



HAL
open science

Modélisation épidémiologique de la dynamique spatio-temporelle des maladies infectieuses à Madagascar : cas du paludisme et du COVID-19

Jean Marius Rakotondramanga

► **To cite this version:**

Jean Marius Rakotondramanga. Modélisation épidémiologique de la dynamique spatio-temporelle des maladies infectieuses à Madagascar : cas du paludisme et du COVID-19. Santé publique et épidémiologie. Sorbonne Université, 2023. Français. NNT : 2023SORUS615 . tel-04606499

HAL Id: tel-04606499

<https://theses.hal.science/tel-04606499>

Submitted on 10 Jun 2024

HAL is a multi-disciplinary open access archive for the deposit and dissemination of scientific research documents, whether they are published or not. The documents may come from teaching and research institutions in France or abroad, or from public or private research centers.

L'archive ouverte pluridisciplinaire **HAL**, est destinée au dépôt et à la diffusion de documents scientifiques de niveau recherche, publiés ou non, émanant des établissements d'enseignement et de recherche français ou étrangers, des laboratoires publics ou privés.

Sorbonne Université

Ecole doctorale Pierre Louis de Santé Publique :

Epidémiologie et sciences de l'information biomédicale

*Equipe UMI 209 Unité de Modélisation Mathématique et Informatique des Systèmes
Complexes (UMMISCO)*

Modélisation épidémiologique de la dynamique spatio- temporelle des maladies infectieuses à Madagascar : cas du paludisme et du COVID-19

Par **Mr Jean Marius RAKOTONDRAMANGA**

Thèse de doctorat de Santé Publique

Spécialité : Biostatistique et Biomathématiques

Dirigée par Benjamin Roche, et co-dirigée par Andres Garchitorea

Présentée et soutenue publiquement le 08 Décembre 2023

Devant un jury composé de :

Mme Lantonirina Ravaoarisoa, Professeure agrégée

Mme Annelise Tran, Directrice de recherche

Mme Elisabeth Delarocque-Astagneau, PU-PH

M. Benjamin Roche, Directeur de recherche

M. Andres Garchitorea, Directeur de recherche

M. Edi Prifti, Directeur de recherche

M. Jordi Landier, Chargé de recherche

Présidente du jury

Rapporteure

Rapporteure

Directeur de thèse

Co-directeur de thèse

Examineur

Examineur



Dédicace

A la mémoire de mes grands-parents, de mon papa, et de ma sœur, qui sont partis trop tôt,

A ma mère,

A ma famille,

A tous les enfants orphelins de Madagascar,

Remerciements

En premier lieu, mes remerciements vont à mes directeurs de recherche, Benjamin Roche et Andres Garchitorena qui m'ont accordé leur confiance et temps, et m'ont guidé au bout de cette thèse. Benjamin, merci de ton investissement et de m'avoir fait partager ta science. Merci d'avoir cru en mes capacités, même si je dois encore m'améliorer pour avoir plus du répondant. Andres, nos entretiens ont toujours été pour moi des moments décisifs, d'orientation dans mes réflexions, d'une pertinence indispensable.

Merci.

Je tiens également à remercier les membres du jury qui ont accepté d'évaluer ce travail.

Je tiens à exprimer mes sincères remerciements à l'ensemble des Directions de l'Ecole Doctorale Pierre Louis de santé publique à Paris (ED 393), de l'Equipe UMI 209 Unité de Modélisation Mathématique et Informatique des Systèmes Complexes (UMMISCO), de l'Institut Pasteur de Madagascar (IPM), de l'Unité d'épidémiologie et de recherche clinique de l'IPM, et de l'Unité MIVEGEC de Montpellier.

Ces travaux n'auraient pu être menés sans le soutien de nombreuses personnes que je remercie tout particulièrement.

A ma famille, qui m'a toujours soutenu et encouragé dans tout ce que j'entreprends.

Merci infiniment.

Production scientifique dans le cadre de la thèse

Publications déjà publiées

Rakotondramanga, J. M., Vigan-Womas, I., Steinhardt, L. C., Harimanana, A., Ravaoarisoa, E., Rasoloharimanana, T. L., Razanatsiorimalala, S., Wesolowski, A., Randrianarivehojosa, M., Roche, B., & Garchitorena, A. (2022). Identification of factors associated with residual malaria transmission using school-based serological surveys in settings pursuing elimination. *Malaria Journal*, 21(1), 242. <https://doi.org/10.1186/s12936-022-04260-0>

Rabarison, J. H., **Rakotondramanga, J. M.***, Ratovoson, R., Masquelier, B., Rasoanomenjanahary, A. M., Dreyfus, A., Garchitorena, A., Rasambainarivo, F., Razanajatovo, N. H., Andriamandimby, S. F., Metcalf, C. J., Lacoste, V., Heraud, J.-M., & Dussart, P. (2023). Excess mortality associated with the COVID-19 pandemic during the 2020 and 2021 waves in Antananarivo, Madagascar. *BMJ Global Health*, 8(7), e011801. <https://doi.org/10.1136/BMJGH-2023-011801>

*Co-premier auteur

Publication en préparation

Rakotondramanga JM, Ratovoson R, Garchitorena A, Roche B, Modelling the impact of screen-and-treat (using RTDs and ACTs) and indoor residual spraying (IRS) strategies on malaria dynamics in southeast of Madagascar (in prep.)

Communications orales ou affichées

Rakotondramanga, J. M., Vigan-Womas, I., Steinhardt, L. C., Harimanana, A., Ravaoarisoa, E., Rasoloharimanana, T. L., Razanatsiorimalala, S., Roche, B., & Garchitorena, A. Identification of factors associated with residual malaria transmission using school-based serological surveys in settings pursuing elimination. Journées Scientifiques du 125^{ème} anniversaire de l'Institut Pasteur de Madagascar, 19-20 octobre 2023 (Poster).

Jean Marius Rakotondramanga, Andres Garchitorena, Benjamin Roche. Les réponses d'anticorps au *Plasmodium falciparum* pour inférer la dynamique de transmission dans les hautes terres de Madagascar. Journées école doctorale St Malo (ED393), SORBONNE UNIVERSITE, 19-20 octobre 2020 (Poster via JITS)

Jean Marius Rakotondramanga, Andres Garchitorena, Benjamin Roche. Les réponses d'anticorps au Plasmodium falciparum pour inférer la dynamique de transmission dans les hautes terres de Madagascar. Journée du département « Processus Écologiques et Évolutifs au sein des Communautés » (PEEC), MIVEGEC Montpellier, 05 octobre 2020 (Présentation orale).

Table des matières

Remerciements	II
Production scientifique dans le cadre de la thèse	III
Table des matières	V
Liste des figures et des tableaux	VII
Liste des abréviations	VIII
1 Introduction.....	1
1.1 Défis et manquements dans la surveillance passive et le contrôle des maladies infectieuses à Madagascar.....	6
1.2 Justification de la thèse.....	10
1.2.1 Problématique.....	10
1.2.2 Objectif général et hypothèses de la thèse.....	11
1.2.3 Les objectifs spécifiques.....	12
1.3 Organisation de la thèse.....	13
2 État de l'Art : Apport de la Modélisation des Maladies Infectieuses dans la Prise de Décision à Madagascar	15
2.1 Contexte.....	16
2.1.1 La modélisation mathématique.....	16
2.1.2 La modélisation statistique.....	17
2.1.3 Les complémentarités des approches statistiques et mathématiques.....	17
2.2 Modèles de dynamique temporelle.....	18
2.2.1 Objectifs et différentes utilisations.....	18
2.2.2 Principaux types de modèles temporels.....	18
2.2.3 Application des modèles temporels au paludisme et au COVID-19	21
2.3 Modèles de dynamique spatiale.....	25
2.3.1 Objectifs et différentes utilisations.....	25
2.3.2 Principaux types de modèles spatiaux.....	25
2.3.3 Application des modèles spatiaux au paludisme et au COVID-19.....	26
2.4 Défis liés aux biais des données de surveillance passive	29
2.5 Conclusion.....	30
3 Chapitre 1 : Identification of factors associated with residual malaria transmission using school-based serological surveys in settings pursuing elimination (Article 1)	31
4 Chapitre 2 : Excess mortality associated with the COVID-19 pandemic during the 2020 and 2021 waves in Antananarivo, Madagascar (Article 2).....	46
5 Synthèse et Discussion	59

5.1	Contributions à la compréhension du paludisme à Madagascar.....	60
5.1.1	Niveau de connaissance sur l'hétérogénéité de la transmission résiduelle.....	60
5.1.2	Comportements d'hôte, exposition aux vecteurs, et recours aux soins	61
	Barrières géographiques, recours aux soins, et prise en charge des cas	61
	Différences d'exposition et d'infection entre classes d'âge	62
5.1.3	Indices environnementaux et climatiques.....	63
5.1.4	Limites méthodologiques de notre étude.....	63
5.1.5	Autres contributions pour caractériser l'épidémiologie du paludisme dans les HTC pendant ma thèse	64
5.2	Contributions à la compréhension du COVID-19 à Madagascar	66
5.2.1	Tendance de la mortalité toutes causes confondues à Antananarivo.....	66
5.2.2	Impact de la pandémie de COVID-19 à Antananarivo.....	67
	Taux de la mortalité.....	67
	Variations et différences en espérance de vie à la naissance.....	68
5.2.3	Forces et faiblesses du système de surveillance hospitalière et communautaire.....	69
5.2.4	Limites et alternatives méthodologiques liées aux sources de données et modèles	70
5.2.5	Autres contributions pour comprendre la dynamique de la première vague de COVID-19 à Madagascar pendant ma thèse	72
5.3	Autres contributions pour comprendre les dynamiques des autres affections ou maladies infectieuses à Madagascar pendant ma thèse	75
6	Conclusion Générale et Perspectives	77
6.1	Perspectives de recherche	81
	Références bibliographiques.....	85
	Informations supplémentaires des chapitres.....	100
	Supplemental files 1 :	101
	Supplemental files 2	120
	ANNEXES : autres contributions en co-auteur pendant la thèse	135
	ANNEXE 1.....	136
	ANNEXE 2.....	147
	ANNEXE 3.....	170
	ANNEXE 4.....	183
	ANNEXE 5.....	190
	ANNEXE 6.....	201
	ANNEXE 7.....	211
	Résumé en français	230
	Résumé en anglais.....	231

Liste des figures et des tableaux

Figure 1 : Maladies infectieuses transmissibles, interactions hôte-pathogène par la flèche plaine (et -vecteur par la flèche en tiret) conditionnées par un environnement favorable (saison, climat, mobilité, etc.).....	2
Figure 2: Flux de données des systèmes de santé (en bleu) face aux défis majeurs des programmes nationaux de contrôle des maladies infectieuses (en rouge).....	3
Figure 3: Evolution des fardeaux dus au paludisme dans les pays de la région africaine de l'OMS, Afrique de l'est et australe, de 2015–2021.....	6
Figure 4: Carte du temps de trajet d'un scénario de déplacement à pied dans le district de Moramanga 2012–2013.....	8
Figure 5: « <i>The Ears of the Hippopotamus</i> » : pour décrire la porosité du système de surveillance passive comme ensemble de gaps à pouvoir contrôler (tester et traiter) les maladies infectieuses.....	10
Figure 6: Les approches de modélisation utilisées dans cette thèse pour estimer le niveau de risque épidémiologique, et évaluer son impact à la population, en considérant la porosité du système de surveillance passive à Madagascar.....	11
Figure 7 : Surveillance d'une épidémie de type syndrome respiratoire aigu sévère à l'aide de données simulées.....	20
Figure 8 : Modèle compartimental proposé par Domenico <i>et al.</i> pour la propagation du COVID-19.....	21
Figure 9 : Cas hebdomadaires de SARS-CoV-2 confirmés en laboratoire à Madagascar du 18 mars–18 septembre 2020.....	23
Figure 10 : L'incidence quotidienne plus faible que prévu peut s'expliquer uniquement par des taux de détection de 0,1–1% des cas ou des efficacités INPs de 30%	24
Figure 11 : Les écozones de la transmission du paludisme à Madagascar, mises à jour sur la base de la carte de prévalence de l'infection <i>Plasmodium falciparum</i> (PfPR).....	26
Figure 12 : Comparaison entre les sources principales (bleu foncé) et l'absence d'importation (gris) et les cas à Antananarivo à partir des données de prévalence.....	27
Figure 13: La proportion des doses totales distribuées par région. En supposant que l'offre totale de vaccins représente 20% de la population totale par différentes stratégies de distribution explorées.....	28
Tableau 1 : Questions de recherche, approches de modélisation épidémiologiques adoptées et données utilisées par Chapitre.....	14
Tableau 2 : Estimation d'excès de mortalité toutes causes de 2020–2021, calculée par le changement relatif utilisant l'algorithme de Farrington et la tendance basale des décès bruts de 2016–2019.....	47

Liste des abréviations

ACT : Combinaison thérapeutique à base d'Artémisinine
AL : Artemether-lumefantrine
anti-PfAMA1 : *P. falciparum apical membrane antigen 1 antibody*
ARIMA : *Autoregressive integrated moving average*
ASAQ : Artesunate-amodiaquine
ASS : Afrique Sub-Saharienne
BMH : Bureau Municipal d'Hygiène
COVID-19 : *Coronavirus Disease 2019*
CRTS : Centres régionaux de transfusion sanguine
CSB : Centre de santé de base
Ct : *Cycle threshold*
CUA : Commune Urbaine d'Antananarivo
EDP: Equations aux dérivées partielles
EDS : Enquête Démographique et de Santé
EM : *Expectation-Maximum*
HTC : Hautes terres centrales
INPs : Interventions non-pharmaceutiques
INSTAT : Institut National de la Statistique
IPM : Institut Pasteur de Madagascar
IRA : Infections respiratoires aiguës
MCE : Méthode *multi-criteria evaluation*
MSANP : Ministère de la Santé Publique de Madagascar
OMS : Organisation Mondiale de la Santé
P. falciparum : *Plasmodium falciparum*
PCR : *Polymerase Chain Reaction*
PID : Pulvérisation intradomiciliaire d'insecticide à effet rémanent
PNLP : Programme Nationale de Lutte contre le Paludisme
PRFI : Pays à revenu faible ou intermédiaire
RT-PCR : *Reverse Transcription-Polymerase Chain Reaction*
SARIMA : *Seasonal autoregressive integrated moving average*
SEIR : Sensible, Exposé, Infectieux et Recouvré/guéri
SIG : Systèmes d'Information Géographique

SIR : Sensible, Infectieux et Recouvré/guéri

TDR : tests de diagnostic rapide

1 Introduction

Pour l'ensemble des pays à revenu faible ou intermédiaire (PRFI), en particuliers les pays d'Afrique Sub-Saharienne (ASS), le contrôle, l'élimination et l'éradication des maladies infectieuses présentent de multiples défis (Ferguson, 2018). Ces défis se reposent d'abord sur la compréhension mécanistique de la transmission des agents pathogènes, au travers de l'écologie d'hôtes (Amambua-Ngwa et al., 2019; Cable et al., 2017) et de vecteurs (Weiss et al., 2015), mais également de l'impact des changements environnementaux, de nature anthropiques ou non (Eikenberry & Gumel, 2018). Mais une diminution du fardeau des maladies infectieuses nécessite également un impact sur des facteurs structurels, tels que les ressources financières (pouvant dépendre des aides internationales), les infrastructures de santé publique, les facteurs socio-économiques et démographiques ou l'éducation (Heesterbeek et al., 2015; Reiner et al., 2013). Cela demande donc une approche novatrice et un investissement supplémentaire, implémentés de façon plus efficace en matière de ressources humaines (aussi bien de façon qualitative que quantitative) et d'infrastructures (en qualité pouvant faire face aux défis de santé publique) (Bonds et al., 2010; Logie et al., 2008).

Généralement, les changements globaux, que ce soit l'altération de la biodiversité d'hôtes potentiels relatifs aux destructions d'habitats au travers la déforestation ou le changement climatique, sont les conséquences des pressions anthropiques exercées par la dynamique démographique rapide, l'urbanisation croissante ou le développement de l'agriculture que les pays connaissent (**Figure 1**) (Albonico et al., 1999; Arisco et al., 2020; Carolan et al., 2014; Zohdy et al., 2016). C'est dans ce contexte qu'il faut placer la lutte contre les maladies infectieuses, qui reste un défi majeur de santé publique tant que les structures de santé offrant des soins hospitaliers ne couvrent pas assez de façon égalitaire les territoires nationaux à cause de leur accès difficiles ou de leur faible développement (plus particulièrement pour les pays d'ASS) (Linard et al., 2012)(Ouma, 2020). De ce fait, ces deux facteurs combinés, aggravés par des situations socio-économiques peu développées, favorisent la persistance des menaces de santé publique (Bonds et al., 2010), surtout pour des groupes de populations fortement vulnérables et exposés à des agents infectieux endémiques comme les parasites *Plasmodium*, ou émergents comme le virus SARS-CoV-2 nécessitant l'application des mesures de contrôle plus adaptées (**Figure 1**).

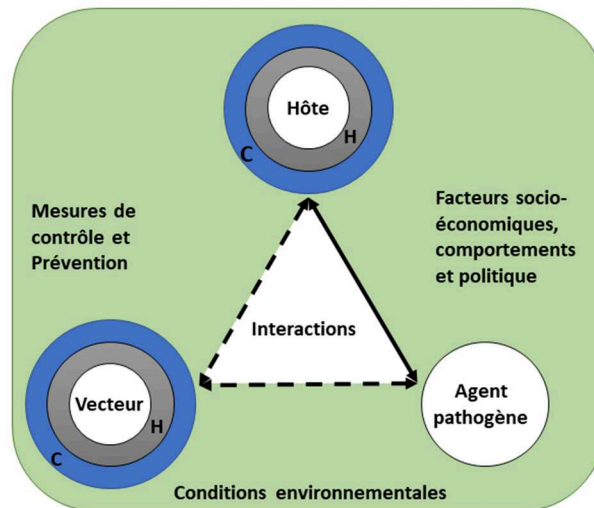


Figure 1 : Maladies infectieuses transmissibles, interactions hôte-pathogène par la flèche pleine (et -vecteur par la flèche en tiret) conditionnées par un environnement favorable (saison, climat, mobilité, etc.) (Breman, 2001; Eikenberry & Gumel, 2018), le contact étroit au sein d'une communauté (C) ou d'un habitat (H), ainsi que la biologie de l'hôte (ou éventuellement du vecteur pour les maladie à transmission vectorielle) (Cauchemez, Temime, et al., 2006).

Source : (Breman, 2001; A. Garchitorena et al., 2017).

Bien que chaque pays possède son propre système de surveillance, le report des données de routine concernant la circulation des maladies infectieuses depuis les centres de santé de base (CSB) jusqu'aux décideurs politiques centraux rencontre plusieurs défis opérationnels et techniques. Le plus important concerne certainement les problèmes de diagnostic des cas, que ce soit faute (i) des signes évocateurs non-spécifiques, (ii) de la disponibilité des tests, et/ou (iii) du manque de formation des agents de santé en capacité d'analyse biologique (World Health Organization (WHO), 2020). En conséquence, les délais de remontée des données sont souvent allongés, engendrant des ripostes tardives. Malgré cela, l'exploitation des données collectées peut être optimisée pour améliorer la prise de décision de santé publique.

En effet, ces données épidémiologiques des patients sont rapportées par les personnels de santé via des systèmes de surveillance dite passive dans une base de données centrale, qui à son tour est utilisée pour divers objectifs, à savoir (de façon non exhaustive) :

1. déterminer les tendances temporelles, notamment à des fins de prédiction,
2. cartographier la distribution géographique de la charge de morbidité dans différentes régions,

3. identifier l'étendue de l'événement épidémique pour pouvoir riposter,
4. évaluer l'efficacité des interventions de contrôle et de prévention des maladies infectieuses.

Le bon rapportage de ces données constitue donc une base importante pour une meilleure prise des décisions relatives à l'allocation des ressources nécessaires (tests de diagnostic, médicaments pour les traitements, et aussi les ressources humaines qu'il faut dans le cadre d'une réponse à une épidémie). La **Figure 2** illustre le flux de données et les obstacles potentiels auxquels sont confrontés les programmes nationaux de contrôle des maladies infectieuses en matière de collecte de données. Elle montre aussi la possibilité que des données additionnelles (données issues de sources parallèles telles que la santé mobile (mHealth), la téléphonie et les données satellitaires et environnementales entre autres) peuvent être utilisées parallèlement aux de sources de données « traditionnelles » (C. O. Buckee et al., 2018). Cependant, à tous les niveaux des programmes nationaux de lutte contre les maladies infectieuses, la capacité des personnels reste un énorme problème pour la surveillance de routine et leurs formations à l'utilisation des nouvelles technologies restent un défi pour la plupart dans les PRFI et les pays d'ASS à cause de leurs faibles niveaux d'éducation qui nécessitent une continuelle remise à niveau (C. O. Buckee et al., 2018).

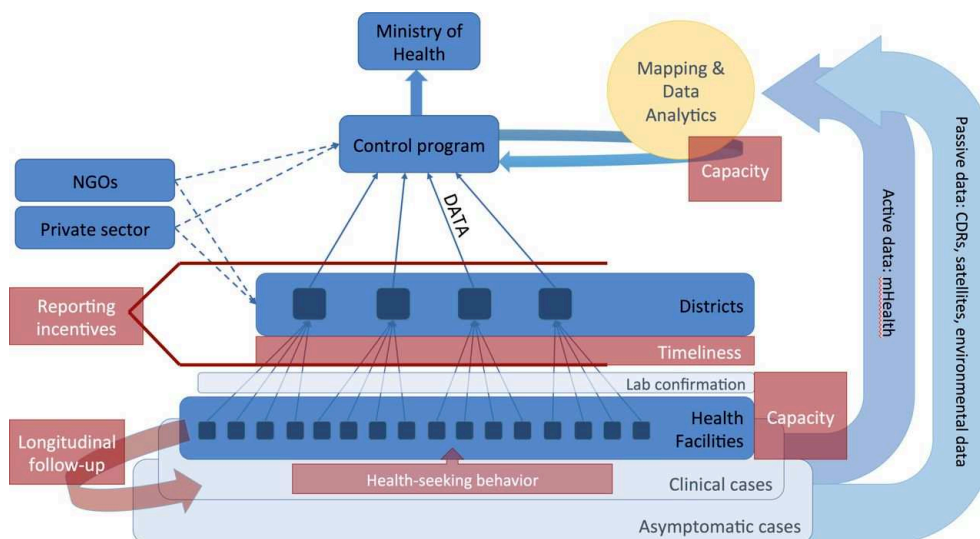


Figure 2: Flux de données des systèmes de santé (en bleu) face aux défis majeurs des programmes nationaux de contrôle des maladies infectieuses (en rouge). À différentes échelles du système de santé, le respect des délais peut être particulièrement problématique pour les menaces émergentes de santé publique qui nécessitent une réactivité importante.

Source : (C. O. Buckee et al., 2018).

Selon une revue systématique sur les objectifs de développement durable N°3 liés à la santé, plusieurs pays d'ASS (y compris Madagascar) ont été classés comme ayant de très faibles probabilités (0%) à atteindre les objectifs moyens projetés des 41 indicateurs composites pour 2030 (GBD 2017 SDG Collaborators, 2018). Pour ce groupe de pays, il a été recommandé d'analyser en profondeur les données désagrégées au niveau sub-national afin de (1) mieux orienter les progrès dans l'atteinte des indicateurs des objectifs de développement durable relatifs à la santé, (2) maximiser les impacts d'interventions (via des méthodes et modèles plus précis), et (3) apporter ainsi des améliorations significatives dans leurs systèmes de santé respectifs (GBD 2017 SDG Collaborators, 2018; Odhiambo et al., 2020). Car, un système de santé fragile et inégalitaire en matière d'accès aux soins a toujours caractérisé ce groupe de pays en plus des multiples menaces de santé publique (exposition aux agents infectieux et faible niveau socio-économique) (Bonds et al., 2018; Linard et al., 2012).

Parmi ces menaces, les pays d'ASS font face, non seulement aux maladies materno-infantiles, mais aussi aux maladies infectieuses pouvant toucher tous les groupes de population. Ces maladies peuvent constituer des risques sanitaires permanent, notamment l'infection à *Plasmodium falciparum* (*P. falciparum*)—l'espèce humaine du parasite la plus répandue, représentant 53,5 millions de cas confirmés en 2021, et à l'origine des formes les plus graves du paludisme en ASS (World Health Organisation, 2022). D'autres maladies infectieuses, plus sporadiques comme la peste ou les infections respiratoires aiguës (IRA) dues aux virus respiratoires tel que le SARS-CoV-2 (Anjorin et al., 2021; Rabarison et al., 2019; R. V. Randremanana et al., 2021; Ratsitorahina et al., 2000), peuvent également faire porter un lourd fardeau aux populations.

Les difficultés de contrôle sont particulièrement criantes pour le cas du paludisme, où plusieurs pays d'ASS n'arrivent pas à contrôler et maîtriser le risque de décès causé par cette maladie parasitaire. Ceci est principalement dû par une prise en charge insuffisamment adaptée des cas (diagnostiquer et traiter) avec: seulement 66,5% des cas de fièvre ont accès au centre de santé, dont une partie (uniquement 56,5%) peuvent à leur tour être correctement diagnostiqués. Aussi, seulement 55,1% de ces cas diagnostiqués positifs avec les tests de diagnostic rapide (TDR) peuvent avoir accès au traitement par la combinaison thérapeutique à base d'Artémisinine (ACT)(World Health Organisation, 2022).

Ce problème de diagnostic et de traitement s'est aussi manifesté lors de la pandémie de COVID-19 (*Coronavirus Disease 2019*). Les pays d'ASS ont fait face à la difficulté de leurs

systèmes de surveillance à pouvoir diagnostiquer correctement et à temps les cas suspects, ainsi qu'à estimer les décès attribuables à cette pandémie. Cette difficulté peut se trouver dans les techniques d'estimation utilisées, mais également dans la disponibilité des données utilisées pour le faire. Car les statistiques officielles souvent utilisées peuvent elles-mêmes comporter des biais en raison de la capacité limitée des tests, soit 1 000 tests maximum par jour pour environ 25,7 millions d'habitants pour Madagascar si on considère l'ensemble de la population comme à risque (Institut National de la Statistique (INSTAT), 2021), du manque de personnel pour effectuer la recherche des contacts (contact tracing), ainsi que des changements dans la politique de dépistage au cours de la pandémie (Randremanana et al., 2021). Il existe également de grandes incertitudes autour des taux de mortalité basales pré-pandémiques en raison du caractère incomplet des systèmes de registre des décès dans les pays d'ASS.

Selon l'Organisation Mondiale de la Santé (OMS), pendant la période pandémique de 2020–2021, environ 82% de cas et 95% de décès dus au paludisme dans le monde ont été survenus la région africaine de l'OMS, avec une hausse allant de 211 millions à 234 millions de cas et de 542 mille à 593 mille décès de 2015–2020 (World Health Organisation, 2022; World Health Organization, 2021). De plus, entre 2020 et 2021, environ 13,4 millions de cas supplémentaires du paludisme (World Health Organisation, 2022), et une augmentation du nombre de décès de 386,4 (IC95%: 307,8–497,8) mille à 597,4 (IC95%: 468,0–784,4) mille auraient été attribuables à la mitigation des efforts de lutte due aux interventions non-pharmaceutiques pour faire face à la pandémie de COVID-19, ayant entraîné 25% de réduction de couverture en antipaludéen (Weiss et al., 2021). Ceci concerne principalement les confinements ayant directement limité l'accès aux tests, les traitements, et les mesures de prévention (par la perturbation des campagnes de pulvérisation intradomiciliaire d'insecticide à effet rémanent (PID) et de distribution de moustiquaires imprégnés d'insecticides) (Bylicka-Szczepanowska & Korzeniewski, 2022; Shi et al., 2021).

1.1 Défis et manquements dans la surveillance passive et le contrôle des maladies infectieuses à Madagascar

Plusieurs pays de la région africaine ont le potentiel d'éliminer le paludisme à moyen ou long terme; le taux d'incidence a été réduit de 372,6 à 233,6 cas pour 1 000 habitants exposés au risque de paludisme entre 2000 et 2020 (World Health Organisation, 2022). Par contre, Madagascar avec 4,9 millions de cas et 12 571 de décès estimés en 2021 fait partie des trois pays de l'Afrique de l'Est et Australe, avec l'Ouganda et le Sud-Soudan, ayant enregistré une hausse des taux d'incidence et de décès du paludisme de 2015–2021, soit de plus de 75% (Figure 3) (World Health Organisation, 2022). Cela prouve que les efforts fournis par Madagascar pour atteindre les objectifs (améliorer la prise en charge d'au moins 95% des cas diagnostiqués et d'assurer la disponibilité permanente des tests de diagnostic et de traitement pour 95% des centres de santé depuis 2013, ainsi que son paquet d'interventions de contrôle) nécessitent une amélioration et une adaptation face aux défis de la lutte contre le paludisme (Programme Nationale de Lutte contre le Paludisme, 2012; Razakamanana et al., 2020; World Health Organization, 2020).

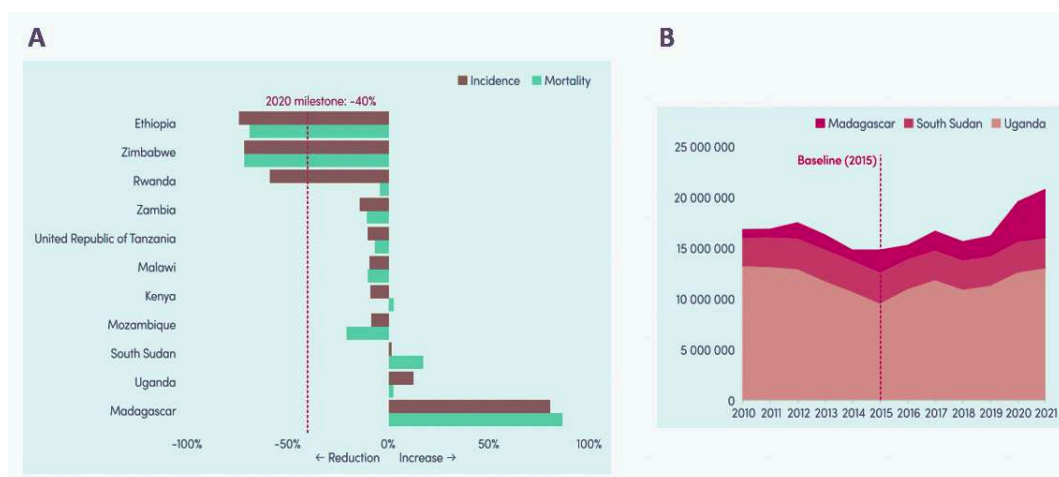


Figure 3: Evolution des fardeaux dus au paludisme dans les pays de la région africaine de l'OMS, Afrique de l'est et australe, de 2015–2021 : A) Variations estimées des taux d'incidence et de mortalité, et B) Nombre de cas estimés dans les pays n'ayant pas enregistré une baisse significative.

Source : (World Health Organisation, 2022)

En effet, selon une enquête récente au niveau national, l'Enquête Démographique et de Santé (EDS) réalisée en 2021 pour les enfants de 5–59 mois sur les 22 régions de Madagascar, 12% des enfants de moins de cinq ans avaient présenté de la fièvre pendant les deux semaines ayant précédé l'enquête. Parmi les enfants ayant eu de la fièvre, 45% d'entre eux ont eu recours au soin et seulement 20% de ces cas de fièvre ont pu être testés au doigt ou au talon. Parmi les enfants traités avec un médicament antipaludique, seulement 55% ont pris un ACT (Institut National de la Statistique (INSTAT) et ICF, 2021). Cependant, d'après les études récentes, le traitement avec ACT en première ligne utilisant l'artesunate-amodiaquine (ASAQ), et en deuxième ligne utilisant l'artemether-lumefantrine (AL) demeure efficace pour traiter les infections à *P. falciparum* à Madagascar (Dentinger et al., 2021; Irinantenaina et al., 2023). S'ajouter à cela, selon l'EDS, la prévalence du paludisme a été estimée à 9% et 2% chez les enfants en milieu rural et urbain, respectivement ; et aussi à 0,7% et 16% chez les enfants des ménages du quintile de bien-être économique le plus élevé et le plus faible, respectivement (Institut National de la Statistique (INSTAT) et ICF, 2021).

Les barrières géographiques constituent un frein majeur à l'accès aux services de santé. Au niveau sub-national, d'après une enquête réalisée en 2013 dans le district de Moramanga se trouvant au nord-est de la capitale, avec une vitesse de marche de 4km/h, les habitants de la partie nord de la zone d'étude doivent parcourir à pied entre 60 et 180 minutes de trajet pour se rendre à la formation sanitaire la plus proche (**Figure 4**). Ce temps de trajet est encore plus élevé dans la majeure partie sud de la zone d'étude, du fait de la rareté des centres de santé. Une partie de la population doit parcourir jusqu'à 5 heures de temps de trajet pour recourir aux soins auprès du centre de santé le plus proche (H. F. A. Ihantamalala, 2013).

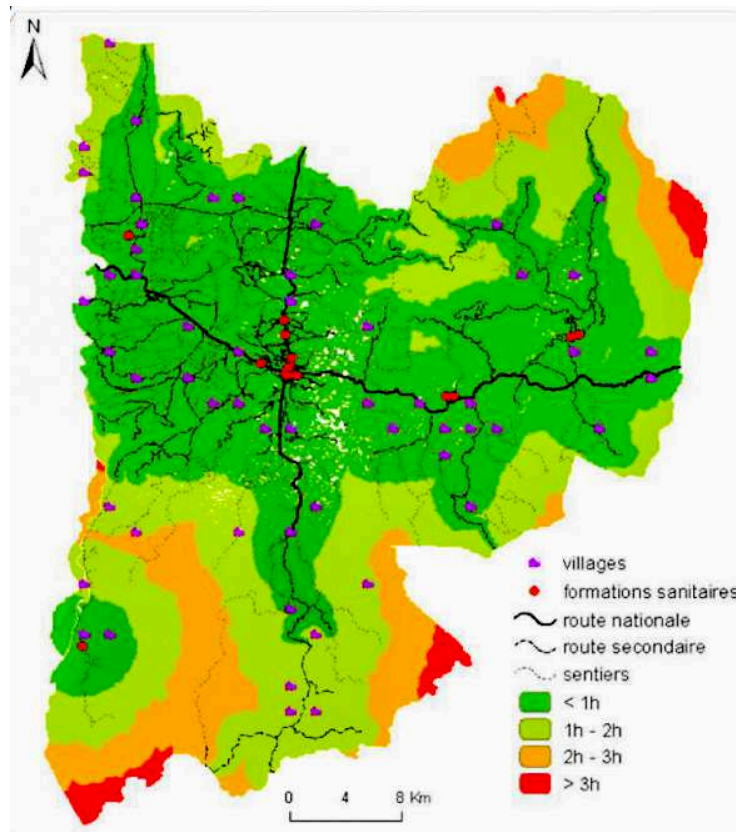


Figure 4: Carte du temps de trajet d'un scénario de déplacement à pied dans le district de Moramanga 2012–2013.

Source : (Ihantamalala FA, Ratovoson R, Mangahasimbola R, 2014)

Ainsi, les cas ni diagnostiqués ni traités, symptomatiques ou asymptomatiques, peuvent activement contribuer à la transmission de l'agent pathogène (Andolina et al., 2021; Rek et al., 2022) et complexifient la lutte contre les maladies infectieuses tels que le paludisme et le COVID-19. Les décès et les fardeaux engendrés par ces maladies au sein de la communauté pourraient échapper aux statistiques des formations sanitaires (Ratovoson, 2020). Selon les estimations de l'OMS, le COVID-19 a causé directement ou indirectement 25 582 décès supplémentaires au cours de la période pandémique 2020–21 à Madagascar (Msemburi et al., 2022). Cependant, au 31 décembre 2021, le Ministère de la Santé Publique de Madagascar (MSANP) avait notifié 1 067 décès dus au COVID-19 pour l'ensemble du pays (Mathieu et al., 2020). Cet écart entre les estimations de l'OMS et les décès notifiés par le MSANP pourrait s'expliquer par le fait que le MSANP n'a notifié que les décès confirmés par les laboratoires effectuant des tests pour les infections à SARS-CoV-2 et n'ayant pas considéré les décès

indirects. Par conséquent, à notre connaissance, le nombre total de décès directs et indirects dus à la pandémie de COVID-19 n'est pas connu ou mal estimé à Madagascar.

D'après les précédentes études basées sur la modélisation, l'impact de la pandémie à Madagascar et celui des interventions de lutte, a été premièrement estimé utilisant des scénarios d'impact des interventions non-pharmaceutiques (INPs) (Evans et al., 2020). En faisant varier le taux de détection des cas et l'effectivité des mesures barrières tout au début de la pandémie, Evans *et al.* a décrit le risque d'augmentation du nombre de décès pouvant être majoritairement attribuable à la pandémie de COVID-19, si de plus les INPs mises en places sont relaxées ou l'accès aux soins ne sont pas continuellement amélioré (Evans et al., 2020). Deuxièmement, une étude de Rasambainarivo *et al.* a simulé l'impact de différentes stratégies de vaccination contre la COVID-19, en évaluant des approches de répartition des doses selon les régions pouvant avoir plus d'impact sur la réduction de taux de mortalité (Rasambainarivo et al., 2022). Ils ont utilisé un modèle mécanistique stochastique structuré par groupe d'âge, et constaté qu'une répartition des doses de vaccins disponibles selon le nombre de population par région pourrait plus baisser les taux de mortalité attribuable au COVID-19.

Cela justifie davantage la nécessité et l'apport que peuvent apporter des approches méthodologiques telle que la modélisation pour mieux comprendre et caractériser les expositions aux risques des maladies infectieuses, tels qu'à l'infection à *P. falciparum* ou à SARS-CoV-2, et aussi évaluer l'impact des interventions de contrôles (pharmaceutiques ou non) pour la population de Madagascar.

1.2 Justification de la thèse

1.2.1 Problématique

Dans la démarche du recours au soin suite à une infection, à l'apparition des symptômes, seuls les cas symptomatiques sont donc testés dans le cadre de la surveillance de routine. Cette approche permet d'identifier et de traiter uniquement les cas symptomatiques, à condition qu'ils soient correctement diagnostiqués, avec un test sensible, et en supposant qu'un médicament ait été administré. En conséquence, seule une infime proportion d'infections au sein de la communauté pourra être enregistrée dans le système de surveillance (Andolina et al., 2021; C. Buckee et al., 2021; Rek et al., 2022). Ainsi, la mortalité et la morbidité engendrées par la maladie, non rapportées, au sein de la communauté peuvent ne pas être enregistrées dans le système de surveillance (Breman, 2001; Ratovoson, 2020). Ce phénomène est représenté par le concept de Breman « *The Ears of the Hippopotamus* », dans le cadre de la surveillance passive du paludisme: qui laisse la majorité de cas infectieux non diagnostiquée ni traitée, et rend difficile le contrôle au sein d'une communauté (**Figure 5**) (Breman, 2001). Dans le cadre de cette thèse, nous le caractérisons par la porosité du système de surveillance passive. Cette dernière est constituée par l'ensemble des manquements à pouvoir contrôler efficacement (tester et traiter) les maladies infectieuses. Cela est due en partie par des infections asymptomatiques ou symptomatiques n'ayant pas accès aux tests ni aux traitements appropriés, des barrières géographiques ou des faibles niveaux socio-économiques.

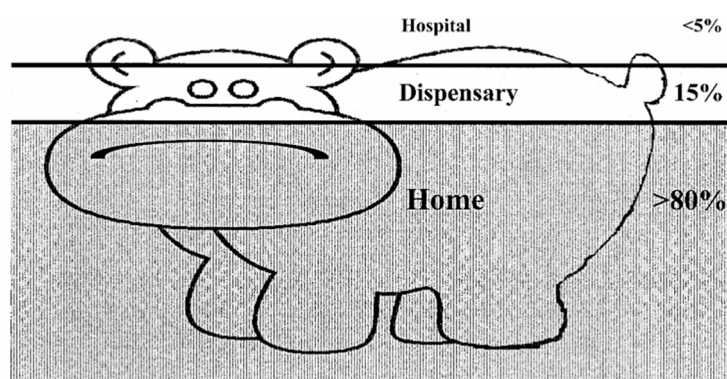


Figure 5: « *The Ears of the Hippopotamus* » : pour décrire la porosité du système de surveillance passive comme un ensemble de gaps à pouvoir contrôler (tester et traiter) les maladies infectieuses, et non seulement dans le cadre du paludisme mais aussi pour les IRA dues au virus respiratoire tel que le SARS-CoV-2.

Source : (Breman, 2001)

Si de plus, le diagnostic moléculaire tel que le test PCR (*Polymerase Chain Reaction*) est demandé pour confirmer le portage de l'infection, comme pour le cas du virus SARS-CoV-2, d'autres barrières liés à l'accessibilité des tests (des ressources techniques et compétences opérationnelles limitées) peuvent constituer des freins supplémentaires et fragiliser davantage le système de surveillance des PRFI (C. O. Buckee et al., 2018; Logie et al., 2008).

1.2.2 Objectif général et hypothèses de la thèse

Dans le cadre de cette thèse, notre objectif consiste à comprendre les dynamiques spatiales ou temporelles des maladies infectieuses malgré la porosité (ensemble de manquements) du système de surveillance passive à Madagascar. Donc, notre hypothèse c'est l'existence de la porosité du système de surveillance passive à Madagascar, altérant l'impact des mesures de contrôle des maladies infectieuses. Pour la tester, des approches de modélisation biostatistique et biomathématique seront adoptées en utilisant des données de mesures indirectes de l'intensité de transmission telles que les mesures d'anticorps du *P. falciparum*, et aussi les excès de mortalité toutes causes pendant la pandémie de COVID-19 (**Figure 6**).

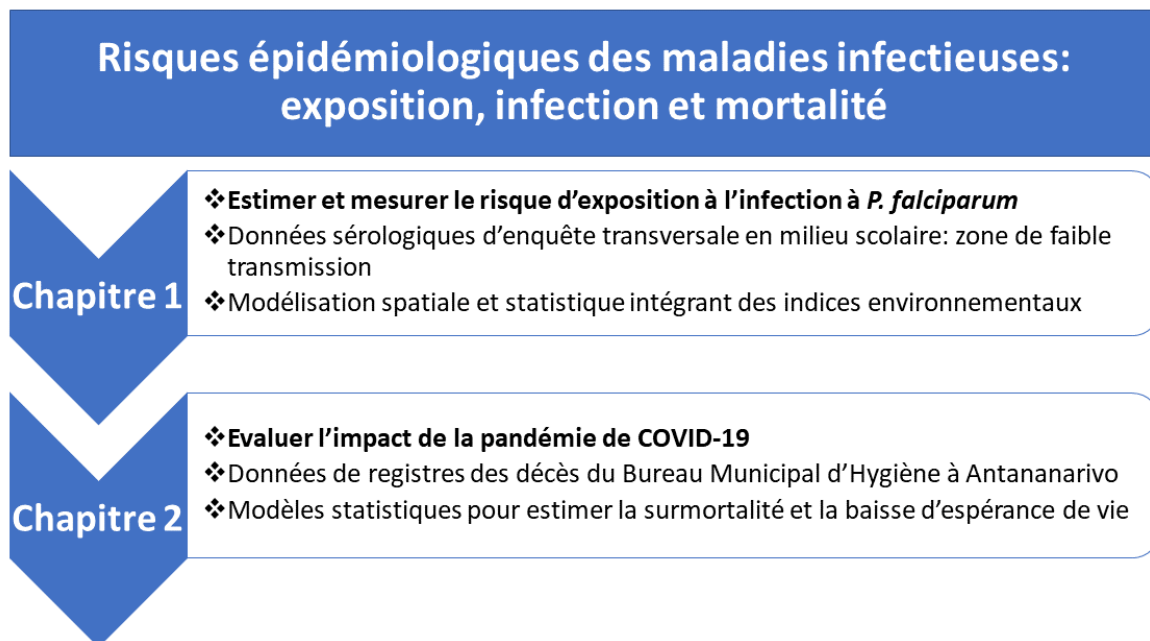


Figure 6: Les approches de modélisation utilisées dans cette thèse pour estimer le niveau de risque épidémiologique, et évaluer son impact à la population, en considérant la porosité du système de surveillance passive à Madagascar.

1.2.3 Les objectifs spécifiques

- i) Identifier des facteurs d'exposition associés à l'infection à *P. falciparum* dans les hautes terres de Madagascar, zone de faible transmission, en 2014 : structurels liés aux offres de soin, et non-modifiables liés à l'environnement et le climat.
- ii) Estimer les excès de mortalité pendant les vagues épidémiques de COVID-19, en 2020–21, dans les cinq arrondissements de la Commune Urbaine d'Antananarivo (CUA), utilisant les données de registres de décès.

1.3 Organisation de la thèse

Précédées par une section d'état de l'art, les questions de recherche, les approches de modélisation épidémiologiques (**Figure 6**) ainsi que les données présentées dans le **Tableau 1**, ci-après, seront abordées, analysées et traitées successivement dans les Chapitres 1 et 2.

Tableau 1 : Questions de recherche, approches de modélisation épidémiologiques adoptées et données utilisées par Chapitre.

Chapitre	Questions	Données utilisées
Chapitre 1	<ul style="list-style-type: none"> ● Détecter et caractériser l'hétérogénéité spatiale de la prévalence de l'infection à <i>P. falciparum</i> et de la séroprévalence de l'anticorps PfAMA1 (anti-PfAMA1, <i>P. falciparum apical membrane antigen 1 antibody</i>) dans les HTC (hautes terres centrales) et les marges, zone de faible transmission, en 2014 ; ● Identifier des facteurs d'exposition associés à l'infection à <i>P. falciparum</i> dans les hautes terres de Madagascar : structurels liés aux offres de soin (accès aux formations sanitaires, prises en charge communautaire, interventions de lutte antivectorielle), et non-modifiables liés à l'environnement et le climat (écologie des vecteurs). 	<ul style="list-style-type: none"> ● Données d'enquête sérologique des écoliers dans les HTC et les marges (Steinhardt et al., 2021); ● Données environnementales et climatiques open source des localités investiguées (Farr et al., 2007; Friedl et al., 2010; Oak Ridge National Laboratory Distributed Active Archive Center (ORNL DAAC), 2018); ● Données de l'OMS sur la location géographique des formations sanitaires publiques desservant les localités investiguées (Maina et al., 2019).
Chapitre 2	<ul style="list-style-type: none"> ● Estimer les excès de mortalité toutes causes hebdomadaires pendant les vagues épidémiques de COVID-19, en 2020–21 ; ● Analyser les associations (synchronisations) entre les données officielles de déclarations de décès dus au COVID-19 versus le taux de mortalité toutes causes ainsi que le taux de positivité hebdomadaire ; ● Evaluer l'évolution de l'espérance de vie par causes de décès pendant la période pandémique de 2020–21. 	<ul style="list-style-type: none"> ● Registres de décès du Bureau Municipal d'Hygiène (BMH), couvrant les cinq arrondissements d'Antananarivo (Masquelier et al., 2019); ● Données officielles de déclaration de décès dus au COVID-19 (Mathieu et al., 2020); ● Données de positivité des tests réalisés à l'Institut Pasteur de Madagascar (IPM) (R. V. Randremanana et al., 2021).

2 État de l'Art : Apport de la Modélisation des Maladies Infectieuses dans la Prise de Décision à Madagascar

Cette revue générale a pour objectif de présenter les différentes approches et l'apport de la modélisation épidémiologique dans la compréhension, la surveillance et le contrôle des maladies infectieuses. Une attention particulière sera portée sur les deux systèmes biologiques étudiés dans le cadre de cette thèse : le paludisme à *P. falciparum* et le COVID-19 à Madagascar. Afin de pouvoir cerner les dynamiques épidémiologiques majeures (de la détection d'une épidémie à l'évaluation d'impact d'interventions de lutte), nous allons nous focaliser sur les modèles mécanistiques permettant la simulation de dynamique temporelle et spatiale, ainsi que les modèles statistiques utilisés dans l'investigation des facteurs de risque des infections aux maladies infectieuses—comme les variables structurantes individuelles (âge de l'hôte, âge de leur infection, leur statut immunologique, etc.) et celles liées à l'environnement ou le climat. Les manquements en matière de données et les perspectives de recherche dont les futures études pourront combler seront par la suite discutés dans les contextes des pays d'ASS.

2.1 Contexte

En général, les défis de la modélisation épidémiologique consistent à comprendre les épidémies passées, à quantifier la dynamique actuelle, et à anticiper les trajectoires futures et les besoins en ressources pour y faire face (Djidjou-Demasse et al., 2020). Deux familles de modèles, souvent complémentaires, constituent alors la pierre angulaire de l'épidémiologie quantitative pour élucider les mécanismes de transmission ainsi que les effets de variables jugées importantes ou liées à la dynamique de l'agent infectieux étudié: il s'agit des modèles mathématiques, reposant sur une modélisation mécanistique des processus impliqués d'une part, et les modèles statistiques, qui permettent de modéliser les données existantes afin d'en comprendre le fonctionnement du système. La différence réside donc dans l'approche, basée sur la caractérisation des processus pour la modélisation mathématique et reposant sur l'analyse des données pour la modélisation statistique.

2.1.1 La modélisation mathématique

Les approches de modélisation mathématique des maladies infectieuses ont été révolutionnées au début du 20ème siècle par les travaux de Ross sur le paludisme (Ross, 1910) et de Kermack et McKendrick sur la théorie mathématique des épidémies et le phénomène de seuil épidémique (Kermack & Mckendrick, 1927). L'objectif de leurs utilisations réside d'abord dans la compréhension du cycle de vie du pathogène, notamment sa transmission, afin ensuite de pouvoir, entre autres choses, évaluer l'efficacité et l'efficacité des mesures de contrôle pour ensuite les améliorer, ou encore de faire une projection future des fardeaux pouvant être engendrés dans la population telle que la mortalité (Bernoulli, 1766; Hamer, 1906). Pour que ces modèles puissent être analysés, ces approches décrivent d'une manière simplifiée les phénomènes biologiques complexes de dynamique de la population d'hôtes, d'agents pathogènes, et aussi de vecteurs pour le cas des maladies à transmission vectorielle tel que le paludisme.

En matière de formalisme, ces modèles font appel, par exemple, à des techniques mathématiques telles que les équations différentielles ordinaires (Wearing et al., 2005), utilisant le temps comme indicateur de variation continu, ou les équations aux dérivées partielles (EDP) considérant l'âge de l'infection comme variable structurante continue (Richard et al., 2021).

2.1.2 La modélisation statistique

Quant aux approches de modélisation statistique, elles s'appliquent tant bien dans les études transversales, en un point de temps donné, et longitudinales (suivi sur une période) que spatiales ou spatio-temporelles (ex. la géostatistique) (R. S. Bivand et al., 2013). De nature probabiliste, les modèles statistiques permettent d'estimer une valeur moyenne pour des paramètres extraits de données qui ne la mesurent pas directement, de quantifier l'incertitude via des intervalles de confiance et des tests d'hypothèse, voire de déduire ou inférer une distribution qui tient compte de la variabilité (Ratovoson, Razafimahatratra, et al., 2022). Toutefois, la capacité d'inférence de ces approches est limitée aux paramètres dont les variations sont relativement bien reflétées dans les données utilisées (Djidjou-Demasse et al., 2020). Pour compenser cela, elles incluent des variables structurantes jugées importantes à la compréhension de cette variation—variables démographiques (âge, sexe), socio-économiques et environnementales voire écologiques d'hôtes, de vecteurs, ou d'agents pathogènes—et permettent d'en sélectionner celles pouvant aider et guider les décideurs de santé publique dans l'orientation de leurs interventions de contrôle (Feachem et al., 2019).

2.1.3 Les complémentarités des approches statistiques et mathématiques

Les approches statistiques et mathématiques sont souvent complémentaires et synergiques. Par exemple, pendant les premières phases épidémiques d'une maladie émergente comme le COVID-19, les analyses statistiques peuvent permettre d'estimer des paramètres clés régissant la dynamique épidémiologique tels que le temps d'incubation (Linton et al., 2020), l'intervalle sériel (Nishiura et al., 2020), le nombre de reproduction de base (Li et al., 2020), ou encore la létalité (pouvant être stratifiée par âge pour indiquer le groupe de la population le plus à risque) (Verity et al., 2020). La bonne estimation de ces paramètres est indispensable à la calibration de modèles mathématiques qui permettent d'effectuer des inférences précoces de l'impact de l'épidémie malgré l'incertitude, l'hétérogénéité et le nombre très limité des données disponibles (Pellis et al., 2020).

2.2 Modèles de dynamique temporelle

2.2.1 Objectifs et différentes utilisations

Afin de comprendre et d'expliquer les phénomènes temporels, les modèles temporels permettent de décrire la dynamique en fonction des données historiques disponibles (Rohani & King, 2010). En se basant sur les données disponibles, l'application des techniques de modélisation temporelles (statistiques ou mathématiques) consiste à répondre principalement aux questions relatives à la prise de décisions de santé publique dans sa temporalité :

- i) l'instant, représenté par un point sur un axe de temps (jour, semaine, mois, année): la date du début de l'épidémie de maladie, le moment du pic épidémique, le début des interventions (fermeture des écoles ou confinement pour altérer la susceptibilité de la population à la transmission);
- ii) la fréquence, la tendance, et la saisonnalité des événements de santé enregistrés: l'incidence et la mortalité;
- iii) l'intervalle de l'occurrence d'un événement de santé, représenté par une période (début, fin) sur un axe de temps: la période d'incubation, pendant laquelle le cas devient infectieux (Linton et al., 2020); et l'intervalle sériel séparant l'apparition de symptômes chez les paires {infecteurs-infectés}(Nishiura et al., 2020).

2.2.2 Principaux types de modèles temporels

Dans le cadre de la surveillance des maladies infectieuses, plusieurs approches statistiques et mathématiques ont été proposées pour détecter et alerter la dynamique temporelle d'une épidémie dans une zone d'endémie ou en pré-élimination.

Les techniques de modélisation temporelle statistique d'une épidémie peuvent être catégorisées en deux « courants dominants » selon le type de processus temporel. D'abord, les processus temps-dépendants, telles les fonctions d'autocorrélation et les modèles de type « autoregressive integrated moving average » (ARIMA) (non-stationnaires au sens de moyenne, comportant de tendance temporelle, mais stationnaires au sens de variance), et ses variants stationnaires (AR, avec composante autorégressive; MA, avec sa composante moyenne mobile; et ARMA, sans la saisonnalité), pour estimer et projeter les taux de mortalité en démographie par exemple (Lee & Carter, 1992). Ensuite, les processus fréquence-dépendants,

telles que les analyses spectrales et celle du périodogramme des séries de Fourier « traditionnelle » visant à subdiviser la variance totale de la série temporelle par d'autres séries avec des propriétés connues, des composantes sinusoïdales avec leurs amplitudes maximales et fréquences respectives (Bjørnstad, 2018; Chatfield & Xing, 2019). Cependant, les méthodes hybrides, dépendantes en temps/fréquence, ont pris de plus en plus d'ampleur sous la forme d'une analyse en ondelettes (Daubechies, 1992). Ce type d'analyse permet non seulement d'étudier les signaux non-stationnaires et les changements dans la dynamique de la maladie, mais aussi de quantifier les changements croisés entre deux séries temporelles—d'une maladie et du signal de son prédicteur, ou d'une même maladie survenue en deux endroits différents—au fil du temps (Cazelles et al., 2007). C'est-à-dire, ces analyses permettent de quantifier l'impact d'un ou de plusieurs facteurs sur la dynamique temporelle d'une maladie ; et elles permettent aussi d'identifier les changements de fréquences au cours du temps (de façon intrinsèque ou à cause de dynamiques des autres facteurs).

Étant intrinsèquement dynamiques, les techniques de modélisation mécanistiques sont souvent utilisées pour modéliser les épidémies au cours du temps. Une utilité majeure de ces modèles est de calculer par exemple le nombre de reproduction, R . Il s'agit en effet de la moyenne des cas secondaires générés à partir d'un cas infectieux. Ce paramètre est une mesure d'importance capitale de la propagation d'une maladie infectieuse au sein d'une communauté d'hôtes. Sa valeur sert à évaluer son potentiel d'invasion ou l'efficacité des mesures de contrôle: une épidémie sous contrôle est caractérisée par $R < 1$, contrairement à une situation épidémique pour laquelle $R > 1$ (Cauchemez, Boelle, et al., 2006). D'un point de vue épidémiologique, R peut être estimé au travers de la recherche des contacts de cas. Néanmoins, ceci est difficilement réalisable et limité par la nature biologique de la transmission (ex. la période d'incubation) et la logistique nécessaire pour le faire. C'est pourquoi des modèles mathématiques et/ou statistiques sont utilisés pour quantifier la valeur prise par R par ajustement aux données populationnelles observées (**Figure 7**) (Cauchemez, Boelle, et al., 2006). En rapport avec le seuil épidémique de Kermack et Mckendrick, on s'intéresse à l'estimation du nombre de reproduction dite basique, R_0 , quand la population est totalement susceptible, et à l'estimation du nombre de reproduction effective, R_e , quand une partie de la population ne pourrait pas être susceptible (ex. immunisée par la vaccination ou susceptibilité différenciée par la stratégie de limitation de contact, cas de la rougeole) (Kermack & Mckendrick, 1927; Metcalf et al., 2011).

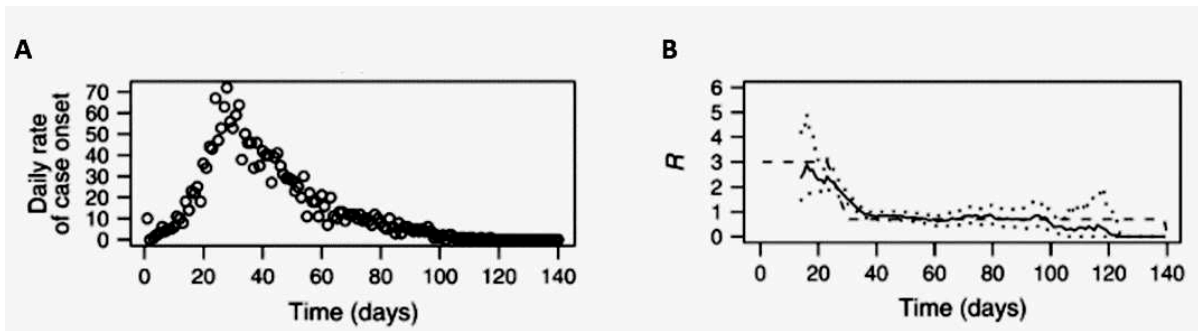


Figure 7 : Surveillance d'une épidémie de type syndrome respiratoire aigu sévère à l'aide de données simulées. A) Taux journalier d'apparition des cas; B) espérance (ligne continue) et intervalle de crédibilité à 95% (ligne pointillée) du nombre de reproduction R obtenu à partir d'une estimation par un modèle hiérarchique Bayésien, et calculés pour les 10 derniers jours d'observation en fonction du temps de la dernière observation.

Source : (Cauchemez, Boelle, et al., 2006)

Les modèles mécanistiques utilisés pour la caractérisation des dynamiques temporelles des épidémies et dans l'estimation des paramètres clés pour leur propagation, tel que la valeur de R , sont souvent des variantes des modèles compartimentaux de type SIR (Susceptibles–Infectieux–Recouvrés). Ils peuvent être complexifiés, par exemple en ajoutant la classe des exposés pour prendre en compte la période de latence avant que le cas ne soit infectieux, le cas des modèles de type SEIR (Susceptibles–Exposés–Infectieux–Recouvrés), ou en ajoutant d'autres classes supplémentaires pendant l'évolution de la maladie telles que proposées par Di Domenico *et al.* (**Figure 8**) (Di Domenico et al., 2020; Ramiadantsoa et al., 2022). Les structures géographiques où vivent des sous-populations, pouvant avoir des caractéristiques démographiques ou d'interactions différentes dans chacune d'elles au sein de la population d'étude, peuvent être modélisées par des mouvements ou interactions entre les sous-populations via des modèles en métapopulation (Linton et al., 2020; Ramiadantsoa et al., 2022).

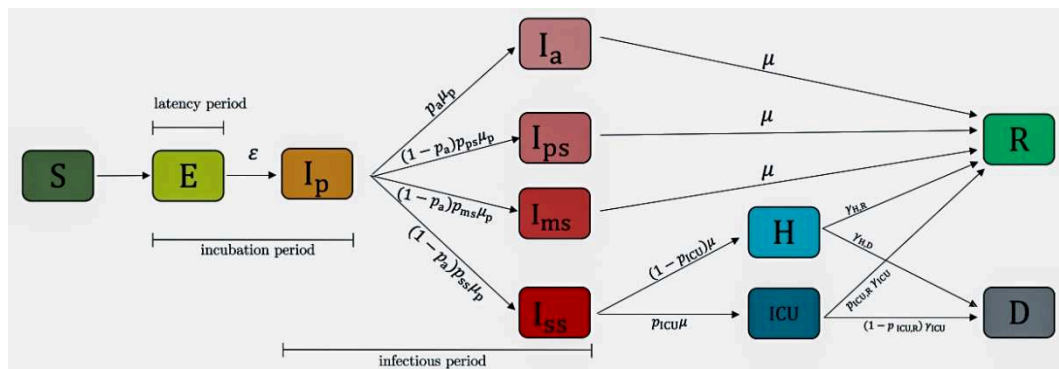


Figure 8 : Modèle compartimental proposé par Domenico *et al.* pour la propagation du COVID-19 (Di Domenico et al., 2020). S = susceptible ; E = exposé ; Ip = infectieux en phase prodromique ; Ia = infectieux asymptomatique ; Ips = infectieux paucysymptomatique; Ims = infectieux symptomatique avec symptômes modérés; Iss = infectieux symptomatique avec symptômes sévères; ICU = cas sévère admis en unité de soins intensifs; H = cas sévère admis à l'hôpital mais pas en soins intensifs; R = guéri; D = décédé. Les lettres à côté des flèches indiquent le taux de transition entre les compartiments du modèle.

Source : (Di Domenico et al., 2020).

Des équations différentielles ordinaires utilisant le temps comme indicateur de variation continue sont utilisées pour modéliser les transitions des individus entre les compartiments, notamment au travers de l'acquisition de l'infection ou du changement d'état lors de l'évolution de la maladie (Di Domenico et al., 2020; Rock et al., 2014). Des modèles plus sophistiqués avec plus de compartiments sont souvent nécessaires pour pouvoir intégrer plus de réalisme dans les processus impliqués aux dynamiques de transmission par l'intégration de l'âge de l'hôte, son niveau d'immunité, l'âge de l'infection, etc.: modèles structurés de force d'infection par groupe d'âge (cas des modèles MSIRV: "*maternally immune*" *M*, "*susceptible*" *S*, "*infected*" *I*, "*recovered*" *R*, et "*vaccinated*" *V*, appliqués à la rougeole) (Metcalf et al., 2012; Rock et al., 2014), ou des modèles intégrant les structures sociales non-homogènes telles que les matrices de contact *Who-Acquires-Infection-From-Whom* (Mossong et al., 2008; Thindwa et al., 2022).

2.2.3 Application des modèles temporels au paludisme et au COVID-19

Etant donné que le paludisme est endémique à Madagascar (Felana A. Ihantamalala et al., 2018), et que son épidémiologie dans l'île est marquée par l'hétérogénéité temporelle et spatiale de sa transmission, les modèles temporels utilisés essaient de caractériser comment la dynamique temporelle change ; ce qui reflète aussi bien les diversités des interactions hôte-parasite-vecteur que les tendances saisonnières liées au climat (Howes et al., 2016; Nguyen et al., 2020). Ce type de modèles, qui divisent l'île par zones écologiques ou par unités administratives, caractérisent les dynamiques saisonnières selon des indicateurs agrégés (incidence moyenne par mois, ratio d'incidence standardisé, indices saisonnières) et montrent les anomalies de cette transmission temporelle à travers l'île (clustering temporel, nombre de flambées épidémiques, modèles de régression spatio-temporelle) (Howes et al., 2016; Felana A. Ihantamalala et al., 2018; Nguyen et al., 2020).

En dehors de la caractérisation de dynamiques temporelles des maladies, d'autres études ont ciblé la prédiction des dynamiques, à la fois à des échelles nationales et locales. Par exemple, Girond et collaborateurs ont développé un système d'alerte précoce sub-national en combinant les données des sites de surveillance sentinelle du paludisme et les prédictions des modèles de type SARIMA (*Seasonal Auto-Regressive Integrated Moving Average*) pour alerter le PNLN en cas de détection de signaux épidémiques, la flambée des cas enregistrés par différentes méthodes de calcul de seuil (Girond et al., 2018). D'autres chercheurs se sont concentrés à prédire les dynamiques au sein des districts sanitaires sur la base de modèles linéaires mixtes généralisés et des variables prédictives (environnementales, socio-démographiques, etc.) à haute résolution (Pourtois et al., 2023).

Une autre utilisation de ces modèles a été dans l'évaluation de l'efficacité des interventions de lutte contre le paludisme. En utilisant les données du programme national entre 2016 et 2021, l'effet des campagnes de PID a été évalué avec des modèles linéaires généralisés, montrant que ces stratégies peuvent réduire l'incidence d'environ 30% (Hilton et al., 2023). En outre, un essai randomisé en grappes a permis d'évaluer l'impact sur la prévalence du paludisme d'une stratégie de dépistage actif suivi de traitement, en parallèle avec la PID, dans le district de Mananjary, zone de forte transmission (Ratovoson, Garchitorena, et al., 2022). Dans ce cas, des modèles d'écart de différences ont été utilisés pour montrer que les interventions étaient associées à une réduction de la prévalence chez les enfants de moins de 15 ans.

Dans le cadre de l'épidémie du COVID-19 à Madagascar, les trois premiers cas confirmés de COVID-19 ont été importés à Antananarivo, la capitale de Madagascar, les 19 et 20 mars 2020 (Randremanana et al., 2021). À la suite de cette notification et dans le but d'arrêter ou d'atténuer le taux de transmission du SARS-CoV-2, le gouvernement malagasy a mis en place des interventions non-pharmaceutiques (INPs) rigoureuses, notamment le port du masque, la fermeture des écoles, l'organisation du travail à domicile pour les travailleurs, la fermeture des bars et des restaurants, et la suspension des loisirs publics (Ratovoson, Razafimahatratra, et al., 2022). La première ville ayant eu la flambée de cas de COVID-19 en dehors de la capitale a été Toamasina, située sur la côte Est, en avril–juin 2020 ; suivie d'Antananarivo, comptant environ 2,6 millions d'habitants, qui a connu sa première vague entre juin et août 2020 (**Figure 9**).

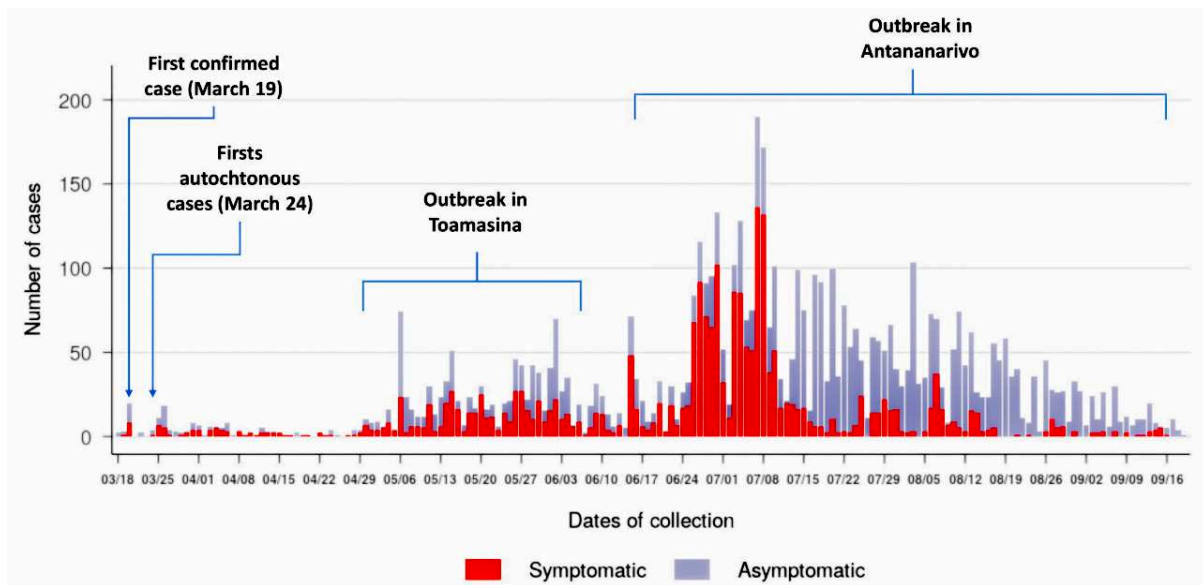


Figure 9 : Cas hebdomadaires de SARS-CoV-2 confirmés en laboratoire à Madagascar du 18 mars–18 septembre 2020.

Source : (Randremanana et al., 2021).

Des analyses descriptives d'échantillons obtenus de la capitale et analysés dans l'Unité de Virologie de l'IPM ont montré que l'épidémie a débuté la semaine 24 (8–14 juin), et elle a culminé la semaine 28 (6–12 juillet) avec un taux de positivité de 50% (Randremanana et al., 2021). En utilisant les modèles basés sur les distributions de probabilités, la période d'incubation, l'intervalle sériel, le taux d'attaque secondaire moyen parmi les contacts étroits, et utilisant un modèle épidémiologique de type SIR, le nombre de reproduction basic R_0 ont été estimés, respectivement, à 4,1 jours (IC95% [0,7–7,5]), 6 jours (IC95% [2,4–9,6]), 38,8% (IC95% [19,5–58,2]) (utilisant les données d'investigation de mars à juin 2020 à Antananarivo) (Ratovoson, Razafimahatratra, et al., 2022), et 2,0 (utilisant les données de surveillance du 15 juin–12 septembre 2020 à Madagascar) (Narison & Maltezos, 2021).

Pendant cette pandémie, les données officielles rapportées par le MSANP n'ont donné qu'un aperçu très partiel de l'épidémie, étant donné le faible taux de détection, 0,1–1% des cas, environ 34,8 tests PCR pour 10 000 habitants (Kousi et al., 2022). Afin de produire des prédictions de l'impact de l'épidémie et des mesures mises en place par le gouvernement malgache malgré ces défis en matière de données disponibles, un modèle mathématique de type SEIR a montré que l'implémentation rapide des INPs a pu avoir une efficacité non-négligeable pendant la première vague épidémique, estimée à 30% (**Figure 10**) (Evans et al., 2020).

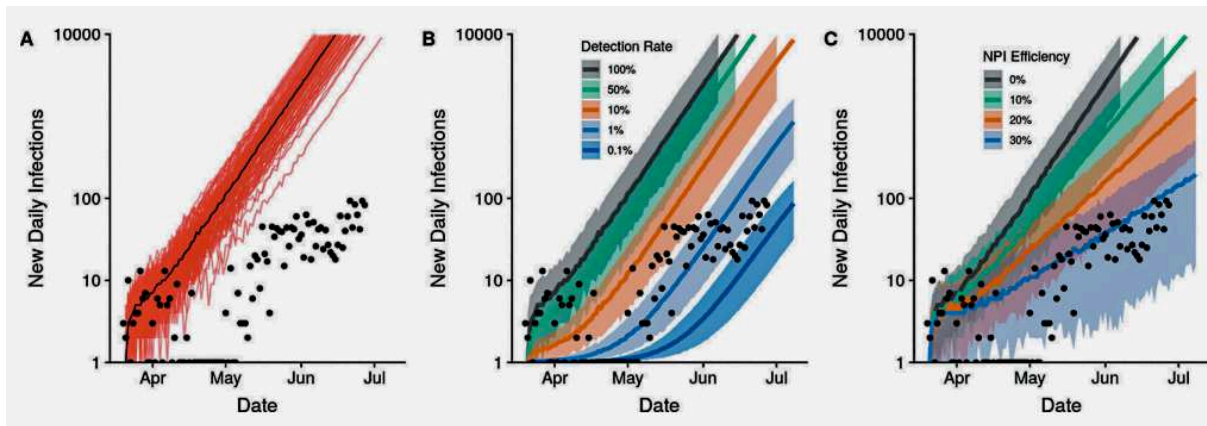


Figure 10 : L'incidence quotidienne plus faible que prévu peut s'expliquer uniquement par des taux de détection de 0,1–1% des cas ou des efficacités INPs de 30% : A) Trajectoires épidémiques prévues par le scénario sans atténuation, B) les gammes des taux de détection ; et C) les gammes des efficacités INPs.

Source : (Evans et al., 2020)

2.3 Modèles de dynamique spatiale

2.3.1 Objectifs et différentes utilisations

Les analyses spatiales permettent d'expliquer les phénomènes et les processus spatiaux derrière les événements de santé ou environnementaux (R. S. Bivand et al., 2013). Dans le cadre de la prise de décision et la réponse aux épidémies des maladies infectieuses, l'analyse spatiale d'indicateurs de santé permet de répondre à plusieurs questions (RICHARDSON, 1992):

- i) Les cas observés se trouvent-ils fréquemment à proximité d'autres cas, certaines zones géographiques ont-elles un nombre de cas différent de celui attendu ?
- ii) Plus généralement, quelles sont les caractéristiques épidémiologiques (facteurs de risque tels que l'âge, le niveau socio-économique, les sources de contamination, ou les hétérogénéités en matière d'accès aux services de santé) de la distribution spatiale de cas observés, ce qui la différencie d'une distribution « aléatoire » ?

2.3.2 Principaux types de modèles spatiaux

Dans la littérature, plusieurs méthodes statistiques ont été utilisées pour cartographier le risque d'infection aux maladies infectieuses. Gaudart *et al.* ont comparé différentes méthodes de détection de cluster du paludisme au Mali dont deux indicateurs globaux : (i) le coefficient de Moran, le coefficient d'autocorrélation qui est classiquement utilisé (Anselin, 1995), (ii) la statistique de Tango, une généralisation spatiale de la statistique du Chi² (Tango, 1995, 2000); et trois méthodes de détection de clusters locaux: (i) l'application locale du coefficient de Moran, introduite par Anselin (Anselin, 1995), (ii) la méthode de balayage, recherchant des regroupements d'unités spatiales (Kulldorff, 1997), et (iii) l'arbre de régression oblique, découpant la zone d'étude en sous-zones de risques différents (J. Gaudart et al., 2007; Jean Gaudart et al., 2005).

Autre que la détection de clusters globaux ou locaux, les modèles linéaires généralisés multiniveaux, à la fois fréquentistes ou bayésiens, sont de plus en plus utilisés pour pouvoir dégager des tendances spatiales ou spatio-temporelles d'incidence ou de prévalence des maladies infectieuses (R. Bivand et al., 2017). Par exemple, Kleinschmidt *et al.* ont combiné un modèle de régression logistique et une analyse de prédiction par géostatistique (krigeage) pour produire une carte des risques de paludisme au Mali (Kleinschmidt et al., 2000).

2.3.3 Application des modèles spatiaux au paludisme et au COVID-19

Dans le cadre de la cartographie du risque de transmission du paludisme à Madagascar, les techniques spatiales (comme les standardisations des taux d'incidence par district et les analyses de cluster) implémentées sur les systèmes d'information géographique (SIG) ont été adoptées par Ihantamalala *et al.* pour élucider des tendances spatiales du risque d'infection palustre de 2010–2014 et par Howes *et al.* pour cartographier et mettre à jour la stratification sub-nationale du risque de paludisme par écozones de 2010–2015 (**Figure 11**) (Howes et al., 2016; Felana A. Ihantamalala et al., 2018).

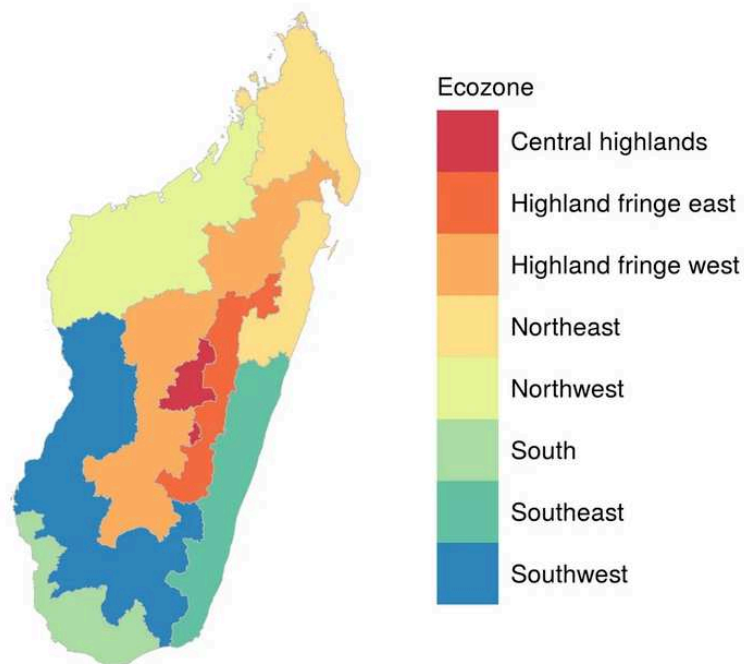


Figure 11 : Les écozones de la transmission du paludisme à Madagascar, mises à jour sur la base de la carte de prévalence de l'infection *Plasmodium falciparum* (*PfPR*) (en fonction des valeurs moyennes par district de 2010–2015 et aux valeurs minimales et maximales de chaque écozone). L'infection à *P. falciparum* dans la tranche d'âge des 2–10 ans (*PfPR*) du Malaria Atlas Project (MAP) a été utilisée pour évaluer les tendances régionales d'infection palustre (Bhatt et al., 2015).

Source : (Howes et al., 2016).

La spatialisation des données d'enquêtes transversales du paludisme à travers de méthodes géostatistiques a permis également de cartographier des indicateurs clés du paludisme; ces indicateurs (ex. les proxys d'abondances de vecteurs) peuvent d'abord être définis par une approche participative avec les décideurs du PNLP avant de proposer des cartes de risque et des activités ciblées selon le contexte géographique considéré (Howes et al., 2019).

Les méthodes d'évaluation multicritère, combinant les techniques de SIG et la méthode basée sur les dires d'experts, ont été utilisées par Rakotoarison *et al.* pour améliorer la compréhension des zones à risque de transmission du paludisme dans les HTC de Madagascar (Rakotoarison *et al.*, 2020). En outre, Ihantamalala *et al.* ont développé un modèle mathématique spatial basé sur la durée moyenne et la fréquence des mouvements entre différentes zones à partir des données des utilisateurs de téléphone mobile, afin d'estimer l'importation des cas de paludisme des zones à forte transmission vers les zones de faible transmission (**Figure 12**) (Felana Angella Ihantamalala *et al.*, 2018).

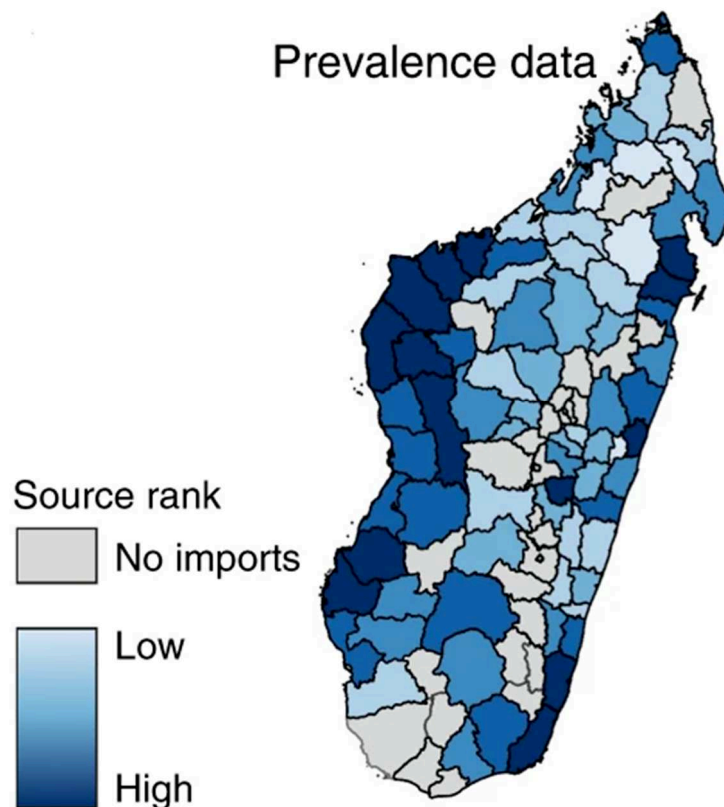


Figure 12 : Comparaison entre les sources principales (bleu foncé) et l'absence d'importation (gris) et les cas à Antananarivo à partir des données de prévalence.

Source : (Felana Angella Ihantamalala *et al.*, 2018).

Quant à la compréhension spatiale du risque de transmission de COVID-19 à Madagascar, celui-ci peut être influencé par la densité de la population, leur mobilité et la durée de trajet entre les zones connectées, ainsi que par des hétérogénéités sub-nationales en matière d'accès aux soins, entre autres (Rice, Annapragada, *et al.*, 2021). Au niveau national, Ramiadantsoa *et al.*, ont modélisé la transmission spatiale de l'épidémie entre les 22 régions de Madagascar à l'aide d'un modèle mathématique de métapopulations pour évaluer l'utilité de

différentes types d'information et méthodes dans la caractérisation du mouvement des populations (basées sur les données mobiles, sur les modèles de gravité, etc.) (Ramiadantsoa et al., 2022). Ils ont démontré que les données actuelles ne permettent pas de modéliser d'une manière fiable les dynamiques spatio-temporelles du COVID-19 à Madagascar. Rasambainarivo *et al.* ont cartographié les distributions proportionnelles des doses de vaccin par différentes stratégies basées sur la pondération par région, en fonction du nombre d'habitants, la distribution des personnes âgées de plus de 60 ans, du nombre de cas de COVID-19 rapportés, ainsi que le nombre de décès causés par le COVID-19 (**Figure 13**) (Rasambainarivo et al., 2022).

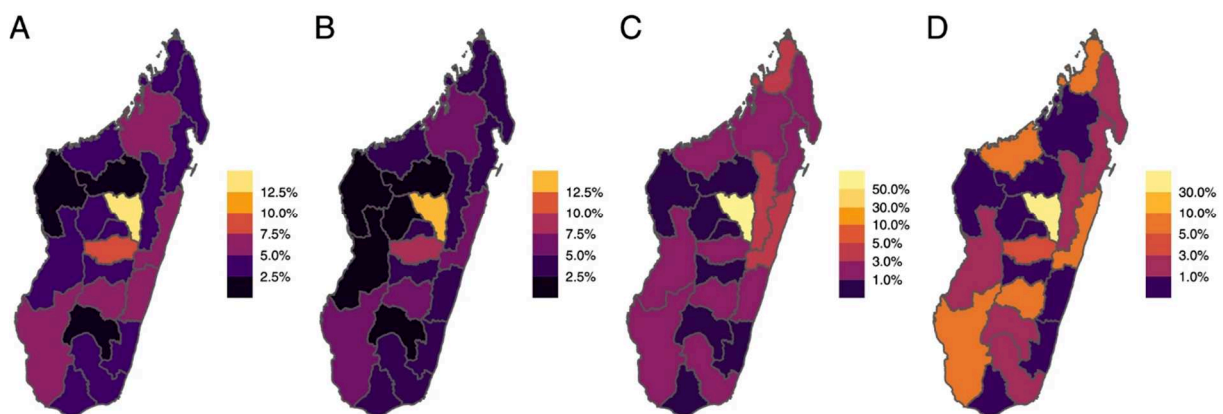


Figure 13: La proportion des doses totales distribuées par région. En supposant que l'offre totale de vaccins représente 20% de la population totale, par différentes stratégies de distribution explorées.

Source : (Rasambainarivo et al., 2022).

Au niveau local, des modèles statistiques ont été utilisés pour décrire les dynamiques spatiales d'infection au COVID-19 pendant les deux premières vagues épidémiques dans le sud-est de Madagascar, ainsi que les facteurs de risque y ont été associés (Andres Garchitorena et al., 2023). Ainsi, Garchitorena *et al.* y ont trouvé que, COVID-19 s'est répandu principalement en fonction des connectivités des localités (proximité par rapport à la route nationale et les routes secondaires) pendant la première vague et la deuxième vague épidémique (Andres Garchitorena et al., 2023).

2.4 Défis liés aux biais des données de surveillance passive

Les sections précédentes montrent des études sur le paludisme et le COVID-19 qui se sont basées, pour une grande majorité, sur les données de la surveillance passive de routine. L'avantage de ces données est qu'elles sont collectées de manière systématique dans les centres de santé de tout le territoire national, mais elles souffrent des biais significatifs. D'abord, une grande proportion des cas de paludisme et de COVID-19 sont asymptomatiques, et pour ceux qui sont symptomatiques, beaucoup ne sont pas diagnostiqués, ce qui rend difficile l'interprétation et la comparabilité des résultats d'incidence (Breman, 2001).

Une solution consiste alors à améliorer la surveillance passive à travers, par exemple, de la mise en place d'une surveillance au niveau communautaire pour le cas du paludisme (Girond et al., 2017), ou encore de compléter cette surveillance passive avec des enquêtes sérologiques combinées avec de la modélisation pour mieux caractériser et comprendre les hétérogénéités de l'intensité de transmission, notamment dans les zones visées pour élimination comme les HTC de Madagascar (Institut National de la Statistique, Programme National de Lutte contre le Paludisme, Institut Pasteur de Madagascar, Antananarivo, Madagascar and ICF International, Calverton, Maryland, 2016; Steinhardt et al., 2021). Ce type de données additionnelles, les données sérologiques, couplées à des modèles statistiques et mathématiques, pourraient réduire les biais liés au faible taux de détection de la surveillance passive.

2.5 Conclusion

Les modèles épidémiologiques quantitatifs, qu'ils soient mathématiques ou statistiques, spatiaux ou temporels, permettent de tester des hypothèses en santé publique et d'éclairer de mécanismes de transmission pour faciliter les activités de contrôle. Des modèles, même lorsqu'ils sont simples, peuvent fournir des éléments de prise de décision très tôt dans l'évolution des épidémies, mais peuvent également être mis à jour ou complexifiés par la suite pour devenir plus précis avec l'arrivée de nouvelles données (issues de la surveillance, d'investigation de terrain ou d'autres études telles que les essais en grappes contrôlés) ou des nouvelles hypothèses afin de pouvoir affiner les stratégies de contrôle (White et al., 2009).

A Madagascar, la modélisation a permis de mieux comprendre les tendances spatiales et temporelles de maladies épidémiques anciennes et nouvelles, telles que le paludisme et le COVID-19, ainsi que de guider leur contrôle. Mais ces maladies sont complexes et dépendent de plusieurs facteurs contexte-spécifiques tels que l'âge, la génétique, le comportement d'hôtes ou de vecteurs (Anderson & May, 1985). Ainsi, plus d'efforts de modélisation sont nécessaires afin d'améliorer notre compréhension de ces systèmes biologiques à Madagascar et d'adapter les activités de surveillance et les stratégies de contrôle de ces deux maladies infectieuses à chaque contexte.

3 Chapitre 1 : Identification of factors associated with residual malaria transmission using school-based serological surveys in settings pursuing elimination (Article 1)

Madagascar, avec 4,9 millions cas et 12 571 décès estimés en 2021 fait partie des trois pays de l’Afrique de l’Est et Australe, avec l’Ouganda et le Sud-Soudan, ayant enregistré une hausse de taux d’incidence et de décès du paludisme de 2015–2021, soit de plus de 75% (**Figure 3**) (World Health Organisation, 2022). Cela prouve que les efforts fournis par Madagascar pour atteindre les objectifs du PNLP—(a) améliorer la prise en charge d’au moins 95% des cas diagnostiqués, et (b) assurer la disponibilité permanente des tests de diagnostic et du traitement pour 95% des formations sanitaires depuis 2013, et du paquet d’interventions de contrôle—nécessitent une amélioration et adaptation dans la lutte contre le paludisme (Programme Nationale de Lutte contre le Paludisme, 2012; Razakamanana et al., 2020; World Health Organization, 2020).

Ce qui justifie le besoin d’utiliser de nouvelles sources de données, combinées avec de la modélisation géostatistique, pour mieux comprendre les dynamiques derrière les faibles taux de détection dans les hautes terres de Madagascar. Car, les poches de transmission résiduelle dans les zones à faible transmission peuvent constituer un obstacle majeur à la réalisation des objectifs d’élimination du paludisme (Rosado et al., 2021). La recherche sur l’hétérogénéité de la transmission du paludisme dans les contextes visant l’élimination est donc importante pour permettre de mieux cibler les activités de contrôle du paludisme.

Ce chapitre a utilisé les données d’une enquête transversale sérologique en milieu scolaire, menée en 2014 dans sept districts des HTC et les marges environnantes, zone de pré-élimination (Steinhardt et al., 2021). Notre étude de séroprévalence portait sur 6 293 écoliers et a permis de caractériser l’hétérogénéité spatiale de transmission du paludisme et de détecter des points chauds de la prévalence d’infection à *P. falciparum* et de l’exposition (mesure d’anticorps PfAMA1) par identification des indices I locaux de Moran. Plus de points chauds d’exposition (de séroprévalence de l’anticorps PfAMA1) ont été observés dans plusieurs districts de la zone par rapport ceux observés par les TDR.

L'utilisation des modèles de régression logistique à effets mixtes, à l'échelle fokontany pour les prévalences et à l'échelle individuelle pour les positivité, a permis de confirmer la persistance des hétérogénéités du risque d'exposition et de transmission au sein de chaque district (fokontany, localité), pouvant être expliquée en partie par l'environnement et le climat (l'altitude, les précipitations, la température, et la couverture végétale), mais aussi par les obstacles géographiques à l'accès aux soins. Les enfants souffrant d'obstacles géographiques à l'accès aux soins, qui vivaient à plus de 5 km des établissements de santé (environ un tiers de la population étudiée), étaient significativement plus exposés à *P. falciparum* ; ce qui pourrait avoir des implications importantes pour les efforts d'élimination du paludisme dans cette zone.


Nos résultats suggèrent, premièrement, que le test et le traitement sous-optimaux des infections à *P. falciparum* dans notre zone d'étude, en raison des obstacles géographiques à l'accès aux soins (Felana Angella Ihantamalala et al., 2021), pourraient entraîner des poches de transmission du paludisme non détectées en compromettant les objectifs d'élimination. Deuxièmement, les études basées sur les TDR conventionnels dans les zones à faible transmission peuvent toujours être menées, même si leurs sensibilités sont parfois discutables selon certains auteurs ; surtout dans le contexte des PRFI qui ne sont pas en mesure d'assumer les coûts opérationnels supplémentaires des études sérologiques (Okell et al., 2009; Okell, Bousema, et al., 2012). D'autres études sont nécessaires pour comprendre davantage le rapport coût-efficacité de techniques de diagnostic plus sensibles pour les infections à faible densité, telles que la PCR (Bousema et al., 2014).

RESEARCH

Open Access



Identification of factors associated with residual malaria transmission using school-based serological surveys in settings pursuing elimination

Jean Marius Rakotondramanga^{1,2,3,4*} , Inès Vigan-Womas^{5,6}, Laura C. Steinhardt⁷, Aina Harimanana¹, Elisabeth Ravaoarisoa⁸, Tsikiniaina L. Rasoloharimanana⁵, Sehen Razanatsiorimalala⁹, Amy Wesolowski¹⁰, Milijaona Randrianarivelosia^{9,11}, Benjamin Roche^{2,4†} and Andres Garchitorena^{1,4†}

Abstract

Background: Targeted research on residual malaria transmission is important to improve strategies in settings pursuing elimination, where transmission reductions prove challenging. This study aimed to detect and characterize spatial heterogeneity and factors associated with *Plasmodium falciparum* infections and exposure, *P. falciparum* apical membrane antigen 1 (PfAMA1) antibody (Ab) response, in the Central Highlands of Madagascar (CHL).

Methods: From May to July 2014, a cross-sectional school-based survey was carried out in 182 *fokontany* (villages) within 7 health districts of the CHL. Rapid diagnostic tests (RDTs) and a bead-based immunoassay including PfAMA1 antigen biomarker were used to estimate malaria prevalence and seroprevalence, respectively. Local Moran's I index was used to detect spatial "hotspots". Remotely sensed environmental data—temperature, vegetation indices, land covers, and elevation—were used in multivariable mixed-effects logistic regression models to characterize factors associated with malaria infection and cumulative exposure.

Results: Among 6,293 school-children ages 2–14 years surveyed, RDT prevalence was low at 0.8% (95% CI 0.6–1.1%), while PfAMA1 Ab seroprevalence was 7.0% (95% CI 6.4–7.7%). Hotspots of PfAMA1 Ab seroprevalence were observed in two districts (Ankazobe and Mandoto). Seroprevalence increased for children living > 5 km from a health centre (adjusted odds ratio (OR) = 1.6, 95% CI 1.2–2.2), and for those experiencing a fever episode in the previous 2 weeks (OR 1.7, 95% CI 1.2–2.4), but decreased at higher elevation (for each 100-m increase, OR = 0.7, 95% CI 0.6–0.8). A clear age pattern was observed whereby children 9–10 years old had an OR of 1.8 (95% CI 1.2–2.4), children 11–12 years an OR of 3.7 (95% CI 2.8–5.0), and children 13–14 years an OR of 5.7 (95% CI 4.0–8.0) for seropositivity, compared with younger children (2–8 years).

Conclusion: The use of serology in this study provided a better understanding of malaria hotspots and associated factors, revealing a pattern of higher transmission linked to geographical barriers in health care access. The integration

[†]Benjamin Roche and Andres Garchitorena share senior authorship

*Correspondence: jean.marius.g@gmail.com

¹ Epidemiology and Clinical Research Unit, Institut Pasteur de Madagascar, Antananarivo, Madagascar

Full list of author information is available at the end of the article



of antibody-assays into existing surveillance activities could improve exposure assessment, and may help to monitor the effectiveness of malaria control efforts and adapt elimination interventions.

Keywords: Malaria, *Plasmodium falciparum*, Antibody, Seroprevalence, AMA1, Spatial analysis, Cluster, Epidemiology, Madagascar

Background

Malaria remains one of the most important causes of morbidity and mortality in sub-Saharan Africa. While many countries in the African region have the potential to eliminate malaria in the medium or long term—malaria case incidence reduced from 363 to 225 cases per 1000 populations at risk in 2000 and 2020, respectively—Madagascar has still been aiming to improve case management for at least 95% of diagnosed cases and to ensure the permanent availability of diagnostic-and-treatment tools for 95% of health facilities since 2013 [1, 2]. Madagascar has a highly heterogeneous distribution of malaria transmission, with areas of high transmission in the east and west coast of the island, and areas of very low and low transmission in the Central Highlands (CHL) and surrounding Fringes areas, respectively [3, 4]. The National Malaria Control Programme (NMCP) has targeted five districts in the highlands for malaria elimination, with the goal to reach zero deaths, and to extend the number of districts targeted for elimination from 5 in 2018 to 13 by 2022, mainly in CHL and surrounding Fringes areas. However, progress so far has been elusive [5].

Characterizing malaria transmission intensity in near-elimination settings using passive surveillance and standard diagnostic methods can be challenging, as asymptomatic infections can outnumber symptomatic infections and are hard to detect with malaria rapid diagnostic tests (RDTs) only [6–8]. Yet, asymptomatic cases with low detectable levels of parasitaemia can constitute potential reservoirs for malaria [6, 8, 9]. In these settings, serological assays for antibody detection can be a powerful tool for estimating cumulative exposure in addition to RDTs and microscopy during large-scale surveillance, such as Malaria Indicator Surveys [10, 11]. Field studies have also shown that the predominant immunoglobulin G (IgG) subclass profiles of *Plasmodium falciparum* are influenced by age and exposure to infection [12]; in particular, IgG-specific antibody responses to *P. falciparum* merozoite antigens—the apical membrane antigen 1 (PfAMA1) and the 19 kDa C-terminal region of the merozoite surface protein 1 (PfMSP1-19)—and other blood-stage antigens can be good biomarkers of *P. falciparum* exposure in populations with low immunity such as children less than 15 years of age [13–15]. Thus, antibody responses against *P. falciparum* antigens, such as

PfAMA1, can be particularly useful and informative to differentiate individuals based on their cumulative exposure, and to aid in characterizing factors associated with spatial heterogeneity in near-elimination settings [16, 17].

In moderate or low malaria transmission settings, characterizing malaria prevalence can yield somewhat homogeneous patterns at higher levels of spatial analysis. Yet, fine-scale population-based parasitaemia data can reveal local spatial heterogeneity in areas previously assumed to have uniform transmission [18]. Country-level surveys like the Demographic and Health Surveys (the finest resolution dataset used for Madagascar) have an average resolution of one cluster per 1000 km² approximately [19]. Data at more granular levels can help to elucidate factors influencing malaria transmission like climate (including temperature, rainfall) and environmental factors (vegetation, elevation, and land covers), guiding district-scale programmatic efforts to control malaria [18]. Such data, when analysed with appropriate methods, can allow identification of malaria transmission hotspots and their characteristics [20], therefore, allowing targeting of transmission residual pockets; which is critical in settings pursuing elimination.

After several years of blanket spraying in the CHL, more targeted indoor residual spraying (IRS) has been applied selectively to epidemic-prone areas since 2003 and insecticide-treated mosquito nets (ITNs) are regularly distributed to the population in mass campaigns into these settings [21]. The World Health Organization (WHO) has recommended at least one ITN per household; in the CHL, ITN ownership and access—the proportion of household members with access to an ITN—were 25% and 16% in 2013, respectively, both the lowest in the country [22]. Moreover, in order to detect and treat cases early, NMCP has implemented the systematic use of RDTs since 2010 for all suspected malaria cases with fever (axillary temperature > 37.5 °C) or history of fever in 2 weeks, but such strategy misses low-density asymptomatic infections that can still contribute to transmission in near elimination settings [6, 23–25].

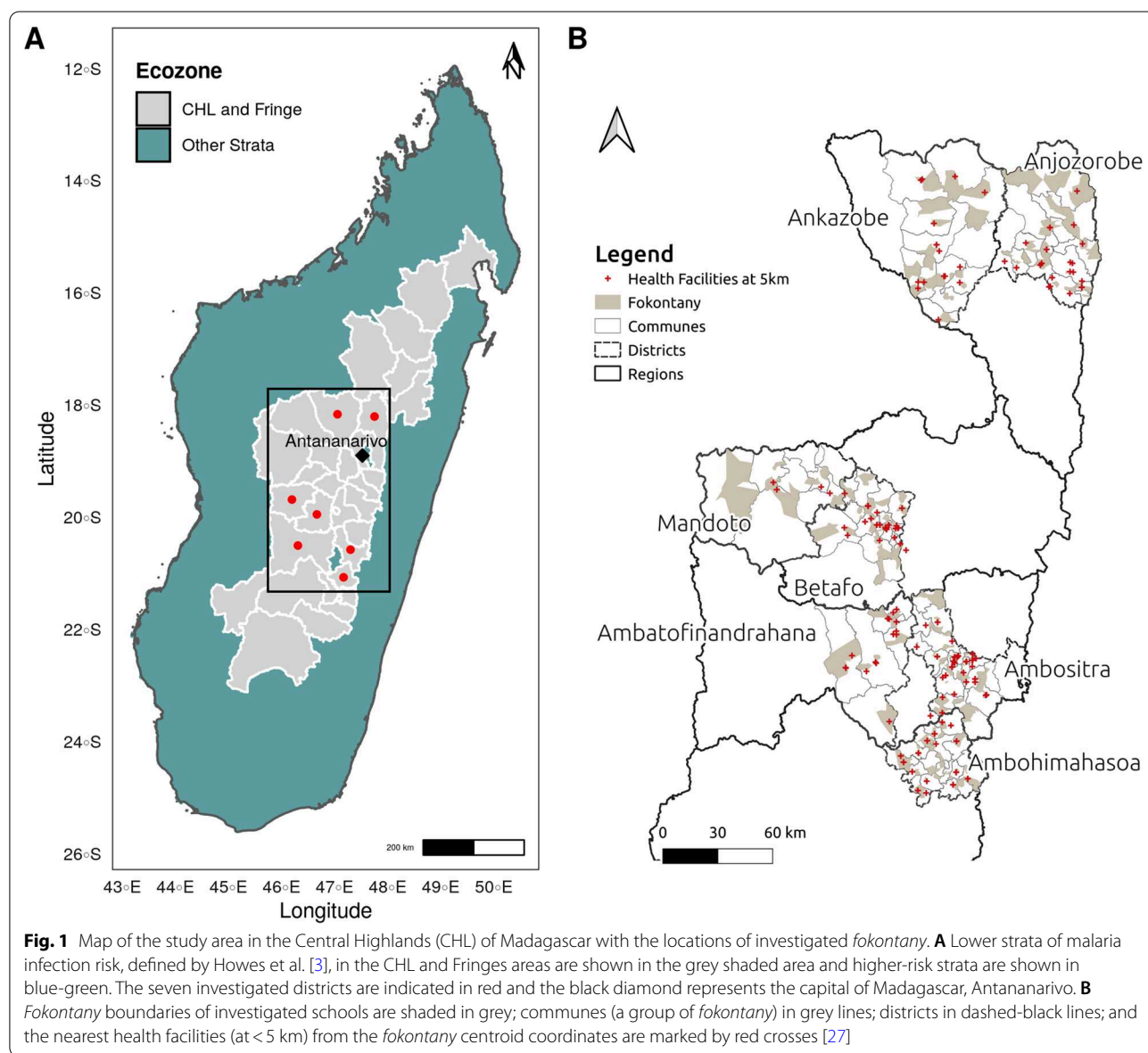
In 2014, a cross-sectional school-based survey was carried out in seven districts of the CHL and surrounding Fringes areas to better characterize malaria transmission via use of serological markers of *P. falciparum* exposure [11]. Results showed that the ability of annual parasite incidence estimates using health

facility routine data of malaria-confirmed patients by RDT to characterize malaria transmission declined at lower transmission levels as compared with a serological approach [11]. Using this dataset, this study expands on the previous analyses and aims (1) to characterize the spatial heterogeneity of malaria transmission intensity and to detect hotspots of both *P. falciparum* infection prevalence and PfAMA1 antibody (Ab) seroprevalence in CHL and surrounding Fringes; and (2) to identify sociodemographic, climatic, and environmental associated factors with such heterogeneity in malaria infection and exposure. These were not elucidated in Steinhardt et al. [11].

Methods

Study area

This study was carried out in 2014 in seven health districts from the CHL and surrounding Fringes areas (Fig. 1A). The health districts targeted were Ankazobe and Anjozorobe to the north of the capital city Antananarivo; Ambatofinandrahana, Ambohimahasoa, Ambositra, Betafo, and Mandoto to the south. The CHL and surrounding Fringes areas are characterized by unstable and episodic malaria transmission. Data from routine surveillance suggested that these areas had the lowest incidence in the country during 2013–2014, as measured by RDT [26], with more than 90% of the malaria infections



occurring in the area due to *P. falciparum* [3]. In 2013, malaria prevalence in children aged 6–59 months, characterized via microscopy, was 0.7% and 2.5%, respectively, in CHL and surrounding Fringes areas [22]. While transmission is low, previous analyses of routine malaria surveillance data have indicated that substantial heterogeneity in malaria transmission exists in the CHL [4], which needs fine-scale risk and exposure assessment to adapt and improve malaria elimination efforts [3].

Data collection

Survey and biological sample collection

To better understand and detect spatial heterogeneity in *P. falciparum* infection in the CHL and surrounding Fringes areas, a school-based seroepidemiological study was carried out from May to July 2014. The study has been described in detail by Steinhardt et al. [11]. Briefly, a cross-sectional survey using bead-based serological multiplex analyses was implemented in low-transmission and elimination settings [17]. In the seven sampled districts, all geographically accessible communes that presented no known safety issues for the study were surveyed, for a total of 93 communes out of 107 (Fig. 1B): for each selected commune, one primary school in proximity of a health facility (within 5 km distance) and one farther away (> 10 km) were selected. Overall, 182 *fokontany* (the smallest administrative unit, ~villages) were considered for investigation (Fig. 1B). Thirty children under 15 years old were selected randomly per school. This age group has been found to reflect populations with low immunity [14, 28, 29]. For each selected child, a questionnaire on demographics, residence, recent symptoms and trips (outside the commune), and household (or community) control measures (bed net use, IRS) was administered to their parent (or guardian).

Malaria RDTs [CareStart Malaria RDT, HRP2/pLDH (Pf/PAN) Combo; Access Bio] were performed with finger prick blood to detect malaria infections in all selected children. Children with a positive RDT were treated with artesunate-amodiaquine with age-appropriate doses, as recommended by national guidelines. Additionally, capillary blood was collected for all children in microvette tubes (Microvette 500 Z-Gel; Sarstedt) for later serological analyses. Collected samples were transported to Institut Pasteur de Madagascar's immunology laboratory in Antananarivo and stored at -20°C until used [11].

Serological data

Laboratory serological analyses were conducted using 5 *P. falciparum* antigens: three soluble recombinant proteins (PF13, PfMSP1, and PfAMA1), and bovine serum albumin-conjugated peptides (PfCSP and PfGLURP) from *P. falciparum*, using procedures previously described

[11, 30, 31]. In short, antigen-coupled beads and plasma were deposited in 96-well plates and analyzed using the Luminex-MAGPIX system and xPONENT 4.1 software. IgG levels were expressed as median fluorescence intensity (MFI). A pool of sera from malaria-immune African adults and plasma samples from malaria-naïve European individuals were included in each assay as positive and negative controls, respectively. Seropositive and seronegative groups were defined from MFI values as previously described [11], using two-component Gaussian mixture model (Additional file 1: Method S1 and Fig. S1).

For the purpose of this study, only the PfAMA1 antibody response was used because: (1) this marker had similar sensitivity and specificity as a latent class antigen modeled in Steinhardt et al. using all 5 previously described antigens [11], and (2) it has been shown to act as biomarker of *P. falciparum* exposure in populations with low immunity such as young children, when previously exposed individuals acquire a long-lived component of the antibody response which increases with age [13, 14].

Environmental and remotely sensed data

Descriptions and resolutions of environmental, climatic, and remotely sensed data are provided in supplemental information (Additional file 1: Table S1). Briefly, temporally dynamic climatic and environmental variables were downloaded from Moderate Resolution Imaging Spectroradiometer (MODIS) satellite data for each investigated *fokontany* [32]. These included the following temperature and vegetation indices (vegetation cover proxies): (1) all 8-days Land Surface Temperature (LST) and emissivity composites; and (2) all 16-days vegetation indices composites—Normalized Difference Vegetation Index (NDVI) and Enhanced Vegetation Index (EVI) [32]. For each of these indices, values matched at one, two and three months prior to the survey date were obtained for each investigated school (within a *fokontany*) [33].

The remaining environmental variables were assumed to be static for each *fokontany* including: (1) The annual MODIS land cover type product for 2014 [34]; (2) elevation, measured from the shuttle radar topography mission elevation surface [35]; and (3) health facilities location in the study area, obtained from recently published data [27]. For land cover data, the international geosphere-biosphere programme legend and class descriptions were used [36], and 5 main classes were utilized: (a) forests, (b) woodlands, (c) grasslands or cereals, (d) wet, croplands or mosaics, and (e) others' class grouping shrublands, wetlands, barren, build-up or water bodies.

Environmental and remotely sensed data processing were performed using standard geographic information

system computational techniques (Additional file 1: Method S2). The R package {MODISTools} was used for downloading and processing of MODIS data, which provides a simplified interface between R software [37] and MODIS land product subsets [32].

Data analyses

Spatial distribution and clustering of P. falciparum infection risk and cumulative exposure

Descriptive and spatial analyses of malaria infection prevalence and PfAMA1 Ab IgG seroprevalence were conducted by *fokontany*. Malaria hotspots were assessed via detection of spatial autocorrelation in the data using the local Moran's I as an indicator of spatial heterogeneity [20]. Logit scale was used to produce more normal distributions of both malaria infection prevalence and PfAMA1 Ab seroprevalence. Empirical neighbourhood of investigated *fokontany* was defined in order to have at least one neighbour and within a maximum distance, approximately 17 km between two farthest *fokontany* (Additional file 1: Fig. S2). Then, global and local Moran's I values were calculated using Monte Carlo simulations ($n=999$) and equal row-standardized spatial weights [38] to test its significance [39]. This test can be interpreted as an indicator of local pockets of non-stationarity, or hotspots, and assesses the influence of a *fokontany* on the magnitude of the global statistic to identify "outliers" [40, 41]. Functions in the R package {spdep} were used to calculate these indices; and a threshold of $p < 0.05$ was chosen to identify significant spatial autocorrelation.

Statistical models to characterize determinants of P. falciparum infection and cumulative exposure by PfAMA1 Ab data

Both *P. falciparum* infection and exposure models were carried out at two levels: (1) at *fokontany* level, to assess the effect of mean temperature and vegetation index—lagged by one month based on univariable analyses of different lagged indices (1–3 months) association with aggregated positivity of malaria infection and exposure, respectively—elevation, percentage of land cover class and distance to health facilities (Additional file 1: Table S1); (2) and at individual-level including additional demographic and household covariates (Additional file 1: Table S2). In both exposure (PfAMA1 response positivity) models the school malaria infection prevalence was included as a potential indicator (mediator) of the seropositivity response and to assess its correlation to detect higher risk *fokontany*.

Mixed-effects binomial logistic regression analyses with two observational-level random effects—to account for within-district and -commune correlations—were used to model *P. falciparum* infection and PfAMA1 Ab

positivity at *fokontany*- and individual-level [42, 43]. Univariable analyses were conducted first to explore the relationship with each of the climatic, environmental, and sociodemographic variables; all covariates which showed significant effects on *P. falciparum* infection positivity (or PfAMA1 Ab seropositivity) in univariable analyses were then included in multivariable analyses. Next, sets of candidate models were compared and ranked using multi-model selection procedures through the R package {MuMIn} according to the lowest second-order Akaike information criterion [44–46] (Additional file 1: Method S3).

Data analyses were carried out using R software v3.6.0 [37] and R package {lme4} [47].

Results

Individual-, household- and fokontany-level characteristics

Overall, 6293 school-children ages 2–14 years were enrolled from 182 *fokontany* where investigated primary schools were located. The median age of participants was 10 years (IQR: 8–11) and 47.4% were male (2984 of 6293). About two-thirds of children sampled (64.7%, 4073 of 6293) were 2–10 years old. Most households (55.4%, 3114 of 5619) in the investigated areas had two or more ITNs for its members (median = 6.0 individuals per household, IQR = 5.0–8.0) (Table 1). A total of 53 (0.8%, 95% CI 0.6–1.1%) children tested positive for malaria by RDT, with no differences between age groups (2–8 years, 9–10 years, 11–12 years and 13–14 years) ($p=0.62$). However, 443 (7.0%, 95% CI 6.4–7.7%) children were seropositive to PfAMA1 antibody with a significant increase in seropositivity across age, both for male and female ($p < 0.001$) (Fig. 2).

Spatial distribution and hotspots of P. falciparum infection prevalence by RDT and of PfAMA1 Ab seroprevalence

Malaria infection by RDT was highest in the *fokontany* located in the northern districts of Ankazobe and Anjozorobe. Overall, only 32 out of 182 *fokontany* had a malaria infection prevalence greater than or equal to 1%, the highest prevalence being 28.1% (Fig. 3A). PfAMA1 Ab seroprevalence was higher than malaria infection prevalence overall (Fig. 2), both in *fokontany* in the northern and western parts of the study site, with higher heterogeneity in its distribution. For instance, PfAMA1 Ab seroprevalence was greater than 12.0% in *fokontany* of 5 different districts across the study area (Ankazobe, Anjozorobe, Mandoto, Betafo and Ambatofinandrahana) (Fig. 3B).

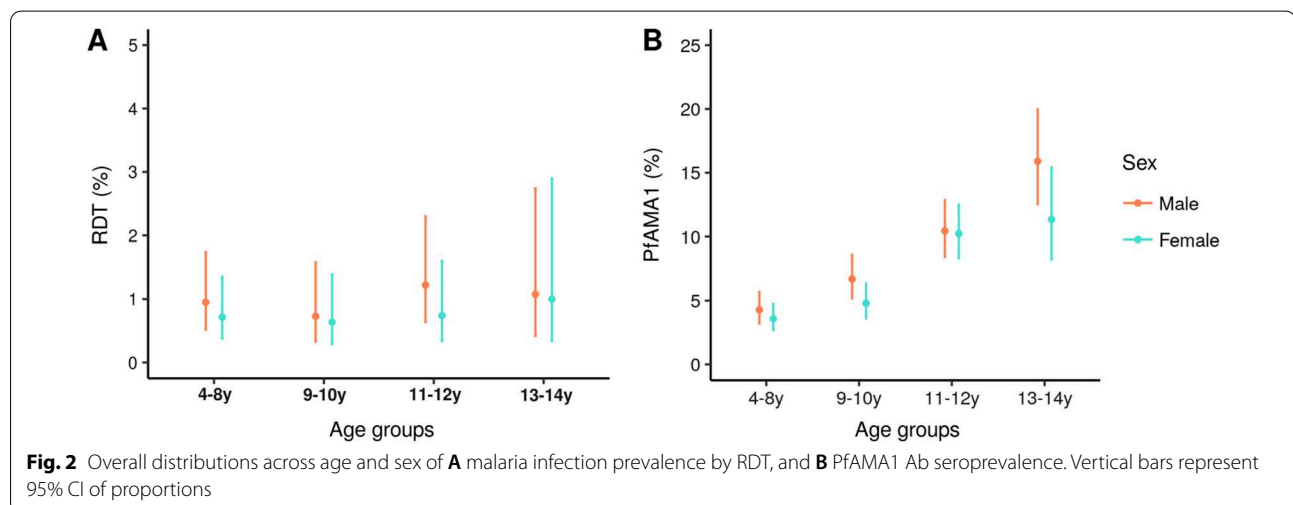
Spatial autocorrelation and hotspots of malaria infection prevalence and PfAMA1 Ab seroprevalence were identified across the study sites. Positive and significant Moran's I indices were found for both *P. falciparum*

Table 1 Characteristics of the study participants (N = 6293), households (N = 5619) and *fokontany* (N = 182)

Fokontany-level variables	Mean (range)	Individual-level variables	n (%)
Climatic, environmental and land cover		RDT positive	53 (0.8)
NDVI lag-1	0.5 (0.3–0.8)	PfAMA1 Ab seropositive	443 (7.0)
LST Day lag-1 (°C)	25.1 (18.1–30.4)	Age (years)	
Forests (%)	1.7 (0.0–65.2)	2–8	2,310 (36.7)
Woodlands (%)	12.2 (0.0–100.0)	9–10	1,763 (28.0)
Grasslands or cereals (%)	80.0 (0.0–100.0)	11–12	1,549 (24.6)
Wet, croplands or mosaics (%)	2.6 (0.0–100.0)	13–14	671 (10.7)
Other land cover classes (%) ^a	0.2 (0.0–20.0)	Sex (male)	2,984 (47.4)
Elevation (m)	1305.3 (773.3–2140.7)	Fever last 2 weeks	481 (7.6)
School RDT prevalence, % (SD)	0.9 (2.8)	Travel in last 2 months	213 (3.4)
PfAMA1 Ab seroprevalence, % (SD)	7.2 (11.0)	Use of ITN last night	2,792 (44.4)
Distance > 5 km from health facility, n (%)	59 (32.4)	Presence of RDT positive household member	24 (0.4)
Household-level variables			
No. of members, mean (SD)	6.5 (2.3)		
No. of ITNs, n (%)			
0	2,148 (38.2)		
1	357 (6.4)		
2–4	2990 (53.2)		
5–10	124 (2.2)		

NDVI Normalized Difference Vegetation Index at the previous month; LST daytime Land Surface Temperature and emissivity composites at the previous month; ITNs insecticide-impregnated mosquito-nets; SD standard deviation

^a Shrublands, wetlands, barren, or water bodies land cover



infection prevalence and Ab seroprevalence, with values of 0.24 ($p=0.001$) and 0.59 ($p=0.001$) respectively, indicative of spatial clustering of areas with similar malaria transmission (high or low). High clusters *fokontany* are the combination of “High-High” or “Low-High” clusters; that represent *fokontany* with expected values (prevalence or seroprevalence) matching with the

weighted mean of each *fokontany*'s neighbours, or those with abnormally observed low but expected high values, respectively (Fig. 3C and D). For *P. falciparum* infection prevalence, hotspots (“High-High” clusters) were identified mostly in one single area in the northern districts of Ankazobe and Anjozorobe (Fig. 3C). Overall, high clusters identified across districts were consistent using

both RDT prevalence or PfAMA1 Ab seroprevalence. However, hotspots of PfAMA1 Ab seroprevalence were not observed in Anjozorobe but rather in the southern district of Mandoto (Fig. 3D). *Fokontany* with seroprevalence greater than 10% were found in Ankazobe and Mandoto (Additional file 1: Fig. S3). Thus, analyses of Abs revealed nearly twice as many hotspots as those based on *P. falciparum* infection prevalence by RDT, suggesting some level of agreement between both detection methods.

Local determinants of *P. falciparum* infection by RDT and exposure by PfAMA1 Ab at the fokontany-level

For *P. falciparum* infection model, univariable analyses at the fokontany-level revealed significant positive associations with longer distance to health facilities, higher temperatures the previous month, and percentage of land cover classes such as grasslands or cereals. Negative associations were observed between *P. falciparum* infection and the *fokontany* at higher elevation, and greater values of NDVI during the previous month. However, the very low RDT prevalence observed in the study population (53 RDT + out of 6,293) prevented finding consistent factors associated in multivariable analyses: only higher temperatures the previous month in a *fokontany* was found as risk factor of malaria infection at fokontany-level (Table 2), and a fever episode in the previous two weeks at individual-level (Additional file 1: Table S5).

For *P. falciparum* exposure (PfAMA1 Ab response) model, univariable analyses at the fokontany-level revealed significant positive associations with distance to health facilities and school RDT prevalence, while associations with environmental and climatic indicators were more variable. Exposure to *P. falciparum* tended to increase with higher temperatures the previous month, and with increased percentage of grasslands or cereals land cover classes in a *fokontany*; while it decreased with higher values of vegetation (NDVI) the previous month, the percentage of woodlands, or elevation (Table 2). After excluding variables with strong collinearity (Additional file 1: Figs. S6 and S7) and adjusting for the effect of other variables in the multivariable model of exposure to *P. falciparum*, living further than 5 km from a health facility was associated with increased odds of exposure (adjusted

odds ratio (OR)=1.6, 95% CI [1.2–2.2]), and every 10% (one unit) increase in school-level RDT prevalence was associated with a doubling in the odds of PfAMA1 Ab response aggregated at fokontany-level (OR=1.9, 95% CI [1.2–3.1]). Out of all the environmental and climatic variables, only elevation was significantly associated with *P. falciparum* exposure, with a 30% decrease in the odds for every 100 m (one unit) increase in elevation (OR=0.7, 95% CI [0.6–0.8]) (Table 2).

No evidence of residual spatial autocorrelation was found in the final multivariable model for PfAMA1 Ab response at the fokontany-level; and no deviance to normal distribution was observed to its residuals (Table 2, Additional file 1: Figs. S8 and S9). That suggests that spatially-structured factors were accounted for in the model of *P. falciparum* exposure risk, or the considered district-and-commune level random effects.

Factors associated with PfAMA1 antibody seropositivity at the individual-level

Individual seropositivity decreased with higher values of vegetation (NDVI) the previous month, the percentage of land cover such as woodlands, and the elevation of *fokontany* (Additional file 1: Table S2). When adjusting for individual-level factors in the multivariable model, distance from health facilities, school-level RDT prevalence, and elevation were remained statistically significant, with similar coefficients as in the *P. falciparum* exposure (PfAMA1 Ab response) model at the fokontany-level (Fig. 4). In addition, the probability of being seropositive increased with age: children aged 9–10 years, 11–12 years and 13–14 years were likely to be more seropositive than youngest 2–8 years group, and the corresponding ORs [95% CI] were, respectively, 1.8 [1.3–2.4], 3.7 [2.8–5.0] and 5.7 [4.0–8.0]. Having a fever episode in the previous two weeks (OR=1.7 [1.2–2.4]) was also identified as risk factor.

Discussion

Pockets of residual transmission in low transmission settings can pose significant challenges to achieving malaria elimination goals [48]. Research on malaria transmission heterogeneity in settings pursuing elimination is therefore important to allow better targeting of malaria

(See figure on next page.)

Fig. 3 Epidemiology and local clustering of *P. falciparum* infection prevalence by RDT and PfAMA1 antibody (Ab) seroprevalence across the study area. **A** Spatial distribution of malaria infection prevalence, and **B** Spatial distribution of PfAMA1 Ab seroprevalence. Dark-maroon colored *fokontany* had higher prevalence and the optimal 5-classes by Jenks classification were used for both malaria infection by RDT and PfAMA1 Ab prevalence. The dark-red diamond represents the capital of Madagascar, Antananarivo. **C** Malaria infection prevalence clusters, and **D** PfAMA1 Ab seroprevalence clusters. “High-High” clusters represent *fokontany* with observed values matching with the weighted mean of each *fokontany*'s neighbours, which is high; “High-Low” clusters are those with abnormally observed high but expected low values; “Low-High” clusters are those with abnormally observed low but expected high values; and no deviance from the stationarity assumption are marked with “none”. These figures are supported by Additional file 1: Fig. S4 and Fig. S5, Additional file 2: Table S3 and Additional file 3: Table S4

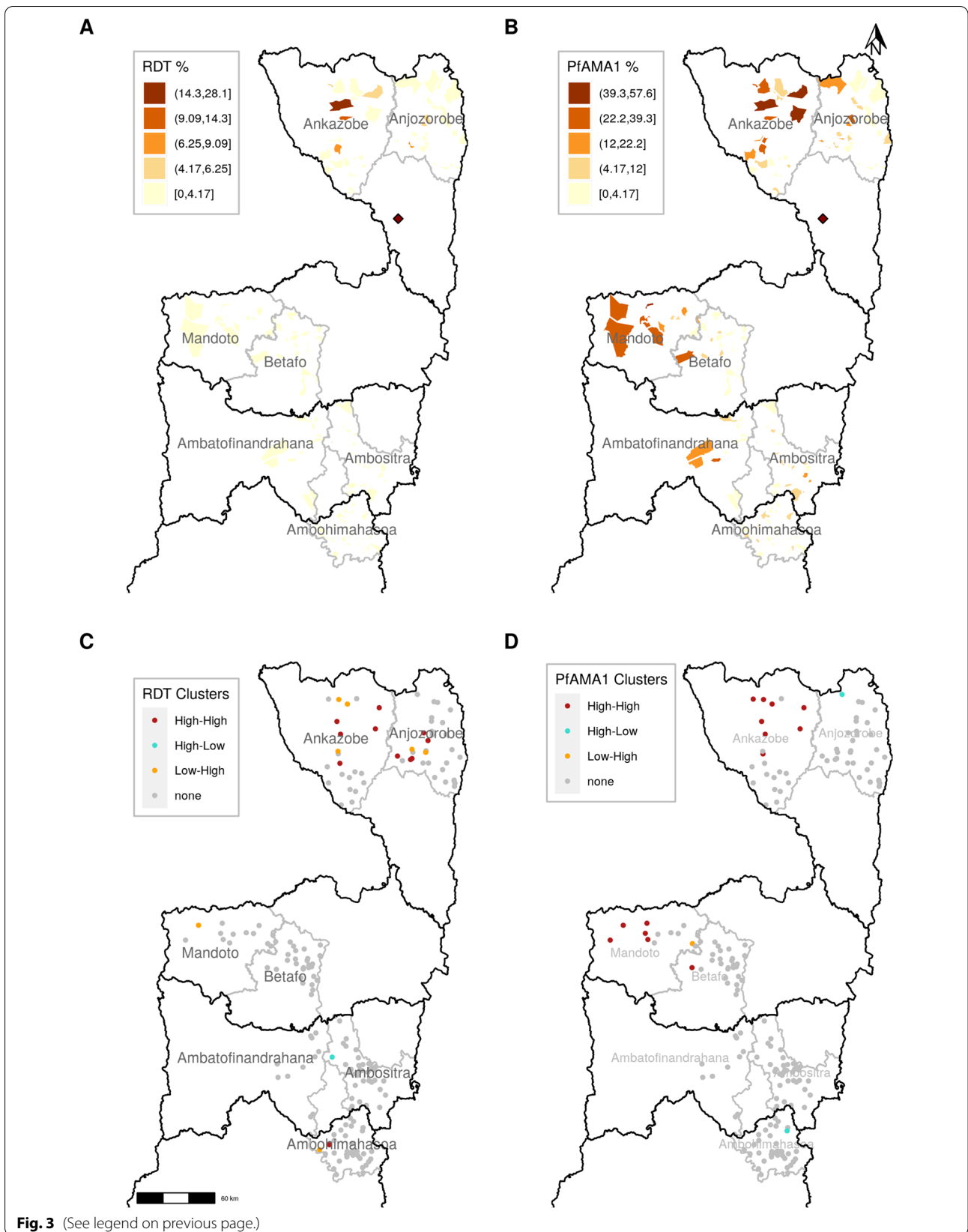


Table 2 *P. falciparum* infection and exposure (PfAMA1 Ab response) model mixed-effects regression models at fokontany-level

Factors associated	<i>P. falciparum</i> infection model				<i>P. falciparum</i> exposure (PfAMA1 Ab response) model			
	Univariable		Multivariable		Univariable		Multivariable	
	OR	95%CI	OR ^e	95%CI	OR	95%CI	OR ^e	95%CI
Health Facilities > 5 km	1.8	1.1–3.1			2.1	1.8–2.6	1.6	1.2–2.2***
School RDT prevalence ^c					4.4	3.5–5.6	1.9	1.2–3.1**
NDVI at lag-1 ^a	0.7	0.6–1.0			0.8	0.7–0.9	1.0	0.8–1.3
LST Day at lag-1 ^b	5.4	3.0–9.7	8.9	2.9–28.0***	4.5	3.7–5.5		
Grasslands or cereals ^c	1.2	1.1–1.4			1.1	1.1–1.2	0.9	0.9–1.0
Forests ^c	0.7	0.3–1.5			0.8	0.7–1.0		
Woodlands ^c	0.8	0.7–1.0	1.2	0.9–1.5	0.9	0.8–0.9		
Wet, croplands or mosaics ^c	0.8	0.5–1.3			0.9	0.8–1.0		
Elevation ^d	0.7	0.6–0.8			0.7	0.6–0.7	0.7	0.6–0.8***

Wald-test approximation was used for CIs (confidence interval) and p-values

NDVI Normalized Difference Vegetation Index at the previous month; LST daytime Land Surface Temperature and emissivity composites at the previous month; OR odds ratio

^a NDVI was scaled 1/10, as one unit increase means 0.1 increase

^b LST Day was scaled in 5 °C unit, as one unit increase means 5° C increase

^c Variables scaled in 10% unit, as one unit increase means 10% increase

^d Elevation scaled in 100 m, as one unit increase means 100 m increase

^e Adjusted odds ratio

***p-value < 0.001; **p-value < 0.01; *p-value < 0.05

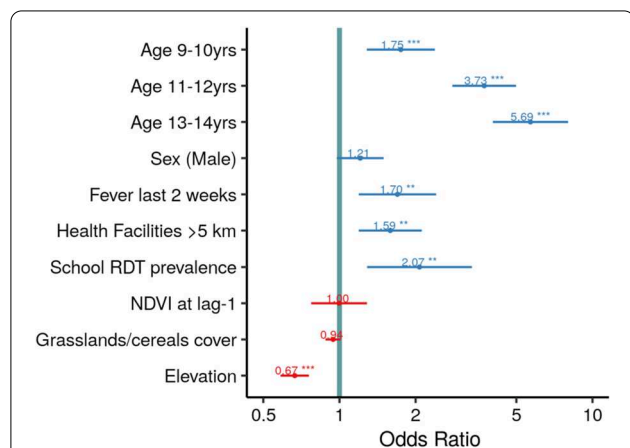


Fig. 4 Factors associated with PfAMA1 Ab seropositivity model of individual-level covariates. Blue- and red-horizontal bars represent the 95% CI of odds ratio (ORs) of each factors with associated positive and negative effect, respectively. The green line represents the ORs value equal to one (1). This figure is supported by Additional file 1: Table S2. NDVI was scaled 1/10, as one unit increase means 0.1 increase. School RDT prevalence and grasslands/cereals cover were scaled in 10% unit, as one unit increase means 10% increase. Elevation was scaled in 100 m, as one unit increase means 100 m increase. Levels of significance are marked with (***) for p < 0.001, (**) for p < 0.01, and (*) for p < 0.05

control activities. Since data collection for this study was conducted, Madagascar and other low-income countries have seen a trend of increasing malaria incidence, which further justifies the need of new approaches to reverse this trend [49]. Using a seroprevalence study of 6293 school-children in the highlands of Madagascar (CHL and Fringe areas) to characterize the spatial heterogeneity of *P. falciparum* infection, approximately 7.0% of children had been exposed to *P. falciparum* according to the Ab response despite a very low prevalence of malaria infection using RDTs (0.8%). Furthermore, hotspots of PfAMA1 Ab seroprevalence were observed in multiple districts in the area, many of which were not observed via malaria RDTs. Exposure to the malarial parasite, as indicated by seroprevalence, increased with a child's age (Fig. 2), for children living further than 5 km from a health facility, and for those experiencing a fever episode in the previous 2 weeks.

Spatial heterogeneity of malaria infection prevalence and PfAMA1 Ab seroprevalence were confirmed across the study sites, revealing an important number of seroprevalence hotspots in districts of the northern and southern part of CHL and Fringe areas of Madagascar. These findings are in accordance with a previous serological study carried out in Madagascar [50], and

similar heterogeneities in malaria transmission were found using routine surveillance data in west Fringes of highlands (Fig. 3) [3, 4]. Factors associated with these spatial heterogeneities were further characterized at the fokontany-level. In this study, two factors associated with *P. falciparum* cumulative exposure at the fokontany and individual levels were school *P. falciparum* infection prevalence by RDT and having a fever in the previous 2 weeks, respectively. This suggests, on one hand, that PfAMA1 Ab may capture additional information on cumulative exposure to malaria parasite in children helping to identify a greater proportion of transmission hotspots; on the other hand, the correlation between RDT and PfAMA1 suggests that conventional RDTs can still be used in settings pursuing elimination, especially in areas with high-density infections [23, 24] not able to afford the additional operational costs of serological studies. Further studies are needed to better understand the cost-effectiveness of more accurate diagnostic techniques for low-density infections such as PCR [51].

Children with geographical barriers in health care access, who lived further than 5 km from health facilities (around one third of the study population) were significantly more exposed to *P. falciparum*, which could have important implications for malaria elimination efforts in these areas. These results suggest that suboptimal testing and treatment of malaria infections in these areas, due to geographic barriers to access health care [52], could result in undetected pockets of malaria transmission that undermine elimination goals. Indeed, previous studies have shown that persistent geographic inequalities in health care access still exist in rural areas of Madagascar, with an exponential decrease in the use of health facilities over the first 5 km [53]. Community health programs can be an effective way to remove geographic barriers to health care access [54], since two community health workers are present in every fokontany independently of their distance to a health facility. However, current national guidelines for community case management of malaria only target children under 5 years, the group at the highest risk of mortality from malaria infections. In this study, this group was found to be least exposed to *P. falciparum* (with zero seropositive to PfAMA1 Ab) although it was not representative of this age group because the study was restricted to school-aged children; and in rural Madagascar, children generally start school at age 5. A sub-analysis of factors associated with exposure of ≤ 5 years children (seroprevalence = 2.6% [5 of 194]) suggests the absence of the barrier of distance to health facilities (Additional file 1: Table S6), which may indicate effective case management but could also be due to small sample sizes for this group. In parallel, this national strategy of malaria community case management leaves out

the vast majority of the population, and current plans to expand it to all ages in Madagascar [55] could, therefore, help address symptomatic malaria cases in these pockets of malaria transmission and accelerate elimination efforts.

Among environmental factors associated with *P. falciparum* cumulative exposure, PfAMA1 Ab response at the fokontany-level was higher at lower elevations, but there was little additional effect of other environmental and climatic factors examined. Elevation is widely used in malaria mapping as an established proxy of malaria transmission due to its association with precipitation and temperature which, along with vegetation cover, are generally found to be important predictors of malaria incidence and transmission, given their role on *Anopheles* spp survival, development, breeding, and biting rates [56–60]. In this setting, elevation was significantly and negatively correlated with temperature and grasslands or cereals land covers, but positively with vegetation cover proxies (NDVI and EVI) (Additional file 1: Fig. S6 and Fig. S7), which might explain why these variables had little to no effect in the final multivariable models (Table 2, Fig. 4).

At the individual level, *P. falciparum* exposure risk increased with age, which could be due to repeated exposure of children—acquiring a long-lived component of the Ab response—to infective female *Anopheles* mosquito bites. Antibody responses are boosted by active *P. falciparum* infections as children get older, which is similar to endemic areas and informative for characterizing spatial heterogeneity [14]. In addition, behaviour and access to protective measures vary for different age groups: given the targeting of children under 5 years and pregnant women in malaria control strategies, net use is especially important in older children and adolescents, but tends to be lowest in these age groups [61–63]. In this setting, 56.4% of children were in households with two or more bed nets, but neither the individual use of an ITN nor the number of ITNs in a household was associated with PfAMA1 Ab seropositivity. Moreover, other studies have found that older children spent more time outdoors in the evening, when *Anopheles* spp biting rates are typically higher, putting them at higher risk for being bitten by infective mosquito than other age groups [64, 65]. That might explain the important role played by these older children and adolescents as reservoirs that could sustain malaria transmission [6], even in very low transmission risk settings of Madagascar (<1% parasite prevalence) as previously highlighted by Kang et al. [33].

This study had several limitations. First, the cross-sectional design reflects a snapshot of children's infection or cumulative exposure, dependent on underlying study setting contexts. Further, these findings might not be representative of other low malaria transmission settings

in the highlands of Madagascar due to their diversity in malaria transmission dynamics (central, fringe east versus fringe west highlands) and vector ecology [26, 66]. Second, since data in this study were collected in 2014, a more recent serological survey could give better information on malaria transmission intensity, to inform how Madagascar should adapt its interventions to reverse the current trend of increasing malaria cases [49].

Conclusions

In this setting, serological markers (PfAMA1 Ab) enabled to highlight hotspots of malaria seroprevalence in multiple districts in the highlands of Madagascar (CHL and Fringe areas)—many of which were not observed via malaria RDTs—and associated factors, revealing a pattern of higher transmission linked to geographical barriers in health care access. Targeting these residual pockets could reduce malaria transmission at the community level [67, 68]. Nevertheless, sub-optimal testing and treatment of malaria infections in CHL and surrounding Fringes areas could undermine elimination efforts by NMCP, at the moment when Madagascar should adapt interventions to face the current challenge of plateauing or increasing malaria cases [5, 49]. Serological markers—especially when used in young children—could add benefits to routine malaria surveillance, provide a good picture of malaria transmission structure [13], and help to support and evaluate community interventions aimed at elimination [15].

Disclaimer

The findings and conclusions in this report are those of the author(s) and do not necessarily represent the official position of the Centers for Disease Control and Prevention.

Abbreviations

P. falciparum: *Plasmodium falciparum*; PfAMA1: *Plasmodium falciparum* Apical membrane antigen 1; Ab: Antibody; RDTs: Rapid diagnostic tests; NMCP: National Malaria Control Program; IgG: Immunoglobulin G; ITNs: Insecticide-treated mosquito nets; IRS: Indoor residual spraying; CHL: Central Highlands of Madagascar; CI: Confidence interval; PCR: Polymerase chain reaction; MODIS: Moderate resolution imaging spectroradiometer; LST: Land Surface Temperature and emissivity composites; NDVI: Normalized Difference Vegetation Index; EVI: Enhanced Vegetation Index; OR: Odds ratios; IQR: Inter-quartile range.

Supplementary Information

The online version contains supplementary material available at <https://doi.org/10.1186/s12936-022-04260-0>.

Additional file 1: Method S1. Two-component gaussian mixture model; **Method S2.** Environmental and remotely sensed data processing; **Method S3.** Mixed-effects binomial logistic regression model frameworks and selection; **Table S1.** List of environmental and climatic data; **Table S2.** Univariable and multivariable *P. falciparum* exposure (PfAMA1 Ab response) model of individual-, household- and fokontany-level

covariates, using mixed-effect logistic regression at district and commune level; **Figure S1.** Cut-off value for PfAMA1 Ab seropositivity (dashed-red line) by using two finite Gaussian mixture models and the serological data (for children and adult participants, $n = 12,770$) described in Steinhart et al. [11]; **Figure S2.** Fokontany neighbour definition by maximum distance, using Great Circle distance around 17 km between two contiguous fokontany; **Figure S3.** Malaria infection prevalence by RDT versus PfAMA1 Ab seroprevalence detected high clusters fokontany across districts. High clusters fokontany are the combination of “High-High” or “Low-High” clusters; that represent fokontany with expected values (prevalence or seroprevalence) matching with the weighted mean of each fokontany's neighbours, or those with abnormally high expected but low expected values, respectively; **Figure S4.** Weighted global Moran's I statistics versus simulated random distribution of logit scale of (A) malaria infection prevalence by RDT ($I = 0.24$), and (B) PfAMA1 Ab seroprevalence ($I = 0.59$); **Figure S5.** Moran Scatterplots of clusters and hotspots of (A) malaria infection prevalence by RDT, and (B) PfAMA1 Ab seroprevalence; **Figure S6.** Pearson's correlation scatterplot and peer's significance of *P. falciparum* infection prevalence by RDT, PfAMA1 Ab seroprevalence and quantitative environmental and climatic covariates. Levels of significance are marked with (***) for $p < 0.001$, (**) for $p < 0.01$, and (*) for $p < 0.05$. Lagged values of temperature and vegetation at 2 and 3 months were less correlated to malaria infection prevalence by RDT and PfAMA1 Ab seroprevalence than one-month lag at fokontany-level; **Figure S7.** Pearson's correlation scatterplot and peers of *P. falciparum* infection prevalence by RDT, PfAMA1 Ab seroprevalence and quantitative environmental and climatic covariates associations. There was high correlation between multiple pairs of covariates such as {NDVI, EVI, forests, woodlands, or grasslands/cereals}, {LST day, LST night, elevation, woodlands or grasslands/cereals} and {grasslands/cereals, wet/croplands/mosaics}; **Table S5.** Univariable and multivariable *P. falciparum* infection model at individual-, household- and fokontany-level covariates using mixed-effect logistic regression at district and commune level; **Figure S8.** *P. falciparum* exposure (PfAMA1 Ab response) model residuals diagnostics of normality at fokontany-level. No significant deviance to normal distribution was observed in PfAMA1 Ab seroprevalence model residuals using Kolmogorov–Smirnov normality test ($p = 0.3$); **Figure S9.** Spatial autocorrelation of residuals diagnostics using Moran's I index of non-spatial *P. falciparum* exposure (PfAMA1 Ab response) model at fokontany-level; **Table S6.** Sub-model for ≤ 5 years old children (seroprevalence = 2.6% [5 of 194]), only variables included in the all participants Ab response model were included: univariable *P. falciparum* exposure (PfAMA1 Ab response) model of individual- and fokontany-level covariates, using binomial logistic regression.

Additional file 2: Table S3. Malaria infection prevalence by RDT measures of local indicators of spatial association.

Additional file 3: Table S4. PfAMA1 Ab seroprevalence measures of local indicators of spatial association.

Acknowledgements

The authors would like to thank to the population of the districts and communes investigated and especially to the children, parents, who participated to the study. We also thank those who facilitated the survey that is heads of communes and fokontany, local administration authorities, and health authorities from Ministry of Public Health of Madagascar. We also thank the National Malaria Control Program and Institut Pasteur de Madagascar survey teams. We especially thank Sixte Zigirumugabe and Jessica Butts of the US President's Malaria Initiative for their guidance in aligning the assessment to on the ground management decisions; Christophe Rogier, Patrice Piola and Thomas Kesteman for their respective valuable advices and input on the study methodology and lab analyses of samples; Anny Randriamoramana and Bienvenue RAHOILJAONA for helpful support on data management supports; and Anthonio RAKOTOARISON and Daouda KASSIE for remotely sensed data analysis advices.

Author contributions

JMR, IV, LCS, BR and AG conceived of the study; IV, AH, ER and MR led investigation and lab analyses of samples; JMR performed the data curation and statistical analyses; JMR drafted the manuscript; AG, BR, IV, LCS, AH, ER, MR and

AW reviewed and contributed to the writing. All authors read and approved the final manuscript.

Funding

This work was supported by the US President's Malaria Initiative program (Grant Number AID-687-G-13-00003 Surveillance and Data for Management Project) and the Institut Pasteur de Madagascar.

Availability of data and materials

The datasets used and/or analysed during the present study are available from the corresponding author upon reasonable request.

Declarations

Ethics approval and consent to participate

The study protocol was approved by the National Ethics Committee of the Ministry of Public Health of Madagascar (approval number CNE 011-MSANP/CE, 26 March 2014) and by the US Centers for Disease Control and Prevention Institutional Review Board. At sampled schools, after explaining the study objectives and procedures, individual, informed consent was obtained from caregivers of sampled school children.

Consent for publication

Not applicable.

Competing interests

The authors do not report any competing interests.

Author details

¹Epidemiology and Clinical Research Unit, Institut Pasteur de Madagascar, Antananarivo, Madagascar. ²IRD, Sorbonne Université, UMMISCO, 93143 Bondy, France. ³Sorbonne Université, ED 393, Paris, France. ⁴MIVEGEC, Université Montpellier, CNRS, IRD, Montpellier, France. ⁵Immunology of Infectious Diseases Unit, Institut Pasteur de Madagascar, Antananarivo, Madagascar. ⁶Immunophysiopathology and Infectious Diseases Department, Institut Pasteur de Dakar, Dakar, Senegal. ⁷Malaria Branch, Division of Parasitic Diseases and Malaria, Center for Global Health, Centers for Disease Control and Prevention, Atlanta, GA, USA. ⁸Faculty of Sciences, University of Antananarivo, Antananarivo, Madagascar. ⁹Unité de Parasitologie, Institut Pasteur de Madagascar, Antananarivo, Madagascar. ¹⁰Department of Epidemiology, Johns Hopkins Bloomberg School of Public Health, Baltimore, MD, USA. ¹¹Faculté Des Sciences, Université de Toliara, 601 Toliara, Madagascar.

Received: 18 March 2022 Accepted: 9 August 2022

Published online: 21 August 2022

References

- WHO. World Malaria Report: 20 years of global progress and challenges. Geneva: World Health Organization; 2020.
- Programme Nationale de Lutte contre le Paludisme. Plan Stratégique de Lutte contre le Paludisme—Madagascar 2013–2017. Antananarivo: Programme Nationale de Lutte contre le Paludisme; 2012.
- Howes RE, Mioramalala SA, Ramiranirina B, Franchard T, Rakotorahalahy AJ, Bisanzio D, et al. Contemporary epidemiological overview of malaria in Madagascar: operational utility of reported routine case data for malaria control planning. *Malar J*. 2016;15:502.
- Ihantamalala FA, Rakotoarimanana FMJ, Ramiadantsoa T, Rakotondramanga JM, Pennober G, Rakotomanana F, et al. Spatial and temporal dynamics of malaria in Madagascar. *Malar J*. 2018;17:58.
- Direction de Lutte contre le Paludisme. Plan Stratégique de Lutte contre le Paludisme—Madagascar 2018–2022. Antananarivo: Direction de Lutte contre le Paludisme; 2017.
- Lindblade KA, Steinhardt L, Samuels A, Kachur SP, Slutsker L. The silent threat: asymptomatic parasitemia and malaria transmission. *Expert Rev Anti Infect Ther*. 2013;11:623–39.
- Lin JT, Saunders DL, Meshnick SR. The role of submicroscopic parasitemia in malaria transmission: what is the evidence? *Trends Parasitol*. 2014;30:183–90.
- Andolina C, Rek JC, Briggs J, Okoth J, Musiime A, Ramjith J, et al. Sources of persistent malaria transmission in a setting with effective malaria control in eastern Uganda: a longitudinal, observational cohort study. *Lancet Infect Dis*. 2021;21:1568–78.
- King CL, Davies DH, Felgner P, Baum E, Jain A, Randall A, et al. Biosignatures of exposure/transmission and immunity. *Am J Trop Med Hyg*. 2015;93:16–27.
- Ashton RA, Kefyalew T, Rand A, Sime H, Asefa A, Makasha A, et al. Geostatistical modeling of malaria endemicity using serological indicators of exposure collected through school surveys. *Am J Trop Med Hyg*. 2015;93:168–77.
- Steinhardt LC, Ravaoarisoa E, Wiegand R, Harimanana A, Hedje J, Cotte AH, et al. School-based serosurveys to assess the validity of using routine health facility data to target malaria interventions in the Central Highlands of Madagascar. *J Infect Dis*. 2021;223:995–1004.
- Tongren JE, Drakeley CJ, McDonald SLR, Reyburn HG, Manjurano A, Nkya WM, et al. Target antigen, age, and duration of antigen exposure independently regulate immunoglobulin G subclass switching in malaria. *Infect Immun*. 2006;74:257–64.
- Akpogheneta OJ, Duah NO, Tetteh KKA, Dunyo S, Lanar DE, Pinder M, et al. Duration of naturally acquired antibody responses to blood-stage *Plasmodium falciparum* is age dependent and antigen specific. *Infect Immun*. 2008;76:1748–55.
- Stanisic DI, Fowkes FJI, Koinari M, Javati S, Lin E, Kiniboro B, et al. Acquisition of antibodies against *Plasmodium falciparum* merozoites and malaria immunity in young children and the influence of age, force of infection, and magnitude of response. *Infect Immun*. 2015;83:646–60.
- Kangoye DT, Noor A, Midega J, Mwangeli J, Mkabili D, Mogeni P, et al. Malaria hotspots defined by clinical malaria, asymptomatic carriage, PCR and vector numbers in a low transmission area on the Kenyan Coast. *Malar J*. 2016;15:213.
- Yman V, White MT, Rono J, Arcà B, Osier FH, Troye-Blomberg M, et al. Antibody acquisition models: a new tool for serological surveillance of malaria transmission intensity. *Sci Rep*. 2016;6:19472.
- Assefa A, Ali Ahmed A, Deressa W, Sime H, Mohammed H, Kebede A, et al. Multiplex serology demonstrate cumulative prevalence and spatial distribution of malaria in Ethiopia. *Malar J*. 2019;18:246.
- Amratia P, Psychas P, Abuaku B, Ahorlu C, Millar J, Oppong S, et al. Characterizing local-scale heterogeneity of malaria risk: a case study in Bunkpurugu-Yunyoo district in northern Ghana. *Malar J*. 2019;18:81.
- Institut National de la Statistique (INSTAT) et ICF Macro. Enquête Démographique et de Santé de Madagascar 2008–2009. Antananarivo: Institut National de la Statistique; 2010.
- Mosha JF, Sturrock HJ, Greenwood B, Sutherland CJ, Gadalla NB, Atwal S, et al. Hot spot or not: a comparison of spatial statistical methods to predict prospective malaria infections. *Malar J*. 2014;13:53.
- WHO for Africa. Implementation of indoor residual spraying of insecticides for malaria control in the WHO African Region Report. Kinshasha: World Health Organization; 2007.
- Institut National de la Statistique (INSTAT), PNLP Madagascar, Institut Pasteur de Madagascar. Malaria Indicator Survey 2013. Calverton: INSTAT, PNLP, IPM et ICF International; 2013.
- Okell LC, Ghani AC, Lyons E, Drakeley CJ. Submicroscopic infection in *Plasmodium falciparum*—endemic populations: a systematic review and meta-analysis. *J Infect Dis*. 2009;200:1509–17.
- Okell LC, Bousema T, Griffin JT, Ouedraogo AL, Ghani AC, Drakeley CJ. Factors determining the occurrence of submicroscopic malaria infections and their relevance for control. *Nat Commun*. 2012;3:1237.
- Wu L, Van Den Hoogen LL, Slater H, Walker PGT, Ghani AC, Drakeley CJ, Okell LC. Comparison of diagnostics for the detection of asymptomatic *Plasmodium falciparum* infections to inform control and elimination strategies. *Nature*. 2015;528:S86–93.
- Arambepola R, Keddie SH, Collins EL, Twohig KA, Bertozzi-Villa A, Chestnutt EG, et al. Spatiotemporal mapping of malaria prevalence in Madagascar using routine surveillance and health survey data. *Sci Rep*. 2020;10:18129.
- Maina J, Ouma PO, Macharia PM, Alegana VA, Mitto B, Fall IS, et al. A spatial database of health facilities managed by the public health sector in sub Saharan Africa. *Sci Data*. 2019;6:134.

28. Stewart L, Gosling R, Griffin J, Gesase S, Campo J, Hashim R, et al. Rapid assessment of malaria transmission using age-specific sero-conversion rates. *PLoS ONE*. 2009;4: e6083.
29. Okebe J, Affara M, Correa S, Muhammad AK, Nwakanma D, Drakeley C, et al. School-based countrywide seroprevalence survey reveals spatial heterogeneity in malaria transmission in the Gambia. *PLoS ONE*. 2014;9: e110926.
30. Perraut R, Richard V, Varela M-L, Trape J-F, Guillotte M, Tall A, et al. Comparative analysis of IgG responses to *Plasmodium falciparum* MSP1p19 and PF13-DBL1 α 1 using ELISA and a magnetic bead-based duplex assay (MAGPIX[®]-Luminex) in a Senegalese meso-endemic community. *Malar J*. 2014;13:410.
31. Kerkhof K, Canier L, Kim S, Heng S, Sochantha T, Sovannaroth S, et al. Implementation and application of a multiplex assay to detect malaria-specific antibodies: a promising tool for assessing malaria transmission in Southeast Asian pre-elimination areas. *Malar J*. 2015;14:338.
32. Oak Ridge National Laboratory Distributed Active Archive Center (ORNL DAAC). MODIS and VIIRS Land Product RESTful Web Service. Oak Ridge: Oak Ridge National Laboratory Distributed Active Archive Center; 2018. <https://doi.org/10.3334/ORNLDAAC/1600>
33. Kang SY, Battle KE, Gibson HS, Ratsimbaoa A, Randrianarivojosia M, Ramboarina S, et al. Spatio-temporal mapping of Madagascar's Malaria Indicator Survey results to assess *Plasmodium falciparum* endemicity trends between 2011 and 2016. *BMC Med*. 2018;16:71.
34. Friedl MA, Sulla-Menasha D, Tan B, Schneider A, Ramankutty N, Sibley A, et al. MODIS Collection 5 global land cover: algorithm refinements and characterization of new datasets. *Remote Sens Environ*. 2010;114:168–82.
35. Farr TG, Rosen PA, Caro E, Crippen R, Duren R, Hensley S, et al. The shuttle radar topography mission. *Rev Geophys*. 2007;45:2004.
36. Loveland TR, Belward AS. The international geosphere biosphere programme data and information system global land cover data set (DIScover). *Acta Astronaut*. 1997;41:681–9.
37. R Core Team. R: a language and environment for statistical computing. Vienna: R Core Team; 2020.
38. Bivand RS, Wong DWS. Comparing implementations of global and local indicators of spatial association. *TEST*. 2018;27:716–48.
39. Bivand RS, Pebesma E, Gómez-Rubio V. Applied spatial data analysis with R. 2nd ed. New York: Springer; 2018. <https://doi.org/10.1007/978-1-4614-7618-4>.
40. Anselin L. Local indicators of spatial association-LISA. *Geogr Anal*. 2010;27:93–115.
41. Getis A, Ord JK. The analysis of spatial association by use of distance statistics. *Geogr Anal*. 1992;24:189–206.
42. Mauny F, Viel JF, Handschumacher P, Sellin B. Multilevel modeling and malaria: a new method for an old disease. *Int J Epidemiol*. 2004;33:1337–44.
43. Harrison XA. A comparison of observation-level random effect and Beta-Binomial models for modelling overdispersion in Binomial data in ecology & evolution. *PeerJ*. 2015;2015: e1114.
44. Bartoń K. MuMIn: Multi-model inference, software. 2020. <https://cran.r-project.org/package=MuMIn>. Accessed 01 Mar 2022.
45. Burnham KP, Anderson DR. Model selection and multimodel inference. 2nd ed. New York: Springer; 2004. <https://doi.org/10.1007/b97636>.
46. Nakagawa S, Schielzeth H. A general and simple method for obtaining R² from generalized linear mixed-effects models. *Methods Ecol Evol*. 2013;4:133–42.
47. Bates D, Mächler M, Bolker BM, Walker SC. Fitting linear mixed-effects models using lme4. *J Stat Softw*. 2015;67: i01.
48. Rosado J, White MT, Longley RJ, Lacerda M, Monteiro W, Brewster J, et al. Heterogeneity in response to serological exposure markers of recent *Plasmodium vivax* infections in contrasting epidemiological contexts. *PLoS Negl Trop Dis*. 2021;15: e0009165.
49. WHO. World Malaria Report 2021. Geneva: World Health Organization; 2021.
50. Razakandrainibe R, Thonier V, Ratsimbaoa A, Rakotomalala E, Ravaoarisoa E, Raherinjafy R, et al. Epidemiological situation of malaria in Madagascar: baseline data for monitoring the impact of malaria control programmes using serological markers. *Acta Trop*. 2009;111:160–7.
51. Bousema T, Okell L, Felger I, Drakeley C. Asymptomatic malaria infections: detectability, transmissibility and public health relevance. *Nat Rev Microbiol*. 2014;12:833–40.
52. Ihantamalala FA, Bonds MH, Randriamihaja M, Rakotonirina L, Herbreteau V, Révillion C, et al. Geographic barriers to establishing a successful hospital referral system in rural Madagascar. *BMJ Glob Health*. 2021;6: e007145.
53. Garchitorena A, Ihantamalala FA, Révillion C, Cordier LF, Randriamihaja M, Razafinjato B, et al. Geographic barriers to achieving universal health coverage: evidence from rural Madagascar. *Health Policy Plan*. 2021;36:1659–70.
54. WHO. Guideline on health policy and system support to optimize community health worker selected highlights. Geneva: World Health Organization; 2012.
55. U. S. President's Malaria Initiative Madagascar. Malaria Operational Plan FY 2020. Pennsylvania: PMI; 2020.
56. Manjurano A, Okell L, Lukindo T, Reyburn H, Olomi R, Roper C, et al. Association of sub-microscopic malaria parasite carriage with transmission intensity in north-eastern Tanzania. *Malar J*. 2011;10:370.
57. Weiss DJ, Mappin B, Dalrymple U, Bhatt S, Cameron E, Hay SI, et al. Re-examining environmental correlates of *Plasmodium falciparum* malaria endemicity: a data-intensive variable selection approach. *Malar J*. 2015;14:68.
58. Guerra CA, Snow RW, Hay SI. Mapping the global extent of malaria in 2005. *Trends Parasitol*. 2006;22:353–8.
59. Paaijmans KP, Thomas MB. The influence of mosquito resting behaviour and associated microclimate for malaria risk. *Malar J*. 2011;10:183.
60. Abiodun GJ, Maharaj R, Witbooi P, Okosun KO. Modelling the influence of temperature and rainfall on the population dynamics of *Anopheles arabiensis*. *Malar J*. 2016;15:364.
61. Korenromp EL, Miller J, Cibulskis RE, Cham MK, Alnwick D. Dye. Monitoring mosquito net coverage for malaria control in Africa: possession vs. use by children under 5 years. *Trop Med Int Health*. 2003;8:693–703.
62. Bernard J, Mtove G, Mandike R, Mtei F, Maxwell C, Reyburn H. Equity and coverage of insecticide-treated bed nets in an area of intense transmission of *Plasmodium falciparum* in Tanzania. *Malar J*. 2009;8:65.
63. Kulkarni MA, Vanden Eng J, Desrochers RE, Hoppe Cotte A, Goodson JL, Johnston A, et al. Contribution of integrated campaign distribution of long-lasting insecticidal nets to coverage of target groups and total populations in malaria-endemic areas in Madagascar. *Am J Trop Med Hyg*. 2010;82:420–5.
64. Braimah N, Drakeley C, Kweka E, Moshia F, Helinski M, Pates H, Maxwell C, Massawe T, Kenward MG, Curtis C. Tests of bednet traps (Mbita traps) for monitoring mosquito populations and time of biting in Tanzania and possible impact of prolonged insecticide treated net use. *Int J Trop Insect Sci*. 2005;25:208–13.
65. Moiroux N, Gomez MB, Pennetier C, Elanga E, Djènonatin A, Chandre F, et al. Changes in *Anopheles funestus* biting behavior following universal coverage of long-lasting insecticidal nets in Benin. *J Infect Dis*. 2010;206:1622–9.
66. Tantely ML, Rakotoniaina JC, Tata E, Andrianaivolambo L, Fontenille D, Elissa N. Modification of *Anopheles gambiae* distribution at high altitudes in Madagascar. *J Vector Ecol*. 2012;37:402–6.
67. Bousema T, Griffin JT, Sauerwein RW, Smith DL, Churcher TS, Takken W, et al. Hitting hotspots: spatial targeting of malaria for control and elimination. *PLoS Med*. 2012;9: e1001165.
68. The malERA Refresh Consultative Panel on Characterising the Reservoir and Measuring Transmission. malERA: an updated research agenda for characterising the reservoir and measuring transmission in malaria elimination and eradication. *PLoS Med*. 2012;14: e1002452.

Publisher's Note

Springer Nature remains neutral with regard to jurisdictional claims in published maps and institutional affiliations.

4 Chapitre 2 : Excess mortality associated with the COVID-19 pandemic during the 2020 and 2021 waves in Antananarivo, Madagascar (Article 2)

La mortalité a considérablement diminué à Madagascar au cours des dernières décennies, l'espérance de vie ayant augmenté de près de 15 ans (de 52 à 66 ans) entre 1990 et 2022 (United Nations Department of Economic and Social Affairs Population Division, 2022). Ces progrès sont en grande partie dus à une baisse rapide de la mortalité des enfants de moins de cinq ans, qui a été réduite de deux tiers au cours de la même période (Sharrow et al., 2022). Plus de trois ans et demi après le début de la pandémie de COVID-19, la charge de la mortalité due cette maladie dans les pays d'ASS reste difficile à quantifier malgré la multitude de méthodes et modèles pour le faire.

Pour évaluer l'impact de la porosité du système de surveillance dans la population de la capitale, nous avons tiré parti du système rigoureux et de longue date d'enregistrement des décès, se trouvant au BMH de la CUA et couvrant à la fois les décès hospitaliers et communautaires. Ce système de notification des décès dispose d'un niveau élevé d'exhaustivité de l'enregistrement des décès, estimé à >90% depuis les années 70 (Masquelier et al., 2019). En se focalisant sur la période pandémique de COVID-19 de 2020–2021, ce chapitre vise à reconstruire les tendances récentes de la mortalité à Antananarivo, et à évaluer les effets de la pandémie de COVID-19 sur la mortalité dans la capitale de Madagascar.



Notre étude dans ce chapitre a permis de mettre en évidence plusieurs pics de surmortalité en 2020–2021, qui ont été associés de manière significative, utilisant les analyses en ondelettes croisées, aux vagues de cas de SARS-CoV-2 signalés. En comparant les tendances durant la période pré-pandémique (2016–2019, utilisées comme tendances basales) avec la période pandémique de 2020–2021, nous avons estimé que la surmortalité toutes causes confondues était de 38,5 et 64,9 pour 100 000 habitants en 2020 et 2021, respectivement. Cette surmortalité a atteint +50% au cours des deux vagues de ces deux premières années (**Table 2**). Nous avons estimé qu'il y avait 1 179 excès de décès sur cette période ; soit une estimation supérieure aux 1 069 décès officiels de COVID-19 notifiés pour l'ensemble du pays par le MSANP à la date du 31 décembre 2021 (Mathieu et al., 2020).

Tableau 2 : Estimation d'excès de mortalité toutes causes de 2020–2021, calculée par le changement relatif utilisant l'algorithme de Farrington et la tendance basale des décès bruts de 2016–2019 (Noufaily et al., 2013)

Year	Relative change level (%)	Nb. of weeks of excess	Expected deaths (2016–2019)		Reported deaths (2020–2021)		Sum excesses death
			Mean	Range (min–max)	Mean	Sum	
2020	< 50	9	144	128–164	188	1 695	244
2020	≥ 50	2	148	142–154	268	536	195
2021	< 50	8	141	123–174	204	1 635	222
2021	≥ 50	4	125	118–139	284	1 135	518
Total		23	140	118–174	217	5 001	1 179

En ce qui concerne l'espérance de vie à la naissance, une baisse substantielle a été observée, diminuant de 0,8 et 1,0 année par rapport à la valeur projetée pour les hommes et les femmes, respectivement, à Antananarivo. Cette baisse de l'espérance de vie est entièrement imputable à l'augmentation du risque de décès chez les hommes et les femmes âgés de plus de 60 ans et aux décès dus au COVID-19, plutôt qu'à l'augmentation d'autres causes de décès. La différence par rapport au sexe trouvée pourrait suggérer des variations de facteurs de risque conduisant à la forme grave de COVID-19, comme par exemple les maladies cardiovasculaires et les comportements à risque des sujets pouvant développer des comorbidités (Cai, 2020; GlobalHealth 5050, 2021).

Excess mortality associated with the COVID-19 pandemic during the 2020 and 2021 waves in Antananarivo, Madagascar

Joelinotahiana Hasina Rabarison,¹ Jean Marius Rakotondramanga ^{1,2}, Rila Ratovoson,¹ Bruno Masquelier,³ Anjaraso Maharavo Rasoanomenjanahary,⁴ Anou Dreyfus,¹ Andres Garchitorena ^{1,5}, Fidisoa Rasambainarivo,^{6,7} Norosoa Harline Razanajatovo,¹ Soa Fy Andriamandimby,¹ C Jessica Metcalf ⁶, Vincent Lacoste,¹ Jean-Michel Heraud ^{1,8}, Philippe Dussart¹

To cite: Rabarison JH, Rakotondramanga JM, Ratovoson R, *et al*. Excess mortality associated with the COVID-19 pandemic during the 2020 and 2021 waves in Antananarivo, Madagascar. *BMJ Glob Health* 2023;**8**:e011801. doi:10.1136/bmjgh-2023-011801

Handling editor Seye Abimbola

► Additional supplemental material is published online only. To view, please visit the journal online (<http://dx.doi.org/10.1136/bmjgh-2023-011801>).

JR and JMR contributed equally.

Received 18 January 2023
Accepted 17 June 2023



© Author(s) (or their employer(s)) 2023. Re-use permitted under CC BY. Published by BMJ.

For numbered affiliations see end of article.

Correspondence to

Dr Jean-Michel Heraud;
jean-michel.heraud@pasteur.fr

ABSTRACT

Introduction COVID-19-associated mortality remains difficult to estimate in sub-Saharan Africa because of the lack of comprehensive systems of death registration. Based on death registers referring to the capital city of Madagascar, we sought to estimate the excess mortality during the COVID-19 pandemic and calculate the loss of life expectancy.

Methods Death records between 2016 and 2021 were used to estimate weekly excess mortality during the pandemic period. To infer its synchrony with circulation of SARS-CoV-2, a cross-wavelet analysis was performed. Life expectancy loss due to the COVID-19 pandemic was calculated by projecting mortality rates using the Lee and Carter model and extrapolating the prepandemic trends (1990–2019). Differences in life expectancy at birth were disaggregated by cause of death.

Results Peaks of excess mortality in 2020–21 were associated with waves of COVID-19. Estimates of all-cause excess mortality were 38.5 and 64.9 per 100 000 inhabitants in 2020 and 2021, respectively, with excess mortality reaching ≥50% over 6 weeks. In 2021, we quantified a drop of 0.8 and 1.0 years in the life expectancy for men and women, respectively attributable to increased risks of death beyond the age of 60 years.

Conclusion We observed high excess mortality during the pandemic period, in particular around the peaks of SARS-CoV-2 circulation in Antananarivo. Our study highlights the need to implement death registration systems in low-income countries to document true toll of a pandemic.

INTRODUCTION

Mortality has declined substantially in Madagascar over the past few decades, with life expectancy increasing by almost 15 years (from 52 to 66 years) between 1990 and 2022.¹ This progress was largely driven by a rapid decline in under-five mortality, which was reduced by two-thirds over the same

WHAT IS ALREADY KNOWN ON THIS TOPIC

⇒ Sub-Saharan countries lag behind the rest of the world in vital statistics leading to the difficulty of collecting information on annual deaths.

WHAT THIS STUDY ADDS

⇒ Our study is one of the firsts conducted in sub-Saharan Africa that made use of a local death notification system to assess the impact of COVID-19 pandemic on mortality and life expectancy in the general population.
⇒ The mortality burden during the COVID-19 pandemic in Antananarivo has been much higher than the official count of COVID-19-related deaths for the entire country.

HOW THIS STUDY MIGHT AFFECT RESEARCH, PRACTICE OR POLICY

⇒ Our study highlights the importance of local sources of death notification to better estimate mortality in the context of an outbreak or a pandemic.

period.² This gain is however fragile, in a country like Madagascar characterised by persistent high rates of poverty, political instability, a weak health system, rapid population growth and scarcity of resources.^{3,4} The recent epidemics of pneumonic plague in 2017 and measles in 2018–19 provide vivid examples of the precariousness of the health situation in the country.^{5,6} The COVID-19 pandemic might have jeopardised the life expectancy gains achieved over the last decades. In many low-income and middle-income countries (LMICs), in particular in sub-Saharan Africa, deaths associated with the COVID-19 remain difficult to estimate, however, mainly due to the absence of a comprehensive and efficient civil registration and vital statistics system.

According to estimates by WHO, when compared with the mortality expected in the absence of the pandemic, COVID-19 caused directly and indirectly, 25 582 additional deaths during the 2020–21 period in Madagascar.⁷ This would represent an increase of approximately 14% over the estimated annual number of deaths in the country.¹ However, as of 31 December 2021, the Malagasy Ministry of Health (MoH) notified 1067 deaths due to COVID-19 for the entire country.⁸ This discrepancy between WHO estimates and the Malagasy MoH deaths could be explained by the fact that the MoH only notified COVID-19 laboratory-confirmed deaths, and left indirect deaths unaccounted for. Moreover, a considerable proportion of deaths occurred outside the healthcare system and were never reported in the official statistics. Consequently, the total number of direct and indirect deaths due to the COVID-19 pandemic is unknown in Madagascar. Epidemiological models such as the WHO model are based on a number of covariates including the reported COVID-19 mortality rate and the COVID-19 positivity rate. But these official statistics can themselves be heavily biased due to limited testing capacity (max 1000 tests/day), insufficient staff to conduct contact tracing and changes in the testing policy during the course of the pandemic.⁹ There are also large uncertainties around pre-pandemic baseline mortality rates due to the incompleteness of death registration systems in LMICs. For example, in Guinea-Bissau, a seroprevalence study in the capital showed that the official number of PCR-confirmed COVID-19 cases greatly underestimated the prevalence of COVID-19 during the pandemic.¹⁰ In Zambia, most deaths due to COVID-19 were detected in the community outside of hospitals and were not tested before death.¹¹

Compared with other African countries, the situation of Madagascar is atypical since the capital city of Antananarivo has a relatively unique system of death notification in place, covering both hospital and community deaths, located at the Bureau Municipal d'Hygiène (BMH) of Antananarivo. An evaluation of this system before the pandemic concluded that high completeness of registration had been achieved over the last decades, with accurate data on the underlying diseases as established by physicians visiting relatives of the deceased or certifying deaths in healthcare facilities.¹² The available registers cover the period 1976–2021 and have previously been analysed to document a mortality crisis due to the resurgence of malaria and an urban famine in the mid-80s,¹³ the excess mortality during the H1N1 pandemic in 2009¹⁴ and the measles outbreak in 2018–19.¹⁵

The objectives of our study were to (i) leverage this death notification system to reconstruct recent mortality trends covering the years 2020 and 2021 in Antananarivo and (ii) assess the effects of the COVID-19 pandemic on mortality in the capital city of Madagascar.

METHODS

Study site and data sources

Since 2016, the National Influenza Centre located at the Institut Pasteur de Madagascar (IPM) has improved the death surveillance system at BMH. This office covers five of the six central districts of Antananarivo city, corresponding to the district of Antananarivo-Renivohitra with a total population of 1.14 million inhabitants according to the 2018 census (online supplemental method S1).¹⁶ The BMH is responsible for delivering and storing death certificates. To date, nine physicians are responsible for home-visits to establish a death certificate indicating the cause of death. The assignment of a cause of death is based on information provided by the family and available medical documentation. If the death occurred at the hospital, the family presents a death certificate signed by a clinician to the BMH. This hospital death certificate also indicates the presumed cause of death. For each death, the register includes the name of the deceased, date of birth, date of death, gender, address, place of death (hospital or home) and cause of death coded according to the International Classification of Diseases (ICD) (currently using the ICD 10th revision). In 2020 and 2021, COVID-19 deaths were coded as 'B97.2' or 'U07', following regulations set by WHO. For deaths that occurred in 2020 and 2021 within hospitals, the certificate also indicates the result of the COVID-19 test. Deaths at home were not tested but diagnosed according to clinical assessment by physicians and according to the epidemiological context. For the study period, we considered all death certificates stored at the BMH between 2016 and 2021. We also resorted to tabulations of deaths by age and sex from 1990 to 2015 to reconstruct trends in mortality over the period pre-pandemic.¹² Using the address of the deceased in the city of Antananarivo from registers of the BMH, we could restrict the analysis to residents of five of the six districts. The sixth district, Ambohimananarina, does not fall in the area covered by the BMH for historical reasons (online supplemental method S1).

Calculation of weekly excess deaths

To calculate weekly excess deaths, we considered calendar weeks (1–52nd) and assessed excess mortality in 2020 and 2021 as the percentage difference between the reported and the average expected number of deaths of the same week, using the relative change measure based on Farrington surveillance algorithm.¹⁷ First, the expected deaths were derived from the period 2016 to 2019, and the corresponding relative change was computed as the difference between the reported count and the upper bound of the 95% CI:

$$\text{Relative change (\%)} = \frac{\{\text{Reported deaths}\} - \{\text{Upper bound of expected deaths}\}}{\{\text{Upper bound of expected deaths}\}} * 100$$

A relative change of 100%, in a given week in 2020 (or 2021), would mean that the death count for that week was double from the expected death count. Based on

the upper bound of the baseline average weekly deaths during 2016–19, excess deaths were then assessed by considering weeks where relative change values were associated with significant positive excess of deaths. In order to classify these relative changes of excess deaths, their estimated values were split in <50% and ≥50% changes.

Second, two sensitivity analyses were performed: (1) to assess the appropriateness of using the relative change in deaths based on Farrington surveillance algorithm instead of the simpler method of relative change (P-scores), which may alter the estimate of excess mortality (online supplemental method S2)¹⁸ and (2) to remove the effects of the 2018–19 measles outbreak, which could have induced large excess mortality in the capital, especially among children and youth.⁶ To do so, for the second sensitivity analysis, weekly deaths were estimated to be the same as historical averages for the same week: using 2016–17 historical data for the October–December 2018 outbreak, and 2016–18 historical data for the January–March 2019 outbreak. Then, the relative changes—as described above—were recalculated considering these adjustments for the baseline years, 2016–19.

Cross-wavelet analyses

Cross-wavelet analyses were used to successively investigate associations between the time series of all-cause deaths over COVID-19 deaths (nationwide),⁸ and of SARS-CoV-2 positivity rate at the IPM laboratory⁹ over all-cause deaths (in Antananarivo). This method is useful for finding the frequency correlation between two non-stationary time series, combining time-frequency analyses and the statistical significance level of the relationships between lead and lag phases.¹⁹ It allows to characterise whether (i) changes in one time series follows or precedes similar changes in the other by a certain amount of time (ie, lead or lag), (ii) similar changes in both time series occur at the same time (ie, synchronous) or (iii) there is no association between the timing of changes in each of the time series. Here, the cross-wavelet analysis was performed twice for scaled time series according to each pair of comparisons of 2020–21 data: all-cause deaths in Antananarivo versus the registered COVID-19-related deaths in the whole country,⁸ and the SARS-CoV-2 positivity rate obtained from the virology unit of the IPM⁹ versus the all-cause deaths in Antananarivo. Using an appropriate combination of parameters, as detailed in the online supplemental method S3 (windows for time and period (scale) smoothing),¹⁹ these analyses can be used to infer the synchrony and association between two time series across time and period, providing wavelet coherence (the equivalent of the coefficient of determination in a statistical model) and phase-difference (angle).²⁰ Further details about the rescaled data and the wavelet analyses coherence and phase-difference can be found in the online supplemental method S3.

Calculation of trends in life expectancy

To construct annual life tables, the populations exposed to the risk of dying were reconstructed from the last three censuses of 1976, 1993 and 2018, assuming a constant rate of growth for each age segment, with growth rates estimated from the two intercensal periods and applied respectively to the periods 1975–1993 and 1993–2021. To calculate the life expectancy loss in 2020 and 2021 due to the COVID-19 pandemic, we projected mortality rates using the model by Lee and Carter and extrapolated the trends observed prepandemic, over the period 1990–2019.²¹ This model uses a singular value decomposition method to synthesise a matrix of logged age-specific mortality rates into three components: (1) an index k_t that reflects the level of mortality (all ages) and varies over time, (2) a general age schedule of mortality (a_x) and (3) a set of constants (b_x) that capture which rates change most rapidly in response to a change in k_t :

$$\log(m_{xt}) = a_x + b_x \cdot k_t + e_{xt}, \text{ where } e_{xt} \sim N(0, \sigma_e^2)$$

This model is widely used for mortality projections. The k_t index is extrapolated using an autoregressive integrated moving average process, while the other two components (a_x and b_x) are held constant; and e_{xt} is the residual at age x and time t . The difference between the observed life expectancy in 2020 and 2021 and the predicted values for these 2 years provided the number of years of life expectancy lost due to the pandemic, and prediction intervals around the life expectancy allowed us to establish whether the trend was significantly deviating from the recent past.

Second, differences in life expectancy at birth between 2019 and 2020–21 are an algebraic function of the differences in the underlying age-specific and cause-specific mortality rates.²² To compute the contribution of each age group and categories of causes of death to the life expectancy difference, we used a decomposition method designed by Arriaga.²³ We first decomposed the difference by age. Then, assuming that the distribution of deaths by cause is constant within each age group, we further disaggregated the contribution within each age group by cause of death, isolating the COVID-19 deaths from all other causes.

All calculations were performed using R statistical software.²⁴ WaveletComp R package was used to perform cross-wavelet coherence analyses.²⁰

Patient and public involvement

Patients and/or the public were not involved in the design, or conduct, or reporting, or dissemination plans of this research.

RESULTS

Temporal trends of crude all-cause mortality in Antananarivo

A total of 45 959 death records, notified to the BMH, were included in our study from 2016 to 2021. Death records averaged 143 (range=118–174) deaths per week during the four prepandemic years (2016–19) considered as our

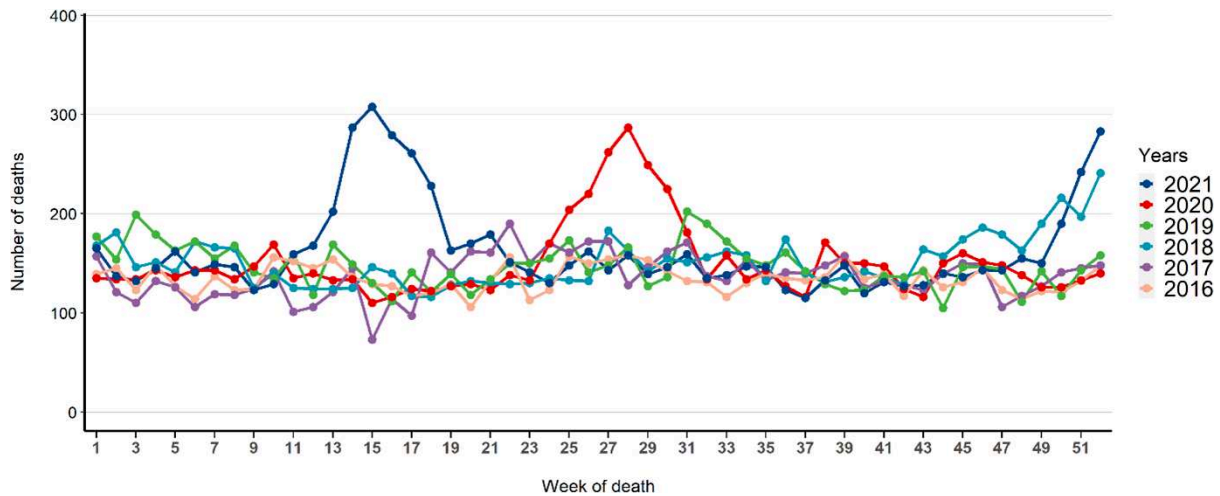


Figure 1 Temporal trends of all-cause crude mortality from 2016 to 2021 in the five central districts of Antananarivo (n=45 959).

baseline period. Before the COVID-19 pandemic period, waves with higher numbers of crude deaths were recorded at the end of 2018, reaching >200 weekly deaths during three consecutive weeks. The excess deaths observed in 2018 could be associated with the measles outbreak that affected the city during the last quarter of 2018.⁶ During the three successive waves of COVID-19, we observed higher peaks of deaths than in previous years, with >200 deaths in weeks 25–30 of 2020 and weeks 13–18 of 2021 as well as in the last weeks of 2021 (51 and 52) (figure 1 and online supplemental tables S1 and S2).

Excess mortality during the 2020–21 waves of COVID-19 infection in Antananarivo

A statistically significant increase in all-cause excess mortality was observed during 23 weeks in 2020 and 2021. During these weeks, we recorded 217 deaths per week on average, representing a 55.0% increase compared with 140 deaths per week over the same weeks during the baseline period (figure 2 and table 1). A total of 1179 all-cause excess deaths were assessed considering only significant relative change measures during the waves of COVID-19 in 2020 and 2021 in Antananarivo (table 1 and figure 2). Excess mortality of <50% was recorded during 9 and 8 weeks, corresponding to 244 and 222 excess deaths, respectively, in 2020 and 2021. In addition, excess deaths of 50% or greater, totalizing 195 and 518 deaths, were detected during 2 and 4 weeks in 2020 and 2021, respectively (table 1 and figure 2A). Normalised by the population size of the five districts of Antananarivo based on the general population census,¹⁶ the number of excess deaths were 38.51 and 64.91 per 100 000 inhabitants in 2020 and 2021, respectively. It is noteworthy that the positivity rate of SARS-CoV-2 virus was >25% during the same periods of the observed excess deaths with a peak reached 1 week before the peak of excess deaths in 2020 and 2021. Excess mortality was observed predominantly in adults aged 15–59 years and older adults aged 60 years and above. For these groups, the excess deaths

seemed to increase with age during the 2020 and 2021 waves of SARS-CoV-2 positivity (figure 2B and online supplemental figure S2). In children and adolescents <15 years, there were very few weeks with excess deaths.

Of note, by adjusting deaths during measles outbreaks (October 2018–March 2019)⁶ from our baseline years, a higher all-cause excess mortality was estimated during waves of COVID-19 in both 2020 and 2021 in Antananarivo: totalling 1500 deaths during 32 weeks (online supplemental figure S3 and online supplemental table S3). Furthermore, by avoiding thresholds in our calculation, all-cause excess mortality was observed during 51 weeks in 2020 (from 1% to 87%) and 2021 (from 2% to 158%)—totalling 2111 deaths and estimated at over 200% for the elderly (80+ years) for each wave (online supplemental figure S4).

Cross-wavelet coherence of SARS-CoV-2 positivity rate and death rate

SARS-CoV-2 test positivity rate by the IPM laboratory and all-cause death rate in Antananarivo, were in phase from June 2020 to September 2021 (online supplemental figure S1A, S1B, S1C, S1D); this was associated with a significant coherence level of ≥ 0.8 ($p < 0.05$), showing that changes in SARS-CoV-2 test positivity rate over time occurred at the same time as equivalent changes in all-cause deaths in Antananarivo during the first wave of COVID-19 (figure 2C). The death rate seemed to slightly precede the SARS-CoV-2 test positivity rate during the growth phase of the first wave of COVID-19, in June 2020.⁹ However, in the second wave of COVID-19, from February 2021 to May 2021, there was a significant lead in the SARS-CoV-2 positivity rate on the death rate (figure 3). In addition, in the first half of 2020, all-cause deaths in Antananarivo and national COVID-19 deaths were not in synchrony (ie, these two time series were out of phase); and the weekly national COVID-19 deaths preceded the Antananarivo deaths (online supplemental figure S3). However, from the second semester of 2020 to September

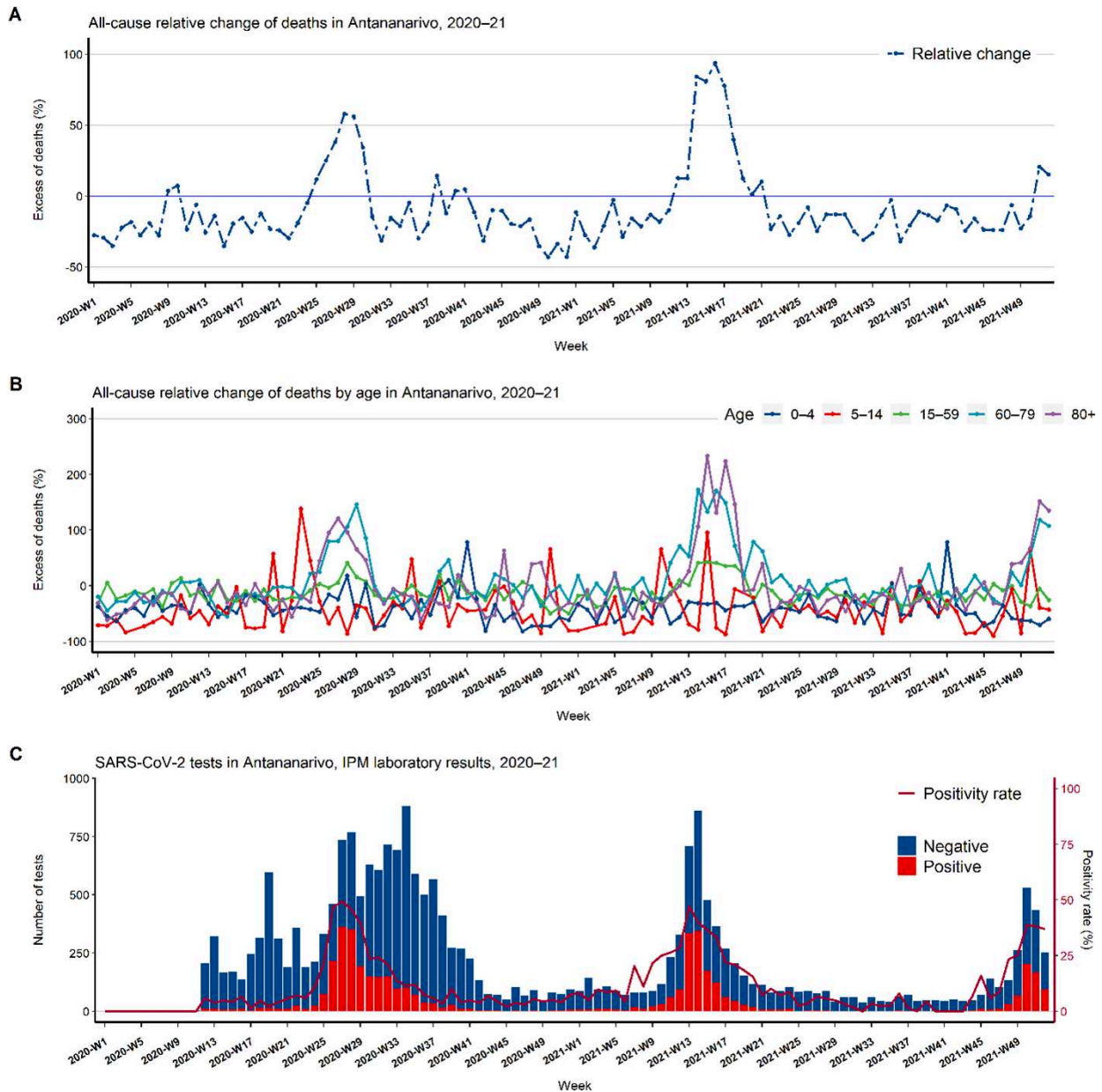


Figure 2 Weekly temporal trends, in five districts of Antananarivo from 2020 to 2021. (A) All-cause excess mortality using 2016–19 crude deaths as baseline years. (B) All-cause excess mortality by age group using 2016–19 crude deaths as baseline years (no death record was observed for age group 5–14 years during 1 week in 2020 and 2 weeks in 2021). (C) SARS-CoV-2 test results and positivity rates (data from the Institut Pasteur de Madagascar (IPM) for Antananarivo).⁹ Supplementary materials representing weekly all-cause deaths by age group (online supplemental table S1) and all-cause excess mortality by sex (online supplemental figure S2) support this figure.

2021, the all-cause deaths in Antananarivo were mainly in phase and preceded the national COVID-19 deaths, with a significant coherence level of ≥ 0.8 ($p < 0.05$), showing that changes in the weekly national COVID-19 deaths occurred at the same time as equivalent changes in all-cause deaths in Antananarivo from second semester of 2020 to September 2021. Additional result interpretations can be found in online supplemental method S3 and online supplemental figure S5.

Changes and differences in life expectancy

For both sexes, life expectancy at birth declined in 2021, compared with the recent past, but the year 2020

was in line with earlier years (figure 4). Male life expectancy has shown very little progress in the capital since 2004, hovering around 63–64 years. Projections (without COVID-19) placed the estimates for 2020 and 2021 at 63.4 and 63.6 years, respectively, compared with the observed values of 63.3 and 62.8. The life expectancy has thus been reduced by 0.1 and 0.8 years for men in 2020 and 2021, respectively. For women, progress has also been very modest since the mid-2000s, with life expectancy appearing to plateau at around 68–69 years. Projections were 68.8 years in 2020 and 69.0 years in 2021, compared with 68.9 and 68.0 observed in the context of

Table 1 Estimated all-cause excess mortality in 2020–21 using relative change and based on 2016–19 baseline of crude deaths data

Year	Relative change level (%)	Nb. of weeks of excess	Expected deaths (2016–19)		Reported deaths (2020–21)		Sum excesses death
			Mean	Range (minimum-maximum)	Mean	Sum	
2020	<50	9	144	128–164	188	1695	244
2020	≥100	2	148	142–154	268	536	195
2021	<50	8	141	123–174	204	1635	222
2021	≥100	4	125	118–139	284	1135	518
Total		23	140	118–174	217	5001	1179

Nb, number.

the pandemic. The levels are therefore virtually the same in 2020, while there is a 1-year drop in life expectancy in 2021. However, for both sexes, the observed drop in 2021 remains within the CIs around the projections, so life expectancy reduction associated with the COVID-19 is not statistically significant. The impact represented by COVID-19 on life expectancy was much smaller than the decline in life expectancy observed in the mid-1980s due to a resurgence of malaria and malnutrition.¹³

Table 2 displays the contributions by age to the differences in life expectancy between the observed life tables and the counterfactual life tables (based on extrapolating prepandemic rates). The contributions by age sum up to the difference in life expectancy at birth. For both sexes, mortality above age 60 years was higher than expected in

2020, with negative contributions of >1 year for men, but this unfavourable development was offset by a faster-than-expected mortality decline below age 60 years. In 2021, the same phenomenon is observed, but the increase in mortality between 60 and 80 years of age is greater. The risk of dying between the ages of 60 and 80 years is 16% higher than expected for women (+20% for men) and the mortality rate above 80 years is 14% higher (+44% for men).

As a result, favourable trends in mortality below the age of 60 years are no longer sufficient to compensate the excess mortality above the age of 60 years and life expectancy is reduced by 0.8 years for men and 1.02 years for women compared with expected levels. In other words, the loss of life expectancy in 2021 is explained exclusively

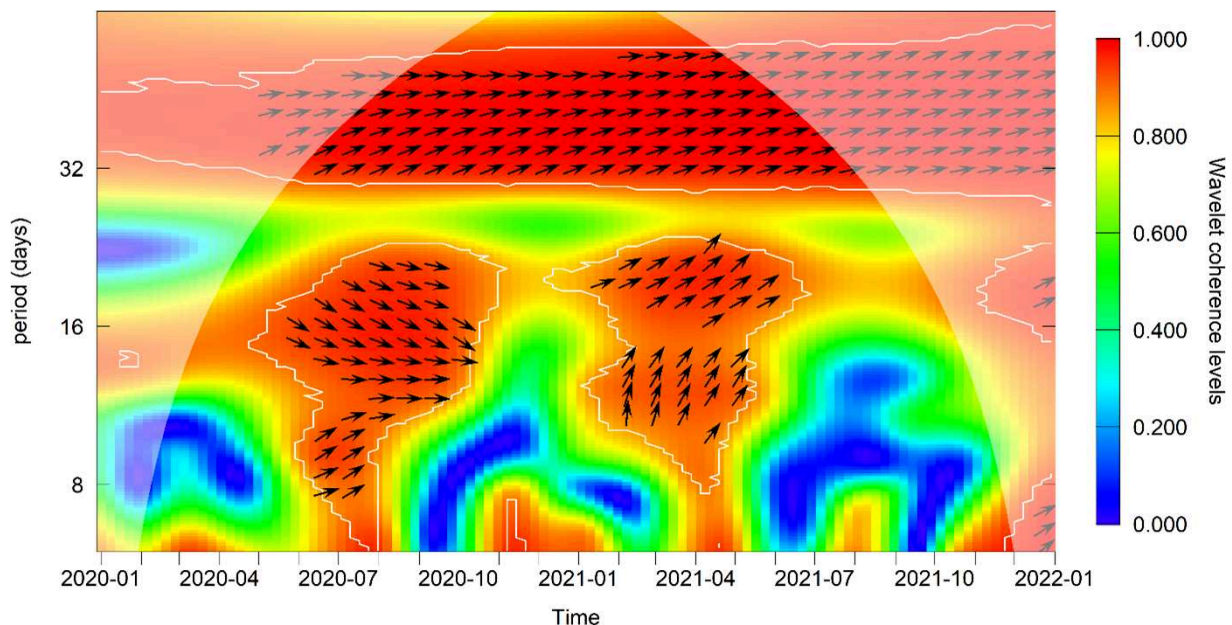


Figure 3 Cross-wavelet coherence and phase-difference of the SARS-CoV-2 positivity rate and all-cause death rate in Antananarivo. These two time series were in phase from June 2020 to September 2021 (phase-differences between 0 and $\frac{\pi}{2}$). During the first wave of COVID-19 (June 2020), the death rate seemed to lead the SARS-CoV-2 positivity rate (phase-differences $-\frac{\pi}{2}$ and 0). In the second wave (February 2021–May 2021), SARS-CoV-2 positivity rate significantly led the death rate (phase-differences between 0 and $\frac{\pi}{2}$). The significant coherence level is ranked from blue (0.0) to red (1.0) colour scale, and statistical significance is marked by the white contour plots, when $p < 0.05$. Supplementary materials representing all-causes deaths (online supplemental figure S1B) and SARS-CoV-2 tests positivity (online supplemental figure S1D), also online supplemental method S3 support the interpretation of this figure.

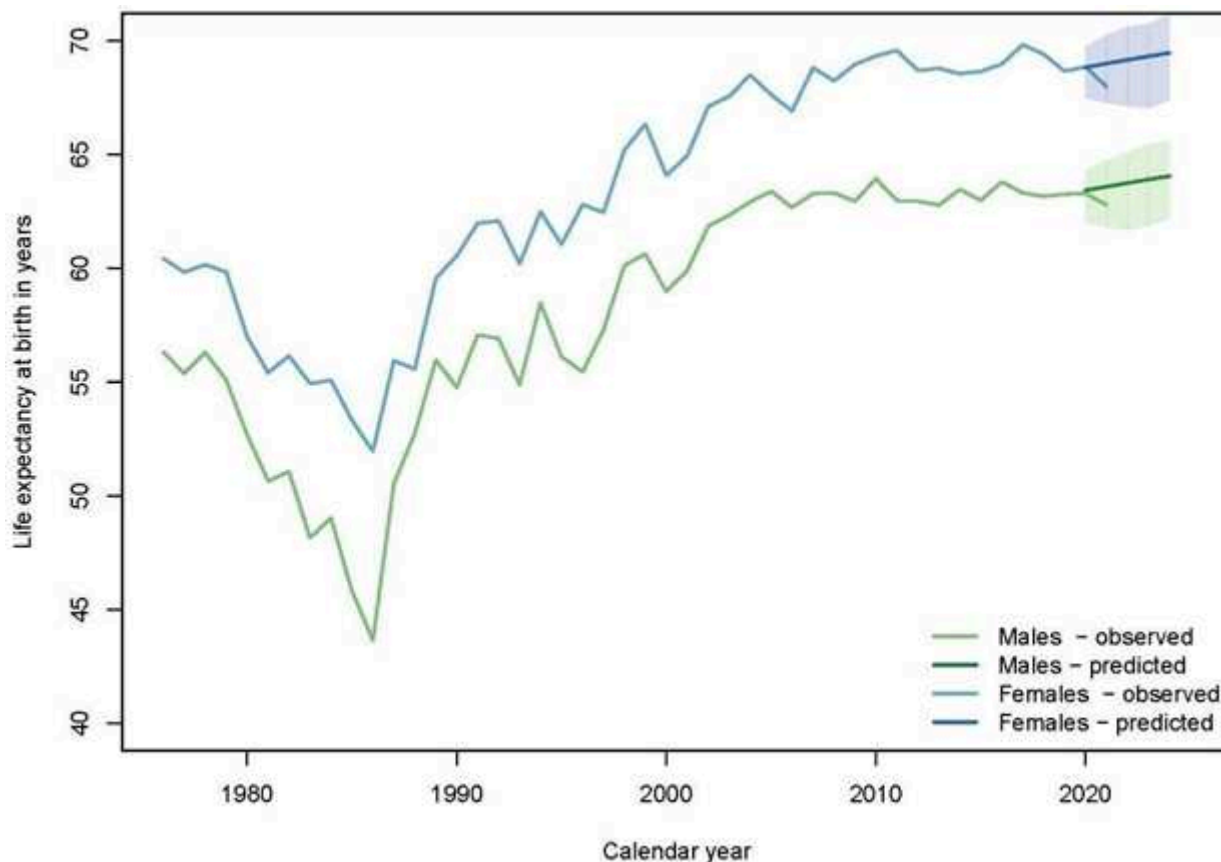


Figure 4 Observed and predicted life expectancy at birth in Antananarivo (1976–2021) for males (green) and females (blue). We projected to 2020–24, the observed life expectancy at birth and the predicted (bold) for both sexes based on the rates measured from 1990 to 2019.

by the sharp increase in a risk of dying above the age of 60 years. In children, youth or adults aged 15–59 years, the various direct or indirect effects of the pandemic (lockdowns, reductions in intervention coverage, etc) did not result in a loss in life expectancy.

We further decomposed the differences in life expectancy at birth between 2019 and 2020, and between 2020 and 2021, by the contribution of different age groups and two categories of causes of death: deaths identified as COVID-19 and all other deaths. From 2020 to 2021, the increase in mortality over age 60 years is attributable to deaths identified as COVID-19 and non-COVID-19 deaths (online supplemental figure S6). Between 2020 and 2021, more years are lost due to the increase in COVID-19-related mortality, for both sexes. The loss of years of life expectancy is concentrated in the 60–79 years age group, with little change in women in non-COVID-19 mortality. Among men, mortality in the age group 35–59 years from non-COVID-19 mortality seems to have improved when compared with 2020, but this could also reflect a more systematic coding of deaths as COVID-19 related (online supplemental table S4).

DISCUSSION

After over three and a half years since the beginning of the pandemic, the mortality burden due to COVID-19

across sub-Saharan Africa remains difficult to quantify. Taking advantage of a longstanding, rigorous death registration system from the city of Antananarivo, our study found several peaks of excess deaths in 2020–21, which were associated significantly with the waves of SARS-CoV-2 reported cases. By comparing trends during the prepandemic period (2016–19) and the pandemic one (2020–21), we estimated that all-cause excess mortality was 38.5 and 64.9 per 100 000 inhabitants in 2020 and 2021, respectively. Excess mortality reached over 50% during both the 2020 and 2021 waves. In sum, we estimated that there were 1179 excess deaths over the 2020–21 period, an estimate which is higher than the official 1069 COVID-19 deaths notified by the MoH for the entire country.⁸ The excess was even higher (1500) when excluding the excess deaths associated with the 2018–19 measles outbreaks, and twofold (2111) when no threshold was included in our calculation of relative change. This excess mortality resulted in a decline in life expectancy of 0.8 years in men and 1.0 years in women in 2021 but this decline is non-significant. The reduction in life expectancy was entirely attributable to increased risks of dying for both men and women above the age of 60 years and due to COVID-19 deaths rather than due to increases in other causes of death.

Table 2 Life expectancy at birth observed in 2019–21, predicted for 2020–21 based on past trends, in the absence of COVID-19, and decomposition of the differences in life expectancy at birth between the observed and predicted estimates

	Observed			Predicted based on 1990–2019		Difference in e0 and contribution in difference by age*	
	2019	2020	2021	2020	2021	2020	2021
Life expectancy at birth (years)							
Male	63.3	63.3	62.8	63.4	63.6	-0.14	-0.80
Female	68.7	68.9	68.0	68.8	69.0	0.03	-1.02
Under-five mortality (5q0—‰)							
Male	40	34	32	45	43	0.76	0.77
Female	38	30	29	39	37	0.58	0.59
Mortality in older children and adolescents (10q5—‰)							
Male	8	7	5	8	8	0.04	0.12
Female	8	4	5	6	6	0.10	0.03
Premature adult mortality ($_{45}q_{15}$ —‰)							
Male	314	314	306	316	316	0.15	0.42
Female	199	201	208	204	204	0.10	-0.04
Old-age mortality ($_{20}q_{60}$ —‰)							
Male	637	683	754	629	627	-0.94	-1.83
Female	517	543	592	513	509	-0.67	-1.38
Mortality rate above age 80 ($_{80}m_{\infty}$ —‰)							
Male	187	200	251	174	174	-0.16	-0.29
Female	170	182	199	174	174	-0.08	-0.22

*The last two columns display the difference in life expectancy at birth between the observed and expected values (in years), and these differences are decomposed into the contributions of the different age-specific rates, using the method by Arriaga.²³ Positive values in these last two columns refer to a decline in mortality, which was faster than expected based on trends in 1990–2019, while negative values refer to a slower progress than expected, or even an increase in mortality, possibly due to COVID-19 deaths.

Interestingly, the death rate mainly preceded the SARS-CoV-2 positivity rate during the first wave of SARS-CoV-2, which may indicate an ‘unsuitable’ screening strategy and the use of a case definition^{9 25} for suspected cases where MoH and WHO guidelines differed.²⁶ This may have led to a mismatch between waves because only few ‘true suspected cases’ were tested. In the second wave of COVID-19 (February–May 2021), the SARS-CoV-2 positivity rate preceded the waves of deaths. This may indicate an improvement in the screening strategy, enabling strong synchrony between laboratory data and virus circulation in Antananarivo, as previously found by Andriamandimby *et al.*²⁵ Indeed, the National Influenza Centre at IPM continued to receive specimens for influenza in 2020 and 2021 and laboratory tests showed no circulation of influenza viruses from March 2020 to mid-July 2021.²⁷ Our results also revealed that in the first half of 2020, the all-cause deaths in Antananarivo and national COVID-19 deaths were not synchronous. This may be explained by the fact that the first large SARS-CoV-2 outbreak occurred in the second highest populated city of Madagascar (Toamasina) in May 2020, followed a few weeks later by a major outbreak in Antananarivo (June 2020).^{9 25}

In the capital city of Antananarivo, we estimated an excess mortality of 38.51 and 64.91 per 100 000 inhabitants

in 2020 and 2021, respectively. These estimates are lower than estimates for Madagascar in a worldwide study using covariates pertaining both to the COVID-19 pandemic and to country-specific health-related metrics (125.4 per 100 000 inhabitants).²⁷ At the level of sub-Saharan African countries, this excess death is comparable to the excess death estimated for Eritrea, Burkina Faso and Ghana.²⁷ Compared with previous crises that have hit the capital city of Madagascar, the mortality shock observed in 2020–21 is less pronounced than other major crisis that have hit Antananarivo before, such as the urban famine and the resurgence of malaria in the mid-1980s. When comparing with the excess death in Antananarivo that occurred during the A(H1N1) pandemic in 2009, a similar impact on elderly people was observed.¹⁴

Our study is among the first to assess the impact of COVID-19 on the life expectancy of a sub-Saharan African population, based on local death registration systems. In contrast to many high-income countries, where reductions of more than an entire year of life expectancy at birth have been documented in 2020,²⁸ we found almost no change for that year (-0.14 for men and +0.03 for women). A faster decline in mortality before age 60 years than expected based on past trends could have offset the unfavourable evolution of mortality beyond age 60 years.

Countries where life expectancy at birth has decreased considerably include Russia, the USA, Italy and Spain²⁹; where populations are older and where baseline mortality rates are much lower in comparison with African populations. Mortality in Madagascar is still highly concentrated in the youngest age groups, and life expectancy remains dominated by variations in the chances of survival among children. Yet, the year 2021 was characterised by a 16% increase in the probability of dying between the ages of 60 and 80 years for women and a 20% increase for men in Antananarivo. The mortality rate over the age of 80 years increased by 14% for women and 44% for men. As observed elsewhere,³⁰ men appeared to have been more affected by the COVID-19 epidemic than women.

Compared with previous years, the excess mortality in Antananarivo was higher in 2021, reaching over 100% for 4 weeks. As a result, a substantial decrease in life expectancy at birth was observed, dropping by 0.8 and 1.0 years below the projected value for males and females, respectively. A similar situation was observed in Brazil where a decline in 2020 life expectancy at birth was estimated at 1.3 years in 2020 vs 1.8 years in the first 4 months of 2021.³¹ Several countries in Eastern Europe and the USA also witnessed sustained loss in life expectancy in 2021.³² Data on the impact of COVID-19 on life expectancy in other sub-Saharan African countries are needed to compare these estimates and shed light on the timing of the mortality shock in this region.

Our results highlight the granularity of Antananarivo's BMH death records as a powerful source to assess the burden of infectious diseases and the strengths and weaknesses of the Malagasy health system to face major threats such as the COVID-19 pandemic. Indeed, the estimated excess mortality in 2020 and 2021 could be due to the difficulty of finding intensive care unit beds for severe infections,³³ with mechanical ventilators and trained personnel, in addition to frequent disruptions in electricity supply observed regularly in LMICs.³⁴ The SARS-CoV-2 Beta variant (B.1.351) circulated in Madagascar from February 2021, preceding the beginning of the peak of mortality in 2021. Results from blood donors confirmed the contribution of this variant in the second COVID-19 wave that started in early 2021.³⁵ The Alpha, Beta and Delta variants of concern were known to be more transmissible and having caused more severe infections than the ancestral SARS-CoV-2.³⁶ In Qatar, patients infected with the Beta variant had an increased risk of progressing to severe disease and death compared with patients infected with the Alpha variant (B.1.1.7).³⁷ This could explain the higher excess of death observed in our study during the second wave when compared with the first one, combined with a vaccination strategy that was not effective at this time.³⁸ Optimal monitoring of variants and more studies on their severity and virulence in the general population are needed to better understand their burden.

Our study has some limitations. First, the Ambohidratrimo district—where the referral centre for severe

COVID-19 infections has been established at the Centre Hospitalier Universitaire Anosiala since 8 July 2020, totaling 442 244 inhabitants according to the 2018 census,¹⁶ does not fall in the six central districts of Antananarivo city nor the area covered by the BMH.³⁹ This may have led to an underestimation of excess mortality using BMH data; although all deaths that occurred among residents of the five central districts should be reported to the BMH, irrespective of the place of the occurrence of the death. Moreover, during the first waves of the pandemic, the virology unit at IPM was mainly focused on the diagnosis of SARS-CoV-2 due to logistic constraints and a lack of human resources, and this may have resulted in an underdiagnosis of other respiratory viral infections responsible for other causes of death. Similarly, a decrease in consultations was observed at health centres during the first and second waves of the pandemic,⁴⁰ which resulted in an under-reporting of other infectious diseases. Second, in our analysis, the estimation of excess mortality focused on the weeks when the excesses were most evident—using Farrington surveillance algorithm,¹⁷ which may induce an underestimation of mortality excess versus relative change method based on of P-scores.¹⁸ The comparison of our results with those of other countries may be biased because of this methodological choice. In other studies, negative binomial or Poisson regression modelling combined with Bayesian approaches or ensemble modelling techniques have been commonly used.^{1 7 27} In addition, between 2016 and 2020, Madagascar experienced other epidemics such as plague and measles that could have had an impact on the mortality of the population of Antananarivo.^{5 6} These epidemics raise our baseline mortality, although we also conducted a sensitivity analysis based on the average number of deaths per week during the pre-COVID-19 period without such peaks, revealing more excesses during the pandemic period.

CONCLUSION

Our findings indicate that the mortality burden of the COVID-19 pandemic in Antananarivo has been much higher than previously estimated, with excess deaths for the capital city being higher than the official count of COVID-19-related deaths for the entire country. The excess mortality was concentrated in older adults, with little impact on mortality among children and young adults. Our study also highlights the importance of local sources of death notification and the need to expand this system to other major cities in the country and use it for real-time surveillance to inform health policy makers. Strengthening local death registration systems in LMICs would allow more precise monitoring of changes in cause-specific mortality associated with COVID-19 and other potential future pandemics.

Author affiliations

¹Institut Pasteur de Madagascar, Antananarivo, Madagascar

²UMMISCO, Bondy, France

³Université Catholique de Louvain Centre de recherche en démographie et sociétés, Louvain la neuve, Belgium

⁴Bureau Municipal d'Hygiène, Commune Urbaine d'Antananarivo, Antananarivo, Madagascar

⁵UMR 224 MIVEGEC, IRD, Montpellier, France

⁶Department of Ecology and Evolutionary Biology, Princeton University, Princeton, New Jersey, USA

⁷Mahaliana Labs SARL, Antananarivo, Madagascar

⁸Institut Pasteur de Dakar, Dakar, Senegal

Twitter C Jessica Metcalf @CJEMetcalf and Jean-Michel Heraud @HeraudJeanMich

Acknowledgements The authors would like to acknowledge the BMH team in the Department of Water, Sanitation and Hygiene and the City of Antananarivo for their support and cooperation in data collection. We thank all involved team members from the Virology and Epidemiology and clinical research units (Mangahasimbola Reziky, Nasolo Frédéric Stanley, Randrianarivony Mamy Thomas desire) at IPM.

Contributors Conceptualisation: JHR, JMR, RR, BM, AD and J-MH. Data curation: JHR, JMR, RR and BM. Formal analysis: JMR and BM. Funding acquisition: RR, BM and J-MH. Methodology: JMR, RR, BM, AG and CJM. Project administration: JHR, AMR, VL, J-MH and PD. Resources: FR, NHR and SFA. Software and visualisation: JMR and BM. Supervision: RR, AG, VL, J-MH and PD. Writing—original draft: JMR, RR, BM, AD and JHR. Writing—review and editing: all authors contributed equally and accept final responsibility to submit for publication. JHR, JMR and BM had full access to the study data. Author acting as guarantor: PD.

Funding This work was supported by the Institut Pasteur de Madagascar (IPM), the Princeton Centre for Health and Wellbeing, the US Centers for Disease Control and Prevention (Cooperative Agreement Number: U51IP000812) and the US Agency for International Development, for Research, Innovation, Surveillance and Evaluation (RISE) Project Cooperative Agreement no. 72068719CA00001.

Disclaimer The funders had no role in study design, data collection and analysis, decision to publish or preparation of the manuscript.

Competing interests None declared.

Patient and public involvement Patients and/or the public were not involved in the design, or conduct, or reporting, or dissemination plans of this research.

Patient consent for publication Not applicable.

Provenance and peer review Not commissioned; externally peer reviewed.

Data availability statement Data are available on reasonable request.

Supplemental material This content has been supplied by the author(s). It has not been vetted by BMJ Publishing Group Limited (BMJ) and may not have been peer-reviewed. Any opinions or recommendations discussed are solely those of the author(s) and are not endorsed by BMJ. BMJ disclaims all liability and responsibility arising from any reliance placed on the content. Where the content includes any translated material, BMJ does not warrant the accuracy and reliability of the translations (including but not limited to local regulations, clinical guidelines, terminology, drug names and drug dosages), and is not responsible for any error and/or omissions arising from translation and adaptation or otherwise.

Open access This is an open access article distributed in accordance with the Creative Commons Attribution 4.0 Unported (CC BY 4.0) license, which permits others to copy, redistribute, remix, transform and build upon this work for any purpose, provided the original work is properly cited, a link to the licence is given, and indication of whether changes were made. See: <https://creativecommons.org/licenses/by/4.0/>.

Author note J-MH and PD authors supervised this work equally.

ORCID iDs

Jean Marius Rakotondramanga <http://orcid.org/0000-0003-0490-7665>

Andres Garchitorena <http://orcid.org/0000-0001-6225-5226>

C Jessica Metcalf <http://orcid.org/0000-0003-3166-7521>

Jean-Michel Heraud <http://orcid.org/0000-0003-1107-0859>

REFERENCES

- Scortichini M, Schneider Dos Santos R, De' Donato F, *et al*. Excess mortality during the COVID-19 outbreak in Italy: a two-stage interrupted time-series analysis. *Int J Epidemiol* 2021;49:1909–17.
- Sharrow D, Hug L, You D, *et al*. Global, regional, and national trends in Under-5 mortality between 1990 and 2019 with scenario-based projections until 2030: a systematic analysis by the UN inter-agency group for child mortality estimation. *Lancet Glob Health* 2022;10:e195–206.
- Barmania S. Madagascar's health challenges. *Lancet* 2015;386:729–30.
- Lang E, Saint-Firmin P, Olivett M, *et al*. Analyse Du Système de Financement de la Santé À Madagascar pour Guider de futures Réformes, Notamment La CSU. Washington, DC. 2018.
- Randremanana R, Andrianaivoarimananana V, Nikolay B, *et al*. Epidemiological characteristics of an urban plague epidemic in Madagascar, August–November, 2017: an outbreak report. *Lancet Infect Dis* 2019;19:537–45.
- Nimpa MM, Andrianirinarison JC, Sodjinou VD, *et al*. Measles outbreak in 2018–2019, Madagascar: epidemiology and public health implications. *Pan Afr Med J* 2020;35:84.
- Msemburi W, Karlinsky A, Knutson V, *et al*. The WHO estimates of excess mortality associated with the COVID-19 pandemic. *Nat* 2022;2022:1–8.
- Kiraevev SR, Mathieu E, Siemens F, *et al*. Lanthanide(III) complexes of Cyclen Triacetates and Triamides bearing tertiary amide-linked antennae. *Molecules* 2020;25:5282.
- Randremanana RV, Andriamandimby S, Rakotondramanga JM, *et al*. The COVID-19 epidemic in Madagascar: clinical description and laboratory results of the first wave, March–September 2020. *Influenza Other Respi Viruses* 2021;15:457–68. 10.1111/irv.12845 Available: <https://onlinelibrary.wiley.com/doi/10.1111/irv.12845>
- Benn CS, Salinha A, Mendes S, *et al*. SARS-Cov-2 Serosurvey among adults involved in Healthcare and health research in guinea-Bissau, West Africa. *Public Health* 2022;203:19–22.
- Mwananyanda L, Gill CJ, MacLeod W, *et al*. Covid-19 deaths in Africa: prospective systematic postmortem surveillance study. *BMJ* 2021;372:n334.
- Masquelier B, Pison G, Rakotonirina J, *et al*. Estimating cause-specific mortality in Madagascar: an evaluation of death notification data from the capital city. *Popul Health Metr* 2019;17:8.
- Waltisperger D, Mesle F, Mandelbaum J. Economic crisis and mortality: the case of Antananarivo, 1976–2000. *Population (English Edition, 2002-)* 2005;60:199.
- Rajatonirina S, Rakotosolobo B, Rakotomanana F, *et al*. Excess mortality associated with the 2009 A(H1N1)V influenza pandemic in Antananarivo, Madagascar. *Epidemiol Infect* 2013;141:745–50.
- Rasambainarivo F, Rasaoanomenjanahary A, Rabarison JH, *et al*. Monitoring for outbreak-associated excess mortality in an African city: detection limits in Antananarivo, Madagascar. *Int J Infect Dis* 2021;103:338–42.
- Institut National de la Statistique. Troisième Recensement général de la population et de l'habitation (Rgph-3). 2021. Available: <https://www.instat.mg/p/resultats-definitifs-du-rgph-3-2018-troisieme-recensement-general-de-la-population-et-de-lhabitation>
- Noufaily A, Enki DG, Farrington P, *et al*. An improved algorithm for outbreak detection in multiple surveillance systems. *Stat Med* 2013;32:1206–22.
- Serfling RE. Methods for current statistical analysis of excess pneumonia-influenza deaths. *Public Health Rep (1896)* 1963;78:494:494–506.:
- Cazelles B, Chavez M, Berteaux D, *et al*. Wavelet analysis of ecological time series. *Oecologia* 2008;156:287–304.
- Roesch A, Schmidbauer H. *WaveletComp: computational wavelet analysis*. 2018.
- Lee RD, Carter LR. Modeling and forecasting U. S. mortality. *J Am Stat Assoc* 1992;87:659.
- Auger N, Feuillet P, Martel S, *et al*. Mortality inequality in populations with equal life expectancy: Arriaga's decomposition method in SAS, STATA, and excel. *Ann Epidemiol* 2014;24:575–80.
- Arriaga EE. Measuring and explaining the change in life expectancies. *Demography* 1984;21:83–96.
- R Core Team. R: A language and environment for statistical computing. 2020. Available: <https://www.r-project.org/>
- Andriamandimby SF, Brook CE, Razanajatovo N, *et al*. Cross-sectional cycle threshold values reflect epidemic Dynamics of COVID-19 in Madagascar. *Epidemics* 2022;38:100533.
- WHO COVID-19: case definitions. 2020. Available: https://apps.who.int/iris/bitstream/handle/10665/333912/WHO-2019-nCoV-Surveillance_Case_Definition-20201-eng.pdf?sequence=1&isAllowed=y
- Wang H, Paulson KR, Pease SA, *et al*. Estimating excess mortality due to the COVID-19 pandemic: a systematic analysis of COVID-19-related mortality, 2020–21. *The Lancet* 2022;399:1513–36.

- 28 Aburto JM, Schöley J, Kashnitsky I, *et al.* Quantifying impacts of the COVID-19 pandemic through life-expectancy losses: a population-level study of 29 countries. *Int J Epidemiol* 2022;51:63–74.
- 29 Islam N, Shkolnikov VM, Acosta RJ, *et al.* Excess deaths associated with COVID-19 pandemic in 2020: age and sex Disaggregated time series analysis in 29 high income countries. *BMJ* 2021;373:n1137.
- 30 Gebhard C, Regitz-Zagrosek V, Neuhauser HK, *et al.* Impact of sex and gender on COVID-19 outcomes in Europe. *Biol Sex Differ* 2020;11:29:29..
- 31 Castro MC, Gurzenda S, Turra CM, *et al.* Reduction in life expectancy in Brazil after COVID-19. *Nat Med* 2021;27:1629–35.
- 32 Schöley J, Aburto JM, Kashnitsky I, *et al.* Life expectancy changes since COVID-19. *Nat Hum Behav* 2022;6:1649–59.
- 33 Madagascar Government. National health emergency. 2021. Available: <https://www.presidence.gov.mg/actualites/conseil-des-ministres/1201-tatitry-ny-filan-kevity-ny-minisitra-natao-tamin-ny-alalan-ny-visioconference-ny-31-martsa-2021.html>
- 34 Gallifant J, Sharell D, Hashmi M, *et al.* Mechanical ventilators for Low- and middle-income countries: informing a context-specific and sustainable design. *Br J Anaesth* 2022;128:e279–81.
- 35 Razafimahatratra SL, Ndiaye MDB, Rasoloharimanana LT, *et al.* Seroprevalence of ancestral and beta SARS-Cov-2 antibodies in Malagasy blood donors. *Lancet Glob Health* 2021;9:e1363–4.
- 36 Davies NG, Jarvis CI, Edmunds WJ, *et al.* Increased mortality in community-tested cases of SARS-Cov-2 lineage B.1.1.7. *Nature* 2021;593:270–4.
- 37 Abu-Raddad LJ, Chemaitelly H, Ayoub HH, *et al.* Severity, Criticality, and fatality of the severe acute respiratory syndrome Coronavirus 2 (SARS-Cov-2) beta variant. *Clin Infect Dis* 2022;75:e1188–91.
- 38 Rasambainarivo F, Ramiadantsoa T, Raherinandrasana A, *et al.* Prioritizing COVID-19 vaccination efforts and dose allocation within Madagascar. *BMC Public Health* 2022;22:1–9.
- 39 Madagascar Government. TATITRY NY FILANKEVITRY NY MINISITRA NATAO TAMIN'NY ALALAN'NY « VISIOCONFERENCE » NY 08 JOLAY 2020. Cons. des Minist. 2020. Available: <https://www.presidence.gov.mg/actualites/conseil-des-ministres/907-tatitry-ny-filankevity-ny-minisitra-natao-tamin-ny-alalan-ny-visioconference-ny-08-jolay-2020.html>
- 40 Rasoanaivo TF, Bourner J, Randriamparany RN, *et al.* The impact of COVID-19 on clinical research for neglected tropical diseases (Ntds): A case study of Bubonic plague. *PLoS Negl Trop Dis* 2021;15:e0010064.

5 Synthèse et Discussion

Ce travail de thèse a passé en revue l'utilisation de la modélisation statistique et mathématique pour mieux comprendre les dynamiques de deux systèmes biologiques, le paludisme et le COVID-19 à Madagascar. La fragilité du système de surveillance passive, appelée ici porosité, est le résultat du niveau très faible d'accès aux soins et du faible système de santé à Madagascar. Ces facteurs laissent ainsi une grande majorité des cas infectieux ni diagnostiqués ni traités, et peuvent même mener à des manquements dans le système de registre municipal de décès quand les décès surviennent au niveau communautaire. Dans ce contexte, cette thèse a proposé des approches de modélisation biostatistique et biomathématiques permettant une meilleure utilisation des mesures indirectes de transmission, comme l'anticorps au *P. falciparum* dans les zones de faible transmission des hautes terres centrales pour le paludisme, et l'excès de mortalité toutes causes pendant la pandémie de COVID-19 à Antananarivo.

5.1 Contributions à la compréhension du paludisme à Madagascar

En utilisant les données d'une enquête transversale sérologique en milieu scolaire menée en 2014 dans sept districts des HTC et les marges environnantes (Steinhardt et al., 2021), l'étude du **Chapitre 1** a caractérisé l'hétérogénéité spatiale de transmission du paludisme et détecté des points chauds de la prévalence d'infection à *P. falciparum* et de l'exposition (mesure d'anticorps PfAMA1). Cette étude a permis d'identifier les facteurs sociodémographiques, climatiques et environnementaux associés à cette hétérogénéité. Ces facteurs n'avaient pas été mis en avant par Steinhardt *et al.* (Steinhardt et al., 2021).

5.1.1 Niveau de connaissance sur l'hétérogénéité de la transmission résiduelle

L'hétérogénéité spatiale de la prévalence de l'infection plasmodiale et de la séroprévalence de l'anticorps PfAMA1 dans des zones visées à l'élimination a été confirmée à travers les sites de l'étude du **Chapitre 1**. Malgré le faible niveau de transmission, l'étude a révélé un nombre important de points chauds de séroprévalence dans les districts de la partie nord et sud des HTC de Madagascar et ses marges, en accord avec une étude sérologique précédente menée à Madagascar (Razakandrainibe et al., 2009). Des hétérogénéités similaires de la transmission du paludisme ont été trouvées en utilisant des données de surveillance de routine entre districts dans la marge ouest des hautes terres (Howes et al., 2016; Felana A. Ihantamalala et al., 2018). D'autres études menées à des échelles spatiales plus fines que celles disponibles par les données de surveillance de routine ont confirmé que les hétérogénéités trouvées au niveau national et sub-national (région, district) persistent à au sein de chaque district (fokontany, localité) (Pourtois et al., 2023; Rice, Golden, et al., 2021).

Dans cette étude, deux facteurs associés à l'exposition cumulative à *P. falciparum* au niveau du fokontany et au niveau individuel étaient respectivement le niveau de prévalence de l'infection à *P. falciparum* par TDR et le fait d'avoir eu de la fièvre au cours des deux semaines précédant l'enquête. Cette corrélation entre le TDR et la réponses d'anticorps PfAMA1 suggère que les TDR conventionnels peuvent encore être utilisés dans les zones visant l'élimination, en particulier dans les zones à forte densité d'infections qui ne sont pas en mesure d'assumer les coûts opérationnels supplémentaires des études sérologiques (Okell et al., 2009; Okell,

Bousema, et al., 2012). Effectivement, d'autres études sont nécessaires pour mieux comprendre le rapport coût-efficacité de techniques de diagnostic plus précises pour les infections à faible densité, telles que la PCR (Bousema et al., 2014).

5.1.2 Comportements d'hôte, exposition aux vecteurs, et recours aux soins

Barrières géographiques, recours aux soins, et prise en charge des cas

Les enfants souffrant d'obstacles géographiques à l'accès aux soins, qui vivaient à plus de 5 km des établissements de santé (environ un tiers de la population étudiée) étaient significativement plus exposés à *P. falciparum*. Cela pourrait avoir des implications importantes pour les efforts d'élimination du paludisme dans ces zones. Ces résultats suggèrent que le dépistage et le traitement sous-optimaux des infections plasmodiales dans ces régions, en raison des obstacles géographiques à l'accès aux soins (Felana Angella Ihantamalala et al., 2021), pourraient entraîner des poches de transmission du paludisme non détectées en compromettant les objectifs d'élimination du PNLP. En effet, le PNLP avait ciblé cinq districts des hautes terres pour l'élimination du paludisme, avec l'objectif d'atteindre zéro décès et d'étendre le nombre de districts ciblés pour l'élimination de 5 (en 2018) à 13 (en 2022), principalement dans les HTC et ses marges (Direction de Lutte contre le Paludisme, 2017). La persistance des barrières géographiques dans l'accès aux soins a été décrite dans de nombreux contextes, y compris dans les zones rurales de Madagascar (Andres Garchitorena et al., 2021), avec une diminution exponentielle de l'utilisation des formations sanitaires après les 5 premiers kilomètres. Bien que des études précédentes ont montré l'impact de ces barrières géographiques sur la prise en charge du paludisme et la performance du système de surveillance à Madagascar (Hyde et al., 2021; Sayre et al., 2021), notre étude est l'une des premières à montrer que ce type de barrières a un impact significatif sur les efforts d'élimination mis en place par le PNLP.

Les programmes de santé communautaire peuvent être un moyen efficace d'éliminer ces barrières géographiques liées à l'accès aux soins (World Health Organization (WHO), 2012), puisque deux agents de santé communautaire sont présents dans chaque fokontany d'après les recommandations nationales, indépendamment de la distance qui les sépare d'une formation sanitaire. Par contre, les directives nationales mises en place ces dernières années pour la prise en charge communautaire des cas de paludisme ne ciblaient que les enfants de moins de 5 ans, le groupe le plus exposé au risque de mortalité lié aux infections palustres. Pourtant, dans notre étude du **Chapitre 1**, ce groupe s'est avéré être le moins exposé à *P. falciparum* (avec zéro

séropositivité à la réponse d'anticorps PfAMA1) ; mais notre étude peut ne pas être représentative de ce groupe d'âge. Car l'étude était seulement limitée aux enfants en âge d'aller à l'école ; et dans les zones rurales de Madagascar, les enfants commencent généralement à aller à l'école à l'âge de 5 ans. Aussi, une sous-analyse des facteurs associés à l'exposition des enfants ≤ 5 ans (séroprévalence = 2,6% [5/194]) a suggéré l'absence de l'obstacle lié à la distance des formations sanitaires. Cela peut indiquer une meilleure gestion des cas de cette catégorie de population, mais pourrait également être dû à la petite taille des échantillons pour ce groupe ($n = 194$).

La stratégie nationale de la prise en charge communautaire des cas de paludisme, qui laissait de côté la grande majorité de la population, est en train d'être étendue à tous les âges à Madagascar, ce qui pourrait donc être un tournant majeur pour aider à traiter les cas symptomatiques de paludisme dans ces poches de transmission (Sayre et al., 2021), et ainsi accélérer les efforts d'élimination dans les hautes terres (U. S. President's Malaria Initiative Madagascar, 2020).

Différences d'exposition et d'infection entre classes d'âge

Au niveau individuel, le risque d'exposition à *P. falciparum* augmente avec l'âge, ce qui pourrait être dû à l'exposition répétée des enfants aux piqûres d'anophèles femelles infectantes. Ces enfants plus âgés pourraient acquérir ainsi une composante à longue durée de vie de la réponse d'anticorps. En effet, selon l'étude de Stanisic *et al.*, les réponses d'anticorps pourraient être stimulées par des infections actives à *P. falciparum* au fur et à mesure que les enfants grandissent, ce qui est similaire aux zones endémiques pouvant permettre de caractériser l'hétérogénéité spatiale de l'exposition (Stanisic et al., 2015).

En outre, le comportement et l'accès aux mesures de protection peuvent varier selon les groupes d'âge : étant donné que les stratégies de lutte contre le paludisme ciblent les enfants de moins de 5 ans et les femmes enceintes, les adolescents peuvent être plus exposés. D'autres facteurs pourraient expliquer cette différence d'exposition (Bernard et al., 2009; Korenromp et al., 2003; Kulkarni et al., 2010). Des études précédentes ont montré que adolescents passaient plus de temps à l'extérieur le soir, lorsque les taux de piqûres d'*Anopheles spp* sont typiquement plus élevés, ce qui les expose à un risque plus élevé d'être piqués par un moustique infectant que les autres groupes de population (Brimmah et al., 2005; Moiroux et al., 2012). Cela pourrait expliquer en partie le rôle important joué par ces adolescents en tant que réservoirs potentiels

pouvant maintenir la transmission du paludisme au sein de la communauté (Lindblade et al., 2013), même dans les zones à très faible risque de transmission de Madagascar (<1% de prévalence parasitaire), comme l'ont souligné précédemment Kang *et al.* (Kang et al., 2018). Par ailleurs, les résultats des études précédentes, quelle que soit la zone étudiée à Madagascar, montrent que, en dehors de l'extension de la prise en charge communautaire du paludisme à tout âge, des stratégies de sensibilisation ciblées pour le groupe des enfants en âge scolaire pourraient contribuer à une meilleure prévention du paludisme et, à terme, à son élimination (Ratovoson, Garchitorena, et al., 2022; Rice, Golden, et al., 2021; Sayre et al., 2021).

5.1.3 Indices environnementaux et climatiques

L'altitude est largement utilisée dans la cartographie du paludisme comme un indicateur établi de la transmission du paludisme en raison de son association avec d'autres variables environnementales et climatiques. Notamment, les précipitations, la température, et la couverture végétale, sont généralement considérées comme des prédicteurs importants de l'incidence et de la transmission du paludisme, étant donné leur rôle sur la survie, le développement, la reproduction et les taux de piquûre des *Anopheles spp* (Abiodun et al., 2016; Guerra et al., 2006; Manjurano et al., 2011; Paaijmans & Thomas, 2011). La zone des HTC, par sa situation en hauteur (au-delà de 1000 mètres au-dessus du niveau de la mer) bénéficie des conditions environnementales moins favorables que le reste de l'île, ce qui explique le plus faible niveau de transmission et qu'elle soit ciblée pour élimination. Dans cette étude, nous avons montré qu'au sein des HTC, des variations des facteurs environnementaux sont toujours associées à l'exposition au *P. falciparum*, et notamment que la réponse d'anticorps PfAMA1 était plus élevée dans les fokontany à basse altitude. L'altitude était négativement corrélée avec la température et les couvertures du sol (de prairies ou de céréales) dans notre zone d'étude, mais elle était positivement corrélée avec les indices de végétation (NDVI et EVI).

5.1.4 Limites méthodologiques de notre étude

Tout d'abord, la conception transversale reflète un instantané de l'infection ou de l'exposition cumulative des enfants. En outre, ces résultats pourraient ne pas être représentatifs d'autres zones à faible transmission du paludisme dans les hautes terres de Madagascar en raison de leur diversité en matière de dynamique de transmission du paludisme et d'écologie des vecteurs (Arambepola et al., 2020; Tantely et al., 2012). Enfin, les données de l'étude du **Chapitre 1** ont été collectées en 2014, donc une enquête sérologique plus récente pourrait

fournir des meilleures informations sur l'intensité de la transmission du paludisme dans le but d'aider le PNLP à adapter ses interventions pour inverser la tendance stagnante ou haussière de l'incidence du paludisme (World Health Organization, 2021).

Nombreux pays de la région africaine ont le potentiel d'éliminer le paludisme à moyen ou long terme, l'incidence des cas de paludisme a été réduite de 372,6 à 233,6 cas pour 1 000 habitants exposés au risque de paludisme en 2000 et 2020, respectivement (World Health Organisation, 2022). Cependant, Madagascar, avec 4,9 millions cas et 12 571 décès estimés en 2021, fait partie des trois pays de l'Afrique de l'Est et Australe (avec l'Ouganda et le Sud-Soudan) ayant enregistré une hausse de taux d'incidence et de décès du paludisme de 2015–2021, soit une hausse de plus de 75% (**Figure 3**) (World Health Organisation, 2022). Ce qui justifie davantage la nécessité de nouvelles approches et outils portés par des modélisateurs pour appuyer le PNLP et ainsi inverser cette tendance haussière.

5.1.5 Autres contributions pour caractériser l'épidémiologie du paludisme dans les HTC pendant ma thèse

En dehors de l'étude présentée dans le Chapitre 1, j'ai également contribué à des analyses épidémiologiques pour d'autres études en tant que coauteur. D'abord, dans l'étude de Steinhardt *et al.* qui a précédé notre étude du Chapitre 1, nous avons fourni des évidence sur l'utilisation des données sérologiques de cinq anticorps au parasite *P. falciparum* dans le but d'estimer la transmission du paludisme au niveau de la commune, où se trouvent les formations sanitaires (**Annexe 1**) (Steinhardt et al., 2021). Dans cette étude, j'ai été impliqué à appliquer des modèles de mélange gaussien basés sur la méthode de clustering utilisant l'algorithme EM (*Expectation-Maximum*) (Dempster et al., 1977) pour subdiviser la population d'étude en sous-groupes des séropositifs (exposés) et séronégatifs (non-exposés) (Arnold et al., 2014; Drakeley et al., 2005; Scrucca et al., 2016). Les statuts de de séropositivité ont été utilisés par d'autres biostatisticiens, co-auteurs de l'étude, pour générer par la suite des taux de séroconversion annuels à l'échelle communale, utilisant des modèles catalytiques réversibles. En bref, cette étude a permis d'identifier les communes à forte transmission et d'évaluer la validité de l'utilisation des données de routine pour cibler la PID. Dans les zones à faible transmission de Madagascar, la sensibilité des données d'incidence issues de la surveillance passive était légèrement supérieure à 70% par rapport aux taux de séroconversion à l'échelle communale utilisés comme référence, permettant d'identifier les 30% de communes ayant la transmission la plus élevée. Cette étude a préconisé que les enquêtes en milieu scolaire présentent l'avantage

d'être relativement rapides et moins coûteuses que les enquêtes auprès des ménages (Steinhardt et al., 2021).

Deuxièmement, dans une étude de Rakotoarison *et al.*, nous avons proposé une méthode *multi-criteria evaluation* (MCE) pour évaluer les risques de transmission de parasite *Plasmodium* par la cartographie et la télédétection (**Annexe 2**) (Rakotoarison et al., 2020). Brièvement, la transmission du paludisme a été déterminée par des critères environnementaux et climatiques parce qu'ils affectent directement le cycle de vie des anophèles et l'écologie du *Plasmodium* qu'elles transmettent (Abiodun et al., 2016; Guerra et al., 2006; Manjurano et al., 2011; Weiss et al., 2015). Dans cette étude, j'ai proposé et mis en œuvre la méthodologie permettant d'agréger le niveau de risque issus de la méthode MCE, de l'échelle du pixel de 30 m vers l'échelle communale, utilisant différentes distributions de probabilité (Weibull, log-normale ou normale), des techniques de *clustering*, et les modèles de mélange gaussien par les méthodes de maximum de vraisemblance basée sur l'algorithme EM (*Expectation-Maximum*) (Arlinghaus & Kerski, 2013; Dempster et al., 1977; Scrucca et al., 2016). La combinaison des SIG et la méthode MCE—une modélisation géostatistique basée sur les dires d'experts—a permis d'améliorer la compréhension des zones à risque de paludisme (Chakhar & Martel, 2003; Wondim et al., 2017; Yankson et al., 2019). La carte des risques qui en résultait a été utilisée pour la prise de décision afin de pouvoir cibler les communes prioritaires pour les campagnes de PID dans les HTC de Madagascar (Rakotoarison et al., 2020).

5.2 Contributions à la compréhension du COVID-19 à Madagascar

Comparée à d'autres pays africains, la situation de Madagascar est atypique puisque la capitale, Antananarivo, dispose d'un système relativement unique de notification des décès, couvrant à la fois les décès hospitaliers et communautaires. Ce système de registre se trouve au BMH de la CUA. Il contribue alors à maintenir un niveau élevé d'exhaustivité de l'enregistrement des décès, estimé à plus de 90% depuis les années 70 (Masquelier et al., 2019).

En effet, les registres qui s'y trouvent, couvrent la période de 1976–2021, et ont pu être analysés auparavant pour documenter une crise de mortalité due à la résurgence du paludisme et à une famine urbaine au milieu des années 80, la surmortalité pendant la pandémie de grippe H1N1 en 2009 et l'épidémie de rougeole en 2018–2019 (RAJATONIRINA et al., 2013; Rasambainarivo et al., 2021; Waltisperger et al., 2005). L'étude de Rasambainarivo *et al.* a d'ailleurs préconisé la robustesse de ce registre pour détecter les anomalies dues à la pandémie de COVID-19 sur les séries de mortalité toutes causes confondues ou par groupe d'âge enregistrées à la capitale de Madagascar (Rasambainarivo et al., 2021).

En se focalisant sur la période pandémique de COVID-19 de 2020–2021, les résultats du **Chapitre 2**, dont je suis co-premier auteur, montrent que ce système de notification des décès permet de reconstruire les tendances récentes de la mortalité couvrant les années 2020 et 2021 à Antananarivo, et d'évaluer les effets de la pandémie de COVID-19 sur la mortalité dans la capitale de Madagascar.

5.2.1 Tendances de la mortalité toutes causes confondues à Antananarivo

Tirant parti d'un système rigoureux et de longue date d'enregistrement des décès dans la ville d'Antananarivo, notre étude a mis en évidence plusieurs pics de surmortalité en 2020–2021, qui ont été associés de manière significative aux vagues de cas de SARS-CoV-2 signalés. En comparant les tendances durant la période pré-pandémique (2016–2019, utilisées comme tendances basales) avec la période pandémique de 2020–2021, nous avons estimé que la surmortalité toutes causes confondues était de 38,5 et 64,9 pour 100 000 habitants en 2020 et 2021, respectivement. La surmortalité a atteint plus de 50% au cours des deux vagues de ces deux premières années. En somme, nous avons estimé qu'il y avait 1 179 excès de décès sur

cette période ; soit une estimation supérieure aux 1 069 décès officiels de COVID-19 notifiés par le MSANP pour l'ensemble du pays à la date du 31 décembre 2021 (Mathieu et al., 2020).

De plus, utilisant deux techniques de sensibilité différentes, l'estimation de l'excès de décès était revue à la hausse. Lorsqu'on excluait les décès en excès associés aux épidémies de rougeole de 2018–2019 dans la tendance basale (Nimpa et al., 2020; Rasambainarivo et al., 2021), par un remplacement par la moyenne hebdomadaire historique, un excès de 1 500 décès a été estimé. L'excès de décès est environ deux fois plus élevé, soit 2 111 décès, lorsqu'on utilisait la méthode du changement relatif utilisant le modèle de régression saisonnière de Serfling (aussi appelé *P-scores*) (Andreasen et al., 2008; Serfling, 1963). Une surmortalité pendant 51 semaines a été observée en 2020 (soit de 1 à 87%) et en 2021 (soit de 2 à 158%); elle a été estimée à plus de 200% pour les personnes âgées (80+ ans) pendant les vagues de 2020 et 2021.

Ces résultats vont dans le même sens que des études précédents, qui avaient prédit un doublement du nombre de décès, attribuables à la pandémie de COVID-19, si les INPs mises en place initialement étaient relaxées (Evans et al., 2020) ou l'accès aux soins n'est pas continuellement amélioré (Msemburi et al., 2022; United Nations Department of Economic and Social Affairs Population Division, 2022). Notre étude est la seule à notre connaissance à avoir estimé d'un point de vue empirique l'impact du COVID-19 en milieu urbain à Madagascar. Une autre étude en milieu rural, dans le district d'Ifanadiana au sud-est du pays, a trouvé que l'effet en matière d'excès de mortalité était même supérieur dans ces zones à ce qu'on a trouvé à Antananarivo (Andres Garchitorena et al., 2023). En utilisant des enquêtes démographiques et de santé au sein d'une cohorte longitudinale, couplée à des analyses de séroprévalence au SARS-CoV-2, cette étude suggère que l'impact indirecte du COVID-19 dans les zones rurales et pauvres aurait pu être très important et doubler le taux de mortalité de groupe d'âge considérés moins à risque, comme ceux entre 30 et 45 ans.

5.2.2 Impact de la pandémie de COVID-19 à Antananarivo

Taux de la mortalité

Il est intéressant de noter qu'en matière de synchronisation (d'après nos analyses par ondelettes croisées), le taux de mortalité à Antananarivo a légèrement précédé le taux de positivité des cas de SARS-CoV-2 diagnostiqués au cours de la première vague. Ce qui pourrait

indiquer une stratégie de dépistage non-optimale ou "inadaptée", et l'utilisation différente d'une définition de cas pour les cas suspects selon les lignes directrices du MSANP et celles de l'OMS (Andriamandimby et al., 2022; R. V. Randremanana et al., 2021; The World Health Organization (WHO), 2020). Cela peut avoir entraîné un décalage entre les vagues de COVID-19 et celle de mortalité ; car seuls quelques "vrais cas suspects" ont été testés faute de faible capacité de test du pays, laissant les autres cas non-diagnostiqués. En effet, les évidences conclues par Evans *et al.* ont expliqué que ce faible taux de détection du virus pouvait expliquer largement le faible nombre de cas rapportés par Madagascar, en présence de l'efficacité des INPs (Evans et al., 2020).

Lors de la deuxième vague du COVID-19, février–mai 2021, le taux de positivité du SARS-CoV-2 a précédé les vagues de décès. Cela pourrait indiquer une amélioration de la stratégie de dépistage, permettant une forte synchronisation entre les données de laboratoire et la circulation dans la communauté du virus à Antananarivo, comme l'avaient déjà constaté Andriamandimby *et al.* (Andriamandimby et al., 2022).

Variations et différences en espérance de vie à la naissance

Par rapport aux années précédentes, la surmortalité à Antananarivo a été plus élevée en 2021, atteignant plus de 50% pendant 4 semaines. En conséquence, une baisse substantielle de l'espérance de vie à la naissance a été observée, diminuant de 0,8 et 1,0 an par rapport à la valeur projetée pour les hommes et les femmes, respectivement. Mais cette baisse n'a pas été statistiquement significative selon le modèle de Lee & Carter utilisé, une variation de modèle de type ARIMA (Lee & Carter, 1992). Une situation similaire a été observée au Brésil, où la baisse de l'espérance de vie à la naissance en 2020 a été estimée à 1,3 an contre 1,8 an au cours des quatre premiers mois de 2021 (Castro et al., 2021). Plusieurs pays d'Europe de l'Est et les États-Unis ont également enregistré une perte soutenue de l'espérance de vie en 2021 (Schöley et al., 2022). Des données sur l'impact du COVID-19 sur l'espérance de vie dans d'autres pays d'Afrique subsaharienne sont nécessaires pour pouvoir comparer ces estimations et mettre en lumière le moment où le choc de mortalité s'est produit dans cette région.

Utilisant les modèles spécifiques aux taux de mortalité par âge ou par cause de décès proposés par Arriaga (Arriaga, 1984; Auger et al., 2014), la réduction de l'espérance de vie est entièrement imputable à l'augmentation du risque de décès chez les hommes et les femmes âgés de plus de 60 ans et aux décès dus au COVID-19, plutôt qu'à l'augmentation d'autres causes de

décès. Les pays où l'espérance de vie à la naissance a considérablement diminué sont la Russie, les Etats-Unis, l'Italie et l'Espagne (Islam et al., 2021); les populations y sont plus âgées et les taux de mortalité basale y sont beaucoup plus faibles que dans les populations africaines. La mortalité à Madagascar est encore fortement concentrée dans les groupes d'âge les plus jeunes, et l'espérance de vie reste dominée par les variations des chances de survie chez les enfants. Cependant, l'année 2021 s'est caractérisée par une augmentation de la probabilité de décéder entre 60 et 80 ans de 16% pour les femmes et de 20% pour les hommes à Antananarivo. Le taux de mortalité au-delà de 80 ans a augmenté de 14% pour les femmes et de 44% pour les hommes. Comme observé dans les pays européens (Gebhard et al., 2020), les hommes semblent avoir été plus touchés par l'épidémie de COVID-19 que les femmes. L'une des explications de cette différence par rapport au sexe serait la différence éventuelle des mécanismes sexospécifiques modulant l'évolution de la maladie, tels que l'expression hormonale des gènes codant pour le virus SARS-CoV-2 (Clinkemalie et al., 2013; Gebhard et al., 2020) ; mais aussi la différence liée aux facteurs de risque de la gravité tels les maladies cardiovasculaires et ses comportements à risque (fumer des cigarettes, boire de l'alcool) pouvant développer des comorbidités (Cai, 2020; GlobalHealth 5050, 2021).

A notre connaissance, notre étude fait partie de l'une des premières à évaluer l'impact du COVID-19 sur l'espérance de vie d'une population d'ASS, sur la base des systèmes locaux d'enregistrement des décès. Contrairement à de nombreux pays à revenu élevé, où des réductions de plus d'une année entière de l'espérance de vie à la naissance ont été documentées en 2020 (Aburto et al., 2022), nous n'avons trouvé pratiquement aucun changement pour cette année-là (-0,14 an pour les hommes et +0,03 an pour les femmes). Une baisse de la mortalité avant 60 ans plus rapide que celle attendue sur la base des tendances passées aurait pu compenser l'évolution défavorable de la mortalité au-delà de 60 ans.

5.2.3 Forces et faiblesses du système de surveillance hospitalière et communautaire

Nos résultats mettent en évidence la granularité des registres de décès du BMH d'Antananarivo en tant que source puissante pour évaluer le fardeau des maladies infectieuses et les forces et faiblesses du système de santé malagasy pour faire face à des menaces majeures telles que la pandémie de COVID-19, également évoquée par des études antérieures (Rasambainarivo *et al.*, 2021). En effet, la surmortalité estimée en 2020 et 2021 pourrait être due à la difficulté de trouver des lits d'hôpitaux dans les unités de soins intensifs, pour les

infections graves nécessitant des ventilations mécaniques (Gouvernement de Madagascar, 2021), et du personnel formé, en plus des interruptions fréquentes de l'approvisionnement en électricité observées régulièrement dans les PRFI (Gallifant et al., 2022).

Le variant Beta (B.1.351) du SARS-CoV-2 a circulé à Madagascar à partir de février 2021, précédant le début du pic de mortalité en 2021. Les résultats obtenus auprès de donneurs de sang ont confirmé la contribution de ce variant à la deuxième vague de COVID-19 qui a commencé au début de 2021 (Razafimahatratra et al., 2021). Les variants Alpha, Beta et Delta concernés étaient connus pour être plus transmissibles et avoir provoqué des infections plus graves que le variant ancestral du SARS-CoV-2 (Davies et al., 2021). Cela pourrait expliquer l'excès de décès plus élevé observé dans notre étude au cours de la deuxième vague par rapport à la première au fur et à mesure de l'évolution de la virulence de virus qui circule, combiné à une stratégie de vaccination qui n'était pas efficace à ce moment-là soit par le retard ou les faibles doses de vaccins alloués (Rasambainarivo et al., 2022).

Une surveillance optimale des variants et des études sur leur gravité ainsi que leur virulence dans la population générale, couplées avec la modélisation spatio-temporelle des taux d'incidence ou de mortalité (Rice, Annapragada, et al., 2021), sont nécessaires pour mieux comprendre les effets distincts de chaque variant sur la santé humaine.

5.2.4 Limites et alternatives méthodologiques liées aux sources de données et modèles

Notre étude du **Chapitre 2** présente certaines limites. Tout d'abord, le district d'Ambohidratrimo—où se trouve le Centre Hospitalier Universitaire Anosiala, centre de référence pour les cas graves de COVID-19 depuis le 8 juillet 2020—totalisant 442 244 habitants selon le recensement de 2018 (Institut National de la Statistique (INSTAT), 2021), ne fait pas partie des six arrondissements de la zone couverte par le BMH (Gouvernement de Madagascar, 2020). Cela a pu conduire à une sous-estimation de la surmortalité à Antananarivo en utilisant que les données du BMH, bien que tous les décès survenus parmi les résidents des cinq arrondissements centraux devraient être rapportés au BMH, quel que soit le lieu de décès. De plus, au cours des premières vagues de la pandémie, l'unité de virologie de l'IPM s'est principalement concentrée sur le diagnostic du SARS-CoV-2 en raison de contraintes logistiques et de management de ressources humaines, ce qui a pu entraîner un sous-diagnostic d'autres infections virales ou respiratoires responsables d'autres causes de décès. De même, une

diminution des consultations a été observée dans les formations de santé au cours des première et deuxième vagues de la pandémie (Rasoanaivo et al., 2021), ce qui a entraîné une sous-déclaration d'autres maladies infectieuses dans le système de surveillance épidémiologique.

Deuxièmement, dans notre analyse, l'estimation de la surmortalité s'est focalisée sur les semaines où les excès étaient les plus évidents, utilisant l'algorithme de surveillance de Farrington (Noufaily et al., 2013). Cela peut induire à une sous-estimation de l'excès de mortalité par rapport à la méthode de variation relative basée sur les *P-scores* (Serfling, 1963). De plus, la comparaison de nos résultats avec ceux d'autres pays peut être biaisée à cause de ce choix méthodologique. D'ailleurs, les modèles de régression binomiale négative ou poissonienne, pouvant être combinés à l'approche bayésienne, ou des techniques de modélisation d'ensemble (*ensemble modelling*) ont été couramment utilisés pour estimer et modéliser la surmortalité (COVID-19 Excess Mortality Collaborators, 2022; Msemburi et al., 2022; United Nations Department of Economic and Social Affairs Population Division, 2022).

Troisièmement, entre 2016 et 2020, Madagascar a connu d'autres épidémies telles que la peste et la rougeole qui auraient pu avoir un impact sur la mortalité de la population d'Antananarivo (Nimpa et al., 2020; R. Randremanana et al., 2019). Ces épidémies ont augmenté la moyenne du taux de mortalité utilisé comme valeur basale de référence de 2016–2019 utilisée dans notre estimation de la surmortalité en 2020–2021. Nos analyses de sensibilité, basées sur le nombre moyen de décès par semaine pendant la période pré-COVID-19 sans prise en compte de tels pics, ont pu donc révéler un excès de décès encore plus important pendant la période pandémique, allant jusqu'à 2 111 d'excès de décès versus 1 179 lorsqu'on utilise l'algorithme de Farrington appliqué sur l'ensemble des données sans correction.

Bien entendu, les résultats présentés dans le **Chapitre 2** ne donnent qu'une image rétrospective et limitée à la ville d'Antananarivo de l'impact de l'épidémie de COVID-19, et d'autres études et modèles complémentaires ont permis d'aborder et comprendre d'autres aspects de la dynamique épidémiologique du COVID-19 à Madagascar. Rasambainarivo *et al.* ont développé et proposé une plateforme en accès ouvert peu après l'introduction du virus en mars 2020 (<https://www.covid19mg.org/>), pour compiler et visualiser les données rapportées publiquement et estimer le R_t à l'aide de méthodes traditionnelles basées sur le taux de croissance appliquées à l'incidence rapportée quotidiennement sur une fenêtre glissante de 7 jours (Abbott et al., 2023; Cori et al., 2013). En s'appuyant sur ces données compilées

d'incidence quotidienne du site (<https://www.covid19mg.org/>) et d'autres sources de données sur la mobilité humaine utilisant la téléphonie mobile, Ramiadantsoa *et al.* ont appliqué un ensemble de modèles mécanistiques de type SEIR en métapopulation, sur 22 les anciennes régions de Madagascar pour expliquer la propagation spatiale du COVID-19 (Ramiadantsoa *et al.*, 2022). Cependant, les incertitudes liées aux tests et à la notification pourraient altérer la robustesse des matrices de mobilité approximatives et la prédiction des trajectoires des pathogènes émergents tel que le COVID-19 ainsi déduite.

5.2.5 Autres contributions pour comprendre la dynamique de la première vague de COVID-19 à Madagascar pendant ma thèse

Étant donné que ma thèse a eu lieu pendant la pandémie de COVID-19, tout en travaillant en tant que modélisateur à l'unité d'épidémiologie et recherche clinique de l'Institut Pasteur de Madagascar, j'ai été mobilisé pour contribuer à la gestion et aux analyses de données de plusieurs autres études sur le COVID-19 à Madagascar. Mes contributions sont résumées dans les paragraphes qui suivent. D'abord, dans l'étude de Randremanana *et al.* de l'**Annexe 3**, nous avons décrit les distributions spatiales et temporelles des premiers cas de COVID-19 à Madagascar selon les tests de positivité en RT-PCR (*Reverse Transcription-Polymerase Chain Reaction*) réalisés à l'IPM, ainsi que les premières interventions déployées par l'Etat pour essayer de maîtriser sa propagation dans l'ensemble du pays : les confinements, les couvre-feux, les restrictions de voyage et la distanciation sociale (R. V. Randremanana *et al.*, 2021). Parmi les facteurs de risque, l'âge (>16 ans) était associé à la probabilité d'avoir un RT-PCR positif, via un modèle de régression logistique multivariée que j'ai appliqué. Les personnes ayant des symptômes tels que de la fièvre, de la toux, et de la fatigue étaient environ deux fois plus susceptibles d'avoir un test positif au SARS-CoV-2. D'autres symptômes, tels que l'écoulement nasal et les maux de tête, ont été associés dans une moindre mesure à la présence de cette infection virale.

Dans l'étude de Schoenhals *et al.* de l'**Annexe 4**, nous avons utilisé des échantillons de sérums des 9 570 donneurs de sang des cinq centres régionaux de transfusion sanguine (CRTS) de Madagascar pour pouvoir estimer les séroprévalences à l'infection à SARS-CoV-2, de mars à novembre 2020 (Schoenhals *et al.*, 2021). Dans les analyses de cette étude, j'ai pu apprendre et appliquer les méthodes de standardisation directe par âge et sexe, utilisant les données démographiques de recensement générale de la population, un modèle de régression multiniveau, et la technique de post-stratification (Breslow & Day, 1987). Ces analyses ont

permis d'estimer la séroprévalence à l'ensemble de la population de ces cinq villes, soit 9,5 millions d'habitants (37% de la population nationale) (Institut National de la Statistique (INSTAT), 2021). Les valeurs de la sensibilité et de la spécificité du test sérologique utilisé ont été ajustées selon la méthode proposée par Uyoga S. *et al.*, notamment le choix des priors naïfs ou non-informationnels pour les paramètres des modèles de régression bayésiens utilisés (Uyoga et al., 2021). La séroprévalence la plus élevée, en étant pondérée par rapport à la population et ajustée à la performance du test, a été observée en septembre 2020 à Antananarivo (43,5% versus 38,5% brute). Les valeurs moyennes des pics de séroprévalence dans les cinq CRTS étaient de 32,1% (séroprévalence brute), 35,7% (standardisée par âge et sexe et ajustée), 36,6% (standardisée par âge et sexe et ajustée) et 37,8% en utilisant le modèle de régression bayésienne à effet aléatoire sur l'âge des donneurs (pondérée en fonction de la population et ajustée). Nos résultats ont aidé à décrire la dynamique de la première vague de SARS-CoV-2 à Madagascar.

Dans l'étude d'Andriamandimby *et al.* de l'**Annexe 5**, nous avons principalement comparé les données d'incidence journalière de la plateforme du site (<https://www.covid19mg.org/>) lors de la première vague épidémique de mars à septembre 2020, avec de nouvelles estimations du taux de croissance épidémique variant dans le temps par l'utilisation de nos données de laboratoire de l'unité de la virologie de l'IPM (Andriamandimby et al., 2022). Une nouvelle méthode basée sur la distribution transversale de la valeur de cycle seuil (appelé *Cycle threshold* ou Ct) des 20 326 tests discrètes de RT-PCR (*Reverse Transcription-Polymerase Chain Reaction*), correspondant au nombre de cycles nécessaires permettant la détection et la quantification du virus SARS-CoV-2 au moment du prélèvement des échantillons, a été proposée (Hay et al., 2021). J'ai été impliqué dans l'analyse statistique qui a indiqué que les valeurs de Ct varient de manière prévisible en fonction du nombre de jours écoulés depuis le début de l'infection. L'application de modèles additifs généralisés (*Generalized additive modeling*) à la fois aux trajectoires d'infection individuelles et aux distributions des valeurs de Ct au niveau de la population a offert un moyen efficace de contrôler ou standardiser la variation du test RT-PCR et de la cible sur diverses plateformes techniques fréquemment utilisées au niveau des laboratoires de virologie. En collaboration avec d'autres modélisateurs, nous avons aussi utilisé un modèle de transmission précédemment développé, de type SEIR (Sensible, Exposé, Infectieux (asymptomatique et symptomatique) et Recouvré/guéri) : plutôt que de supposer que tous les individus infectieux (classe des Infectieux) contribuaient de manière égale à la transmission dans le cadre de la modélisation

compartimentale, le modèle de Hay *et al.* utilisé intègre la cinétique virale intra-hôte, pouvant décrire la trajectoire moyenne de la charge virale d'un patient infecté par le SARS-CoV-2 (indiquée par la valeur Ct) tout au long de l'évolution de l'infection au sein de la classe des Infectieux (Hay et al., 2021). Cela a permis d'exploiter ces données de cinétiques virales pour calibrer les modèles épidémiologiques à l'échelle de la population. Via ce modèle, la tendance de la trajectoire des valeurs de Ct s'est maintenue même après avoir contrôlé les effets de l'âge et de l'état des symptômes. Ainsi, ces résultats ont permis de valider l'applicabilité de la valeur de Ct en tant qu'indicateur du moment de l'infection.

5.3 Autres contributions pour comprendre les dynamiques des autres affections ou maladies infectieuses à Madagascar pendant ma thèse

Pendant l'épidémie de peste pulmonaire (PP) d'une ampleur inhabituelle en 2017, touchant la ville d'Antananarivo et les districts aux alentours, j'ai été mobilisé pour appuyer l'unité peste de l'IPM au management, aux analyses, et à la publication de données de surveillance épidémiologique en co-premier auteur, présentées dans l'**Annexe 6** (R. Randremanana et al., 2019). Les cas cliniquement suspects de peste ont été notifiés au Laboratoire central de la peste de l'IPM (Antananarivo, Madagascar), où des échantillons biologiques ont été analysés. Sur la base des 2 414 cas enregistrés entre le 1er août et le 26 novembre 2017, les caractéristiques épidémiologiques de cette épidémie ont été évaluées. Les cas ont été classés comme suspectés, probables ou confirmés sur la base des résultats de trois types de tests de diagnostic (test de diagnostic rapide, méthodes moléculaires et culture) selon les recommandations de l'OMS. En bref, l'ampleur de l'épidémie de PP a probablement été moins importante que ne le suggèrent les notifications issues du système de surveillance, puisque seuls 23% des cas notifiés de PP avaient plus d'un test positif au laboratoire, et les résultats de laboratoire étant disponibles pour plus de 99% des cas. L'étendue spatiale de l'épidémie semble avoir été relativement restreinte, 84% des cas confirmés ou probables de PP ayant été observés dans les deux principales villes urbaines (la ville d'Antananarivo et les districts aux alentours, et la ville de Toamasina) d'après l'analyse spatiale utilisant les techniques de clustering (Bjørnstad & Falck, 2001; MORAN, 1950). Avec une période de génération de 5 jours, l'analyse temporelle, utilisant les modèles de croissance exponentielle proposés par Wallinga et Lipsitch (Wallinga & Lipsitch, 2006) et Nishiura (Nishiura, 2006), appliquées à l'incidence rapportée quotidiennement au début de l'épidémie, a révélé que la croissance des cas confirmés ou probables de PP a été rapide, mais une partie de cette croissance a pu être due à une augmentation des déclarations grâce à l'amélioration de la surveillance par la recherche des contacts et à la sensibilisation accrue lors de la riposte. Les facteurs qui pourraient expliquer la sur-déclaration des cas de PP comprenaient le manque d'expérience clinique dans les zones nouvellement touchées, et la difficulté du diagnostic clinique dans un contexte où les signes respiratoires peuvent être causés par d'autres agents pathogènes en circulation. Les analyses de cette épidémie ont confirmé le risque important pour la santé

publique de la réémergence de la PP dans les zones urbaines et son potentiel d'expansion rapide. Les leçons tirées de nos résultats sur le diagnostic clinique et biologique, la définition des cas, la surveillance épidémiologique, et la gestion logistique de la riposte, ont constitué les piliers de l'amélioration du système de surveillance, de l'investigation de la peste, ainsi que des efforts de réponse à Madagascar et ailleurs (Demeure et al., 2019; ten Bosch et al., 2022; World Health Organization (WHO), 2021).

Dans le cadre d'une autre étude sur la qualité microbiologique de l'eau, j'ai également contribué à l'analyse des tendances temporelles à long terme de la qualité de l'eau approvisionnée à Antananarivo, une analyse de données de surveillance de 1985–2017 (Bastaraud et al., 2020). Dans cette étude de Bastaraud *et al.* de l'**Annexe 7**, nous avons caractérisé et mesuré les interactions entre les indices environnementaux et climatiques et le système d'approvisionnement en eau de la population de la capitale. Au total, 25 467 échantillons d'eau ont été prélevés chaque semaine en différents points du système d'approvisionnement en eau potable. Les échantillons ont été analysés pour les coliformes totaux, *Escherichia coli*, les entérocoques intestinaux, et les spores de clostridies sulfito-réductrices. Les analyses biologiques ont trouvé 981 échantillons positifs pour un des indicateurs, répartis de manière inégale dans le temps. Quatre périodes majeures ont été identifiées par la méthode des points de rupture, au cours desquelles la série temporelle des contaminations présentait des changements dans le niveau et le profil, et dans le schéma mensuel de la contamination, avec plus d'effets directs des précipitations sur la qualité de l'eau potable. Les résultats de la modélisation ont montré des décalages significativement différents entre les indicateurs de présence de bactéries après les précipitations cumulées, variant de 4 à 8 semaines. Ses analyses ont révélé que la qualité bactériologique de l'eau distribuée à Antananarivo s'est progressivement dégradée pendant les années de l'étude, de 1985–2017. En effet, les infrastructures d'approvisionnement n'ont pas suivi la croissance démographique, et le déséquilibre entre la capacité de production et la demande en eau est devenu critique, avec un impact sérieux sur la qualité de l'eau fournie et le portage de virus entéropathogènes ou non entéropathogènes (Razanajatovo et al., 2023). La modernisation de la station d'épuration en 1993 a eu un impact positif à long terme sur la qualité de l'eau potable, principalement en diminuant les contaminations par les coliformes totaux. Une modernisation appropriée du processus de filtration pourrait être efficace pour améliorer la qualité microbiologique de l'eau dans le système d'approvisionnement.

6 Conclusion Générale et Perspectives

A travers cette thèse, les travaux menés nous ont permis non seulement de comprendre les dynamiques de deux systèmes biologiques, le paludisme et le COVID-19 à Madagascar, mais aussi d'analyser le niveau de risques suite aux efforts de contrôle, et les impacts de ces deux maladies dans la population. En somme, malgré la porosité du système de surveillance passive laissant une grande majorité des cas symptomatiques ou asymptomatiques non diagnostiqués, altérant les efforts de lutte par les programmes nationaux de contrôle, les approches de modélisation biostatistique et biomathématiques, basées sur (ou validées par) les données d'investigation (ou de surveillance) à l'échelle fine, ont été proposées et adoptées dans les chapitres de cette thèse afin de pouvoir, successivement, (i) estimer et mesurer l'exposition au parasite *P. falciparum*, et (ii) évaluer l'impact de la pandémie de COVID-19 dans la population de Madagascar.

Depuis 2008, le PNLN ont permis la mise à l'échelle des TDRs et la prise en charge communautaire des cas de paludisme, par le déploiement des agents de santé communautaires jouant le rôle du premier front, pouvant diagnostiquer et traiter à temps les cas symptomatiques simples via les ACTs, avant les formations sanitaires publiques (Programme Nationale de Lutte contre le Paludisme, 2012). Notre étude du **Chapitre 1** a caractérisé l'hétérogénéité spatiale de transmission du paludisme et détecté des points chauds de la prévalence d'infection à *P. falciparum* et de l'exposition (mesure d'anticorps PfAMA1). Nos résultats ont confirmé la persistance au sein de chaque district (fokontany, localité) des hétérogénéités du risque d'exposition et de transmission au niveau national et subnational (région, district) aussi trouvée par d'autres études (Pourtois et al., 2023; Rice, Golden, et al., 2021). Cela a été expliqué en partie par l'environnement, l'altitude ; mais aussi par des obstacles géographiques à l'accès aux soins qui sont souvent associés à l'exposition au *P. falciparum* et au risque de transmission. Ainsi, les études basés sur les TDR conventionnels dans les zones à faible transmission, même avec des sensibilités parfois discutables selon certains auteurs, peuvent toujours être menées, surtout dans le contexte des pays d'ASS qui ne sont pas en mesure d'assurer les coûts opérationnels supplémentaires des études sérologiques, et aussi dans les zones à forte densité d'infections (Okell et al., 2009; Okell, Bousema, et al., 2012). D'autres études sont nécessaires pour mieux comprendre le rapport coût-efficacité des techniques de diagnostic plus précises pour les infections à faible densité, telles que la PCR (Bousema et al., 2014).

Depuis les investigations et la collecte de données utilisées dans notre étude de ce chapitre, 2014, nombreux pays de la région africaine de l’OMS ont le potentiel d’éliminer le paludisme à moyen ou long terme, et le taux d’incidence de cette maladie parasitaire a été réduite de 372,6 à 233,6 cas pour 1 000 habitants exposés au risque de paludisme de 2000–2020 (World Health Organisation, 2022). Cependant, Madagascar, avec 4,9 millions cas et 12 571 décès estimés en 2021, fait partie des trois pays de l’Afrique de l’Est et Australe (avec l’Ouganda et le Sud-Soudan) ayant enregistré une hausse des taux d’incidence et de décès du paludisme de 2015–2021 (World Health Organisation, 2022). Ce qui justifie davantage la nécessité des études sur l’évaluation d’impact des interventions menées par le PNLP telles que la prise en charge des cas au niveau communautaire et les lutttes antivectorielles, les campagnes de PID.

L’étude du **Chapitre 1** fait partie des premières visant à montrer que les barrières liées à l’accès aux soins (tests par les TDR et traitement pas les ACTs), utilisant les approches de modélisation statistiques et spatiales, peuvent avoir un impact considérable à altérer les efforts d’élimination et de contrôle du paludisme par le PNLP à Madagascar. Ces barrières à l’accès aux tests et aux traitements ont été trouvées d’avoir laissé le groupe des enfants en âge de scolarisation fortement exposés et à risque par rapport à l’ensemble de la population. Par conséquent, les adolescents pourraient jouer un rôle important en tant que réservoirs potentiels pouvant maintenir la transmission du paludisme au sein de la communauté (Lindblade et al., 2013).

Dans le cadre de la lutte contre les maladies infectieuses, les cas ni diagnostiqués ni traités, symptomatiques ou asymptomatiques, peuvent activement contribuer à la transmission de l’agent pathogène (Andolina et al., 2021; Rek et al., 2022) et complexifier la mise en place des stratégies de contrôle tels que le paludisme et le COVID-19. Pour évaluer l’impact de la porosité du système de surveillance dans la population de la capitale, nous avons tiré parti du système rigoureux et de longue date d’enregistrement des décès, se trouvant au BMH de la CUA. Notre étude du **Chapitre 2** a mis en évidence plusieurs pics de surmortalité en 2020–2021, qui ont été associés de manière significative aux vagues de cas de SARS-CoV-2. En comparant les tendances durant la période pré-pandémique de 2016–2019 et la période pandémique de 2020–2021, nous avons estimé que la surmortalité toutes causes confondues était de 38,5 et 64,9 pour 100 000 habitants en 2020 et 2021, respectivement. Au total, 1 179 excès de décès ont été estimés pendant cette période pandémique de COVID-19. Pendant la

première vague en 2020, un faible taux de détection du virus SARS-CoV-2 trouvé pourrait entraîner un décalage entre les vagues de COVID-19 et celle de mortalité, laissant plusieurs cas non-diagnostiqués et entraînant un faible nombre de cas rapportés le MSANP (Evans et al., 2020). Lors de la deuxième vague du COVID-19, février–mai 2021, une amélioration du système de surveillance, par la stratégie de dépistage, a été constatée, le taux de positivité du SARS-CoV-2 a précédé les vagues de décès, par une forte synchronisation, montrant la nécessité prépondérante de la capacité de diagnostic et l'importance capitale des données de laboratoire pour évaluer l'impact de la circulation virus dans la population (Andriamandimby et al., 2022).

En ce qui concerne l'espérance de vie à la naissance, une baisse substantielle a été observée, diminuant de 0,8 et 1,0 année par rapport à la valeur projetée pour les hommes et les femmes, respectivement, à Antananarivo. Cette baisse de l'espérance de vie est entièrement imputable à l'augmentation du risque de décès chez les hommes et les femmes âgés de plus de 60 ans et aux décès dus au COVID-19, plutôt qu'à l'augmentation d'autres causes de décès. En effet, le taux de mortalité au-delà de 80 ans a augmenté de 14% pour les femmes et de 44% pour les hommes. L'un des facteurs de cette différence serait la différence éventuelle liées aux facteurs de risque conduisant à la forme grave de COVID-19, tels que les maladies cardiovasculaires et les comportements à risque des sujets pouvant développer des comorbidités (Cai, 2020; GlobalHealth 5050, 2021).

Notre étude du **Chapitre 2** fait partie de l'une des premières à notre connaissance (i) à avoir estimé d'un point de vue empirique l'impact du COVID-19 à la population urbaine des pays d'ASS, notamment à la capitale, à Antananarivo, et aussi (ii) à évaluer son impact sur l'espérance de vie, sur la base des systèmes locaux d'enregistrement des décès. Contrairement à la situation de nombreux pays à revenu élevé (Aburto et al., 2022), l'impact de la pandémie de COVID-19 à l'espérance de vie a été atténué à Madagascar en 2020 (similaire aux autres PRFI), soit de -0,14 an pour les hommes et +0,03 an pour les femmes. Ce qui peut être expliqué par les dynamiques d'indicateurs démographiques bien avant l'arrivée de la pandémie, les données pré-pandémiques étant utilisées comme les tendances basales de nos estimations. En effet, d'après les statistiques nationales, le taux de mortalité des enfants de moins de 5 ans a légèrement connu une baisse : il a été estimé à 94‰ naissances vivantes en 2003–04 pour atteindre un taux estimé à 75‰ en 2021 (Ratovoson, 2020); mais cette baisse n'a pas été

poursuivie dans la dernière décennie de 2008–09 à 2021, variant de 72‰ à 75‰ (Institut National de la Statistique (INSTAT) et ICF, 2021).

Au cours de cette thèse, j'ai développé une expérience sur diverses études, en rapport à la thèse (**Chapitre 1 à 2**) ou d'autres études en collaboration (**Annexe 1 à 7**) : en biostatistique, biomathématiques, et épidémiologie ; ce qui m'ont conduit des théories/connaissances aux pratiques pouvant aider dans la prise de décision en santé publique. J'ai pu m'apercevoir que la qualité des données d'enquête ou de registres hospitaliers ou communautaires et la persistance des analyses de modélisation proposées (statistiques ou mécanistiques/mathématiques) sont indissociables de toute étude épidémiologique pour pouvoir tirer des leçons et faire des recommandations dans l'amélioration du système de santé publique. C'est pourquoi l'épidémiologie et la santé publique sont pluridisciplinaires et nécessitent de s'allier à d'autres scientifiques spécialisés dans des domaines variés en relation directe ou indirecte à la santé ou la société, tels que la nutrition, l'éducation et l'économie. Cet enjeu de la discipline explique aussi sa complexité de mise en œuvre dans le cadre de la lutte contre les maladies infectieuses, notamment le cas des pays à revenu faible ou intermédiaire. Dans le cadre de cette thèse, ou dans les études menées en parallèles avec ma thèse, nous avons collaboré avec des chercheurs en écologie de la santé, des immunologistes, des démographes, des virologistes, des géographes, des data managers, des techniciens de recherche clinique, des entomologistes, des épidémiologistes, des parasitologues et des personnels du Ministère de la santé publique. On comprend ainsi que les collaborations multiples sont au cœur des études en épidémiologie et santé publique.

6.1 Perspectives de recherche

Dans la perspective d'aborder davantage les questions non couvertes dans cette thèse, alors qu'elles demeurent prépondérantes et primordiales pour réussir la lutte contre le paludisme à Madagascar, nous recommandons quatre axes méthodologiques suivants :

Axe 1: Estimer l'impact et l'efficacité de la stratégie de dépistage actif (tester et traiter), ainsi que l'évolution de dynamique de transmission du paludisme dans le sud-est de Madagascar, district de Mananjary, zone de forte transmission, en 2017 (Ratovoson, Garchitorena, et al., 2022). Car, des études visant (i) à évaluer et quantifier l'impact des prises en communautaires, via des modèle statistiques comme celle de (Ratovoson, Garchitorena, et al., 2022) ou des modèles mécanistiques, en cours de développement au sein de notre équipe, ou (ii) à investiguer les rôles adolescents à arborer et à transmettre le parasite *Plasmodium* aux vecteurs (Andolina et al., 2021; Rek et al., 2022; Stone et al., 2015), sont plus que nécessaires pour renverser la tendance haussière de l'incidence du paludisme à Madagascar (World Health Organisation, 2022).

Il s'agit d'un projet d'article en perspective. Cette étude devra permettre d' :

- explorer les pistes de modélisation pouvant estimer la réduction de la transmissibilité par différentes zones d'interventions suite à la réduction de la durée moyenne d'infectiosité, par la surveillance active des cas symptomatiques et le traitement par ACT, et aussi estimer l'impact des campagnes de PID par la réduction de la durée de vie moyenne des anophèles vectrices;
- estimer l'impact des interventions basées sur un modèle de transmission structuré par groupe d'âge, via des scénarios d'impacts de la réduction de la fréquence de visite (pour traiter plus), du prolongement de la durée de l'intervention de la prise en charge active, et du prolongement de l'efficacité des PID par des campagnes répétées pour maintenir l'efficacité de l'insecticide à pouvoir baisser la population des vecteurs;
- avoir une idée sur combinaison optimale des mesures de contrôle pouvant aider les futures études et, par la suite, le PNLP, à baisser le niveau de risque de transmission dans les districts à forte transmission.

Axe 2 : Utilisation des données de surveillance pour la modélisation de l'impact des interventions de lutte du PNLP. Peut-on utiliser les données issues de surveillance de routine pour évaluer l'efficacité des interventions mises en place pour baisser ou interrompre la transmission du paludisme dans les différents districts de Madagascar ?

- La première étape de cette étude vise à sélectionner les formations sanitaires en prenant en compte des écozones et des interventions mesurables mises en place par le PNLP, ainsi que leurs performances à fournir des données « de qualité ».
- La deuxième étape consistera à appliquer la modélisation statistique, dont l'objectif est d'évaluer l'efficacité des interventions de lutte mises en place pour baisser la transmission du paludisme tout en tenant compte des caractéristiques environnementales et climatiques. Des analyses spatio-temporelles sont proposées pour estimer les relations et effets des variations des indices environnementaux et climatiques aux risques du paludisme (*rate ratios*) de chaque site par rapport aux districts les moins à risque, ceux des HTC (ex. : *Generalized Linear Mixed Model*, *Generalized Additive Mixed Model* ou *Distributed lag non-linear models*) (Ateba et al., 2020; Hastie & Tibshirani, 1986; Pedersen et al., 2019). Il s'agira de construire des combinaisons des indices les plus pertinents : indices des interventions combinant les campagnes de moustiquaires imprégnées d'insecticide à longue durée d'action et des PID, la disponibilité des TDRs et les ACTs; et les indices environnementaux et climatiques (couverture végétale/NDVI, température, humidité, précipitation, altitude et démographie).
- La troisième étape, pourra consister, via un modèle mathématique (Fang et al., 2016; Okell, Paintain, et al., 2012), à questionner comment améliorer les interventions de lutte à plus impacter et baisser le niveau de risque de la transmission du paludisme dans les districts les plus à risque en considérant leurs environnements. Des scénarii d'effets des interventions de lutte seront simulés moyennant les gradients de conditions environnementales et climatiques, définies comme favorables et utilisées en tant que proxy de vecteurs, et leurs relations linéaires ou non (Evans et al., 2020).

Axe 3 : Modèle de coût-efficacité de lutte contre le paludisme pour les PRFI.

Etant de formation initiale en mathématiques appliquées à la finance, je souhaite proposer un modèle de coût-efficacité, basé sur le modèle de Parham et Hughes (Parham &

Hughes, 2015; Stuckey et al., 2014), pour pouvoir aider et orienter les stratégies du PNLP, via l'estimation de :

- Le coût par an par régions et/ou par écozones des interventions ;
- La projection des coûts budgétaires visant l'efficacité des interventions additionnelles en tenant compte des tendances par régions et/ou écozones de l'incidence du paludisme ;
- L'achèvement des objectifs stratégiques visés par le PNLP selon le budget disponible, utilisant des techniques d'optimisation avec des contraintes budgétaires et logistiques afférentes.

Des collaborations avec d'autres unités et équipes de recherche peuvent être envisagées en concertations avec le PNLP et le MSANP.

Axe 4 : Etude observationnelle rétrospective de co-circulation (co-endémicité) des maladies infectieuses à Madagascar : exemple du paludisme et du COVID-19 (ou du paludisme et d'autres maladies parasitaires comme la bilharziose).

Selon l'OMS, pendant la période pandémique de 2020–2021, environ 13,4 millions de cas supplémentaires du paludisme en 2020 et 2021 (World Health Organisation, 2022), et une augmentation d'environ 100% de décès en 2020 (Weiss et al., 2021) auraient été attribuables à la mitigation des efforts de lutte due aux interventions non-pharmaceutiques pour faire face à la pandémie de COVID-19. Ceci concerne principalement les mesures de préventions tels que les confinements ayant directement limité l'accès aux tests, les traitements, et les mesures de prévention (par la perturbation des campagnes de PID et de moustiquaires imprégnées d'insecticide à longue durée d'action) (Bylicka-Szczepanowska & Korzeniewski, 2022; Shi et al., 2021).

En choisissant un site ou une ville, à la fois avec une transmission endémique du paludisme et ayant subie des vagues de COVID-19 (ex. Toamasina, Morondava ou Antsohihy), je souhaite évaluer l'impact du COVID-19 à la mitigation des interventions de lutte contre le paludisme via :

- une analyse en ondelettes croisées comme celles proposées dans le Chapitre 2 (Cazelles et al., 2007; Grinsted et al., 2004);

- ou un modèle mécanistique stochastique structuré par groupe d'âge de type SEIR (Abbate et al., 2020; Domenech de Cellès et al., 2021; Sow et al., 2016).

Références bibliographiques

- Abbate, J. L., Becquart, P., Leroy, E., Ezenwa, V. O., & Roche, B. (2020). Exposure to Ebola virus and risk for infection with malaria parasites, rural Gabon. *Emerging Infectious Diseases*, *26*(2), 229–237. <https://doi.org/10.3201/eid2602.181120>
- Abbott, S., Funk, S., Hickson, J., Badr, H. S., Monticone, P., Ellis, P., Azam, J., Munday, J., Allen, J., Johnson, A., Pearson, C. A. B., actions-user, Chapman, L., DeWitt, M., Bosse, N., & Meakin, S. (2023). *epiforecasts/EpiNow2: 1.4.0 release*. <https://doi.org/10.5281/ZENODO.8380568>
- Abiodun, G. J., Maharaj, R., Witbooi, P., & Okosun, K. O. (2016). Modelling the influence of temperature and rainfall on the population dynamics of *Anopheles arabiensis*. *Malaria Journal*, *15*(1), 364. <https://doi.org/10.1186/s12936-016-1411-6>
- Abu-Raddad, L. J., Chemaitelly, H., Ayoub, H. H., Yassine, H. M., Benslimane, F. M., Al Khatib, H. A., Tang, P., Hasan, M. R., Coyle, P., AlMukdad, S., Al Kanaani, Z., Al Kuwari, E., Jeremijenko, A., Kaleeckal, A. H., Latif, A. N., Shaik, R. M., Abdul Rahim, H. F., Nasrallah, G. K., Al Kuwari, M. G., ... Bertollini, R. (2022). Severity, Criticality, and Fatality of the Severe Acute Respiratory Syndrome Coronavirus 2 (SARS-CoV-2) Beta Variant. *Clinical Infectious Diseases*, *75*(1), e1188–e1191. <https://doi.org/10.1093/CID/CIAB909>
- Aburto, J. M., Schöley, J., Kashnitsky, I., Zhang, L., Rahal, C., Missov, T. I., Mills, M. C., Dowd, J. B., & Kashyap, R. (2022). Quantifying impacts of the COVID-19 pandemic through life-expectancy losses: a population-level study of 29 countries. *International Journal of Epidemiology*, *51*(1), 63–74. <https://doi.org/10.1093/ije/dyab207>
- Aguiar-Conraria, L., & Soares, M. J. (2011). The Continuous Wavelet Transform: A Primer (Issue 16/2011). <https://econpapers.repec.org/RePEc:nip:nipewp:16/2011> (Accessed le 20 octobre 2023)
- Akpotheneta, O. J., Duah, N. O., Tetteh, K. K. A., Dunyo, S., Lanar, D. E., Pinder, M., & Conway, D. J. (2008). Duration of naturally acquired antibody responses to blood-stage *Plasmodium falciparum* is age dependent and antigen specific. *Infection and Immunity*, *76*(4), 1748–1755. <https://doi.org/10.1128/IAI.01333-07>
- Albonico, M., De Giorgi, F., Razanakolona, J., Raveloson, A., Sabatinelli, G., Pietra, V., & Modiano, D. (1999). Control of epidemic malaria on the Highlands of Madagascar. *Parassitologia*, *41*(1–3), 373–376. <http://www.ncbi.nlm.nih.gov/pubmed/10697886>
- Amambua-Ngwa, A., Amenga-Etego, L., Kamau, E., Amato, R., Ghansah, A., Golassa, L., Randrianarivojosia, M., Ishengoma, D., Apinjoh, T., Maïga-Ascofaré, O., Andagalu, B., Yavo, W., Bouyou-Akotet, M., Kolapo, O., Mane, K., Worwui, A., Jeffries, D., Simpson, V., D’Alessandro, U., ... Djimde, A. A. (2019). Major subpopulations of *Plasmodium falciparum* in sub-Saharan Africa. *Science*, *365*(6455), 813–816. <https://doi.org/10.1126/science.aav5427>
- Amratia, P., Psychas, P., Abuaku, B., Ahorlu, C., Millar, J., Oppong, S., Koram, K., & Valle, D. (2019). Characterizing local-scale heterogeneity of malaria risk: A case study in Bunkpurugu-Yunyoo district in northern Ghana. *Malaria Journal*, *18*(1), 81. <https://doi.org/10.1186/s12936-019-2703-4>
- Anderson, R. M., & May, R. M. (1985). Vaccination and herd immunity to infectious diseases. *Nature* *1985* *318*:6044, *318*(6044), 323–329. <https://doi.org/10.1038/318323a0>
- Andolina, C., Rek, J. C., Briggs, J., Okoth, J., Musiime, A., Ramjith, J., Teyssier, N., Conrad, M., Nankabirwa, J. I., Lanke, K., Rodriguez-Barraquer, I., Meerstein-Kessel, L., Arinaitwe, E., Olwoch, P., Rosenthal, P. J., Kanya, M. R., Dorsey, G., Greenhouse, B., Drakeley, C., ... Bousema, T. (2021). Sources of persistent malaria transmission in a setting with effective malaria control in eastern Uganda: a longitudinal, observational cohort study. *The Lancet Infectious Diseases*, *21*(11), 1568–1578. [https://doi.org/10.1016/s1473-3099\(21\)00072-4](https://doi.org/10.1016/s1473-3099(21)00072-4)
- Andreasen, V., Viboud, C., & Simonsen, L. (2008). Epidemiologic Characterization of the 1918 Influenza Pandemic Summer Wave in Copenhagen: Implications for Pandemic Control Strategies. *The Journal of Infectious Diseases*, *197*(2), 270–278. <https://doi.org/10.1086/524065>
- Andriamandimby, S. F., Brook, C. E., Razanajatovo, N., Randriambolamanantsoa, T. H., Rakotondramanga, J. M., Rasambainarivo, F., Raharimanga, V., Razanajatovo, I. M., Mangahasimbola, R., Razafindratsimandresy, R., Randrianarisoa, S., Bernardson, B., Rabarison, J. H., Randrianarisoa, M., Nasolo, F. S., Rabetombosoa, R. M., Ratsimbazafy, A. M., Raharinosy, V., Rabemananjara, A. H., ... Dussart, P. (2022). Cross-sectional cycle threshold values reflect epidemic dynamics of COVID-19 in Madagascar. *Epidemics*, *38*, 100533. <https://doi.org/10.1016/j.epidem.2021.100533>
- Anjorin, A. A., Abioye, A. I., Asowata, O. E., Soipe, A., Kazeem, M. I., Adesanya, I. O., Raji, M. A., Adesanya, M., Oke, F. A., Lawal, F. J., Kasali, B. A., & Omotayo, M. O. (2021). Comorbidities and the COVID-19 pandemic dynamics in Africa. *Tropical Medicine & International Health*, *26*(1), 2–13. <https://doi.org/10.1111/TMI.13504>

- Anselin, L. (1995). Local Indicators of Spatial Association-LISA. *Geographical Analysis*, 27(2), 93–115. <https://doi.org/10.1111/j.1538-4632.1995.tb00338.x>
- Arambepola, R., Keddie, S. H., Collins, E. L., Twohig, K. A., Amratia, P., Bertozzi-Villa, A., Chestnutt, E. G., Harris, J., Millar, J., Rozier, J., Rumisha, S. F., Symons, T. L., Vargas-Ruiz, C., Andriamananjara, M., Rabeherisoa, S., Ratsimbaoa, A. C., Howes, R. E., Weiss, D. J., Gething, P. W., & Cameron, E. (2020). Spatiotemporal mapping of malaria prevalence in Madagascar using routine surveillance and health survey data. *Scientific Reports*, 10(1), 18129. <https://doi.org/10.1038/s41598-020-75189-0>
- Arisco, N. J., Rice, B. L., Tantely, L. M., Girod, R., Emile, G. N., Randriamady, H. J., Castro, M. C., & Golden, C. D. (2020). Variation in Anopheles distribution and predictors of malaria infection risk across regions of Madagascar. *Malaria Journal*, 19(1), 348. <https://doi.org/10.1186/s12936-020-03423-1>
- Arlinghaus, S. L., & Kerski, J. J. (2013). Spatial Mathematics. In *Spatial Mathematics*. CRC Press. <https://doi.org/10.1201/b15049>
- Arnold, B. F., Priest, J. W., Hamlin, K. L., Moss, D. M., Colford, J. M., & Lammie, P. J. (2014). Serological Measures of Malaria Transmission in Haiti: Comparison of Longitudinal and Cross-Sectional Methods. *PLOS ONE*, 9(4), e93684. <https://doi.org/10.1371/JOURNAL.PONE.0093684>
- Arriaga, E. E. (1984). Measuring and explaining the change in life expectancies. *Demography*, 21(1), 83–96. <https://doi.org/10.2307/2061029>
- Ashton, R. A., Kefyalew, T., Rand, A., Sime, H., Assefa, A., Mekasha, A., Edosa, W., Tesfaye, G., Cano, J., Teka, H., Reithinger, R., Pullan, R. L., Drakeley, C. J., & Brooker, S. J. (2015). Geostatistical modeling of malaria endemicity using serological indicators of exposure collected through school surveys. *American Journal of Tropical Medicine and Hygiene*, 93(1), 168–177. <https://doi.org/10.4269/ajtmh.14-0620>
- Assefa, A., Ali Ahmed, A., Deressa, W., Sime, H., Mohammed, H., Kebede, A., Solomon, H., Teka, H., Gurralla, K., Matei, B., Wakeman, B., Wilson, G. G., Sinha, I., Maude, R. J., Ashton, R., Cook, J., Shi, Y. P., Drakeley, C., Von Seidlein, L., ... Hwang, J. (2019). Multiplex serology demonstrate cumulative prevalence and spatial distribution of malaria in Ethiopia. *Malaria Journal*, 18(1), 246. <https://doi.org/10.1186/s12936-019-2874-z>
- Ateba, F. F., Febrero-Bande, M., Sagara, I., Sogoba, N., Touré, M., Sanogo, D., Diarra, A., Magdalene Ngitah, A., Winch, P. J., Shaffer, J. G., Krogstad, D. J., Marker, H. C., Gaudart, J., & Doumbia, S. (2020). Predicting Malaria Transmission Dynamics in Dangassa, Mali: A Novel Approach Using Functional Generalized Additive Models. *International Journal of Environmental Research and Public Health*, 17(17), 6339. <https://doi.org/10.3390/ijerph17176339>
- Auger, N., Feuillet, P., Martel, S., Lo, E., Barry, A. D., & Harper, S. (2014). Mortality inequality in populations with equal life expectancy: Arriaga's decomposition method in SAS, Stata, and Excel. *Annals of Epidemiology*, 24(8), 575-580.e1. <https://doi.org/10.1016/j.annepidem.2014.05.006>
- Barmania, S. (2015). Madagascar's health challenges. *The Lancet*, 386(9995), 729–730. [https://doi.org/10.1016/S0140-6736\(15\)61526-4](https://doi.org/10.1016/S0140-6736(15)61526-4)
- Bartoń, K. (2020). *MuMIn: Multi-model inference, software*. <https://cran.r-project.org/package=MuMIn> (Accessed le 20 octobre 2023)
- Bastaraud, A., Perthame, E., Rakotondramanga, J.-M., Mahazasoatra, J., Ravaonindrina, N., & Jambou, R. (2020). The impact of rainfall on drinking water quality in Antananarivo, Madagascar. *PLOS ONE*, 15(6), e0218698. <https://doi.org/10.1371/journal.pone.0218698>
- Bates, D., Mächler, M., Bolker, B., & Walker, S. (2015). Fitting Linear Mixed-Effects Models Using lme4. *Journal of Statistical Software*, 67(1). <https://doi.org/10.18637/jss.v067.i01> (Accessed le 20 octobre 2023)
- Benn, C. S., Salinha, A., Mendes, S., Cabral, C., Martins, C., Nielsen, S., Fisker, A. B., Schaltz-Buchholzer, F., Jørgensen, C. S., & Aaby, P. (2022). SARS-CoV-2 serosurvey among adults involved in healthcare and health research in Guinea-Bissau, West Africa. *Public Health*, 203, 19–22. <https://doi.org/10.1016/J.PUHE.2021.11.013>
- Bernard, J., Mtove, G., Mandike, R., Mtei, F., Maxwell, C., & Reyburn, H. (2009). Equity and coverage of insecticide-treated bed nets in an area of intense transmission of Plasmodium falciparum in Tanzania. *Malaria Journal*, 8(1), 65. <https://doi.org/10.1186/1475-2875-8-65>
- Bernoulli, D. (1766). Essai d'une nouvelle analyse de la mortalité causée par la petite vérole, et des avantages de l'inoculation pour la prévenir. *History of Actuarial Science*, 8, 1766. https://gallica.bnf.fr/ark:/12148/bpt6k3558n/f220.image.r=daniel_bernoulli
- Bhatt, S., Weiss, D. J., Cameron, E., Bisanzio, D., Mappin, B., Dalrymple, U., Battle, K. E., Moyes, C. L., Henry, A., Eckhoff, P. A., Wenger, E. A., Briët, O., Penny, M. A., Smith, T. A., Bennett, A., Yukich, J., Eisele, T. P., Griffin, J. T., Fergus, C. A., ... Gething, P. W. (2015). The effect of malaria control on Plasmodium falciparum in Africa between 2000 and 2015. *Nature*, 526(7572), 207–211. <https://doi.org/10.1038/nature15535>
- Bivand, R. S., Pebesma, E., & Gómez-Rubio, V. (2013). *Applied Spatial Data Analysis with R* (2nd ed.). Springer New York. <https://doi.org/10.1007/978-1-4614-7618-4>

- Bivand, R. S., & Wong, D. W. S. (2018). Comparing implementations of global and local indicators of spatial association. *TEST*, 27(3), 716–748. <https://doi.org/10.1007/s11749-018-0599-x>
- Bivand, R., Sha, Z., Osland, L., & Thorsen, I. S. (2017). A comparison of estimation methods for multilevel models of spatially structured data. *Spatial Statistics*, 21, 440–459. <https://doi.org/10.1016/j.spasta.2017.01.002>
- Bjørnstad, O. N. (2018). Time-Series Analysis. *Epidemics, Use R!*, 95–115. https://doi.org/10.1007/978-3-319-97487-3_6
- Bjørnstad, O. N., & Falck, W. (2001). Nonparametric spatial covariance functions: Estimation and testing. *Environmental and Ecological Statistics*, 8(1), 53–70. <https://doi.org/10.1023/A:1009601932481>
- Bonds, M. H., Keenan, D. C., Rohani, P., & Sachs, J. D. (2010). Poverty trap formed by the ecology of infectious diseases. *Proceedings of the Royal Society B: Biological Sciences*, 277(1685), 1185–1192. <https://doi.org/10.1098/rspb.2009.1778>
- Bonds, M. H., Ouenzar, M. A., Garchitorena, A., Cordier, L. F., McCarty, M. G., Rich, M. L., Andriamihaja, B., Haruna, J., & Farmer, P. E. (2018). Madagascar can build stronger health systems to fight plague and prevent the next epidemic. *PLoS Neglected Tropical Diseases*, 12(1), e0006131. <https://doi.org/10.1371/journal.pntd.0006131>
- Bousema, T., Griffin, J. T., Sauerwein, R. W., Smith, D. L., Churcher, T. S., Takken, W., Ghani, A., Drakeley, C., & Gosling, R. (2012). Hitting hotspots: Spatial targeting of malaria for control and elimination. *PLoS Medicine*, 9(1), 1–7. <https://doi.org/10.1371/journal.pmed.1001165>
- Bousema, T., Okell, L., Felger, I., & Drakeley, C. (2014). Asymptomatic malaria infections: Detectability, transmissibility and public health relevance. In *Nature Reviews Microbiology* (Vol. 12, Issue 12, pp. 833–840). Nature Publishing Group. <https://doi.org/10.1038/nrmicro3364>
- Braimah, N., Drakeley, C., Kweka, E., Mosha, F., Helinski, M., Pates, H., Maxwell, C., Massawe, T., Kenward, M. G., & Curtis, C. (2005). Tests of bednet traps (Mbita traps) for monitoring mosquito populations and time of biting in Tanzania and possible impact of prolonged insecticide treated net use. *International Journal of Tropical Insect Science*, 25(3), 208–213. <https://doi.org/10.1079/IJT200576>
- Breman, J. (2001). The ears of the hippopotamus: manifestations, determinants, and estimates of the malaria burden. *The American Journal of Tropical Medicine and Hygiene*, 64(1_suppl), 1–11. <https://doi.org/10.4269/ajtmh.2001.64.1>
- Breslow, N. E., & Day, N. E. (1987). Statistical methods in cancer research. Volume II--The design and analysis of cohort studies. *IARC Scientific Publications*, 82, 1–406.
- Buckee, C., Noor, A., & Sattenspiel, L. (2021). Thinking clearly about social aspects of infectious disease transmission. *Nature 2021 595:7866*, 595(7866), 205–213. <https://doi.org/10.1038/s41586-021-03694-x>
- Buckee, C. O., Cardenas, M. I. E., Corpuz, J., Ghosh, A., Haque, F., Karim, J., Mahmud, A. S., Maude, R. J., Mensah, K., Motaze, N. V., Nabaggala, M., Metcalf, C. J. E., Mioramalala, S. A., Mubiru, F., Peak, C. M., Pramanik, S., Rakotondramanga, J. M., Remera, E., Sinha, I., ... Zaw, W. (2018). Productive disruption: opportunities and challenges for innovation in infectious disease surveillance. *BMJ Global Health*, 3(1), e000538. <https://doi.org/10.1136/bmjgh-2017-000538>
- Burnham, K.P. and Anderson, D. R. (2004). *Model Selection and Multimodel Inference* (K. P. Burnham & D. R. Anderson (eds.); 2nd ed.). Springer New York. <https://doi.org/10.1007/b97636>
- Bylicka-Szczepanowska, E., & Korzeniewski, K. (2022). Asymptomatic Malaria Infections in the Time of COVID-19 Pandemic: Experience from the Central African Republic. *International Journal of Environmental Research and Public Health*, 19(6). <https://doi.org/10.3390/ijerph19063544>
- Cable, J., Barber, I., Boag, B., Ellison, A. R., Morgan, E. R., Murray, K., Pascoe, E. L., Sait, S. M., Wilson, A. J., & Booth, M. (2017). Global change, parasite transmission and disease control: lessons from ecology. *Philosophical Transactions of the Royal Society of London. Series B, Biological Sciences*, 372(1719). <https://doi.org/10.1098/rstb.2016.0088>
- Cai, H. (2020). Sex difference and smoking predisposition in patients with COVID-19. *The Lancet Respiratory Medicine*, 8(4), e20. [https://doi.org/10.1016/S2213-2600\(20\)30117-X](https://doi.org/10.1016/S2213-2600(20)30117-X)
- Carolan, K., Ebong, S. M. A., Garchitorena, A., Landier, J., Sanhueza, D., Texier, G., Marsollier, L., Gall, P. Le, Guégan, J. F., & Seen, D. Lo. (2014). Ecological niche modelling of Hemipteran insects in Cameroon; The paradox of a vector-borne transmission for Mycobacterium ulcerans, the causative agent of Buruli ulcer. *International Journal of Health Geographics*, 13(1). <https://doi.org/10.1186/1476-072X-13-44>
- Castro, M. C., Gurzenda, S., Turra, C. M., Kim, S., Andrasfay, T., & Goldman, N. (2021). Reduction in life expectancy in Brazil after COVID-19. *Nature Medicine 2021 27:9*, 27(9), 1629–1635. <https://doi.org/10.1038/s41591-021-01437-z>
- Cauchemez, S., Boelle, P.-Y., Donnelly, C. A., Ferguson, N. M., Thomas, G., Leung, G. M., Hedley, A. J., Anderson, R. M., & Valleron, A.-J. (2006). Real-time estimates in early detection of SARS. *Emerging Infectious Diseases*, 12(1), 110–113. <https://doi.org/10.3201/eid1201.050593>
- Cauchemez, S., Temime, L., Guillemot, D., Varon, E., Valleron, A.-J., Thomas, G., & Boëlle, P.-Y. (2006).

- Investigating Heterogeneity in Pneumococcal Transmission. *Journal of the American Statistical Association*, 101(475), 946–958. <https://doi.org/10.1198/016214506000000230>
- Cazelles, B., Chavez, M., Bertheaux, D., Ménard, F., Vik, J. O., Jenouvrier, S., & Stenseth, N. C. (2008). Wavelet analysis of ecological time series. *Oecologia*, 156(2), 287–304. <https://doi.org/10.1007/S00442-008-0993-2>
- Cazelles, B., Chavez, M., De Magny, G. C., Guégan, J. F., & Hales, S. (2007). Time-dependent spectral analysis of epidemiological time-series with wavelets. *Journal of the Royal Society Interface*, 4(15), 625. <https://doi.org/10.1098/RSIF.2007.0212>
- Chakhar, S., & Martel, J.-M. (2003). *Enhancing Geographical Information Systems Capabilities with Multi-Criteria Evaluation Functions*. <https://api.semanticscholar.org/CorpusID:54584578>
- Chatfield, C., & Xing, H. (2019). The Analysis of Time Series. In *The Analysis of Time Series*. Seventh edition. Boca Raton, Florida : Chapman and Hall/CRC. <https://doi.org/10.1201/9781351259446>
- Clinckemalie, L., Spans, L., Dubois, V., Laurent, M., Helsen, C., Joniau, S., & Claessens, F. (2013). Androgen Regulation of the TMPRSS2 Gene and the Effect of a SNP in an Androgen Response Element. *Molecular Endocrinology*, 27(12), 2028–2040. <https://doi.org/10.1210/ME.2013-1098>
- Cori, A., Ferguson, N. M., Fraser, C., & Cauchemez, S. (2013). A New Framework and Software to Estimate Time-Varying Reproduction Numbers During Epidemics. *American Journal of Epidemiology*, 178(9), 1505–1512. <https://doi.org/10.1093/aje/kwt133>
- COVID-19 Excess Mortality Collaborators. (2022). Estimating excess mortality due to the COVID-19 pandemic: a systematic analysis of COVID-19-related mortality, 2020–21. *The Lancet*, 399(10334), 1513–1536. [https://doi.org/10.1016/S0140-6736\(21\)02796-3](https://doi.org/10.1016/S0140-6736(21)02796-3)
- Daubechies, I. (1992). Ten Lectures on Wavelets. In *Ten Lectures on Wavelets*. Society for Industrial and Applied Mathematics. <https://doi.org/10.1137/1.9781611970104>
- Davies, N. G., Jarvis, C. I., van Zandvoort, K., Clifford, S., Sun, F. Y., Funk, S., Medley, G., Jafari, Y., Meakin, S. R., Lowe, R., Quaife, M., Waterlow, N. R., Eggo, R. M., Lei, J., Koltai, M., Krauer, F., Tully, D. C., Munday, J. D., Showering, A., ... Keogh, R. H. (2021). Increased mortality in community-tested cases of SARS-CoV-2 lineage B.1.1.7. *Nature* 2021 593:7858, 593(7858), 270–274. <https://doi.org/10.1038/s41586-021-03426-1>
- Demeure, C. E., Dussurget, O., Mas Fiol, G., Le Guern, A. S., Savin, C., & Pizarro-Cerdá, J. (2019). Yersinia pestis and plague: an updated view on evolution, virulence determinants, immune subversion, vaccination, and diagnostics. *Genes and Immunity*, 20(5), 357–370. <https://doi.org/10.1038/s41435-019-0065-0>
- Dempster, A. P., Laird, N. M., & Rubin, D. B. (1977). Maximum Likelihood from Incomplete Data Via the EM Algorithm. *Journal of the Royal Statistical Society: Series B (Methodological)*, 39(1), 1–22. <https://doi.org/10.1111/j.2517-6161.1977.tb01600.x>
- Dentinger, C. M., Rakotomanga, T. A., Rakotondrandriana, A., Rakotoarisoa, A., Rason, M. A., Moriarty, L. F., Steinhart, L. C., Kapesa, L., Razafindrakoto, J., Svigel, S. S., Lucchi, N. W., Udhayakumar, V., Halsey, E. S., & Ratsimbaoa, C. A. (2021). Efficacy of artesunate-amodiaquine and artemether-lumefantrine for uncomplicated Plasmodium falciparum malaria in Madagascar, 2018. *Malaria Journal*, 20(1), 432. <https://doi.org/10.1186/s12936-021-03935-4>
- Di Domenico, L., Pullano, G., Sabbatini, C. E., Boëlle, P.-Y., & Colizza, V. (2020). Impact of lockdown on COVID-19 epidemic in Île-de-France and possible exit strategies. *BMC Medicine*, 18(1), 240. <https://doi.org/10.1186/s12916-020-01698-4>
- Direction de Lutte contre le Paludisme. (2017). Ministère de la santé publique de Madagascar. *PLAN STRATEGIQUE DE LUTTE CONTRE LE PALUDISME – MADAGASCAR 2018-2022*.
- Djidjou-Demasse, R., Selinger, C., & Sofonea, M. T. (2020). Épidémiologie mathématique et modélisation de la pandémie de Covid-19 : enjeux et diversité. *Revue Francophone Des Laboratoires*, 2020(526), 63–69. [https://doi.org/10.1016/S1773-035X\(20\)30315-4](https://doi.org/10.1016/S1773-035X(20)30315-4)
- Domenech de Cellès, M., Casalegno, J.-S., Lina, B., & Opatowski, L. (2021). Estimating the impact of influenza on the epidemiological dynamics of SARS-CoV-2. *PeerJ*, 9, e12566. <https://doi.org/10.7717/peerj.12566>
- Drakeley, C. J., Corran, P. H., Coleman, P. G., Tongren, J. E., McDonald, S. L. R., Carneiro, I., Malima, R., Lusingu, J., Manjurano, A., Nkya, W. M. M., Lemnge, M. M., Cox, J., Reyburn, H., & Riley, E. M. (2005). Estimating medium- and long-term trends in malaria transmission by using serological markers of malaria exposure. *Proceedings of the National Academy of Sciences of the United States of America*, 102(14), 5108–5113. <https://doi.org/10.1073/pnas.0408725102>
- Eikenberry, S. E., & Gumel, A. B. (2018). Mathematical modeling of climate change and malaria transmission dynamics: a historical review. *Journal of Mathematical Biology*, 77(4), 857–933. <https://doi.org/10.1007/s00285-018-1229-7>
- Evans, M. V., Garchitorena, A., Rakotonanahary, R. J. L., Drake, J. M., Andriamihaja, B., Rajaonarifara, E., Ngonghala, C. N., Roche, B., Bonds, M. H., & Rakotonirina, J. (2020). Reconciling model predictions with low reported cases of COVID-19 in Sub-Saharan Africa: insights from Madagascar. *Global Health*

- Action*, 13(1). <https://doi.org/10.1080/16549716.2020.1816044>
- Fang, L.-Q., Yang, Y., Jiang, J.-F., Yao, H.-W., Kargbo, D., Li, X.-L., Jiang, B.-G., Kargbo, B., Tong, Y.-G., Wang, Y.-W., Liu, K., Kamara, A., Dafaé, F., Kanu, A., Jiang, R.-R., Sun, Y., Sun, R.-X., Chen, W.-J., Ma, M.-J., ... Cao, W.-C. (2016). Transmission dynamics of Ebola virus disease and intervention effectiveness in Sierra Leone. *Proceedings of the National Academy of Sciences*, 113(16), 4488–4493. <https://doi.org/10.1073/pnas.1518587113>
- Farr, T. G., Rosen, P. A., Caro, E., Crippen, R., Duren, R., Hensley, S., Kobrick, M., Paller, M., Rodriguez, E., Roth, L., Seal, D., Shaffer, S., Shimada, J., Umland, J., Werner, M., Oskin, M., Burbank, D., & Alsdorf, D. E. (2007). The shuttle radar topography mission. *Reviews of Geophysics*, 45(2), 2004. <https://doi.org/10.1029/2005RG000183>
- Feachem, R. G. A., Chen, I., Akbari, O., Bertozzi-Villa, A., Bhatt, S., Binka, F., Boni, M. F., Buckee, C., Dieleman, J., Dondorp, A., Eapen, A., Sekhri Feachem, N., Filler, S., Gething, P., Gosling, R., Haakenstad, A., Harvard, K., Hatefi, A., Jamison, D., ... Mpanju-Shumbusho, W. (2019). Malaria eradication within a generation: ambitious, achievable, and necessary. *Lancet (London, England)*, 394(10203), 1056–1112. [https://doi.org/10.1016/S0140-6736\(19\)31139-0](https://doi.org/10.1016/S0140-6736(19)31139-0)
- Ferguson, N. M. (2018). Challenges and opportunities in controlling mosquito-borne infections. *Nature* 2018 559:7715, 559(7715), 490–497. <https://doi.org/10.1038/s41586-018-0318-5>
- Friedl, M. A., Sulla-Menashe, D., Tan, B., Schneider, A., Ramankutty, N., Sibley, A., & Huang, X. (2010). MODIS Collection 5 global land cover: Algorithm refinements and characterization of new datasets. *Remote Sensing of Environment*, 114(1), 168–182. <https://doi.org/10.1016/j.rse.2009.08.016>
- Gallifant, J., Sharell, D., Hashmi, M., Riviello, E. D., Schultz, M. J., Ulisubisya, M. M., & Formenti, F. (2022). Mechanical ventilators for low- and middle-income countries: informing a context-specific and sustainable design. *British Journal of Anaesthesia*, 128(4), e279–e281. <https://doi.org/10.1016/j.bja.2022.01.007>
- Garchitorena, A., Sokolow, S. H., Roche, B., Ngonghala, C. N., Jocque, M., Lund, A., Barry, M., Mordecai, E. A., Daily, G. C., Jones, J. H., Andrews, J. R., Bendavid, E., Luby, S. P., LaBeaud, A. D., Seetah, K., Guégan, J. F., Bonds, M. H., & De Leo, G. A. (2017). Disease ecology, health and the environment: a framework to account for ecological and socio-economic drivers in the control of neglected tropical diseases. *Philosophical Transactions of the Royal Society B: Biological Sciences*, 372(1722), 20160128. <https://doi.org/10.1098/rstb.2016.0128>
- Garchitorena, Andres, Ihantamalala, F. A., Révillion, C., Cordier, L. F., Randriamihaja, M., Razafinjato, B., Rafenoarivamalala, F. H., Finnegan, K. E., Andrianirinarison, J. C., Rakotonirina, J., Herbreteau, V., & Bonds, M. H. (2021). Geographic barriers to achieving universal health coverage: evidence from rural Madagascar. *Health Policy and Planning*, 36(10), 1659–1670. <https://doi.org/10.1093/heapol/czab087>
- Garchitorena, Andres, Rasoloharimanana, L. T., Rakotonanahary, R. J., Evans, M. V., Miller, A. C., Finnegan, K. E., Cordier, L. F., Cowley, G., Razafinjato, B., Randriamanambintsoa, M., Andrianambinina, S., Popper, S. J., Hotahiene, R., Bonds, M. H., & Schoenhals, M. (2023). Morbidity and mortality burden of COVID-19 in rural Madagascar: results from a longitudinal cohort and nested seroprevalence study. *International Journal of Epidemiology*. <https://doi.org/10.1093/ije/dyad135>
- Gaudart, J., Giorgi, R., Poudiougou, B., Touré, O., Ranque, S., Doumbo, O., & Demongeot, J. (2007). Spatial cluster detection without point source specification: the use of five methods and comparison of their results. *Revue d'Epidemiologie et de Sante Publique*, 55(4), 297–306. <https://doi.org/10.1016/j.respe.2007.04.003>
- Gaudart, Jean, Poudiougou, B., Ranque, S., & Doumbo, O. (2005). Oblique decision trees for spatial pattern detection: Optimal algorithm and application to malaria risk. *BMC Medical Research Methodology*, 5(1), 22. <https://doi.org/10.1186/1471-2288-5-22>
- GBD 2017 SDG Collaborators. (2018). Measuring progress from 1990 to 2017 and projecting attainment to 2030 of the health-related Sustainable Development Goals for 195 countries and territories: a systematic analysis for the Global Burden of Disease Study 2017. *The Lancet*, 392(10159), 2091–2138. [https://doi.org/10.1016/S0140-6736\(18\)32281-5](https://doi.org/10.1016/S0140-6736(18)32281-5)
- Gebhard, C., Regitz-Zagrosek, V., Neuhauser, H. K., Morgan, R., & Klein, S. L. (2020). Impact of sex and gender on COVID-19 outcomes in Europe. *Biology of Sex Differences* 2020 11:1, 11(1), 1–13. <https://doi.org/10.1186/S13293-020-00304-9>
- Getis, A., & Ord, J. K. (2010). The Analysis of Spatial Association by Use of Distance Statistics. In *Advances in Spatial Science* (Vol. 61, Issue 24, pp. 127–145). https://doi.org/10.1007/978-3-642-01976-0_10
- Girond, F., Madec, Y., Kesteman, T., Randrianariveolosia, M., Randremanana, R., Randriamampionona, L., Randrianasolo, L., Ratsitorahina, M., Herbreteau, V., Hedje, J., Rogier, C., & Piola, P. (2018). Evaluating Effectiveness of Mass and Continuous Long-lasting Insecticidal Net Distributions Over Time in Madagascar: A Sentinel Surveillance Based Epidemiological Study. *EClinicalMedicine*, 1, 62–69. <https://doi.org/10.1016/j.eclinm.2018.07.003>
- Girond, F., Randrianasolo, L., Randriamampionona, L., Rakotomanana, F., Randrianariveolosia, M.,

- Ratsitorahina, M., Brou, T. Y., Herbreteau, V., Mangeas, M., Zigiugabe, S., Hedje, J., Rogier, C., & Piola, P. (2017). Analysing trends and forecasting malaria epidemics in Madagascar using a sentinel surveillance network: a web-based application. *Malaria Journal*, *16*(1), 72. <https://doi.org/10.1186/s12936-017-1728-9>
- GlobalHealth 5050. (2021). *The Sex, Gender and COVID-19 Project | Global Health 50/50*. The Sex, Gender and COVID-19 Project. <https://globalhealth5050.org/the-sex-gender-and-covid-19-project/> (Accessed le 20 octobre 2023)
- Gouvernement de Madagascar. (2020). *TATITRY NY FILANKEVITRY NY MINISITRA NATAO TAMIN'NY ALALAN'NY « VISIOCONFERENCE » NY 08 JOLAY 2020*. Conseil Des Ministres. <https://www.presidence.gov.mg/actualites/conseil-des-ministres/907-tatitry-ny-filankevity-ny-minisitranatao-tamin-ny-alalan-ny-visioconference-ny-08-jolay-2020.html> (Accessed le 20 octobre 2023)
- Gouvernement de Madagascar. (2021). *Urgence sanitaire nationale*. Conseil Des Ministres. <https://www.presidence.gov.mg/actualites/conseil-des-ministres/1201-tatitry-ny-filan-kevity-ny-minisitranatao-tamin-ny-alalan-ny-visioconference-ny-31-martsa-2021.html> (Accessed le 20 octobre 2023)
- Grinsted, A., Moore, J. C., & Jevrejeva, S. (2004). Application of the cross wavelet transform and wavelet coherence to geophysical time series. *Nonlinear Processes in Geophysics*, *11*(5/6), 561–566. <https://doi.org/10.5194/npg-11-561-2004>
- Guerra, C. A., Snow, R. W., & Hay, S. I. (2006). Mapping the global extent of malaria in 2005. *Trends in Parasitology*, *22*(8), 353–358. <https://doi.org/10.1016/j.pt.2006.06.006>
- Hamer, W. H. (1906). The Milroy Lectures ON EPIDEMIC DISEASE IN ENGLAND—THE EVIDENCE OF VARIABILITY AND OF PERSISTENCY OF TYPE. *The Lancet*, *167*(4305), 569–574. [https://doi.org/10.1016/S0140-6736\(01\)80187-2](https://doi.org/10.1016/S0140-6736(01)80187-2)
- Harrison, X. A. (2015). A comparison of observation-level random effect and Beta-Binomial models for modelling overdispersion in Binomial data in ecology & evolution. *PeerJ*, *2015*(7), e1114. <https://doi.org/10.7717/peerj.1114>
- Hastie, T., & Tibshirani, R. (1986). [Generalized Additive Models]: Rejoinder. *Statistical Science*, *1*(3), 314–318. <https://doi.org/10.1214/ss/1177013609>
- Hay, J. A., Kennedy-Shaffer, L., Kanjilal, S., Lennon, N. J., Gabriel, S. B., Lipsitch, M., & Mina, M. J. (2021). Estimating epidemiologic dynamics from cross-sectional viral load distributions. *Science*, *373*(6552). <https://doi.org/10.1126/science.abh0635>
- Heesterbeek, H., Anderson, R. M., Andreasen, V., Bansal, S., De Angelis, D., Dye, C., Eames, K. T. D., Edmunds, W. J., Frost, S. D. W., Funk, S., Hollingsworth, T. D., House, T., Isham, V., Klepac, P., Lessler, J., Lloyd-Smith, J. O., Metcalf, C. J. E., Mollison, D., Pellis, L., ... Viboud, C. (2015). Modeling infectious disease dynamics in the complex landscape of global health. *Science*, *347*(6227). <https://doi.org/10.1126/science.aaa4339>
- Hilton, E. R., Rabeherisoa, S., Ramandimbiarajaona, H., Rajaratnam, J., Belemvire, A., Kapesa, L., Zohdy, S., Dentinger, C., Gandaho, T., Jacob, D., Burnett, S., & Razafinjato, C. (2023). Using routine health data to evaluate the impact of indoor residual spraying on malaria transmission in Madagascar. *BMJ Global Health*, *8*(7), e010818. <https://doi.org/10.1136/BMJGH-2022-010818>
- Howes, R. E., Hawa, K., Andriamamonjy, V. F., Franchard, T., Miarambola, R., Mioramalala, S. A., Rafamatanantsoa, J. F., Rahantamalala, M. A. M., Rajaobary, S. H., Rajaonera, H. D. G., Rakotonindrainy, A. P., Rakotoson Andrianjatonavalona, C., Randriamiarinjatovo, D. N. A. L., Randrianasolo, F. M., Ramasy Razafindratovo, R. M., Ravaoarimanga, M., Ye, M., Gething, P. W., & Taylor, C. A. (2019). A stakeholder workshop about modelled maps of key malaria indicator survey indicators in Madagascar. *Malaria Journal*, *18*(1), 1–10. <https://doi.org/10.1186/s12936-019-2729-7>
- Howes, R. E., Mioramalala, S. A., Ramiranirina, B., Franchard, T., Rakotorahalahy, A. J., Bisanzio, D., Gething, P. W., Zimmerman, P. A., & Ratsimbao, A. (2016). Contemporary epidemiological overview of malaria in Madagascar: operational utility of reported routine case data for malaria control planning. *Malaria Journal*, *15*(1), 502. <https://doi.org/10.1186/s12936-016-1556-3>
- Hyde, E., Bonds, M. H., Ihantamalala, F. A., Miller, A. C., Cordier, L. F., Razafinjato, B., Andriambolamanana, H., Randriamanambintsoa, M., Barry, M., Andrianirinarison, J. C., Andriamananjara, M. N., & Garchitorea, A. (2021). Estimating the local spatio-temporal distribution of malaria from routine health information systems in areas of low health care access and reporting. *International Journal of Health Geographics*, *20*(1), 8. <https://doi.org/10.1186/s12942-021-00262-4>
- Ihantamalala FA, R. Ratovoson, R. Mangahasimbola, F. Rakotomanana. Modélisation de l'accessibilité aux soins dans les centres de santé de base publiques, Moramanga, Madagascar, *Revue d'Épidémiologie et de Santé Publique*, *62* (5) 2014, S189-S190. <https://doi.org/10.1016/j.respe.2014.06.060>
- Ihantamalala, Felana A., Rakotoarimanana, F. M. J., Ramiadantsoa, T., Rakotondramanga, J. M., Pennober, G., Rakotomanana, F., Cauchemez, S., Metcalf, C. J. E., Herbreteau, V., & Wesolowski, A. (2018). Spatial and temporal dynamics of malaria in Madagascar. *Malaria Journal*, *17*(1), 58.

- <https://doi.org/10.1186/s12936-018-2206-8>
- Ihantamalala, Felana Angella, Bonds, M. H., Randriamihaja, M., Rakotonirina, L., Herbreteau, V., Révillion, C., Rakotoarimanana, S., Cowley, G., Andriatiana, T. A., Mayfield, A., Rich, M. L., Rakotonanahary, R. J., Finnegan, K. E., Ramarson, A., Razafinjato, B., Ramiandrisoa, B., Randrianambinina, A., Cordier, L. F., & Garchitorena, A. (2021). Geographic barriers to establishing a successful hospital referral system in rural Madagascar. *BMJ Global Health*, 6(12), 2021.08.06.21261682. <https://doi.org/10.1136/bmjgh-2021-007145>
- Ihantamalala, Felana Angella, Herbreteau, V., Rakotoarimanana, F. M. J., Rakotondramanga, J. M., Cauchemez, S., Rahoilijaona, B., Pennober, G., Buckee, C. O., Rogier, C., Metcalf, C. J. E., & Wesolowski, A. (2018). Estimating sources and sinks of malaria parasites in Madagascar. *Nature Communications*, 9(1), 3897. <https://doi.org/10.1038/s41467-018-06290-2>
- Ihantamalala, H. F. A. (2013). Détermination des bassins de recrutement des patients dans les structures sanitaires périphériques, Moramanga, Madagascar. (Master 2: Télé-détection et risques naturels) [Université de La Réunion]
- Institut National de la Statistique, Programme National de Lutte contre le Paludisme, Institut Pasteur de Madagascar, Antananarivo, Madagascar and ICF International, Calverton, Maryland, U. (2016). *Madagascar, Enquête sur les Indicateurs du Paludisme*. 33–45. <http://dhsprogram.com/pubs/pdf/MIS17/MIS17.pdf>
- Institut National de la Statistique (INSTAT). (2021). *TROISIEME RECENSEMENT GENERAL DE LA POPULATION ET DE L'HABITATION (RGPH-3)*. https://madagascar.unfpa.org/sites/default/files/pub-pdf/resultat_globaux_rgph3_tome_01.pdf (Accessed le 20 octobre 2023)
- Institut National de la Statistique (INSTAT) et ICF. (2021). *Enquête Démographique et de Santé à Madagascar, 2021 : Indicateurs Clés*. https://www.unicef.org/madagascar/media/7286/file/INSTAT_EDSMD-V_Indicateurs-cl%C3%83%C2%A9s.pdf (Accessed le 20 octobre 2023)
- Institut National de la Statistique (INSTAT) et ICF Macro. (2010). *Enquête Démographique et de Santé de Madagascar 2008-2009*. <https://dhsprogram.com/methodology/survey/survey-display-296.cfm> (Accessed le 20 octobre 2023)
- Irinantenaina, J., Carn, G., Ny, D., Randriamiarinjatovo, A. L., Harimanana, A. N., Razanatsiorimalala, S., Ralemary, N., Randriarison, M., Razafinjato, C., Hotahiene, R., & Randrianarivojosia, M. (2023). Therapeutic efficacy and safety of artesunate + amodiaquine and artemether + lumefantrine in treating uncomplicated *Plasmodium falciparum* malaria in children on the rainy south-east coast of Madagascar. *Parasite*, 30, 32. <https://doi.org/10.1051/PARASITE/2023034>
- Islam, N., Jdanov, D. A., Shkolnikov, V. M., Khunti, K., Kawachi, I., White, M., Lewington, S., & Lacey, B. (2021). Effects of covid-19 pandemic on life expectancy and premature mortality in 2020: time series analysis in 37 countries. *BMJ*, 375. <https://doi.org/10.1136/BMJ-2021-066768>
- Kang, S. Y., Battle, K. E., Gibson, H. S., Ratsimbaoa, A., Randrianarivojosia, M., Ramboarina, S., Zimmerman, P. A., Weiss, D. J., Cameron, E., Gething, P. W., & Howes, R. E. (2018). Spatio-temporal mapping of Madagascar's Malaria Indicator Survey results to assess *Plasmodium falciparum* endemicity trends between 2011 and 2016. *BMC Medicine*, 16(1), 1–15. <https://doi.org/10.1186/s12916-018-1060-4>
- Kangoye, D. T., Noor, A., Midega, J., Mwongeli, J., Mkabili, D., Mogeni, P., Kerubo, C., Akoo, P., Mwangangi, J., Drakeley, C., Marsh, K., Bejon, P., & Njuguna, P. (2016). Malaria hotspots defined by clinical malaria, asymptomatic carriage, PCR and vector numbers in a low transmission area on the Kenyan Coast. *Malaria Journal*, 15(1), 1–13. <https://doi.org/10.1186/s12936-016-1260-3>
- Kerkhof, K., Canier, L., Kim, S., Heng, S., Sochantha, T., Sovannaroth, S., Vigan-Womas, I., Coosemans, M., Sluydts, V., Ménard, D., & Durnez, L. (2015). Implementation and application of a multiplex assay to detect malaria-specific antibodies: a promising tool for assessing malaria transmission in Southeast Asian pre-elimination areas. *Malaria Journal*, 14(1). <https://doi.org/10.1186/s12936-015-0868-z>
- Kermack, W. O., & McKendrick, A. G. (1927). A contribution to the mathematical theory of epidemics. *Proceedings of the Royal Society of London. Series A, Containing Papers of a Mathematical and Physical Character*, 115(772), 700–721. <https://doi.org/10.1098/rspa.1927.0118>
- King, C. L., Davies, D. H., Felgner, P., Baum, E., Jain, A., Randall, A., Tetteh, K., Drakeley, C. J., & Greenhouse, B. (2015). Biosignatures of Exposure/Transmission and Immunity. *The American Journal of Tropical Medicine and Hygiene*, 93(3), 16–27. <https://doi.org/10.4269/ajtmh.15-0037>
- Kleinschmidt, I., Bagayoko, M., Clarke, G. P. Y., Craig, M., & Le Sueur, D. (2000). A spatial statistical approach to malaria mapping. *International Journal of Epidemiology*, 29(2), 355–361. <https://doi.org/10.1093/ije/29.2.355>
- Korenromp, E. L., Miller, J., Cibulskis, R. E., Cham, M. K., Alnwick, D., & Dye, C. (2003). Monitoring mosquito net coverage for malaria control in Africa: Possession vs. use by children under 5 years. *Tropical Medicine and International Health*, 8(8), 693–703. <https://doi.org/10.1046/j.1365-3156.2003.01084.x>
- Kousi, T., Vivacqua, D., Dalal, J., James, A., Câmara, D. C. P., Botero Mesa, S., Chimbetete, C., Impouma, B.,

- Williams, G. S., Mboussou, F., Mlanda, T., Bukhari, A., Keiser, O., Abbate, J. L., & Hofer, C. B. (2022). COVID-19 pandemic in Africa's island nations during the first 9 months: a descriptive study of variation in patterns of infection, severe disease, and response measures. *BMJ Global Health*, 7(3), e006821. <https://doi.org/10.1136/BMJGH-2021-006821>
- Kulkarni, M. A., Vanden Eng, J., Desrochers, R. E., Cotte, A. H., Goodson, J. L., Johnston, A., Wolkon, A., Erskine, M., Berti, P., Rakotoarisoa, A., Ranaivo, L., & Peat, J. (2010). Contribution of integrated campaign distribution of long-lasting insecticidal nets to coverage of target groups and total populations in malaria-endemic areas in Madagascar. *American Journal of Tropical Medicine and Hygiene*, 82(3), 420–425. <https://doi.org/10.4269/ajtmh.2010.09-0597>
- Kulldorff, M. (1997). A spatial scan statistic. *Communications in Statistics - Theory and Methods*, 26(6), 1481–1496. <https://doi.org/10.1080/03610929708831995>
- Lang E., P. Saint-Firmin, A. Olivetti, M. Rakotomalala, A. D. (2018). *Analyse du système de financement de la santé à Madagascar pour guider de futures réformes, notamment la CSU*. https://pdf.usaid.gov/pdf_docs/PA00T152.pdf (Accessed le 20 octobre 2023)
- Lee, R. D., & Carter, L. R. (1992). Modeling and Forecasting U. S. Mortality. *Journal of the American Statistical Association*, 87(419), 659. <https://doi.org/10.2307/2290201>
- Li, Q., Guan, X., Wu, P., Wang, X., Zhou, L., Tong, Y., Ren, R., Leung, K. S. M., Lau, E. H. Y., Wong, J. Y., Xing, X., Xiang, N., Wu, Y., Li, C., Chen, Q., Li, D., Liu, T., Zhao, J., Liu, M., ... Feng, Z. (2020). Early Transmission Dynamics in Wuhan, China, of Novel Coronavirus-Infected Pneumonia. *New England Journal of Medicine*, 382(13), 1199–1207. <https://doi.org/10.1056/NEJMOA2001316>
- Lin, J. T., Saunders, D. L., & Meshnick, S. R. (2014). The role of submicroscopic parasitemia in malaria transmission: What is the evidence? *Trends in Parasitology*, 30(4), 183–190. <https://doi.org/10.1016/j.pt.2014.02.004>
- Linard, C., Gilbert, M., Snow, R. W., Noor, A. M., & Tatem, A. J. (2012). Population distribution, settlement patterns and accessibility across Africa in 2010. *PLoS ONE*, 7(2). <https://doi.org/10.1371/journal.pone.0031743>
- Lindblade, K. A., Steinhart, L., Samuels, A., Kachur, S. P., & Slutsker, L. (2013). The silent threat: Asymptomatic parasitemia and malaria transmission. *Expert Review of Anti-Infective Therapy*, 11(6), 623–639. <https://doi.org/10.1586/eri.13.45>
- Linton, N., Kobayashi, T., Yang, Y., Hayashi, K., Akhmetzhanov, A., Jung, S., Yuan, B., Kinoshita, R., & Nishiura, H. (2020). Incubation Period and Other Epidemiological Characteristics of 2019 Novel Coronavirus Infections with Right Truncation: A Statistical Analysis of Publicly Available Case Data. *Journal of Clinical Medicine*, 9(2), 538. <https://doi.org/10.3390/jcm9020538>
- Logie, D. E., Rowson, M., & Ndagije, F. (2008). Innovations in Rwanda's health system: looking to the future. *The Lancet*, 372(9634), 256–261. [https://doi.org/10.1016/S0140-6736\(08\)60962-9](https://doi.org/10.1016/S0140-6736(08)60962-9)
- Loveland, T. R., & Belward, A. S. (1997). The international geosphere biosphere programme data and information system global land cover data set (DIScover). *Acta Astronautica*, 41(4–10), 681–689. [https://doi.org/10.1016/S0094-5765\(98\)00050-2](https://doi.org/10.1016/S0094-5765(98)00050-2)
- Maina, J., Ouma, P. O., Macharia, P. M., Alegana, V. A., Mitto, B., Fall, I. S., Noor, A. M., Snow, R. W., & Okiro, E. A. (2019). A spatial database of health facilities managed by the public health sector in sub Saharan Africa. *Scientific Data*, 6(1), 134. <https://doi.org/10.1038/s41597-019-0142-2>
- Manjurano, A., Okell, L., Lukindo, T., Reyburn, H., Olomi, R., Roper, C., Clark, T. G., Joseph, S., Riley, E. M., & Drakeley, C. (2011). Association of sub-microscopic malaria parasite carriage with transmission intensity in north-eastern Tanzania. *Malaria Journal*, 10(1), 370. <https://doi.org/10.1186/1475-2875-10-370>
- Masquelier, B., Pison, G., Rakotonirina, J., & Rasoanomenjanahary, A. (2019). Estimating cause-specific mortality in Madagascar: an evaluation of death notification data from the capital city. *Population Health Metrics*, 17(1), 8. <https://doi.org/10.1186/s12963-019-0190-z>
- Mathieu, E., Ritchie, H., Rodés-Guirao, L., Appel, C., Giattino, C., Hasell, J., Macdonald, B., Dattani, S., Beltekian, D., Ortiz-Ospina, E., & Roser, M. (2020). *Coronavirus pandemic (COVID-19): Australia: Coronavirus Pandemic Country Profile*. OurWorldInData.Org. <https://ourworldindata.org/coronavirus> (Accessed le 20 octobre 2023)
- Mauny, F., Viel, J. F., Handschumacher, P., & Sellin, B. (2004). Multilevel modelling and malaria: A new method for an old disease. *International Journal of Epidemiology*, 33(6), 1337–1344. <https://doi.org/10.1093/ije/dyh274>
- Metcalf, C. J. E., Graham, A. L., Huijben, S., Barclay, V. C., Long, G. H., Grenfell, B. T., Read, A. F., & Bjørnstad, O. N. (2011). Partitioning regulatory mechanisms of within-host malaria dynamics using the effective propagation number. *Science*, 333(6045), 984–988. <https://doi.org/10.1126/science.1204588>
- Metcalf, C. J. E., Lessler, J., Klepac, P., Morice, A., Grenfell, B. T., & Bjørnstad, O. N. (2012). Structured models of infectious disease: Inference with discrete data. *Theoretical Population Biology*, 82(4), 275–

282. <https://doi.org/10.1016/j.tpb.2011.12.001>
- Moiroux, N., Gomez, M. B., Pennetier, C., Elanga, E., Djènontin, A., Chandre, F., Djègbé, I., Guis, H., & Corbel, V. (2012). Changes in anopheles funestus biting behavior following universal coverage of long-lasting insecticidal nets in benin. *Journal of Infectious Diseases*, 206(10), 1622–1629. <https://doi.org/10.1093/infdis/jis565>
- MORAN, P. A. P. (1950). Notes on continuous stochastic phenomena. *Biometrika*, 37(1–2), 17–23.
- Mosha, J. F., Sturrock, H. J., Greenwood, B., Sutherland, C. J., Gadalla, N. B., Atwal, S., Hemelaar, S., Brown, J. M., Drakeley, C., Kibiki, G., Bousema, T., Chandramohan, D., & Gosling, R. D. (2014). Hot spot or not: a comparison of spatial statistical methods to predict prospective malaria infections. *Malaria Journal*, 13(1), 53. <https://doi.org/10.1186/1475-2875-13-53>
- Mosson, J., Hens, N., Jit, M., Beutels, P., Auranen, K., Mikolajczyk, R., Massari, M., Salmaso, S., Tomba, G. S., Wallinga, J., Heijne, J., Sadkowska-Todys, M., Rosinska, M., & Edmunds, W. J. (2008). Social Contacts and Mixing Patterns Relevant to the Spread of Infectious Diseases. *PLOS Medicine*, 5(3), e74. <https://doi.org/10.1371/JOURNAL.PMED.0050074>
- Msemburi, W., Karlinsky, A., Knutson, V., Aleshin-Guendel, S., Chatterji, S., & Wakefield, J. (2022). The WHO estimates of excess mortality associated with the COVID-19 pandemic. *Nature* 2022, 1–8. <https://doi.org/10.1038/s41586-022-05522-2>
- Mwananyanda, L., Gill, C. J., Macleod, W., Kwenda, G., Pieciak, R., Mupila, Z., Lapidot, R., Mupeta, F., Forman, L., Ziko, L., Etter, L., & Thea, D. (2021). Covid-19 deaths in Africa: prospective systematic postmortem surveillance study. *BMJ*, 372. <https://doi.org/10.1136/BMJ.N334>
- Nakagawa, S., & Schielzeth, H. (2013). A general and simple method for obtaining R² from generalized linear mixed-effects models. *Methods in Ecology and Evolution*, 4(2), 133–142. <https://doi.org/10.1111/j.2041-210x.2012.00261.x>
- Narison, S., & Maltezos, S. (2021). Scrutinizing the spread of COVID-19 in Madagascar. *Infection, Genetics and Evolution*, 87, 104668. <https://doi.org/10.1016/j.meegid.2020.104668>
- Nguyen, M., Howes, R. E., Lucas, T. C. D., Battle, K. E., Cameron, E., Gibson, H. S., Rozier, J., Keddie, S., Collins, E., Arambepola, R., Kang, S. Y., Hendriks, C., Nandi, A., Rumisha, S. F., Bhatt, S., Mioramalala, S. A., Nambinisoa, M. A., Rakotomanana, F., Gething, P. W., & Weiss, D. J. (2020). Mapping malaria seasonality in Madagascar using health facility data. *BMC Medicine*, 18(1), 26. <https://doi.org/10.1186/s12916-019-1486-3>
- Nimpa, M. M., Andrianirinarison, J. C., Sodjinou, V. D., Douba, A., Masembe, Y. V., Randriatsarafara, F., Ramamonjisoa, C. B., Rafalimanantsoa, A. S., Razafindratsimandresy, R., Ndiaye, C. F., & Rakotonirina, J. (2020). Measles outbreak in 2018-2019, Madagascar: epidemiology and public health implications. *PAMJ*. 2020; 35:84, 35(84). <https://doi.org/10.11604/PAMJ.2020.35.84.19630>
- Nishiura, H. (2006). Epidemiology of a primary pneumonic plague in Kantoshu, Manchuria, from 1910 to 1911: statistical analysis of individual records collected by the Japanese Empire. *International Journal of Epidemiology*, 35(4), 1059–1065. <https://doi.org/10.1093/IJE/DYL091>
- Nishiura, H., Linton, N. M., & Akhmetzhanov, A. R. (2020). Serial interval of novel coronavirus (COVID-19) infections. *International Journal of Infectious Diseases*, 93, 284–286. <https://doi.org/10.1016/j.ijid.2020.02.060>
- Noufaily, A., Enki, D. G., Farrington, P., Garthwaite, P., Andrews, N., & Charlett, A. (2013). An improved algorithm for outbreak detection in multiple surveillance systems. *Statistics in Medicine*, 32(7), 1206–1222. <https://doi.org/10.1002/sim.5595>
- Oak Ridge National Laboratory Distributed Active Archive Center (ORNL DAAC). (2018). *MODIS and VIIRS Land Product Subsets RESTful Web Service*. ORNL Distributed Active Archive Center. <https://doi.org/10.3334/ORNLDAAC/1600>
- Odiambo, J. N., Kalinda, C., MacHaria, P. M., Snow, R. W., & Sartorius, B. (2020). Spatial and spatio-temporal methods for mapping malaria risk: A systematic review. *BMJ Global Health*, 5(10), e002919. <https://doi.org/10.1136/bmjgh-2020-002919>
- Okebe, J., Affara, M., Correa, S., Muhammad, A. K., Nwakanma, D., Drakeley, C., & D'Alessandro, U. (2014). School-based countrywide seroprevalence survey reveals spatial heterogeneity in malaria transmission in the Gambia. *PLoS ONE*, 9(10), e110926. <https://doi.org/10.1371/journal.pone.0110926>
- Okell, L. C., Bousema, T., Griffin, J. T., Ouedraogo, A. L., Ghani, A. C., & Drakeley, C. J. (2012). Factors determining the occurrence of submicroscopic malaria infections and their relevance for control. *Nature Communications*, 3(1), 1237. <https://doi.org/10.1038/ncomms2241>
- Okell, L. C., Ghani, A. C., Lyons, E., & Drakeley, C. J. (2009). Submicroscopic infection in plasmodium falciparum-endemic populations: A systematic review and meta-analysis. *Journal of Infectious Diseases*, 200(10), 1509–1517. <https://doi.org/10.1086/644781>
- Okell, L. C., Paintain, L. S., Webster, J., Hanson, K., & Lines, J. (2012). From intervention to impact: modelling the potential mortality impact achievable by different long-lasting, insecticide-treated net delivery

- strategies. *Malaria Journal*, 11(1), 327. <https://doi.org/10.1186/1475-2875-11-327>
- Ouma, P. E. O. (2020). Spatial Access to Comprehensive Emergency Obstetric and Neonatal Care and Its Relationship to Mortality at the Regional Level in Sub-Saharan Africa and at a National Level in Kenya. *PQDT - Global*, 296. <https://doi.org/10.21954/ou.ro.000120d4>
- Paaijmans, K. P., & Thomas, M. B. (2011). The influence of mosquito resting behaviour and associated microclimate for malaria risk. In *Malaria Journal* (Vol. 10, Issue 1, pp. 1–7). BioMed Central. <https://doi.org/10.1186/1475-2875-10-183>
- Parham, P. E., & Hughes, D. A. (2015). Climate influences on the cost-effectiveness of vector-based interventions against malaria in elimination scenarios. *Philosophical Transactions of the Royal Society B: Biological Sciences*, 370(1665), 1–15. <https://doi.org/10.1098/rstb.2013.0557>
- Pedersen, E. J., Miller, D. L., Simpson, G. L., & Ross, N. (2019). Hierarchical generalized additive models in ecology: an introduction with mgcv. *PeerJ*, 7, e6876. <https://doi.org/10.7717/peerj.6876>
- Pellis, L., Cauchemez, S., Ferguson, N. M., & Fraser, C. (2020). Systematic selection between age and household structure for models aimed at emerging epidemic predictions. *Nature Communications*, 11(1), 906. <https://doi.org/10.1038/s41467-019-14229-4>
- Perraut, R., Richard, V., Varela, M.-L., Trape, J.-F., Guilloitte, M., Tall, A., Toure, A., Sokhna, C., Vigan-Womas, I., & Mercereau-Puijalon, O. (2014). Comparative analysis of IgG responses to Plasmodium falciparum MSP1p19 and PF13-DBL1 α 1 using ELISA and a magnetic bead-based duplex assay (MAGPIX®-Luminex) in a Senegalese meso-endemic community. *Malaria Journal*, 13(1). <https://doi.org/10.1186/1475-2875-13-410>
- Pourtois, J. D., Tallam, K., Jones, I., Id, E. H., Chamberlin, A. J., Evans Id, M. V., Ihantamalala, F. A., Cordier, L. F., Né Dicte, B., Razafinjato, R., Rakotonanahary, R. J. L., Tsirinomen'ny Aina, A., Soloniaina, P., Raholiarimanana, S. H., Razafinjato, C., Bonds, M. H., De Leo, G. A., Sokolow, S. H., & Garchitorenaid, A. (2023). Climatic, land-use and socio-economic factors can predict malaria dynamics at fine spatial scales relevant to local health actors: Evidence from rural Madagascar. *PLOS Global Public Health*, 3(2), e0001607. <https://doi.org/10.1371/JOURNAL.PGPH.0001607>
- Programme Nationale de Lutte contre le Paludisme. (2012). Ministère de la santé publique de Madagascar. *PLAN STRATEGIQUE DE LUTTE CONTRE LE PALUDISME – MADAGASCAR 2013-2017*.
- QGIS Team Development. (2019). v3.10. *Open Source Geospatial Foundation Project*. <http://qgis.osgeo.org/en/site/>
- R Core Team. (2020). *R: A language and environment for statistical computing*. <https://www.r-project.org/>
- Rabarison, J. H., Tempia, S., Harimanana, A., Guillebaud, J., Razanajatovo, N. H., Ratsitorahina, M., & Heraud, J. M. (2019). Burden and epidemiology of influenza- and respiratory syncytial virus-associated severe acute respiratory illness hospitalization in Madagascar, 2011–2016. *Influenza and Other Respiratory Viruses*, 13(2), 138–147. <https://doi.org/10.1111/irv.12557>
- RAJATONIRINA, S., RAKOTOSOLOFO, B., RAKOTOMANANA, F., RANDRIANASOLO, L., RATSITOHARINA, M., RAHARINANDRASANA, H., HERAUD, J.-M., & RICHARD, V. (2013). Excess mortality associated with the 2009 A(H1N1)v influenza pandemic in Antananarivo, Madagascar. *Epidemiology and Infection*, 141(4), 745–750. <https://doi.org/10.1017/S0950268812001215>
- Rakotoarison, H. A., Rasamimalala, M., Rakotondramanga, J. M., Ramiranirina, B., Franchard, T., Kapesa, L., Razafindrakoto, J., Guis, H., Tantely, L. M., Girod, R., Rakotoniaina, S., Baril, L., Piola, P., & Rakotomanana, F. (2020). Remote Sensing and Multi-Criteria Evaluation for Malaria Risk Mapping to Support Indoor Residual Spraying Prioritization in the Central Highlands of Madagascar. *Remote Sensing*, 12(10), 1585. <https://doi.org/10.3390/rs12101585>
- Ramiadantsoa, T., Metcalf, C. J. E., Raheerinandrasana, A. H., Randrianarisoa, S., Rice, B. L., Wesolowski, A., Randriatsarafara, F. M., & Rasambainarivo, F. (2022). Existing human mobility data sources poorly predicted the spatial spread of SARS-CoV-2 in Madagascar. *Epidemics*, 38, 100534. <https://doi.org/10.1016/j.epidem.2021.100534>
- Randremanana, R., Andrianaivoarimanana, V., Nikolay, B., Ramasindrazana, B., Paireau, J., ten Bosch, Q. A., Rakotondramanga, J. M., Rahajandraibe, S., Rahelinirina, S., Rakotomanana, F., Rakotoarimanana, F. M., Randriamampionona, L. B., Razafimbiana, V., De Dieu Randria, M. J., Raberahona, M., Mikaty, G., Le Guern, A.-S., Rakotonjanabelo, L. A., Ndiaye, C. F., ... Rajerison, M. (2019). Epidemiological characteristics of an urban plague epidemic in Madagascar, August–November, 2017: an outbreak report. *The Lancet Infectious Diseases*, 19(5), 537–545. [https://doi.org/10.1016/S1473-3099\(18\)30730-8](https://doi.org/10.1016/S1473-3099(18)30730-8)
- Randremanana, R. V., Andriamandimby, S., Rakotondramanga, J. M., Razanajatovo, N. H., Mangahasimbola, R. T., Randriambolamanantsoa, T. H., Ranaivoson, H. C., Rabemananjara, H. A., Razanajatovo, I., Razafindratsimandresy, R., Rabarison, J. H., Brook, C. E., Rakotomanana, F., Rabetombosoa, R. M., Razafimanjato, H., Ahyong, V., Raharinosy, V., Raharimanga, V., Raharinantoanina, S. J., ... Heraud, J. (2021). The COVID-19 epidemic in Madagascar: clinical description and laboratory results of the first wave, march–september 2020. *Influenza and Other Respiratory Viruses*, 15(4), 457–468.

<https://doi.org/10.1111/irv.12845>

- Rasambainarivo, F., Ramiadantsoa, T., Raheerinandrasana, A., Randrianarisoa, S., Rice, B. L., Evans, M. V., Roche, B., Randriatsarafara, F. M., Wesolowski, A., & Metcalf, J. C. (2022). Prioritizing COVID-19 vaccination efforts and dose allocation within Madagascar. *BMC Public Health* 22:1, 22(1), 1–9. <https://doi.org/10.1186/S12889-022-13150-8>
- Rasambainarivo, F., Rasoanomenjanahary, A., Rabarison, J. H., Ramiadantsoa, T., Ratovoson, R., Rendremanana, R., Randrianarisoa, S., Rajeev, M., Masquelier, B., Heraud, J. M., Metcalf, C. J. E., & Rice, B. L. (2021). Monitoring for outbreak-associated excess mortality in an African city: Detection limits in Antananarivo, Madagascar. *International Journal of Infectious Diseases*, 103, 338–342. <https://doi.org/10.1016/j.ijid.2020.11.182>
- Rasoanaivo, T. F., Bourner, J., Randriamparany, R. N., Gamana, T. M., Andrianaivoarimanana, V., Rahevivo, M. H., Randriamampionona, H., Rajerison, M., Raberahona, M., Salam, A. P., Edwards, T., Olliaro, P. L., & Rendremanana, R. V. (2021). The impact of COVID-19 on clinical research for Neglected Tropical Diseases (NTDs): A case study of bubonic plague. *PLOS Neglected Tropical Diseases*, 15(12), e0010064. <https://doi.org/10.1371/JOURNAL.PNTD.0010064>
- Ratovoson, R. (2020). *Mortalité et santé à Madagascar : la transition sanitaire dans la zone de Moramanga, Madagascar* (Issue 2020SORUS423) [Sorbonne Université]. <https://theses.hal.science/tel-03584660>
- Ratovoson, R., Garchitorea, A., Kassie, D., Ravelonarivo, J. A., Andrianaranjaka, V., Razanatsiorimalala, S., Razafimandimby, A., Rakotomanana, F., Ohlstein, L., Mangahasimbola, R., Randrianarisoa, S. A. N., Razafindrakoto, J., Dentinger, C. M., Williamson, J., Kapesa, L., Piola, P., Randrianarivojosia, M., Thwing, J., Steinhardt, L. C., & Baril, L. (2022). Proactive community case management decreased malaria prevalence in rural Madagascar: results from a cluster randomized trial. *BMC Medicine* 20:1, 20(1), 1–15. <https://doi.org/10.1186/S12916-022-02530-X>
- Ratovoson, R., Razafimahatratra, R., Randriamanantsoa, L., Raberahona, M., Rabarison, H. J., Rahaingovahoaka, F. N., Andriamasy, E. H., Herindrainy, P., Razanajatovo, N., Andriamandimby, S. F., Dussart, P., Schoenhals, M., Randria, M. J. de D., Heraud, J. M., & Rendremanana, R. V. (2022). Household transmission of COVID-19 among the earliest cases in Antananarivo, Madagascar. *Influenza and Other Respiratory Viruses*, 16(1), 48–55. <https://doi.org/10.1111/irv.12896>
- Ratsitorahina, M., Chanteau, S., Rahalison, L., Ratsifasoamanana, L., & Boisier, P. (2000). Epidemiological and diagnostic aspects of the outbreak of pneumonic plague in Madagascar. *Lancet*, 355(9198), 111–113. [https://doi.org/10.1016/S0140-6736\(99\)05163-6](https://doi.org/10.1016/S0140-6736(99)05163-6)
- Razafimahatratra, S. L., Ndiaye, M. D. B., Rasoloharimanana, L. T., Dussart, P., Sahondranirina, P. H., Randriamanantany, Z. A., & Schoenhals, M. (2021). Seroprevalence of ancestral and Beta SARS-CoV-2 antibodies in Malagasy blood donors. *The Lancet Global Health*, 9(10), e1363–e1364. [https://doi.org/10.1016/S2214-109X\(21\)00361-2](https://doi.org/10.1016/S2214-109X(21)00361-2)
- Razakamanana, M. V., Audibert, M., Andrianantoandro, V. T., & Harimanana, A. (2020). Impact et efficience de l'intégration du diagnostic et du traitement de la pneumonie dans la prise en charge communautaire du paludisme à Madagascar. *Revue Économique*, Vol. 71(1), 5–30. <https://doi.org/10.3917/reco.711.0005>
- Razakandrainibe, R., Thonier, V., Ratsimbasoa, A., Rakotomalala, E., Ravaoarisoa, E., Raheerinjafy, R., Andrianantenaina, H., Voahanginirina, O., Rahasana, T. E., Carod, J. F., Domarle, O., & Menard, D. (2009). Epidemiological situation of malaria in Madagascar: Baseline data for monitoring the impact of malaria control programmes using serological markers. *Acta Tropica*, 111(2), 160–167. <https://doi.org/10.1016/j.actatropica.2009.04.007>
- Razanajatovo, I. M., Andrianomiadana, L., Habib, A., Randrianarisoa, M. M., Razafimanjato, H., Rakotondrainipiana, M., Andriantsalama, P., Randriamparany, R., Andriamandimby, S. F., Vonaesch, P., Sansonetti, P. J., Lacoste, V., Rendremanana, R. V., Collard, J. M., & Heraud, J. M. (2023). Factors Associated with Carriage of Enteropathogenic and Non-Enteropathogenic Viruses: A Reanalysis of Matched Case-Control Data from the AFRIBIOTA Site in Antananarivo, Madagascar. *Pathogens*, 12(8), 1009. <https://doi.org/10.3390/PATHOGENS12081009>
- Reiner, R. C., Perkins, T. A., Barker, C. M., Niu, T., Chaves, L. F., Ellis, A. M., George, D. B., Le Menach, A., Pulliam, J. R. C., Bisanzio, D., Buckee, C., Chiyaka, C., Cummings, D. A. T., Garcia, A. J., Gatton, M. L., Gething, P. W., Hartley, D. M., Johnston, G., Klein, E. Y., ... Smith, D. L. (2013). A systematic review of mathematical models of mosquito-borne pathogen transmission: 1970–2010. In *Journal of the Royal Society Interface* (Vol. 10, Issue 81, p. 20120921). The Royal Society. <https://doi.org/10.1098/rsif.2012.0921>
- Rek, J., Blanken, S. L., Okoth, J., Ayo, D., Onyige, I., Musasizi, E., Ramjith, J., Andolina, C., Lanke, K., Arinaitwe, E., Olwoch, P., Collins, K. A., Kanya, M. R., Dorsey, G., Drakeley, C., Staedke, S. G., Bousema, T., & Conrad, M. D. (2022). Asymptomatic School-Aged Children Are Important Drivers of Malaria Transmission in a High Endemicity Setting in Uganda. *The Journal of Infectious Diseases*, 226(4), 708–713. <https://doi.org/10.1093/infdis/jiac169>

- Rice, B. L., Annapragada, A., Baker, R. E., Bruijning, M., Dotse-Gborgbortsi, W., Mensah, K., Miller, I. F., Motaze, N. V., Raheerinandrasana, A., Rajeev, M., Rakotonirina, J., Ramiadantsoa, T., Rasambainarivo, F., Yu, W., Grenfell, B. T., Tatem, A. J., & Metcalf, C. J. E. (2021). Variation in SARS-CoV-2 outbreaks across sub-Saharan Africa. *Nature Medicine*, 27(3), 447–453. <https://doi.org/10.1038/s41591-021-01234-8>
- Rice, B. L., Golden, C. D., Randriamady, H. J., Rakotomalala, A. A. N. A., Vonona, M. A., Anjaranirina, E. J. G., Hazen, J., Castro, M. C., Metcalf, C. J. E., & Hartl, D. L. (2021). Fine-scale variation in malaria prevalence across ecological regions in Madagascar: a cross-sectional study. *BMC Public Health*, 21(1), 1018. <https://doi.org/10.1186/s12889-021-11090-3>
- Richard, Q., Alizon, S., Choisy, M., Sofonea, M. T., & Djidjou-Demasse, R. (2021). Age-structured non-pharmaceutical interventions for optimal control of COVID-19 epidemic. *PLoS Computational Biology*, 17(3), e1008776. <https://doi.org/10.1371/journal.pcbi.1008776>
- RICHARDSON, S. (1992). Modélisation statistique des variations géographiques en épidémiologie. *Revue d'épidémiologie et de Santé Publique*, 40(1), 33–45.
- Rock, K., Brand, S., Moir, J., & Keeling, M. J. (2014). Dynamics of infectious diseases. In *Reports on Progress in Physics* (Vol. 77, Issue 2, p. 51). Institute of Physics Publishing. <https://doi.org/10.1088/0034-4885/77/2/026602>
- Roesch, A., & Schmidbauer, H. (2018). *WaveletComp: Computational Wavelet Analysis*. <https://cran.r-project.org/package=WaveletComp>
- Rogier, E., Wiegand, R., Moss, D., Priest, J., Angov, E., Dutta, S., Journel, I., Jean, S. E., Mace, K., Chang, M., Lemoine, J. F., Udhayakumar, V., & Barnwell, J. W. (2015). Multiple comparisons analysis of serological data from an area of low Plasmodium falciparum transmission. *Malaria Journal*, 14(1). <https://doi.org/10.1186/s12936-015-0955-1>
- Rohani, P., & King, A. A. (2010). Never mind the length, feel the quality: The impact of long-term epidemiological data sets on theory, application and policy. In *Trends in Ecology and Evolution* (Vol. 25, Issue 10, pp. 611–618). Elsevier Current Trends. <https://doi.org/10.1016/j.tree.2010.07.010>
- Rosado, J., White, M. T., Longley, R. J., Lacerda, M., Monteiro, W., Brewster, J., Sattabongkot, J., Guzman-Guzman, M., Llanos-Cuentas, A., Vinetz, J. M., Gamboa, D., & Mueller, I. (2021). Heterogeneity in response to serological exposure markers of recent Plasmodium vivax infections in contrasting epidemiological contexts. *PLOS Neglected Tropical Diseases*, 15(2), e0009165. <https://doi.org/10.1371/journal.pntd.0009165>
- Ross, R. (1910). The Prevention of Malaria. *Nature*, 85(2148), 263–264. <https://doi.org/10.1038/085263a0>
- Sayre, D., Steinhardt, L. C., Irinantenaina, J., Dentinger, C., Rasoanaivo, T. F., Kapesa, L., Razafindrakoto, J., Legrand, A., Prada, N., Gutman, J., Lewis, L., Mangahasimbola, R. T., Andriamananjara, M., Ravaoarinosy, A. V., Ralemary, N., Garchitorea, A., & Harimanana, A. (2021). Baseline malaria prevalence and care-seeking behaviours in rural Madagascar prior to a trial to expand malaria community case management to all ages. *Malaria Journal*, 20(1), 1–13. <https://doi.org/10.1186/s12936-021-03956-z>
- Schoenhals, M., Rabenindrina, N., Rakotondramanga, J. M., Dussart, P., Randremanana, R., Heraud, J. M., Andriamandimby, S. F., Sahondranirina, P. H., Vololoniaina, M. C. A., Randriatsarafara, F. M., Rasolofo, V., Randriamanantany, Z. A., & Spiegel, A. (2021). SARS-CoV-2 antibody seroprevalence follow-up in Malagasy blood donors during the 2020 COVID-19 Epidemic. *EBioMedicine*, 68, 103419. <https://doi.org/10.1016/j.ebiom.2021.103419>
- Schöley, J., Aburto, J. M., Kashnitsky, I., Kniffka, M. S., Zhang, L., Jaadla, H., Dowd, J. B., & Kashyap, R. (2022). Life expectancy changes since COVID-19. *Nature Human Behaviour* 2022, 1–11. <https://doi.org/10.1038/s41562-022-01450-3>
- Scrucca, L., Fop, M., Murphy, T. B., & Raftery, A. E. (2016). Mclust 5: Clustering, classification and density estimation using Gaussian finite mixture models. *R Journal*, 8(1), 289–317. <https://doi.org/10.32614/rj-2016-021>
- Serfling, R. E. (1963). Methods for Current Statistical Analysis of Excess Pneumonia-Influenza Deaths. *Public Health Reports (1896-1970)*, 78(6), 494. <https://doi.org/10.2307/4591848>
- Sharrow, D., Hug, L., You, D., Alkema, L., Black, R., Cousens, S., Croft, T., Gaigbe-Togbe, V., Gerland, P., Guillot, M., Hill, K., Masquelier, B., Mathers, C., Pedersen, J., Strong, K. L., Suzuki, E., Wakefield, J., & Walker, N. (2022). Global, regional, and national trends in under-5 mortality between 1990 and 2019 with scenario-based projections until 2030: a systematic analysis by the UN Inter-agency Group for Child Mortality Estimation. *The Lancet Global Health*, 10(2), e195–e206. [https://doi.org/10.1016/S2214-109X\(21\)00515-5](https://doi.org/10.1016/S2214-109X(21)00515-5)
- Shi, B., Zheng, J., Xia, S., Lin, S., Wang, X., Liu, Y., Zhou, X. N., & Liu, J. (2021). Accessing the syndemic of COVID-19 and malaria intervention in Africa. *Infectious Diseases of Poverty*, 10(1). <https://doi.org/10.1186/S40249-020-00788-Y>
- Sow, A., Loucoubar, C., Diallo, D., Faye, O., Ndiaye, Y., Senghor, C. S., Dia, A. T., Faye, O., Weaver, S. C., Diallo, M., Malvy, D., & Sall, A. A. (2016). Concurrent malaria and arbovirus infections in Kedougou,

- southeastern Senegal. *Malaria Journal*, 15(1), 47. <https://doi.org/10.1186/s12936-016-1100-5>
- Stanisic, D. I., Fowkes, F. J. I., Koinari, M., Javati, S., Lin, E., Kiniboro, B., Richards, J. S., Robinson, L. J., Schofield, L., Kazura, J. W., King, C. L., Zimmerman, P., Felger, I., Siba, P. M., Mueller, I., & Beeson, J. G. (2015). Acquisition of antibodies against Plasmodium falciparum merozoites and malaria immunity in young children and the influence of age, force of infection, and magnitude of response. *Infection and Immunity*, 83(2), 646–660. <https://doi.org/10.1128/IAI.02398-14>
- Steinhardt, L. C., Ravaoarisoa, E., Wiegand, R., Harimanana, A., Hedje, J., Cotte, A. H., Zigirumugabe, S., Kesteman, T., Rasoloharimanana, T. L., Rakotomalala, E., Randriamoramana, A. M., Rakotondramanga, J. M., Razanatsiorimalala, S., Mercereau-Puijalon, O., Perraut, R., Ratsimbasoa, A., Butts, J., Rogier, C., Piola, P., ... Vigan-Womas, I. (2021). School-Based Serosurveys to Assess the Validity of Using Routine Health Facility Data to Target Malaria Interventions in the Central Highlands of Madagascar. *Journal of Infectious Diseases*, 223(6), 995–1004. <https://doi.org/10.1093/infdis/jiaa476>
- Stewart, L., Gosling, R., Griffin, J., Gesase, S., Campo, J., Hashim, R., Masika, P., Mosha, J., Bousema, T., Shekalaghe, S., Cook, J., Corran, P., Ghani, A., Riley, E. M., & Drakeley, C. (2009). Rapid assessment of malaria transmission using age-specific sero-conversion rates. *PLoS ONE*, 4(6). <https://doi.org/10.1371/journal.pone.0006083>
- Stone, W., Gonçalves, B. P., Bousema, T., & Drakeley, C. (2015). Assessing the infectious reservoir of falciparum malaria: past and future. *Trends in Parasitology*, 31(7), 287–296. <https://doi.org/10.1016/J.PT.2015.04.004>
- Stuckey, E. M., Stevenson, J., Galactionova, K., Baidjoe, A. Y., Bousema, T., Odongo, W., Kariuki, S., Drakeley, C., Smith, T. A., Cox, J., & Chitnis, N. (2014). Modeling the cost effectiveness of malaria control interventions in the highlands of western Kenya. *PLoS ONE*, 9(10). <https://doi.org/10.1371/journal.pone.0107700>
- Tango, T. (1995). A class of tests for detecting ‘general’ and ‘focused’ clustering of rare diseases. *Statistics in Medicine*, 14(21–22), 2323–2334. <https://doi.org/10.1002/sim.4780142105>
- Tango, T. (2000). A test for spatial disease clustering adjusted for multiple testing. *Statistics in Medicine*, 19(2), 191–204. [https://doi.org/10.1002/\(SICI\)1097-0258\(20000130\)19:2<191::AID-SIM281>3.0.CO;2-Q](https://doi.org/10.1002/(SICI)1097-0258(20000130)19:2<191::AID-SIM281>3.0.CO;2-Q)
- Tantely, M. L., Rakotoniaina, J. C., Tata, E., Andrianaivolambo, L., Fontenille, D., & Elissa, N. (2012). Modification of Anopheles gambiae distribution at high altitudes in Madagascar. *Journal of Vector Ecology*, 37(2), 402–406. <https://doi.org/10.1111/j.1948-7134.2012.00244.x>
- ten Bosch, Q., Andrianaivoarimanana, V., Ramasindrazana, B., Mikaty, G., Rakotonanahary, R. J. L., Nikolay, B., Rahajandraibe, S., Feher, M., Grassin, Q., Paireau, J., Rahelinirina, S., Rendremanana, R., Rakotoarimanana, F., Melocco, M., Rasolofo, V., Pizarro-Cerdá, J., Le Guern, A.-S., Bertherat, E., Ratsitorahina, M., ... Cauchemez, S. (2022). Analytical framework to evaluate and optimize the use of imperfect diagnostics to inform outbreak response: Application to the 2017 plague epidemic in Madagascar. *PLOS Biology*, 20(8), e3001736. <https://doi.org/10.1371/journal.pbio.3001736>
- The malERA Refresh Consultative Panel on Characterising the Reservoir and Measuring Transmission. (2017). malERA: An updated research agenda for characterising the reservoir and measuring transmission in malaria elimination and eradication. *PLOS Medicine*, 14(11), e1002452. <https://doi.org/10.1371/journal.pmed.1002452>
- The World Health Organization (WHO). (2020). *WHO COVID-19: Case Definitions*. https://apps.who.int/iris/bitstream/handle/10665/333912/WHO-2019-nCoV-Surveillance_Case_Definition-20201-eng.pdf?sequence=1&isAllowed=y (Accessed le 20 octobre 2023)
- Thindwa, D., Jambo, K. C., Ojal, J., MacPherson, P., Dennis Phiri, M., Pinsent, A., Khundi, M., Chiume, L., Gallagher, K. E., Heyderman, R. S., Corbett, E. L., French, N., & Flasche, S. (2022). Social mixing patterns relevant to infectious diseases spread by close contact in urban Blantyre, Malawi. *Epidemics*, 40, 100590. <https://doi.org/10.1016/j.epidem.2022.100590>
- Tongren, J. E., Drakeley, C. J., McDonald, S. L. R., Reyburn, H. G., Manjurano, A., Nkya, W. M. M., Lemnge, M. M., Gowda, C. D., Todd, J. E., Corran, P. H., & Riley, E. M. (2006). Target antigen, age, and duration of antigen exposure independently regulate immunoglobulin G subclass switching in malaria. *Infection and Immunity*, 74(1), 257–264. <https://doi.org/10.1128/IAI.74.1.257-264.2006>
- U. S. President’s Malaria Initiative Madagascar. (2020). Malaria Operational Plan FY 2020. Retrieved from (www.pmi.gov). In *Report*. <https://www.pmi.gov/where-we-work/madagascar/> (Accessed le 20 octobre 2023)
- United Nations Department of Economic and Social Affairs Population Division. (2022). *World Population Prospects 2022: Summary of Results*. UN DESA/POP/2022/TR/NO. 3. https://www.un.org/development/desa/pd/sites/www.un.org.development.desa.pd/files/wpp2022_summary_of_results.pdf (Accessed le 20 octobre 2023)
- Uyoga, S., Adetifa, I. M. O., Otiende, M., Yegon, C., Agweyu, A., Warimwe, G. M., & Scott, J. A. G. (2021). Prevalence of SARS-CoV-2 Antibodies From a National Serosurveillance of Kenyan Blood Donors,

- January-March 2021. *JAMA*, 326(14), 1436–1438. <https://doi.org/10.1001/JAMA.2021.15265>
- Verity, R., Okell, L. C., Dorigatti, I., Winskill, P., Whittaker, C., Imai, N., Cuomo-Dannenburg, G., Thompson, H., Walker, P. G. T., Fu, H., Dighe, A., Griffin, J. T., Baguelin, M., Bhatia, S., Boonyasiri, A., Cori, A., Cucunubá, Z., FitzJohn, R., Gaythorpe, K., ... Ferguson, N. M. (2020). Estimates of the severity of coronavirus disease 2019: a model-based analysis. *The Lancet Infectious Diseases*, 20(6), 669–677. [https://doi.org/10.1016/S1473-3099\(20\)30243-7](https://doi.org/10.1016/S1473-3099(20)30243-7)
- Wallinga, J., & Lipsitch, M. (2006). How generation intervals shape the relationship between growth rates and reproductive numbers. *Proceedings of the Royal Society B: Biological Sciences*, 274(1609), 599–604. <https://doi.org/10.1098/RSPB.2006.3754>
- Waltisperger, D., Mesle, F., & Mandelbaum, J. (2005). Economic Crisis and Mortality: The Case of Antananarivo, 1976-2000. *Population (English Edition, 2002-)*, 60(3), 199. <https://doi.org/10.2307/4148193>
- Wearing, H. J., Rohani, P., & Keeling, M. J. (2005). Appropriate Models for the Management of Infectious Diseases. *PLOS Medicine*, 2(7), e174. <https://doi.org/10.1371/JOURNAL.PMED.0020174>
- Weiss, D. J., Bertozzi-Villa, A., Rumisha, S. F., Amratia, P., Arambepola, R., Battle, K. E., Cameron, E., Chestnutt, E., Gibson, H. S., Harris, J., Keddie, S., Millar, J. J., Rozier, J., Symons, T. L., Vargas-Ruiz, C., Hay, S. I., Smith, D. L., Alonso, P. L., Noor, A. M., ... Gething, P. W. (2021). Indirect effects of the COVID-19 pandemic on malaria intervention coverage, morbidity, and mortality in Africa: a geospatial modelling analysis. *The Lancet Infectious Diseases*, 21(1), 59–69. [https://doi.org/10.1016/S1473-3099\(20\)30700-3](https://doi.org/10.1016/S1473-3099(20)30700-3)
- Weiss, D. J., Mappin, B., Dalrymple, U., Bhatt, S., Cameron, E., Hay, S. I., & Gething, P. W. (2015). Re-examining environmental correlates of Plasmodium falciparum Malaria endemicity: A data-intensive variable selection approach. *Malaria Journal*, 14(1), 1–18. <https://doi.org/10.1186/s12936-015-0574-x>
- White, L. J., Maude, R. J., Pongtavornpinyo, W., Saralamba, S., Aguas, R., Van Effelterre, T., Day, N. P., & White, N. J. (2009). The role of simple mathematical models in malaria elimination strategy design. *Malaria Journal*, 8(1), 212. <https://doi.org/10.1186/1475-2875-8-212>
- Wondim, K. Y., Alemayehu, E. B., & Abebe, W. B. (2017). Malaria Hazard and Risk Mapping Using GIS Based Spatial Multicriteria Evaluation Technique (SMCET) in Tekeze Basin Development Corridor, Amhara Region, Ethiopia. *Journal of Environment and Earth Science*, 7(5), 76–87. <https://iiste.org/Journals/index.php/JEES/article/view/36981>
- World Health Organisation. (2022). *World malaria report 2022*. Geneva: World Health Organization, 73(1), 2013–2015. <https://www.who.int/teams/global-malaria-programme/reports/world-malaria-report-2022>
- World Health Organization. (2020). *World Malaria Report: 20 years of global progress and challenges*. In *World Health: Vol. WHO/HTM/GM* (Issue December). <https://www.who.int/publications/i/item/9789240015791>
- World Health Organization. (2021). *World Malaria Report 2021*. Geneva: World Health Organization
- World Health Organization (WHO). (2012). WHO Guideline on Health Policy And System Support to Optimize Community Health Worker Selected highlights. In *WHO Guideline on Health Policy And System Support to Optimize Community Health Worker Selected highlights*.
- World Health Organization (WHO). (2020). *Adapter les interventions de lutte contre le paludisme dans le contexte de la COVID-19*. Geneva: World Health Organization
- World Health Organization (WHO). (2021). Revision of the international definition of plague cases – Révision de la définition internationale des cas de peste. *Weekly Epidemiological Record = Relevé Épidémiologique Hebdomadaire*, 96(24), 238–240.
- World Health Organization (WHO) for Africa. (2007). *Implementation of Indoor Residual Spraying of Insecticides for Malaria Control in the WHO African Region Report* (Issue November). https://www.afro.who.int/sites/default/files/2017-06/report_on_the_implementation_of_irs_in_the_african_region_2007.pdf (Accessed le 20 octobre 2023)
- Wu, L., Van Den Hoogen, L. L., Slater, H., Walker, P. G. T., Ghani, A. C., Drakeley, C. J., & Okell, L. C. (2015). Comparison of diagnostics for the detection of asymptomatic Plasmodium falciparum infections to inform control and elimination strategies. *Nature*, 528(7580), S86–S93. <https://doi.org/10.1038/nature16039>
- Yankson, R., Anto, E. A., & Chipeta, M. G. (2019). Geostatistical analysis and mapping of malaria risk in children under 5 using point-referenced prevalence data in Ghana. *Malaria Journal*, 18(1). <https://doi.org/10.1186/s12936-019-2709-y>
- Yman, V., White, M. T., Rono, J., Arcà, B., Osier, F. H., Troye-Blomberg, M., Boström, S., Ronca, R., Rooth, I., & Färnert, A. (2016). Antibody acquisition models: A new tool for serological surveillance of malaria transmission intensity. *Scientific Reports*, 6(1), 19472. <https://doi.org/10.1038/srep19472>
- Zohdy, S., Derfus, K., Headrick, E. G., Andrianjafy, M. T., Wright, P. C., & Gillespie, T. R. (2016). Small-scale land-use variability affects Anopheles spp. distribution and concomitant Plasmodium infection in humans

and mosquito vectors in southeastern Madagascar. *Malaria Journal*, 15(1), 1–9.
<https://doi.org/10.1186/S12936-016-1164-2>

Informations supplémentaires des chapitres

Supplemental files 1 :

Identification of factors associated with residual malaria transmission using school-based serological surveys in settings pursuing elimination

Jean Marius Rakotondramanga^{1,2,3,4*}, Inès Vigan-Womas^{5,6}, Laura C. Steinhardt⁷, Aina Harimanana¹, Elisabeth Ravaoarisoa⁸, Tsikiniaina L Rasoloharimanana⁶, Sehen Razanatsiorimalala⁹, Amy Wesolowski¹⁰, Milijaona Randrianariveლოსია^{9,11}, Benjamin Roche^{2,4¶}, Andres Garchitorenna^{1,4¶}

Author details

¹ Epidemiology and Clinical Research Unit, Institut Pasteur de Madagascar, Antananarivo, Madagascar.

² IRD, Sorbonne Université, UMMISCO, Bondy F-93143, France.

³ Sorbonne Université, ED 393, Paris, France

⁴ MIVEGEC, Univ. Montpellier, CNRS, IRD, Montpellier, France.

⁵ Immunology of Infectious Diseases Unit, Institut Pasteur de Madagascar, Antananarivo, Madagascar.

⁶ Institut Pasteur de Dakar, Immunophysiology and Infectious Diseases Department, Dakar, Senegal.

⁷ Malaria Branch, Division of Parasitic Diseases and Malaria, Center for Global Health, Centers for Disease Control and Prevention, Atlanta, Georgia, USA.

⁸ Faculty of Sciences, University of Antananarivo, Antananarivo, Madagascar.

⁹ Malaria Research Unit, Institut Pasteur de Madagascar, Antananarivo, Madagascar.

¹⁰ Department of Epidemiology, Johns Hopkins Bloomberg School of Public Health, Baltimore, MD, USA.

¹¹ Faculté des Sciences, Université de Toliara, 601, Toliara, Madagascar.

*Corresponding author

Email: jean.marius.g@gmail.com

¶ These authors share senior authorship

Method S1 Two-component gaussian mixture model

To dichotomize seropositivity, log-transformed of median fluorescence intensity (MFI) values were assumed to have two underlying components for seronegative and seropositive groups (Rogier et al., 2015). Two finite mixture models with a Gaussian distribution were fitted by maximum likelihood estimation using expectation-maximum algorithm with the R package {flexmix}. This statistical approach has been used on samples from other low-endemicity settings without requiring antibody responses from a reference population (Assefa et al., 2019; Dempster et al., 1977; Steinhardt et al., 2021). BSA (GeneCust) described in and based on Steinhardt et al. was used as carrier control. Due to skewness in all participants' data distribution, negative values of {MFI minus BSA-background} were recoded to 1 to accommodate to the log transformation (to have more normal distribution); then all participants could be included in the study (Assefa et al., 2019; Steinhardt et al., 2021). A cut-off value for seropositivity, the junction of lower and upper Gaussian distributions, was determined to characterize seronegative (unexposed) and seropositive (exposed) populations—instead of using the commonly used mean + 3*SD cut-off (dashed-orange line) which requires an appropriate unexposed reference population (**Fig. S1**).

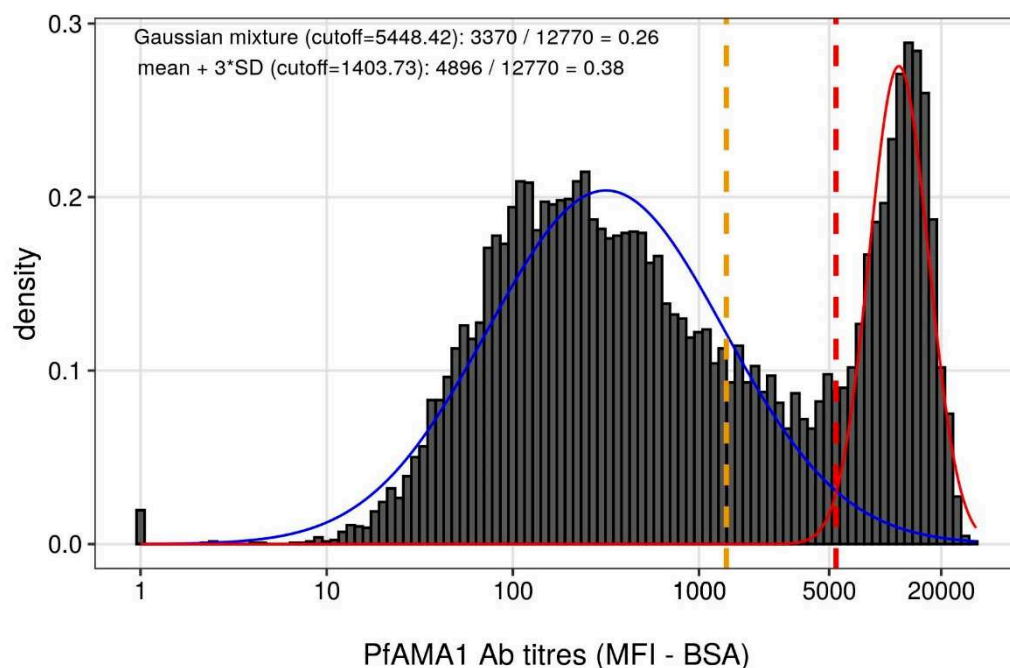


Fig. S1 Cut-off value for PfAMA1 Ab seropositivity (dashed-red line) by using two finite Gaussian mixture models and the serological data (for children and adult participants, $n = 12,770$) described in Steinhardt et al. (Steinhardt et al., 2021).

Table S1 List of environmental and climatic data

Data	Description	Dynamic in models	Round 1 selected for <i>Pf.</i> infection and exposure (PfAMA1 Ab response) model	Resolution (Unit)	Source
Distance >5 km from health facility	Calculated using Euclidean distance (>5 km, nearly 5 km in travel distance) from each fokontany centroid to the nearest health facility in QGIS	Static	Yes	Binary (km)	WHO recently published data (Maina et al., 2019; QGIS Team Development, n.d.)
Elevation	Measured from the SRTM elevation surface	Static	Yes	90 m	SRTM derivative (Farr et al., 2007)
NDVI	NDVI (Normalized Difference Vegetation Index)	Monthly ^f	Lagged by 1 month prior surveys	16-days at 250 m	MODIS product of MOD13Q1 (Kang et al., 2018; Oak Ridge National Laboratory Distributed Active Archive Center (ORNL DAAC), 2018)
EVI	EVI (Enhanced Vegetation Index)	Monthly ^f	No	16-days at 250 m	MODIS product of MOD13Q1 (Kang et al., 2018; Oak Ridge National Laboratory Distributed Active Archive Center (ORNL DAAC), 2018)
QA for NVDI or EVI*	Used for NDVI or EVI quality assessment reliability	Monthly ^f	No	16-days at 250 m	MODIS product of MOD13Q1 (Kang et al., 2018; Oak Ridge National Laboratory Distributed Active Archive Center (ORNL DAAC), 2018)
LST Day	Day-time Land Surface Temperature (LST) and emissivity composites	Monthly ^f	Lagged by 1 month prior surveys	8-days at 1 km	MODIS product of MOD11A2 (Kang et al., 2018; Oak Ridge National Laboratory Distributed Active Archive Center (ORNL DAAC), 2018)
LST Night	Night-time LST and emissivity composites	Monthly ^f	No	8-days at 1 km	MODIS product of MOD11A2 (Kang et al., 2018; Oak Ridge National Laboratory Distributed Active Archive Center (ORNL DAAC), 2018)

QA for LST Day*	Used for LST Day quality assessment reliability	Monthly ^f	No	8-days at 1 km	MODIS product of MOD11A2 (Kang et al., 2018; Oak Ridge National Laboratory Distributed Active Archive Center (ORNL DAAC), 2018)
QA for LST Night*	Used for LST Night quality assessment reliability	Monthly ^f	No	8-days at 1 km	MODIS product of MOD11A2 (Kang et al., 2018; Oak Ridge National Laboratory Distributed Active Archive Center (ORNL DAAC), 2018)
Forests	IGBP forests legend and class	Annual ^h	Yes	Annual ^h at 500 m	MODIS product of MCD12Q1 (Friedl et al., 2010)
Woodlands	IGBP woodlands legend and class	Annual ^h	Yes	Annual ^h at 500 m	MODIS product of MCD12Q1 (Friedl et al., 2010)
Grasslands/cereals	IGBP grasslands or cereals legend and class	Annual ^h	Yes	Annual ^h at 500 m	MODIS product of MCD12Q1 (Friedl et al., 2010)
Wet/croplands/mosaics	IGBP wet, croplands or mosaics legend and class	Annual ^h	Yes	Annual ^h at 500 m	MODIS product of MCD12Q1 (Friedl et al., 2010)
Others' land cover classes	Others IGBP legends and class	Annual ^h	No	Annual ^h at 500 m	MODIS product of MCD12Q1 (Friedl et al., 2010)

QGIS: QGIS Team Development Open Source Geospatial Foundation Project ; SRTM: SRTM Shuttle Radar Topography Mission ; MODIS: Moderate Resolution

Imaging Spectroradiometer ; *QA: Quality Assessment reliability index ; IGBP: International Geosphere-Biosphere Programme ; ^fOne, two and three month prior survey ; ^h2014

Method S2 Environmental and remotely sensed data processing

Temporally dynamic climatic and environmental, (1) all 8-days Land Surface Temperature (LST) and emissivity composites (day-time and night-time LST products of MOD11A2 band at 1 km spatial resolution), and (2) all 16-days vegetation indices composites (Normalized Difference Vegetation Index (NDVI) and Enhanced Vegetation Index (EVI) of MOD13Q1 band at 250 m spatial resolution) (Oak Ridge National Laboratory Distributed Active Archive Center (ORNL DAAC), 2018), indices' values were first rasterized. Then, they were masked with corresponding quality assessment reliability composites to set and unsure "nodata" removing (such as due to cloud cover), and cropped with the fokontany boundary (only the pixels with majority surface superimpose the fokontany polygons were considered). For computational use, all pixel values at specific dates—depending on the temporal data resolution: 3 or 4 dates for temperatures, and 2 dates per month for vegetation indices—of each indices were aggregated to obtain median value at fokontany-level; and mean of monthly values from multiple raster images were calculated.

The MODIS land cover type product (MCD12Q1, at annual and 500 m spatial resolution) for 2014: (a) forests, (b) woodlands, (c) grasslands or cereals, (d) croplands or mosaics, and (e) others' class grouping shrublands, wetlands, barren or water bodies were processed differently. The land cover class values were first rasterized and cropped with the fokontany boundary (only the pixels with majority surface superimpose the fokontany polygons were considered). Then, the percentage of fokontany i , area occupied by land cover class j , were calculated using (Eq. 1):

$$\{Landcover\}_i(\%) = \frac{100 * \{Numberofpixels\}_{ij}}{\{Numberofallpixels\}_i} \quad (\text{Eq. 1})$$

For elevation data, mean values per fokontany were used.

QGIS software v3.10, was used to calculate the Euclidean distance from each fokontany centroid to the nearest health facility via use of World Health Organization localization data (Maina et al., 2019; QGIS Team Development, n.d.).

**Neighbor definition by maximum distance:
Great Circle distance ~17km**

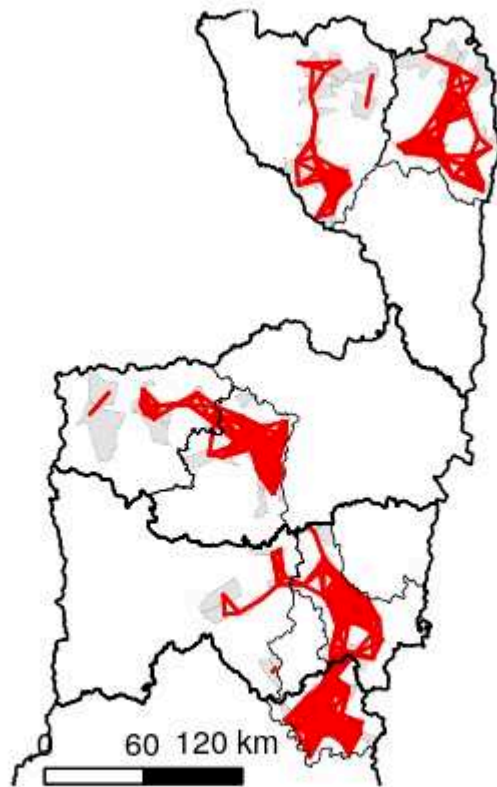


Fig. S2 Fokontany neighbour definition by maximum distance, using Great Circle distance around 17 km between two contiguous fokontany.

Method S3 Mixed-effects binomial logistic regression model frameworks and selection

Mixed-effects binomial logistic regression models with district- and commune-level random effects were fitted to model *P. falciparum* infection at fokontany-level (Eq. 2) or at individual-level (Eq. 3), and PfAMA1 Ab response at fokontany-level (Eq. 4) or seropositivity at individual-level (Eq. 5) (Harrison, 2015; Mauny et al., 2004), using R package {lme4} (Bates et al., 2015):

Random effects were treated as nested for the analyses to model the overdispersion and give more accurate estimates of standard errors (Harrison, 2015; Mauny et al., 2004), because each fokontany (n = 182) or individual (n = 6,293) was surveyed only within one commune (n = 93) and one district (n = 7):

(i) *P. falciparum* infection model at fokontany-level :

$$\begin{aligned} \text{logit}(pi) = & \alpha_{ijk} + \beta_0 + \beta_1\{\text{distance} > 5\text{km}\} + \beta_2\{\text{forests}\} + \beta_3\{\text{woodlands}\} + \\ & \beta_4\{\text{grasslands/cereals}\} + \beta_5\{\text{wet/croplands/mosaics}\} + \beta_6\{\text{elevation}\} + \\ & \beta_7\{\text{NDVI, lag} - 1\} + \beta_8\{\text{LST, lag} - 1\} + \beta_9\{(\text{NDVI, lag} - 1) * (\text{LST, lag} - 1)\} + \\ & \beta_{10}\{(\text{NDVI, lag} - 1) * (\text{grasslands/cereals})\} + \epsilon_i; \end{aligned} \quad (\text{Eq. 2})$$

where p , i , j and k are respectively the aggregated *P. falciparum* infection, the fokontany-, commune- and district-indices;

$$\epsilon_i \sim \text{Normal}(0, \sigma_\epsilon^2).$$

(ii) *P. falciparum* infection model at individual-level :

$$\begin{aligned} \text{logit}(pi) = & \alpha_{ijk} + \beta_0 + \beta_1\{\text{agegroup}\} + \beta_2\{\text{sex}\} + \beta_3\{\text{fiver}\} + \beta_4\{\text{trip}\} + \beta_5\{\text{netuse}\} + \\ & \beta_6\{\text{netnumber}\} + \beta_8\{\text{distance} > 5\text{km}\} + \beta_9\{\text{forests}\} + \beta_{10}\{\text{woodlands}\} + \\ & \beta_{11}\{\text{grasslands/cereals}\} + \beta_{12}\{\text{wet/croplands/mosaics}\} + \beta_{13}\{\text{elevation}\} + \\ & \beta_{14}\{\text{NDVI, lag} - 1\} + \beta_{15}\{\text{LST, lag} - 1\} + \beta_{16}\{(\text{NDVI, lag} - 1) * (\text{LST, lag} - 1)\} + \\ & \beta_{17}\{(\text{NDVI, lag} - 1) * (\text{grasslands/cereals})\} + \epsilon_i; \end{aligned} \quad (\text{Eq. 3})$$

where p , i , j and k are respectively the *P. falciparum* infection positivity, the individual-, commune- and district-indices;

$$\epsilon_i \sim Normal(0, \sigma_{\epsilon}^2).$$

(iii) *P. falciparum* exposure (PfAMA1 Ab response) model at fokontany-level :

$$\begin{aligned} \text{logit}(\text{seroposi}) = & \alpha_{ijk} + \beta_0 + \beta_1\{\text{distance} > 5\text{km}\} + \beta_2\{\text{forests}\} + \\ & \beta_3\{\text{woodlands}\} + \beta_4\{\text{grasslands/cereals}\} + \beta_5\{\text{wet/croplands/mosaics}\} + \\ & \beta_6\{\text{elevation}\} + \beta_7\{\text{NDVI, lag} - 1\} + \beta_8\{\text{LST, lag} - 1\} + \beta_9\{(\text{NDVI, lag} - 1) * \\ & (\text{LST, lag} - 1)\} + \beta_{10}\{(\text{NDVI, lag} - 1) * (\text{grasslands/cereals})\} + \beta_{11}\{pi\} + \epsilon_i; \end{aligned} \quad (\text{Eq. 4})$$

where p , $seropos$, i , j and k are respectively the School RDT prevalence, the aggregated PfAMA1 Ab response, the *fokontany*-, commune- and district-indices;

$$\epsilon_i \sim Normal(0, \sigma_{\epsilon}^2).$$

(iv) *P. falciparum* exposure (PfAMA1 Ab response) model at individual-level :

$$\begin{aligned} \text{logit}(\text{seroposi}) \\ = & \alpha_{ijk} + \beta_0 + \beta_1\{\text{agegroup}\} + \beta_2\{\text{sex}\} + \beta_3\{\text{fiver}\} + \beta_4\{\text{trip}\} + \beta_5\{\text{netuse}\} \\ & + \beta_6\{\text{netnumber}\} + \beta_7\{\text{RDTpositive} \in \text{household}\} + \beta_8\{\text{distance} > 5\text{km}\} \\ & + \beta_9\{\text{forests}\} + \beta_{10}\{\text{woodlands}\} + \beta_{11}\{\text{grasslands/cereals}\} \\ & + \beta_{12}\{\text{wet/croplands/mosaics}\} + \beta_{13}\{\text{elevation}\} + \beta_{14}\{\text{NDVI, lag} - 1\} \\ & + \beta_{15}\{\text{LST, lag} - 1\} + \beta_{16}\{(\text{NDVI, lag} - 1) * (\text{LST, lag} - 1)\} \\ & + \beta_{17}\{(\text{NDVI, lag} - 1) * (\text{grasslands/cereals})\} + \beta_{18}\{pi\} + \epsilon_i; \end{aligned} \quad (\text{Eq. 5})$$

where p , $seropos$, i , j and k are respectively the School RDT prevalence, the PfAMA1 Ab response, the individual-, commune- and district-indices;

$$\epsilon_i \sim Normal(0, \sigma_{\epsilon}^2).$$

Then, the following inclusion rules and multi-model selection procedures were applied using R package {MuMIn} (Bartoń, 2020; Burnham, K.P. and Anderson, 2004): (a) all covariates which showed significant effects on outcome variables (*P. falciparum* infection and exposure (PfAMA1 Ab response), both at *fokontany*- and individual-level) in univariable analyses were then included in multivariable analyses; (b) one of correlated pairs of quantitative environmental and climatic covariates was excluded from the same model candidate to avoid multicollinearity by using internal arguments (subset) of *MuMIn::pdredge* function {NDVI exclusive-or woodlands}, {temperature exclusive-or grasslands/cereals}, {temperature exclusive-or elevation}, and {woodlands exclusive-or grasslands/cereals} (Additional file 1: **Fig. S7**); (c) the interaction terms {NDVI * temperature} or {NDVI * “grasslands/cereals land cover”} were also included to all model candidates to assess its effects; and (d) sets of candidate models—for *P. falciparum* infection at *fokontany*-level (Eq. 2) and individual-level (Eq. 3), or for PfAMA1 Ab response at *fokontany*-level (Eq. 4) and individual-level (Eq. 5)—were then compared and ranked one-by-one according to the lowest information criteria (AICc, Second-order Akaike Information Criterion) to provide an absolute value for the model fit (Bartoń, 2020; Burnham, K.P. and Anderson, 2004; Nakagawa & Schielzeth, 2013).

Fixed-effect coefficients were transformed to obtain odds ratios $\{OR = \exp(\beta)\}$ —exponentiated model coefficients which reflect the ratio of change in outcome variable (*P. falciparum* infection or exposure) associated with each explanatory variable increase—in order to facilitate interpretation of results according the appropriate used scales.

The final model of *P. falciparum* exposure (PfAMA1 Ab response) at *fokontany*-level was checked for unaccounted spatial autocorrelation in the model residuals using Moran’s I index.

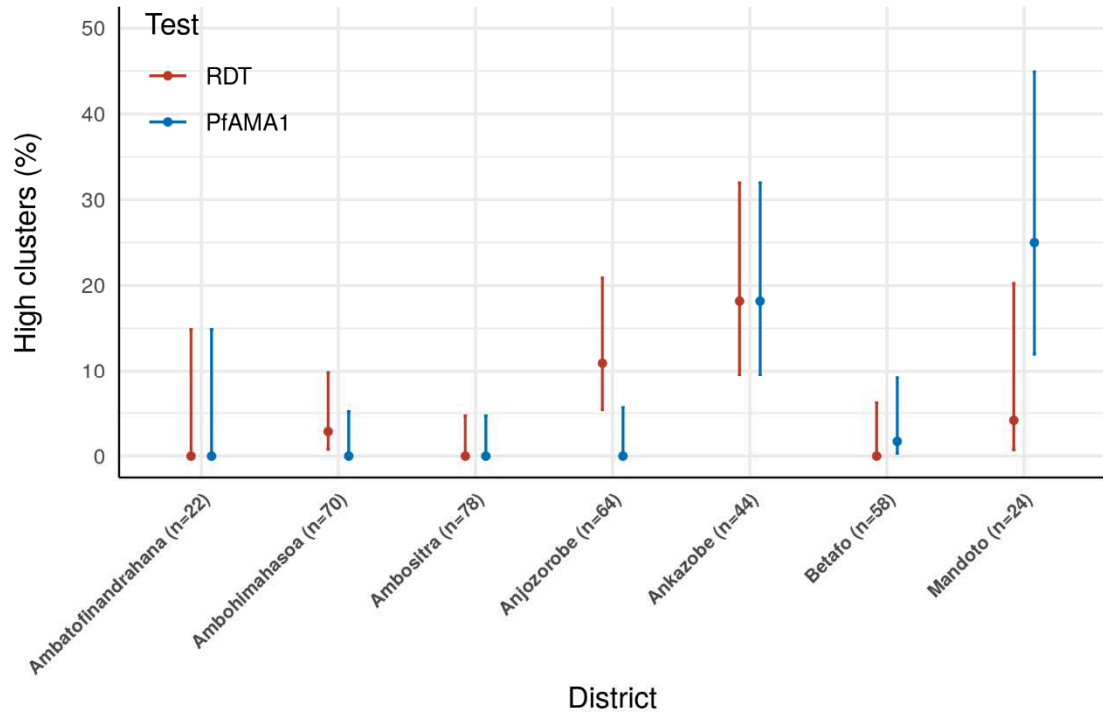


Fig. S3 Malaria infection prevalence by RDT versus PfAMA1 Ab seroprevalence detected high clusters fokontany across districts. High clusters fokontany are the combination of “High-High” or “Low-High” clusters; that represent fokontany with expected values (prevalence or seroprevalence) matching with the weighted mean of each fokontany’s neighbours, or those with abnormally high expected but low expected values, respectively.

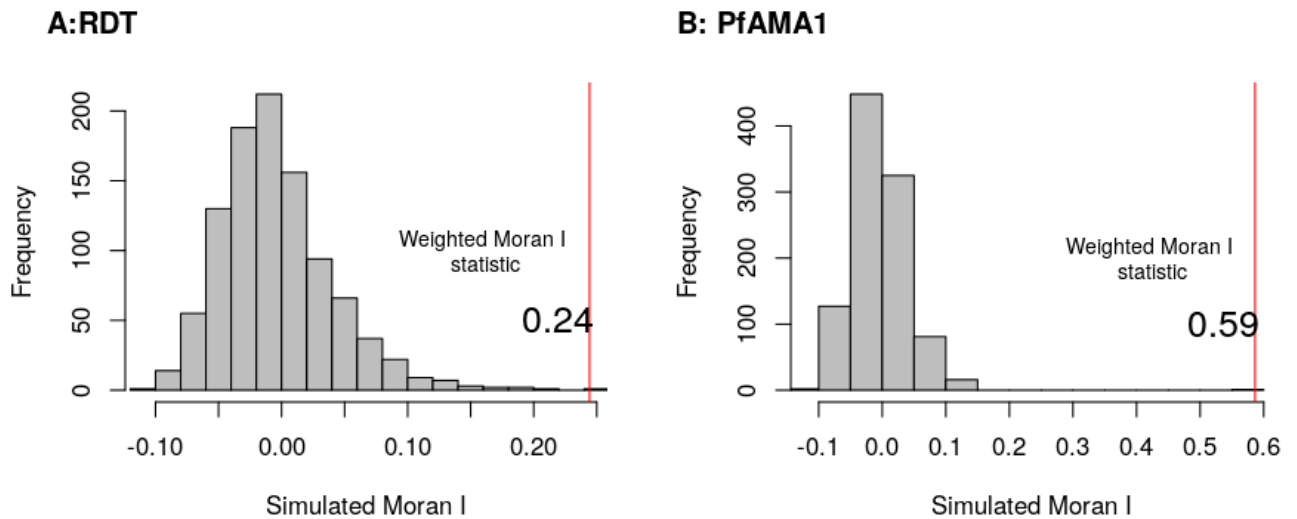


Fig. S4 Weighted global Moran's I statistics versus simulated random distribution of logit scale of (A) malaria infection prevalence by RDT ($I = 0.24$), and (B) PfAMA1 Ab seroprevalence ($I = 0.59$)

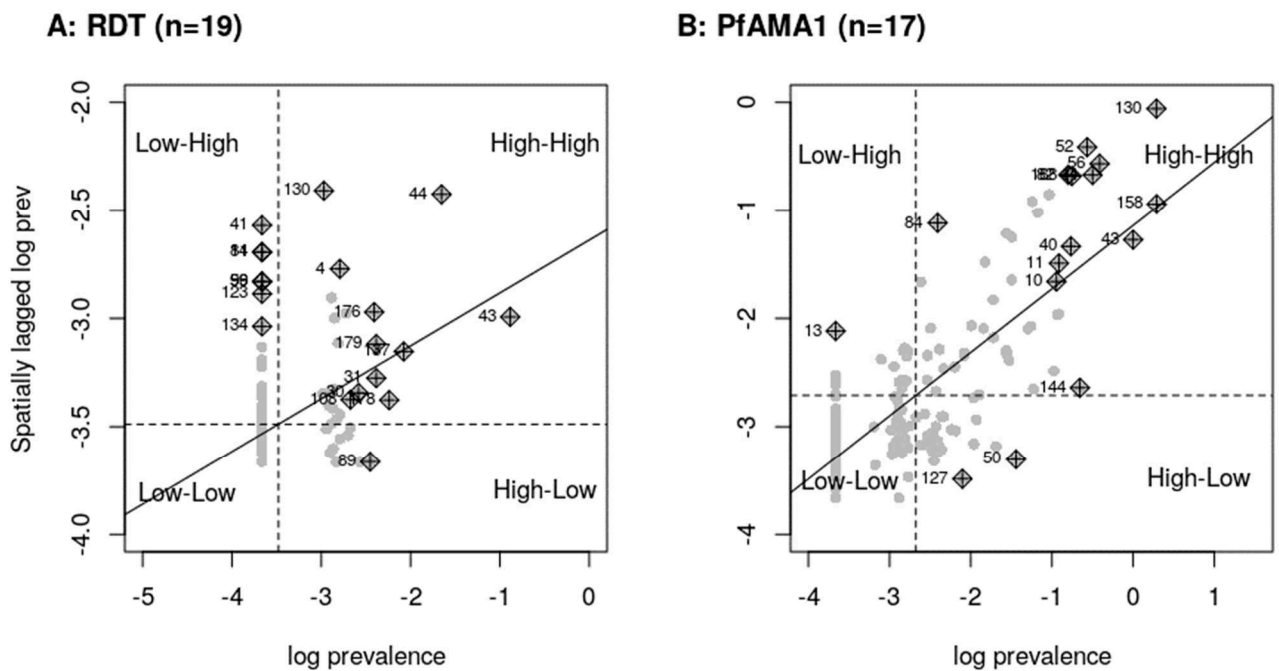


Fig. S5 Moran Scatterplots of clusters and hotspots of (A) malaria infection prevalence by RDT, and (B) PfAMA1 Ab seroprevalence.

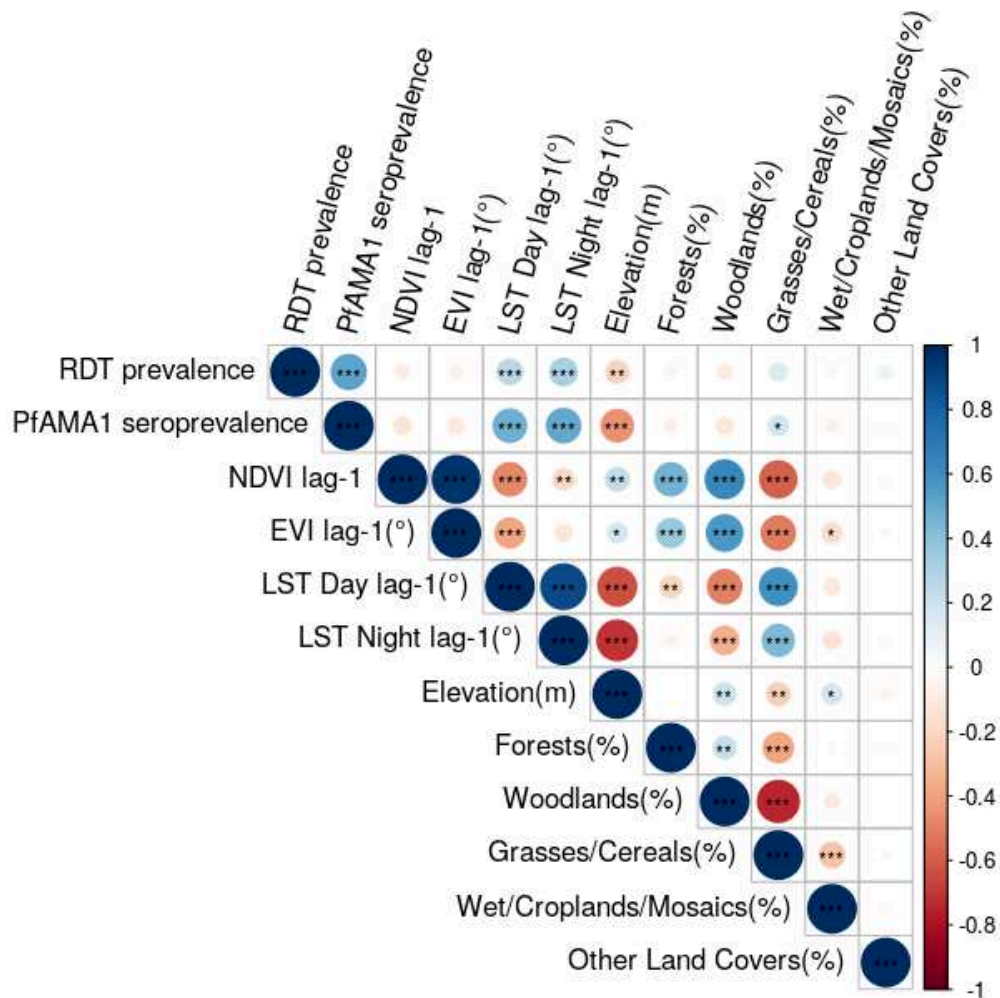


Fig. S6 Pearson's correlation scatterplot and peer's significance of *P. falciparum* infection prevalence by RDT, PfAMA1 Ab seroprevalence and quantitative environmental and climatic covariates. Levels of significance are marked with (***) for $p < 0.001$, (**) for $p < 0.01$, and (*) for $p < 0.05$. Lagged values of temperature and vegetation at 2 and 3 months were less correlated to malaria infection prevalence by RDT and PfAMA1 Ab seroprevalence than one-month lag at fokontany-level .

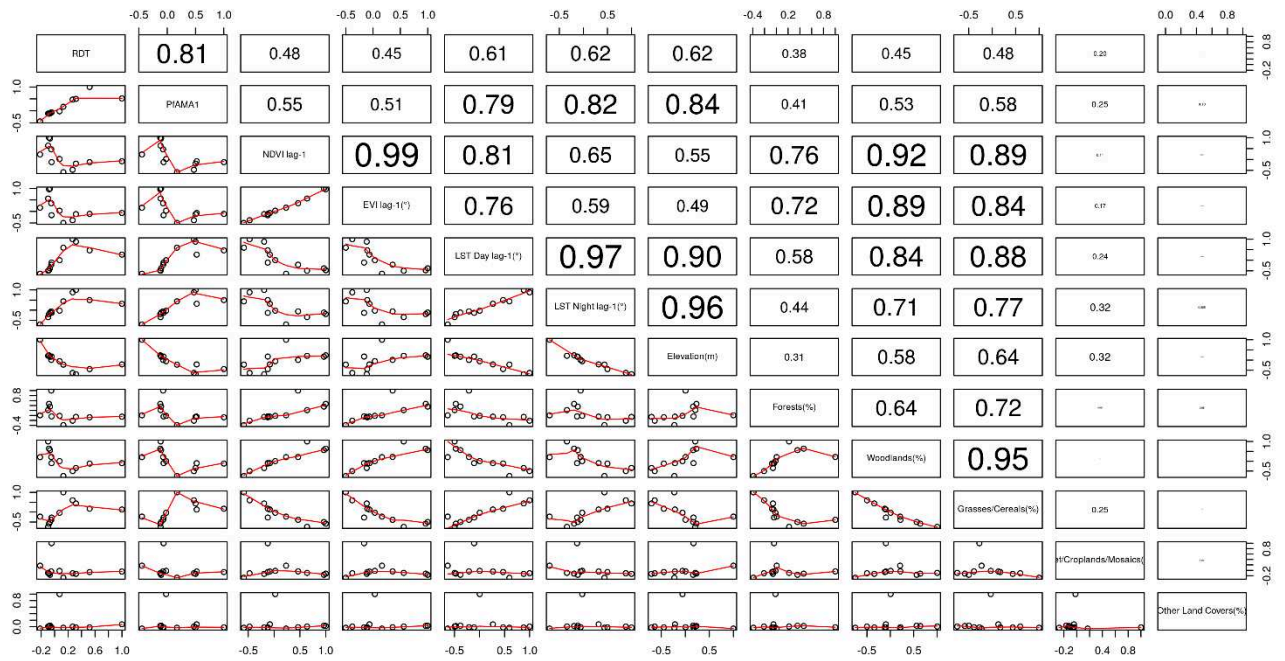


Fig. S7 Pearson's correlation scatterplot and peers of *P. falciparum* infection prevalence by RDT, PfAMA1 Ab seroprevalence and quantitative environmental and climatic covariates associations.

There was high correlation between multiple pairs of covariates such as {NDVI, EVI, forests, woodlands, or grasslands/cereals}, {LST day, LST night, elevation, woodlands or grasslands/cereals} and {grasslands/cereals, wet/croplands/mosaics}

Table S2 Univariable and multivariable *P. falciparum* exposure (PfAMA1 Ab response) model of individual-, household- and fokontany-level covariates, using mixed-effect logistic regression at district and commune level

Factors associated	<i>P. falciparum</i> exposure (PfAMA1 Ab response) model			
	Univariable		Multivariable	
	OR	95% CI	OR	95% CI
Individual level				
Age (years)				
2–8 (Ref.)	1		1	
9–10	1.5	1.1–2.0	1.8	1.2–2.4***
11–12	2.8	2.2–3.7	3.7	2.8–5.0***
13–14	4.0	2.9–5.4	5.7	4.0–8.0***
Sex				
Female (Ref.)	1			
Male	1.3	1.1–1.6	1.2	1.0–1.5
Fever last 2 weeks	1.7	1.3–2.3	1.7	1.2–2.4**
Trip last 2 months	1.0	0.6–1.7		
Last night use of ITN	2.0	1.7–2.5		
Household level				
No. of ITN				
[0,1]	1			
(1,4]	2.7	2.1–3.4		
(4,10]	4.3	2.7–7.0		
Presence of RDT positive household member	5.5	2.3–13.4		
Fokontany level				
Health Facilities >5 km	2.1	1.7–2.6	1.6	1.2–2.1**
School RDT prevalence ^k	4.4	3.5–5.6	2.1	1.3–3.3**
NDVI at lag-1 ⁿ	0.8	0.7–0.9	1.0	0.8–1.3
LST Day at lag-1 ^l	4.5	3.7–5.4		
Grasslands or cereals ^k	1.1	1.1–1.2	0.9	0.9–1.0
Forests ^k	0.8	0.7–1.0		
Woodlands ^k	0.9	0.8–0.9		
Wet, croplands or mosaics ^k	0.9	0.8–1.0		
Elevation ^e	0.7	0.6–0.7	0.7	0.6–0.8***

NDVI: Normalized Difference Vegetation Index at the previous month

LST: daytime Land Surface Temperature and emissivity composites at the previous month

^η NDVI was scaled 1/10, as one unit increase means 0.1 increase

[¶] LST Day was scaled in 5 °C unit, as one unit increase means 5 °C increase

^κ Variables scaled in 10% unit, as one unit increase means 10% increase

^ε Elevation scaled in 100 m, as one unit increase means 100 m increase

OR: odds ratio; *** p-value < 0.001; ** p-value < 0.01; * p-value < 0.05; Wald-test approximation was used for CIs (confidence interval) and p-values

Ref.: Reference; ITN: Insecticide-impregnated mosquito-nets

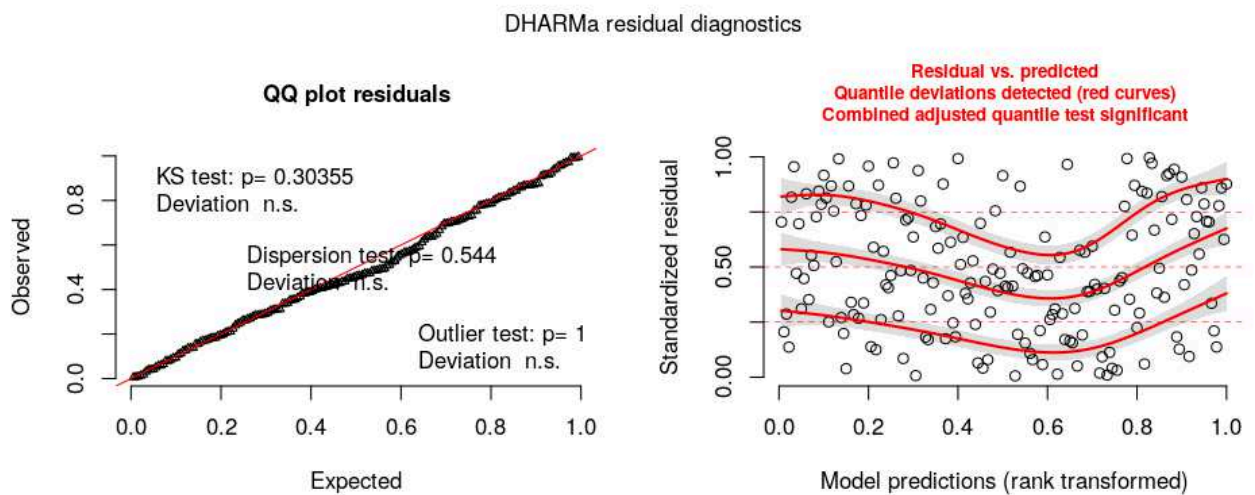


Fig. S8 *P. falciparum* exposure (PfAMA1 Ab response) model residuals diagnostics of normality at fokontany-level. No significant deviance to normal distribution was observed PfAMA1 Ab response model residuals using Kolmogorov–Smirnov normality test ($p = 0.3$).

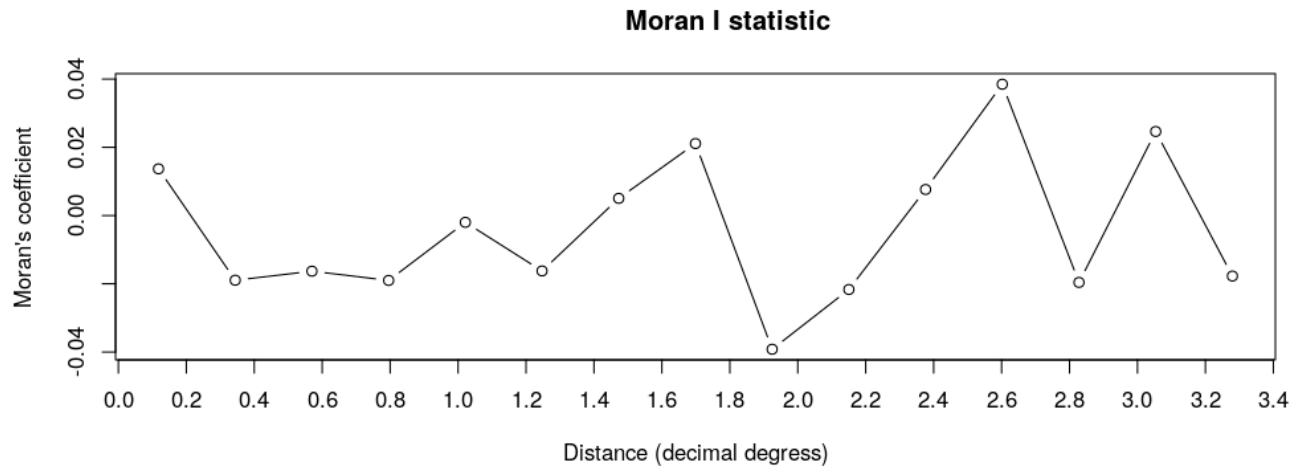


Fig. S9 Spatial autocorrelation of residuals diagnostics using Moran's I index of non-spatial *P. falciparum* exposure (PfAMA1 Ab response) model at fokontany-level.

Table S5 Univariable and multivariable *P. falciparum* infection model at individual-, household- and fokontany-level covariates using mixed-effect logistic regression at district and commune level

Factors associated	<i>P. falciparum</i> infection model			
	Univariable		Multivariable	
	OR	95% CI	OR	95% CI
Individual level				
Age (years)				
2–8 (Ref.)	1			
9–10	0.8	0.4–1.7		
11–12	1.2	0.6–2.3		
13–14	1.3	0.5–3.0		
Sex				
Female (Ref.)	1			
Male	1.3	0.8–2.3		
Fever last 2 weeks	8.9	5.1–15.6	9.9	5.2–18.9***
Trip last 2 months	0.6	0.1–4.0		
Last night use of ITN	1.5	0.9–2.6		
Household level				
No. of ITN				
[0,1]	1			
(1,4]	2.21	1.2–4.1		
(4,10]	1.2	0.2–9.3		
Fokontany level				
Health Facilities >5 km	1.8	1.1–3.1		
NDVI at lag-1 [¶]	0.7	0.5–0.9		
LST Day at lag-1 [¶]	38.1	11.2–129.6	118.0	10.4–1.3e+03***
Grasslands or cereals ^κ	1.3	1.1–1.6		
Forests ^κ	0.7	0.3–1.5		
Woodlands ^κ	0.7	0.6–0.9	1.1	0.8–1.5
Wet, croplands or mosaics ^κ	0.8	0.5–1.3		
Elevation ^ε	0.7	0.6–0.8		

NDVI: Normalized Difference Vegetation Index at the previous month

LST: daytime Land Surface Temperature and emissivity composites at the previous month

[¶] NDVI was scaled 1/10, as one unit increase means 0.1 increase

[¶] LST Day was scaled in 5 °C unit, as one unit increase means 5 °C increase

^κ Variables scaled in 10% unit, as one unit increase means 10% increase

^ε Elevation scaled in 100 m, as one unit increase means 100 m increase

OR: odds ratio; *** p-value <0.001; ** p-value < 0.01; * p-value < 0.05; Wald-test approximation was used for CIs (confidence interval) and p-values

Ref.: Reference; ITN: Insecticide-impregnated mosquito-nets

Table S6 Sub-model for ≤5 years old children (seroprevalence = 2.6% [5 of 194]), only variables included in the all participants Ab response model were included: univariable *P. falciparum* exposure (PfAMA1 Ab response) model of individual- and fokontany-level covariates, using binomial logistic regression

Factors associated	<i>P. falciparum</i> exposure (PfAMA1 Ab response) model	
	Univariable	
	OR	95% CI
Individual level		
Sex		
Female (Ref.)	1	
Male	0.4	0.0–3.7
Fever last 2 weeks	1.9	0.2–17.8
Fokontany level		
Health Facilities >5 km	2.0	0.3–12.4
School RDT prevalence ^κ	0.8	0.0–52.1
NDVI at lag-1 ^η	2.1	0.9–5.0
Grasslands or cereals ^κ	0.8	0.7–1.0
Elevation ^ε	1.2	0.7–1.9

NDVI: Normalized Difference Vegetation Index at the previous month

^η NDVI was scaled 1/10, as one unit increase means 0.1 increase

^κ Variables scaled in 10% unit, as one unit increase means 10% increase

^ε Elevation scaled in 100 m, as one unit increase means 100 m increase

OR: odds ratio; *** p-value <0.001; ** p-value < 0.01; * p-value < 0.05; Wald-test approximation was used for CIs (confidence interval) and p-values

Ref.: Reference; ITN: Insecticide-impregnated mosquito-nets

Supplemental files 2

Supplementary materials

Excess mortality associated with the COVID-19 pandemic during the 2020 and 2021 waves in

Antananarivo, Madagascar

J.H. Rabarison MD^{1*}, J.M. Rakotondramanga MSc^{2,3,4,5*}, R. Ratovoson PhD^{2#}, B. Masquelier PhD⁶, A.M. Rasoanomenjanahary MD⁷, A. Dreyfus PhD², A. Garchitorena PhD^{2,5}, F. Rasambainarivo PhD^{8,9}, N.H. Razanajatovo PhD¹, S.F. Andriamandimby PhD¹, C.J.E. Metcalf PhD^{8,10}, V. Lacoste PhD¹, J-M. Heraud PhD^{1q\$#}, P. Dussart PhD^{1\$}

Content

Supplementary Methods S1–S3

Supplementary Figures S1–S6

Supplementary Tables S1–S4

Supplementary Methods

Method S1. The Bureau Municipal d'Hygiène (BMH) of Antananarivo

This office was created in 1916 and covers five of the six central districts of Antananarivo-city, corresponding to the district of Antananarivo-Renivohitra. Its role has been to provide free consultations, conduct vaccination campaigns, manage malaria prophylaxis, and isolate patients with highly infectious diseases. Since 1921, the BMH has also been in charge of home verification of deaths. Historically, this system of death verification was motivated by recurrent plague epidemics but was maintained for the purpose of disease and outbreak surveillance. The 6th district (Ambohimananarina) does not fall in the area covered by the BMH for historical reasons; this locality was an autonomous urban commune under the 1st Republic, from 1958–72. Community and hospital deaths are recorded in a single register as they are reported to the BMH. These certificates are mandatory to obtain burial authorization. This system contributes to maintaining a high completeness of death registration, estimated at over 90% since the 1970s. (Masquelier et al., 2019)

Method S2: Relative change method based on P-scores

The expected deaths were derived from the period 2016 to 2019, and the corresponding relative change was computed as follows: (Serfling, 1963)

$$\text{Relative change}(\%) = \frac{\{\text{Reported deaths}\} - \{\text{Average expected deaths}\}}{\{\text{Average expected deaths}\}} * 100.$$

A relative change of 100%, in a given week in 2020 (or 2021), would mean that the death count for that week was double from the expected death count.

Method S3: Mathematical background to cross-wavelet analyses

Cross-wavelet analyses were performed twice in order to detect and quantify the existing relationships between (1) the log-transformed of all-cause deaths in Antananarivo and national COVID-19 deaths (supplementary Figure S1A and S1C), (Mathieu et al., 2020) and (2) the transformed square root of SARS-CoV-2 test positivity rate by the IPM laboratory and all-cause death rate in Antananarivo, (Supplementary Figure S1B and S1D), as non-stationary time series. The concepts of cross-wavelet coherency and wavelet phase difference are natural generalizations of the basic wavelet analysis tools that enable us to appropriately deal and conclude with the time-frequency dependencies between two time series. (Aguiar-Conraria & Soares, 2011)

Cross-Wavelet Transform (XWT) of two time series, $x(t)$ and $y(t)$ is defined as

$$W_{xy} = W_x W_y ,$$

Where W_x and W_y are the wavelet transforms of x and y , respectively. The cross-wavelet power (XWP) is

$$(XWP)_{xy} = |W_{xy}|.$$

Here, we can interpret the wavelet power spectrum to depict the local variance of a time series; the cross-wavelet power of two time series depicts the local covariance between these time series at each time and frequency (the inverse form of scale/period). Furthermore, the cross-wavelet power informs us about a quantified indication of the similarity of power between two time series.

Then, given two time series $x(t)$ and $y(t)$, their complex wavelet coherency can be defined as ρ_{xy} by:

$$\rho_{xy} = \frac{S(W_{xy})}{[S(|W_x|^2)S(|W_y|^2)]^{1/2}},$$

where S denotes a smoothing operator in both time and scale (period). Without the smoothing, coherency would be identically one at all scales and times. That needs an appropriate choice of parameters combination. So, Bartlett window was used both for smoothing in time and scale (period) direction, without a detrending technique but with a default method of generating surrogate time series, white-noise.(Cazelles et al., 2008)

Then, the complex wavelet coherency can be written in polar form, as $\rho_{xy} = |\rho_{xy}|e^{i\Phi_{xy}}$:(Roesch & Schmidbauer, 2018)

- The absolute value of the complex wavelet coherency is called the wavelet coherency and is defined as,

$$Coherency = R_{xy} = \frac{|S(W_{xy})|}{[S(|W_x|^2)S(|W_y|^2)]^{1/2}},$$

with $0 \leq R_{xy} \leq 1$ across time and scale direction.

Thus, the cross-wavelet coherence of a complex wavelet is,

$$Coherence = Coherency^2$$

- The angle of the complex coherency is called phase-difference (phase lead of x over y), i.e.

$$\Phi_{xy} = \left(\frac{\Im(S(W_{xy}))}{\Re(S(W_{xy}))} \right).$$

Thus, a phase-difference of zero indicates that the time series move together at the specified time-frequency; if $\Phi_{xy} \in \left(0, \frac{\pi}{2}\right)$, then the series move in phase, but x leads y ; if $\Phi_{xy} \in \left(\frac{-\pi}{2}, 0\right)$, then it is y that is leading x . A phase-difference of π (or $-\pi$) indicates an anti-phase relation; if $\Phi_{xy} \in \left(\frac{\pi}{2}, \pi\right)$, then y is leading; x is leading if $\Phi_{xy} \in \left(-\pi, -\frac{\pi}{2}\right)$. This is illustrated by arrows directions as in Figure 3.(Roesch & Schmidbauer, 2018)

Supplementary Figures

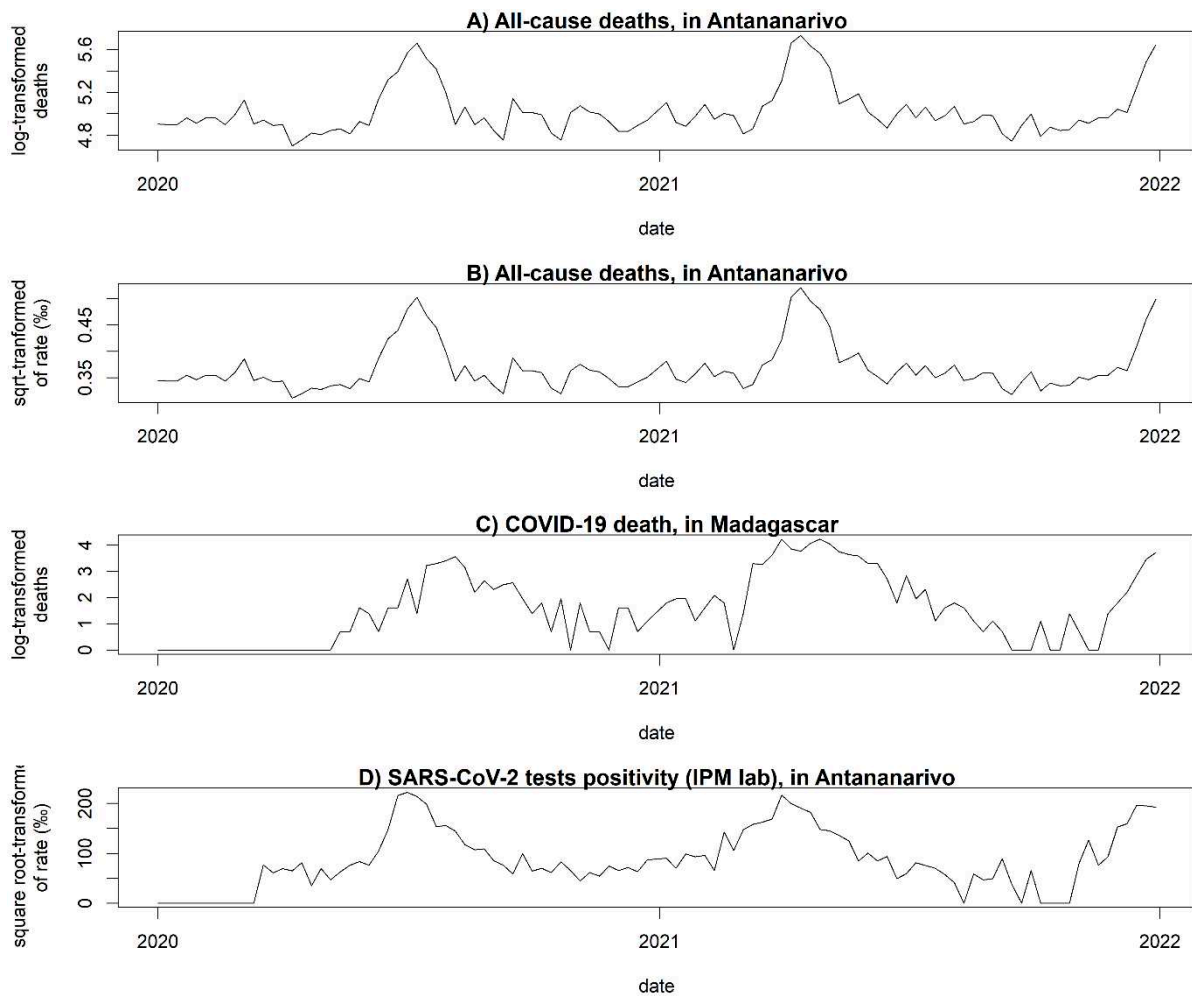


Figure S1. Temporal trends from 2020–21 of transformed data used for the wavelet analyses, cross-wavelet coherence and phase-difference: the log-transformed of all-cause deaths in Antananarivo and national COVID-19 deaths (panels A and C),(Mathieu et al., 2020) and the square root-transformed of SARS-CoV-2 test positivity rate by the IPM laboratory and all-cause death rate in Antananarivo (panels B and D).

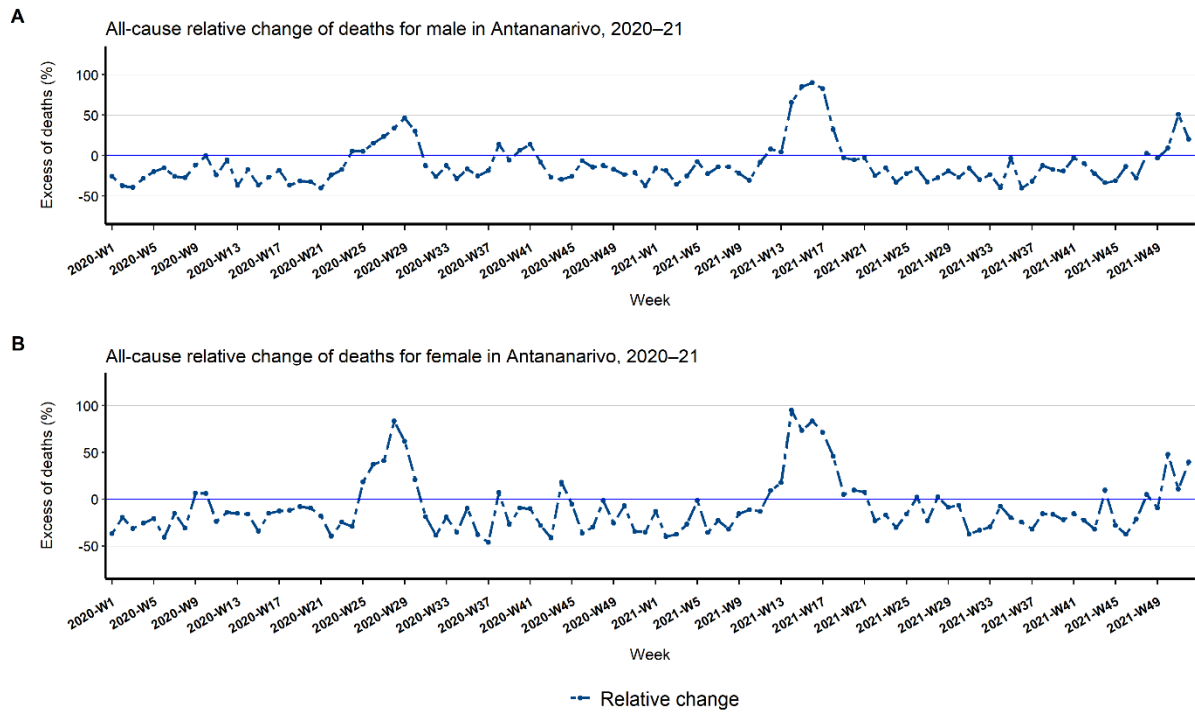


Figure S2: Weekly excess mortality by sex: for (A) Male and (B) Female deaths.

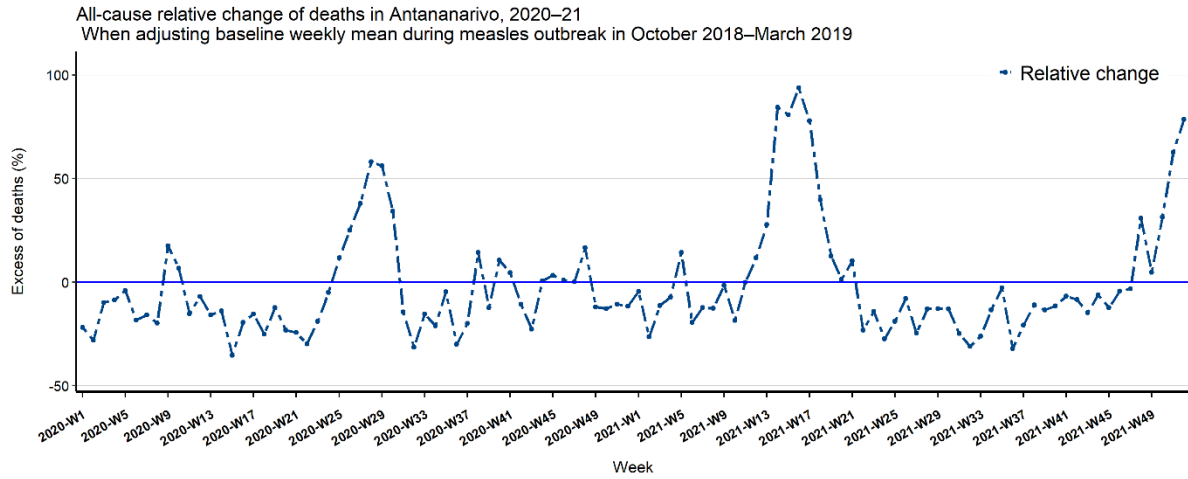


Figure S3. Weekly temporal trends, in five districts of Antananarivo from 2020–21. All-causes excess deaths were calculated using 2016–19 adjusted deaths as baseline (death from October 2018 to March 2019 was not considered due to measles outbreak affecting Antananarivo). Significant all-cause excess mortality was estimated during waves of COVID-19 in both 2020 and 2021 in Antananarivo: totalling 1,499 deaths for 32 weeks. (95 % CI is indicated in grey)

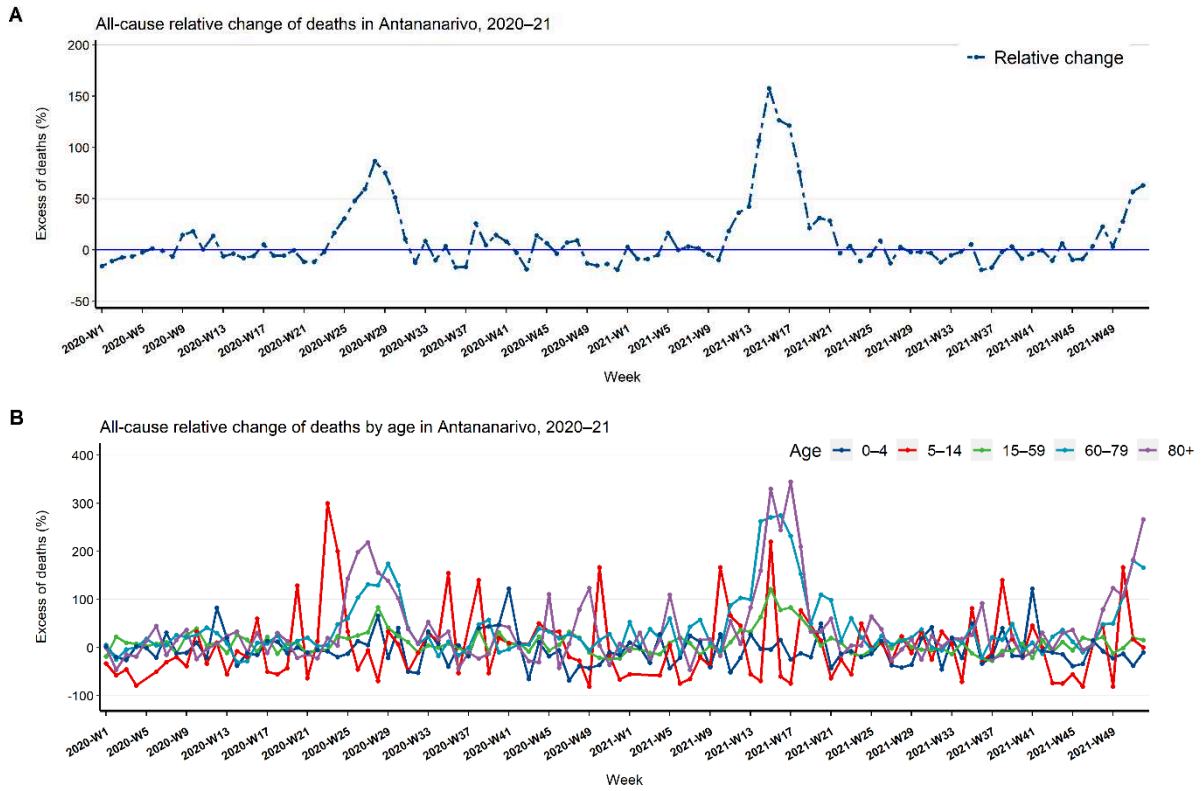


Figure S4. Weekly temporal trends using a relative change method based on P-scores, in five districts of Antananarivo from 2020–21. (a) All-cause excess mortality using 2016–19 crude deaths as baseline years, totalling 2,111 deaths for 51 weeks. **(b)** All-cause excess mortality by age group using 2016–19 crude deaths as baseline years; the excess mortality was estimated at over 200% for the elderly (80+) for each wave (no death record was observed for age group 5–14 age during one week in 2020 and two weeks in 2021). Supplementary Table S1 Supplementary materials representing weekly all-cause deaths by age group supports this figure.

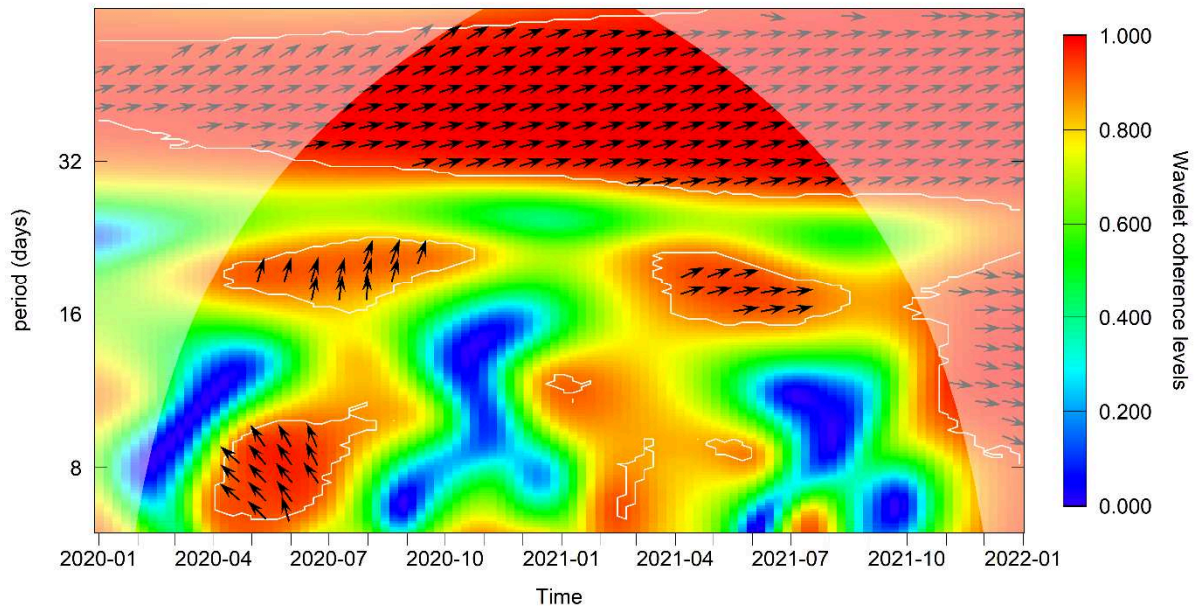


Figure S5: Cross-wavelet coherence and phase-difference of the all-cause deaths in Antananarivo and national COVID-19 deaths. (Mathieu et al., 2020) This figure shows that these two time series were out of phase, phase-differences $\in \left(\frac{\pi}{2}, \pi\right)$; and the weekly national COVID-19 deaths led the Antananarivo deaths. However, from the 2nd half of 2020 to September 2021, the all-cause deaths in Antananarivo were mainly in phase and led the national COVID-19 deaths, phase-differences $\in \left(0, \frac{\pi}{2}\right)$. The significant coherence level is ranked from blue–red colour scale, and statistically significant wavelet coherence is marked by the white contour plots when p-value < 0.05 . This figure is supported by the Method S3, Figure S1A and S1C.

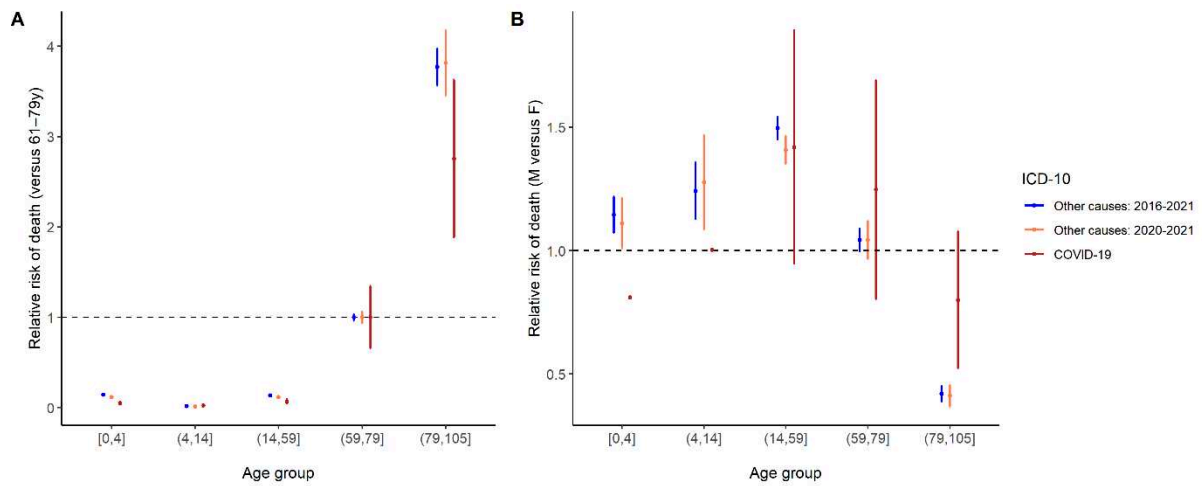


Figure S6. Relative risk ratios of COVID-19 and other causes of death, for each age group, (A) versus 60–79y, and (B) for Male (versus Female). The vertical bars represent confidence intervals. In 2020–2021, COVID-19 infection induced a significantly higher risk of death for the elderly aged 80+ compared to persons aged 60–79 years of age, with a risk ratio (RR) = 2.8 (IC95% 1.9–3.6) (panel A). A similar relative risk of dying from COVID-19 was observed for men and women in these two age groups, in comparison to other causes of deaths in the same period. That showed lesser risk for men 80+ years of age, RR = 0.4 (0.36–0.46) (panel B).

Supplementary Tables

Table S1: Weekly mortality data in Antananarivo, 2016–2021.

Year	Age	Mean	SD
2016	[0,4]	11.1	4.74
2016	(4,14]	3.02	1.63
2016	(14,59]	61.27	7.97
2016	(59,79]	33.17	5.87
2016	(79,105]	12.4	3.81
2017	[0,4]	11.73	3.75
2017	(4,14]	2.9	1.49
2017	(14,59]	62.31	12.15
2017	(59,79]	35.83	7.48
2017	(79,105]	12.25	4.41
2018	[0,4]	17	10.14
2018	(4,14]	3.92	2.51
2018	(14,59]	68.87	15.96
2018	(59,79]	37.69	8.43
2018	(79,105]	12.5	3.62
2019	[0,4]	16.12	5.9
2019	(4,14]	3.98	1.96
2019	(14,59]	69.23	11.44
2019	(59,79]	42.62	8.04
2019	(79,105]	15.19	4.29
2020	[0,4]	13.21	4.13
2020	(4,14]	3.18	1.82
2020	(14,59]	70.62	12.99
2020	(59,79]	46.96	19.25
2020	(79,105]	16.63	9.38
2021	[0,4]	12.75	3.92
2021	(4,14]	2.96	1.63
2021	(14,59]	71.21	15.09
2021	(59,79]	57.29	25.45
2021	(79,105]	19.1	9.49

Table S2: Weekly mortality data and excess deaths in Antananarivo, 2020-2021. Data shows estimated all-age excess mortality using positive lower bounds of relative change, the difference between weekly reported deaths in 2020–2021 and the upper bounds of 95%CI of the average expected deaths.

Week	Year	Reported deaths	Average expected deaths (2016–2019)			Death excesses by relative change
			Mean	CI Low	CI Up	
1	2020	135	160.25	134.22	186.28	-27.53
2	2020	134	150.25	110.81	189.69	-29.36
3	2020	134	144.50	82.02	206.98	-35.26
4	2020	143	152.50	121.41	183.59	-22.11
5	2020	136	139.25	111.80	166.70	-18.42
6	2020	143	141.00	83.80	198.20	-27.85
7	2020	143	144.25	111.40	177.10	-19.26
8	2020	134	143.50	101.07	185.93	-27.93
9	2020	147	128.50	115.22	141.78	3.68
10	2020	169	143.25	128.94	157.56	7.26
11	2020	135	134.25	91.96	176.54	-23.53
12	2020	140	123.25	97.29	149.21	-6.18
13	2020	133	142.00	104.82	179.18	-25.77
14	2020	134	138.75	121.79	155.71	-13.94
15	2020	110	119.50	68.64	170.36	-35.43
16	2020	116	123.25	102.57	143.93	-19.41
17	2020	124	118.00	89.36	146.64	-15.44
18	2020	122	129.50	95.91	163.09	-25.20
19	2020	127	134.25	123.59	144.91	-12.36
20	2020	129	129.50	91.10	167.90	-23.17
21	2020	123	139.25	116.03	162.47	-24.29
22	2020	138	156.25	115.99	196.51	-29.78
23	2020	133	135.75	107.33	164.17	-18.98
24	2020	170	145.75	112.54	178.96	-5.01
25	2020	204	156.00	129.31	182.69	11.66
26	2020	220	148.75	121.45	176.05	24.97
27	2020	262	164.25	138.58	189.92	37.95
28	2020	287	153.75	125.93	181.57	58.07
29	2020	249	142.00	124.52	159.48	56.13
30	2020	225	148.75	129.86	167.64	34.22
31	2020	181	164.00	116.39	211.61	-14.47
32	2020	134	153.50	111.23	195.77	-31.55
33	2020	158	145.50	104.14	186.86	-15.45
34	2020	134	149.25	128.65	169.85	-21.11

35	2020	143	138.25	126.46	150.04	-4.69
36	2020	127	152.75	124.10	181.40	-29.99
37	2020	116	138.75	132.47	145.03	-20.02
38	2020	171	136.00	122.44	149.56	14.33
39	2020	150	143.25	115.53	170.97	-12.27
40	2020	150	131.00	117.07	144.93	3.50
41	2020	147	135.75	131.00	140.50	4.63
42	2020	124	127.50	115.00	140.00	-11.43
43	2020	116	143.00	116.34	169.66	-31.63
44	2020	150	131.75	96.90	166.60	-9.96
45	2020	160	150.25	121.89	178.61	-10.42
46	2020	151	156.75	125.61	187.89	-19.63
47	2020	148	138.00	87.97	188.03	-21.29
48	2020	138	126.25	87.07	165.43	-16.58
49	2020	126	145.25	95.89	194.61	-35.26
50	2020	126	148.75	75.48	222.02	-43.25
51	2020	133	154.25	108.00	200.50	-33.67
52	2020	140	173.75	102.02	245.48	-42.97
1	2021	165	160.25	134.22	186.28	-11.42
2	2021	137	150.25	110.81	189.69	-27.78
3	2021	132	144.50	82.02	206.98	-36.23
4	2021	145	152.50	121.41	183.59	-21.02
5	2021	162	139.25	111.80	166.70	-2.82
6	2021	141	141.00	83.80	198.20	-28.86
7	2021	149	144.25	111.40	177.10	-15.87
8	2021	146	143.50	101.07	185.93	-21.48
9	2021	123	128.50	115.22	141.78	-13.25
10	2021	129	143.25	128.94	157.56	-18.13
11	2021	159	134.25	91.96	176.54	-9.93
12	2021	168	123.25	97.29	149.21	12.59
13	2021	202	142.00	104.82	179.18	12.73
14	2021	287	138.75	121.79	155.71	84.32
15	2021	308	119.50	68.64	170.36	80.79
16	2021	279	123.25	102.57	143.93	93.84
17	2021	261	118.00	89.36	146.64	77.98
18	2021	228	129.50	95.91	163.09	39.80
19	2021	163	134.25	123.59	144.91	12.48
20	2021	170	129.50	91.10	167.90	1.25

21	2021	179	139.25	116.03	162.47	10.18
22	2021	151	156.25	115.99	196.51	-23.16
23	2021	141	135.75	107.33	164.17	-14.11
24	2021	130	145.75	112.54	178.96	-27.36
25	2021	148	156.00	129.31	182.69	-18.99
26	2021	162	148.75	121.45	176.05	-7.98
27	2021	143	164.25	138.58	189.92	-24.71
28	2021	158	153.75	125.93	181.57	-12.98
29	2021	139	142.00	124.52	159.48	-12.84
30	2021	146	148.75	129.86	167.64	-12.91
31	2021	159	164.00	116.39	211.61	-24.86
32	2021	135	153.50	111.23	195.77	-31.04
33	2021	138	145.50	104.14	186.86	-26.15
34	2021	147	149.25	128.65	169.85	-13.45
35	2021	146	138.25	126.46	150.04	-2.69
36	2021	123	152.75	124.10	181.40	-32.20
37	2021	115	138.75	132.47	145.03	-20.71
38	2021	133	136.00	122.44	149.56	-11.08
39	2021	148	143.25	115.53	170.97	-13.44
40	2021	120	131.00	117.07	144.93	-17.20
41	2021	131	135.75	131.00	140.50	-6.76
42	2021	127	127.50	115.00	140.00	-9.28
43	2021	128	143.00	116.34	169.66	-24.55
44	2021	140	131.75	96.90	166.60	-15.96
45	2021	136	150.25	121.89	178.61	-23.86
46	2021	143	156.75	125.61	187.89	-23.89
47	2021	143	138.00	87.97	188.03	-23.95
48	2021	155	126.25	87.07	165.43	-6.30
49	2021	150	145.25	95.89	194.61	-22.92
50	2021	190	148.75	75.48	222.02	-14.42
51	2021	242	154.25	108.00	200.50	20.70
52	2021	283	173.75	102.02	245.48	15.28

Table S3. Estimated all-cause excess mortality in 2020–2021. Relative changes and expected deaths were calculated based on 2016–2019 baseline mortality adjusted by deaths during measles outbreaks (October 2018 to March 2019).

Year	Relative change level (%)	Nb. of weeks of excess	Adjusted expected deaths (2016–2019) ¹		Reported deaths (2020–2021)		Sum death excesses
			Mean	Range (min-max)	Mean	Sum	
2020	< 50	14	139	114-164	174	2,442	297
2020	≥ 50	2	148	142-154	268	536	195
2021	< 50	10	129	114-139	177	1,767	272
2021	≥ 50	6	132	118-150	277	1,66	736
Total		32	137	114-164	200	6,405	1,500

¹ Expected deaths were adjusted with deaths occurring during measles outbreak (October 2018-March 2019).
Nb=number

Table S4: Contribution of deaths identified as COVID-19 and those associated with other causes of deaths to changes in life expectancy at birth between 2019 and 2020, and between 2020 and 2021.

Age group	Males: $e_0(2020) - e_0(2019)$		Females: $e_0(2020) - e_0(2019)$		Males: $e_0(2021) - e_0(2020)$		Females: $e_0(2021) - e_0(2020)$	
	Covid-19 deaths	All other causes	Covid-19 deaths	All other causes	Covid-19 deaths	All other causes	Covid-19 deaths	All other causes
0-1	0.00	0.22	-0.01	0.07	0.00	0.01	0.00	0.06
1-4	0.00	0.19	0.00	0.44	0.00	0.12	0.00	0.03
5-14	0.00	0.08	0.00	0.21	0.00	0.05	0.00	-0.06
15-34	-0.02	0.04	-0.02	0.04	-0.04	0.08	-0.03	0.09
35-59	-0.13	0.27	-0.11	0.09	-0.31	0.62	-0.27	0.13
60-79	-0.17	-0.30	-0.19	-0.10	-0.48	-0.24	-0.55	-0.11
80+	-0.02	-0.04	-0.03	-0.09	-0.06	-0.09	-0.14	0.00
Total	-0.35	0.45	-0.36	0.66	-0.90	0.55	-0.99	0.13

The e_{xt} is the residual at age x and time t .

ANNEXES : autres contributions en co-auteur pendant la thèse

ANNEXE 1

Steinhardt, L. C., Ravaoarisoa, E., Wiegand, R., Harimanana, A., Hedje, J., Cotte, A. H., Zigirumugabe, S., Kesteman, T., Rasoloharimanana, T. L., Rakotomalala, E., Randriamoramana, A. M., Rakotondramanga, J. M., Razanatsiorimalala, S., Mercereau-Puijalon, O., Perraut, R., Ratsimbaoa, A., Butts, J., Rogier, C., Piola, P., ... Vigan-Womas, I. (2021). School-Based Serosurveys to Assess the Validity of Using Routine Health Facility Data to Target Malaria Interventions in the Central Highlands of Madagascar. *Journal of Infectious Diseases*, 223(6), 995–1004. <https://doi.org/10.1093/infdis/jiaa476>

School-Based Serosurveys to Assess the Validity of Using Routine Health Facility Data to Target Malaria Interventions in the Central Highlands of Madagascar

Laura C. Steinhardt,^{1,9} Elisabeth Ravaoarisoa,^{3,4} Ryan Wiegand,¹ Aina Harimanana,⁵ Judith Hedje,^{1,6} Annett H. Cotte,^{1,2} Sixte Zigirumugabe,^{6,7} Thomas Kesteman,^{3,8} Tsikiniaina L. Rasoloharimanana,⁹ Emma Rakotomalala,⁹ Anny M. Randriamoramana,⁵ Jean-Marius Rakotondramanga,⁵ Sehen Razanatsiorimalala,³ Odile Mercereau-Puijalon,¹⁰ Ronald Perraut,¹¹ Arsène Ratsimbaoa,^{12,13,14} Jessica Butts,^{1,2} Christophe Rogier,^{14,15} Patrice Piola,^{5,16} Milijaona Randrianarivojosia,³ and Inès Vigan-Womas⁹

¹Division of Parasitic Diseases and Malaria, Center for Global Health, Centers for Disease Control and Prevention, Atlanta, Georgia, USA, ²U.S. President's Malaria Initiative, Centers for Disease Control and Prevention, Atlanta, Georgia, USA, ³Malaria Research Unit, Institut Pasteur de Madagascar, Antananarivo, Madagascar, ⁴Faculty of Sciences, University of Antananarivo, Antananarivo, Madagascar, ⁵Epidemiology Unit, Institut Pasteur de Madagascar, Antananarivo, Madagascar, ⁶US President's Malaria Initiative, Antananarivo, Madagascar, ⁷United States Agency for International Development, Washington, District of Columbia, USA, ⁸Fondation Merieux, Lyon, France, ⁹Immunology of Infectious Diseases Unit, Institut Pasteur de Madagascar, Antananarivo, Madagascar, ¹⁰Parasites and Insect Vectors Department, Institut Pasteur, Paris, France, ¹¹Immunology Unit, Institut Pasteur de Dakar, Dakar, Senegal, ¹²National Malaria Control Program of Madagascar, Ministry of Public Health, Antananarivo, Madagascar, ¹³Faculty of Medicine, University of Antananarivo, Antananarivo, Madagascar, ¹⁴L'Institut Hospitalo-Universitaire en Maladies Infectieuses de Marseille, Marseille, France, ¹⁵Institut Pasteur de Madagascar, Antananarivo, Madagascar, and ¹⁶Epidemiology and Public Health Unit, Institut Pasteur du Cambodge, Phnom Penh, Cambodia

Background. In low-malaria–transmission areas of Madagascar, annual parasite incidence (API) from routine data has been used to target indoor residual spraying at subdistrict commune level. To assess validity of this approach, we conducted school-based serological surveys and health facility (HF) data quality assessments in 7 districts to compare API to gold-standard commune-level serological measures.

Methods. At 2 primary schools in each of 93 communes, 60 students were randomly selected with parents and teachers. Capillary blood was drawn for rapid diagnostic tests (RDTs) and serology. Multiplex bead-based immunoassays to detect antibodies to 5 *Plasmodium falciparum* antigens were conducted, and finite mixture models used to characterize seronegative and seropositive populations. Reversible catalytic models generated commune-level annual seroconversion rates (SCRs). HF register data were abstracted to assess completeness and accuracy.

Results. RDT positivity from 12 770 samples was 0.5%. Seroprevalence to tested antigens ranged from 17.9% (MSP-1) to 59.7% (PF13). Median commune-level SCR was 0.0108 (range, 0.001–0.075). Compared to SCRs, API identified 71% (95% confidence interval, 51%–87%) of the 30% highest-transmission communes; sensitivity declined at lower levels. Routine data accuracy did not substantially affect API performance.

Conclusions. API performs reasonably well at identifying higher-transmission communes but sensitivity declined at lower transmission levels.

Keywords. serology; school-based surveys; malaria; Madagascar; stratification.

Although malaria has declined in Madagascar in the last 2 decades, transmission has increased recently, with increasing focal outbreaks in the last several years [1–5]. Indoor residual spraying (IRS) campaigns with effective insecticides are one of the primary approaches for vector control to reduce malaria burden and prevent outbreaks in epidemic-prone areas. The Central Highlands (CHL) of Madagascar represent an area of unstable malaria transmission >800 meters in altitude

that is prone to malaria epidemics. Generalized IRS, that is spraying all houses in all communes (a subdistrict administrative unit) within targeted districts, was carried out using dichlorodiphenyltrichloroethane (DDT) in the CHL from 1993 until 1998; from 1999 to 2007, focalized spraying (only certain communes per district) took place using DDT until 2003 and pyrethroids thereafter.

After the Ministry of Health declared in 2005 a goal of malaria elimination in Madagascar, generalized IRS in the CHL was restarted in 2008 and soon expanded to the Fringe areas surrounding the CHL, using pyrethroid insecticides (CHL where long-lasting insecticidal nets [LLINs] were not distributed) and carbamates (Fringe areas with LLIN distributions). After 4 years of generalized district-wide spraying, declining resources forced Madagascar to switch to focalized spraying in the CHL/Fringe areas, targeting subdistrict-level communes in 2012. Health facility (HF)-confirmed malaria case data were used to identify and prioritize

Received 2 March 2020; editorial decision 23 July 2020; accepted 28 July 2020; published online August 6, 2020.

Correspondence: Laura Steinhardt, PhD, MPH, Malaria Branch, Division of Parasitic Diseases and Malaria, Center for Global Health, Centers for Disease Control and Prevention, 1600 Clifton Road, NE, Mailstop A-06, Atlanta, GA 30329 (LSteinhardt@cdc.gov).

The Journal of Infectious Diseases® 2020;XX:1–10

Published by Oxford University Press for the Infectious Diseases Society of America 2020. This work is written by (a) US Government employee(s) and is in the public domain in the US. DOI: 10.1093/infdis/jiaa476

approximately 30% of communes (within the 33 districts) with the highest malaria incidence in 2011 for focalized spraying.

Using routine malaria case data for stratifying communes by transmission intensity for focalized IRS is potentially problematic because of variable quality and completeness of HF data [6]. In addition, rates of care-seeking in the formal public sector are generally low in Madagascar [7], with only 35.2% of febrile children <5 years old taken to public facilities or community health workers [8]; this rate is 36.0% in the CHL but only 20.1% in the surrounding Fringe areas, where part of the study took place. Accurate stratification of malaria transmission intensity is important for targeting interventions, especially as countries pursue malaria elimination [9]. Better understanding the validity of HF malaria case data for targeting IRS to higher-transmission areas is an important programmatic exercise as countries decide how to deploy more effectively and efficiently limited vector control resources.

Serological markers of malaria exposure can detect malaria hotspots in low-transmission settings [10–12]. Longer-lived antibodies to malaria, such as AMA-1 and MSP-1, can persist over time and represent a more stable measure of malaria transmission compared to parasite prevalence, which can vary substantially between and within transmission seasons [13, 14]. Serology has recently been shown to be a valid tool for measuring variation in local transmission intensity from samples collected in communities [15] and HFs [16]. School-based surveys are significantly less expensive than household surveys [17, 18], and serological measures from school-attending children can be valid for generalizing serological estimates to the surrounding commune [19].

We conducted school-based serological and parasite prevalence surveys to assess the validity of using HF malaria case data to target communes for focalized IRS in Madagascar.

METHODS

Study Sites

Malaria transmission in the CHL is unstable and episodic. In the Fringe areas, approximately 500 to 1000 meters in altitude, transmission patterns are seasonal, lasting from November to May (rainy season). In 2013, malaria prevalence in children aged 6–59 months was 0.7% and 2.5% by microscopy in the CHL and Fringe areas, respectively [8, 20]. Beginning in 2008, 32 districts in the CHL and Fringe areas, covering 29% of Madagascar's 114 districts, received IRS. The study area included 7 districts, 2 in the CHL (Ambohimahaso, Ambositra) not covered by LLIN distributions, and 5 in the Fringe areas (Ambatofinandrahana, Anjozorobe, Ankazobe, Betafo, and Mandoto), covered by LLIN distributions, which had all undergone 4 consecutive years of blanket (district-wide) IRS, plus 2 years of focalized spraying, by the time of the survey in May 2014 (Figure 1). These 7 districts comprise 107 communes. Each commune has an average of 14.6 primary schools (average of 154 children per school).

Each commune has at least 1 primary health center, or *centre de santé de base* (CSB), and in most cases 2 lower-level health centers, which should be staffed by a paramedical worker and an assistant, and serve approximately 4000 people. Midlevel health centers should be staffed by a medical doctor, nurse, and midwife, and serve approximately 8000 people. Unfilled positions and frequent absenteeism mean that few are fully staffed. During data collection in May–July 2014, 14 of the 107 communes were not accessible due to insecurity or inaccessibility (eg, heavy rains, lack of roads), leaving 93 communes able to be surveyed.

Data Collection

School-Based Serological Surveys

Within each commune, each public primary school was mapped by Euclidean distance to the midlevel CSB (or lower-level CSB if there was no midlevel CSB in the commune); 1 nearby primary school within 5 km of the midlevel CSB and 1 far primary school (>10 km distance), each with enrolment of at least 50 children, were randomly selected to ensure balance regarding healthcare

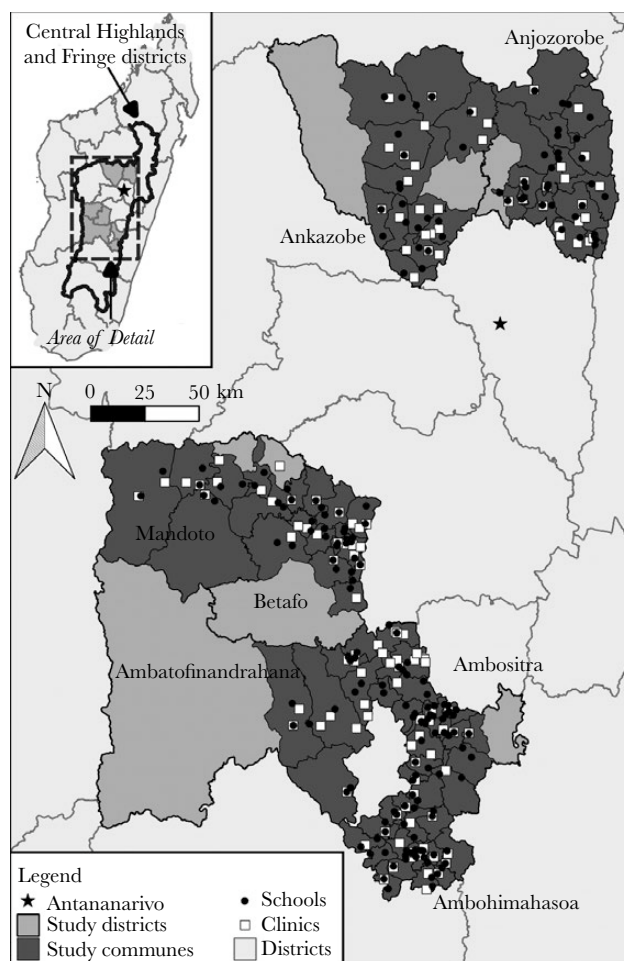


Figure 1. Map of sampled districts, schools, and health facilities. Source: Database of Global Administrative Areas (GADM) and QGIS.

access. Sampled schools were contacted in advance and parents invited to attend on the day of the survey. Thirty children with parents present (6 children from each of the 5 class levels) and their parents were randomly sampled per school. All teachers present were sampled. If parents brought younger children with them, they were also included if parents consented. A total of 120 children, parents, and teachers were targeted per commune based on simulations that indicated a sample size of 100 observations or greater with a seroconversion rate (SCR) of 0.05 and a seroreversion rate of 0.01 had a small expected bias for estimating the SCR (Wiegand, personal communication).

A brief questionnaire on demographics, residence, bed net use, and recent travel history for the parent and child was administered to parents and teachers. Finger prick blood was collected for malaria rapid diagnostic tests (RDTs) (CareStart Malaria RDT, HRP2/pLDH [Pf/PAN] Combo; Access Bio). Approximately 300–500 μ L of capillary blood was collected in microvette tubes (Microvette 500 Z-Gel; Sarstedt) for later serological analysis. The microvettes were centrifuged for 10 minutes at 8000 rpm and stored at -20°C until use. Results of RDTs were disclosed to individuals or their guardian; individuals with a positive RDT were given artesunate-amodiaquine (ASAQ) according to national guidelines. The first treatment dose was administered at the school, and parents were instructed on how to give/take the remaining ASAQ doses at home.

Health Facility Data Quality Assessments

Survey teams visited all open and accessible public lower-level and midlevel CSBs in the 7 districts (estimated total of 179) to conduct rapid data quality assessments. The purpose of this exercise was to explore how varying degrees of data quality affect utility of routine data for estimating malaria transmission intensity. Clinical register data were abstracted for 4 preselected months and assessed for completeness. Register data reporting accuracy was assessed through comparisons with health management information system (HMIS) data (full details in the [Supplementary Materials](#)).

Routine Malaria Data

Routine data on HF-based RDT-confirmed malaria cases in 2013 were obtained from the National Malaria Control Program (NMCP) and divided by the estimated commune-level population to calculate the annual parasite incidence (API). For IRS targeting, the NMCP primarily used rank-ordered commune API, selecting communes with APIs in the highest 30% (due to budgetary constraints), although occasionally RDT test-positivity or whether a commune had submitted a malaria epidemic alert in the previous year were considered as well.

Serological Analysis

Three soluble recombinant proteins (PF13, PfMSP1, and PfAMA1) and 2 bovine serum albumin (BSA)-conjugated

peptides (PfcSP and PfGLURP) from *Plasmodium falciparum* were included. BSA (GeneCust) was used as carrier control. Full details of the antigen preparation are in the [Supplementary Materials](#). Carboxylated magnetic MagPlex beads (Luminex) were covalently coupled with recombinant proteins, peptide-BSA complexes, or BSA as background control using the xMAP Antibody Coupling Kit (Luminex) following manufacturers' instructions, and using procedures previously described [21–23]. Antigen-coupled beads and plasma were deposited in 96-well plates (additional details in [Supplementary Materials](#)) and analyzed using the Luminex-MAGPIX system (Luminex) and xPONENT 4.1 software. IgG levels were expressed as median fluorescence intensity (MFI). A pool of sera from malaria-immune African adults and plasma samples from malaria-naive European individuals were included in each assay as positive and negative controls, respectively.

Data Analyses

Full details on statistical methods can be found in the [Supplementary Materials](#). Briefly, finite mixture models were used to determine which participants were considered negative (unexposed) and positive (exposed) for each antigen. MFI values were \log_{10} -transformed due to skewness in all distributions; participants with negative MFI- background values were recoded to 1 so all participants could be included. Using MFI data for all *P. falciparum* antigens, a latent class model was fit to determine an overall *P. falciparum* seropositivity latent variable for each participant. Seropositivity status from the latent class model was then used in reversible catalytic models to calculate SCRs for each commune.

Given the right-skewed distributions of both API and SCR, values of each measure were \log_{10} -transformed in analyses. All communes had 0.1 added to incidence values prior to transformation to include communes with zero incidence. Relationships between commune-level SCRs, as a gold standard, and APIs were assessed via regression models. All models attempted were univariable models with \log_{10} -transformed API as the outcome variable and \log_{10} -transformed SCR as the predictor. Different models were attempted and best-fitting regression models were used (see [Supplementary Materials](#)). Final models either included \log_{10} -transformed SCR as a linear term or as piecewise linear with 2 intercepts and slopes.

The sensitivity and specificity of API for correctly identifying the 30% of communes with the most intense transmission according to SCR were assessed. This process was then duplicated for other percentages of communes with highest transmission by SCR. Sensitivity and specificity were separately evaluated for the subsets of districts with lower ($n = 3$) and higher ($n = 4$) accuracy and completeness scores. Prevalence estimate confidence intervals across communes used the delta method to account for clustering at the school level or Wilson method [24] when no participants were positive. Analyses were carried out

in R and QGIS version 2.18.1 (QGIS Development Team) was used for mapping, and the 5% level of significance was used.

Ethics Approval and Consent to Participate

The study protocol was approved by the National Ethics Committee of the Ministry of Public Health of Madagascar (approval number CNE 011-MSANP/CE, 26 March 2014) and by the US Centers for Disease Control and Prevention Institutional Review Board. At sampled schools, after explaining the study objectives and procedures, individual, informed consent was obtained from caregivers of sampled students, younger children, and from teachers. Assent was obtained from students aged 7–17 years old.

RESULTS

Survey teams visited 185 schools (2/commune) of an estimated 1372 public primary schools and 141 HFs of an estimated 179 HFs in the 93 accessible communes (Supplementary Figure 1). Altogether, 6447 children and 6448 parents and teachers were surveyed, and 12 770 of the 12 895 (99.0%) surveyed participants had complete serology and demographic data. Most participants were either school aged (5–14 years old, 49.2%) or older than 20 years (48.8%) (Table 1).

Overall RDT positivity was very low at 0.5% and ranged from 0% to 13.3% by commune (Table 1, Supplementary Table 1, and Figure 2). Of the 93 communes surveyed, 68 (73%) had zero positive RDTs (Supplementary Table 1). Seropositivity to the *P. falciparum* antigens ranged from 17.9% of participants seropositive for PfMSP1 to 59.7% seropositive to PF13 (Table 1). Median SCRs by commune for the *P. falciparum* antigens followed the same trend as overall mean seropositivity, with PfMSP1, PfAMA1, PfCSP, PfGLURP, and PF13 having increasing values of median SCR/seropositivity (Table 1). Seropositivity for the *P. falciparum* latent antigen was 24.3% overall, ranging by commune from 2.0% to 67.2% (Table 1 and Supplementary Table 1). The SCR for the *P. falciparum* latent antigen had a median of 0.010 across communes, ranging from 0.001 to 0.075 (Table 1 and Figure 2). Commune-level API for 2013 from HF data ranged from 0.0 to 177.3 positive RDTs per 1000 population (Supplementary Table 1), with a median of 0 positive RDTs per 1000.

Routine Data Quality

Missingness of data in register fields was able to be assessed at 140 HFs in 91 communes, and data quality assessments were able to be conducted at HFs in 89 communes (HFs were inaccessible in 2 communes and HMIS data were not available for accuracy comparisons in an additional 2 communes). Missingness of the 4 register fields assessed was very low (average 1.9% missingness across all communes; range, 0.0%–23.6%) (Supplementary Table 2). It was not possible to gauge completeness of malaria data in terms of entire HFs not

Table 1. Characteristics of Sampled Individuals and Communes

Characteristic	Sample	Positive RDT	Serological Outcomes							API
			PfMSP1	PfAMA1	PfCSP	PfGLURP	PF13	Pf Latent Antigen ^a		
<i>Individual data</i>										
Age, y	n (%)	n	% (95% CI)	Seropositivity, % (95% CI)						
2–4	24 (0.2)	0	0.0 (0.0–17.2)	4.2 (0.1–22.7)	0.0 (0.0–17.2)	12.5 (2.0–35.6)	29.2 (13.6–49.4)	25.0 (10.3–45.7)	0.0 (0.0–17.2)	...
5–9	3071 (24.1)	22	0.7 (0.3–1.3)	6.9 (5.6–8.4)	4.0 (3.0–5.3)	13.2 (11.9–14.5)	34.6 (30.6–38.7)	47.0 (45.0–49.1)	3.3 (2.4–4.5)	...
10–14	3204 (25.1)	32	1.0 (0.6–1.6)	8.8 (7.3–10.4)	10.0 (7.6–12.7)	18.0 (16.4–19.7)	40.0 (35.8–44.3)	55.3 (53.0–57.5)	76 (5.6–9.9)	...
15–19	241 (1.9)	1	0.4 (0.0–2.3)	10.0 (6.2–15.0)	12.9 (7.8–19.6)	29.0 (23.4–35.2)	42.3 (34.3–50.7)	56.0 (49.2–62.7)	12.4 (7.3–19.4)	...
20+	6230 (48.8)	13	0.2 (0.1–0.4)	28.4 (25.2–31.8)	46.3 (41.9–50.8)	44.7 (41.6–47.8)	72.0 (68.5–75.4)	68.5 (65.8–71.0)	43.8 (39.3–48.5)	...
Female	8071 (63.2)	33	0.4 (0.2–0.7)	17.3 (15.2–19.7)	26.9 (23.9–30.1)	30.6 (28.5–32.6)	55.3 (51.9–58.7)	59.3 (57.3–61.3)	24.8 (21.8–28.0)	...
Total	12 770 (100.0)	68	(0.5)	17.9	26.3	30.1	54.3	59.7	24.3	...
<i>Commune data</i>										
n	Median (min, max)	Seroconversion Rate, Median (min, max)								
93	0.00 (0.00–13.3)	0.006 (0.001–0.056)	0.011 (0.002–0.078)	0.013 (0.006–0.068)	0.037 (0.011–0.524)	0.090 (0.047–0.256)	0.01 (0.001–0.075)	0.0 (0.0–177.3)	0.0 (0.0–177.3)	0.0 (0.0–177.3)

API derived from health management information system data; all other measures derived from survey data.

Abbreviations: API, annual parasite incidence; Pf, *Plasmodium falciparum*; RDT, rapid diagnostic test

^aPf latent antigen created from latent class analysis of all *Plasmodium falciparum* antigens.

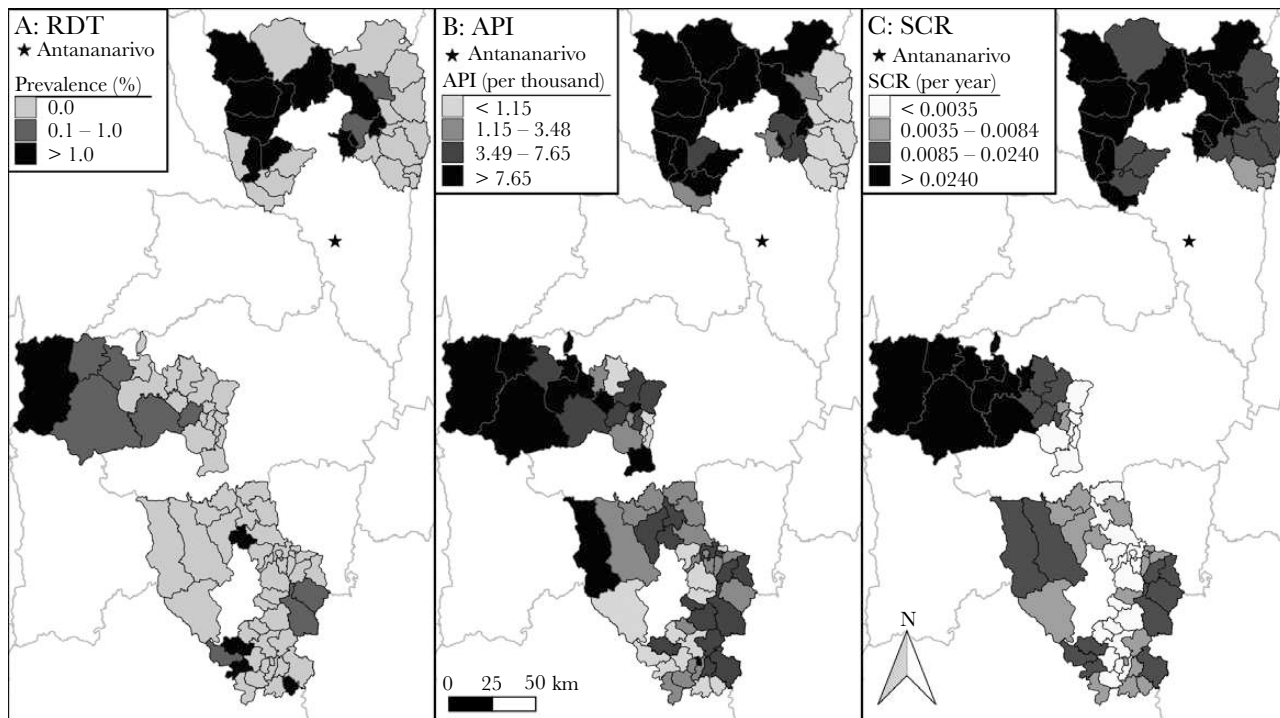


Figure 2. Maps of commune-level RDT prevalence (A), 2013 health facility API (B), and SCR for the Pf latent antigen (C). Abbreviations: API, annual parasite incidence; RDT, rapid diagnostic test; SCR, seroconversion rate. Source: Database of Global Administrative Areas (GADM) and QGIS.

reporting into the HMIS, as only HF reporting data were included as a denominator and no master list beyond this existed.

Data accuracy, however, was much poorer, with a 34.4% mean absolute value discordance (range by commune, 0.0%–275%) between register tallies and numbers reported in HMIS for indicators examined (number of consultations, number of RDTs done, and number of positive RDTs). Overall district data quality scores combining data missingness and accuracy indicated that 6 of 7 districts had roughly similar quality scores; 1 district (Mandoto) had much worse scores (Supplementary Table 3). Weights for the data quality were then calculated as $1/(1 + \text{mean proportion discordance})$. The median weight was 0.834 with a range from 0.267 to 1.000.

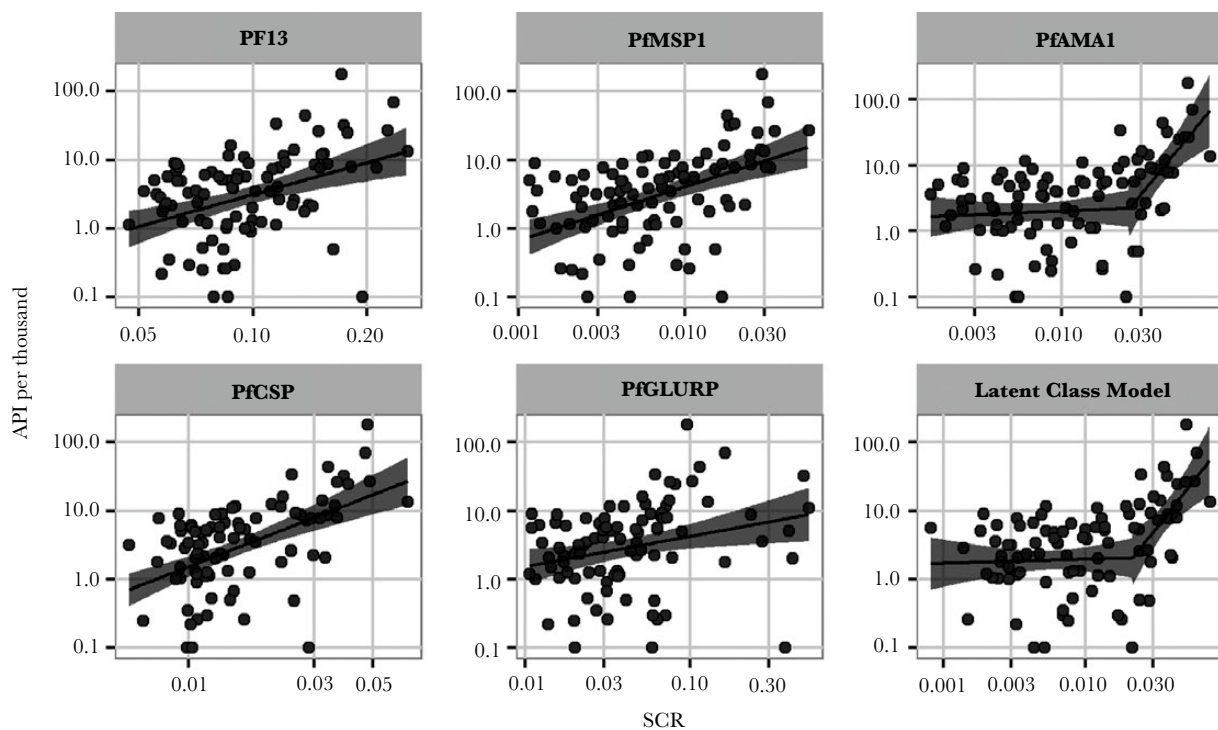
Relationship Between HF Incidence and Seropositivity Measures

The Akaike information criterion and Bayesian information criterion values indicated that spatial models did not provide a better fit but those accounting for commune-level data quality through an accuracy weight provided a marginally better fit (Supplementary Table 4). The final models selected were linear models for PF13, PfMSP1, PfCSP, and PfGLURP and piecewise linear models for PfAMA1 and the latent antigen (Figure 3). All models incorporated the data quality weights. For the 4 antigens with linear models, there was a significant positive relationship between SCR and API, although with wide variability and confidence intervals. For PfAMA1 and the *P. falciparum* latent antigen, there was a relatively flat relationship at lower levels of

SCR (up to 0.0263 and 0.0219 for PfAMA1 and latent antigen, respectively), after which there was a significant positive relationship between SCR and API (Figure 3).

Using commune-level SCRs as a gold standard, we identified the 30% of communes with the highest malaria transmission. Using each commune's API, the sensitivity of detecting the top 30% ranged from 60.7% to 75.0%, and specificity ranged from 83.1% to 89.2%, depending on the antigen used (Figure 4). Sensitivity and specificity of API were 71% (95% confidence interval [CI], 51%–87%) and 88% (95% CI, 77%–95%), respectively, using the *P. falciparum* latent antigen as a gold standard (Figure 4). The performance of API versus gold standard SCRs, as measured by area under the curve (AUC), typically improved when targeting the highest transmission communes (eg, the top 10% or 20%, according to SCR); sensitivity of API and AUC declined, although specificity remained relatively constant, when targeting a broader band of communes (eg, the top 50% or 60%) (Table 2). However, variability in the AUC and sensitivity does not allow us to conclude that 1 quantile has a stronger association with SCR values.

To further explore the impact of data quality on performance of API for targeting high-transmission communes, we calculated sensitivity and specificity of API for identifying the top 30% of communes after stratifying by district quality (4 districts with higher quality versus 3 districts with lower quality), as well as for all districts except Mandoto, the outlying, low-data-quality district. Using API only in districts with higher-quality



Marker	Term	Intercept (95% CI)	Slope (95% CI)	Difference (95% CI)	Changepoint (95% CI)
PF13		2.05 (1.26–2.83)	1.55 (0.79–2.31)		
PfMSP1		2.18 (1.51–2.85)	0.78 (0.48–1.08)		
PfAMA1	Segment 1	0.52	0.11 (–0.33–0.54)	2.98 (1.15–4.80)	–1.59 (–1.76 to –1.43)
PfAMA1	Segment 2	5.26	3.08 (1.31–4.85)		
PfCSP		3.18 (2.25–4.11)	1.49 (0.99–2.00)		
PfGLURP		1.07 (0.58–1.55)	0.44 (0.10–0.78)		
Latent class model	Segment 1	0.41	0.06 (–0.37–0.49)	2.56 (1.03–4.10)	–1.67 (–1.86 to –1.48)
Latent class model	Segment 2	4.68	2.62 (1.15–4.09)		

Figure 3. Best-fitting regression models (above) and coefficients (below) for SCRs of different antibodies versus API. Abbreviations: API, annual parasite incidence; CI, confidence interval; SCR, seroconversion rate.

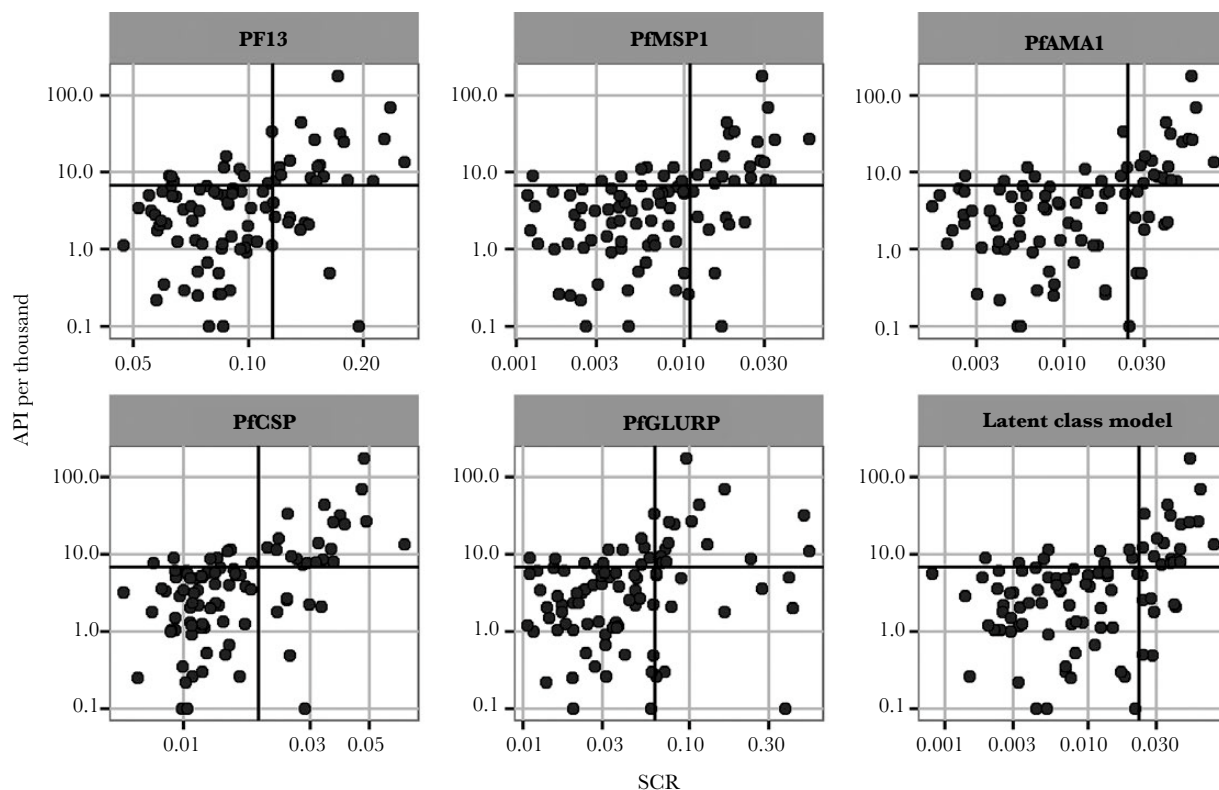
data did not improve prediction of higher-transmission communes ([Supplementary Figure 2](#)).

DISCUSSION

Similar to other settings [25–29], antibody data were much more sensitive and informative than RDT positivity, which was extremely low: only 25 of 93 (27%) communes had any positive RDTs among surveyed participants. Serological data were used in this study as a gold standard for assessing validity of using routine data from the HMIS to target higher-transmission communes for IRS. Previous studies have indicated high

correlations between SCRs and clinical malaria incidence in cohort studies [16], as well as between SCRs and the entomological inoculation rate [14, 30], which has traditionally been the gold standard measure of malaria transmission.

The overall SCR for the study area for the latent antigen of 0.010 translates into roughly 1 seroconversion per 100 population per year. This is low and expected, given the low overall API from HF data in the study area of 3.5 reported cases per 1000 population. However, serological data revealed wide heterogeneity among the communes, where SCRs ranged from 0.001 to 0.075. Our inclusion of several antigens, which might represent



Marker	Sensitivity (95% CI)	Specificity (95% CI)	SCR*	API*
PF13	68 (48–84)	86 (75–93)	0.116	6.77
PfMSP1	71 (51–87)	88 (77–95)	0.011	6.77
PfAMA1	68 (48–84)	86 (75–93)	0.024	6.77
PfCSP	75 (55–89)	89 (79–96)	0.019	6.77
PfGLURP	61 (41–78)	83 (72–91)	0.062	6.77
Latent class model	71 (51–87)	88 (77–95)	0.023	6.77

Figure 4. Sensitivity and specificity of API versus gold standard SCR for detecting 30% highest transmission communes. Horizontal and vertical lines represent API and SCR, respectively, for the top 30% communes. * SCR and API values represent cutoff for top 30% communes. Abbreviations: API, annual parasite incidence; CI, confidence interval; SCR, seroconversion rate.

different exposure histories, has been recommended for maximizing the utility of serology for malaria [30], and latent class analysis has been proposed as an approach to combine results from multiple tests when no gold standard exists [31, 32]. The latent class analysis analyzed the quantitative MFI values from the 5 antigens instead of using the binary classifications from each antigen. Therefore, this approach avoided the loss of information created from a binary classification for each antigen.

In our study area within the low-transmission CHL and Fringes areas, we found that API is relatively good at identifying higher-transmission communes, or hotspots, but sensitivity

of this measure degrades at lower transmission levels, that is when trying to detect a larger percentage of communes as ranked by SCR. It should be noted that these findings are in the context of relatively low levels of public sector HF utilization in Madagascar (only 35.8% of children aged 6–59 months with fever were taken to the public sector for care according to a 2016 survey [20]) and poor data quality in the HMIS [6]. Interestingly, data quality did not appear to modify substantially the relationship between API and SCRs. Few studies have looked at the relationship between API from routine data and seropositivity. One study in a very low-transmission area of

Table 2. Sensitivity, Specificity, and AUC of API Versus SCRs of Various *Plasmodium falciparum* Antigens, at Different Quantiles of the SCR

Percentage of Highest Communes ^a	SCR Threshold ^b	API Threshold ^c	AUC (95% CI)	Sensitivity (95% CI)	Specificity (95% CI)
PF13					
50	0.0903	5.15	72 (62–83)	61 (46–74)	79 (66–89)
40	0.099	6.83	73 (62–84)	57 (41–73)	88 (79–95)
30	0.1157	7.6	77 (65–89)	68 (50–86)	89 (82–95)
20	0.1371	7.6	79 (65–94)	79 (58–95)	85 (77–92)
10	0.162	7.6	76 (52–99)	80 (50–100)	78 (70–87)
PfMSP1					
50	0.0064	5.02	73 (63–84)	65 (52–78)	81 (68–91)
40	0.0083	6.18	75 (63–86)	62 (46–78)	88 (79–95)
30	0.0109	6.83	81 (69–92)	71 (54–86)	88 (80–95)
20	0.0171	7.6	89 (79–98)	84 (68–100)	86 (78–93)
10	0.0249	7.64	93 (87–99)	100 (100–100)	83 (75–90)
PfAMA1					
50	0.0114	5.02	74 (64–84)	65 (52–78)	81 (70–91)
40	0.0167	6.83	76 (65–87)	59 (43–76)	89 (80–96)
30	0.0239	6.83	76 (64–88)	68 (50–86)	86 (77–94)
20	0.0313	7.6	87 (77–96)	84 (68–100)	86 (78–93)
10	0.0427	7.6	93 (87–99)	100 (100–100)	81 (72–89)
PfCSP					
50	0.0133	6.18	77 (68–87)	59 (43–74)	94 (85–100)
40	0.0151	6.18	78 (68–88)	62 (46–78)	88 (79–95)
30	0.0191	6.83	82 (70–93)	75 (57–89)	89 (82–95)
20	0.0262	6.83	83 (71–96)	84 (68–100)	84 (76–92)
10	0.0338	11.52	97 (94–100)	90 (70–100)	95 (90–99)
PfGLURP					
50	0.0371	6.83	71 (60–82)	50 (35–65)	89 (79–98)
40	0.0505	6.83	73 (61–85)	59 (43–76)	89 (80–96)
30	0.0621	7.6	74 (62–87)	61 (43–79)	86 (77–94)
20	0.0723	7.74	76 (62–90)	63 (42–84)	85 (77–93)
10	0.1254	8.51	63 (42–84)	50 (20–80)	81 (72–88)
Pf latent antigen					
50	0.0097	5.02	73 (63–84)	65 (50–78)	81 (68–91)
40	0.0136	6.83	74 (62–85)	59 (43–76)	89 (80–96)
30	0.0227	6.83	81 (70–92)	71 (54–89)	88 (78–95)
20	0.0297	6.83	89 (81–98)	89 (74–100)	85 (77–93)
10	0.0405	7.74	88 (76–100)	90 (70–100)	83 (75–90)

Abbreviations: AUC, area under the curve; API, annual parasite incidence; Pf, *Plasmodium falciparum*; SCR, seroconversion rate.

^aPercentage of highest communes refers to the highest X% of communes by transmission level assessed by SCR (eg, the highest 20% of communes). For each antigen, 46 were above the 50% SCR threshold, 37 above the 40% SCR threshold, 28 above the 30% SCR threshold, 19 above the 20% SCR threshold, and 10 above the 10% threshold, although it should be noted that these communes differ by antigen, which gives different results.

^bSCR threshold is the value that splits the communes such that the number of communes to be identified matches the percentage in the first column.

^cAPI threshold was determined by Youden index (see [Supplementary Material](#)).

South Africa found no significant linear relationship between seroprevalence and historical ward-level malaria incidence [33].

This study had several limitations. We were only able to sample 2 schools (from an average of 14) per commune, thus our use of SCR as the gold standard for transmission intensity in

this study relies on several assumptions, including that school-children and their parents accurately represent commune transmission and that the 2 sampled schools are representative of the commune. Although appropriate for a low-transmission setting, the use of finite mixture models to produce seropositivity cutoffs assumes only 2 underlying components when in reality there could be more than that [34]. Further, our sample included only a handful of children younger than 5 years, who might be most informative for assessing recent transmission. However, lack of data from the youngest age group should in theory have affected only the confidence intervals on the SCRs but not the SCRs themselves [35]. Another potential limitation is that routine data for only the previous year (2013) were used to calculate the API for comparison with the SCR, which might reflect more cumulative exposure than simply the previous year; however, comprehensive routine malaria data were not available before this and some studies have shown that several of the antibodies assessed have very short half-lives in children [36, 37]. Finally, community-level data were not captured during this time period in the routine data system. However, this should not compromise the utility of APIs as a relative measure of transmission intensity if the proportion of cases seen in the community does not vary substantially by commune.

Despite its limitations, this study provides important information on the validity of routine data to characterize relative malaria transmission intensity at subdistrict levels. Reassuringly, despite imperfect routine data, API performed reasonably well for identifying the highest-transmission communes. In many cases, routine data are the most readily-available—and sometimes the *only* available—information that program managers have for stratification efforts. Malaria program managers in Madagascar are increasingly using routine data to assess trends and predict and prevent outbreaks at the facility and commune level, as cases have increased nationwide beginning in 2017. In response to findings from this study, managers have also worked to improve the quality of routine data especially in outbreak-prone, low-transmission areas.

CONCLUSIONS

This study used serological data from multiple *P. falciparum* antibodies to estimate commune-level malaria transmission for identifying the highest-transmission communes, and for evaluating the validity of using routine data to target IRS. In low-transmission settings of Madagascar, API had a sensitivity of slightly above 70% compared to gold standard commune SCRs for identifying the 30% of communes with highest transmission. API performed better at differentiating communes on the higher end of transmission, but its performance declined when trying to target a greater percentage of communes. Factoring in data quality did not appear to change substantially the relationship between API and SCR. Although school-based surveys have the advantage of being relatively rapid and less costly than

household surveys (total cost for this survey was approximately US \$300 000), program managers must weigh their costs against using existing routine data or other less costly measures such as climate and vegetation data, which are increasingly being used to predict malaria transmission.

Supplementary Data

Supplementary materials are available at *The Journal of Infectious Diseases* online. Consisting of data provided by the authors to benefit the reader, the posted materials are not copyedited and are the sole responsibility of the authors, so questions or comments should be addressed to the corresponding author.

Notes

Acknowledgments. We express our gratitude to the population of the districts and communes investigated and especially to the children, parents, guardians, and teachers who participated to the study. We also thank those who facilitated the survey, that is heads of communes and *fokontany*, local administration authorities, and health authorities from Ministry of Health and National Malaria Control Program. We also thank the survey teams.

Disclaimer. The findings and conclusions in this report are those of the authors and do not necessarily represent the views of the Centers for Disease Control and Prevention.

Financial support. This work was supported by the US President's Malaria Initiative program (grant number AID-687-G-13-00003 Surveillance and Data for Management Project).

Potential conflicts of interest. All authors: No reported conflicts of interest. All authors have submitted the ICMJE Form for Disclosure of Potential Conflicts of Interest. Conflicts that the editors consider relevant to the content of the manuscript have been disclosed.

Presented in part: 64th Annual Meeting of the American Society of Tropical Medicine and Hygiene, 25–29 October 2015, Philadelphia, PA.

References

1. World Health Organization (WHO). World malaria report 2017. Geneva, Switzerland: WHO, 2017.
2. World Health Organization (WHO). World malaria report 2018. Geneva, Switzerland: WHO, 2018.
3. Howes RE, Mioramalala SA, Ramiranirina B, et al. Contemporary epidemiological overview of malaria in Madagascar: operational utility of reported routine case data for malaria control planning. *Malar J* 2016; 15:502.
4. Ihantamalala FA, Rakotoarimanana FMJ, Ramiadantsoa T, et al. Spatial and temporal dynamics of malaria in Madagascar. *Malar J* 2018; 17:58.
5. Kang SY, Battle KE, Gibson HS, et al. Spatio-temporal mapping of Madagascar's malaria indicator survey results to assess *Plasmodium falciparum* endemicity trends between 2011 and 2016. *BMC Med* 2018; 16:71.
6. Ly M, N'Gbichi J-M, Lippeveld T, Ye Y. Rapport d'évaluation de la performance du système d'information sanitaire de routine (SISR) et de la surveillance intégrée de la maladie et la riposte (SIMR). Chapel Hill, NC: MEASURE Evaluation, 2016.
7. Mattern C, Pourette D, Raboanary E, et al. "Tazomoka is not a problem". Local perspectives on Malaria, fever case management and bed net use in Madagascar. *PLoS One* 2016; 11:e0151068.
8. Institut National de la Statistique (INSTAT), Programme National de Lutte Contre le Paludisme (PNLP), Institut Pasteur de Madagascar IPM), ICF International. Madagascar. Enquete sur les indicateurs du paludisme 2013. Antananarivo, Madagascar and Calverton, MD: INSTAT, PNL, IPM, ICF International, 2013.
9. World Health Organization (WHO). A framework for malaria elimination. Geneva, Switzerland: WHO, 2017.
10. Bousema T, Drakeley C, Gesase S, et al. Identification of hot spots of malaria transmission for targeted malaria control. *J Infect Dis* 2010; 201:1764–74.
11. Bousema T, Griffin JT, Sauerwein RW, et al. Hitting hotspots: spatial targeting of malaria for control and elimination. *PLoS Med* 2012; 9:e1001165.
12. Lynch CA, Cook J, Nanyunja S, et al. Application of serological tools and spatial analysis to investigate malaria transmission dynamics in highland areas of Southwest Uganda. *Am J Trop Med Hyg* 2016; 94:1251–8.
13. Corran P, Coleman P, Riley E, Drakeley C. Serology: a robust indicator of malaria transmission intensity? *Trends Parasitol* 2007; 23:575–82.
14. Drakeley CJ, Corran PH, Coleman PG, et al. Estimating medium- and long-term trends in malaria transmission by using serological markers of malaria exposure. *Proc Natl Acad Sci U S A* 2005; 102:5108–13.
15. Satoguina J, Walther B, Drakeley C, et al. Comparison of surveillance methods applied to a situation of low malaria prevalence at rural sites in The Gambia and Guinea Bissau. *Malar J* 2009; 8:274.
16. Stewart L, Gosling R, Griffin J, et al. Rapid assessment of malaria transmission using age-specific sero-conversion rates. *PLoS One* 2009; 4:e6083.
17. Gitonga CW, Karanja PN, Kihara J, et al. Implementing school malaria surveys in Kenya: towards a national surveillance system. *Malar J* 2010; 9:306.
18. Brooker S, Kolaczinski JH, Gitonga CW, Noor AM, Snow RW. The use of schools for malaria surveillance and programme evaluation in Africa. *Malar J* 2009; 8:231.
19. Stevenson JC, Stresman GH, Gitonga CW, et al. Reliability of school surveys in estimating geographic variation in malaria transmission in the western Kenyan highlands. *PLoS One* 2013; 8:e77641.

20. Institut National de la Statistique (INSTST), Programme National de Lutte Contre le Paludisme (PNLP), Institut Pasteur de Madagascar (IPM), ICF International. Enquete sur les indicateurs du paludisme a Madagascar 2016. Antananarivo, Madagascar and Rockville, MD: INSTAT, PNL, IPM, ICF International, **2017**.
21. Kerkhof K, Canier L, Kim S, et al. Implementation and application of a multiplex assay to detect malaria-specific antibodies: a promising tool for assessing malaria transmission in Southeast Asian pre-elimination areas. *Malar J* **2015**; 14:338.
22. Perraut R, Richard V, Varela ML, et al. Comparative analysis of IgG responses to *Plasmodium falciparum* MSP1p19 and PF13-DBL1 α 1 using ELISA and a magnetic bead-based duplex assay (MAGPIX[®]-Luminex) in a Senegalese meso-endemic community. *Malar J* **2014**; 13:410.
23. Perraut R, Varela M, Mbengue B, Guillotte M, Mercereau-Puijalon O, Vigan-Womas I. Standardization of a multiplex magnetic bead-based for simultaneous detection of IgG to *Plasmodium* antigens. *J Immunol Tech Infect Dis* **2015**; 4:1–8.
24. Wilson EB. Probable inference, the law of succession, and statistical inference. *J Am Stat Assoc* **1927**; 22:209–12.
25. Kattenberg JH, Erhart A, Truong MH, et al. Characterization of *Plasmodium falciparum* and *Plasmodium vivax* recent exposure in an area of significantly decreased transmission intensity in central Vietnam. *Malar J* **2018**; 17:180.
26. Birhanu Z, Yihdego YY, Yewhalaw D. Quantifying malaria endemicity in Ethiopia through combined application of classical methods and enzyme-linked immunosorbent assay: an initial step for countries with low transmission initiating elimination programme. *Malar J* **2018**; 17:152.
27. Nyunt MH, Soe TN, Shein T, et al. Estimation on local transmission of malaria by serological approach under low transmission setting in Myanmar. *Malar J* **2018**; 17:6.
28. Sáenz FE, Arévalo-Cortés A, Valenzuela G, et al. Malaria epidemiology in low-endemicity areas of the northern coast of Ecuador: high prevalence of asymptomatic infections. *Malar J* **2017**; 16:300.
29. Stevenson JC, Stresman GH, Baidjoe A, et al. Use of different transmission metrics to describe malaria epidemiology in the highlands of western Kenya. *Malar J* **2015**; 14:418.
30. Greenhouse B, Smith DL, Rodríguez-Barraquer I, Mueller I, Drakeley CJ. Taking sharper pictures of malaria with CAMERAs: combined antibodies to measure exposure recency assays. *Am J Trop Med Hyg* **2018**; 99:1120–7.
31. van Smeden M, Naaktgeboren CA, Reitsma JB, Moons KG, de Groot JA. Latent class models in diagnostic studies when there is no reference standard—a systematic review. *Am J Epidemiol* **2014**; 179:423–31.
32. Wiegand RE, Cooley G, Goodhew B, et al. Latent class modeling to compare testing platforms for detection of antibodies against the *Chlamydia trachomatis* antigen Pgp3. *Sci Rep* **2018**; 8:4232.
33. Biggs J, Raman J, Cook J, et al. Serology reveals heterogeneity of *Plasmodium falciparum* transmission in north-eastern South Africa: implications for malaria elimination. *Malar J* **2017**; 16:48.
34. Rogier E, Wiegand R, Moss D, et al. Multiple comparisons analysis of serological data from an area of low *Plasmodium falciparum* transmission. *Malar J* **2015**; 14:436.
35. Sepúlveda N, Drakeley C. Sample size determination for estimating antibody seroconversion rate under stable malaria transmission intensity. *Malar J* **2015**; 14:141.
36. Akpogheneta OJ, Duah NO, Tetteh KK, et al. Duration of naturally acquired antibody responses to blood-stage *Plasmodium falciparum* is age dependent and antigen specific. *Infect Immun* **2008**; 76:1748–55.
37. Kinyanjui SM, Conway DJ, Lanar DE, Marsh K. IgG antibody responses to *Plasmodium falciparum* merozoite antigens in Kenyan children have a short half-life. *Malar J* **2007**; 6:82.

ANNEXE 2

Rakotoarison, H. A., Rasamimalala, M., Rakotondramanga, J. M., Ramiranirina, B., Franchard, T., Kapesa, L., Razafindrakoto, J., Guis, H., Tantely, L. M., Girod, R., Rakotoniaina, S., Baril, L., Piola, P., & Rakotomanana, F. (2020). Remote Sensing and Multi-Criteria Evaluation for Malaria Risk Mapping to Support Indoor Residual Spraying Prioritization in the Central Highlands of Madagascar. *Remote Sensing*, *12*(10), 1585.
<https://doi.org/10.3390/rs12101585>

Article

Remote Sensing and Multi-Criteria Evaluation for Malaria Risk Mapping to Support Indoor Residual Spraying Prioritization in the Central Highlands of Madagascar

Hobiniaina Anthonio Rakotoarison ^{1,2,3,4,*}, **Mampionona Rasamimalala** ¹,
Jean Marius Rakotondramanga ¹, **Brune Ramiranirina** ⁵, **Thierry Franchard** ⁵, **Laurent Kapesa** ⁶,
Jocelyn Razafindrakoto ⁶, **Hélène Guis** ^{1,7,8,9}, **Luciano Michaël Tantely** ¹⁰, **Romain Girod** ¹⁰,
Solofoarisoa Rakotoniaina ⁴, **Laurence Baril** ^{1,11}, **Patrice Piola** ¹² and **Fanjaso Rakotomanana** ¹

- ¹ Epidemiology and Clinical Research Unit, Institut Pasteur de Madagascar, 101 Antananarivo, Madagascar; rasamimalala@gmail.com (M.R.); rjmarius@pasteur.mg (J.M.R.); helene.guis@cirad.fr (H.G.); lbaril@pasteur-kh.org (L.B.); fanja@pasteur.mg (F.R.)
 - ² Centre de coopération Internationale en Recherche Agronomique pour le Développement (CIRAD), Unité Mixte de Recherche Territoires, Environnement, Télédétection et Information Spatiale (UMR TETIS), 34398 Montpellier, France
 - ³ Unité Mixte de Recherche Territoires, Environnement, Télédétection et Information Spatiale (UMR TETIS), Université de Montpellier, Institut des sciences et industries du vivant et de l'environnement (AgroParisTech), Centre de coopération Internationale en Recherche Agronomique pour le Développement (CIRAD), Centre National de la Recherche Scientifique (CNRS), Institut national de recherche pour l'agriculture, l'alimentation et l'environnement (INRAE), F-34090 Montpellier, France
 - ⁴ Laboratoire de Géophysique de l'Environnement et Télédétection (LGET), Institut et Observatoire de Géophysique d'Antananarivo (IOGA), Université d'Antananarivo, 101 Antananarivo, Madagascar; solofoarisoa@gmail.com
 - ⁵ National Malaria Control Program (NMCP), Ministry of Public Health, 101 Antananarivo, Madagascar; brune.estelle2@gmail.com (B.R.); franchtee@gmail.com (T.F.)
 - ⁶ United States Agency for International Development (USAID) Madagascar/President Malaria Initiative (PMI), Health Population and Nutrition Office (HPN), 101 Antananarivo, Madagascar; lkapesa@usaid.gov (L.K.); jrazafindrakoto@usaid.gov (J.R.)
 - ⁷ Centre de coopération Internationale en Recherche Agronomique pour le Développement (CIRAD), Unité Mixte de Recherche Animal, Santé, Territoires, Risques et Ecosystèmes (UMR ASTRE), 101 Antananarivo, Madagascar
 - ⁸ Centre de coopération Internationale en Recherche Agronomique pour le Développement (CIRAD), Institut national de recherche pour l'agriculture, l'alimentation et l'environnement (INRAE), Université de Montpellier, Unité Mixte de Recherche Animal, Santé, Territoires, Risques et Ecosystèmes (UMR ASTRE), F-34090 Montpellier, France
 - ⁹ Foibem-pirenena momba ny Fikarohana ampiarina amin'ny Fampanandrosoana ny eny Ambanivohitra—Département de Recherche Zootechnique, Vétérinaire et Piscicole (FOFIFA-DRZVP), 101 Antananarivo, Madagascar
 - ¹⁰ Medical Entomology Unit, Institut Pasteur de Madagascar, 101 Antananarivo, Madagascar; lucinambi@pasteur.mg (L.M.T.); rgirod@pasteur.mg (R.G.)
 - ¹¹ Institut Pasteur du Cambodge, 99 Phnom Penh, Cambodia
 - ¹² Epidemiology and Public Health Unit, Institut Pasteur du Cambodge, 99 Phnom Penh, Cambodia; ppiola@pasteur-kh.org
- * Correspondence: a.rakotoarison@gmail.com; Tel.: +261-34-33-792-59

Received: 30 March 2020; Accepted: 13 May 2020; Published: 16 May 2020

Abstract: The National Malaria Control Program (NMCP) in Madagascar classifies Malagasy districts into two malaria situations: districts in the pre-elimination phase and districts in the control phase. Indoor residual spraying (IRS) is identified as the main intervention means to control malaria in the Central Highlands. However, it involves an important logistical mobilization and thus necessitates prioritization of interventions according to the magnitude of malaria risks. Our objectives were to map the malaria transmission risk and to develop a tool to support the Malagasy Ministry of Public Health (MoH) for selective IRS implementation. For the 2014–2016 period, different sources of remotely sensed data were used to update land cover information and substitute in situ climatic data. Spatial modeling was performed based on multi-criteria evaluation (MCE) to assess malaria risk. Models were mainly based on environment and climate. Three annual malaria risk maps were obtained for 2014, 2015, and 2016. Annual parasite incidence data were used to validate the results. In 2016, the validation of the model using a receiver operating characteristic (ROC) curve showed an accuracy of 0.736; 95% CI [0.669–0.803]. A free plugin for QGIS software was made available for NMCP decision makers to prioritize areas for IRS. An annual update of the model provides the basic information for decision making before each IRS campaign. In Madagascar and beyond, the availability of the free plugin for open-source software facilitates the transfer to the MoH and allows further application to other problems and contexts.

Keywords: remote sensing; spatial modeling; multi-criteria evaluation; malaria; Madagascar

1. Introduction

Malaria is an infectious disease transmitted by female *Anopheles* mosquitoes. It remains a major global public health concern. In 2018, worldwide malaria cases were estimated at about 228 million, 93% of which were reported in the African Region [1]. The Roll Back Malaria (RBM) partnership has defined a global framework to end malaria [2].

As the fourth-highest cause of both morbidity in health centers and mortality in hospitals, malaria remains a public health issue in Madagascar. Until 2013, the confirmed number of simple cases of malaria in health facilities annually represented 6.5% of all outpatient consultations. This proportion was 5.6% in 2016 [3]. In Madagascar, the prevalence varied greatly according to the epidemiological facies of malaria: from 1% in the Central Highlands (CHL), to 5% in the sub-desert facies, and to 9% in the Tropical and Equatorial facies, where transmission is high and perennial [4]. Unlike eastern and western coastal areas of Madagascar, the CHL are characterized by seasonal and unstable malaria transmission. Historically, malaria in the CHL of Madagascar has been marked by deadly epidemics. During the last major epidemic in the CHL, in 1988, malaria caused an estimated 25,000 deaths [5]. Human in-country mobility is increasing between high malaria transmission and low transmission areas. A sentinel network of fever surveillance shows the persistence of malaria transmission in stable areas [6].

In high malaria prevalence areas, the main malaria control measures implemented by the Malagasy National Malaria Control Program (NMCP) are the use of insecticide-treated nets (ITN) and ProActive Community Treatment (Pro-ACT). In areas of low malaria prevalence, as in the CHL, control differs and relies essentially on indoor residual spraying (IRS) [7,8]. Global funds and other institutions, such as the President Malaria Initiative (PMI)/USAID help to fight malaria in high burden countries [9]. The NMCP benefits from those financial supports [10]. In 2015, the Malagasy Ministry of Public Health (MoH) declared that six out of 31 districts in the CHL are in the pre-elimination phase. These districts are those with a rapid diagnostic test (RDT) positivity rate under 5% in the general population [4]. It becomes crucial to consolidate these achievements and to extend new areas towards the pre-elimination phase.

For Madagascar, the implementation of IRS implies a heavy logistical mobilization and an adapted financial support mostly depending on external funding. To control the malaria epidemic in the central highlands in the late 1980s, five years of full insecticide campaign coverage were

implemented. Annual programs of indoor residual spraying of DDT were carried out between December 1993 and January 1998 in most rural areas at altitudes of 1000–1500 m. This strategy helped to stop this deadly epidemic [11,12]. Since 1999, rotational and selective interventions were carried out [12,13] based on the incidence of malaria observed during the year preceding the transmission season. Some IRSs have been carried out in response to epidemics. For IRS campaigns in the CHL, the NMCP advocates an alternation of two years of total coverage and two years of selective IRS. This strategy aims to reduce IRS coverage and instead enhance selective interventions. In a context of limited resources, optimizing malaria control targets becomes essential for countries like Madagascar. Given that allocated resources will not cover costs for total coverage of IRS, the aim is to prioritize areas with the highest malaria transmission risk.

Several methods have been used to map malaria risk. GIS-based spatial modeling techniques were adopted by Rincón-Romero and Londoño for malaria risk mapping in Columbia and by Ferrao et al. in Mozambique [14,15]. Others promote spatial statistical approaches to map malaria risk. For example, Kleinschmidt et al. combined a logistic regression model and geostatistical analysis to produce a malaria risk map in Mali [16]. Yankson et al. used model-based geostatistical methods to map malaria risk in children under five in Ghana [17]. Hanaf-Bojd et al., Wondim et al., and Ali and Ahmad used the multi-criteria evaluation (MCE) method to map malaria risk in the South of Iran, Ethiopia, and West Bengal, respectively [18–20].

As for most, if not all, vectors, environmental and climatic factors play a critical role in the *Anopheles* life cycle and in the maintenance of malaria transmission. The environmental temperature impacts the internal temperature of mosquitoes [21]. The environmental conditions also considerably impact breeding sites. Wetlands, for example, are crucial for the development of the larvae of *Anopheles* [22,23]. The changes of environment and climate can also induce changes in vector behavior [24,25].

To overcome the lack of entomological data on malaria vector distribution at the scale of the country, a suitable habitat for *Anopheles* can be characterized by using an environmental proxy [26–29]. The malaria patterns depend on location and availability of breeding sites that can be recovered using spatial information [30,31].

Several risk factors of malaria have been identified in the literature, mainly through a statistical modeling approach [32,33]. Environment and climate data, such as distance from water bodies, temperature, elevation, drainage density, rainfall, and land use/land cover, are widely used because they are closely linked to malaria and its vectors. Other methods, such as the use of MCE, can be developed when epidemiological and/or entomological data are too scarce to develop statistical models [34–36].

MCE is a common method for assessing and aggregating many criteria [34,37–39]. In order to form a single index of evaluation and to provide necessary information for decision makers, MCE basically consists of combining information from several criteria. It is considered a semi-quantitative method using a participative approach where stakeholders bring their knowledge and expertise [40].

The combination of the geographical information system (GIS) approach and MCE began in the 1990s, with full integration by Eastman [41]. This combination is widely used as a decision support tool [34,42,43]. In Madagascar, where field malaria data is limited, Rakotomanana et al. used an MCE approach to evaluate malaria risk in six zones of the CHL [22]. Their study is based on environmental factors such as temperature, elevation, and rice fields as model input data. Landsat 7, Spot 4, and radar images were used to map rice fields. Yet, inhabited areas, which represent the vulnerable population, and precipitation were not taken into consideration. Furthermore, as the method can only be carried out by GIS specialists, the map has not been updated since 2007.

The main objective of this study is to map malaria risk in all CHL communes, taking into account the vulnerable population, and then validate the results by comparing them to epidemiological data. A second objective is to develop a “user-friendly” tool, enabling regular updating of risk maps, to support Malagasy MoH for selective IRS implementation.

2. Materials and Methods

2.1. Study Area

The CHL are located in the central plateau of Madagascar. They encompass 97,000 km² and include 31 districts (Figure 1), representing 27% of the country's districts. The west side presents a smooth slope, whereas the east presents an abrupt slope towards the coastal regions. The altitude of the CHL ranges from 200 to 2700 m. The average annual temperature is 20 °C and the climate is subdivided into two seasons: rainy season (October to May) and dry season (June to September). In the CHL, the average annual precipitation is between 800 and 1500 mm. The CHL have the highest human density in Madagascar. Almost half of Malagasy people live in the CHL. In 2014, the population in the CHL was estimated at 9,200,000 inhabitants, with an annual growth rate of 2.8%. More than 80% of Malagasy people live in rural areas. The main activities of the population are agriculture and livestock farming. Rice is the main food and rice fields are highly abundant in Madagascar, especially in the CHL.

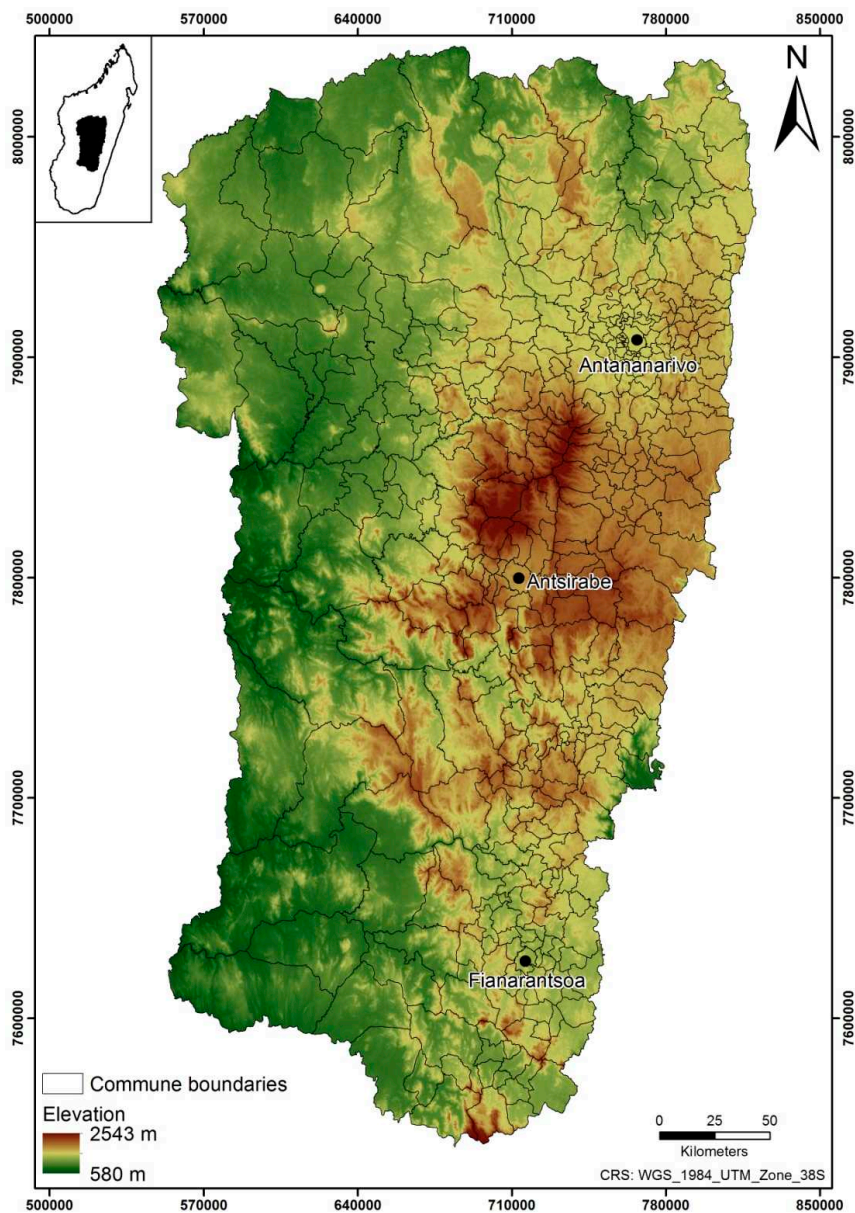


Figure 1. Central highlands (CHL) of Madagascar.

2.2. Land Cover Update

A total of 18 images from the Landsat 8 sensor, with 30 m spatial resolution, were used to update the land cover map from 2014 to 2016. Images were downloaded from the United States Geological Survey (USGS) earth explorer website (<https://earthexplorer.usgs.gov/>). The object-based image analysis (OBIA) classification approach was used. Unlike the standard per pixel approach, the OBIA approach does not treat the pixels one by one, but in context by grouping pixels within objects based on their spectral value, size, shape, and context [44]. Firstly, an object segmentation of images was performed in order to group all pixels having the same radiometric characteristics. Then, the segmented images were classified into nine classes through a membership rule-based method where each segment attribute had conditions to respect. Specifically, each land cover class was classified according to pre-defined rules. The implementation of these rules was based on thresholds (Table 1).

Table 1. Classification parameters for land cover.

Classes	Parameters
Rice field	GLCM contrast ≤ 70 ; LWM ≤ 75 ; Mean layer ≤ 85
Water body	NDWI > 0.37 ; Sum of reflectance ($\Sigma (b_2, b_3, b_4)$) < 204
Hydrographic network	Brightness > 65 ; LWM < 56 ; NDVI < 0
Wet cultivation	$-0.15 < \text{NDVI} < -0.01$
Other	Everything that is not assigned to the above four classes

Note: GLCM (Gray Level Co-Occurrence Matrix), LWM (Land and Water Masks) = $b_5 / (b_3 + 0.0001) \times 100$, NDVI (Normalized Difference Vegetation Index), b_2 : blue band, b_3 : green band, b_4 : red band, b_5 = near infrared band (Spectral band).

As *Anopheles* breed in various areas, four land cover classes were identified as areas for mosquito development that were considered potential breeding sites: rice field, water body, hydrographic network, wet cultivation [45].

A post-classification phase was performed to assess the accuracy of the classification results. The ground truth data were obtained from field missions in five districts of the CHL during rainy season. Three confusion matrices were generated in order to represent the misclassification, as well as classification accuracy for 2014, 2015, and 2016. Cohen's Kappa index was calculated for each confusion matrix to test for the concordance of the classification.

2.3. Spatial Multi Criteria Evaluation

Three yearly malaria risk models were established following the workflow shown in Figure 2 using six criteria involved in malaria risk.

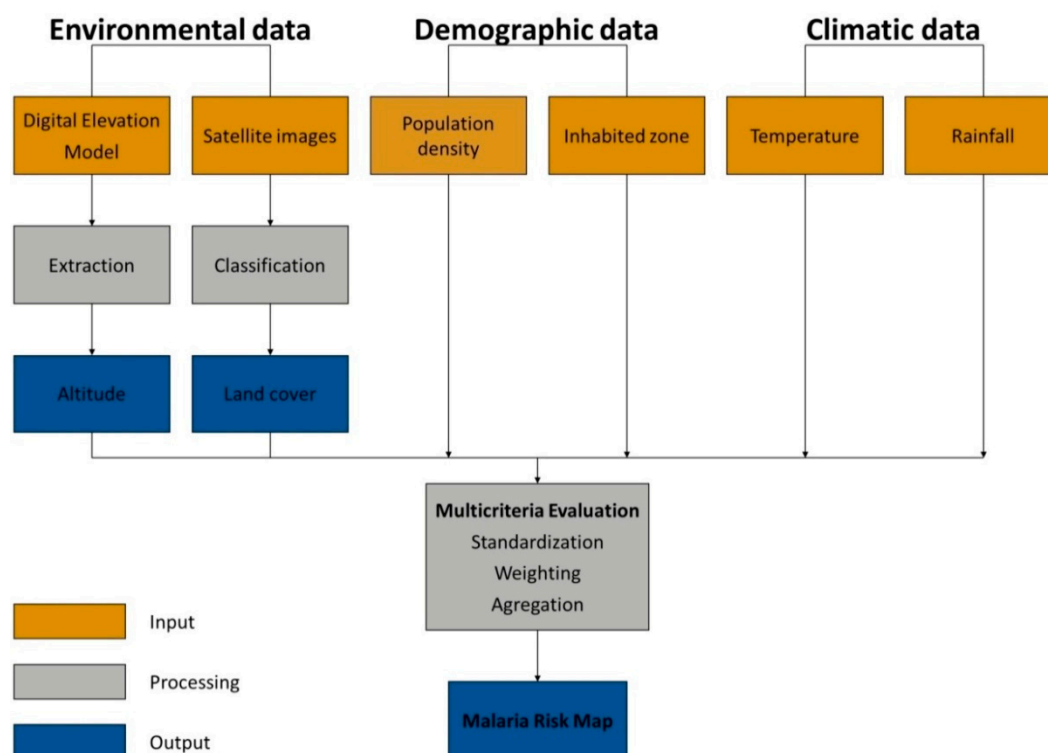


Figure 2. Workflow of the adopted spatial multi-criteria evaluation (MCE) process.

2.3.1. Criteria Identification and Differentiation

The choice of the criteria was based on a literature review and seven expert opinions (epidemiologists, entomologist, a doctor, geomaticians, and a modeler).

Inhabited zone: Malaria only occurs in inhabited areas as humans are the only reservoir of malaria. Village locations, in vector format (point type), were extracted from the database of the Malagasy Cartographic Institute named “Foiben-Taosarintanin’i Madagasikara” (FTM) in 2000. In order to obtain updated village locations, these were combined with data gathered from OpenStreetMap (<https://www.openstreetmap.org/>) and data obtained from 2013 to 2016 field missions. A 1 km buffer, representing inhabited areas, was created from the previously combined data and then rasterized to a 30 m spatial resolution.

Population density: The last national population census campaigns took place in 1993 and 2018, but data from the latter is not yet accessible. Given the lack of updated data, the population density was extracted from the WorldPop project database (www.worldpop.org.uk). WorldPop is an open-access library providing population data with a spatial resolution of 100 m. The 2010 population density was used for the 2014 model, while data of 2015 were used for 2015 and 2016 models. Since data with better resolution do not exist at the present time, a resampling to 30 m was performed.

Elevation: Elevation is important in malaria risk assessment because it is directly related to temperature, and impacts the life cycle of the mosquito vectors [46–48] and the development of *Plasmodium* species, which are the parasites responsible for malaria disease. Elevation data were obtained from digital terrain models provided by the Shuttle Radar Topography Mission (SRTM) campaign held in 2000. The SRTM data for CHL, with a spatial resolution of 30 m, was downloaded from the USGS Earth explorer website (<https://earthexplorer.usgs.gov/>). Two tile sets of SRTM images (SRTM_46_16 and SRTM_46_17) were used to cover all CHL.

Temperature: Temperature influences mosquito development and longevity [49,50]. The hot and rainy season lasts from October to May in Madagascar. During this period, the population densities of *Anopheles* and malaria cases are high. Mean temperatures for this timeframe, from 2014 to 2016, were computed. The USGS, through the International Research Institute (IRI) library

(<http://iridl.ldeo.columbia.edu/>), provides temperature data every eight days with a spatial resolution of 1 km. This source platform allowed extracting a 30 m spatial resolution through its expert mode tool.

Precipitation: Rainfall influences the availability of mosquito breeding sites; it may predict vector abundance [51,52]. Rain increases the chance of larval habitat availability; however, excessive rainfall can cause leaching of larval breeding sites. Daily precipitation with a spatial resolution of 12 km data was obtained from the IRI website (<http://iridl.ldeo.columbia.edu/>) provided by the United States National Oceanic and Atmospheric Administration (US NOAA) agency. These were GeoTIFF raster images, in which values are expressed in millimeters of rain. Using the same expert mode feature as for temperature, a resolution of 30 m was extracted. Total precipitation during the October to May period was calculated for each studied year by adding daily values during the eight months.

Distance to wetland: Extracted from the updated land cover for 2014 to 2016, at a resolution of 30 m, distance to wetland was used as an environmental determinant of malaria transmission risk. Agricultural parcels, standing water, and streams are considered as potential mosquito breeding sites [53]. A maximum distance of 5 km from wetlands was formed to take into consideration mosquito blood meal seeking and resting areas [54]. It was considered that the malaria risk decreased progressively as distance increased within the buffer.

2.3.2. Factor Standardization

Criteria were categorized and divided into constraints and factors. Constraints are defined as masks that consider whether a zone will be part of the calculation [22]. The process uses a Boolean function by classifying the criteria into suitable or not suitable areas (Table 2). Eastman described factors as criteria that define a certain degree of aptitude for all regions [55]. In this study, factors are expressed by continuous values and act in a progressive way on the aptitude following fuzzy logic functions (Table 3).

Table 2. Constraint descriptions and parameters.

Criteria	Description
Inhabited zone	BF: recoded to 1 for inhabited areas that are potentially at risk, and to 0 for uninhabited area that are not at risk
Elevation	BF: recoded to 0 for elevation <1000 m (permanent risk) and >1500 m (no risk); recoded to 1 for elevation between 1000 m and 1500 m
Population density	BF: recoded to 1 in areas with $d < 800$ pop/km ² and to 0 in areas with $d \geq 800$ pop/km ²

Note: BF (Boolean function), d (Population Density).

Table 3. Threshold for the fuzzy logic function used in the spatial MCE models.

Criteria	Function	Control Points			
		a	b	c	d
Population density	Decreasing sigmoid	-	-	$400 \leq d < 800$	$d \geq 800$
Elevation	Increasing sigmoid	500	1500	-	-
Distance to wetland	Decreasing sigmoid	-	-	1000	5000
Precipitation	Symmetric sigmoid	0	80	1000	2000
Temperature	Symmetric sigmoid	18	28	32	35

Note: d is in population per km². Elevation and distance to wetland are in meters (m). Precipitation is in millimeters (mm). Temperature is in degrees Celsius (°C).

Each factor was integrated into a GIS and mapped. Factors were quantitative variables (e.g., temperature, elevation) and measured in various units (e.g., degrees Celsius, meters). Standardization was performed to bring the factors on a continuous scale of aptitude, ranging from least aptitude (0) to most aptitude (255). Standardization enables the comparison and combination of

factors for each pixel in the study area. The fuzzy logic functions were used to represent the transition between the totally unsuitable and the fully suitable to better represent real life settings [56]. Here, factors were defined using sigmoid membership functions (increasing, decreasing, or symmetrical). Functions and parameters are presented in Table 3.

2.3.3. Factor Weighting

The second step of the MCE consisted in weighting factors, i.e., assigning weights to each standardized factor according to their degree of relevance. To determine the weight of each factor, an analytical hierarchy process (AHP) was implemented [57]. This method consists of a pair-wise comparison of the factors [22,57]. Weights assigned to each factor are determined by experts' contribution using Saaty's continuous rating scale [57]. Experts were asked to compare factors two by two and to determine their importance. As per this scale, factors were rated as: 9 for extremely more important, 7 for very highly more important, 5 for highly more important, 3 for moderately more important or 1 for equally important than the second factor. Inversely, less important factors were assigned a score of: 1/3 for moderately less important, 1/5 for much less important, 1/7 for very much less important or 1/9 for extremely less important. This procedure generates a table of the pair-wise comparison of all factors. In this table, the sum of the weights of all factors equals 1. The pair-wise comparison used in this study is detailed in Supplementary File (Table S1). The consistency of the comparison is then assessed by computing the consistency ratio (CR). This corresponds to the probability that ratings were randomly generated. The consistency of the rating is considered acceptable when $CR < 0.1$ [58].

2.3.4. Criteria Aggregation

A weighted linear combination (WLC) aggregation of criteria was the last step of the MCE. It consisted of multiplying the weights from the weighting of each standardized factor and then summing them. To exclude unsuitable areas, i.e., areas where there was no risk of malaria, this sum was multiplied with Boolean constraints. The aggregation of criteria per Equation (1) resulted in a gradient risk map of malaria, per pixel of 30 m.

$$S = \sum_{i=1}^n w_i X_i \prod_{j=1}^m C_j, \quad (1)$$

where S is the aptitude for an event, W_i is the weight of factor i , X_i is the factor i , C_j it the constraint j , n is the number of factors, and m is the number of constraints.

Malaria risk models were constructed for the years 2014, 2015, and 2016.

As the NMCP uses communes as the scale for IRS intervention in Madagascar, risk gradient per pixel was therefore aggregated by commune.

Aggregation of pixel risk values at commune level was carried out following three steps. Firstly, to determine the probability distribution of gradients per pixel, using the maximum likelihood method, six candidate distributions (normal, log-normal, geometric, gamma, Poisson, and Weibull) were tested in 100 randomly selected communes. Secondly, outlier values were detected according to the respective distribution selected per commune and corrected with the confidence interval of the crude mean to derive an adjusted mean. Finally, the optimal class number to perform the Jenks natural breaks algorithm of commune-level risk gradients was determined through the Gaussian mixture model [59,60].

2.3.5. Validation of the Model Framework

Model output was compared to data on Annual Parasite Incidence (API) provided by the NMCP. These data record the incidence rate of malaria per commune and per year. API validation data was only available for 208 communes and for 2015.

The area under the curve (AUC) of the receiver operating characteristic (ROC) curve was used to assess the model performance. The perfect model shows a value of 1.0 in the ROC curve [61]. We used the 2015 API data to validate the output of the model for the 2016 IRS campaign. The 2015 API

in each commune, corresponding to observed values, was recoded as a binary variable to compute the AUC ROC: API <1‰ was considered as low incidence and API ≥1‰ as high incidence. Sensitivity and specificity were computed using the best cut-off of the classified malaria risk map (Figure 4).

2.4. Uncertainty Analyses

Uncertainty analyses were performed to verify the stability of the model. Indeed, the parameters used in the development of the model mainly depended on the choice of experts, as well as on the literature. These analyses consisted of varying the weights of the various standardized factors of the model, and checking the impact of these variations on the standard deviation of model output. Ten variations of the initial weights corresponding to 10 different expert choices (test at ±5%, ±10%, ±15%, ±20%, and ±25%) were simulated. The adjusted weights were calculated using Equation (2):

$$w_i = (1 - w_m) * \frac{w_{i0}}{1 - w_{m0}}, 1 \leq i \leq n, i \neq m, \quad (2)$$

where w_{i0} and w_{m0} are, respectively, the weights of the i th risk factor and, in the base model, of the main changing risk [62–64].

2.5. Plugin Development

In order to provide a dynamic, simple, and free decision support tool for the NMCP, an extension of the QGIS 2.x software, called “MCE for Public Health”, was developed. The Python programming language was used because it is the most suitable language for QGIS. To make the tool more efficient, all calculations were performed with the application programming interface and Geospatial Data Abstraction Library (GDAL) of QGIS. Qt Designer Software was used to design the graphical user interface (GUI) [65]. It was designed to be ergonomic, easy to use, and to prevent user typing errors [65].

2.6. Change Detection

In order to evaluate the density of change in the different zone surfaces (with a 30 m step), in terms of area at risk, a change detection process was carried out. It was applied to the 2014, 2015, and 2016 spatial models. According to Singh, change detection can be defined as a process identifying state changes of an object and/or phenomenon on different dates [66]. For this study, image differencing was adopted. It consists of evaluating the difference, pixel by pixel, between two images at different dates. This method is thoroughly explained by Singh [66]. The risk gradient, per class, was calculated in order to appreciate the tendency of each risk class from one year to another. Through this method, zones subjected to changes had different statistics than those that had not changed. A risk gradient with a declining surface shows negative pixel values, while gradients that have an increased surface have positive values.

3. Results

3.1. Land Cover Updating

The application of the OBIA classification method, through the membership rules, allowed classifying the land cover in the CHL. The classification showed that the rice fields and wet cultivation classes represented 17% in 2014, 27% in 2015, and 11% in 2016. The water body and hydrographic networks classes covered 6%, 6%, and 5%, respectively, in 2014, 2015, and 2016. The remainder is covered by the “other” class, which includes bare soils, built-up areas, and clouds.

Based on the strength of agreement established by Landis and Kock, the results of the land cover classifications for 2014, 2015, and 2016 were statistically satisfactory (Table 4) [67].

Table 4. Cohen’s Kappa index for 2014, 2015, and 2016 land cover classifications.

	Kappa Index
Land cover classification (2014)	0.7741
Land cover classification (2015)	0.7438
Land cover classification (2016)	0.8320

3.2. Malaria Risk Model

According to their respective experiences, experts working on the malaria program parameters in relation to the transmission of malaria attributed the weights of each standardized factor (Table 5). The CR for the pair-wise comparison matrix (Table S1) showed a value of 0.06, which indicates that the conducted comparison was consistent. Population density was considered to be the most important factor in malaria risk, followed in decreasing order of importance by distance from wetlands, temperature, the altitude, and precipitation.

Table 5. Factor weights.

Factors	Weights
Population density	0.4990
Distance to wetland	0.1824
Temperature	0.1698
Elevation	0.0910
Precipitation	0.0577

The MCE, through the application of the WLC, allowed having a malaria risk map with a gradient ranging from 0 to 255 for each pixel of 30 m spatial resolution. Areas with a value of 0 had the lowest risk, while areas with a suitability of 255 had the highest risk. Figure 3 presents the different maps of malaria transmission risk for 2014, 2015, and 2016, with a 30 m pixel scale. Figure 4 shows the 2016 spatial model map, adjusted to the commune scale. Three distributions were found to best fit the commune-level risk (Weibull, log-normal, and normal). According to the adjusted mean and available malaria incidence data for validation, three optimal classes were selected to categorize the risk values. CHL presented 60%, 32%, and 8% of communes with high (rating of 3), moderate (rating of 2), and low malaria (rating of 1) risk, respectively. The central and eastern parts of the CHL were dominated by communes at a high risk of malaria. Communes with low risk were located on the western side of the CHL and the other communes had a moderate malaria risk.

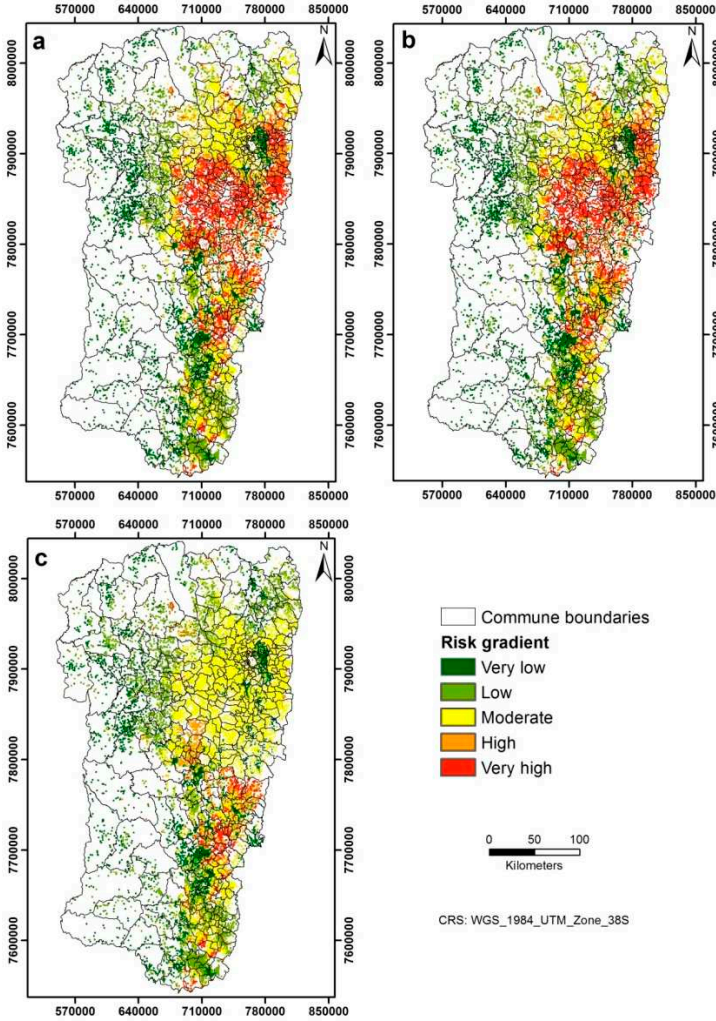


Figure 3. Suitability maps for Malaria. (a) 2014; (b) 2015; and (c) 2016.

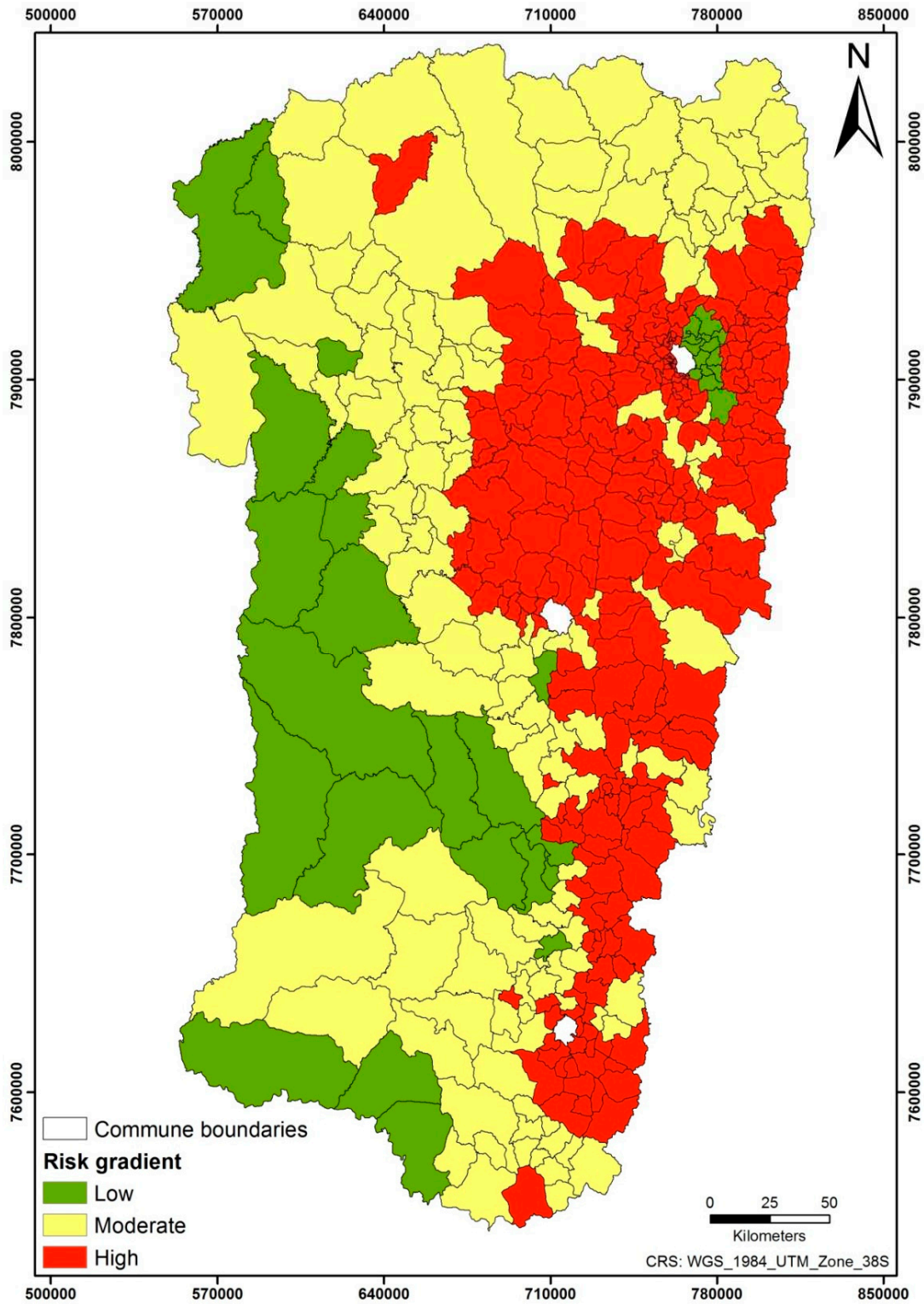


Figure 4. Suitability map in 2016 adjusted to a commune scale.

Giving the lack of API validation data, only the malaria risk model of 2016 was validated. Validation showed an acceptable fitting with an AUC of 0.736 (95% confidence intervals (CI): [0.669–0.803]) (Figure 5) [68]. Table 6 shows the results of ROC analysis. Using a rating of 2 as a threshold, a sensitivity of 0.91 (11 positive cases were missed) and a specificity of 0.43 (49 negative cases labeled as high risk) were obtained. By applying this cut-off, 91% of the communes were identified as high risk by the model.

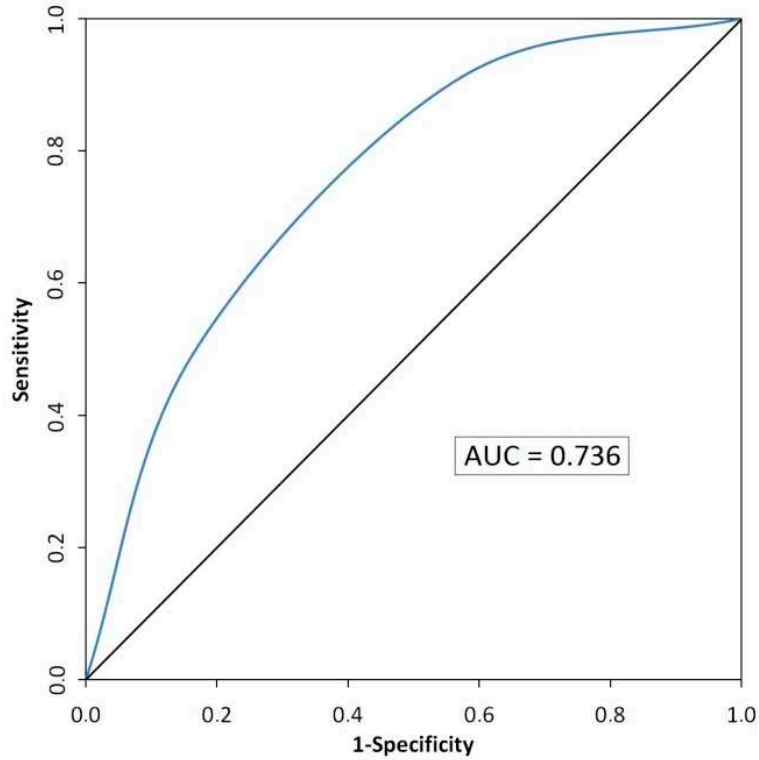


Figure 5. Receiver operating characteristic (ROC) curve of the malaria risk model. Blue line and black diagonal line represent the ROC of the model and the random ROC, respectively.

Table 6. Results of ROC analysis.

2016 Model Output	2015 Annual Parasite Incidence	
	High	Low
High	TP: 111	FP: 49
Low	FN: 11	TN: 37
Accuracy: 0.712		
Sensitivity: 0.910		
Specificity: 0.430		

Note: TP (True Positive), TN (True Negative), FP (False Positive), FN (False Negative), Accuracy = $(TN + TP)/(TN + TP + FN + FP)$, Sensitivity = $TP/(TP + FN)$, Specificity = $TN/(TN + FP)$.

3.3. Uncertainty Analysis

The CHL uncertainty map (Figure 6) showed that the maximum value of standard deviation was significantly below 0.1, indicating a robust model [63,64]. Calculated standard deviations revealed values around the mean, demonstrating that the risk model of malaria remains stable even when the weights assigned to each standardized factor are changed by the stakeholders.

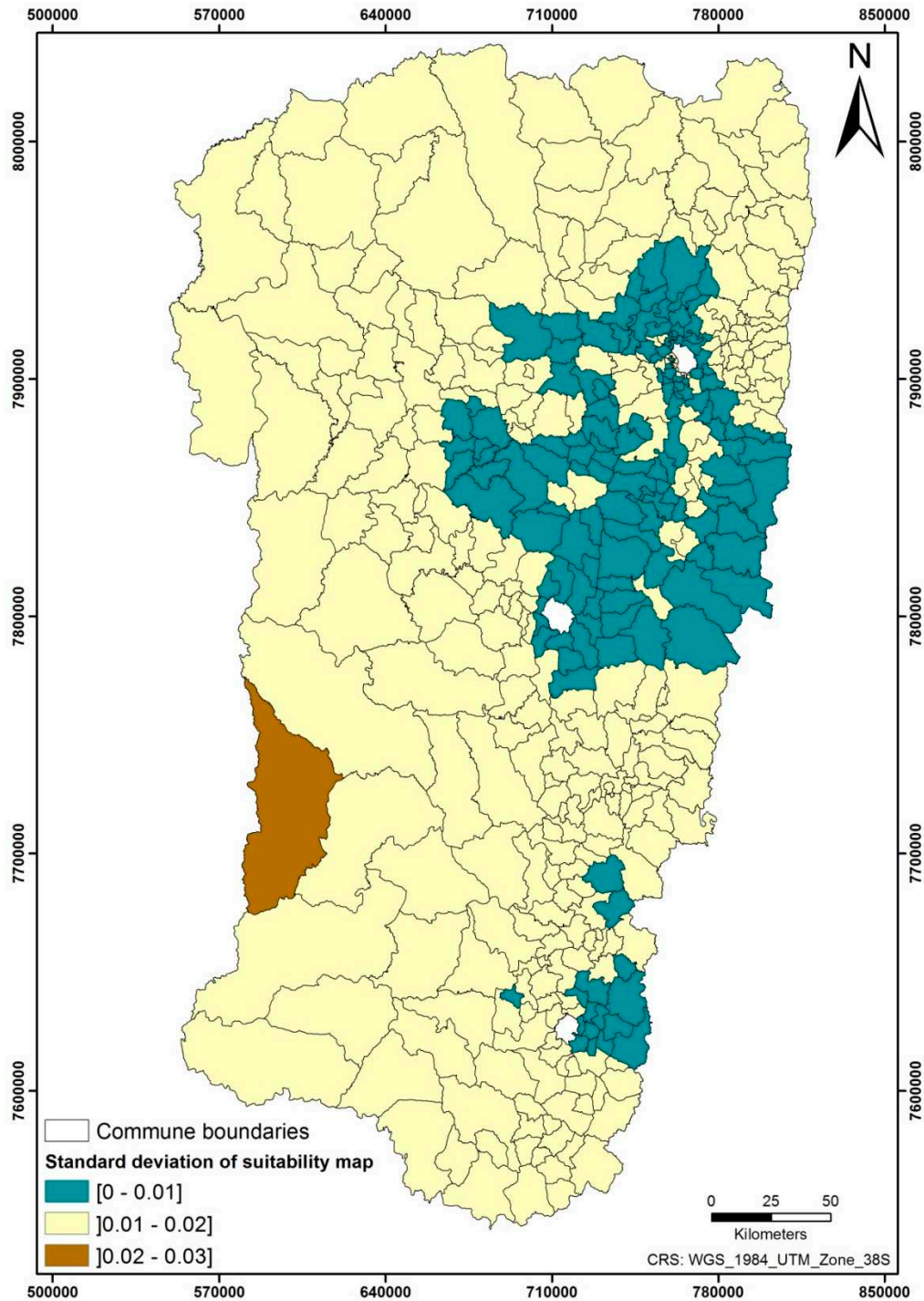


Figure 6. Uncertainty map.

3.4. "MCE for Public Health" Plugin

The plugin is an interactive tool, adapted for the QGIS 2.x version: a dynamic, free, and open source semi-automatic tool. It groups the main steps for MCE evaluation: reclassification of constraints, normalization, computing weight for each factor using a pair-wise comparison matrix, and aggregation of factors. The plugin runs for a maximum of 10 constraints and 15 factors. It can support four raster formats of input and output data: rst (idrisi format), gtiff (GeoTIFF format), img (erdas imagine format), and jpeg. The Full MCE plugin file is available on GitHub (<https://github.com/SaGEOTeam/FullMCE>). The plugin is presented both in French and English. Figure 7 shows the main interface of the developed plugin.

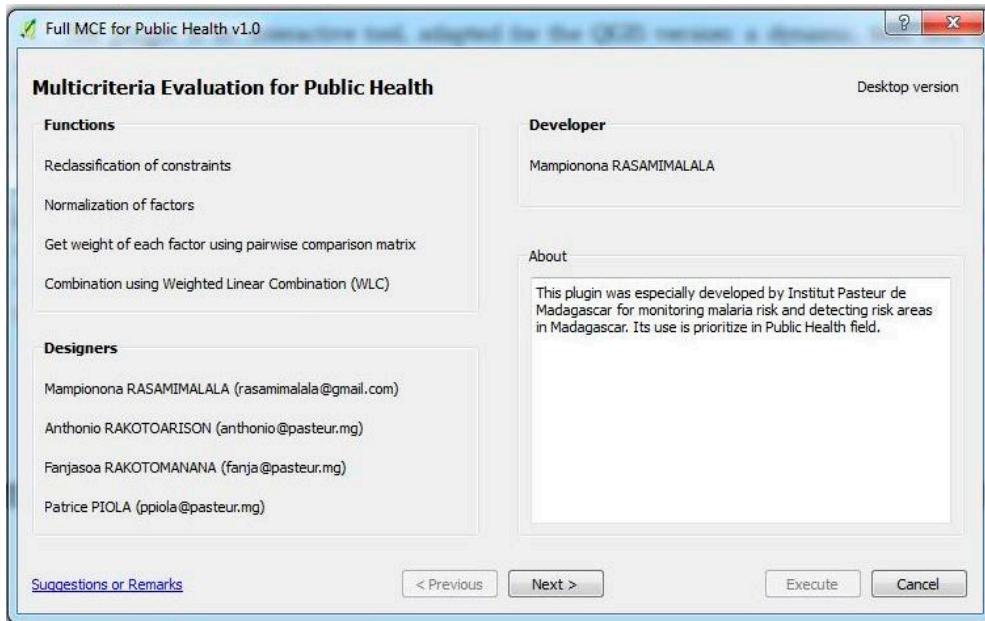


Figure 7. Interface of the developed multi-criteria evaluation (MCE) plugin.

3.5. Change Detection on Models

Two change detections of malaria risk were carried out to determine if the risk category had changed. The results of the image differencing technique, for 2015–2014 and 2016–2015, were two images with pixel coded in three categories: increase in risk, no change, and decrease in risk (Figure 8).

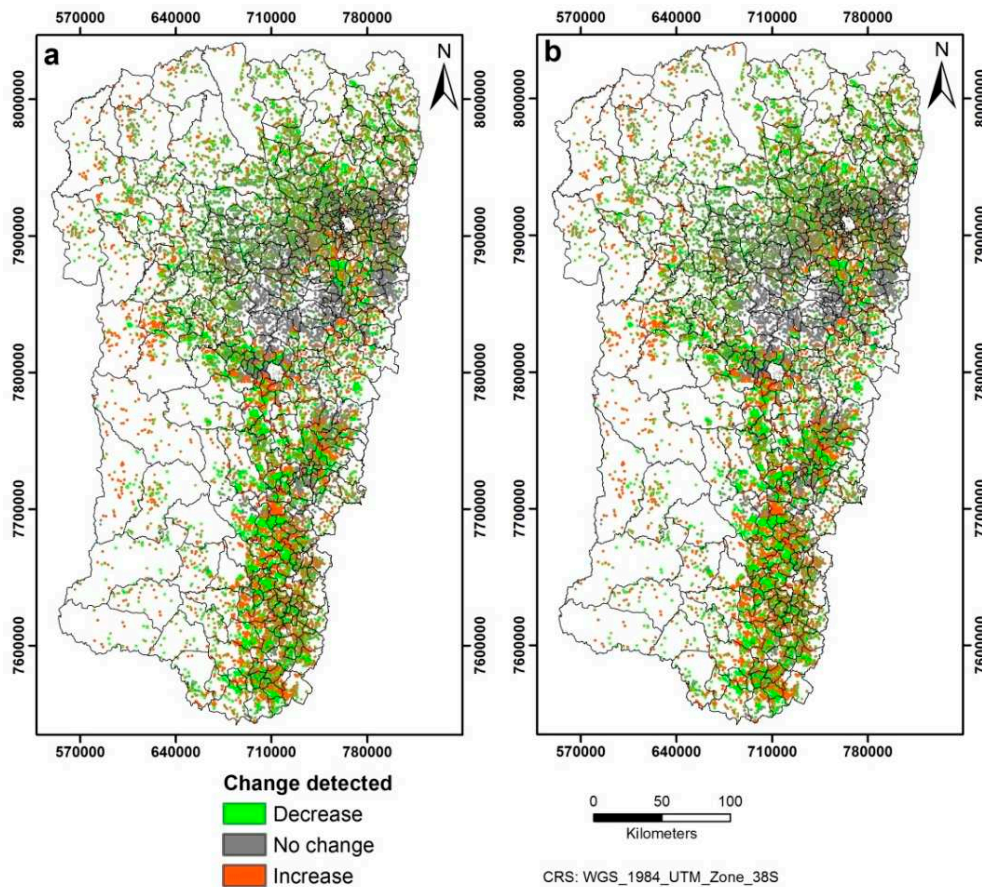


Figure 8. Change detection of suitability models. (a) 2015–2014, (b) 2016–2015.

Based on the three risk models, at pixel scale, Table 7 shows the changes on the risk surface of 2015–2014 and those of 2016–2015. Between 2014 and 2015, 64% of the surfaces in the study area were subject to risk change where 35% affected the transition to a higher risk than in 2014. Between 2015 and 2016, 89% of the surface changed risk with 61% surfaces subject to a decrease in risk. The models have not changed significantly between 2014 and 2015. From 2015 to 2016, the drastic decrease in rainfall and wetland during the malaria transmission season led to a decrease of the high-risk class of the model and a subsequent increase of the moderate class.

Table 7. Surface affected by changes resulting from the image differencing method.

	Surface 2015–2014 (km ²)	Surface 2016–2015 (km ²)
decrease	12,198.96	21,435.32
no change	12,334.38	3883.71
increase	10,086.82	9301.13
Total	34,620.16	34,620.16

4. Discussion

The MCE method had previously been carried out in six areas of the Malagasy CHL [22]. Here, the model is improved by including all areas of the CHL and by taking into account rainfall and population distribution. The comparison of available API data with the risk model enabled an assessment of the accuracy of MCE in this study. Validation of the malaria risk model showed a good result. For the first time, to our knowledge, the development of the “Full MCE” plugin enables non-specialists, such as staff of the Malagasy NMCP, to carry out a complete MCE approach with a free spatial decision tool. This initiative allowed the use of a single software platform to perform all the MCE treatments. In April 2019, NMCP and other stakeholders (Ministry of Public Health, Ministry of Agriculture, universities and research institutes) from 10 countries were trained to use the plugin and the tool was distributed to them. An update with the latest version 3.x of QGIS is currently in progress to allow a wider diffusion.

The availability of Landsat 8 images allowed updating the Malagasy CHL land cover map with a medium spatial resolution of 30 m. The previous land cover map had dated from 2009. Although the OBIA approach is better suited for images at a high spatial resolution, it is also currently used for images with medium spatial resolution such as Landsat images [69,70]. At the scale of the present study (i.e., commune scale), the results obtained from the Landsat 8 images seem appropriate.

The MCE approach is a knowledge-based and pragmatic method adapted to situations in which there is a lack of data. This method is rapid and easy to implement [36]. It is an alternative to a statistical method requiring large datasets and is adaptable and/or transposable to different areas [36] with particular aspects of malaria transmission. AHP is a method which is very commonly used [22,63,64,71] to weigh factors in MCE. It greatly facilitates the work assigned to experts as (i) pair-wise comparisons are easier to carry out for experts than simultaneous comparison of all factors, and (ii) it is simpler to compare factors using qualitative ordinal variables (“extremely more important than”, etc.) rather than defining precise weights. AHP also has the advantage of enabling an easy assessment of the ratings consistency through the CR.

Most studies on spatial modeling of malaria transmission risk [22,72] do not take into account the human reservoir aspect in the models. Previously, only population density was used, while this variable supports all pixels across the entire study area, even uninhabited areas. The notion of reservoir is however important in terms of risk of disease and particularly in public health [73,74]. The particularity of the present model is that it takes into account only the areas where the population is present, which represent a potential human reservoir.

GIS-based decision support was recently used to target IRS control programs in Zambia [75,76]. Chanda et al. used epidemiological and entomological data to determine areas that needed interventions [75]. In Madagascar, the geographical extent coupled with the issue of being landlocked make routine surveillance and data collection system difficult. Despite efforts from the

NMCP stakeholders, complete and up-to-date data are usually not available before elaborating the annual IRS target. The present model shows that MCE approaches overcome these difficulties.

However, the present study has some limitations that need to be mentioned. Data collection on climate and demography was difficult in Madagascar, whether free or paid. Indeed, the number of meteorological stations is not sufficient for national use, and their interpolation may have a direct impact on the result. The scarcity of meteorological stations imposed us to use remotely sensed substitute data. The IRI for Climate and Society provided a solution to this issue by integrating climate and environmental data from various sources [77]. Forecast climate data was previously used to predict malaria risks in the African region [28,77,78]. Dambach et al. confirmed the role of land surface temperature and rainfall in mosquito density [79].

Datasets used to compute malaria risk were not always available at similar scales. Population data was only available with a spatial scale of 100 m. Lack of access to high spatial resolution data is frequent in low income countries and considerably hinders the quality of produced risk maps. Furthermore, using datasets with different spatial resolutions is clearly not ideal, and it is recommended to downgrade the resolution of all datasets to the lowest spatial resolution. Here, we took the risk to resample datasets to 30 m but finally produced an operational risk map at the commune level (i.e., with a much coarser resolution than the one used for the datasets). The latest general population censuses in Madagascar were conducted in 1993 and in 2018 but results of the latter are not yet available. When the 2018 Malagasy population census data is released, updated population density maps with finer resolution will be produced and should considerably improve incidence and prevalence estimates, as well as risk maps produced in Madagascar (including the malaria maps derived from this work).

The available API data, required for model validation, did not cover the entire study area. Only about half of the study area had complete data covering the period of malaria transmission. This lack of API data could significantly impact the accuracy of the model validation.

In our study, malaria control data, such as recent IRS campaigns, were not taken into account. It can be hypothesized that they impacted malaria transmission data (API) and thus model validation. Since these intervention data influence malaria suitability, they can easily be considered in future malaria risk model constructions.

Despite these limitations, the tool synthesizes current knowledge on malaria transmission in the Malagasy CHL. Based on the available data, it provided information that was useful to decision makers. An improved version of the map could be made if better data and knowledge were available.

From the perspective of spatial modeling of malaria risk in other regions, particularly in coastal areas, it would be interesting to produce a risk map at the national level. Madagascar is currently divided into five malaria transmission strata (CHL, fringes, East, West, and desert south) [80,81]. These strata represent endemic areas (coasts) and low transmission areas (CHL and fringes). These areas differ according to their transmission intensity, ecozone, and vectors [80]. The development of a model for the other epidemiological facies might require using different variables or different weights. These variables and parameters need to be determined by experts.

This study focuses on mapping malaria risk in CHL, an area with low transmission. Population movement flow is an important factor impacting malaria risk because malaria risk increases in areas receiving people from high transmission zones [81]. In 2017, Girond et al. developed an early warning system. It used new technologies for early detection and forecasting of malaria based on a Malagasy sentinel surveillance system [82]. This early warning system combined with our spatial model would allow a more accurate mapping of malaria risk and better predictions of epidemics.

5. Conclusions

Malaria transmission is limited by environmental and climatic criteria because they directly affect the life cycle of *Anopheles* and the *Plasmodium* they transmit. GIS combined with MCE, through their capacity for storage, data management, analysis, modeling, and mapping of spatially referenced data, is a useful tool to apprehend spatial decision issues [83]. This combination has

improved the understanding of areas at risk of malaria. The resulting risk map is used for decision making to target priority communes to focus IRS campaigns in Madagascar. The “Full MCE for Public Health” tool, which is dynamic, fast, and easy to use, should be easily appropriated by decision makers to prioritize IRS, and its flexibility makes it easy to use in other contexts: for other diseases and for other countries, to simulate various scenarios. It will be useful to a much wider community of stakeholders involved in risk assessment, especially in areas where data is lacking.

Supplementary Materials: The following are available online at www.mdpi.com/2072-4292/12/10/1585/s1, Table S1: Pair-wise comparison matrix of the standardized factors associated with malaria risk.

Author Contributions: Conceptualization: H.A.R., F.R., and P.P.; Methodology: H.A.R., F.R., M.R., J.M.R., T.F., and B.R.; Software: H.A.R. and M.R.; Validation: H.A.R., M.R., and J.M.R.; Formal analysis: H.A.R., M.R., J.M.R., and F.R.; Investigation: H.A.R., M.R., J.M.R., and F.R.; Resources: T.F. and B.R.; Data curation: H.A.R., M.R., and J.M.R.; Writing—original draft: H.A.R., M.R., J.M.R., and F.R.; Writing—review and editing: H.A.R., M.R., J.M.R., B.R., T.F., L.K., J.R., H.G., L.M.T., R.G., S.R., L.B., P.P., and F.R.; Supervision: F.R., H.G., S.R., P.P., and L.B.; Project administration: F.R., P.P., and L.B.; Funding acquisition: F.R. and P.P. All authors have read and agreed to the published version of the manuscript.

Funding: This research was funded by the United States Agency for International Development (USAID), grant number AID-687-G-13-00003. APC was funded by ANISETTE, a project supported by the French Space Agency, CNES (DAR 4800001029).

Acknowledgments: The authors would like to thank Annelise Tran from Cirad for comments and reviewing the manuscript.

Conflicts of Interest: The authors declare no conflicts of interest.

References

1. World Health Organization. *World Malaria Report 2019*; World Health Organization: Geneva, Switzerland, 2019.
2. Roll Back Malaria. *RBM Partnership Strategic Plan 2018–2020*; RBM partnership to end malaria: Geneva, Switzerland, 2018.
3. Direction de Lutte contre le Paludisme. *Plan Stratégique National de lutte contre le paludisme 2018-2022*; Direction de Lutte contre le Paludisme: Antananarivo, Madagascar, 2017.
4. INSTAT. *Enquête sur les indicateurs du Paludisme à Madagascar—Rapport Final 2016*; INSTAT: Calverton, MD, USA, 2017.
5. Mouchet, J.; Baudon, D. *Rapport de Mission d’expertise sur le Paludisme à Madagascar (Région des Hauts Plateaux)*; Ministère de la Coopération et du Développement : Paris, France, 1988.
6. Randrianasolo, L.; Raolina, Y.; Ratsitorahina, M.; Ravolomanana, L.; Andriamandimby, S.; Heraud, J.; Rakotomanana, F.; Ramanjato, R.; Randrianarivo-Solofoniaina, A.E.; Richard, V. Sentinel surveillance system for early outbreak detection in Madagascar. *BMC Public Health* **2010**, *10*, doi:10.1186/1471-2458-10-31.
7. Rabarijaona, L.P.; Rabe, T.; Ranaivo, L.H.; Raharimalala, L.A.; Rakotomanana, F.; Rakotondraibe, E.M.; Ramarosandratana, B.; Rakotoson, J.D.; Rakotonjanabelo, L.A.; Tafangy, P.B. Paludisme sur les Hautes Terres Centrales de Madagascar: Stratégies de lutte. *Méd. Trop.* **2006**, *66*, 504–512.
8. Ratovonjato, J.; Randrianarivojosia, M.; Rakotondrainibe, M.E.; Raharimanga, V.; Andrianaivolambo, L.; Le Goff, G.; Rogier, C.; Ariey, F.; Boyer, S.; Robert, V. Entomological and parasitological impacts of indoor residual spraying with DDT, alphacypermethrin and deltamethrin in the western foothill area of Madagascar. *Malar. J.* **2014**, *13*, doi:10.1186/1475-2875-13-21.
9. The Global Fund. *The Global Fund 2016 Annual Financial Report*; The Global Fund: Geneva, Switzerland, 2017.
10. PMI. *Malaria Operational Plan FY 2018*; PMI: Washington, WA, USA, 2018.
11. Jambou, R.; Ranaivo, L.; Raharimalala, L.; Randrianarivo, J.; Rakotomanana, F.; Modiano, D.; Pietra, V.; Boisier, P.; Rabarijaona, L.; Rabe, T.; et al. Malaria in the highlands of Madagascar after five years of indoor house spraying of DDT. *Trans. R. Soc. Trop. Med. Hyg.* **2001**, *95*, 14–18, doi:10.1016/s0035-9203(01)90317-7.

12. Robert, V.; Le Goff, G.; Andrianaivolambo, L.; Randimby, F.M.; Domarle, O.; Randrianariveolosia, M.; Raharimanga, V.; Raveloson, A.; Ravaonjanahary, C.; Arie, F. Moderate transmission but high prevalence of malaria in Madagascar. *Int. J. for Parasitol.* **2006**, *36*, 1273–1281, doi:10.1016/j.ijpara.2006.06.005.
13. Nepomichene, T.; Tata, E.; Boyer, S. Malaria case in Madagascar, probable implication of a new vector, *Anopheles coustani*. *Malar. J.* **2015**, *14*, 475, doi:10.1186/s12936-015-1004-9.
14. Rincón-Romero, M.E.; Londoño, J.E. Mapping malaria risk using environmental and anthropic variables. *Rev. Bras. Epidemiol.* **2009**, *12*, 338–354, doi:10.1590/S1415-790X2009000300005.
15. Ferrao, J.L.; Niquisse, S.; Mendes, J.M.; Painho, M. Mapping and Modelling Malaria Risk Areas Using Climate, Socio-Demographic and Clinical Variables in Chimoio, Mozambique. *Int. J. Environ. Res. Public Health* **2018**, *15*, 795, doi:10.3390/ijerph15040795.
16. Kleinschmidt, I.; Bagayoko, M.; Clarke, G.P.Y.; Craig Le Sueur, D. A spatial statistical approach to malaria mapping. *Int. J. Epidemiol.* **2000**, *29*, 355–361, doi:10.1093/ije/29.2.355.
17. Yankson, R.; Anto, E.A.; Chipeta, M.G. Geostatistical analysis and mapping of malaria risk in children under 5 using point-referenced prevalence data in Ghana. *Malar. J.* **2019**, *18*, 67, doi:10.1186/s12936-019-2709-y.
18. Hanaf-Bojd, A.A.; Vatandoost, H.; Oshaghi, M.A.; Charrahy, Z.; Haghdoost, A.A.; Zamani, G.; Abedi, F.; Sedaghat, M.M.; Soltani, M.; Shahi, M.; et al. Spatial analysis and mapping of malaria risk in an endemic area, south of Iran: A GIS based decision making for planning of control. *Acta Trop.* **2012**, *122*, 132–137; doi:10.1016/j.actatropica.2012.01.003.
19. Wondim, Y.K.; Alemayehu, E.B.; Abebe, W.B. Malaria Hazard and Risk Mapping Using GIS Based Spatial Multicriteria Evaluation Technique (SMCET) in Tekeze Basin Development Corridor, Amhara Region, Ethiopia. *J. Environ. Earth Sci.* **2017**, *7*, 5.
20. Ali, S.K.A.; Ahmad, A. Mapping of mosquito-borne diseases in Kolkata Municipal Corporation using GIS and AHP based decision making approach. *Spat. Inf. Res.* **2019**, *27*, 351–372, doi:10.1007/s41324-019-00242-8.
21. Reinhold, J.M.; Lazzari, C.R.; Lahondère, C. Effects of the Environmental Temperature on *Aedes aegypti* and *Aedes albopictus* Mosquitoes: A Review. *Insects* **2018**, *9*, 158, doi:10.3390/insects9040158.
22. Rakotomanana, F.; Rendremanana, R.V.; Rabarijaona, L.P.; Duchemin, J.B.; Ratovonjato, J.; Arie, F.; Rudant, J.P.; Jeanne, I. Determining areas that require indoor insecticide spraying using Multi Criteria Evaluation, a decision-support tool for malaria vector control programmes in the Central Highlands of Madagascar. *Int. J. Health Geogr.* **2007**, *6*, doi:10.1186/1476-072X-6-2.
23. Zahouli, J.B.Z.; Koudou, B.G.; Müller, P.; Malone, D.; Tano, Y.; Utzinger, J. Effect of land-use changes on the abundance, distribution, and host-seeking behavior of *Aedes arbovirus* vectors in oil palm-dominated landscapes, southeastern Côte d'Ivoire. *PLoS ONE* **2017**, *12*, e0189082, doi:10.1371/journal.pone.0189082.
24. Gimonneau, G.; Bouyer, J.; Morand, S.; Besansky, N.J.; Diabate, A.; Simard, F. A behavioral mechanism underlying ecological divergence in the malaria mosquito *Anopheles gambiae*. *Behav. Ecol.* **2010**, *21*, 1087–1092, doi:10.1093/beheco/arq114.
25. Paaajmans, K.P.; Thomas, M.B. The influence of mosquito resting behaviour and associated microclimate for malaria risk. *Malar. J.* **2011**, *10*, doi:10.1186/1475-2875-10-183.
26. Tran, A.; Ponçon, N.; Toty, C.; Linard, C.; Guis, H.; Ferré, J.B.; Lo Seen, D.; Roger, F.; de la Rocque, S.; Fontenille, D.; et al. Using remote sensing to map larval and adult populations of *Anopheles hyrcanus* (Diptera: Culicidae) a potential malaria vector in Southern France. *Int. J. Health Geogr.* **2008**, *7*, 9; doi:10.1186/1476-072X-7-9.
27. Machault, V.; Vignolles, C.; Borchi, F.; Vounatsou, P.; Pages, F.; Briolant, S.; Lacaux, J.P.; Rogier, C. The use of remotely sensed environmental data in the study of malaria. *Geospat. Health* **2011**, *5*, 151–168, doi:10.4081/gh.2011.167.
28. Machault, V.; Vignolles, C.; Pagès, F.; Gadiaga, L.; Tourre, Y.M.; Gaye, A.; Sokhna, C.; Trape, J.-F.; Lacaux, J.-P.; Rogier, C. Risk mapping of *Anopheles gambiae* s.l. densities using remotely-sensed environmental and meteorological data in an urban area: Dakar, Senegal. *PLoS ONE*. **2012**, *7*, doi:10.1371/journal.pone.0050674.
29. Tokarz, R.; Novak, R.J. Spatial-temporal distribution of *Anopheles* larval habitats in Uganda using GIS/remote sensing technologies. *Malar. J.* **2018**, *17*, 420, doi:10.1186/s12936-018-2567-z.

30. Booman, M.; Durrheim, D.N.; La Grange, K.; Martin, C.; Mabuza, A.M.; Zitha, A.; Mbokazi, F.M.; Fraser, C.; Sharp, B.L. Using a geographical information system to plan a malaria control programme in South Africa. *Bull. World Health Organ.* **2000**, *78*, 1438–1444.
31. Carter, R.; Mendis, K.N.; Roberts, D. Spatial targeting of interventions against malaria. *Bull. World Health Organ.* **2000**, *78*, 1401–1411.
32. Samadoulougou, S.; Maheu-Giroux, M.; Kirakoya-Samadoulougou, F.; De Keukeleire, M.; Castro, M.C.; Robert, A. Multilevel and geo-statistical modeling of malaria risk in children of Burkina Faso. *Parasites Vectors* **2014**, *7*, 350, doi:10.1186/1756-3305-7-350.
33. Millar, J.; Psychas, P.; Abuaku, B.; Ahorlu, C.; Amratia, P.; Koram, K.; Oppong, S.; Valle, D. Detecting local risk factors for residual malaria in northern Ghana using Bayesian model averaging. *Malar. J.* **2018**, *17*, 343, doi:10.1186/s12936-018-2491-2.
34. Hongoh, V.; Hoen, A.G.; Aenishaenslin, C.; Waub, J.-P.; Bélanger, D.; Michel, P. The Lyme-MCDA Consortium. Spatially explicit multi-criteria decision analysis for managing vector-borne diseases. *Int. J. Health Geogr.* **2011**, *10*, 70, doi:10.1186/1476-072X-10-70.
35. Chevalier, V.; Trevenec, C.; Gély, M.; Pinto, J.; Tran, A. Spatial multi-criteria evaluation: A promising methodology for identifying areas at risk of Rift Valley fever. *EMPRES-Anim. Health* **2014**, *360*, 14–16.
36. Tran, A.; Roger, F. Strengthening health decision-making at the territorial level: Operational support for spatial multi-criteria evaluation. *CIRAD Montp. Perspect.* **2018**, *46*, 1–4, doi:10.19182/agritrop/00022.
37. Chandio, I.A.; Matori, A.N.B.; Yusof, K.B.W.; Talpur, M.A.H. Validation of Multi-Criteria Decision Analysis model of land suitability analysis for sustainable hillside development. *Eur. J. Sci. Res.* **2013**, *109*, 342–349.
38. Cinelli, M.; Coles, S.R.; Kirwan, K. Analysis of the potentials of multi criteria decision analysis methods to conduct sustainability assessment. *Ecol. Indic.* **2014**, *46*, 138–148, doi:10.1016/j.ecolind.2014.06.011.
39. Dehe, B.; Bamford, D. Development, test and comparison of two Multiple Criteria Decision Analysis (MCDA) models: A case of healthcare infrastructure location. *Expert Syst. Appl.* **2015**, *42*, 6717–6727, doi:10.1016/j.eswa.2015.04.059.
40. Thiery, Y.; Malet, J.-P.; Maquaire, O. Test of fuzzy logic rules for landslide susceptibility assessment. In Proceedings of the International Conference on Spatial Analysis and Geomatics, Strasbourg, France, 11–13 September 2006.
41. Eastman, J.R.; Jin, W.; Kyem, P.A.K.; Toledano, J. Raster procedures for multi-criteria/multi-objective decisions. *Photogramm. Eng. Remote Sens.* **1995**, *61*, 539–547.
42. Malczewski, J. GIS-based multicriteria decision analysis: A survey of the literature. *Int. J. Geogr. Inf. Sci.* **2006**, *20*, 703–726, doi:10.1080/13658810600661508.
43. Pechanec, V.; Machar, I. Implementation of decision support tools in ArcGIS and IDRISI and their environmental applications. *Int. J. Circuits Syst. Signal Process.* **2014**, *8*, 388–398.
44. Benz, U.C.; Hofmann, P.; Willhauck, G.; Lingenfelder, I.; Heynen, M. Multi-resolution, object-oriented fuzzy analysis of remote sensing data for GIS-ready information. *ISPRS J. Photogramm. Remote Sens.* **2004**, *58*, 239–258, doi:10.1016/j.isprsjprs.2003.10.002.
45. Carnevale, P.; Robert, V. *Les anopheles Biologie, transmission du Plasmodium et lutte antivectorielle*; IRD: Marseille, France, 2009.
46. Afrane, Y.A.; Githeko, A.; Yan, G. The ecology of *Anopheles* mosquitoes under climate change: Cases studies from the effects of environmental changes in East Africa highlands. *Ann. N.Y. Acad. Sci.* **2012**, *1249*, 204–210, doi:10.1111/j.1749-6632.2011.06432.x.
47. Beck-johnson, L.M.; Nelson, W.A.; Paaijmans, K.P.; Read, A.F.; Thomas, M.B.; Bjørnstad, O.N. The effect of temperature on *Anopheles* mosquito population dynamics and the potential for malaria transmission. *PLoS ONE* **2013**, *8*, doi:10.1371/journal.pone.0079276.
48. Ewing, D.A.; Cobbold, C.A.; Purse, B.V.; Nunn, M.A.; White, S.M. Modelling the effect of temperature on the seasonal population dynamics of temperate mosquitoes. *J. Theor. Biol.* **2016**, *400*, 65–79, doi:10.1016/j.jtbi.2016.04.008.
49. Depinay, J.O.; Mbogo, C.M.; Killeen, G.; Knols, B.; Beier, J.; Carlson, J.; Dushoff, J.; Billingsley, P.; Mwambi, H.; Githure, J.; et al. A simulation model of African *Anopheles* ecology and population dynamics for the analysis of malaria transmission. *Malar. J.* **2004**, *3*, doi:10.1186/1475-2875-3-29.

50. Paaijmans, K.P.; Imbahale, S.S.; Thomas, M.B.; Takken, W. Relevant microclimate for determining the development rate of malaria mosquitoes and possible implications of climate change. *Malar. J.* **2010**, *9*, 196, doi:10.1186/1475-2875-9-196.
51. Galardo, A.K.R.; Zimmerman, R.H.; Lounibos, L.P.; Young, L.J.; Galardo, C.D.; Arruda, M.; D'Almeida Couto, A.A.R. Seasonal abundance of anopheline mosquitoes and their association with rainfall and malaria along the Matapi River, Amap, Brazil. *Med. Vet. Entomol.* **2009**, *23*, 335–349, doi:10.1111/j.1365-2915.2009.00839.x.
52. Kelly-hope, L.A.; Hemingway, J.; Mckenzie, F.E. Environmental factors associated with the malaria vectors *Anopheles gambiae* and *Anopheles funestus* in Kenya. *Malar. J.* **2009**, *8*, 1–8, doi:10.1186/1475-2875-8-268.
53. Ravoniharimelina, B.; Romi, R.; Sabatinelli, G. Etude longitudinale sur les gîtes larvaires d'*Anopheles gambiae* s. l. dans un canton de la province d'Antananarivo (Hautes Terres Centrales de Madagascar). *Ann. Parasitol. Hum. Comp.* **1992**, *67*, 26–30, doi:10.1051/parasite/199267126.
54. Kaufmann, C.; Briegel, H. Flight performance of the malaria vectors *Anopheles gambiae* and *Anopheles atroparvus*. *J. Vector Ecol.* **2004**, *29*, 140–153.
55. Eastman, J.R. Multi-criteria evaluation and GIS. In *Geographical Information Systems*; John Wiley and Sons: Hoboken, NJ, USA, 1999; pp. 493–502, ISBN 978-0-470-87002-0.
56. Jensen, J.R. *Introductory Digital Image Processing*; Prentice Hall: Upper Saddle River, NJ, USA, 2005; ISBN 0131453610.
57. Saaty, T.L. A scaling method for priorities in hierarchical structures. *J. Math. Psychol.* **1977**, *15*, 234–281, doi:10.1016/0022-2496(77)90033-5.
58. Saaty, T.L. How to make a decision: The Analytic Hierarchy Process. *Eur. J. Oper. Res.* **1990**, *48*, 9–26, doi:10.1016/0377-2217(90)90057-I.
59. Arlinghaus, S.L.; Kerski, J.J. *Spatial Mathematics: Theory and Practice through Mapping*; Taylor & Francis Group: Boca Raton, FL, USA, 2014.
60. Scrucca, L.; Fop, M.; Murphy, T.B.; Raftery, A.E. mclust 5: Clustering, Classification and Density Estimation Using Gaussian Finite Mixture Models. *R J.* **2016**, *8*, 289, doi:10.32614/RJ-2016-021.
61. Nandi, A.; Shakoor, A. A GIS-based landslide susceptibility evaluation using bivariate and multivariate statistical analyses. *Eng. Geol.* **2009**, *110*, 11–20, doi:10.1016/j.enggeo.2009.10.001.
62. Ligmann-zielinska, A.; Jankowski, P. Spatially-explicit integrated uncertainty and sensitivity analysis of criteria weights in multicriteria land suitability evaluation. *Environ. Model. Softw.* **2014**, *57*, 235–247, doi:10.1016/j.envsoft.2014.03.007.
63. Paul, M.C.; Goutard, F.L.; Roulleau, F.; Holl, D.; Thanapongtharm, W.; Roger, F.L.; Tran, A. Quantitative assessment of a spatial multicriteria model for highly pathogenic avian influenza H5N1 in Thailand, and application in Cambodia. *Sci. Rep.* **2016**, *6*, doi:10.1038/srep31096.
64. Tran, A.; Trevennec, C.; Lutwama, J.; Sserugga, J.; Gély, M.; Pittiglio, C.; Pinto, J.; Chevalier, V. Development and assessment of a geographic knowledge-based model for mapping suitable areas for rift valley fever transmission in Eastern Africa. *PLoS Negl. Trop. Dis.* **2016**, *10*, e0004999, doi:10.1371/journal.pntd.0004999.
65. Summerfield, M. *Rapid GUI Programming with Python and Qt*, 1st ed.; Prentice Hall: Upper Saddle River, NJ, USA, 2007; ISBN 0-13-235418-9.
66. Singh, A. Digital change detection techniques using remotely-sensed data. *Int. J. Remote Sens.* **1989**, *10*, 989–1003, doi:10.1080/01431168908903939.
67. Landis, J.R.; Koch, G.G. The Measurement of Observer Agreement for Categorical Data. *Biometrics* **1977**, *33*, 159–174, doi:10.2307/2529310.
68. Hosmer, D.W.; Lemeshow, S. *Applied Logistic Regression*, 2nd ed.; Chapter 5; John Wiley and Sons: New York, NY, USA, 2000; pp. 160–164; ISBN 0471356328.
69. Kindu, M.; Schneider, T.; Teketay, D.; Knoke, T. Land Use/Land Cover change analysis using object-based classification approach in Munessa-Shashemene landscape of the Ethiopian Highlands. *Remote Sens.* **2013**, *5*, 2411–2435, doi:10.3390/rs5052411.
70. Phiri, D.; Morgenroth, J. Developments in Landsat land cover classification methods: A review. *Remote Sens.* **2017**, *9*, 796, doi:10.3390/rs9090967.

71. Bhatt, B.; Joshi, J. Analytical hierarchy process modeling for malaria risk zones in Vadodara district, Gujarat. *Int. Arch. Photogramm. Remote Sens. Spat. Inf. Sci.* **2014**, *XL-8*, 171–176, doi:10.5194/isprsarchives-XL-8-171-2014.
72. Ahmed, A. GIS and remote sensing for malaria risk mapping, Ethiopia. *ISPRS Tech. Comm. VIII Symp.* **2014**, *XL-8*, 155–161, doi:10.5194/isprsarchives-XL-8-155-2014.
73. Lawpoolsri, S.; Chavez, I.F.; Yimsamran, S.; Puangsa-art, S.; Thanyavanich, N.; Maneeboonyang, W.; Chaimungkun, W.; Singhasivanon, P.; Maguire, J.H.; Hungerford, L.L. The impact of human reservoir of malaria at a community-level on individual malaria occurrence in a low malaria transmission setting along the Thai-Myanmar border. *Malar. J.* **2010**, *9*, 143, doi:10.1186/1475-2875-9-143.
74. Ouédraogo, A.L.; Gonçalves, B.P.; Gnémé, A.; Wenger, E.A.; Guelbeogo, M.W.; Ouédraogo, A.; Gerardin, J.; Bever, C.A.; Lyons, H.; Pitroipa, X.; et al. Dynamics of the human infectious reservoir for malaria determined by mosquito feeding assays and ultrasensitive malaria diagnosis in Burkina Faso. *J. Infect. Dis.* **2016**, *213*, 90–99, doi:10.1093/infdis/jiv370.
75. Chanda, E.; Mukonka, V.M.; Mthembu, D.; Kamuliwo, M.; Coetzer, S.; Shinondo, C.J. Using a Geographical Information System based decision support to enhance malaria vector control in Zambia. *J. Trop. Med.* **2012**, *1*, doi:10.1155/2012/363520.
76. Pinchoff, J.; Larsen, D.A.; Renn, S.; Pollard, D.; Fornadel, C.; Maire, M.J.; Sikaala, C.; Sinyangwe, C.; Winters, B.; Bridges, D.J.; et al. Targeting indoor residual spraying for malaria using epidemiological data: A case study of the Zambia experience. *Malar. J.* **2016**, *15*, doi:10.1186/s12936-015-1073-9.
77. Landman, W.A. How the International Research Institute fo Climate and Society has contributed towards seasonal climate foecast modelling and operations in South Africa. *Earth Perspect.* **2014**, *1*, 1–13, doi:10.1186/2194-6434-1-22.
78. Gaudart, J.; Touré, O.; Dessay, N.; Dicko, A.L.; Ranque, S.; Forest, L.; Demongeot, J.; Doumbo, O.K. Modelling malaria incidence with environmental dependency in a locality of Sudanese savannah area, Mali. *Malar. J.* **2009**, *8*, doi:10.1186/1475-2875-8-61.
79. Dambach, P.; Machault, V.; Lacaus, J.-P.; Vignolles, C.; Sié, A.; Sauerborn, R. Utilization of combined remote sensing techniques to detect environmental variables influencing malaria vector densities in rural West Africa. *Int. J. Health Geogr.* **2012**, *11*, doi:10.1186/1476-072X-11-8.
80. Howes, R.E.; Mioramalala, S.A.; Ramiranirina, B.; Franchard, T.; Rakotorahalahy, A.J.; Bisanzio, D.; Gething, P.W.; Zimmerman, P.A.; Ratsimbao, A. Contemporary epidemiological overview of malaria in Madagascar: Operational utility of reported routine case data for malaria control planning. *Malar. J.* **2016**, *15*, 502, doi:10.1186/s12936-016-1556-3.
81. Ithantamalala, F.A.; Rakotoarimanana, F.M.J.; Ramiadantsoa, T.; Rakotondramanga, J.M.; Pennober, G.; Rakotomanana, F.; Simon Cauchemez, C.J. Spatial and temporal dynamics of malaria in Madagascar. *Malar. J.* **2018**, *17*, 58, doi:10.1186/s12936-018-2206-8.
82. Girond, F.; Randrianasolo, L.; Randriamampionona, L.; Rakotomanana, F.; Randrianarivelosoa, M.; Ratsitorahina, M.; Brou, T.Y.; Herbreteau, V.; Mangeas, M.; Zigiumugabe, S.; et al. Analysing trends and forecasting malaria epidemics in Madagascar using a sentinel surveillance network: A web-based application. *Malar. J.* **2017**, *16*, 72, doi:10.1186/s12936-017-1728-9.
83. Chakhar, S. Enhancing Geographical Information Systems Capabilities with Multi-Criteria Evaluation Functions. *J. Geogr. Inf. Decis. Anal.* **2003**, *7*, 47–71.



ANNEXE 3

Randremanana, R. V., Andriamandimby, S., Rakotondramanga, J. M., Razanajatovo, N. H., Mangahasimbola, R. T., Randriambolamanantsoa, T. H., Ranaivoson, H. C., Rabemananjara, H. A., Razanajatovo, I., Razafindratsimandresy, R., Rabarison, J. H., Brook, C. E., Rakotomanana, F., Rabetombosoa, R. M., Razafimanjato, H., Ahyong, V., Raharinosy, V., Raharimanga, V., Raharinantoanina, S. J., ... Heraud, J. (2021). The COVID-19 epidemic in Madagascar: clinical description and laboratory results of the first wave, march-september 2020. *Influenza and Other Respiratory Viruses*, 15(4), 457–468. <https://doi.org/10.1111/irv.12845>

The COVID-19 epidemic in Madagascar: clinical description and laboratory results of the first wave, march-september 2020

Rindra Vatosoa Randremanana¹ | Soa-Fy Andriamandimby² |
 Jean Marius Rakotondramanga¹  | Norosoa Harline Razanajatovo² |
 Rezyky Tiandraza Mangahasimbola¹ | Tsiry Hasina Randriambolamanantsoa² |
 Hafaliana Christian Ranaivoson² | Harinirina Aina Rabemananjara² | Iony Razanajatovo² |
 Richter Razafindratsimandresy² | Joelinotahiana Hasina Rabarison² | Cara E. Brook³ |
 Fanjasoa Rakotomanana¹ | Roger Mario Rabetombosa¹ | Helisoa Razafimanjato² |
 Vida Ahyong⁴ | Vololoniaina Raharinosy² | Vaomalala Raharimanga¹ | Sandratana
 Jonhson Raharintoanina² | Mirella Malala Randrianarisoa¹ | Barivola Bernardson¹ |
 Laurence Randrianasolo¹ | Léa Bricette Nirina Randriamampionona⁵ | Cristina M. Tato⁴ |
 Joseph L. DeRisi⁴ | Philippe Dussart²  | Manuela Christophère Vololoniaina⁵ |
 Fidiniaina Mamy Randriatsarafara⁵ | Zely Arivelo Randriamanantany⁵ |
 Jean-Michel Heraud² 

¹Epidemiology and Clinical Research Unit, Institut Pasteur de Madagascar, Antananarivo, Madagascar

²Virology Unit, Institut Pasteur de Madagascar, Antananarivo, Madagascar

³University of California Berkeley, Berkeley, CA, USA

⁴Chan Zuckerberg Biohub, San Francisco, CA, USA

⁵Ministry of Public Health, Government of the Republic of Madagascar, Antananarivo, Madagascar

Correspondence

Jean-Michel Heraud, Virology Department, Institut Pasteur de Dakar, BP 220, Dakar, 12900, Senegal.
 Email: jean-michel.heraud@pasteur.fr

Present address

Jean-Michel Heraud, Virology Department, Institut Pasteur de Dakar, Dakar, Senegal

Funding information

United States Agency for International Development, Grant/Award Number: Cooperation Agreement 72068719CA00001; World Health

Abstract

Background: Following the first detection of SARS-CoV-2 in passengers arriving from Europe on 19 March 2020, Madagascar took several mitigation measures to limit the spread of the virus in the country.

Methods: Nasopharyngeal and/or oropharyngeal swabs were collected from travelers to Madagascar, suspected SARS-CoV-2 cases and contact of confirmed cases. Swabs were tested at the national reference laboratory using real-time RT-PCR. Data collected from patients were entered in an electronic database for subsequent statistical analysis. All distribution of laboratory-confirmed cases were mapped, and six genomes of viruses were fully sequenced.

Results: Overall, 26,415 individuals were tested for SARS-CoV-2 between 18 March and 18 September 2020, of whom 21.0% (5,553/26,145) returned positive. Among laboratory-confirmed SARS-CoV-2-positive patients, the median age was 39 years (IQR: 28-52), and 56.6% (3,311/5,553) were asymptomatic at the time of sampling. The probability of testing positive increased with age with the highest adjusted odds ratio of 2.2 [95% CI: 1.9-2.5] for individuals aged 49 years and more. Viral strains sequenced belong to clades 19A, 20A and 20B indicative of several independent introduction of viruses.

This is an open access article under the terms of the Creative Commons Attribution License, which permits use, distribution and reproduction in any medium, provided the original work is properly cited.

© 2021 The Authors. *Influenza and Other Respiratory Viruses* Published by John Wiley & Sons Ltd.

Organization; Innovative Genomics Institute; U.S. Department of Health and Human Services, Grant/Award Number: IDSEP190051-01-0200; National Center for Immunization and Respiratory Diseases, Grant/Award Number: U5/IP000812-05; Bill and Melinda Gates Foundation, Grant/Award Number: GCE/ID OPP1211841; Chan Zuckerberg Biohub

Conclusions: Our study describes the first wave of the COVID-19 in Madagascar. Despite early strategies in place Madagascar could not avoid the introduction and spread of the virus. More studies are needed to estimate the true burden of disease and make public health recommendations for a better preparation to another wave.

KEYWORDS

COVID-19, epidemiology, madagascar, pandemic, SARS-CoV-2, Surveillance

1 | INTRODUCTION

In December 2019, a new coronavirus later named SARS-CoV-2 emerged in the city of Wuhan (province of Hubei), China, causing deadly pneumonia.^{1,2} Since then, this virus has spread worldwide and the World Health Organizations (WHO) declared coronavirus disease 2019 (COVID-19), the disease resulting from SARS-CoV-2 infection, a global pandemic on 11 March 2020.³ Despite many efforts from countries to contain the spread at the national level, the epidemic is still ongoing in many countries, including those in Africa, although the African epidemic has been somewhat blunted in comparison with European countries and other territories.^{4,5} At the time of submission (31 December 2020), COVID-19 has resulted in more than 83 million cases and 1,8 million deaths worldwide.⁵ In Africa, the number of cases (2,76) and deaths (65 468) represents a small fraction of the global data. With the exception of anosmia and ageusia in some patients, COVID-19 is non-specific and similar to many other respiratory viruses.^{6,7} Therefore, laboratory confirmation is required to positively identify a case.

Madagascar is a large island located in the South-West of the Indian Ocean with an estimated population of about 27 million, most of whom (65%) inhabit rural areas.⁸ International connection through air-traffic remains limited with fewer than 50 international flights per week and around 500 000 passengers annually.⁸ In order to mitigate the introduction of SARS-CoV-2 to Madagascar from patients arriving from affected countries, the Institut Pasteur de Madagascar established a real-time RT-PCR detection platform in country as early as 29 January 2020, thanks to technical support from the Hong Kong University—Pasteur Research Pole.⁹

Following an increasing number of cases in Europe and Asia, one of the regions with high volume of travellers, the Malagasy Government screened all incoming international travellers from 12 to 20 March 2020 and eventually decided to close the country to all air-traffic on 20 March 2020. After the detection of the first SARS-CoV-2 case in Madagascar from an incoming traveller on 19 March 2020, other non-pharmaceutical interventions were adopted, including curfew, stay-at-home order, closure of non-essential businesses and social distancing in order to prevent or limit the spread of the virus in the country.

The objective of the current study was to describe the epidemiology of the first epidemic wave of SARS-CoV-2 affecting Madagascar from 18 March to 18 September 2020, and in particular the proportion of asymptomatic positive cases since the national strategy was to test both travellers and contacts regardless of the presence of symptoms at the time of sampling.

2 | MATERIALS AND METHODS

2.1 | Study subject and specimen collection

Specimen were collected from different types of individuals:

- Passengers. Following the strategy from the Ministry of Public Health (MPH), all passengers arriving from Europe and China, from 12 to 20 March (2020) were screened for SARS-CoV-2 regardless of symptoms at the time of sampling.
- Contacts of positive cases regardless of symptoms at the time of sampling. Contacts were defined as anyone who had direct contact or was within 1 metre of a SARS-CoV-2-infected person for at least 15 minutes even if that person had no symptoms (household members, other family contacts, visitors, neighbours, colleagues, teachers, co-workers) according to the MPH case definition based on WHO guidelines.¹⁰
- Suspected SARS-CoV-2 cases. After community transmission was demonstrated in one region or locality in Madagascar, all patients visiting hospitals and clinics with symptoms related to COVID-19 infection were sampled. Additionally, our existing Influenza Surveillance System (ISS) was extended to include monitoring of COVID-19 based on recommendations from the WHO¹¹⁻¹³: patients visiting clinics or hospitals within the ISS network were sampled if presenting with influenza-like illness (ILI) or severe acute respiratory infection (SARI) as per the revised WHO case definitions.¹⁴ Patients that presented with solely anosmia and/or ageusia were also considered as COVID-19 suspected cases. From each suspected case, demographic and clinical information was collected.
- We also received a high number of specimens from public clinics that were opened during the epidemic offering free sampling and screening test. Convenient specimens were also received from public and private institutions.

2.2 | Viral detection

Nasopharyngeal and/or oropharyngeal swabs were taken and were placed into viral transport media and transported at 4°C to the Virology Unit (National Influenza Centre) at the Institut Pasteur de Madagascar (IPM). Specimens were stored at 4°C before nucleic acid extraction and real-time RT-PCR processing. Due to the scarcity of reagents available, specimens were tested using different methods upon availability of reagents. Overall, five real-time RT-PCR

protocols recommended by WHO were used for the detection of the novel coronavirus 2019^{15,16}: Charité—Universitätsmedizin Berlin,¹⁷ Hong Kong University,⁹ Da An gene (Da An Gene Co., Ltd. Sun Yat-sen University, Guangzhou, China), LightMix® SarbecoV E-gene plus EAV control (TIB Biolmol, Berlin, Germany), and TaqPath™ COVID-19 Combo kit (Life Technologies Ltd, Paisley, UK). For clinicians in need of rapid results for patients in the emergency care unit/intensive care unit, specimens were tested using Xpert Xpress SARS-CoV-2 cartridges (Cepheid, Sunnyvale, CA, USA), a rapid PCR-based assay. All tests were performed in accordance with the protocols available provided by the WHO¹⁵ and manufacturer's instructions for use.

2.3 | Full Genome sequencing and genomic analysis

Methods for generating full genome sequences from SRAS-CoV-2 strains circulating in Madagascar and subsequent genomic analysis are detailed in Supplementary file.

2.4 | Data management and analyses

The data included in the record form accompanying the biological samples were collected and managed using REDCap electronic data capture tools hosted at IPM.^{18,19} REDCap (Research Electronic Data Capture) is a secure, web-based software platform designed to support data capture for research studies, providing 1) an intuitive interface for validated data capture; 2) audit trails for tracking data manipulation and export procedures; 3) automated export procedures for seamless data downloads to common statistical packages; and 4) procedures for data integration and interoperability with external sources. In our analyses, all continuous variables are expressed as median with interquartile range (IQR); categorical variables are presented as percentage, subject to a chi-squared test. All statistical analysis was performed in R²⁰ and at individual level, and *P-value* < .05 was considered statistically significant. We carried out a mapping of the geographical distribution of confirmed cases according to the health district where the sample collection originated from.

2.5 | Patient Consent Statement

All data used by this study were from state-wide surveillance of a notifiable disease and were de-identified.

3 | RESULTS

3.1 | Characteristics of patients and specimens

From 25 January to 15 March 2020, 96 suspected cases were sampled and all tested negative. The vast majority of these suspected cases

tested had a travel history in China and particularly originated from the Hubei Province (personal communication). On 16 March 2020, following the increasing number of cases that occurred in Europe and specifically in Italy, Spain and France, the Government took the decision to test all passengers that have arrived in Madagascar since 12 March 2020, from an affected area. The first imported SARS-CoV-2 case in Madagascar was then laboratory-confirmed on 19 March 2020. Thereafter, several imported cases from passengers were detected. The first laboratory-confirmed cases without a travel history, therefore considered to be community transmission, were detected on 25 March 2020. Although some cases are still being detected in December 2020, our study focuses on the first six months, or the “first wave,” of the pandemic in Madagascar (ie from 18 March to 18 September 2020).

Overall, we received specimens from 26,468 individuals of which 26,415 (99.8%) were tested for SARS-CoV-2 (remaining specimens were rejected for non-conformity). Among individuals tested, 21.0% (5,553/26,415) were positive (Table 1). The median age of patients from whom specimens were collected was 37 years (IQR: 26-49 years) and 52.9% were male (13,817/26,138) when excluding missing data on sex. The age distribution of patients from whom specimens were collected was different than the age distribution of the overall Malagasy population, with more individuals over 20 years sampled. (22,397/25,928) (Table 1). Most of the individuals sampled (76.0%; 19,718/25,928) and those who tested positive (77.3%; 4,257/5,507) were aged from 20 to 59 years old and positivity rate increased with age (Figure S1). Among SARS-CoV-2-confirmed cases, the sex ratio (M/F) was 1.05 (2,826/2,686) (Table 1). The median age of positive patients was 39 years (IQR: 28-52 years) and ranged from 1 week to 93 years. When looking at passenger, suspected cases and contact of confirmed cases, we found that positivity rates was 11.2% (98/878), 23.5% (3,819/16,219) and 17.6% (1,636/9,318), respectively (Table S1).

3.2 | Clinical symptoms of patients

We found that 75.2% (19,864/26,415) of patients tested declared no symptom at the time of sampling. The proportion of asymptomatic individuals was 56.6% (3,311/5,553) among laboratory-confirmed cases (Table 1). The most common symptoms of illness onset among confirmed cases were cough (27.2%), fever (18.7%), weakness (14.7%), runny nose (13.3%) and headache (13.1%) (Table S2; Table 2). In multiple logistic regression, age and the five most common symptoms observed in confirmed cases were associated with SARS-CoV-2 positivity. The probability of having a positive RT-PCR increased with age (Figure S1). Compared to individuals less than 16 years, individuals aged 16 and above had higher probability to have a positive RT-PCR. The adjusted odds ratios (aOR) were 1.8 [95% CI: 1.6-2.1]) for individuals aged 16 to 49 years and 2.2 [95% CI: 1.9-2.5]) for individuals aged 50 years and more. We estimated that, compared to individuals without fever, individuals with fever were two times more likely to have a positive RT-PCR (aOR_{1.9} [95% CI:

Total	Positive		Negative		Total		P-value [*]
	5 553	%	20 862	%	26 415	%	
Sex							.008
Male	2 826	50.9	10 991	52.7	13 817	52.3	
Female	2 686	48.4	9 635	46.2	12 321	46.6	
Missing	41	0.7	236	1.1	277	1.0	
Age (Years)							<.001
0-4	78	1.4	728	3.5	806	3.1	
5-14	191	3.4	1 104	5.3	1 295	4.9	
15-19	268	4.8	1 162	5.6	1 430	5.4	
20-29	1 116	20.1	4 270	20.5	5 386	20.4	
30-39	1 131	20.4	4 503	21.6	5 634	21.3	
40-49	1 142	20.6	3 782	18.1	4 924	18.6	
50-59	868	15.6	2 906	13.9	3 774	14.3	
>59	713	12.8	1 966	9.4	2 679	10.1	
Missing	46	0.8	441	2.1	487	1.8	
Symptomatic							<.001
Yes	2 242	40.4	4 309	20.7	6 551	24.8	
No	3 311	56.6	16 553	79.3	19 864	75.2	

*Pearson's chi-squared tests were performed (P -values < .05 were considered significant)

1.7-2.1]), while those with cough and weakness were, respectively, 1.8 and 1.4 times more likely to test positive (aOR cough = 1.8 [95% CI: 1.7-2.0]; aOR weakness = 1.4 [95% CI: 1.3-1.6]). Those with runny nose and headache had respective aORs of 1.3 [95% CI: 1.1-1.5] and 1.2 [95% CI: 1.1-1.3].

3.3 | Circulation of SARS-CoV-2 in Madagascar

During the first wave of the epidemic, the virus spread in almost all regions of Madagascar (Figure 1). At the national level, active circulation of the virus in the community was observed in a first surge from May to June followed by a second but more intense surge from the end of June to the end of July (Figure 2). These two consecutive peaks were driven by community outbreaks occurring in two highly populated regions of the country (Toamasina and Antananarivo) (Figure 3). The first city affected was Toamasina, located on the East coast, the second most populated city of Madagascar and the main seaport of the country. In this city, sporadic cases were detected from 16 March to 26 April 2020 from individuals with (i) a history of travel in countries with SARS-CoV-2 community transmission or (ii) contacts with travellers that tested positive. During week 18 (27 April to 03 May 2020), several clusters of cases were detected, many among the employees of a large mining company. From these clusters, the virus quickly spreads into the community, causing an ensuing outbreak, which lasted for 8 weeks (from 27 April to 21 June 2020) (Figure 3A). During that period, the peak of cases was observed during week 20 (mid-May). The positivity rate reached 43.2% on week 21 (18-24 May

2020) and decreased thereafter. The second city affected was Antananarivo, the capital city of Madagascar with around 2.6 million inhabitants. The epidemic started in Antananarivo during week 24 (8-14 June 2020) (Figure 3B). The epidemic peaked on week 28 (6-12 July 2020) with the positivity rate of about 50%. Although cases were still detected at the end of our study, the positivity rate was below 10% by end of August and the number of daily cases was below 10 by week 38 (14-20 September 2020).

3.4 | Monitoring of COVID-19 through the Influenza Surveillance System

A proportion of the overall specimens received during the COVID-19 epidemic were acquired through the extension of the ISS to include SARS-CoV-2. Although our SARI surveillance system only detected a few COVID-19 cases (with very few samples received from May to July and only two SARI-derived SARS-CoV-2-confirmed cases in August and September), the ILI system sourced a substantial number of COVID-19-positive samples (Figure 4). Overall, among ILI suspected cases, 35.0% (205/584) of them were found positive for SARS-CoV-2. The peak positivity rate reached 69.2% (164/237) in July and decreased thereafter.

3.5 | Genetic characteristics of the newly introduced SARS-CoV-2 virus in Madagascar

The entire genomes of the 10th and 19th cases of SARS-CoV-2 detected in Madagascar (from 20 and 22 March 2020) were obtained on

TABLE 1 Laboratory results of all individual tested at IPM for SARS-CoV-2 by gender, age group and occurrence of symptoms

TABLE 2 Association of RT-PCR results with age, sex and clinical symptoms. Only data from individuals with no missing information (ie age sex and symptoms) were included

Covariates	RT-PCR results		OR (95% CI)	aOR (95% CI)	P-value*
	POS (5 472)	NEG (20 268)			
Age (%)					
<16yrs	312 (5.7)	2,006 (9.9)	1	1	
16-49yrs	3 586 (65.5)	13 422 (66.2)	1.7 (1.5-1.9)	1.8 (1.6-2.1)	< 0.001
>49yrs	1 574 (28.8)	4 840 (23.9)	2.1 (1.8-2.4)	2.2 (1.9-2.5)	< .001
Sex (%)					
Female	2 672 (48.8)	9 468 (46.7)	1	1	
Male	2 800 (51.2)	10 800 (53.3)	0.9 (0.9-1.0)	0.9 (0.9-1.0)	.05
Cough (%)					
No	3 984 (72.8)	17 924 (88.4)	1	1	
Yes	1 488 (27.2)	2 344 (11.6)	2.9(2.7-3.1)	1.8 (1.7-2.0)	< .001
Fever (%)					
No	4 447 (81.3)	18 932 (93.4)	1	1	
Yes	1 025 (18.7)	1 336 (6.6)	3.3 (3.0-3.6)	1.9 (1.7-2.1)	< .001
Weakness					
No	4 668 (85.3)	19 131 (94.4)	1	1	
Yes	804 (14.7)	1 137 (5.6)	2.9 (2.6-3.2)	1.4 (1.3-1.6)	< .001
Runny nose					
No	4 743 (86.7)	18 908 (93.3)	1	1	
Yes	729 (13.3)	1 360 (6.7)	2.1 (1.9-2.3)	1.2 (1.1-1.3)	.003
Headache					
No	4 755 (86.9)	19 180 (94.6)	1	1	
Yes	717 (13.1)	1 088 (5.4)	2.7 (2.4-2.9)	1.3 (1.1-1.5)	< .001

Abbreviation: OR, Crude Odd ratio; aOR, Adjusted Odd ratio.

*Pearson's chi-squared tests were performed (*P*-values < .05 were considered significant).

an Illumina platform (iSeq100) and deposited in the GISAID EpiCoV™ database (EPI_ISL_508862|2020-03-20, EPI_ISL_508863|2020-03-22). The patients from which both genomes were obtained arrived from France (Paris) on 18 and 19 March 2020. The analysis of the complete genome of both samples revealed a sequence homology of 99.92% when compared to the reference virus originated from Wuhan (hCov-19/Wuhan/WIV04/2019). These two viruses belong to the clade 20A, lineage B.1 (Figure S2), which was prevalent in Europe at the time of introduction.²¹ Several amino acid substitutions were observed at the following sites: the viral Spike glycoprotein (D614G), accompanied (as is customary to this clade) by a C-to-T mutation in the 5' untranslated region at position 241, a synonymous C-to-T mutation at position 3037, a non-synonymous C-to-T mutation at position 14 408 in the RNA-dependent RNA polymerase gene (ORF1b-Nsp12:P314L) and a non-synonymous G-to-T mutation at position 25 563 (Orf3a: Q57H) (Table S3). In addition to these common mutations, both early sequences also exhibited C-to-T mutations at positions 2416 and 5884.

Two additional samples collected on 26 March 2020 from the beginning of the outbreak in Toamasina were sequenced (EPI_ISL_677635/2020-03-26, EPI_ISL_677636/2020-03-26) from two mining workers that were also housemate, and who had travelled to Madagascar from the Philippines. These sequences demonstrated

a sequence homology of 99.98% when compared to the reference virus (hCov-19/Wuhan/WIV04/2019); they cluster in a rare Asian subclade within Nextstrain clade 19A (Figure S2), which has been previously described circulating in India with links to Indonesia.²² The Toamasina sequences share four mutations with this previously characterized Indian subclade: a non-synonymous C-to-A mutation at position 6312 (Orf1a-Nsp3: T2016K), the common G-to-T mutation at position 11 803 (Orf1a-Nsp12: L3606F), a non-synonymous C-to-T mutation at position 13 730 (Orf1b-RdRp: A88V), a C-to-T spike protein mutation at position 23 929 and a non-synonymous C-to-T mutation at position 28 311 (N: P13L and Orf9b: P10S) (Table S3). In addition, they also show a C-to-T mutation at position 19 524 and a non-synonymous G-to-A mutation at position 1268 (Orf1a-Nsp2: D335N).

Finally, we have recently begun sequencing samples from later in the Madagascar epidemic, including one sample collected from Toamasina in May (GISAID EPI_ISL_625456/2020-05-04) and another from Antananarivo in September (EPI_ISL_677634/2020-09-16). Both of these sequences belong to Nextstrain clade 20B, lineage B.1.1 (Figure S2), which is distinguished from the four common mutations that define clade 20A by an additional three consecutive mutations: G-to-A at position 28 881, G-to-A at 28 882 and G-to-C at 28 883. The September sample (EPI_ISL_677634)

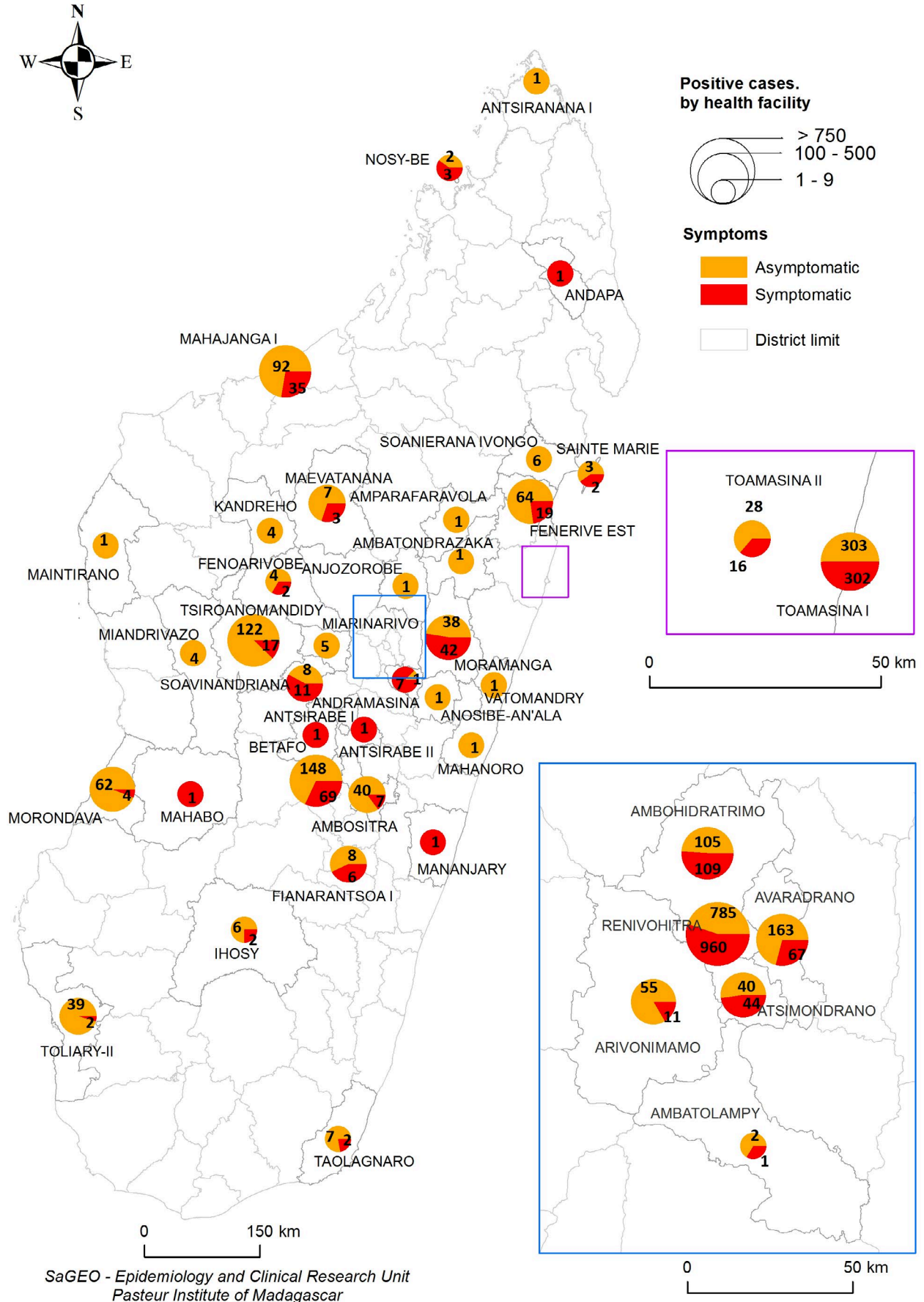


FIGURE 1 Distribution of positive cases in Madagascar from 18 March to 18 September 2020. Pies shows the numbers of symptomatic (red) and asymptomatic (orange) SARS-CoV-2 laboratory-confirmed cases. Pie size is proportional to the total number of cases per region

SaGEO - Epidemiology and Clinical Research Unit
 Pasteur Institute of Madagascar

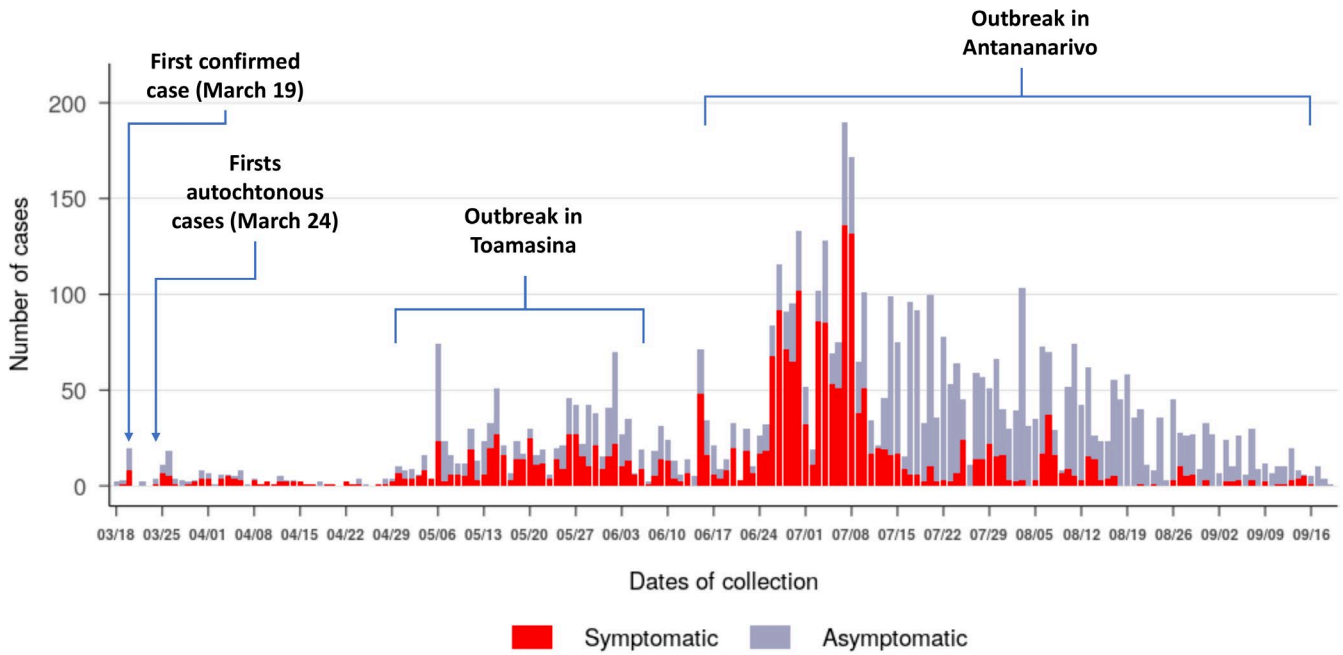


FIGURE 2 Weekly SARS-CoV-2 laboratory-confirmed cases in Madagascar from 18 March to 18 September 2020. SARS-CoV-2-positive cases are represented according symptoms presented at the time of collection (n = 5 553)

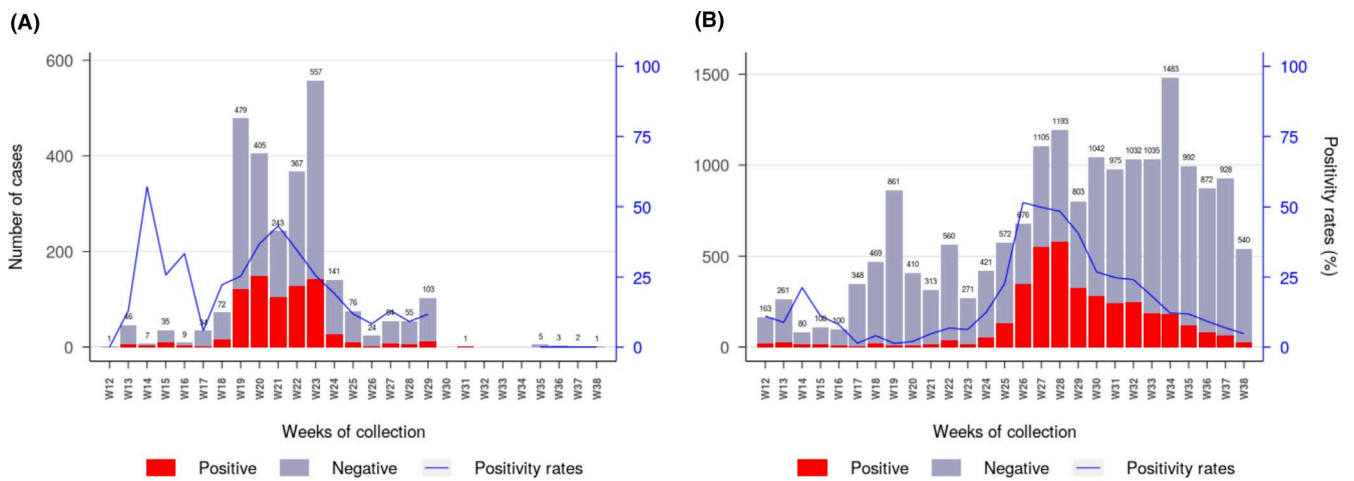


FIGURE 3 Weekly laboratory results and positivity rate for SARS-CoV-2 in Toamasina (A) and Antananarivo (B) regions from week 12 to week 38. For the Toamasina Region, specimens (n = 2 720) originated from two health districts (Toamasina I and Toamasina II). For Antananarivo region, specimens (n = 17 613) originated from five health districts (Andramasina, Ambohidratrimo, Antananarivo-Avaradrano, Antananarivo-Atsimondrano, and Antananarivo-Renivohitra districts). (remark: week 12 started on 16th of March and week 38 ended on 20th of September 2020)

also shows numerous downstream mutations within lineage 20B, including five non-synonymous mutations in Orf1a-Nsp3 (C6027T: P1921L), Orf1a-Nsp6 (C11514T: T3750I), the Spike glycoprotein (C20703T: V3G and C21575T: L5F) and Orf3a (G25599T: W69C) (Table S3).

4 | DISCUSSION

Like many countries in sub-Saharan Africa, Madagascar quickly imposed a border closure and a lockdown of the capital city following

the first detected case of COVID-19. To limit the spread and contain the epidemic, the MPH commissioned testing of all passengers arriving from affected countries (mainly Europe) from 12 March to the date of closure of air-traffic (20 March 2020). All identified and reachable air-passengers that arrived in Madagascar during that period were sampled and tested independently of clinical signs. Some of them were quarantined upon arrival, while others were tested retrospectively after returning home for several days with their relatives. Despite attempts to prevent introductions, the first locally acquired cases were detected on 25 March 2020, suggestive of introductions prior to border closure. Nevertheless,

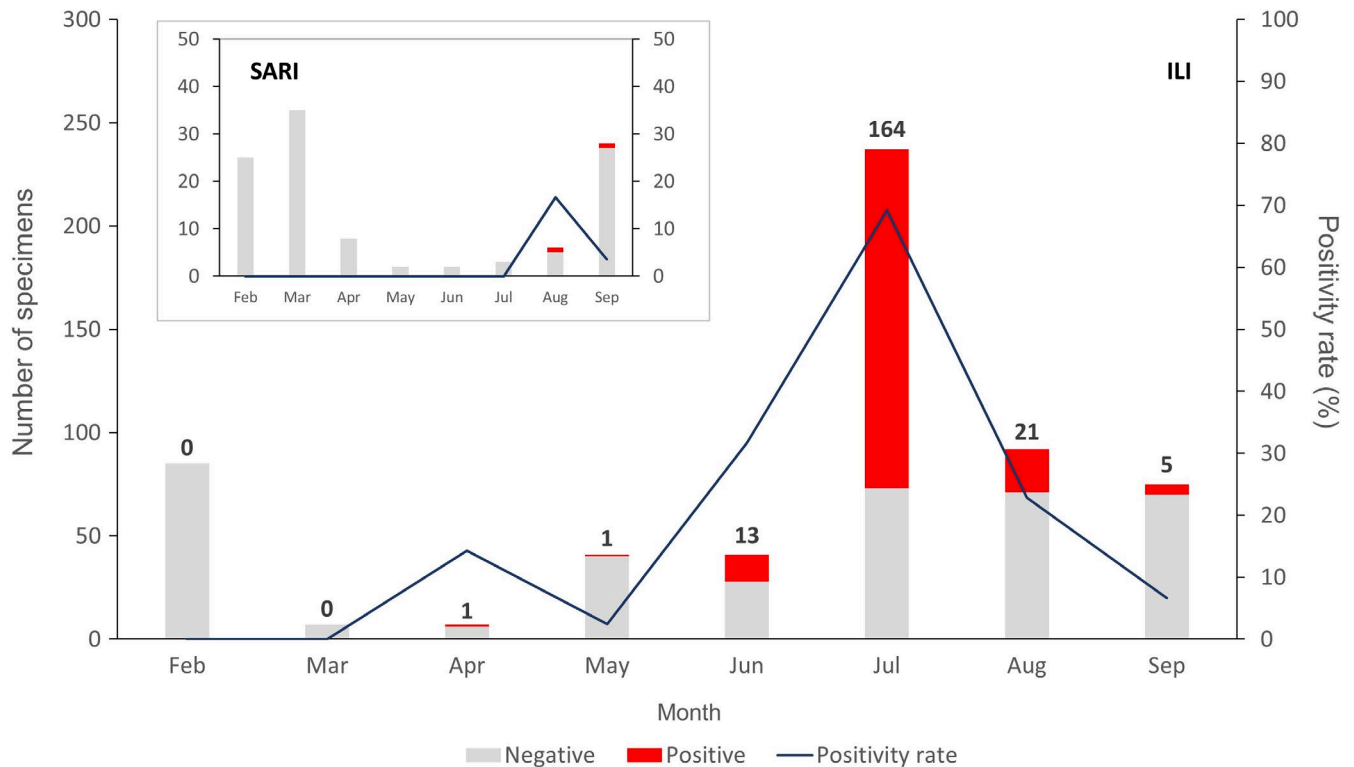


FIGURE 4 Monthly laboratory results from the Severe Acute Surveillance Infection (SARI) and Influenza-Like Illness (ILI) surveillance in Madagascar from February to September 2020. Each bar represents the total number of negative cases (grey) and SARS-CoV-2-positive cases (red). Numbers above bars indicate the number of positives. The dark blue line represents the positivity rate

community transmission remained limited until the end of April, with only sporadic cases detected, followed by strong measures to isolate patients, and trace and test all contacts. Unfortunately, in May 2020, an increasing number of cases from several clusters were detected in Toamasina, the second highest populated city of the country. The outbreak started initially among the several hundred employees of a large mining company that operates in the city. Despite efforts to contain the outbreak, the virus rapidly spread throughout the city and neighbouring region. This outbreak lasted for 8 weeks (from 27 April to 21 June 2020). Following this major outbreak in Toamasina, cases began to rise in the capital of Antananarivo during the first week of June. Sequence data are not yet resolved sufficiently to determine if the outbreak affecting Antananarivo was a consequence of individuals arriving from Toamasina despite regional containment measures or if it resulted from low-level circulation within Antananarivo following the first introductions in March. As May to September marks the dry, cold season in the Madagascar highlands, climate may have also played a role in amplifying the epidemic; indeed, previous studies have shown that active circulation of influenza viruses in Madagascar and particularly in Antananarivo is observed between May to September during the dry and cold season in the highlands.²³⁻²⁵ Further sequencing of SARS-CoV-2 isolates will be critical to “tracing” the spread of these two different outbreaks.

Overall, the total number of laboratory-confirmed cases of COVID-19 in Madagascar as of 20 September 2020 (16,020, a third

of which were detected in part with this study) remained low per inhabitant, when compared to Europe and the Americas.²⁶ Within Africa, Madagascar is among the ten countries reporting the highest number of cases of COVID-19 but is still reporting far fewer cases than the northern African countries, as well as South Africa.^{26,27} Several reasons could explain this result. First, almost 65% of Madagascar's inhabitants live in rural settings,⁸ and the population is, on average, very young (median age = 20.3 years). In our study, SARS-CoV-2 infected patients aged less than 20 years represented only 9.4% of all positive cases. This particularity may have limited the spread of COVID-19 as suggested by the modelling study conducted by Diop *et al.*²⁸ Secondly, it is possible that the total number of confirmed cases of COVID-19 in Madagascar is underestimated and/or underreported due to several factors, including (i) the testing capacity of labs that could not exceed 1,000 tests/day, (ii) insufficient staff to conduct efficient contact tracing and (iii) behavioral resistance to healthcare seeking in the population. Limited healthcare seeking behaviour often presents challenges to efforts to estimate the burden of diseases in sub-Saharan and other low-income countries.^{29,30} Resistance to seeking health care can have many drivers, but recent studies have shown a reduction in patient presentation in clinics or hospitals during the COVID-19 pandemic and associated lockdown.³¹⁻³³ An ongoing serological survey among blood donors in Madagascar should be able to address the true burden of COVID-19.

For future monitoring of SARS-CoV-2 circulation, WHO has recently recommended that countries extend the Influenza

Surveillance System (ISS) to include COVID-19.¹³ In Madagascar, an effective ISS has been in place for decades and was used effectively to detect and monitor the last pandemic virus A/H1N1pdm09 in Madagascar.^{11,12} Although the ISS was disrupted during the first few weeks of the COVID-19 epidemic, due to a lack of personal protective equipment for clinicians and their excessive workload, it was rapidly reinstated and has been used thereafter for effective monitoring of SARS-CoV-2 circulation in the Madagascar community. Indeed, 3.7% (207/5,553) of all COVID-19 cases considered in this study were sampled in the ISS. The ISS was also responsible for identification of the first cases of COVID-19 in some of Madagascar's cities (ie Antsirabe and Toamasina). Interestingly, both positivity rate and total case number for COVID-19 in the ISS peaked in July 2020, mirroring the peak witnessed in the national data published by the MPH, which reported a peak of 614 daily cases on July 22.⁵ This finding demonstrates the importance and public value of the WHO recommendation to extend national ISS to include COVID-19, as emphasized in a recent publication.^{13,34}

In our study, we found that the median age of positive COVID-19 cases in Madagascar was 39 years (IQR: 28-52 years), with most positive patients aged 20 years and older (90.6%). Nevertheless, the positivity rates increased with age. These findings are similar to those previously observed in other low-income countries like Algeria, Nigeria and Pakistan,³⁵⁻³⁷ but show an average infection distribution that is younger than that previously reported from Wuhan (median age = 59 years).³⁸ These differences likely reflect both the younger age structure of the Madagascar population (median age = 20.3 years) and the national strategy aimed at testing both patients presenting to clinics with pneumonia, as well as travellers and contacts regardless of symptoms at the time of sampling. Indeed, 60% of positive cases in our study declared no symptoms at the time of sampling. This proportion of patient may have impact on the spread of the epidemic. Children under 15 years of age represented only 4.4% of all positive SARS-CoV-2 cases in Madagascar, consistent with global patterns showing lower infection rates in children, and in contrast to previously described patterns of respiratory virus circulation in Madagascar.^{24,25,39,40}

Regarding clinical signs, although symptoms of COVID-19 are considered to be non-specific, the five most common clinical manifestations (fever, cough, weakness, headache and runny nose) were significantly associated with SARS-CoV-2 infection in our study. Indeed, a recently published article from one Antananarivo hospital leveraged this finding to adopt a clinical screening score used to assess the probability of COVID-19 infection.⁴¹

Initial sequence data indicate multiple introduction events of SARS-CoV-2 to Madagascar, with sequences derived from a largely Asian clade of the virus sourcing the initial outbreak in Toamasina, and sequences derived from at least two primarily European clades of the virus sourcing the subsequent outbreak in the capital city of Antananarivo. Notably, the initial SARS-CoV-2 sequences from Toamasina lacked the D614G mutation that has been shown to enhance SARS-CoV-2 transmissibility,⁴² while those sequences from Antananarivo contained it. Further sequencing of additional isolates

from these disparate introduction events in Madagascar should allow us to compare the persistence, duration and transmission capacity of these different SARS-CoV-2 lineages. It is important to highlight that the G204R mutation found in both of the later epidemic sequences (EPI_ISL_625456 and EPI_ISL_677634) may affect the binding of primers used in the China CDC assay for N-gene detection.¹⁶ This information will need to be addressed in ongoing surveillance. It highlights the need to utilise multiple genetic targets for PCR testing, as well as the importance of periodic genome sequencing of circulating strains to quickly identify any mutation that might affect molecular testing.

Our study has some limitations. Beginning in May 2020, the Madagascar MPH decreed that samples from hospitalized patients should also be tested in public laboratories. Subsequent to this decree, other laboratories began to receive samples not included in these analyses. Additionally, during the first month of our current study, we tested mostly international travellers returning from affected areas, as well as their contacts regardless of symptoms. As such, our data do not represent the full spectrum of clinical cases in Madagascar. In contrast, however, these findings underline the importance of asymptomatic transmission for SARS-CoV-2. The role of asymptomatic carriers in the epidemiology of the current pandemic is disputed, but recent paper estimates that half of the overall transmission of SARS-CoV-2 are coming from infected patient that present no symptoms.^{43,44} Ongoing studies are currently collecting information on a follow-up cohort of infected patients and their households and contacts to elucidate more thoroughly the epidemiology of this first wave of SARS-CoV-2 in Madagascar. If the role of asymptomatic in the transmission is confirmed, health authorities should consider these population of infected individuals to contain the spread of the virus by increasing the proportion of asymptomatic patients being tracked and screened.

In conclusion, despite strong interventions to prevent and contain the spread of the COVID-19 epidemic in Madagascar (including lockdowns, curfews, travel restrictions and social distancing), Madagascar was unable to avoid the introduction and the spread of the virus in the country. Nonetheless, these strategies may have helped delay the onset of the epidemic and allowed the MPH to prepare for the response, especially in health districts with limited infrastructure for severe case management. Indeed, the strategy to test specimen from passengers, contacts of confirmed case regardless of symptoms allowed the detection of a substantial proportion of SARS-CoV-2 cases (respectively 11.2% and 17.5%) and conduct the health authorities to the isolate those individuals that could have spread the virus in the community. It is yet too early to estimate the true impact of prevention measures taken at both the national and local level on the spread of COVID-19 in Madagascar. Further work is needed to determine if various interventions effectively delayed the spread of SARS-CoV-2 in country or successfully reduced the magnitude of the epidemic. Ongoing studies (seroprevalence surveys, first few hundred cases and contact analyses, and genomic epidemiology) will support efforts to estimate the burden of disease, various epidemiological

parameters (eg RO, clinical attack rate, immune response...), and underreporting of cases and inform public health strategies critical to avoiding or reducing the impact of subsequent waves of infection on the health systems and the economy of a country with limited resources.

ACKNOWLEDGEMENTS

We thank all staff from the Ministry of Public Health including the clinicians and nurses from the different University Hospitals, in particular in Antananarivo (Joseph Raseta Befelatanana, Joseph Ravoahangy Andrianavalona, Anosiala and Andohatapenaka), and Toamasina (Analakininina and Morafeno). We are in debt to all staff from the Institut Pasteur de Madagascar for their dedicated work during this pandemic. We received technical support from The Institut Pasteur International Network, the United Nations Children's Fund (UNICEF), the AFRICA CDC and the Jack Ma Foundation. This study received financial support from the World Health Organization (WHO), the US Centers for Disease Control and Prevention (US CDC: Grant#U5/IP000812-05), the United States Agency for International Development (USAID: Cooperation Agreement 72068719CA00001), the Office of the Assistant Secretary for Preparedness and Response in the US Department of Health and Human Services (DHHS: grant number IDSEP190051-01-0200), the Bill & Melinda Gates Foundation (GCE/ID OPP1211841), the Chan Zuckerberg Biohub, and the Innovative Genomics Institute at UC Berkeley. The contents are the responsibility of the authors and do not necessarily reflect the views of the WHO, US CDC, USAID, US DHHS, the Government of the United States of America, the UNICEF, the Bill & Melinda Gates Foundation, the Chan Zuckerberg Biohub, or the Innovative Genomics Institute.

CONFLICT OF INTEREST

All authors declare that they have no commercial or other associations that may pose a conflict of interest.

AUTHOR CONTRIBUTION


Rindra Vatosoa Randremanana: Conceptualization (lead); Data curation (supporting); Formal analysis (equal); Funding acquisition (lead); Investigation (equal); Methodology (lead); Supervision (lead); Writing-original draft (equal); Writing-review & editing (lead). **Soa-Fy Andriamandimby:** Data curation (supporting); Formal analysis (supporting); Methodology (supporting); Supervision (equal); Validation (equal); Writing-review & editing (equal). **Jean Marius Rakotondramanga:** Data curation (lead); Formal analysis (equal); Methodology (supporting); Software (equal); Validation (equal); Visualization (equal); Writing-original draft (supporting); Writing-review & editing (supporting). **Noroso Harline Razanajatovo:** Data curation (supporting); Formal analysis (equal); Methodology (equal); Supervision (supporting); Validation (equal); Writing-review & editing (supporting). **Reziky Tiandraza Mangahasimbola:** Software (lead); Supervision (supporting); Writing-review & editing (supporting). **Tsiry Hasina Randriambolanantsoa:** Formal analysis (equal); Investigation (supporting); Methodology (supporting); Validation

(supporting); Writing-review & editing (supporting). **Hafaliana Christian Ranaivoson:** Data curation (equal); Formal analysis (equal); Writing-review & editing (supporting). **Harinirina Aina Rabemananjara:** Formal analysis (equal); Investigation (supporting); Methodology (supporting); Writing-review & editing (supporting). **Iony Razanajatovo:** Formal analysis (supporting); Methodology (supporting); Supervision (equal); Validation (equal). **Richter Razafindratsimandresy:** Supervision (equal); Validation (equal); Writing-review & editing (supporting). **Joelinotahina Hasina Rabarison:** Data curation (equal); Formal analysis (supporting); Investigation (equal); Supervision (supporting); Writing-review & editing (supporting). **Cara E Brook:** Data curation (supporting); Formal analysis (supporting); Funding acquisition (supporting); Software (supporting); Visualization (supporting); Writing-review & editing (equal). **Fanjasoa Rakotomanana:** Software (equal); Visualization (equal); Writing-review & editing (supporting). **Roger Mario Rabetombosoa:** Investigation (supporting); Resources (supporting); Supervision (supporting). **Helisoa Razafimanjato:** Data curation (supporting); Formal analysis (equal); Methodology (supporting); Validation (equal). **Vida Ahyong:** Data curation (supporting); Formal analysis (supporting); Software (supporting); Validation (supporting). **Vololoniaina Raharinosy:** Formal analysis (supporting); Methodology (supporting); Validation (supporting). **Vaomalala Raharimanga:** Data curation (supporting); Investigation (supporting); Supervision (supporting). **Sandratana Jonhson Raharinantoanina:** Formal analysis (supporting); Investigation (lead); Supervision (supporting); Validation (supporting). **Mirella Malala Randrianarisoa:** Data curation (supporting); Investigation (supporting). **Barivola Bernardson:** Investigation (supporting); Supervision (supporting). **Laurence Randrianasolo:** Investigation (equal); Project administration (equal); Resources (equal); Supervision (supporting). **Léa Bricette Nirina Randriamampionona:** Investigation (equal); Project administration (supporting); Resources (equal); Supervision (supporting); Validation (supporting). **Cristina M. Tato:** Data curation (supporting); Funding acquisition (supporting); Project administration (supporting); Software (supporting); Validation (supporting); Writing-review & editing (supporting). **Joseph L. DeRisi:** Data curation (supporting); Funding acquisition (supporting); Resources (supporting); Validation (supporting); Writing-review & editing (equal). **Manuela Christophère Vololoniaina:** Resources (lead); Supervision (equal); Validation (supporting); Writing-review & editing (supporting). **Fidiniaina Mamy Randriatsarafara:** Investigation (equal); Resources (lead); Supervision (equal); Writing-review & editing (supporting). **Zely Arivelo Randriamanantany:** Conceptualization (supporting); Investigation (lead); Project administration (equal); Resources (lead); Supervision (supporting); Writing-review & editing (supporting). **Jean-Michel Heraud:** Conceptualization (lead); Data curation (equal); Formal analysis (equal); Funding acquisition (equal); Investigation (equal); Methodology (equal); Project administration (lead); Resources (lead); Supervision (equal); Validation (supporting); Writing-original draft (lead); Writing-review & editing (lead).

PEER REVIEW

The peer review history for this article is available at <https://publons.com/publon/10.1111/irv.12845>.

ORCID

Jean Marius Rakotondramanga  <https://orcid.org/0000-0003-0490-7665>

Philippe Dussart  <https://orcid.org/0000-0002-1931-3037>

Jean-Michel Heraud  <https://orcid.org/0000-0003-1107-0859>

REFERENCES

- Wu F, Zhao S, Yu B, et al. A new coronavirus associated with human respiratory disease in China. *Nature*. 2020;579(7798):265-269.
- Zhou P, Yang XL, Wang XG, et al. A pneumonia outbreak associated with a new coronavirus of probable bat origin. *Nature*. 2020;579(7798):270-273.
- The World Health Organization (WHO). WHO Director-General's opening remarks at the media briefing on COVID-19 - 11 March 2020. 2020. <https://www.who.int/director-general/speeches/detail/who-director-general-s-opening-remarks-at-the-media-briefing-on-covid-19--11-march-2020>
- Dong E, Du H, Gardner L. An interactive web-based dashboard to track COVID-19 in real time. *Lancet Infect Dis*. 2020;20(5):533-534.
- Worldometers.info. COVID-19 CORONAVIRUS PANDEMIC Dover, Delaware, USA. 2020 updated 30 November 2020. <https://www.worldometers.info/coronavirus/>
- Huang C, Wang Y, Li X, et al. Clinical features of patients infected with 2019 novel coronavirus in Wuhan, China. *Lancet*. 2020;395(10223):497-506.
- Patel A, Charani E, Ariyanayagam D, et al. New-onset anosmia and ageusia in adult patients diagnosed with SARS-CoV-2 infection. *Clin Microbiol Infect*. 2020.
- The US. Central Intelligence Agency (CIA). The World Factbook - Africa -. Madagascar. 2020. <https://www.cia.gov/library/publications/the-world-factbook/geos/ma.html>
- Chu DKW, Pan Y, Cheng SMS, et al. Molecular diagnosis of a novel coronavirus (2019-nCoV) causing an outbreak of pneumonia. *Clin Chem*. 2020;66(4):549-555.
- The World Health Organization (WHO). WHO COVID-19: Case Definitions 2020. https://apps.who.int/iris/bitstream/handle/10665/333912/WHO-2019-nCoV-Surveillance_Case_Definition-2020.1-eng.pdf?sequence=1&isAllowed=y
- Rajatonirina S, Heraud JM, Orelle A, et al. The spread of influenza A(H1N1)pdm09 virus in Madagascar described by a sentinel surveillance network. *PLoS One*. 2012;7(5):e37067.
- Rakotoarisoa A, Randrianasolo L, Tempia S, et al. Evaluation of the influenza sentinel surveillance system in Madagascar, 2009-2014. *Bull World Health Organ*. 2017;95(5):375-381.
- The World Health Organization (WHO). Maintaining surveillance of influenza and monitoring SARS-CoV-2 - adapting Global Influenza Surveillance and Response System (GISRS) and sentinel systems during the COVID-19 pandemic: Interim guidance. Geneva: World Health Organization; 2020 (WHO/2019-nCoV/Adapting_GISRS/2020.1). 2020. <https://apps.who.int/iris/handle/10665/336689>
- Fitzner J, Qasmieh S, Mounts AW, et al. Revision of clinical case definitions: influenza-like illness and severe acute respiratory infection. *Bull World Health Organ*. 2018;96(2):122-128.
- The World Health Organization (WHO). Molecular assays to diagnose COVID-19: Summary table of available protocols 2020 <https://www.who.int/publications/m/item/molecular-assays-to-diagnose-covid-19-summary-table-of-available-protocols>
- The World Health Organization (WHO). Molecular assays to diagnose COVID-19: Summary table of available protocols 2020. <https://www.who.int/publications/m/item/molecular-assays-to-diagnose-covid-19-summary-table-of-available-protocols>
- Corman VM, Landt O, Kaiser M, et al. Detection of 2019 novel coronavirus (2019-nCoV) by real-time RT-PCR. *Euro Surveill*. 2020;25(3):2000045.
- Harris PA, Taylor R, Minor BL, et al. The REDCap consortium: Building an international community of software platform partners. *J Biomed Inform*. 2019;95:103208.
- Harris PA, Taylor R, Thielke R, Payne J, Gonzalez N, Conde JG. Research electronic data capture (REDCap)—a metadata-driven methodology and workflow process for providing translational research informatics support. *J Biomed Inform*. 2009;42(2):377-381.
- R Core Team. *R: A language and environment for statistical computing*. Vienna, Austria: R Foundation for Statistical Computing; 2013. <https://www.R-project.org>
- Mercatelli D, Giorgi FM. Geographic and genomic distribution of SARS-CoV-2 mutations. *Front Microbiol*. 2020;11:1800.
- Banu S, Jolly B, Mukherjee P, et al. A distinct phylogenetic cluster of indian severe acute respiratory syndrome coronavirus 2 isolates. *open forum Infect Dis*. 2020;7(11):ofaa434.
- Alonso WJ, Guillebaud J, Viboud C, et al. Influenza seasonality in Madagascar: the mysterious African free-runner. *Influenza Other Respir Viruses*. 2015;9(3):101-109.
- Razanajatovo NH, Guillebaud J, Harimanana A, et al. Epidemiology of severe acute respiratory infections from hospital-based surveillance in Madagascar, November 2010 to July 2013. *PLoS One*. 2018;13(11):e0205124.
- Razanajatovo NH, Richard V, Hoffmann J, et al. Viral etiology of influenza-like illnesses in Antananarivo, Madagascar, July 2008 to June 2009. *PLoS One*. 2011;6(3):e17579.
- The World Health Organization (WHO). Weekly epidemiological update - 21 September 2020 2020. <https://www.who.int/publications/m/item/weekly-epidemiological-update--21-september-2020>
- Massinga Loembe M, Tshangela A, Salyer SJ, Varma JK, Ouma AEO, Nkengasong JN. COVID-19 in Africa: the spread and response. *Nat Med*. 2020;26(7):999-1003.
- Diop BZ, Ngom M, Poug e Biyong C, Poug e Biyong JN. The relatively young and rural population may limit the spread and severity of COVID-19 in Africa: a modelling study. *BMJ Glob Health*. 2020;5:e002699.
- Adedokun ST, Yaya S. Factors influencing mothers' health care seeking behaviour for their children: evidence from 31 countries in sub-Saharan Africa. *BMC Health Serv Res*. 2020;20(1):842.
- Noordam AC, Carvajal-Velez L, Sharkey AB, Young M, Cals JW. Care seeking behaviour for children with suspected pneumonia in countries in sub-Saharan Africa with high pneumonia mortality. *PLoS One*. 2015;10(2):e0117919.
- Baugh JJ, White BA, McEvoy D, et al. The cases not seen: Patterns of emergency department visits and procedures in the era of COVID-19. *Am J Emerg Med*. 2020. <https://doi.org/10.1016/j.ajem.2020.10.081>. [Epub ahead of print].
- Hautz WE, Sauter TC, Exadaktylos AK, Krummrey G, Schaub S, Muller M. Barriers to seeking emergency care during the COVID-19 pandemic may lead to higher morbidity and mortality - a retrospective study from a Swiss university hospital. *Swiss Med Wkly*. 2020;150:w20331.
- Thornton J. Covid-19: A&E visits in England fall by 25% in week after lockdown. *BMJ*. 2020;369:m1401.
- Chotpitayasunondh T, Fischer TK, Heraud JM, et al. Influenza and COVID-19: What does co-existence mean? *Influenza Other Respir Viruses*. 2020. <https://doi.org/10.1111/irv.12824>. [Epub ahead of print].
- Lounis M. Epidemiology of coronavirus disease 2020 (COVID-19) in Algeria. *New Microbes New Infect*. 2021;39:100822.
- Elimian KO, Ochu CL, Ilori E, et al. Descriptive epidemiology of coronavirus disease 2019 in Nigeria, 27 February-6 June 2020. *Epidemiol Infect*. 2020;148:e208.
- Khan M, Khan H, Khan S, Nawaz M. Epidemiological and clinical characteristics of coronavirus disease (COVID-19) cases at a screening clinic during the early outbreak period: a single-centre study. *J Med Microbiol*. 2020;69(8):1114-1123.

38. Li Q, Guan X, Wu P, et al. Early transmission dynamics in Wuhan, China, of novel coronavirus-infected pneumonia. *N Engl J Med*. 2020;382(13):1199-1207.
39. Rabarison JH, Tempia S, Harimanana A, et al. Burden and epidemiology of influenza- and respiratory syncytial virus-associated severe acute respiratory illness hospitalization in Madagascar, 2011–2016. *Influenza Other Respir Viruses*. 2019;13(2):138-147.
40. Rauf A, Abu-Izneid T, Olatunde A, et al. COVID-19 Pandemic: Epidemiology, Etiology, Conventional and Non-Conventional Therapies. *Int J Environ Res Public Health*. 2020;17(21):8155.
41. Raberahona M, Rakotomalala R, Rakotomijoro E, et al. Clinical and epidemiological features discriminating confirmed COVID-19 patients from SARS-CoV-2 negative patients at screening centres in Madagascar. *Int J Infect Dis*. 2020;103:6-8.
42. Plante JA, Liu Y, Liu J, et al. Spike mutation D614G alters SARS-CoV-2 fitness and neutralization susceptibility. *bioRxiv*. 2020. <https://doi.org/10.1101/2020.09.01.278689>. [Epub ahead of print].
43. Luo T, Cao Z, Wang Y, Zeng DD, Zhang Q. Role of Asymptomatic COVID-19 Cases in Viral Transmission: Findings from a Hierarchical Community Contact Network Model. <https://doi.org/10.2139/ssrn.3676211>
44. Johansson MA, Quandelacy TM, Kada S, et al. SARS-CoV-2 Transmission From People Without COVID-19 Symptoms. *JAMA Netw Open*. 2021;4(1):e2035057. <https://doi.org/10.1001/jamanetworkopen.2020.35057>

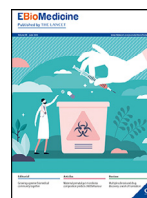
SUPPORTING INFORMATION

Additional supporting information may be found online in the Supporting Information section.

How to cite this article: Randremanana RV, Andriamandimby S-F, Rakotondramanga JM. The COVID-19 epidemic in Madagascar: clinical description and laboratory results of the first wave, march-september 2020. *Influenza Other Respir Viruses*. 2021;00:1-12. <https://doi.org/10.1111/irv.12845>

ANNEXE 4

Schoenhals, M., Rabenindrina, N., Rakotondramanga, J. M., Dussart, P., Rendremanana, R., Heraud, J. M., Andriamandimby, S. F., Sahondranirina, P. H., Vololoniaina, M. C. A., Randriatsarafara, F. M., Rasolofo, V., Randriamanantany, Z. A., & Spiegel, A. (2021). SARS-CoV-2 antibody seroprevalence follow-up in Malagasy blood donors during the 2020 COVID-19 Epidemic. *EBioMedicine*, 68, 103419.
<https://doi.org/10.1016/j.ebiom.2021.103419>



Research paper

SARS-CoV-2 antibody seroprevalence follow-up in Malagasy blood donors during the 2020 COVID-19 Epidemic



Matthieu Schoenhals^{a,*}, Niry Rabenindrina^a, Jean Marius Rakotondramanga^a, Philippe Dussart^a, Rindra Randremanana^a, Jean-Michel Heraud^{a,†}, Soa Fy Andriamandimby^a, Paquerette Hanitriniala Sahondranirina^b, Manuela Christophère Andriamahatana Vololoniaina^b, Fidiniana Mamy Randriatsarafara^b, Voahangy Rasolofo^a, Zely Arivelo Randriamanantany^{b,‡}, André Spiegel^{a,‡}

^a Institut Pasteur de Madagascar, Madagascar

^b Ministry of Public Health of Madagascar, Madagascar

ARTICLE INFO

Article History:

Received 19 February 2021

Revised 11 May 2021

Accepted 14 May 2021

Available online 4 June 2021

Keywords:

Madagascar

SARS-CoV-2 Seroprevalence

Blood donors

ABSTRACT

Background: The incidence of the 2020 COVID-19 epidemic in Africa seems to be different from that of the rest of the world, however its true extent is probably underestimated. Conducting population based sero-surveys during the epidemic has moreover been extremely challenging, driving our group and others to study blood donor samples.

Methods: We collected regional epidemiological COVID-19 surveillance data, and simultaneously monitored anti-SARS-CoV-2 antibody seroprevalences monthly throughout the epidemic in 5 major Region-associated Blood Transfusion Centres of Madagascar over a period of 9 months.

Findings: Soon after attaining the first epidemic peaks between May and August 2020, both crude and population-weighted test-performance-adjusted seroprevalences of anti-SARS-CoV-2 antibodies was in Malagasy blood donors rapidly increased up to over 40% positivity.

Interpretation: These findings suggest a high cumulative incidence of infection and seroconversion, which may have contributed to the observed deceleration of infection rates, but was not sufficient to prevent the second epidemic wave that struck Madagascar in Spring 2021.

Funding: This project was funded by the United States Agency for International Development.

© 2021 The Author(s). Published by Elsevier B.V. This is an open access article under the CC BY-NC-ND license (<http://creativecommons.org/licenses/by-nc-nd/4.0/>)

1. Introduction

As of February 2021, more than one hundred million people have been infected with SARS-CoV-2 worldwide, and over 2.3M deaths have been reported, 2.7M cases and 68,487 deaths in Africa. Despite available data suggesting that the incidence of COVID-19 in Africa is different from that of the rest of the world the extent of this epidemic is probably underestimated [1].

On March 19th 2020, Madagascar identified its first case of COVID-19. Restrictions across the country were quickly adopted on March 21st in order to slow the epidemic down, simultaneously however limiting the conduct of population-based surveys. Despite these restrictions, Madagascar has experienced the epidemic in different

locations, particularly in Toamasina (April-June 2020) and Antananarivo (June-August 2020). The state of health emergency was ended October 18th, and a series of relief measures was gradually implemented.

In a mixed context of aging immunity and new variants circulation, Madagascar was struck once again by an epidemic wave in Spring 2021. The Ministry of Health in Madagascar notified as of February the 15th 2021, 38,874 confirmed cases and 716 deaths linked to COVID-19 [1].

In Europe, the first epidemic wave would have affected around 5% of the population in Spain [2] and 4.4% in France and up to 10% in certain regions [3].

Anti-SARS-CoV-2 antibody detection makes it possible to define cumulative incidence of infection, confirming both symptomatic and asymptomatic infections. However due to difficulties to conduct of population based sero-surveys during the epidemic, several countries have monitored seroprevalences in blood donors [4,5]. Kenya has reported 5.2% seropositivity for antibodies to SARS-CoV-2, with the

* Corresponding author at: Institut Pasteur de Madagascar, Madagascar.

E-mail address: schoenhals@pasteur.mg (M. Schoenhals).

‡ Institut Pasteur de Dakar

† ZAR and AS contributed equally

Research in Context

Evidence before this study

We searched PubMed for research articles published from database inception until May 10th, 2021, with no language restrictions, using the terms “SARS-CoV-2” and “seroprevalence”. Seven hundred and twenty-seven peer-reviewed publications were available. Many described serosurvey results and meta-analysis that estimate regional seroprevalence rates in humans of SARS-CoV-2 antibodies. Only 27 publications were available when adding “Africa” to the search terms. None of these articles described simultaneous epidemiological COVID-19 surveillance data, and anti-SARS-CoV-2 antibody seroprevalences monitoring throughout an entire epidemic wave (before, during and after).

SARS-CoV-2 antibodies' seroprevalences have been reported in November 2020 to reach over 40% in one province of Northern Italy and in Manaus, Brazil. As for Africa, S. Uyoga *et al.* recently described that SARS-CoV-2 exposure of blood donors in Kenya was more extensive (around 10%) than indicated by case-based surveillance and closer to cumulative incidence of infection.

Added value of this study

We report for the first time the seroprevalences of anti-SARS-CoV-2 IgG antibodies amongst blood donors in Madagascar during the outbreak and how they sharply increased from 0% to 40%. This sudden increase was associated with a concomitant reduction in the virus circulation. This reproducible pattern was found in all 5 investigated regions of the country and 5 major cities amongst which its capital Antananarivo, home to 1,275,000 inhabitants. What seemed to be protective immunity however did not last and Madagascar has since undergone a second major epidemic wave.

Implications of all the available evidence

Simultaneous analysis of epidemiological COVID-19 surveillance data and anti-SARS-CoV-2 antibody seroprevalences monitoring throughout the entire epidemic remain paramount in understanding the dynamics of the pandemic. This is all the more true in countries where containment and lockdown measures could not be applied, and considering the high proportion of asymptomatic COVID-19 cases. Results of such studies will be useful for authorities to guide public health decisions.

2. Methods

2.1. Sample collection

Plasma or serum samples were collected in 5 out of 7 Regional Blood Transfusion Centres (RBTCs) of Madagascar for which it was possible to collect samples throughout the epidemic, and despite drastic travel restrictions. These 5 centres are localised in 5 out of 6 most populated cities of Madagascar, 36% of the Malagasy population lives in these 5 Regions (Supplementary Figure S1). The samples used come from venous blood samples intended for different quality control steps (blood counts, HIV and HCV serologies) from blood bags collected in blood banks and then for destruction.

Samples were collected twice a month from March to November at RBTC Antananarivo, and from June to November at RBTC Toamasina, Fianarantsoa, Toliara and Mahajanga. For each sample, the blood donor's gender, age, occupation and date of collection were collected.

Plasma samples from Antananarivo were aliquoted at the Joseph Ravoahangy Andrianavalona Hospital (HJRA) in 1mL cryotubes, then stored at -20°C, and analysed at the Infectious Diseases Immunology Unit of the Pasteur Institute of Madagascar.

Plasma samples from the provinces were aliquoted in RBTCs, shipped at a positive temperature between 0 and 4°C in 1mL cryotubes, then stored at -80°C until analysis at the Immunology of Infectious Diseases Unit of the Institut Pasteur in Madagascar.

Duplicates as well as samples from donors under the age of 18 were eliminated from the study. All Collected samples were analysed.

2.2. Serology

Semi-quantitative indirect ELISA for detection of anti-SARS-CoV-2 IgG – The ELISA kit used, ID Screen® SARS-CoV-2-N IgG Indirect ELISA (ID.Vet, Grabels, France) of semi-quantitative type, demonstrates the antibodies (IgG) directed against the nucleocapsid (N) of the SARS-CoV-2 in human serum or plasma.

Briefly, and following the manufacturer's instructions the samples to be tested and the controls were distributed in wells of the microplate coated with a purified recombinant antigen of the N protein. After washing, a protein G conjugate labelled with peroxidase (HRP), recognising total human IgGs (IgG1, IgG2, IgG3, IgG4), but not binding to IgA, nor to IgM and IgE, was distributed in the wells, forming an antigen-antibody-conjugate-HRP complex. After removing the excess conjugate and washing, the developing solution (TMB) was added. The reaction was then stopped and the microplate is read at a wavelength of 450 nm.

According to the manufacturer, the kit used has a specificity of 99.8% (95% CI 99.3 - 99.9) and a sensitivity of 95.2% (95% CI 95.2 - 100) (Sensitivity study performed on 41 hospitalised RT-PCR positive samples > 15 days after first symptom presentation. Specificity study performed on 1247 French Blood donor samples collected before 2017. S/P threshold 40%) [7].

According to internal studies, the kit used has a specificity of 99.6% (95% CI 99.1- 99.8), and a sensitivity of 92.6% (95% CI 76.6-98.7). The sensitivity study was performed on 27 serum samples from hospitalised patients with positive SARS-CoV-2 RT-PCR, collected more than 28 days after onset of symptoms. Specificity study was performed on 1,251 Blood donor samples collected before the COVID-19 epidemic. S/P threshold of 40% was used according to manufacturer instruction.

Results interpretation – For each sample, the “S / P” “Sample / Positive control” ratio, expressed as a percentage (S/P%) was calculated with the formula:

$$S/P = \frac{DO_{\text{sample}} - DO_{\text{CTRL-}}}{DO_{\text{CTRL+}} - DO_{\text{CTRL-}}}$$

The negative control used contains a matrix based on bovine serum albumin, while the positive control of human origin, contains anti-SARS-Cov-2 IgG in a standardised quantity.

peaks up to almost 10% observed in the 3 highly urbanised regions. In the United States, the seroprevalence was monitored in dialysis patients and estimated in July at 9.3%, with peaks observed at 33.6% in New York City, an epidemic hotspot [6]. However, unlike in most European countries, blood donors in Madagascar are often family members or acquaintances of those in need of blood thus may come from different socio-economic and socio-cultural backgrounds of the general population.

As soon as the circumstances allowed us to do so (March for Antananarivo capital city, and from June for regions out of Antananarivo), serum samples were collected monthly until November 2020 in 5 of the country's Regional Blood Transfusion Centres (RBDCs) (Supplementary Figure S1) and analysed for the presence of anti-SARS-CoV-2 IgGs (anti-N) using a highly specific and sensitive ELISA kit. This serological data was then compared to COVID-19 epidemiological surveillance data (See materials and methods section) collected by the Ministry of Public Health for the corresponding regions.

Samples showing an S/P:

- Below 40% are considered negative.
- Greater than or equal to 40% were considered positive.

Relative levels of anti-SARS-Cov-2 IgGs from samples considered positive are S/P values of samples greater than or equal to 40%.

2.3. Epidemiological surveillance data

The monthly seroprevalence rates observed in each of the RBTC were compared with the epidemic dynamics described, in each administrative region to which the RBTC belongs, by the number of cases confirmed by SARS-CoV-2 RT-PCR and the positivity rate (number of confirmed cases by SARS-CoV-2 RT-PCR / numbers of SARS-CoV-2 RT-PCRs performed).

All the surveillance data for the Analamanga (Antananarivo), Haute Matsiatra (Fianarantsoa), Atsinanana (Toamasina), Boeny (Mahajanga) and Atsimo Andrefana (Toliara) regions were obtained from the Department of Health Watch, Epidemiological and Response Surveillance (DVSSER): number of SARS-CoV-2 RT-PCRs performed by four laboratories for the whole country, number of confirmed cases by SARS-CoV-2 RT-PCR and RT-PCR positive rate (Case confirmation rate).

2.4. Statistical analysis and modeling

To allow direct standardisation of estimated seroprevalences in RBTC donors, we tabulated seropositive results by gender, age and region, because the study was a non-random sample of the population. We then calculated standardised prevalence estimates [8] using population data from the 2018 Malagasy Population and Housing Census [9]. We used direct standardisation on the observed seroprevalence and population weights in 250 gender-age-month-CRTS strata: gender (n=2), age (n=4), month and CRTS (n=5). Some age groups or genders may not have investigated at certain months in specific RBTCs due to low sample size. Only investigated age and gender groups were considered for direct standardisation, Bayesian multilevel regression modeling, and post-stratification.

Monthly prevalence estimates calculated using multilevel regression and post-stratification (MLRP) were used to account for differences in the sample and the regional populations [4]. To predict stratum (age-gender) prevalence for MLRP we fitted a Bayesian logistic regression model by month using the rjags package (version 4.3.0) in R, that included gender as a fixed effect, and age as a random effect; except for Mahajanga in September when only the 18-24 age group was represented. A fixed effect model on gender was then fitted. We used vague or weakly informative priors for all parameters [4,10].

Analysis was conducted in R (R Core Team, 2014) URL <http://www.R-project.org/> or using GraphPad Prism version 8.0. Statistical tests are mentioned, confidence intervals calculated using Wilson/Brown method.

2.5. Ethics

This study was authorised by the Ministry of Health of Madagascar and by the BioMedical Research Ethics Committee (CERBM) that informed the investigators it required neither the approval of the committee nor specific donor consent (CERBM: IOR0000851) (Authorisation N°205-MSANP/SG/AGMED/CERBM). Blood donors are advised their blood may be tested for surveillance purposes.

2.6. Role of funders

This project was funded by the United States Agency for International Development (USAID) cooperation agreement 72068719CA00001

and supported by the Institut Pasteur de Madagascar, and by the French Ministry for Europe and Foreign Affairs through the REPAIR Covid-19-Africa project coordinated by the Pasteur International Network association. The contents are the responsibility of the authors and do not necessarily reflect the views of USAID and the United States Government.

3. Results

The first epidemic peak took place in May in the Atsinanana region, case confirmation rates reaching 30%. The Analamanga region (including Antananarivo) subsequently reached its peak in July. Eighty two percent of cases were confirmed between July and August (n=9,570) and case confirmation rate reached 41.8% in July. The Boeny region was also reached in July (case confirmation rate 30.5%) and Haute Matsiatra region and Atsimo Andrefana were reached early August (respectively 60 cases and 52 cases diagnosed in July and August). (Fig. 1 Table S1).

Toamasina RBTC sample collection was initiated in June 2020. Samples were 39.0% positive for anti-SARS-CoV-2 antibodies, then increased to 43.4% in July and stabilised around 40% in August, before decreasing in September to 29.1%, 26.1% in October and 18.4% in November (Fig. 1, Table S2 Panel a).

Antananarivo samples had very low seroprevalences (mean 0.4%) from March to May (n=1,251), then started to increase reaching 38.5% in September (n=483) (Fig. 1 Table S2 Panel a). As among Toamasina blood donors, a seroprevalence slight decrease was observed in October and November (down to 31.3%).

In Mahajanga, Fianarantsoa and Toliara RBTCs, the first samples collected in June and July showed no to low seropositivity then sharply increased in Mahajanga to 35.5% (n=107) in August (stabilising at 37.7% in September). Toliara and Fianarantsoa however showed a milder increase stabilising around 20% in September. Seroprevalences then decreased in Mahajanga and Fianarantsoa and seemed to stabilise just around 20% in Toliara, suggesting residual virus circulation in later months (Fig. 1 Table S2 Panel a).

Compared with the 2018 Malagasy Population and Housing Census [9], our participants were older (mean age 32 yo versus 22 yo in the census) and more commonly males (80.2% males in our study versus 49.3% in the census) (Supplementary Table S3). Only Mahajanga showed mild differences when performing bivariate seropositivity analysis according to the demographic characteristics of the population and the month of sample collection in the 5 RBTCs from March to November 2020 (Supplementary Table S4).

Nevertheless, we adjusted the prevalence estimates for the demographics of the sample using poststratification, and for the sensitivity and specificity of the test as described by Uyoga S. et al. [4]. Population-weighted and test-performance-adjusted seroprevalence in Antananarivo was highest in September (43.5% vs crude 38.5%), reached 51.2% in Toamasina in July (vs crude 43.4%), 21.9% in Fianarantsoa in September (vs crude 18.5%), 27.7% in Toliara in October (vs crude 22.3%) and 44.5% in August in Mahajanga, whereas the crude peak only happened in September (37.7%). It is noteworthy however that only the 18-24 age group was represented in Mahajanga in September, and that a fixed effect model on gender was thus fitted (Supplementary Table S2 Panel a, b, c).

Test-performance-adjusting using in-house calculated specificity (99.6%, 95% CI 99.1- 99.8) and sensitivity (92.6%, 95% CI 76.6- 98.7), had very little effect when compared to manufacture values: Mean values of peak seroprevalences in the 5 RBTCs were 32.1% (crude seroprevalence), 35.7% (Standardised, population-weighted, manufacture test-performance-adjusted), 36.6% (Standardised, population-weighted, in-house test-performance-adjusted) and 37.8% using the Bayesian model (population-weighted and manufacture test-performance-adjusted) (Supplementary Table S2 Panels a, b, data not shown and c).

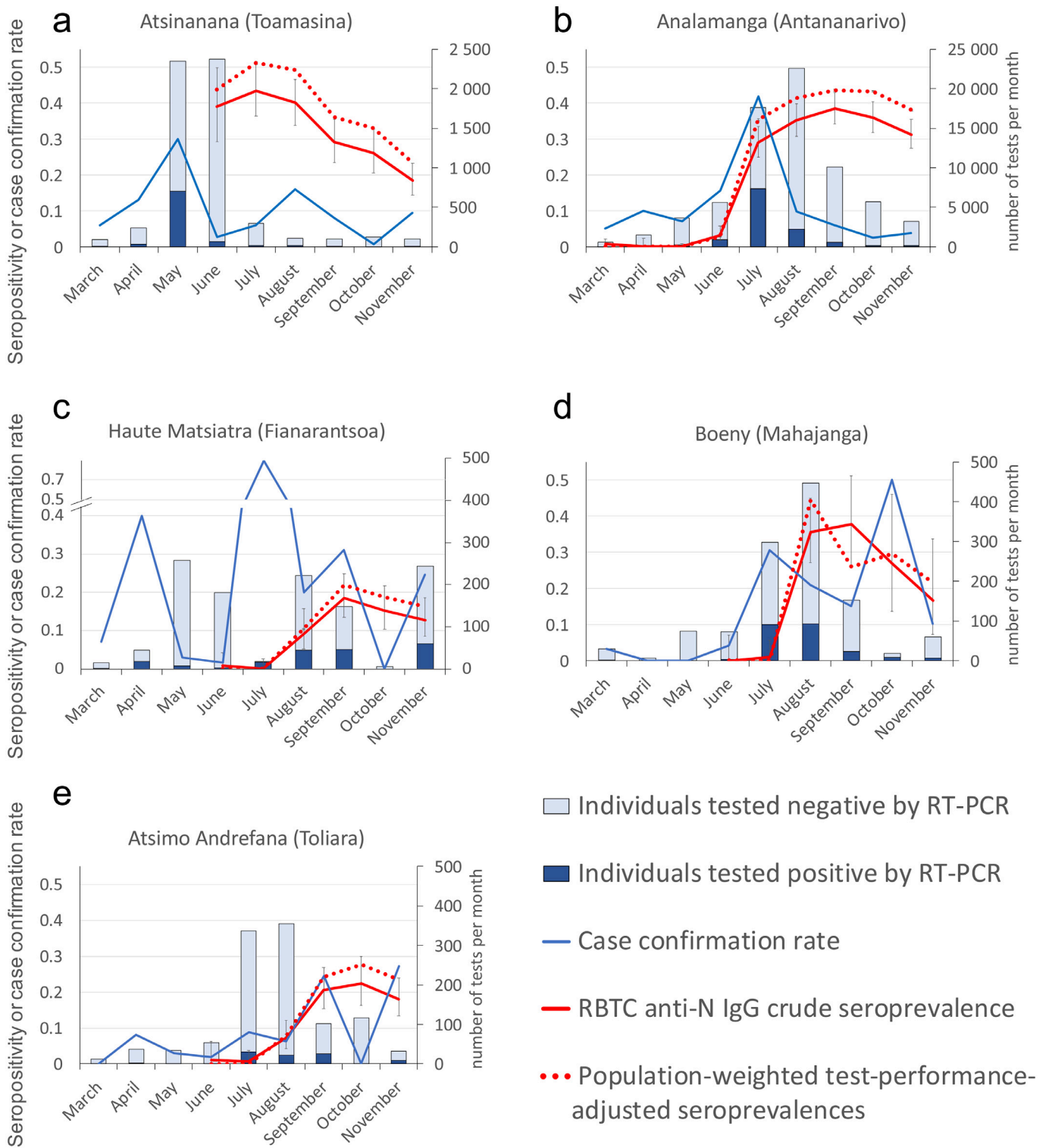


Fig. 1. Monthly anti-SARS-CoV-2 IgG seropositivity in blood donors (crude seroprevalences and Bayesian model population-weighted and manufacture test-performance-adjusted) and epidemiological indicators in regions of Madagascar; a – Atsinanana, b – Analamanga, c – Haute Matsiatra, d – Boeny and e – Atsimo Andrefana. Light blue bars: COVID-19 suspected individuals tested negative for SARS-CoV-2 by RT-PCR; Dark blue bars: COVID-19 suspected individuals tested positive for SARS-CoV-2 by RT-PCR; Blue line: SARS-coV-2 case confirmation rate; Red line: anti-N IgG crude seroprevalence among RBTC collected samples (95% confidence interval); Dotted red line: population-weighted test-performance adjusted seroprevalences (95% confidence interval). (For interpretation of the references to colour in this figure legend, the reader is referred to the web version of this article.)

4. Discussion

Blood donors represent a simple, accessible and inexpensive means of collecting samples from an adult (over 18 yo) population. SARS-CoV-2 hospitalised patients do not commonly require blood

transfusion. Blood donor exposure is thus not particularly biased in this respect. Young male samples are however over-represented, most importantly in Tulear (92.2%) and Toamasina (90.1%) due to the conditions associated with donating blood (blood donation is only allowed after a non-donation period of 3 months for males and 4

months for females. The donor must have a weight greater than 50 kg, be non -pregnant, -breastfeeding, -menstruation -use of implant or injectable contraceptive).

Several factors may affect the accuracy of our seroprevalence estimates. Half of the population of Madagascar is outside the age range sampled in this study (Age and gender distribution of RBTC sampled population in comparison with the overall age-sex distribution of the regions' adult population is represented in Supplementary Fig. S2), and the seroprevalence in children, that represent 50% of the Malagasy population [9], and older adults is thought to be low [2]. Moreover, the more prudent fraction of the population avoiding exposure may not be properly represented in our sampled population. However, our sampling may as well be underestimating seroprevalences as potential donors are excluded from giving blood if they have not been healthy for at least a few weeks. Last, antibodies specific to the nucleocapsid antigen are known to disappear early [11,12], resulting in low seroprevalences only a few month after exposure. Our analysis is consequently not entirely representative, even after population-weighting and test-performance-adjusting.

An important indicator during an epidemic is the number of confirmed cases. This is not absolutely relevant in Madagascar, where the number of tests performed is not large enough to reflect the true incidence of the disease. Indeed, the strategy in Madagascar was at first to detect early virus circulation. It then evolved with the epidemic to test predominantly people coming to hospitals to be diagnosed and obtain medical care consequently testing distinct populations. Case confirmation rates thus appears to be the best indicator of the epidemic dynamics, provided that the number of tests carried out monthly is sufficiently large, as it is the case in Antananarivo and Toamasina. Regions such as Haute Matsiatra, Boeny and Atsimo Andrafana did not show stable testing capacity resulting in surprisingly variable case confirmation rates from one month to the other (Fig. 1 Panels c, d and e). Whatever the setting however, seroprevalences increase after the first notified cases and reach a plateau, providing good indicators for both cumulative incidence and progression during the epidemic.

Correcting seroprevalences using either population-weighted, test-performance direct standardisation or the Bayesian model generated seroprevalences extremely close to crude values. The maximal seroprevalence of anti-SARS-CoV-2 antibodies fluctuates around 40% among blood donors from Toamasina, Antananarivo and Mahajanga, which is at least 4-fold higher than the post-epidemic seroprevalences described elsewhere in particular in Kenya, whose blood donors are as in Madagascar predominantly males aged less than 45 years. This high rate suggests a greater spread of the virus in Madagascar and is likely linked to an incomplete observance by the population of restrictions imposed by the health authorities due to difficult economic conditions in certain populational categories. Assuming seroprevalences in the whole population of the 5 regions (9.5M inhabitants, 37% of the country's population) were identical to those from their paired blood donors, which is certainly not the case, as only 20-25 % of regions' population live in these 5 regional capital cities, we estimated 3.6M individuals (900 000 if considering the Capital cities only) would have been infected by SARS-CoV-2, in comparison to 12,930 notified cases reported during the study period in these regions.

The COVID-19 epidemic occurred sequentially in the 5 different regions of our study. We observed a slowdown in the spread of the virus concurrent with 40% population seropositivity. Decreased infection rates were seen as early as June in Toamasina, by the end of July in Antananarivo, began in Mahajanga at the end of August. Finally, the low seroprevalences in blood donors of Toliara and Fianarantsoa at the end of September could suggest a slower progression of the pandemic in these provinces. Seroprevalence monitoring of collected blood donor samples and epidemiological indicators obtained until the end of November do not indicate a recirculation of the virus 5-7 months after the first epidemic peak.

Seroprevalences drop from September to November 2020, and most importantly in Toamasina (from 29.1% to 18.4%), after 3 months of seroprevalences of anti-SARS-CoV-2 antibodies in over 40% of donors. This drop has already been described elsewhere [11,13–15], in particular as in our case when the antigenic target is the Nucleocapsid (N) protein of SARS-CoV-2. Indeed, the anti-N antibody levels of seropositive donors from Toamasina drop significantly from August to September and October to November 2020, as more and more seropositive individuals approach the seropositivity threshold (Supplementary Fig. S3).

Each component of SARS-CoV-2 immune memory seems to exhibit distinct kinetics: Sero-neutralizing ability decrease has been documented in the first 2 months after infection, particularly after mild COVID-19 [15], others have shown that neutralizing antibodies are stably found for at least 5-7 months after infection with SARS-CoV-2 [14]. Spike-specific memory B cells however have been found more abundant at 6 months than at 1 month, and with no apparent half-life at 5+ months post-infection, unlike SARS-CoV-2-specific CD4+ T cells and CD8+ T cells that seem to decline with half-lives of 3 to 5 months [16].

Natural reinfections, which occur when humoral and cellular immunity are insufficient, seem to be a common feature for all human seasonal coronaviruses after the 12th month post-infection [17], suggesting a non-permanent protective immunity. This could also be the case with SARS-CoV-2 infections, even though currently circulating strains of SARS-CoV-2 are not very variable, unless the Spike-specific memory B cells developed during COVID-19 turn out to be long-lived or very long-lived, as observed after other infections as multi-decade old smallpox vaccination memory B cells [18] or influenza memory B cells [19]. However, correlates of protection against SARS-CoV-2 and the longevity of the immune response are still not well understood.

This study however has limitations, as longitudinal data was not accessible in Madagascar during this epidemic, resulting in a multi-cross-sectional young population overrepresenting males. Drops in infection rates could be due to factors unrelated to seropositivity, such as seasonality [20], social interventions, or awareness of danger leading to behaviour changes [21].

The pandemic however has evolved with a resurgence in peaks happening throughout the world, and new variants seemingly affecting its course as in Manaus, Brazil. High seroprevalences and attack rates as high as 75% were described after the first epidemic peak [22], but this city was devastated by a second peak in December. Preliminary data suggesting 42% of samples collected mid-December contained a new viral lineage called P.1 [23]. One possibility is that in some people, P.1 could elude the human immune response triggered by the lineage that ravaged the city earlier in 2020. As in Brazil, high seroprevalence rates were not sufficient to prevent a second epidemic wave from happening. Aging immunity and new variants circulation have led Madagascar to be struck by a second major peak in Spring 2021.

Our data describes the dynamics of the first peak in SARS-CoV-2 in Madagascar, in which we observed a drop in circulation of the virus concurrent with a peak of 40% anti-SARS-CoV-2 seropositivity. This seemingly high natural immunisation rate was however clearly not enough to provide permanent immunity, a substantial proportion of the population having remained susceptible or regained susceptibility to infection. Population vaccination should be intensified, and early detection of new variants having the potential to affect the course of the epidemic continuously monitored, for immediate public health decision-making.

Contributors

Conceptualisation and methodology: MS, ZAR, AS. Investigation: NR, MS. Formal analysis: MS, JMR, RR, MCAV. (MS, NR and JMR have verified the underlying data). Resources and funding acquisition: MS,

VR, ZAR, AS. Supervision: MS, ZAR, AS. Writing – Original draft preparation: MS, PD, RR, AS. Writing – Review and editing: all authors.

Data sharing

Data will be made available with publication (ELISA data and de-identified participant age and gender) upon request to the corresponding author.

Declaration of Competing Interest

All authors declare no competing interests.

Acknowledgments

We thank the blood donors and RBTC staff who supported this work, importantly Drs Jocelyne Nirina ANDRIAMBELO (RBTC Toamasina), Léa Isabelle RAMANDIMBISOA (RBTC Toliara), Michael Marie Osé HARIOLY NIRINA (NRTC Antananarivo), Dr Danielle FITAHIANA (RBTC Fianarantsoa) and Pr Tahiry RABENANDRIANINA (RBTC Mahajanga).

We thank the Immunology of Infectious Diseases unit staff for performing assays, as well as the 4 laboratories in Madagascar where RT-PCRs were run particularly the IPM virology unit.

We express our gratitude to the National Institute of Statistics of Madagascar and its Director General Isaora Zefania ROMALAHY, for sharing with us the 2020 demographics of Madagascar [9].

Supplementary materials

Supplementary material associated with this article can be found, in the online version, at [doi:10.1016/j.ebiom.2021.103419](https://doi.org/10.1016/j.ebiom.2021.103419).

References

- [1] World Health Organization. WHO Coronavirus Disease (COVID-19) Dashboard. <https://covid19.who.int>. <https://covid19.who.int>.
- [2] Pollán M, Pérez-Gómez B, Pastor-Barriuso R, et al. Prevalence of SARS-CoV-2 in Spain (ENE-COVID): a nationwide, population-based seroepidemiological study. *Lancet* 2020;396:535–44.
- [3] Salje H, Kiem CT, Lefrancq N, et al. Estimating the burden of SARS-CoV-2 in France. *Science* (80-) 2020;369:208–11.
- [4] Uyoga S, Adetifa IMO, Karanja HK, et al. Seroprevalence of anti-SARS-CoV-2 IgG antibodies in Kenyan blood donors. *Science* (80-) 2020.
- [5] Filho LA, Szwarcwald CL, Mateos S de OG, et al. Seroprevalence of anti-SARS-CoV-2 among blood donors in Rio de Janeiro, Brazil. *Rev Saude Publica* 2020;54:1–10.
- [6] Anand S, Montez-Rath M, Han J, et al. Prevalence of SARS-CoV-2 antibodies in a large nationwide sample of patients on dialysis in the USA: a cross-sectional study. *Lancet* 2020;6736:1–10.
- [7] ID.VET. ID Screen SARS-CoV-2-N IgG Indirect. *SARSCOVS2 version 0419FR DOC_107142020*.
- [8] Breslow NE, Day NE, Cancer IA for R on. *Statistical methods in cancer research Volume II—the design and analysis of cohort studies* (IARC Scientific Publications). 1986.
- [9] Institut National de la Statistique (INSTAT) de Madagascar. Résultats définitifs du RGPH-3. Résultats Définitifs du RGPH-3 Tome 1 2 2020 <https://www.instat.mg/recensement-general-de-la-population-et-de-lhabitat-rgph/resultats-definitifs-rgph-3/>.
- [10] Gelman A, Hill J. *Data Analysis Using Regression and Multilevel/Hierarchical (Analytical Methods for Social researchchical)*. Cambridge Univ Press; 2006.
- [11] Ripperger TJ, Uhrlaub JL, Watanabe M, et al. Orthogonal SARS-CoV-2 serological assays enable surveillance of low prevalence communities and reveal durable humoral immunity. *Immunity* 2020. doi: [10.1016/j.immuni.2020.10.004](https://doi.org/10.1016/j.immuni.2020.10.004).
- [12] Gudbjartsson DF, Norddahl GL, Melsted P, et al. Humoral immune response to SARS-CoV-2 in Iceland. *N Engl J Med* 2020. doi: [10.1056/nejmoa2026116](https://doi.org/10.1056/nejmoa2026116).
- [13] Kutsuna S, Asai Y, Matsunaga A. Loss of Anti-SARS-CoV-2 Antibodies in Mild Covid-19. *N Engl J Med* 2020;383:1–4.
- [14] Ibarrondo FJ, Fulcher JA, Goodman-Meza D, et al. Rapid decay of Anti-SARS-CoV-2 antibodies in persons with mild covid-19. *N Engl J Med* 2020;1:10–2.
- [15] Long QX, Tang XJ, Shi QL, et al. Clinical and immunological assessment of asymptomatic SARS-CoV-2 infections. *Nat Med* 2020;26:1200–4.
- [16] Dan JM, Mateus J, Kato Y, et al. Immunological memory to SARS-CoV-2 assessed for greater than six months after infection. *bioRxiv* 2020.
- [17] Edridge AW, Kaczorowska JM, Hoste AC, et al. Coronavirus protective immunity is short-lasting. *medRxiv* 2020.05.11.20086439.
- [18] Crotty S, Felgner P, Davies H, Glidewell J, Villarreal L, Ahmed R. Cutting edge: long-term B cell memory in humans after smallpox vaccination. *J Immunol* 2003;171:4969–73.
- [19] Yu X, Tsibane T, McGraw PA, et al. Neutralizing antibodies derived from the B cells of 1918 influenza pandemic survivors. *Nature* 2008. doi: [10.1038/nature07231](https://doi.org/10.1038/nature07231).
- [20] Merow C, Urban MC. Seasonality and uncertainty in global COVID-19 growth rates. *Proc Natl Acad Sci U S A* 2020. doi: [10.1073/pnas.2008590117](https://doi.org/10.1073/pnas.2008590117).
- [21] Mercker M, Betzin U, Wilken D. What influences COVID-19 infection rates: a statistical approach to identify promising factors applied to infection data from Germany. *medRxiv*. doi: [10.1101/2020.04.14.20064501](https://doi.org/10.1101/2020.04.14.20064501).
- [22] Buss LF, Prete CA, Abraham CMM, et al. Three-quarters attack rate of SARS-CoV-2 in the Brazilian Amazon during a largely unmitigated epidemic. *Science* (80-) 2020:eabe9728.
- [23] Faria NR, Claro IM, Candido D, et al. Genomic characterisation of an emergent SARS-CoV-2 lineage in Manaus: preliminary findings. *Virological* 2021 <https://virological.org/t/genomic-characterisation-of-an-emergent-sars-cov-2-lineage-in-manaus-preliminary-findings/586>.

ANNEXE 5

Andriamandimby, S. F., Brook, C. E., Razanajatovo, N.,
Randriambolamanantsoa, T. H., Rakotondramanga, J. M.,
Rasambainarivo, F., Raharimanga, V., Razanajatovo, I. M.,
Mangahasimbola, R., Razafindratsimandresy, R., Randrianarisoa,
S., Bernardson, B., Rabarison, J. H., Randrianarisoa, M., Nasolo,
F. S., Rabetombosoa, R. M., Ratsimbazafy, A. M., Raharinosy, V.,
Rabemananjara, A. H., ... Dussart, P. (2022). Cross-sectional
cycle threshold values reflect epidemic dynamics of COVID-19 in
Madagascar. *Epidemics*, 38, 100533.
<https://doi.org/10.1016/j.epidem.2021.100533>



Cross-sectional cycle threshold values reflect epidemic dynamics of COVID-19 in Madagascar

Soa Fy Andriamandimby^{a,*}, Cara E. Brook^{b,1}, Norosoa Razanajatovo^a,
Tsiry H. Randriambolamanantsoa^a, Jean-Marius Rakotondramanga^c, Fidisoa Rasambainarivo^d,
Vaomalala Raharimanga^c, Iony Manitra Razanajatovo^a, Reziky Mangahasimbola^c,
Richter Razafindratsimandresy^a, Santatra Randrianarisoa^e, Barivola Bernardson^c,
Joelinotahiana Hasina Rabarison^a, Mirella Randrianarisoa^c, Frédéric Stanley Nasolo^a,
Roger Mario Rabetombosa^c, Anne-Marie Ratsimbazafy^a, Vololoniaina Raharinosy^a,
Aina H. Rabemananjara^a, Christian H. Ranaivoson^a, Helisoa Razafimanjato^a,
Rindra Randremanana^{a,c,2}, Jean-Michel Héraud^{f,2,3}, Philippe Dussart^{a,2}

^a Virology Unit, Institut Pasteur de Madagascar, Madagascar

^b Department of Ecology and Evolution, University of Chicago, United States

^c Epidemiology and Clinical Research Unit, Institut Pasteur de Madagascar, Madagascar

^d Department of Ecology and Evolutionary Biology, Princeton University, United States

^e Department of Veterinary Sciences and Medicine, University of Antananarivo, Madagascar

^f Virology Unit, Institut Pasteur of Dakar, Senegal

ARTICLE INFO

Keywords:

COVID-19

LMIC

Madagascar

Africa

Cycle threshold value

Cross-sectional data

ABSTRACT

As the national reference laboratory for febrile illness in Madagascar, we processed samples from the first epidemic wave of COVID-19, between March and September 2020. We fit generalized additive models to cycle threshold (C_t) value data from our RT-qPCR platform, demonstrating a peak in high viral load, low- C_t value infections temporally coincident with peak epidemic growth rates estimated in real time from publicly-reported incidence data and retrospectively from our own laboratory testing data across three administrative regions. We additionally demonstrate a statistically significant effect of duration of time since infection onset on C_t value, suggesting that C_t value can be used as a biomarker of the stage at which an individual is sampled in the course of an infection trajectory. As an extension, the population-level C_t distribution at a given timepoint can be used to estimate population-level epidemiological dynamics. We illustrate this concept by adopting a recently-developed, nested modeling approach, embedding a within-host viral kinetics model within a population-level Susceptible-Exposed-Infectious-Recovered (SEIR) framework, to mechanistically estimate epidemic growth rates from cross-sectional C_t distributions across three regions in Madagascar. We find that C_t -derived epidemic growth estimates slightly precede those derived from incidence data across the first epidemic wave, suggesting delays in surveillance and case reporting. Our findings indicate that public reporting of C_t values could offer an important resource for epidemiological inference in low surveillance settings, enabling forecasts of impending incidence peaks in regions with limited case reporting.

* Corresponding author.

E-mail address: soafy@pasteur.mg (S.F. Andriamandimby).

¹ Lead authors contributed equally.

² These senior authors contributed equally to this work.

³ Present address: Virology Department, Institut Pasteur de Dakar.

1. Introduction

Madagascar reported its first case of coronavirus disease 2019 (COVID-19) on 19 March 2020, in part with a government-sponsored surveillance platform testing all incoming international travelers (Randremanana et al., 2021). Subsequent to this introduction, the first wave of the COVID-19 epidemic was geographically staggered, with early cases in May 2020 largely concentrated in the eastern city of Toamasina, part of the Atsinanana administrative region, followed by a more severe outbreak which peaked in July 2020 in the capital city of Antananarivo, part of the Analamanga administrative region. Test positive rates exceeded 50% at the epidemic peak for both regions and at the national level, indicating widespread underreporting (Chitwood et al., 2020), a common feature of COVID-19, for which some 20–40% of infections are thought to be entirely asymptomatic (Oran and Topol, 2020; Mizumoto et al., 2020; Nishiura et al., 2020; Treibel et al., 2020). Early reporting on the first epidemic wave in Madagascar indicated an extremely high (56.6%) proportion of asymptomatic cases, based on targeted surveillance of symptomatic patients and their contacts (Randremanana et al., 2021).

Madagascar closed its borders to international air travel on 20 March 2020 and, subsequent to identification of the first case, implemented several non-pharmaceutical interventions aimed at curbing epidemic spread, including non-essential business closures, curfews, stay-at-home orders, and mandates for social distancing. These restrictions were relaxed after the first epidemic subsided in September 2020 but have since been re-implemented in the face of a second epidemic wave. In other regions of the globe, widespread efforts to estimate the effective reproduction number, R_t , for COVID-19 at national, regional, and local levels (Abbott et al., 2020b) have been used to inform public health interventions and retrospectively assess their effectiveness (Gostic et al., 2020): disease transmission rates are increasing at $R_t > 1$ and decreasing at $R_t < 1$. Estimation of R_t , or its related counterpart, r , the epidemic growth rate (Wallinga and Lipsitch, 2007; Park et al., 2020), from available case count data is challenged by limitations or variability in surveillance, uncertainty surrounding the shape of disease parameter distributions, and delays in reporting (Gostic et al., 2020). Despite the enormity of these challenges in the limited surveillance settings common to many lower- and middle-income countries (LMICs), real-time estimation of R_t from COVID-19 case-counts has been attempted for most regions of the globe (Abbott et al., 2020b) and has been implemented locally in Madagascar (Rasambainarivo et al., 2020; Raherinirina et al., 2021a,b; Narison and Maltezos, 2021).

Recent methodological advances have introduced a new resource to the epidemiological toolkit by which to conduct real time estimation of epidemic trajectories (Hay et al., 2021), one that leverages the often-discarded cycle threshold, or C_t , value, that is returned as an inverse log-10 measure of viral load from all RT-qPCR-based platforms (Tom and Mina, 2020). After observing that SARS-CoV-2 viral loads—and, as a consequence RT-qPCR C_t values—demonstrate a predictable trajectory following the onset of infection (Chen and Li, 2020; Jacot et al., 2020; Borremans et al., 2020), Hay et al., 2021 showed that the C_t value can be used as a biomarker of time since infection and, consequently, be leveraged to back-calculate infection incidence, in a manner analogous to previous work leveraging serological titer information in other systems (Borremans et al., 2016; Hay et al., 2020; Salje et al., 2018). Probabilistically, a randomly-selected infection is more likely to be early in its infection trajectory when identified during a growing epidemic and later in its trajectory in a declining epidemic (Wallinga and Lipsitch, 2007; Rydevik et al., 2016), and as a consequence, the population-level distribution of C_t values for any viral infection is expected to shift across the duration of an epidemic. Indeed, low- C_t -high-viral-load infections have been observed to coincide with growing COVID-19 epidemics and high- C_t -low-viral-load infections with declining epidemics in several settings (Jacot et al., 2020; Moraz et al., 2020; Walker et al., 2020). Exploiting this phenomenon, Hay et al.

developed a method that embeds a within-host, viral kinetics model in a population-level disease transmission model to derive epidemic trajectories from cross-sectional C_t samples. Because this method depends on quantitative information captured in the biological sample itself, rather than the relationship between case count and reporting date, C_t value estimation more accurately predicts true epidemic trajectories than traditional incidence estimation in settings with uneven surveillance (Hay et al., 2021).

During the early phase of the COVID-19 epidemic in Madagascar, the Virology Unit laboratory (National Influenza Centre) at the Institut Pasteur of Madagascar (IPM) processed the majority of all SARS-CoV-2 testing samples derived from 114 districts across 6 major provinces in the country. Consistent with findings reported elsewhere (Jacot et al., 2020; Moraz et al., 2020; Walker et al., 2020), we observed a population-level decline in C_t values derived from RT-qPCR-testing in our laboratory, coincident with the epidemic peak across the first wave of COVID-19 in Madagascar. We here adopt the methods presented by Hay et al. (2021) to estimate COVID-19 epidemic growth rates at the national level (2018 population \sim 26 million (INSTAT Madagascar., 2018)) and in two major administrative regions of Madagascar: Atsinanana (east coast of Madagascar; 2018 population \sim 1.5 million (INSTAT Madagascar., 2018)) and Analamanga (including Antananarivo, capital city; 2018 population \sim 3.6 million (INSTAT Madagascar., 2018)). We evaluate the robustness of this C_t -based method in comparison with epidemic growth rates derived from more traditional case-count methods applied to the same regions and at the national level. Atsinanana and Analamanga comprised the geographic epicenter of the first COVID-19 wave in Madagascar but also the source of the majority of samples sent for testing. Given that vast majority of testing resources across the duration of the Madagascar pandemic have been concentrated in Antananarivo (Rakotonanahary et al., 2021), ‘national’ reported trends may belie temporally lagged disease dynamics in more rural regions of the country. We advocate for more widespread C_t reporting from rural areas, as our analysis indicates that C_t -based R_t estimation could be a particularly robust method of inferring epidemiological trajectories in low-surveillance settings.

2. Materials and methods

2.1. IPM SARS-CoV-2 C_t data

Methods for collection, transport, and processing of SARS-CoV-2 testing samples at IPM have been previously described (Randremanana et al., 2021). Briefly, nasopharyngeal and oropharyngeal swabs were collected at local administrative hospitals in viral transport medium and transported at 4 °C to our laboratory for testing. Between 18 March and 30 September 2020, we conducted 34,563 RT-qPCR tests targeting the E, N, Orf1a/b, or S gene of SARS-CoV-2. These tests were carried out across 20,326 discrete samples (many of which were tested across multiple platforms targeting multiple genes), and 17,499 discrete patients, a subset of whom were tested at multiple timepoints. Earlier in March 2020, the Madagascar Ministry of Public Health screened all travelers entering the country in an effort to prevent the introduction of COVID-19 to Madagascar (Randremanana et al., 2021). Despite these efforts, the first infection with SARS-CoV-2 was first confirmed in Madagascar on 19 March 2020, after which testing efforts were refocused to screen contacts of confirmed cases, as well as any patients reporting to clinics or hospitals with symptoms aligned with pre-existing surveillance systems for influenza-like illness (ILI) and severe acute respiratory infection (SARI), following guidelines from WHO (WHO, 2020). IPM has processed samples from ILI and SARI surveillance platforms in Madagascar for over a decade; in April 2020, we added SARS-CoV-2 to the routine screening of incoming specimens (Randremanana et al., 2021; Rakotoarisoa et al., 2017; Guillebaud et al., 2018).

Due to a dearth of available reagents in the early stages of the

epidemic, our lab used seven different WHO-recommended kits and corresponding protocols (The World Health Organization (WHO), 2020) to assay infection in these samples (Randremanana et al., 2021): Charity Berlin (Corman et al., 2020), Hong Kong University (Chu et al., 2020), Da An gene (Da An Gene Co., Ltd. Sun Yatsen University, Guangzhou, China), LightMix® SarbeCoV E-gene plus EAV control (TIB Biolmol, Berlin, Germany), SarbeCoV TibMolBiol (TIB Biolmol, Berlin, Germany), TaqPath™ COVID-19 Combo kit (Life Technologies Ltd, Paisley, UK), and GeneXpert (Cepheid, Sunnyvale, CA, USA).

Some 9493 of those tests, corresponding to 5310 individuals, were RT-qPCR positive for SARS-CoV-2 infection based on the cut-off positive value for the test in question (Charity Berlin: ≤ 38 ; Hong Kong: ≤ 40 ; Da An: ≤ 40 ; LightMix SarbeCoV/SarbeCoV TibMolBiol ≤ 38 ; TaqPath ≤ 37 for 2 of 3 targets; GeneXpert: ≤ 40). All analyses presented in this paper are derived from these positive test results, as C_t -values were not reliably recorded following negative results. We further subset our data as appropriate for each analysis of interest.

2.2. Estimating growth rates from IPM case data

We first sought to obtain an estimate of new daily cases reported from our laboratory to the Malagasy government between 18 March and

30 September 2020. To this end, we reduced our dataset to include only sampling from the first reported positive test date for each unique patient; we assumed that reinfection was unlikely within the short duration of our study and that any subsequent positive tests were reflective of longer-duration infections in repeatedly sampled individuals. A patient was considered “positive” for SARS-CoV-2 infection if any test for any SARS-CoV-2 target was positive, and the results of the other samples were not inconsistent with this finding. We then summed cases by date at the national level and for two administrative regions (Atsinanana and Analamanga) that reported the majority of total cases across the study period overall. In total, 5276 cases were reported from our laboratory across the study period at the national level, 3505 in Analamanga region and 758 in Atsinanana. Daily cases for the two target regions and for the nation at large are summarized in Fig. 1.

We applied the opensource R-package EpiNow2 (Abbott et al., 2020a) to the daily incidence data to estimate the epidemic growth rate for COVID-19 across the study period. EpiNow2 builds on previous R_t estimation packages (Cori et al., 2013), using a non-stationary Gaussian process model to estimate the instantaneous time-varying reproduction number, R_t , and the corresponding time-varying epidemic growth rate, r , while incorporating uncertainty in the generation interval. Following best recommended practices (Gostic et al., 2020), we modeled the

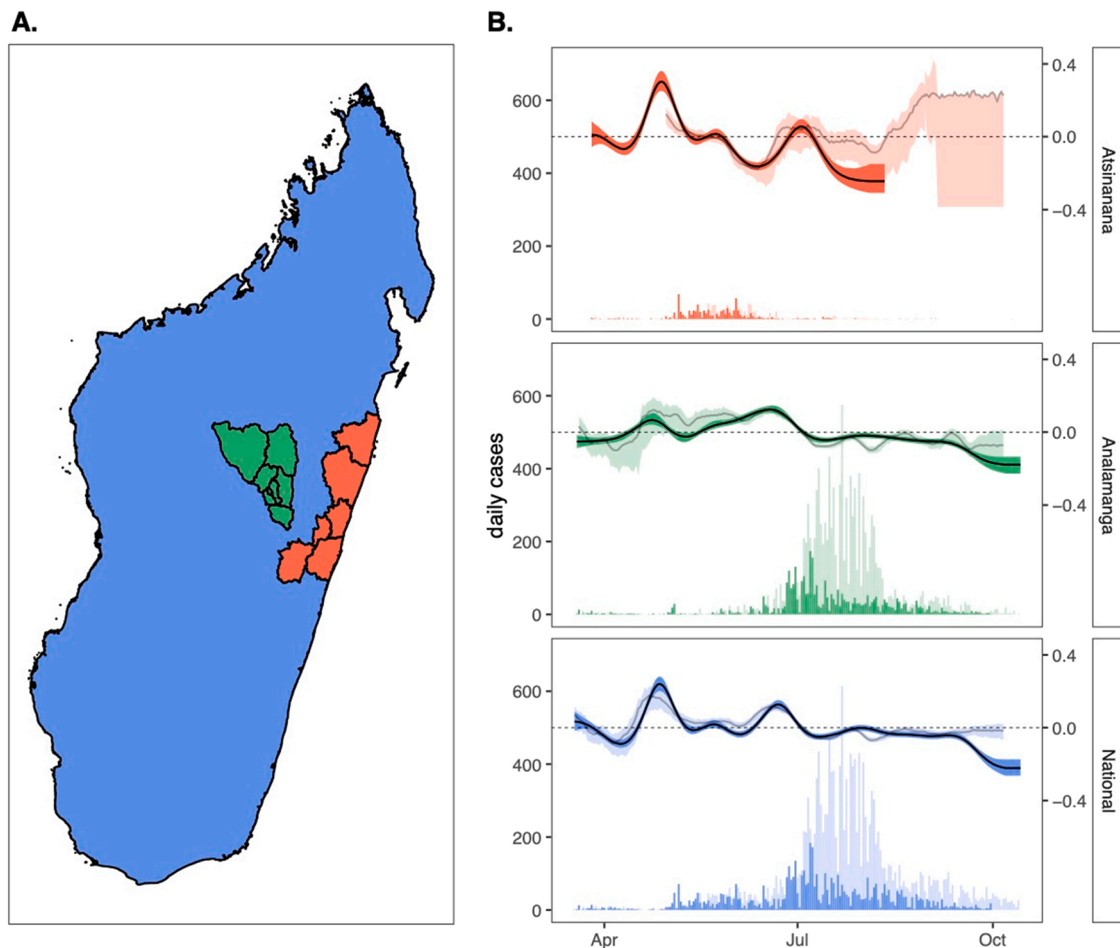


Fig. 1. Epidemic growth rate estimates from case count data across the first wave of COVID-19 in Madagascar. (A.) Map of Madagascar, colored by regions of case count tabulation, showing the Atsinanana region (orange), the Analamanga region (green), and the National region (blue); note that data analyzed at the National level includes data from both Atsinanana and Analamanga regions, as well as the rest of Madagascar. (B.) Time series of new case incidence lefthand y-axis across the first wave of COVID-19 in Madagascar (18 March – 30 September 2020), across three focal regions. Darker shading shows data derived from the IPM RT-qPCR platform, while lighter shading depicts data nationally reported and consolidated on (Rasambainarivo et al., 2020). Righthand y-axis shows corresponding epidemic growth rate computed from case count data in EpiNow2 (Abbott et al., 2020a), with darker line corresponding to computation from IPM data and lighter line to computation from publicly reported data; background shading around each line depicts the corresponding 50% quantile by EpiNow2 (Abbott et al., 2020a). (For interpretation of the references to color in this figure legend, the reader is referred to the web version of this article.)

SARS-CoV-2 incubation period as a log-normal distribution with a mean of 1.621 days ($sd = 0.064$) and a standard deviation of 0.418 days ($sd = 0.061$) (Lauer et al., 2020) and the generation time interval as a gamma distribution with a mean of 3.635 ($sd = 0.71$) and a standard deviation of 3.075 (0.77) (Ganyani et al., 2020). Since the IPM testing data reported the actual date of sample collection, no reporting delay was incorporated in our growth rate estimation.

2.3. Epidemic trajectories from publicly reported data

To compare our laboratory-derived epidemic growth estimates with those undertaken in real time in Madagascar, we collaborated with colleagues who recorded data on the number of new PCR-confirmed cases reported daily on national television by the Ministry of Health of the Government of Madagascar across the duration of the first epidemic wave. From these daily case estimates, we used the EpiNow2 package (Abbott et al., 2020a) to again estimate the epidemic growth rate across the same study period, assuming the same incubation period and general time interval referenced above (Lauer et al., 2020; Ganyani et al., 2020). For these estimates, we followed methods outlined in (Abbott et al., 2021), to additionally model a reporting delay from a log-normal distribution fit to 100 subsamples with 1000 bootstraps from a publicly available linelist that collates data globally for COVID-19 cases for which both infection onset and notification dates are available (Xu et al., 2020).

2.4. Standardizing C_t values across tests and targets

In our next series of analyses, we leveraged information captured in the individual C_t value returned from each positive test. To control for extensive variation in qPCR test and target (each of which reported varying thresholds for positivity), we carried out in vitro experiments using SARS-CoV-2 isolates from infected patients reporting similar C_t values on the TaqPath platform at the time of sampling. Briefly, three SARS-CoV-2 isolates (designated hCoV-19/Madagascar/IPM-00754/2021, hCoV-19/Madagascar/IPM-01263/2021 and hCoV-19/Madagascar/IPM-01315/2021) were obtained and cultured in Vero cells as previously described (Auerswald et al., 2021). Upon infection with SARS-CoV-2, the culture medium was replaced by infection medium containing DMEM, 5% FBS, antibiotics, 2.5 $\mu\text{g}/\text{ml}$ Amphotericin B (Gibco) and 16 $\mu\text{g}/\text{ml}$ TPCK-trypsin (Gibco). Virus-containing supernatants, as determined by the presence of cytopathic effect (CPE), were harvested 7 days after infection by centrifugation at 1500 r.p.m. for 10 min. RNA was subsequently extracted from supernatant and subjected to serial dilutions and subsequent testing on six of the seven RT-qPCR platforms used in our population-level dataset (LightMix SarbeCoV and SarbeCoV TibMolBioI were considered equivalent and tested only using the current version of the kit: SarbeCoV TibMolBioI). We fit linear mixed effect regression models in the lme4 (Bates et al., 2015) package in R to the resulting C_t curves returned from each testing platform across the dilution series and used the fitted slope and y-intercept of each regression equation to reproject all C_t values in our dataset to correspond to results returned from the TaqPath N gene test. We report, analyze, and visualize these TaqPath N-corrected C_t values in all analyses. We selected the TaqPath N gene C_t as the basis for reporting because our laboratory adopted the TaqPath assay for exclusive use after supply chains stabilized nine months into the pandemic; of the three targets returned from the TaqPath assay, the N-gene is the most common target across other SARS-CoV-2 diagnostic platforms (Kubina and Dziedzic, 2020).

2.5. Generalized additive modeling of the longitudinal C_t distribution by region

After observing a population-level dip in the average C_t value recovered from our testing platform, roughly coincident with the

epidemic peak in the three regions of interest, we asked the broad question, *what is the population level time-trend of SARS-CoV-2 C_t values across these three regions?* To address this question, we compiled all positive tests from the first date of positive testing for each patient, recording the date, region, test, and target that corresponded to each corrected C_t value, in addition to the numerical ID and the symptom status (asymptomatic, symptomatic, or unknown) of the patient from which it was derived. Symptom statuses were recorded by medical staff at the timepoint of sampling and merely indicated whether or not the patient presented with symptoms; thus, ‘asymptomatic’ classification did exclude the possibility that the same patient reported symptoms at later or earlier timepoints across the course of infection. The resulting data consisted of 8055 discrete C_t values, corresponding to 5280 patients, most of whom were tested using multiple tests and/or gene targets of interest. C_t values for these positive test results ranged from 6.36 to 39.91. When reprojected to TaqPath N levels, the range shifted from 7.82 to 39.99, such that 507 C_t values classed as “positive” by the cutoff thresholds on other platforms exceeded the $C_t \leq 37$ threshold for positivity on the TaqPath platform. These samples were nonetheless retained for generalized additive modeling (GAM) of longitudinal C_t trends but GAM-projected C_t values still exceeding the TaqPath cutoff were later excluded in mechanistic modeling of transmission trends fitted to positive data.

Using the mgcv package (Wood, 2001) in the R statistical program, we next fit a GAM in the gaussian family to the response variable of corrected C_t value, incorporating a numerical thinplate smoothing predictor of date, and random effects on the categorical variables of test (Charity Berlin, Hong Kong, Da An, LightMix SarbeCoV, SarbeCoV TibMolBio, TaqPath, or GeneXpert), target (E,N,Orf1a/b, or S), and individual patient ID. We refit the model to three different subsets of the data, encompassing the Atsinanana and Analamanga regions, as well as the entire National data as a whole. We then used the resulting fitted GAMs to simulate population-level C_t distributions for each date in our dataset, excluding the effects of test and target in the predict.gam function from mgcv. This produced a test- and target-controlled average C_t estimate for each positive patient at the timepoint of sampling. We used these GAM-simulated C_t distributions to carry out mechanistic model fitting in subsequent analyses, as described below, excluding 15 patients with C_t projections > 37 , which exceeded the positive threshold for the TaqPath N gene assay.

2.6. Generalized additive modeling of C_t value since time of infection onset

To validate observations from the literature which indicate that the viral load and corresponding C_t value follow a predictable trajectory after the onset of SARS-CoV-2 infection (Chen and Li, 2020; Jacot et al., 2020) within our own study system, we next concentrated analyses on a subset of 4822 C_t values (corresponding to 2842 unique samples derived from 2404 unique patients), for which the timing of symptom onset was also recorded. For each of these samples, we randomly drew a corresponding incubation time from the literature-derived log-normal distribution above (Lauer et al., 2020) to approximate the timing of infection onset. To answer the question, *how does C_t vary with time since symptom onset?*, we fit a GAM in the gaussian family to the resulting data with a response variable of C_t and a numerical thinplate smoothing predictor of days since infection onset, as well as random effects of test, target, and patient ID. After fitting, we used the predict.gam function from the mgcv package, excluding the effects of target and test, to produce a distribution of C_t values corresponding to times since symptom onset (one per each unique patient ID). We used these C_t trajectories to estimate parameters for the within-host viral kinetics model described in final methods section below.

2.7. Generalized additive modeling of the relationship between C_t value and symptom status

We next asked the question, *does C_t value vary in symptomatic vs. asymptomatic cases?*

Our first investigation of this question required only reconsideration of the individual trajectory GAM described above to include additional predictor variables of age and symptom status, in addition to days since infection onset, target, and test. Since symptom status was recorded only at the first timepoint of sampling for each individual, we limited our individual trajectory dataset to a 4072 datapoint subset of C_t values from 2404 discrete patients reporting both date of symptom/infection onset and symptom status at the timepoint of sampling; as mentioned previously, ‘asymptomatic’ classification in our dataset included patients reporting symptoms from earlier or later timepoints prior to or following the sampling date. Thus, this GAM tested whether symptom status and C_t value interacted merely as a function of the timing since symptom onset (e.g. high C_t values were recovered from patients either very early or late in their infection trajectory), or whether independent interactions between symptomatic vs. asymptomatic infections and C_t were also present, while also controlling for age.

After observing results, we extended this analysis by applying another GAM in the gaussian family to a 7937 datapoint subset of the data used to model longitudinal C_t trajectories at the National level, which additionally reported symptom status (symptomatic vs. asymptomatic) at the timepoint of first sampling for 5202 unique patients. Corrected C_t values in this data subset ranged between 7.82 and 39.99. This GAM incorporated a response variable of C_t and random effects predictor smoothing terms of symptom status, test, target, and patient ID, as well as a numerical smoothing predictor for age of the infected patient.

2.8. Estimating epidemic growth rates from cross-sectional C_t values

Finally, following newly-developed methods (Hay et al., 2021), we sought to estimate the epidemic growth rate across our three regions of interest using cross-sectional C_t distributions and compare these results against estimates derived from the case count methods described above. In their original paper, Hay et al. (2021) applied two population-level models (a Susceptible-Exposed-Infectious-Recovered [SEIR] model and a more flexible Gaussian process [GP] model) to a time-series of infected cases from the Brigham and Women’s Hospital, Boston, MA, each reporting a quantitative estimate of viral load by C_t value. Rather than assuming all infectious (“I” class) individuals contributed equally to onward transmission, as is standard in compartmental modeling, Hay et al. (2021) nested a separate within-host viral kinetics model describing the mean trajectory a SARS-CoV-2-infected patient’s viral load (as indicated by C_t -value) across the timecourse of infection within their infectious (I) class. By fitting this within-host model to the quantitative data encapsulated in a C_t -value datapoint, the authors were able to back-infer the duration of time since the original infection occurred and the trajectory of viral load-dependent infectiousness for each positive patient, allowing for accurate estimation of epidemic trajectories independent of delays and biases in reporting (Hay et al., 2021).

To this end, we adopted the method developed in Hay et al. (2021), first fitting the within-host viral kinetics model to the test- and target-controlled C_t values produced from the above GAM describing C_t as a function of time since infection. We used the resulting parameter estimates as informed priors (Table S1) which we next incorporated into the same two population-level SARS-CoV-2 transmission models defined by Hay et al (2021), here applied to our time series data across the three Madagascar regions: a compartmental SEIR model and a GP model, which makes no assumptions about the specific mechanisms underlying an epidemic trajectory beyond the correlation of cases from one time-step to the next. Given uncertainty in the epidemiology underlying COVID-19 dynamics in Madagascar and other parts of Africa (Evans

et al., 2020), we anticipated that the GP model would offer the most flexible fit to the data. Beyond the viral kinetics parameters, we adopted less-constrained priors from the original paper (Hay et al., 2021) for other epidemiological parameters included in both population-level models (Table S1), then re-fit both transmission models in turn to cross-sectional weekly C_t distributions derived from the Atsinanana, Analamanga, and National-level datasets. We fit both models to each dataset using an MCMC algorithm derived from `lazymcmc` R-package (Hay, 2020), as described in the original paper (Hay et al., 2021), applying the default algorithm to the GP fit and a parallel tempering algorithm able to accurately parse multimodal posterior distributions to the SEIR fit. Four MCMC chains were run for 500,000 iterations in the case of the GP model and three MCMC chains for 80,000 iterations each in the case of the SEIR model, then evaluated for convergence via manual inspection of the resulting trace plots and verification that the potential scale reduction factor, had a value < 1.1 and the effective population size had a value > 200 for all parameters estimated.

After confirming chain convergence, we computed epidemic growth rates from the resulting estimated infection time series and compared results with those derived using more traditional case count methods outlined above. Code and supporting datasets needed to reproduce all analyses are available for download on our opensource GitHub repository at: github.com/carabrook/Mada-Ct-Distribute.

3. Results

3.1. Epidemic trajectories from case count data

The first wave of COVID-19 infections in Madagascar, between March and September 2020, was characterized by two subsequent outbreaks: one early, May 2020 peak centered in the eastern port city of Toamasina (region Atsinanana), followed by a second peak in July centered in the capital city of Antananarivo (region Analamanga) (Fig. 1) (Randremana et al., 2021). Estimation of the epidemic growth rate showed broad agreement in trends at both the national and regional levels, whether computed from IPM testing data assuming perfect reporting of testing date, or from publicly reported national data, including a reporting delay parameterized from a global opensource database (Fig. 1) (Xu et al., 2020). Since IPM data comprised just over 30% of nationally reported data throughout the first six months of the Madagascar epidemic, this concurrence in growth rates was unsurprising but nonetheless validates the applicability of the globally parameterized reporting delay for use in Madagascar. In both datasets, we estimated the national level epidemic growth rate to be increasing in the months preceding the two epidemic sub-peaks (in April and in June) and declining beginning in mid-July after the last peak in national case counts (Fig. 1). When IPM data were considered at the regional level, we discovered the April peak to be concentrated in Atsinanana, preceding the Toamasina outbreak and the June peak to be concentrated in Analamanga preceding the Antananarivo outbreak. Growth rate estimation from publicly reported data confirmed this pattern for Analamanga but was not possible for the Atsinanana region due to a lack of clarity in regional reporting; indeed, nearly 70% of nationally reported data in the public dataset were derived from the Analamanga region.

3.2. Standardizing C_t values across tests and targets

All RT-qPCR platforms used in our laboratory demonstrated increases in C_t value corresponding to 10-fold dilutions of RNA extracted from the original virus isolate (Table S2), though the estimated slope and y-intercept of each regression varied across the tests and targets considered, with the steepest slope recovered from GeneXpert N-gene tests and the shallowest from the Hong Kong ORF1a/b kits (Fig. S1, Table S3). We used the corresponding slope and y-intercept for each test and platform to transform C_t values in all subsequent analyses into values predicted for a TaqPath N-gene platform.

3.3. Longitudinal population-level trends in SARS-CoV-2 C_t values across the epidemic wave

We observed a population-level dip in C_t values obtained from our SARS-CoV-2 RT-qPCR platform concurrent with the regional peak in cases in May for Atsinanana and June for Analamanga, with both peaks observable in the National data (Fig. 2A). GAMs fit to Atsinanana, Analamanga, and National data subsets explained, respectively, 98.8%, 98.9%, and 98.9% of the deviation in the data (Table S4). All three GAMs demonstrated statistically significant effects of date, test, and individual patient ID, which contributed to the total deviance capture by each model. GAMs fit to the Analamanga and National data subsets showed an additional significant effect of target on the C_t value. Partial effects plots were computed from the resulting GAMs (Fig. S2) following methods described in (Mollentze and Streicker, 2020) and demonstrated no significant effects of any particular test or target gene. In general, most variation in C_t value beyond that of the individual patient was driven by the significant effect of date across all regions (Table S4).

3.4. Individual trends in SARS-CoV-2 C_t values across the trajectory of infection

The SARS-CoV-2 C_t value also demonstrated a predictable trajectory from the timing of onset of infection. Our GAM fit to data reporting a date of symptom onset (which we converted to a date of infection onset) and incorporating a predictor smoothing term of days since infection onset, and random effects of test, target, and patient ID explained 92.7% of the deviance in the data and demonstrated statistically significant

effects of all predictor variables, including days since infection onset (Table S5). These findings confirmed that C_t value can be used as a biomarker of time since infection, validating the applicability of methods outlined in (Hay et al., 2021) for our Madagascar data.

3.5. Relationship between symptom status and SARS-CoV-2 C_t value

As an extension of the individual trajectory analysis, we hypothesized that C_t value would likely be linked to symptom status, since many infection trajectories begin with a brief presymptomatic phase, progress to symptom presentation, then become asymptomatic during recovery (Chen and Li, 2020; Jacot et al., 2020). The first GAM we employed to address this question considered age and symptom status as additional predictor variables in our individual trajectory analysis. This final GAM explained 98.5% of the deviation in the data and included significant effects of days since infection onset, symptom status, test, target, and patient ID (Table S5). Despite the significance of symptom status as a predictor variable in the GAM overall, partial effects plots demonstrated no significant association between asymptomatic status and high C_t values or symptomatic status and low C_t values, while controlling for age (Fig. 2B–D). These results suggest that, in our dataset, C_t value varies predictably with an individual's infection trajectory regardless of symptom classification or age of the patient, further validating its adoption as a robust biomarker of time since infection (Table S5).

We additionally extended this analysis to our National-level C_t dataset, including a predictor variable of symptom status, in addition to test, target, patient age, and patient ID in longitudinal GAMs. This model explained 98.9% of the deviation witnessed in the data, including

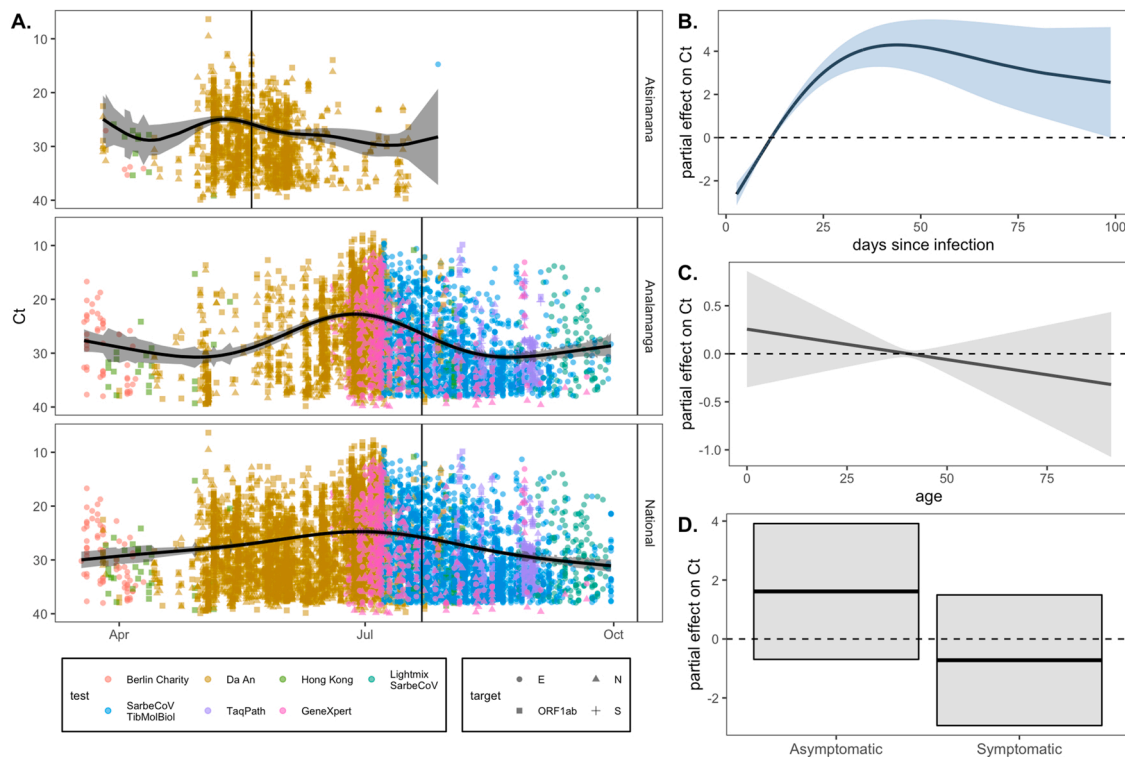


Fig. 2. RT-qPCR SARS-CoV-2 C_t value as a biomarker of population-level epidemic pace and individual infection trajectory. (A.) Population-level SARS-CoV-2 corrected C_t values from IPM RT-qPCR platform across three Madagascar regions from March–September 2020. C_t values are colored by the test and shaped by the target from which they were derived (legend), though note that all C_t values were first corrected to TaqPath N gene range. The vertical, black line gives the date of peak case counts per region in the IPM dataset, from which these C_t values were derived (May 20, 2020 for Atsinanana and July 22, 2020 for both Analamanga and National). The black, horizontal curve gives the output from a gaussian GAM fit to these data (Table S4), excluding the effects of target and test, which were also included as predictors in the model; 95% confidence intervals by standard error are shown in translucent shading. Partial effects of each predictor are visualized in Fig. S2. Righthand plots visualize partial effects of (B.) days since infection, (C.) patient age, and (D.) patient symptom status on C_t value from our individual trajectory GAM (Table S5). Significant predictors are depicted in light blue and non-significant in gray (Table S5). (For interpretation of the references to color in this figure legend, the reader is referred to the web version of this article.)

significant effects of test, target, patient ID, and symptom status (Table S6). Test and target were here included as control variates only and cannot be considered for prediction, as both co-varied with date, which was not used as a predictor in this model. In this model, partial effects plots indicated a significant association of asymptomatic status with high C_t values and symptomatic status with low C_t values (Fig. S3), even when controlling for effects of age; as this larger dataset did not report date of symptom/infection onset, it is likely that this association co-varied with the timing of infection onset, suggesting that previous reports of a high proportion of asymptomatic infections in Madagascar (Randremarana et al., 2021) could reflect a high proportion of pre- or post-symptomatic infections.

3.6. Epidemiological dynamics inferred from cross-sectional C_t distributions

After confirming the predictable pattern of C_t value across an individual's infection trajectory, and the predictable decline in population-level C_t in conjunction with the epidemic peak, we used our individual trajectory GAM to simulate a distribution of C_t values across a 50-day duration of infection and fit the within-host viral kinetics model described in (Hay et al., 2021) to the resulting data (Fig. S4). The model demonstrated a good fit to the data, and estimated posterior distributions for viral kinetics parameters were largely on par with those used previously in models of SARS-CoV-2 dynamics in Massachusetts, though the modal C_t value at peak viral load was slightly lower in our Madagascar dataset (Fig S4; Table S1).

After fitting the within-host model, we next used longitudinal population-level GAMs (Fig. S2) to generate weekly cross-sectional C_t

distributions, controlled for test and target, across our three regions of interest. As expected, weekly cross-sectional C_t distributions demonstrated a shift across the duration of the epidemic wave; with lower C_t values temporally correlated with high growth rates estimated from case count data (Fig. 3).

Finally, we used the viral kinetics posterior distributions resulting from the within-host viral kinetics model fit as prior inputs into SEIR and GP population-level epidemiological models, which we fit to the weekly cross-sectional C_t data. MCMC chains generated in the fitting process demonstrated good convergence (Fig. S5, Tables S7 and S8) and produced posterior distributions for all parameters on par with those estimated in previous work (Table S1, Fig. S6), which effectively recaptured cross-sectional C_t value histograms across the target timeseries in all three regions (Figs. 3, S7–S9) (Hay et al., 2021). From the resulting fitted models, we simulated epidemic incidence curves, which we used to compute growth rate estimates across the duration of the first epidemic wave in each of the three regions (Fig. 4). We compared these estimates to growth rates inferred from case count data; patterns from both SEIR and GP models were largely complementary, though, as expected, the more flexible GP model demonstrated less extreme variation in epidemic growth rate. Both C_t -model fits demonstrated similar patterns to epidemic trajectories estimated from incidence data, with increasing growth rates in the months preceding both epidemic sub-peaks (April and June) and decreasing growth rates beginning in July. Nonetheless, growth rate estimates derived from the C_t model slightly preceded those estimated from case count data. The C_t model fits further predicted uncertainty in growth rate directionality towards the end of the study period for the Analamanga and National-level data, while incidence estimation projected decreasing cases at this time. This finding suggests

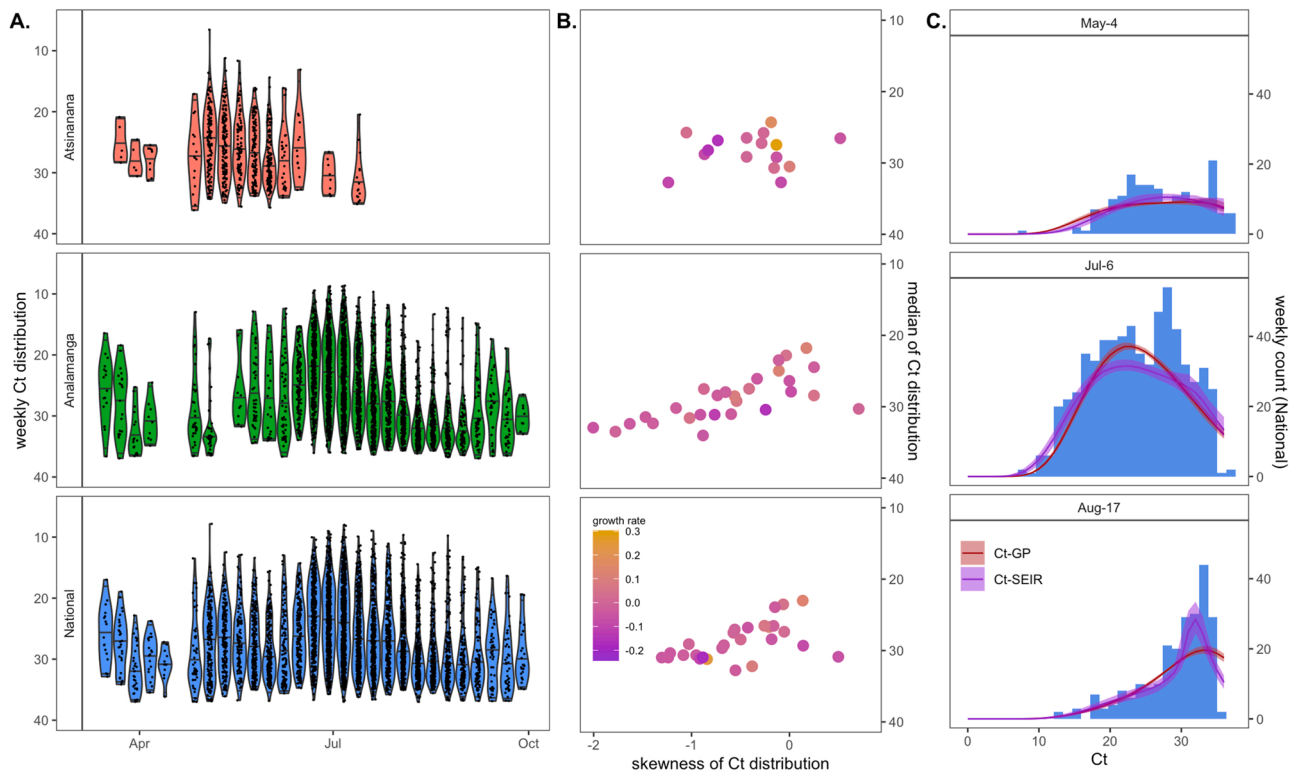


Fig. 3. Population-level C_t distribution reflects epidemic dynamics of the first wave of COVID-19 across three Madagascar regions. (A.) Simulated weekly C_t distributions by Madagascar region, derived from population-level longitudinal GAMs (Fig. 2A), excluding random effects of test and target. (B.) Higher skew and lower median C_t from each cross-sectional C_t distribution in (A.) were loosely associated with higher epidemic growth rates from the corresponding week, here derived from EpiNow2 estimation from IPM case count data (Fig. 1B.) (C.) Cross-sectional C_t distributions from Analamanga time series in (A.) were fit via Gaussian process (GP) and SEIR mechanistic models incorporating a within-host viral kinetics model. Modeled C_t distributions are shown as solid lines (GP = red; SEIR = purple), with 95% quantiles in surrounding sheer shading. Both models effectively recapture the shape of the C_t histogram as it changes (skews left) across the duration of the first epidemic wave. Model fits to the full time series of C_t histograms across all three regions are visualized in Figs. S7–S9. (For interpretation of the references to color in this figure legend, the reader is referred to the web version of this article.)

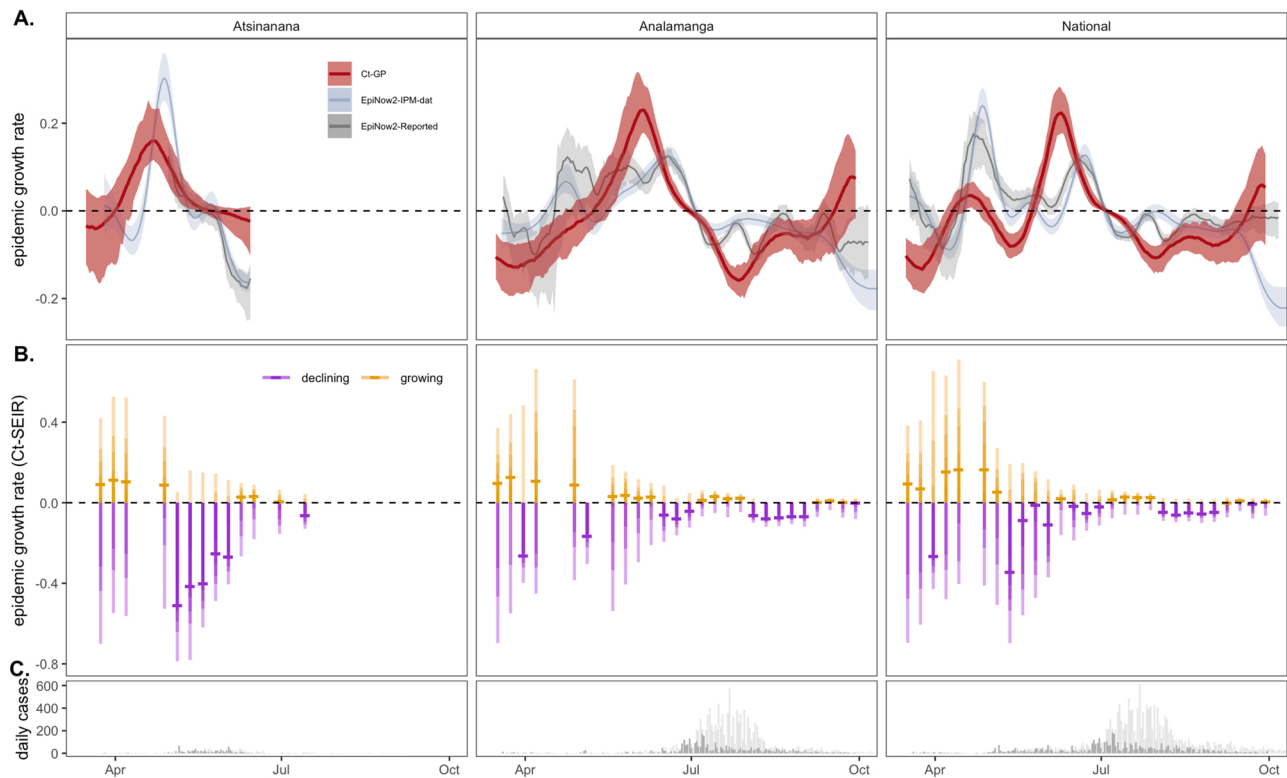


Fig. 4. Epidemic growth rate estimates from mechanistic model fits to population-level C_t distributions across the first wave of COVID-19 in three Madagascar regions. (A.) Comparison of COVID-19 epidemic growth rates from March–September 2020, estimated from IPM (blue) and publicly reported (gray) case count data using EpiNow2 (Abbott et al., 2020a) with estimates derived from Gaussian process (GP; red) mechanistic model fit to the time series of C_t distributions (Fig. 3A). Median growth rates are shown as solid lines, with 50% quantile on case-based estimates and 95% quantile of the posterior distributions from C_t -based estimates in corresponding sheer shading. (B.) Growth rate estimates from individual SEIR C_t -model fits to each C_t -distribution shown in Fig. 3A; median growth rates are given as horizontal dashes, with the 95%, 70%, 50%, and 20% of the posterior distribution indicated by progressively darker coloring. Estimates > 0 (indicating growing epidemics) are depicted in gold and < 0 (indicating declining epidemics) in purples. (C.) Raw case count data from the time series (dark = IPM data; light = publicly reported data) is shown for reference. (For interpretation of the references to color in this figure legend, the reader is referred to the web version of this article.)

that cross-sectional C_t distributions indicated a possible epidemic resurgence which was overlooked by growth rates estimated from declining incidence. If incidence declined in part due to declining surveillance, as was the reality at the end of Madagascar’s first epidemic wave (Randremanana et al., 2021), only the C_t method remained robust to the possibility of epidemic renewal.

4. Conclusions

Real-time estimation of epidemiological parameters, including the time-varying effective reproduction number, R_b , and the related instantaneous epidemic growth rate, r , has played an important role in guiding public health interventions and policies across many epidemic outbreaks, including COVID-19 (Cauchemez et al., 2006; Kucharski et al., 2020; Pan et al., 2020). In Madagascar, an opensource platform (Rasambainarivo et al., 2020) was developed shortly after the introduction of COVID-19 in March 2020, to collate and visualize publicly reported data and estimate R_t using traditional methods applied to daily reported incidence (Abbott et al., 2020a; Cori et al., 2013). We here compare the results from this platform applied to the first epidemic wave in Madagascar, with new estimates of the time-varying epidemic growth rate applied to our own laboratory data across the first epidemic wave—including those derived using a novel method based on the cross-sectional C_t value distribution at the time of sampling (Hay et al., 2021).

We find our new estimates to be largely congruent with those predicted from publicly reported data, demonstrating a pattern of increasing epidemic growth rates prior to a peak in cases, which occurred first in May 2020 in the Atsinanana region, followed by a

second outbreak in July 2020 in the Analamanga region. Critically, our growth rate estimates derived using novel methods applied to the C_t distribution over time slightly precede those estimated from incidence data. As previous work has demonstrated C_t estimation to offer a more robust approximation of true dynamics under limited surveillance scenarios (Hay et al., 2021), these findings suggest that incidence-based methods to estimate epidemic trajectories in Madagascar may be underestimating the true pace of the epidemic, likely as a result of underreporting. Additionally, C_t -based methods adopted by a single laboratory allow for estimation of epidemic growth rates even in the absence of publicly reported case counts: in October 2020, the Malagasy Ministry of Health shifted its daily COVID-19 case notifications to weekly, interfering with incidence-based approaches to estimate epidemic trajectories (Rasambainarivo et al., 2020). C_t -based approaches, instead, should be robust to this variation in reporting, offering a powerful tool for public health efforts in low surveillance settings. Indeed, our analysis demonstrates that C_t -based epidemic growth rates show uncertain directionality towards the end of the first wave of COVID-19 in Madagascar, presaging eventual epidemic resurgence, while incidence-based rates categorically declined due to both truly declining cases and declining surveillance. Incidence-based growth rate estimation ceased during the continued limited surveillance period from October 2020 through March 2021 (Rasambainarivo et al., 2020); had C_t -based methods been available at the time, it is possible that the current second wave could have been predicted and mitigated by earlier rollout of public health interventions.

Statistical analysis of our C_t data indicates that C_t values vary predictably with days since onset of infection, allowing viral kinetics data to be leveraged for population-level estimation of epidemiological

patterns. In our system, this pattern held even after controlling for the effects of age and symptom status on the C_t trajectory, further validating the applicability of C_t value as an indicator of time since infection. Nonetheless, in future work, it may be possible to fit unique viral kinetics trajectories for different classes of people; for example, older age cohorts or cohorts of people infected with more transmissible variants may be better represented by lower average C_t trajectories than the population as a whole (Jacot et al., 2020; Kidd et al., 2021). Our application of generalized additive models to both individual infection trajectory and population-level C_t distributions offers an effective means by which to control for variation in test and target across diverse RT-qPCR platforms to generate C_t values for epidemiological inference which represent a reliable average of population-level patterns overall.

We acknowledge the limitations of our current method, especially as it relates to testing biases. Nearly two-thirds of both case data and C_t -value data were derived from Madagascar's Analamanga region, including the capital city of Antananarivo; as such, national trends are strongly influenced by the Antananarivo epidemic and may belie more time-lagged dynamics in more rural, less connected regions of the country. Nonetheless, these biases are unlikely to seriously impact inference from the early stages of the Madagascar epidemic, which began with an introduction event in Antananarivo (Randremanana et al., 2021), and despite the concentration of testing resources in the Analamanga (Rakotonanahary et al., 2021), our C_t -based estimation methods applied to the national dataset were nonetheless able to detect the epidemic in the Atsinanana region, too. During the earliest phases of the epidemic in Madagascar, testing resources were limited in our laboratory, which may have additionally biased sample intake towards high-viral-load, low- C_t -value cases that could bias epidemiological inference towards increasing growth rates even after the epidemic has, in reality, already begun to decline. As the epidemic ensued, however, the Madagascar Ministry of Health focused sampling on symptomatic patients and their suspected contacts, leading to a high proportion (56.6%) of reported asymptomatic infections in our dataset (Randremanana et al., 2021), which may have instead prematurely biased inference towards a declining epidemic. Nonetheless, our C_t -based projections of epidemic trajectories do not appear to underestimate realized trends, suggesting that our method was robust to these inconsistencies.

We apply a novel method leveraging within-host viral load data that is currently largely overlooked in the epidemiological literature to describe the dynamics of the first wave of COVID-19 in Madagascar. Our approach validates an important new tool for epidemiological inference of ongoing epidemics, particularly applicable to limited surveillance settings characteristic of many lower- and middle- income countries. We advocate for public release of real time data describing the C_t value distribution, in addition to daily case counts, to improve epidemiological inference to guide public health response and intervention.

CRediT authorship contribution statement

Soa Fy Andriamandimby: Conceptualization, Validation, Formal analysis, Investigation, Resources, Data curation, Writing – review and editing, Supervision, Project administration. **Cara E. Brook:** Conceptualization, Methodology, Software, Formal analysis, Writing – original draft, Visualization. **Noroso Razanajatovo:** Investigation, Validation, Resources, Supervision, Project administration. **Tsiry H. Randriambolamanantsoa:** Investigation, Resources. **Jean-Marius Rakotondramanga:** Data curation, Supervision. **Fidisoa Rasambainarivo:** Resources. **Vaomalala Raharimanga:** Data curation, Supervision. **Iony Manitra Razanajatovo:** Investigation, Validation, Resources, Supervision, Project administration. **Reziky Mangahasimbola:** Data curation, Supervision. **Richter Razafindratsimandresy:** Investigation, Validation, Resources, Supervision, Project administration. **Santatra Randrianarisoa:** Resources. **Barivola Bernardson,** Data curation, Supervision. **Joelinotahiana Hasina Rabarison:** Investigation,

Validation, Resources, Supervision, Project administration. **Mirella Randrianarisoa:** Data curation, Supervision. **Frédéric Stanley Nasolo:** Data curation. **Roger Mario Rabetombosoa:** Data curation, Supervision. **Anne-Marie Ratsimbazafy:** Investigation. **Vololoniaina Raharinosy:** Investigation. **Aina H. Rabemananjara:** Investigation. **Christian H. Ranaivoson:** Investigation. **Helisoa Razafimanjato:** Investigation. **Rindra Randremanana:** Supervision. **Jean-Michel Héraud:** Funding acquisition, Supervision, Validation, Resources, Project administration. **Philippe Dussart:** Supervision, Resources, Project administration.

Declaration of Competing Interest

The authors declare that they have no known competing financial interests or personal relationships that could have appeared to influence the work reported in this paper.

Acknowledgments

This work was supported by the US National Institutes of Health [1R01AI29822-01] United States; the Bill & Melinda Gates Foundation, Seattle, WA [GCE OPP1211841] - United States; the Innovative Genomics Institute at UC Berkeley, Berkeley, CA [COVID-19 Rapid Response Grant] and the Chan Zuckerberg Biohub (gift for COVID-19 response efforts). The authors thank Malavika Rajeev, Tanjona Ramiadantsoa, and Benjamin Rice for help in establishing the Madagascar COVID-19 dashboard.

Appendix A. Supplementary material

Supplementary data associated with this article can be found in the online version at doi:10.1016/j.epidem.2021.100533.

References

- Abbott, S., Hellewell, J., Sherratt, K., Gostic, K., Hickson, J., Badr, H.S., DeWitt, M., Thompson, R., EpiForecasts, Funk, S., 2020a. EpiNow2: Estimate Real-Time Case Counts and Time-varying Epidemiological Parameters.
- Abbott, S., Hellewell, J., Thompson, R.N., Sherratt, K., Gibbs, H.P., Bosse, N.I., Munday, J.D., Meakin, S., Doughty, E.L., Chun, J.Y., Chan, Y.-W.D., Finger, F., Campbell, P., Endo, A., Pearson, C.A.B., Gimma, A., Russell, T., Modelling Group, C.C., Flasche, S., Kucharski, A.J., Eggo, R.M., Funk, S., 2020b. Temporal Variation in Transmission During the COVID-19 Outbreak.
- Abbott, S., Hellewell, J., Thompson, R.N., Sherratt, K., Gibbs, H.P., Bosse, N.I., Munday, J.D., Meakin, S., Doughty, E.L., Chun, J.Y., Chan, Y.D., Finger, F., Campbell, P., Endo, A., Pearson, C.A.B., Gimma, A., Russell, T., Covid, C., Flasche, S., Kucharski, A.J., Eggo, R.M., Funk, S., 2021. Estimating the time-varying reproduction number of SARS-CoV-2 using national and subnational case counts. *Wellcome Open Res.* 1–10.
- Auerswald, H., Yann, S., Dul, S., In, S., Dussart, P., Martin, N.J., Karlsson, E.A., Garcia-Rivera, J.A., 2021. Assessment of inactivation procedures for SARS-CoV-2. *J. Gen. Virol.* 102, 1–5. <https://doi.org/10.1099/JGV.0.001539>.
- Bates, D., Mächler, M., Bolker, B.M., Walker, S.C., 2015. Fitting linear mixed-effects models using lme4. *J. Stat. Softw.* 67, 1–48. <https://doi.org/10.18637/jss.v067.i01>.
- Borremans, B., Gamble, A., Prager, K.C., Helman, S.K., McClain, A.M., Cox, C., Savage, V., Lloyd-Smith, J.O., 2020. Quantifying antibody kinetics and rna detection during early-phase SARS-CoV-2 infection by time since symptom onset. *ELife* 9, 1–27. <https://doi.org/10.7554/ELIFE.60122>.
- Borremans, B., Hens, N., Beutels, P., Leirs, H., Reijnders, J., 2016. Estimating time of infection using prior serological and individual information can greatly improve incidence estimation of human and wildlife infections. *PLoS Comput. Biol.* 12, e1004882 <https://doi.org/10.1371/journal.pcbi.1004882>.
- Cauchemez, S., Boëlle, P.Y., Donnelly, C.A., Ferguson, N.M., Thomas, G., Leung, G.M., Hedley, A.J., Anderson, R.M., Valleron, A.J., 2006. Real-time estimates in early detection of SARS. *Emerg. Infect. Dis.* 12, 110–113. <https://doi.org/10.3201/eid1201.050593>.
- Chen, Y., Li, L., 2020. SARS-CoV-2: virus dynamics and host response. *Lancet Infect. Dis.* 2019 (2019–2020) [https://doi.org/10.1016/S1473-3099\(20\)30235-8](https://doi.org/10.1016/S1473-3099(20)30235-8).
- Chitwood, M.H., Russi, M., Gunasekera, K., Havumaki, J., Pitzer, V.E., Warren, J.L., Weinberger, D.M., Cohen, T., Menzies, N.A., 2020. Menzies3, Bayesian nowcasting with adjustment for delayed and incomplete reporting to estimate COVID-19 infections in the United States. *MedRxiv* 20, 1–6. <https://doi.org/10.18907/jjrs.20.7.624.5>.
- Chu, D.K.W., Pan, Y., Cheng, S.M.S., Hui, K.P.Y., Krishnan, P., Liu, Y., Ng, D.Y.M., Wan, C.K.C., Yang, P., Wang, Q., Peiris, M., Poon, L.L.M., 2020. Molecular diagnosis

- of a novel coronavirus (2019-nCoV) causing an outbreak of pneumonia. *Clin. Chem.* 66, 549–555. <https://doi.org/10.1093/clinchem/hvaa029>.
- Cori, A., Ferguson, N.M., Fraser, C., Cauchemez, S., 2013. A new framework and software to estimate time-varying reproduction numbers during epidemics. *Am. J. Epidemiol.* 178, 1505–1512. <https://doi.org/10.1093/aje/kwt133>.
- Corman, V.M., Landt, O., Kaiser, M., Molenkamp, R., Meijer, A., Chu, D.K.W., Bleicker, T., Brünink, S., Schneider, J., Schmidt, M.L., Mulders, D.G.J.C., Haagmans, B.L., Van Der Veer, B., Van Den Brink, S., Wijsman, L., Goderski, G., Romette, J.L., Ellis, J., Zambon, M., Peiris, M., Goossens, H., Reusken, C., Koopmans, M.P.G., Drosten, C., 2020. Detection of 2019 novel coronavirus (2019-nCoV) by real-time RT-PCR. *Eurosurveillance* 25. <https://doi.org/10.2807/1560-7917.ES.2020.25.3.2000045>.
- Evans, M.V., Garchitorena, A., Rakotonanahary, R.J.L., Drake, J.M., Andriamihaja, B., Rajaonarifara, E., Ngonghala, C.N., Roche, B., Bonds, M.H., Rakotonirina, J., 2020. Reconciling model predictions with low reported cases of COVID-19 in Sub-Saharan Africa: insights from Madagascar. *Glob. Health Action* 13. <https://doi.org/10.1080/16549716.2020.1816044>.
- Ganyani, T., Kremer, C., Chen, D., Torneri, A., Faes, C., Wallinga, J., Hens, N., 2020. Estimating the generation interval for coronavirus disease (COVID-19) based on symptom onset data, March 2020. *Eurosurveillance* 25, 1–8. <https://doi.org/10.2807/1560-7917.ES.2020.25.17.2000257>.
- Gostic, K.M., McGough, L., Baskerville, E.B., Abbott, S., Joshi, K., Tedijanto, C., Kahn, R., Niehus, R., Hay, A., De Salazar, P.M., Hellewell, J., Meakin, S., Munday, J.D., Bosse, N.I., Sherrat, K., Thompson, R.N., White, L.F., Huisman, J.S., Scire, J., Bonhoeffer, S., Stadler, T., Wallinga, J., Funk, S., Lipsitch, M., Cobey, S., 2020. Practical considerations for measuring the effective reproductive number. *Rt. PLoS Comput. Biol.* 16, e1008409. <https://doi.org/10.1371/journal.pcbi.1008409>.
- Guillebaud, J., Bernardson, B., Randriambolanantsoa, T.H., Randrianasolo, L., Randriamampionona, J.L., Marino, C.A., Rasolofy, V., Randrianarivelosia, M., Vigan-Womas, I., Stivaktas, V., Venter, M., Piola, P., Héraud, J.M., 2018. Study on causes of fever in primary healthcare center uncovers pathogens of public health concern in Madagascar. *PLoS Negl. Trop. Dis.* 12, 1–15. <https://doi.org/10.1371/journal.pntd.0006642>.
- Hay, J.A., Kennedy-Shaffer, L., Kanjilal, S., Lennon, N.J., Gabriel, S.B., Lipsitch, M., Mina, M.J., 2021. Estimating epidemiologic dynamics from cross-sectional viral load distributions. *Science* (80-).
- Hay, J.A., Minter, A., Ainslie, K.E.C., Lessler, J., Yang, B., Cummings, D.A.T., Kucharski, A.J., Riley, S., 2020. An open source tool to infer epidemiological and immunological dynamics from serological data: serosolver. *PLoS Comput. Biol.* 16, 1–24. <https://doi.org/10.1371/journal.pcbi.1007840>.
- Hay, J., 2020. lazymcmc. (<https://github.com/jameshay218/lazymcmc>).
- Jacot, D., Greub, G., Jaton, K., Opota, O., 2020. Viral load of SARS-CoV-2 across patients and compared to other respiratory viruses. *Microbes Infect.* 22, 617–621. <https://doi.org/10.1016/j.micinf.2020.08.004>.
- Kidd, M., Richter, A., Best, A., Cumley, N., Mirza, J., Percival, B., Mayhew, M., Megram, O., Ashford, F., White, T., Moles-Garcia, E., Crawford, L., Bosworth, A., Atabani, S.F., Plant, T., McNally, A., 2021. S-Variant SARS-CoV-2 lineage B.1.1.7 is associated with significantly higher viral load in samples tested by TaqPath Polymerase Chain Reaction. *J. Infect. Dis.* 223. <https://doi.org/10.1093/infdis/jiab082>.
- Kubina, R., Dziedzic, A., 2020. Molecular and serological tests for COVID-19. A comparative review of SARS-CoV-2 coronavirus laboratory and point-of-care diagnostics. *Diagnostics* 10.
- Kucharski, A.J., Russell, T.W., Diamond, C., Liu, Y., Edmunds, J., Funk, S., Eggo, R.M., Sun, F., Jit, M., Munday, J.D., Davies, N., Gimma, A., van Zandvoort, K., Gibbs, H., Hellewell, J., Jarvis, C.I., Clifford, S., Quilty, B.J., Bosse, N.I., Abbott, S., Klepac, P., Flasche, S., 2020. Early dynamics of transmission and control of COVID-19: a mathematical modelling study. *Lancet Infect. Dis.* 20, 553–558. [https://doi.org/10.1016/S1473-3099\(20\)30144-4](https://doi.org/10.1016/S1473-3099(20)30144-4).
- Lauer, S.A., Grantz, K.H., Bi, Q., Jones, F.K., Zheng, Q., Meredith, H.R., Azman, A.S., Reich, N.G., Lessler, J., 2020. The incubation period of coronavirus disease 2019 (COVID-19) from publicly reported confirmed cases: estimation and application. *Ann. Intern. Med.* 172, 577–582. <https://doi.org/10.7326/M20-0504>.
- Mizumoto, K., Kagaya, K., Zarebski, A., Chowell, G., 2020. Estimating the asymptomatic proportion of coronavirus disease 2019 (COVID-19) cases on board the Diamond Princess cruise ship, Yokohama, Japan, 2020. *Eurosurveillance* 25, 1–5. <https://doi.org/10.2807/1560-7917.ES.2020.25.10.2000180>.
- Mollentze, N., Streicker, D.G., 2020. Viral zoonotic risk is homogenous among taxonomic orders of mammalian and avian reservoir hosts. *Proc. Natl. Acad. Sci.* 1–8. <https://doi.org/10.1073/pnas.1919176117>.
- Moraz, M., Jacot, D., Papadimitriou-Olivigeris, M., Senn, L., Greub, G., Jaton, K., Opota, O., 2020. Universal admission screening strategy for COVID-19 highlighted the clinical importance of reporting SARS-CoV-2 viral loads. *New Microbes New Infect.* 38, 100820. <https://doi.org/10.1016/j.nmi.2020.100820>.
- Narison, S., Maltzoz, S., 2021. Scrutinizing the spread of COVID-19 in Madagascar. *Infect. Genet. Evol.* 87, 104668. <https://doi.org/10.1016/j.meegid.2020.104668>.
- Nishiura, H., Kobayashi, T., Miyama, T., Suzuki, A., Jung, S. mok, Hayashi, K., Kinoshita, R., Yang, Y., Yuan, B., Akhmetzhanov, A.R., Linton, N.M., 2020. Estimation of the asymptomatic ratio of novel coronavirus infections (COVID-19). *Int. J. Infect. Dis.* 94, 154–155. <https://doi.org/10.1016/j.ijid.2020.03.020>.
- Oran, D.P., Topol, E.J., 2020. Prevalence of asymptomatic SARS-CoV-2 infection: a narrative review. *Ann. Intern. Med.* 173, 362–367. <https://doi.org/10.7326/M20-3012>.
- Pan, A., Liu, L., Wang, C., Guo, H., Hao, X., Wang, Q., Huang, J., He, N., Yu, H., Lin, X., Wei, S., Wu, T., 2020. Association of public health interventions with the epidemiology of the COVID-19 outbreak in Wuhan, China. *JAMA J. Am. Med. Assoc.* 323, 1915–1923. <https://doi.org/10.1001/jama.2020.6130>.
- Park, S.W., Bolker, B.M., Champredon, D., Earn, D.J.D., Li, M., Weitz, J.S., Grenfell, B.T., Dushoff, J., 2020. Reconciling early-outbreak estimates of the basic reproductive number and its uncertainty: framework and applications to the novel coronavirus (SARS-CoV-2) outbreak. *J. R. Soc. Interface* 17, 20200144.
- Raherinirina, A., Fandresena, T.S., Hajalalaina, A.R., Rabetafika, H., Rakotoarivelo, R.A., Rafamatanantsoa, F., 2021a. Probabilistic modelling of COVID-19 dynamic in the context of Madagascar. *Open J. Model. Simul.* 09, 211–230. <https://doi.org/10.4236/ojmsi.2021.93014>.
- Raherinirina, A., Rafamatanantsoa, F., Fandresena, T.S., Rakotoarivelo, R.A., 2021b. Mathematical model and non-pharmaceutical control of the coronavirus 2019 disease in Madagascar. *Open J. Model. Simul.* 09, 259–274. <https://doi.org/10.4236/ojmsi.2021.93017>.
- Rakotoarisoa, A., Randrianasolo, L., Tempia, S., Guillebaud, J., Razanajatovo, N., Randriamampionona, L., Piola, P., Halm, A., Heraud, J.-M., 2017. Evaluation of the influenza sentinel surveillance system in Madagascar, 2009–2014. *Bull. World Health Organ.* 95, 375–381. (<http://www.who.int/entity/bulletin/volumes/95/5/16-171280.pdf?%0Ahttp://ovidsp.ovid.com/ovidweb.cgi?T=JS&PAGE=reference&D=EM&NEWS=N&AN=615951962>).
- Rakotonanahary, R.J.L., Andriambolanana, H., Razafinjato, B., Razafanomezanjanahary, E.M., Ramanandrisoiy, V., Ralaivavikoa, F., Tsinimomen'ny Aina, A., Rahajatiaina, L., Rakotonirina, L., Haruna, J., Cordier, L.F., Murray, M.B., Cowley, G., Jordan, D., Krasnow, M.A., Wright, P.C., Gillespie, T.R., Docherty, M., Loyd, T., Evans, M.V., Drake, J.M., Ngonghala, C.N., Rich, M.L., Popper, S.J., Miller, A.C., Ihanamalala, F.A., Randrianambalina, A., Ramandrisoa, B., Rakotozafy, E., Rasolofomanana, A., Rakotozafy, G., Andriamahatana Vololoniaina, M.C., Andriamihaja, B., Garchitorena, A., Rakotonirina, J., Mayfield, A., Finnegan, K.E., Bonds, M.H., 2021. Integrating health systems and science to respond to COVID-19 in a model district of rural Madagascar. *Front. Public Health* 9, 1–10. <https://doi.org/10.3389/fpubh.2021.654299>.
- Randremanana, R., Andriamandimby, S., Rakotondramanga, J.M., Razanajatovo, N., Mangahasimbola, R., Randriambolanantsoa, T., Ranaivoson, H., Rabemananjara, H., Razanajatovo, I., Rabarison, J., Brook, C., Rakotomanana, F., Rabarimbosoa, R., Razafimanjato, H., Ahyong, V., Raharinosy, V., Raharimanga, V., Raharintanoaina, S., Randrianarisoa, M., Bernardson, B., Randrianasolo, L., Randriamanantany, Z., Heraud, J., Biohub, C.Z., 2021. The COVID-19 Epidemic in Madagascar: Clinical Description and Laboratory Results of the First Wave, March–September 2020. *Influenza Other Respiratory Viruses*, 00, pp. 1–12.
- Rasambainarivo, F., Ramiadantsoa, T., Randrianarisoa, S., Rajeev, M., Rice, B., Metcalf, C.J., 2020. COVID-19 Madagascar Dashboard.
- Rydevik, G., Innocent, G.T., Marion, G., Davidson, R.S., White, P.C.L., Billinis, C., Barrow, P., Mertens, P.P.C., Gavier-Widén, D., Hutchings, M.R., 2016. Using combined diagnostic test results to hindcast trends of infection from cross-sectional data. *PLoS Comput. Biol.* 12, 1–19. <https://doi.org/10.1371/journal.pcbi.1004901>.
- Salje, H., Cummings, D.A.T., Rodriguez-Barraquer, I., Katzelnick, L.C., Lessler, J., Klungthong, C., Thaisomboonsuk, B., Nisalak, A., Weg, A., Ellison, D., Macareo, L., 2018. Reconstruction of antibody dynamics and infection histories to evaluate dengue risk. *Nature* 557, 719–723. <https://doi.org/10.1038/s41586-018-0157-4>.
- The World Health Organization (WHO), 2020. Molecular Assays to Diagnose COVID-19: Summary Table of Available Protocols. (n.d.). (<https://www.who.int/publications/m/item/molecular-assays-to-diagnose-covid-19-summary-table-of-available-protocols>).
- Tom, M.R., Mina, M.J., 2020. To interpret the SARS-CoV-2 test, consider the cycle threshold value. *Clin. Infect. Dis.* 71, 2252–2254. <https://doi.org/10.1093/cid/ciaa619>.
- Treibel, T.A., Manisty, C., Burton, M., McKnight, A., Lambourne, J., Augusto, J.B., Couto-Parada, X., Cutino-Moguel, T., Noursadeghi, M., Moon, J.C., 2020. COVID-19: PCR screening of asymptomatic health-care workers at London hospital. *Lancet* 395, 1608–1610. [https://doi.org/10.1016/S0140-6736\(20\)31100-4](https://doi.org/10.1016/S0140-6736(20)31100-4).
- Walker, A.S., Pritchard, E., House, T., Robotham, J.V., Birrell, P.J., Bell, J.I., Newton, J. N., Farrar, J., Diamond, I., Studley, R., Hay, J., 2020. Viral Load in Community SARS-CoV-2 Cases Varies Widely and Temporally.
- Wallinga, J., Lipsitch, M., 2007. How generation intervals shape the relationship between growth rates and reproductive numbers. *Proc. R. Soc. B Biol. Sci.* 274, 599–604. <https://doi.org/10.1098/rspb.2006.3754>.
- T.W.H.O. (WHO), 2020. Maintaining Surveillance of Influenza and Monitoring SARS-CoV-2 – Adapting Global Influenza Surveillance and Response System (GISRS) and Sentinel Systems during the COVID-19 Pandemic: Interim Guidance. Geneva.
- Wood, S.N., 2001. mgcv: GAMs and generalized ridge regression for R. *R News* 1/2, 20–24.
- Xu, B., Gutierrez, B., Mekaru, S., Sewalk, K., Goodwin, L., Loskill, A., Cohn, E.L., Hsuen, Y., Hill, S.C., Cobo, M.M., Zarebski, A.E., Li, S., Wu, C.H., Hulland, E., Morgan, J.D., Wang, L., O'Brien, K., Scarpino, S.V.V., Brownstein, J.S., Pybus, O.G., Pigott, D.M., Kraemer, M.U.G., 2020. Epidemiological data from the COVID-19 outbreak, real-time case information. *Sci. Data* 7, 1–6. <https://doi.org/10.1038/s41597-020-0448-0>.
- https://madagascar.unfpa.org/sites/default/files/pub-pdf/resultat_globaux_rgph3_tome_01.pdf. (2018). (Accessed 03 Dec 2021).

ANNEXE 6

Randremanana, R., Andrianaivoarimanana, V., Nikolay, B.,
Ramasindrazana, B., Paireau, J., ten Bosch, Q. A.,
Rakotondramanga, J. M., Rahajandraibe, S., Rahelinirina, S.,
Rakotomanana, F., Rakotoarimanana, F. M., Randriamampionona,
L. B., Razafimbia, V., De Dieu Randria, M. J., Raberahona, M.,
Mikaty, G., Le Guern, A.-S., Rakotonjanabelo, L. A., Ndiaye, C.
F., ... Rajerison, M. (2019). Epidemiological characteristics of an
urban plague epidemic in Madagascar, August–November, 2017:
an outbreak report. *The Lancet Infectious Diseases*, 19(5), 537–
545. [https://doi.org/10.1016/S1473-3099\(18\)30730-8](https://doi.org/10.1016/S1473-3099(18)30730-8)

Epidemiological characteristics of an urban plague epidemic in Madagascar, August–November, 2017: an outbreak report



Rindra Randremanana*, Voahangy Andrianaivoarimanana*, Birgit Nikolay*, Beza Ramasindrazana*, Juliette Paireau*, Quirine Astrid ten Bosch*, Jean Marius Rakotondramanga*, Soloandry Rahajandraibe, Soanandrasana Rahelinirina, Fanjasoa Rakotomanana, Feno M Rakotoarimanana, Léa Bricette Randriamampionona, Vaoary Razafimbria, Mamy Jean De Dieu Randria, Mihaja Raberahona, Guillain Mikaty, Anne-Sophie Le Guern, Lamina Arthur Rakotonjanabelo, Charlotte Faty Ndiaye, Voahangy Rasolofo, Eric Bertherat†, Maherisoa Ratsitorahina†, Simon Cauchemez‡, Laurence Barilt, André Spiegel†, Minoarisoa Rajerison†

Summary

Background Madagascar accounts for 75% of global plague cases reported to WHO, with an annual incidence of 200–700 suspected cases (mainly bubonic plague). In 2017, a pneumonic plague epidemic of unusual size occurred. The extent of this epidemic provides a unique opportunity to better understand the epidemiology of pneumonic plagues, particularly in urban settings.

Methods Clinically suspected plague cases were notified to the Central Laboratory for Plague at Institut Pasteur de Madagascar (Antananarivo, Madagascar), where biological samples were tested. Based on cases recorded between Aug 1, and Nov 26, 2017, we assessed the epidemiological characteristics of this epidemic. Cases were classified as suspected, probable, or confirmed based on the results of three types of diagnostic tests (rapid diagnostic test, molecular methods, and culture) according to 2006 WHO recommendations.

Findings 2414 clinically suspected plague cases were reported, including 1878 (78%) pneumonic plague cases, 395 (16%) bubonic plague cases, one (<1%) septicaemic case, and 140 (6%) cases with unspecified clinical form. 386 (21%) of 1878 notified pneumonic plague cases were probable and 32 (2%) were confirmed. 73 (18%) of 395 notified bubonic plague cases were probable and 66 (17%) were confirmed. The case fatality ratio was higher among confirmed cases (eight [25%] of 32 cases) than probable (27 [8%] of 360 cases) or suspected pneumonic plague cases (74 [5%] of 1358 cases) and a similar trend was seen for bubonic plague cases (16 [24%] of 66 confirmed cases, four [6%] of 68 probable cases, and six [2%] of 243 suspected cases). 351 (84%) of 418 confirmed or probable pneumonic plague cases were concentrated in Antananarivo, the capital city, and Toamasina, the main seaport. All 50 isolated *Yersinia pestis* strains were susceptible to the tested antibiotics.

Interpretation This predominantly urban plague epidemic was characterised by a large number of notifications in two major urban areas and an unusually high proportion of pneumonic forms, with only 23% having one or more positive laboratory tests. Lessons about clinical and biological diagnosis, case definition, surveillance, and the logistical management of the response identified in this epidemic are crucial to improve the response to future plague outbreaks.

Funding US Agency for International Development, WHO, Institut Pasteur, US Department of Health and Human Services, Laboratoire d'Excellence Integrative Biology of Emerging Infectious Diseases, Models of Infectious Disease Agent Study of the National Institute of General Medical Sciences, AXA Research Fund, and the INCEPTION programme.

Copyright © The Author(s). Published by Elsevier Ltd. This is an Open Access article under the CC BY-NC-ND 4.0 license.

Introduction

Plague, a disease caused by a Gram-negative bacillus *Yersinia pestis*, has been linked to three major historical pandemics with devastating impacts on human populations.¹ Plague can manifest itself through different clinical presentations. Bubonic plague is the most common form and is acquired through bites from fleas that serve as vectors between reservoirs (wildlife or commensal rodents) and humans. A small number of bubonic plague cases might develop into secondary pneumonic plague through septicaemic spread. Although there is generally no onward transmission from bubonic

plague cases, interhuman transmission from pneumonic plague cases to close contacts can occur through droplet spread.² Bubonic plague cases are characterised by fever and painful lymphadenitis in the area of the fleabite, whereas pneumonic plague cases are characterised by sudden fever, cough, and symptoms of lower respiratory tract infections, often with haemoptysis as the disease progresses. Prompt treatment with appropriate antibiotics is usually effective; however, case fatality rates (CFRs) have remained high, at about 10% and 40% in previous bubonic plague and pneumonic plague epidemics, respectively, as reported by WHO.³

Lancet Infect Dis 2019

Published Online

March 28, 2019

[http://dx.doi.org/10.1016/S1473-3099\(18\)30730-8](http://dx.doi.org/10.1016/S1473-3099(18)30730-8)

See Online/Comment

[http://dx.doi.org/10.1016/S1473-3099\(18\)30794-1](http://dx.doi.org/10.1016/S1473-3099(18)30794-1)

*Contributed equally

†Equal senior contribution

Epidemiology and Clinical Research Unit

(R Randremanana PhD, J M Rakotondramanga MSc, F Rakotomanana PhD, F M Rakotoarimanana MD, L Baril MD) and Plague Unit (V Andrianaivoarimanana PhD, B Ramasindrazana PhD, S Rahelinirina PhD, M Rajerison PhD), Institut Pasteur de Madagascar (V Rasolofo PhD, A Spiegel MD), Antananarivo, Madagascar; Mathematical Modelling of Infectious Diseases Unit, Institut Pasteur, UMR 2000, CNRS, Paris, France (B Nikolay PhD, J Paireau PhD, Q A ten Bosch PhD, S Cauchemez PhD);

Environment and Infectious Risks Research Unit, Laboratory for Urgent Response to Biological Threats (ERI-CIBU) (G Mikaty PhD) and Yersinia Research Unit, National Reference Laboratory for Plague, WHO Collaborating Centre (A-S Le Guern PharmD), Institut Pasteur, Paris, France; Central Laboratory for Plague (S Rahajandraibe MSc) and Directorate of Health and Epidemiological Surveillance (L B Randriamampionona MD, V Razafimbria MD, M Ratsitorahina MD), Ministry of Public Health, Antananarivo, Madagascar; Department of Infectiology, University Hospital Joseph Raseta Befelatanana, Antananarivo, Madagascar (Prof M J De Dieu Randria MD,

M Raberahona MD); WHO, Antananarivo, Madagascar (LA Rakotonjanabelo MSc, Prof C F Ndiaye MD); and WHO, Geneva, Switzerland (E Bertherat MD)

Correspondence to: Dr Simon Cauchemez, Mathematical Modelling of Infectious Diseases Unit, Institut Pasteur, Paris 75015, France simon.cauchemez@pasteur.fr

Research in context

Evidence before this study

Madagascar accounts for 75% of plague cases reported to WHO globally, with an annual incidence of 200–700 cases (mainly bubonic plague). In 2017, a pneumonic plague epidemic of unusual size, timing, and geographical location occurred. On July 13, 2018, we searched Web of Science for articles published in English between Jan 1, 2017, and July 13, 2018, with the terms “plague” and “Madagascar” in the title. We found 20 publications, including seven news items, five perspective articles discussing the response to the epidemic, and six articles presenting research unrelated to the 2017 plague epidemic in Madagascar. One article estimated the basic reproduction number of pneumonic plague in the 2017 epidemic from an analysis of preliminary data extracted from situation reports. Another article evaluated the risks of exportation. We identified no detailed descriptions of the 2017 epidemic.

Added value of this study

In this study, we present the epidemiology and transmission dynamics of the 2017 plague epidemic in Madagascar.

This predominantly urban epidemic was characterised by many notified cases, with a quarter classified as confirmed or probable cases, and an unusually high proportion of pneumonic forms. The study provides a unique opportunity to better understand the epidemiological characteristics of pneumonic plague in a densely populated urban setting. The outbreak also illustrates the many challenges associated with the control of plague in Madagascar.

Implications of all the available evidence

This epidemic confirmed the significant public health risk of re-emergence of pneumonic plague in urban areas and its potential for rapid expansion. Lessons learned from this epidemic concerning clinical and biological diagnosis, case definition, surveillance, and logistical management of the response will form the basis for improved plague investigation and response efforts in Madagascar and beyond.

Since the 1990s, plague has been considered a re-emerging disease.^{4–6} A few countries continue to report plague cases annually and, despite surveillance and response efforts, Madagascar accounts for 75% of plague cases reported to WHO.³ Between 2010 and 2015, 200–700 suspected cases (about 55% of which were laboratory confirmed) were reported annually to the Central Laboratory for Plague (WHO collaborating centre) at the Institut Pasteur de Madagascar (Antananarivo, Madagascar), with a CFR of 20%. Most of these notifications (>75%) were bubonic plague cases from rural areas of the central highlands, where plague is endemic and seasonal, with cases typically occurring between October and April.³ Small outbreaks of pneumonic plague were reported in 1997, 2011, and 2015 in rural areas of Madagascar (14–20 cases)^{7–9} and in 2004 in Antananarivo (81 notified cases restricted mainly to one commune in the capital; Rajerison M, unpublished).

Between late August and November, 2017, Madagascar had an unprecedented plague epidemic with a large volume of notifications, a predominance of pneumonic forms, and multiple geographic foci, including two main urban areas—Antananarivo, the capital (with around 2·8 million inhabitants), and Toamasina, the main seaport (with around 290 000 inhabitants). The index case was a 31-year-old man who died from respiratory distress on Aug 28, 2017, while travelling in a bush taxi between the middle-west central highlands (Ankazobe) and the coastal town of Toamasina. Two fellow passengers from the taxi subsequently died on Sept 2, 2017, in Toamasina, and Sept 3, 2017, in Antananarivo, presumably contributing to further disease transmission in both cities. The first laboratory-confirmed pneumonic plague case was a 47-year-old woman from Antananarivo

who was linked to the Toamasina cluster and died on Sept 11, 2017, confirming the suspicion of a pneumonic plague outbreak. WHO was notified by the Malagasy Ministry of Public Health on Sept 13, 2017, as per 2005 international health regulations, and the potential for a large-scale epidemic in an urban context prompted a large international response.^{10,11}

The objective of this report is to describe the epidemiological characteristics of this epidemic. Before this report, our knowledge of pneumonic plague was largely based on a few small rural outbreaks or century-old information.^{2,7–9,12–14} The extent of this epidemic therefore provides a unique opportunity to better understand the epidemiology of pneumonic plagues, particularly in urban settings. For completeness, we also describe bubonic plague over the same period, even though the trends were similar to those of previous years and represent the endemic background observed every year in Madagascar.

Methods

Data collection, biological analyses, and case classification

This is a retrospective observational study based on national surveillance data. The plague national surveillance system in Madagascar requires health-care professionals to notify suspected cases, on the basis of clinical presentation, to the Malagasy Ministry of Public Health and Institut Pasteur de Madagascar, where the Central Laboratory for Plague records the details on case notification forms and analyses biological samples for laboratory confirmation.

Case notification forms contained information on symptoms on admission, demographics (age, sex, occupation, and residence), the reporting health facility, key dates (symptom onset, clinical examination, and

sample collection), use of medication before admission, vital status, and type of laboratory samples collected. For cases without a notification form or with substantial missing information, the epidemiological team at Institut Pasteur de Madagascar followed up with the notifying health-care professionals.

Biological samples (bubo aspirates for bubonic plague, sputum for pneumonic plague, and liver or lung puncture from deceased patients) were collected by health-care workers or physicians from suspected plague cases. Biological diagnosis of plague was done at the Central Laboratory for Plague by rapid diagnostic tests,¹⁵ molecular biology,^{16,17} and culture¹⁸ (appendix). At the beginning of the pneumonic plague epidemic, molecular biology, on the basis of conventional PCR targeting the *pla* gene, was used for *Y pestis* confirmation.^{16,17} However, as the implemented protocol lacked specificity, this was replaced by real-time PCR (rtPCR) targeting the *pla* and *cafI* genes¹⁹ on Nov 3, 2017. Furthermore, conventional PCR targeting the *pla*, *cafI*, and *inv* genes²⁰ was done on samples with inconclusive rtPCR results based on a new decision tree (appendix). All samples received before this date were retested using these new protocols over the months of November, and December, 2017. Cases were classified as suspected, probable, or confirmed based on the results of three types of diagnostic tests (rapid diagnostic test, molecular methods, and culture) according to 2006 WHO recommendations (table 1).²¹ Point-of-care testing using rapid diagnostic tests was also done in public health-care centres as recommended by the Plague National Control Program. Because of insufficient experience of health-care staff operating in newly affected districts, the results of these tests were not considered, except when no other test could be done at the Central Laboratory for Plague.

Isolated *Y pestis* strains were tested for susceptibility to streptomycin, co-trimoxazole, tetracycline, ciprofloxacin, gentamicin, and chloramphenicol following Clinical Laboratory Standards guidelines.^{23,24}

We used the collated database (Institut Pasteur de Madagascar database) of epidemiological, clinical, and laboratory data describing cases with disease onset between Aug 1, and Nov 26, 2017, since the pneumonic plague epidemic was officially declared over on Nov 27, 2017. Patients with a missing onset date were included if the date of clinical examination, sample collection, or sample receipt was within the epidemic period.

The data reported here are part of the plague national surveillance system and no specific additional ethics approval was necessary. All information on individual patients has been anonymised for presentation.

Treatment of cases

Treatment of suspected cases and preventive measures were implemented without waiting for biological confirmation. Although intramuscular high-dose streptomycin

	Definition
Suspected cases	All clinically suspected plague cases that meet the clinical and epidemiological criteria as per WHO recommendations*
Probable cases†	Clinically suspected cases with positive rapid diagnostic test or positive molecular biology, and culture negative or not done
Confirmed cases	Clinically suspected cases with positive rapid diagnostic tests and positive molecular biology, or positive culture
Case definitions made on the basis of 2006 WHO recommendations, ²¹ using three diagnostic tests done at Institut Pasteur de Madagascar—rapid diagnostic tests, molecular biology (following the algorithm detailed in the appendix), and culture. Serologies (anti-F1 IgG detection) were not done during the epidemic period. *Compatible clinical presentation (fever, sepsis syndrome, lymphadenopathy, or acute pneumonitis) and epidemiological features (such as exposure to infected animals or humans, evidence of flea bites, or residence in or travel to a known endemic focus within the previous 10 days). ^{21,22} †For a single pneumonic plague case, none of the three diagnostic tests could be done at Institut Pasteur de Madagascar, but the rapid diagnostic test done at the health-care centre was positive and associated with clinical symptoms of plague; this case was classified as probable.	

Table 1: Case definitions

is the recommended first-line treatment for plague, fluoroquinolones are sometimes used to avoid potential side-effects of streptomycin.²⁵ We describe the use of antibiotics with known effect on *Y pestis*, including tetracyclines (doxycycline), sulfamides (co-trimoxazole), aminoglycosides (streptomycin, amikacin, or gentamicin), and fluoroquinolones (ciprofloxacin or ofloxacin) as reported by the notification forms. See Online for appendix

Several control measures were put in place to contain the outbreak. These included the set-up and strengthening of effective triage measures and treatment centres for patients with plague, post-exposure antibiotic prophylaxis for contacts of all suspected cases, follow-up of these contacts to ensure rapid isolation and treatment, strengthening of surveillance through a range of activities, such as active case finding, air, ground, and seaport screening, and the set-up of an alert phone line, and appropriate and wide-ranging health promotion, social mobilisation, and community communication activities to the population. In the context of a condition such as plague, which carries potential stigma, health education messages were particularly important to strengthen early warning and ensure that patients sought care early. Finally, the widespread use of antibiotics in the community might have also contributed to reduction of community transmission.

Statistical analysis

We produced epidemic curves, sociodemographic and clinical case characteristics, and CFR estimates of plague cases according to case classification and clinical form. We then focused analyses on confirmed or probable cases (ie, cases with at least one positive laboratory test).

We explored potential differences in the CFR over time. Geographical zones were classified as Antananarivo area (urban community of Antananarivo and the three neighbouring districts), Toamasina district, endemic zone (plague-endemic districts²⁶ apart from Antananarivo area), or other. To investigate risk factors of death among confirmed cases, we estimated CFRs and exact binomial

	Pneumonic plague			Bubonic plague		
	Confirmed (n=32)	Probable (n=386)	Suspected (n=1460)	Confirmed (n=66)	Probable (n=73)	Suspected (n=256)
Sex						
Male	23 (72%)	195/381 (51%)	819/1443 (57%)	39 (59%)	41/72 (57%)	145/254 (57%)
Female	9 (28%)	186/381 (49%)	624/1443 (43%)	27 (41%)	31/72 (43%)	109/254 (43%)
Age (years)						
0–4	5/31 (16%)	89/377 (24%)	407/1444 (28%)	4 (6%)	12/70 (17%)	34/252 (13%)
5–14	3/31 (10%)	42/377 (11%)	152/1444 (11%)	26 (39%)	29/70 (41%)	99/252 (39%)
15–49	19/31 (61%)	206/377 (55%)	758/1444 (52%)	33 (50%)	26/70 (37%)	108/252 (43%)
≥50	4/31 (13%)	40/377 (11%)	127/1444 (9%)	3 (5%)	3/70 (4%)	11/252 (4%)
Use of antibiotics with effect on <i>Yersinia pestis</i> before clinical examination*	8 (25%)	70 (18%)	221 (15%)	14 (21%)	14 (19%)	62 (24%)
Time to clinical examination (days)	1.5 (0.0–3.0)	1.0 (0.0–3.0)	1.0 (1.0–3.0)	1.0 (1.0–2.0)	1.0 (1.0–3.0)	1.0 (0.0–2.3)
Fever (≥37.5°C)	21/28 (75%)	220/329 (67%)	771/1288 (60%)	52/53 (98%)	47/60 (78%)	182/231 (79%)
Pulmonary symptoms						
Cough	26 (81%)	268/354 (76%)	977/1370 (71%)	9/56 (16%)	10/54 (19%)	15/233 (6%)
Chest pain	16 (50%)	127/348 (36%)	429/1366 (31%)	3/53 (6%)	1/54 (2%)	8/233 (3%)
Haemoptysis	15/31 (48%)	118/349 (34%)	461/1361 (34%)	0	0	2/233 (1%)
Adenopathy	1/25 (4%)	12/338 (4%)	34/1338 (3%)	66 (100%)	70/70 (100%)	249/249 (100%)
Fatal outcome	8 (25%)	27/360 (8%)	74/1358 (5%)	16 (24%)	4/68 (6%)	6/243 (2%)

Data are n (%), n/N (%), or median (IQR). In addition to the cases in this table, there was one case of septicaemic plague and 140 cases whose clinical form was not specified (appendix). Characteristics of confirmed or probable cases are presented in the appendix. Some individuals had missing case characteristics; the total number of observations by characteristic might therefore not add up to the total number of cases. *Cases without any reported treatment probably include cases with missing information.

Table 2: Characteristics of pneumonic plague and bubonic plague cases

95% CIs by sociodemographic, clinical, and epidemiological factors. Because of the small number of confirmed cases, we described trends in the data but could not assess statistical evidence for differences. We explored if similar trends were present for the larger number of confirmed or probable cases, for which we estimated risk ratios (RR) of death and 95% CIs using a log-binomial regression model (appendix). We did a survival analysis to investigate the potential effects of censoring (eg, deaths that occurred after case reporting) and evaluated the effect of inclusion of cases with unspecified clinical forms on CFR estimates among confirmed or probable cases (appendix). We estimated survival probability by days since onset of illness on the basis of a generalisation of the Kaplan-Meier curve. We compared the time to death among confirmed or probable pneumonic plague and bubonic plague cases with a weighted log-rank test.

We used a simple exponential growth model to compute the doubling time (ie, the time it takes for the number of cases to double) of confirmed and confirmed or probable cases in the growing phase of the pneumonic plague epidemic, for the whole country and for the Antananarivo area.²⁷ We derived upper bound estimates for the reproduction number of pneumonic plague (ie, the average number of people infected by a pneumonic plague case; appendix).

We mapped the spatial distribution of confirmed or probable cases using districts of residence (n=114) as

geographical scales, with an analysis of spatial clustering (appendix).

Role of the funding source

The funders of the study had no role in study design, data collection, data analysis, data interpretation, or writing of the report. The corresponding author had full access to all the data in the study and had final responsibility for the decision to submit for publication.

Results

Between Aug 1, and Nov 26, 2017, 2414 plague cases were reported, including 1878 (78%) pneumonic plague cases, 395 (16%) bubonic plague cases, one (<1%) septicaemic case, and 140 (6%) cases with unspecified clinical form (table 2; appendix). 66 additional cases with missing dates were not included in our study. Case notification forms were available for 2266 (94%) of 2414 cases and biological samples were available for 2405 (>99%) of 2414 cases. 32 (2%) of 1878 notified pneumonic plague cases were confirmed and 386 (21%) were probable. 66 (17%) of 395 notified bubonic plague cases were confirmed and 73 (18%) were probable.

After an initial phase with low numbers of notified cases, the weekly number of notified pneumonic plague cases increased markedly at the end of September, 2017, reaching its peak (423 cases) in the week beginning Oct 2, 2017 (figure 1). The number of bubonic plague cases peaked at

the same time as pneumonic plague cases, with 245 (62%) notifications occurring in October, 2017 (figure 1).

The median age of confirmed pneumonic plague cases was 26 years (IQR 15–28) and 23 (72%) of 32 patients were male (table 2). Most confirmed pneumonic plague cases reported cough (26 [81%] of 32 cases), and around half of cases had chest pain (16 [50%] of 32 cases) and haemoptysis (15 [48%] of 31 cases). Eight (25%) of 32 confirmed pneumonic plague cases reported use of antibiotics active on *Y pestis* before clinical examination (table 2). The frequency of symptoms in probable pneumonic plague cases often fell between the frequency in confirmed and suspected pneumonic plague cases (eg, prevalence of cough, 26 [81%] of 32 confirmed cases, 268 [76%] of 354 probable cases, and 977 [71%] of 1370 suspected cases; prevalence of fever, 21 [75%] of 28 confirmed cases, 220 [67%] of 329 probable cases, and 771 [60%] of 1288 suspected cases; table 2).

Among confirmed bubonic plague cases, the median age was 15 years (IQR 8–20) and 39 (59%) of 66 cases were male. Fever was reported in 52 (98%) of 53 confirmed cases, 47 (78%) of 60 probable cases, and 182 (79%) of 231 suspected bubonic plague cases (table 2).

Characteristics of confirmed or probable cases are presented in the appendix.

The CFR was higher among confirmed cases (eight [25%] of 32 cases) than probable (27 [8%] of 360 cases) or suspected pneumonic plague cases (74 [5%] of 1358 cases; table 2), and a similar trend was seen for bubonic plague cases (16 [24%] of 66 confirmed cases, four [6%] of 68 probable cases, and six [2%] of 243 suspected cases; table 2). CFR estimates for probable cases were similar regardless of which diagnostic test was positive (appendix). The CFR among confirmed, probable, and suspected pneumonic and bubonic plague cases was stable over time (figure 2). Cases with unspecified clinical form had a high CFR (78 [92%] of 85 cases; appendix).

The risk of death for confirmed pneumonic plague cases tended to be higher among cases with chest pain than others (seven [44%] of 16 cases vs one [6%] of 16 cases; appendix), among cases with haemoptysis than others (six [40%] of 15 cases vs two [13%] of 16 cases), and among cases in the endemic zone than in Antananarivo area (five [50%] of ten cases vs three [17%] of 18 cases). The risk of death for confirmed bubonic plague cases tended to increase with time to clinical examination (five [13%] of 38 cases with 0 to 1 days vs eight [40%] of 20 cases with 2 to 4 days; appendix). The analysis of risk factors of death among confirmed or probable cases showed similar trends, but did not support a higher risk of death among cases with chest pain or haemoptysis (appendix).

All deaths among confirmed or probable cases occurred within 8 days of symptom onset (figure 2), with a median delay from onset to death of 1 day for pneumonic plague cases and 2 days for bubonic plague cases (weighted log-rank test $p=0.12$).

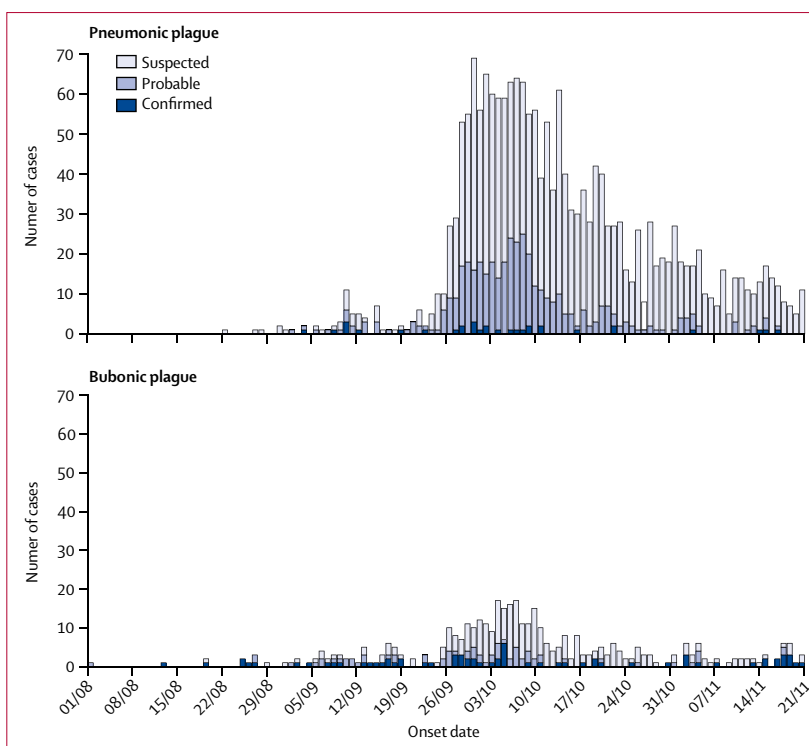


Figure 1: Daily number of notified plague cases over time (onset date) by case classification

Numbers of pneumonic plague (A) and bubonic plague (B) cases. Onset dates were imputed for 140 pneumonic plague and 22 bubonic plague cases. Seven pneumonic plague and two bubonic plague cases with missing onset, clinical examination, and sample collection dates are not shown.

Between Sept 13, and Oct 9, 2017, the number of confirmed or probable pneumonic plague cases doubled on average every 5 days (95% CI 4–6) in the whole country and in Antananarivo area (appendix). The reproduction number of pneumonic plague was estimated to be 1.6 or less (appendix).

The spatial distribution of confirmed or probable cases is shown in figure 3. Pneumonic plague mainly affected the urban centres of Antananarivo (288 [69%] of 418 cases) and Toamasina (63 [15%] of 418 cases), and showed substantial spatial clustering (appendix). 131 (94%) of 139 confirmed or probable bubonic plague cases were observed in plague-endemic districts (31 in Antananarivo area and 100 outside).

50 *Y pestis* strains were isolated (41 bubonic plague, eight pneumonic plague, and one unspecified form). All isolated strains were susceptible to the tested antibiotics.

Discussion

In this study, we described the epidemiology of the 2017 plague epidemic in Madagascar. This predominantly urban epidemic was characterised by many notified cases, with a quarter of cases classified as confirmed or probable, and an unusually high proportion of pneumonic forms. This study provides a unique opportunity to better understand the epidemiological characteristics

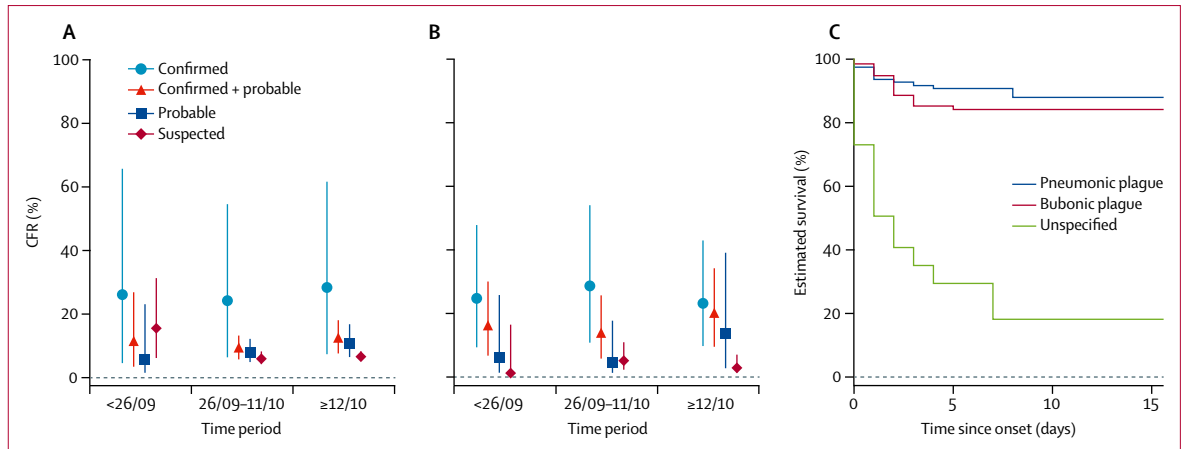


Figure 2: CFRs by time period among confirmed, probable, and suspected pneumonic plague (A) and bubonic plague (B) cases, and probability of survival by days since symptom onset for confirmed or probable cases (C)
Plots represent CFR and 95% CIs for confirmed, probable, and suspected cases by time period of the epidemic (initial, rapid growth, and control phase). CFR=case fatality ratio.

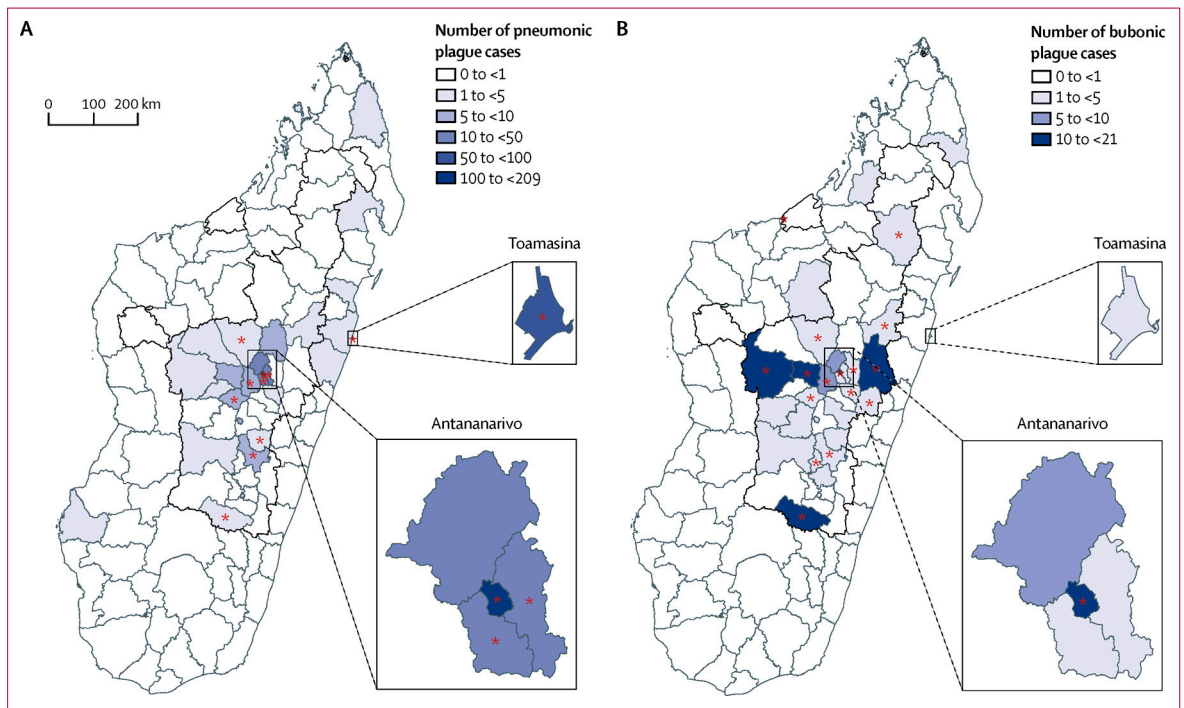


Figure 3: Spatial distribution of confirmed or probable plague cases
Number of pneumonic plague cases per district (A). Number of bubonic plague cases per district (B). Red stars indicate districts with at least one confirmed case. The solid black line delimits the endemic districts.

of pneumonic plague in a densely populated urban setting. The outbreak also illustrates the many challenges associated with control of plague in Madagascar.

The epidemic was characterised by exceptionally large numbers of pneumonic plague case notifications (1878 in 2017 vs 83 per year on average in 2010–15), although the number of notified bubonic plague cases remained similar to that of recent years.³ The rapid increase in notified cases, particularly of pneumonic form, at the

end of September, 2017, prompted a large national and international multisectoral response, the creation of a national emergency task force, and a joint response plan to curtail the epidemic.¹⁰ The urban nature of the epidemic, its multiple foci, and the potential for international human-to-human spread, as well as the potentially high lethality, required rapid and sustained multipronged efforts. The outbreak also had a substantial impact on society (eg, school closure) and travel and

trade for Madagascar (eg, implementation of airport screening measures—some airlines cancelled flights). The large number of suspected cases was a major hurdle for logistical management of the different aspects of the response.

This outbreak was the first time that the Central Laboratory for Plague had received such a large number of pneumonic plague samples, which raised several challenges for laboratory confirmation of cases. The tests initially used by the Central Laboratory for Plague had mainly been done on bubonic plague samples and their performance on primary pneumonic plague samples had not been evaluated. Testing the presence of *Y pestis* is much more challenging for pneumonic plague because of the quality of sputum samples and the contamination of samples by the commensal flora of the upper respiratory tract. For example, the insufficient specificity of conventional *pla* PCR on pneumonic plague samples led to rapid implementation of improved molecular diagnostics. Samples collected before Nov 3, 2017, were retrospectively retested in November, and December, 2017, with the upgraded molecular biology techniques. The higher specificity of these techniques led to a decrease in the final number of confirmed or probable cases compared with previous reports during the outbreak, particularly for pneumonic plague cases.¹⁰

Therefore, the magnitude of the pneumonic plague epidemic is likely to have been smaller than suggested by notifications, since only 23% of notified pneumonic plague cases had more than one positive laboratory test, with laboratory results available for more than 99% of cases. The spatial extent of the pneumonic plague epidemic appears to have been relatively restricted, with 84% of the confirmed or probable pneumonic plague cases observed in the initial two main urban transmission sites (Antananarivo area and Toamasina). With a doubling time of 5 days, the growth in confirmed or probable pneumonic plague cases was fast, but part of that growth might have been due to increased reporting thanks to enhanced contact tracing and a rise in public awareness. Factors that might explain over-reporting of pneumonic plague cases include little clinical experience in newly affected areas (pneumonic plague is rare and few clinicians in Madagascar had first-hand experience of it), and difficulty of clinical diagnosis in a context in which respiratory signs can be caused by other circulating pathogens (eg, a concomitant outbreak of bronchiolitis among children). Indeed, patients with pneumonic plague initially present with mostly non-specific upper respiratory symptoms, such as cough, fever, and headache, and differential diagnosis is therefore difficult on clinical grounds, particularly in the early stages of disease. Some similarities to this outbreak can be seen in an outbreak of pneumonic plague in India in 1994 that resulted in more than 6000 notifications for less than 300 confirmed or probable cases.²⁸ In this Indian

epidemic, experts recommended that suspected cases with negative biological test results should remain classified as suspected.²² Overall, more than 99% of suspected cases tested negative on both rapid diagnostic tests and PCR (with a culture that was either negative or not done). Investigating these negative cases more thoroughly in future outbreaks, and revising guidelines accordingly, might help better characterise the true magnitude of plague outbreaks.

In a context such as this, in which confirmatory diagnostics are challenging, it remains difficult to precisely quantify the prevalence of plague among notified cases. For example, newly implemented rtPCR targeting two genes is expected to be highly specific but could have insufficient sensitivity. Therefore, the true prevalence of plague in notified pneumonic plague cases is likely to lie somewhere between that of confirmed and probable cases, and also justifies why we did our analyses on confirmed cases and on confirmed or probable cases as a joint group. This theory was corroborated by the fact that numbers for demographic, clinical, and epidemiological characteristics of probable cases often fell between those for confirmed and suspected cases.

The CFRs of suspected (5%), probable (8%), and confirmed (25%) pneumonic plague cases differed markedly. These differences might be due to various reasons, including a proportion of false positives among probable cases, a lower probability of being diagnosed as a confirmed case among non-deaths, since sputum samples have a lower yield than do lung or liver samples, which are only taken from dead individuals (appendix), and early and frequent antibiotic use (because of frequent self-medication facilitated by the availability of antibiotics without a prescription) and better clinical care, which might both reduce the probability of confirmation (ie, hence cases are probable) and increase the likelihood of survival (hence lower CFR). These factors might also partly explain why the CFR did not substantially change with the response. Better access to health care and more intensive use of antibiotics in cities (that were predominantly affected by pneumonic plague) might partly explain why the CFR of pneumonic plague cases was lower in cities than in the endemic zone, and why pneumonic plague cases were not more severe than bubonic plague cases, as is typically observed. The CFR was particularly high in cases with unspecified clinical form, most of whom died before the history of symptoms could be accurately reported. No nosocomial cases were identified using the notification forms; assessment of the post-epidemic serological status of exposed health-care workers is ongoing.

Serology was not done because the collection of blood samples was restricted by logistical constraints and was not recommended by the Plague National Control Program in this epidemic context. Serological examination of recovered patients with pneumonic plague is ongoing during post-epidemic investigations.

We can only speculate about the factors that led to such an unprecedented outbreak. The early start might have been induced by changes in the demography or behaviour of the reservoir (potentially due to climatic or ecological variations), which could have increased the risk of contact with humans. Detection of pneumonic plague cases can be more challenging in the middle of the austral winter because of the concomitant circulation of other respiratory diseases with similar symptoms. Once plague reaches multiple locations, including urban centres with high population densities, management and control of the epidemic becomes much more challenging. The lower median age for bubonic plague cases might be explained by behavioural factors—young adults are more involved in agricultural activities, exposing them to contact with rodents and fleas, and children spend more time close to the floor than do adults, leading to greater exposure to flea bites.

There are several limitations to this study. The samples and data used were collected during the response to a major epidemic and should be interpreted in this context. For example, information on pre-examination treatment was collected as free text and absence of treatment could not be distinguished from missing information. Acquiring information from severely ill cases is difficult and the quality of collected data might be affected by outcome, potentially leading to some reporting biases.

Despite these challenges, our study provides invaluable information about the characteristics, epidemiology, and transmission dynamics of pneumonic plague. This epidemic illustrates the difficulty in adapting medical and public health responses during an epidemic of unusual magnitude and clinical form, in predominantly urban areas. In such an emergency context, national and international multidisciplinary mobilisation is important to support real-time surveillance capacity, improved microbiological testing, community sensitisation, and protection of health-care workers. Structures and strengthened surveillance mechanisms put in place during the epidemic now need to be optimised to strengthen national and international response capacities in case of another urban outbreak. Additionally, multidisciplinary research programmes to improve diagnostic algorithms, alternatives to aminoglycoside-based treatment, immune response mechanisms in humans, and studies disentangling causes for re-emergence²⁹ are required.

Overall, this epidemic confirmed the significant public health risk of re-emergence of pneumonic plague in urban areas and its potential for rapid expansion. Lessons learned from this epidemic will form the basis for improved plague investigation and response efforts in Madagascar and beyond.

Contributors

VA, BR, SRaha, SRAhe, GM, A-SLG, and MRaj did the laboratory tests. RR, VA, SRaha, FR, FMR, LBR, VRaz, LB, and MRaj contributed to the data collection and management (including the geographical information

system). MJDDR and MRab contributed to patient clinical management and expertise. BN, JP, JMR, QAtB, and SC analysed the data. BN, JP, SC, LB, and MRaj wrote the first draft of the manuscript. RR, VA, LAR, CFN, EB, VRas, LB, AS, and MRaj coordinated the response. All authors critically commented on the manuscript and approved the final version.

Declaration of interests

We declare no competing interests.

Acknowledgments

This work received financial support from the US Agency for International Development (grant no AID-687-G-13-0003) for the implementation of the quantitative PCR technique (equipment and consumables) and financing for the additional human resources needed by the Central Laboratory for Plague and Epidemiology Units at Institut Pasteur de Madagascar (Antananarivo, Madagascar). WHO provided funding for the acquisition of new equipment to accelerate rapid diagnostic test production and secured biological sample transportation between health-care facilities and the Central Laboratory for Plague. The Central Laboratory for Plague also received financial support from the Department of International Affairs of the Institut Pasteur (Paris, France) through a cooperative agreement with the Office of the Assistant Secretary for Preparedness and Response in the US Department of Health and Human Services (project ASIDE; grant number IDSEP140020-01-00). The Mathematical Modelling of Infectious Diseases Unit received financial support from the Investissement d'Avenir programme, the Laboratoire d'Excellence Integrative Biology of Emerging Infectious Diseases programme (grant no ANR-10-LABX-62-IBEID), the Models of Infectious Disease Agent Study of the National Institute of General Medical Sciences, the AXA Research Fund, and the INCEPTION programme. We thank for their continuous support during the epidemic the other team members of the Institut Pasteur de Madagascar laboratories (from the Virology, Experimental Bacteriology, Infectious Diseases Immunology, and Malaria Research Units, the Clinical Biology Laboratory, and the Hygiene, Food and Environment Laboratory), members of the supporting research units at Institut Pasteur Paris (Cellule d'Intervention Biologique d'Urgence, the Epidemiology of Emerging Infectious Diseases Unit, and the Molecular Genetics of RNA Viruses Unit), experts deployed through the Global Outbreak Alert Response Network (GOARN), and all the colleagues who were instrumental in improving and implementing epidemiological and laboratory surveillance, and who supported the epidemic response efforts.

References

- Perry RD, Fetherston JD. *Yersinia pestis*—etiologic agent of plague. *Clin Microbiol Rev* 1997; **10**: 35–66.
- Kool JL. Risk of person-to-person transmission of pneumonic plague. *Clin Infect Dis* 2005; **40**: 1166–72.
- Plague around the world, 2010–2015. *Wkly Epidemiol Rec* 2016; **91**: 89–93.
- Duplantier JM, Duchemin JB, Chanteau S, Carniel E. From the recent lessons of the Malagasy foci towards a global understanding of the factors involved in plague reemergence. *Vet Res* 2005; **36**: 437–53.
- Migliani R, Chanteau S, Rahalison L, et al. Epidemiological trends for human plague in Madagascar during the second half of the 20th century: a survey of 20 900 notified cases. *Trop Med Int Health* 2006; **11**: 1228–37.
- Chanteau S, Ratsitorahina M, Rahalison L, et al. Current epidemiology of human plague in Madagascar. *Microbes Infect* 2000; **2**: 25–31.
- Ratsitorahina M, Chanteau S, Rahalison L, Ratsifasoamanana L, Boissier P. Epidemiological and diagnostic aspects of the outbreak of pneumonic plague in Madagascar. *Lancet* 2000; **355**: 111–13.
- Ramasindrazana B, Andrianaivoarimanana V, Rakotondramanga JM, Birdsall DN, Ratsitorahina M, Rajerison M. Pneumonic plague transmission, Moramanga, Madagascar, 2015. *Emerg Infect Dis* 2017; **23**: 521–24.
- Richard V, Riehm JM, Herindrainy P, et al. Pneumonic plague outbreak, northern Madagascar, 2011. *Emerg Infect Dis* 2015; **21**: 8–15.
- WHO Regional Office for Africa. Plague outbreak in Madagascar. External situation report 13. Nov 27, 2017. <https://apps.who.int/iris/bitstream/handle/10665/259514/Ex-PlagueMadagascar27112017.pdf;jsessionid=07EAA452DA9053F9F79F45FF326D5D20?sequence=1> (accessed Feb 22, 2019).

- 11 Mead PS. Plague in Madagascar—a tragic opportunity for improving public health. *N Engl J Med* 2018; **378**: 106–08.
- 12 Bertherat E, Thullier P, Shako JC, et al. Lessons learned about pneumonic plague diagnosis from two outbreaks, Democratic Republic of the Congo. *Emerg Infect Dis* 2011; **17**: 778–84.
- 13 Teh WL. Plague in the Orient with special reference to the Manchurian outbreaks. *J Hyg (Lond)* 1922; **21**: 62–76.
- 14 Viselsteer AJ. The pneumonic plague epidemic of 1924 in Los Angeles. *Yale J Biol Med* 1974; **47**: 40–54.
- 15 Chanteau S, Rahalison L, Ralafiarisoa L, et al. Development and testing of a rapid diagnostic test for bubonic and pneumonic plague. *Lancet* 2003; **361**: 211–16.
- 16 Hinnebusch J, Schwan TG. New method for plague surveillance using polymerase chain reaction to detect *Yersinia pestis* in fleas. *J Clin Microbiol* 1993; **31**: 1511–14.
- 17 Pouillot F, Derbise A, Kukkonen M, Foulon J, Korhonen TK, Carniel E. Evaluation of O-antigen inactivation on *Pla* activity and virulence of *Yersinia pseudotuberculosis* harbouring the pPla plasmid. *Microbiology* 2005; **151**: 3759–68.
- 18 Rasoamanana B, Rahalison L, Raharimanana C, Chanteau S. Comparison of *Yersinia* CIN agar and mouse inoculation assay for the diagnosis of plague. *Trans R Soc Trop Med Hyg* 1996; **90**: 651.
- 19 Loiez C, Herwegh S, Wallet F, Armand S, Guinet F, Courcol RJ. Detection of *Yersinia pestis* in sputum by real-time PCR. *J Clin Microbiol* 2003; **41**: 4873–75.
- 20 Tsukano H, Itoh K, Suzuki S, Watanabe H. Detection and identification of *Yersinia pestis* by polymerase chain reaction (PCR) using multiplex primers. *Microbiol Immunol* 1996; **40**: 773–75.
- 21 International meeting on preventing and controlling plague: the old calamity still has a future. *Wkly Epidemiol Rec* 2006; **81**: 278–84.
- 22 WHO. Interregional meeting on prevention and control of plague. Geneva: World Health Organization, 2008.
- 23 Clinical and Laboratory Standards Institute. M11-S23. Performance standards for antimicrobial disk susceptibility tests. Approved standard—eleventh edition. January 2012. <https://www.researchgate.net/file.PostFileLoader.html?id=58139aa4615e27240754da03&assetKey=AS%3A422233756704774%401477679780485> (accessed Feb 22, 2019).
- 24 Galimand M, Carniel E, Courvalin P. Resistance of *Yersinia pestis* to antimicrobial agents. *Antimicrob Agents Chemother* 2006; **50**: 3233–36.
- 25 Rajerison M, Ratsitoharina M, Andrianaivoarimanana V. Plague. In: Farrar J, Hotez PJ, Junghanss T, Kang G, Lalloo D, White NJ (eds). *Manson's Tropical Diseases*. Philadelphia: Saunders, 2014: 404–09.
- 26 Andrianaivoarimanana V, Kreppel K, Elissa N, et al. Understanding the persistence of plague foci in Madagascar. *PLoS Negl Trop Dis* 2013; **7**: e2382.
- 27 Wallinga J, Lipsitch M. How generation intervals shape the relationship between growth rates and reproductive numbers. *Proc Biol Sci* 2007; **274**: 599–604.
- 28 Mavalankar DV. Indian 'plague' epidemic: unanswered questions and key lessons. *J R Soc Med* 1995; **88**: 547–51.
- 29 Stenseth NC, Atshabar BB, Begon M, et al. Plague: past, present, and future. *PLoS Med* 2008; **5**: e3.

ANNEXE 7

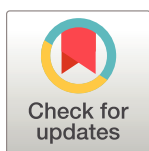
Bastaraud, A., Perthame, E., Rakotondramanga, J.-M., Mahazosaotra, J., Ravaonindrina, N., & Jambou, R. (2020). The impact of rainfall on drinking water quality in Antananarivo, Madagascar. *PLOS ONE*, 15(6), e0218698.
<https://doi.org/10.1371/journal.pone.0218698>

RESEARCH ARTICLE

The impact of rainfall on drinking water quality in Antananarivo, Madagascar

Alexandra Bastaraud¹, Emeline Perthame², Jean-Marius Rakotondramanga³, Jackson Mahazosaotra¹, Noro Ravaonindrina¹, Ronan Jambou^{4*}

1 Food Hygiene and Environment Laboratory, Institut Pasteur of Madagascar, Antananarivo, Madagascar, **2** The Center of Bioinformatics, Biostatistics and Integrative Biology (C3BI), Institut Pasteur Paris, Paris, France, **3** Epidemiology Department Institut Pasteur of Madagascar, Antananarivo, Madagascar, **4** Global Health Department, Institut Pasteur Paris, Paris, France

* rjambou@pasteur.fr

Abstract

Low-income cities that are subject to high population pressure and vulnerable to climate events often have a low capacity to continuously deliver safe drinking water. Here we reported the results of a 32-year survey on the temporal dynamics of drinking water quality indicators in the city of Antananarivo. We analyzed the long-term evolution of the quality of the water supplied and characterized the interactions between climatic conditions and the full-scale water supply system. A total of 25,467 water samples were collected every week at different points in the supplied drinking water system. Samples were analyzed for total coliforms (TC), *Escherichia coli* (EC), intestinal Enterococci (IE), and Spores of Sulphite-Reducing Clostridia (SSRC). Nine-hundred-eighty-one samples that were identified as positive for one or more indicators were unevenly distributed over time. The breakpoint method identified four periods when the time series displayed changes in the level and profile of contamination (i) and the monthly pattern of contamination (ii), with more direct effects of rainfall on the quality of supplied drinking water. The modeling showed significantly different lags among indicators of bacteria occurrence after cumulative rainfall, which range from 4 to 8 weeks. Among the effects of low-income urbanization, a rapid demographic transition and the degradation of urban watersheds have gradually affected the quality of the water supplied and resulted in the more direct effects of rainfall events. We focused on the need to adopt an alternative perspective of drinking water and urban watersheds management.

OPEN ACCESS

Citation: Bastaraud A, Perthame E, Rakotondramanga J-M, Mahazosaotra J, Ravaonindrina N, Jambou R (2020) The impact of rainfall on drinking water quality in Antananarivo, Madagascar. PLoS ONE 15(6): e0218698. <https://doi.org/10.1371/journal.pone.0218698>

Editor: Christopher Staley, University of Minnesota Twin Cities, UNITED STATES

Received: June 6, 2019

Accepted: April 6, 2020

Published: June 15, 2020

Copyright: © 2020 Bastaraud et al. This is an open access article distributed under the terms of the [Creative Commons Attribution License](https://creativecommons.org/licenses/by/4.0/), which permits unrestricted use, distribution, and reproduction in any medium, provided the original author and source are credited.

Data Availability Statement: The data underlying the results presented in the study are available from JIRAMA (<http://www.jirama.mg/>). They are public third party data available through regular request to the office. Requests can be sent to: dexo-dgo@jirama.mg. The person in charge of the data is the head of the data unit: pascale.rakotomahanina@jirama.mg.

Funding: The author(s) received no specific funding for this work.

Introduction

A poor capacity to provide safe drinking water, regardless of weather conditions, is of growing concern in low-income areas vulnerable to climate change [1,2]. Indeed, some parts of the world are expected to experience an increase in the frequency and intensity of precipitation and will find it increasingly difficult to limit the impact of storms [3], such as flooding or heavy run-off [4,5]. These events are associated with elevated turbidity [6–8] and dissolved organic matter in water sources [9], which can overwhelm treatment plans [10]. The high

Competing interests: The authors have declared that no competing interests exist.

levels of suspended solids limit the proper progress of the clarification steps and reduce the efficiency of chlorination. Indeed, extreme rainfall regimes are likely to be associated with drinking water contaminations [6,10], and this is predicted to be worsened by climate change [11]. Contaminated water is the main cause of diarrhea in children, and it is evident that an integrated approach to improving water supply will have an impact on the health of the population [12].

However, the relationship between rainfall patterns and microbial water quality is complex, involving an interplay between the type of water supply, the type of water source, and the treatment technology applied to water [13]. Also, susceptibility to climate change is reinforced by rapid and unplanned urbanization, poor sanitation, erosion, and low level of maintenance of the supply network [14]. Thus, the nature and the depth of the link between rainfall and water quality is not expected to be stationary. Rather, these should vary with the infrastructure and environmental changes, the time scale of study (yearly, season or day to day), and the rainfall patterns. Rainfall is a seasonal phenomenon with significant inter-annual variability [15] related to climate variations [16], extreme climatic events [6], intra-annual variability or distribution of water [17], change in duration of spells of continuous rain or no-rain events, and the total amount of water delivered during each wet spell [15]. Combined or selective impacts of these factors also depend on the catchment's characteristics.

Due to its diverse landscape, Madagascar is exposed to a variety of weather and climate phenomena [18]. The capital of Madagascar (Commune Urbaine d'Antananarivo–CUA) has experienced rapid urbanization due to the arrival of an additional 100,000 inhabitants per year. This population growth has increased the technical constraints on infrastructure and local services that were already deficient [19]. Water supply in Madagascar dates only from the colonial period (1952) and has been outpaced by urban expansion and population growth. Consequently, home connections are still limited, and a network of about 900 standpipes (public water fountains) supplies un-piped households. In this context, storm events, heavy rainfall, and runoff can increase water turbidity and microbiological contamination [20]. Un- or insufficiently filtered, inadequately, and even adequately disinfected drinking water is thus susceptible to microbiological contamination [21]. Water utilities are required to monitor microbial indicators to assess the effectiveness of the treatment process (i.e., spores of *Clostridia*), the safety of end drinking water (i.e., *Escherichia coli*, intestinal enterococci), and the biological stability of microorganism communities in piped water (i.e., total coliforms) [21]. All changes impacting the water source or the treatment process can affect these indicators and the drinking water quality. Exploring the interaction between precipitation events and urban water supply systems will highlight monitoring needs and priorities for improving water production.

Due to its geographic setting, its demographic burden, and its environmental transition, Antananarivo is a suitable example for setting up new strategies to survey water treatment based on predictive mathematic models. Predictive models could also be used to adapt the activities of dispensaries based on the burden of diarrhea. First, we analyzed how the water quality had evolved over the last 30 years, and then how the rainfall pattern has impacted long-term water quality in the supply system under environmental and technical shifts. We also focused on the current week-to-week relationship between rainfall patterns characteristics and water quality to determine the main factors regulating water contamination.

Materials and methods

CUA and its drinking-water supply system

Site of study. Antananarivo is located in the central highlands of Madagascar at 1,300 m above sea level (18°55' S latitude and 47°32' Longitude). The city is nestled among twelve hills

and lies in the natural floodplain of the Ikopa River, which skirts the city to the south and west (Fig 1). The river and its tributaries play an important role in rice-dominated agricultural production. The metropolitan area spreads over 220 km², with an estimated population of 3,058 million inhabitants in 2018 [22]. This area currently experiences significant challenges due to flooding during the rainy season.

Climate. Antananarivo experiences a subtropical highland climate, warm and temperate classified as Cwb by the Köppen-Geiger system [23]. Summers are rainy, with most of the precipitations falling in December, January, and February. The winters are dry, especially in June, July, and August. The dry season occurs from May to September (i.e., from week no.14 to no.40), and the wet season from November to April (i.e., from week no.41 to no.13). From 1985 to 2017, the annual average of rainfall was above 1500 mm with extremes in January (above 300 mm) and June (less than 10 mm). The city of Antananarivo has experienced cyclones over the past 20 years, including Geralda in January 1994, Giovanna in February 2012, and Enawo in January 2017. These induced severe flooding as in February 2015 and 2016.

Water supply. In 2015, according to the National Water and Electricity Utility (JIRAMA), the whole drinking water supply system represents 1000 km of pipes for 80,000 subscribers (supply rate 56.8%). Water is provided by the Ikopa River, whose flow is diverted to the 1.41 km³ artificial Mandrozeza Lake from where water is pumped [24]. Two water stations, Mandrozeza I and II, with a daily production of 93,000 and 62,000 m³ per day (m³/d) respectively, supply 30 reservoirs. The treatment process includes coagulation, flocculation, decantation, filtration, chlorination, and neutralization steps [25].

Data collection

Water sampling and analysis. Four different points in the network (e.g. piped households, administrative buildings, standpipes, water tanks) were randomly investigated daily, five days a week. Each sample was collected in 500 ml sterile containers with 10 mg sodium thiosulfate and stored at 4 to 10°C until processing at the Institute Pasteur laboratory within 18 to 24 hours. Microbial water quality was assessed by enumerating samples contaminated or not by microbial indicators, including *Escherichia coli* (EC) and Total Coliform count (TC); intestinal enterococci (IE); spores of Sulfite-Reducing Clostridia (SSRC) [26]. From 1985 to 2014 (August), the laboratory used standardized methods based on the filtration of 100 milliliters (ml) of sample for testing EC, TC [27,28] and IE [29,30]. Since August 2014, the IDEXX Quanti-Tray methods were performed for testing IE [31], EC and TC [32]. From 1985 to June 2010 and after August 2016, the detection and enumeration of the spores of sulfite-reducing anaerobes (SSRC) required an enrichment of 20 ml of sample in a liquid medium [33]. From July 2010 to July 2016, the 100 ml filtration method was preferred for testing SSRC, resulting in a five-fold increase in test volume [34]. Criteria for a negative sample is set to “undetectable microorganism in any 100 ml” and in any “20 ml for SSRC”.

Temporal patterns of microbial water quality are expressed as the frequency of positive samples reported to the total number of samples collected during the period (monthly and weekly) over 32 years (from 1985 to 2017, except 2009 due to the insurrectional crisis). Monthly series had 6.41% missing values, and weekly series had 18.69% missing values. The missing values were mainly due to the interval between analysis service contracts or weeks during which samples were not taken (technical problems or weeks not working). For multivariate analysis, missing data were replaced by the median of the related month for monthly series and of the related week for weekly series.

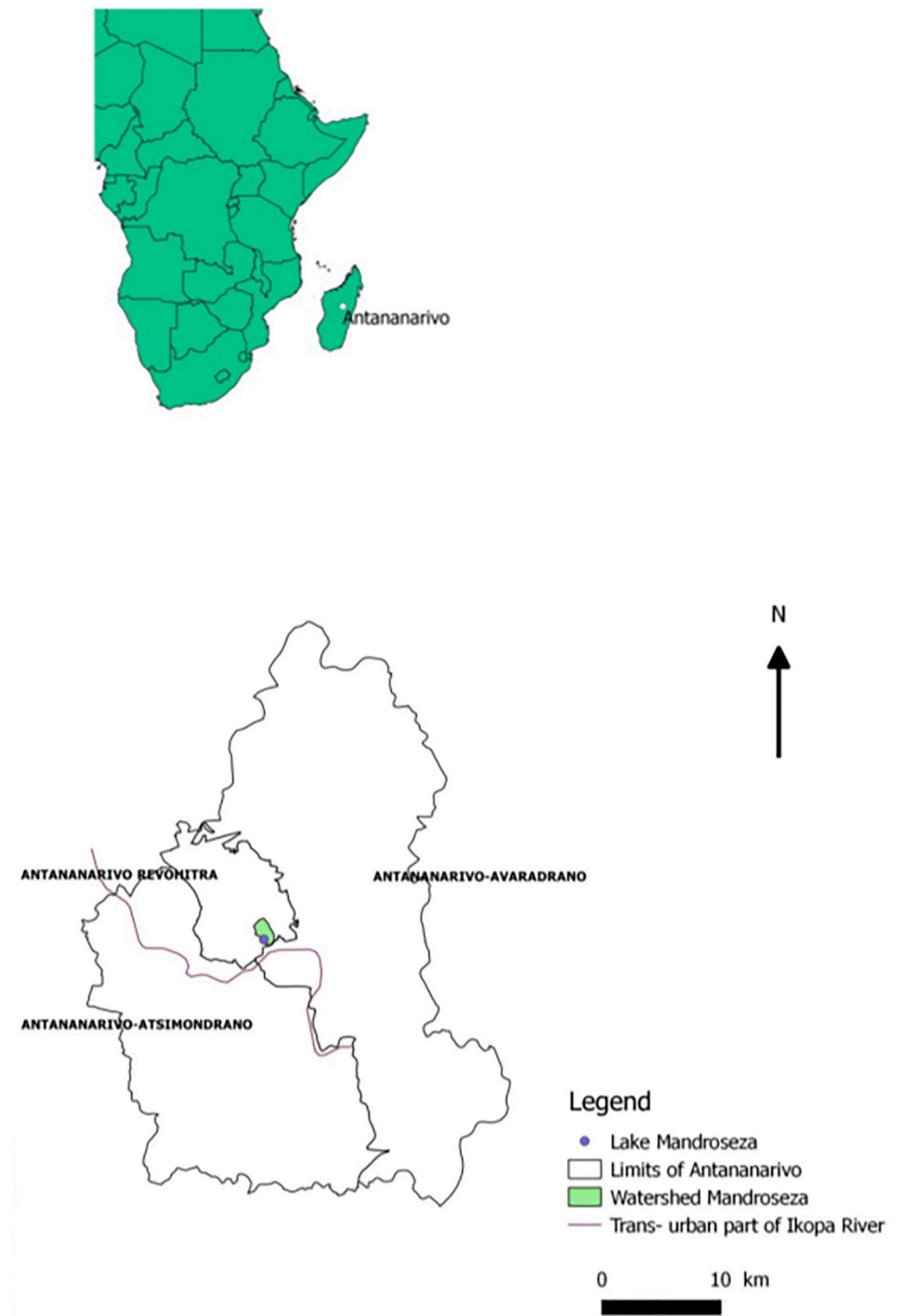


Fig 1. Location of Mandrozeza Lake inside the limits of Antananarivo. The file in “Africa map” created from OpenStreetMap databank are licensed under the Open Database 1.0 License. Administrative boundaries were from data OCHA (office for the coordination of Humanitarian Affairs) <https://data.humadata.org/dataset/madagascar-administrative-level-0-4-boundaries>. Watercourse layers are OpenSource databases from <https://www.openstreetmap.org>. OpenStreetMap[®] is *open data*, licensed under the Open Data Commons Open Database License (ODbl) by the OpenStreetMap Foundation (OSMF). The final map was prepared with own tiles under “ARCGIS software”.

<https://doi.org/10.1371/journal.pone.0218698.g001>

Rainfall data. From 1985 to 2017, monthly rainfall was collected from the data from *Direction Générale de la Météorologie*. Daily rainfall (available from 2007 to 2017) was collected from the IRI-International Research Institute for climate and society. To have the same time-step for rainfalls and contamination, these data were summarized as cumulative rainfall by month or by week.

Statistical analysis

Breakpoint detection method. To detect specific periods or obvious trends within contamination markers and rainfall time series, we applied a breakpoint detection method implemented in the *Strucchange* R package [35]. We used the method of simultaneous estimation of multiple breakpoints proposed by Bai and Perron in 2003 [36]. The method was run using the default parameters of breakpoints function, and the number of periods was estimated by minimizing the BIC (Bayesian Information Criterion).

Fourier analysis. To test if the variable “month” affects the contamination markers and rainfall pattern, we applied a Fourier transform to each variable using the *TSA* (Time Series Analysis) R package [37]. The computed periodograms from this transformation were tested. If there is a month effect in the time series, the periodogram should have a peak at time 12 (corresponding to 12 months). The significance of the amplitude of the periodogram at time 12 is tested using a permutation test (i.e., comparison with a random sequence with a significance level at 0.05) [38]. All p-values are available in the supporting information (S1 Table).

Hierarchical clustering. To check for similar current profiles of contamination, we focused on data from the last period provided by statistical analysis of contamination change. We applied a hierarchical clustering algorithm with Euclidean distance and Ward distance. The clustering was applied to the four contamination markers (IE, EC, TC, and SSRC). Total contamination was not used for clustering to avoid collinearity with IE, TC, EC, and SSRC. Rainfall and total contamination were added to the graphical representation for interpretation.

Auto-regressive integrated moving average (ARIMA) models. To investigate the specific relationship between drinking water contamination and rainfall, we have run three models following: a “naive” model (i) that consists of forecasting the contamination of a given week by the mean of the previous corresponding weeks. This model does not account for the effect of rainfall and is used as a benchmark for further comparisons: any prediction model achieving higher prediction error is not relevant. Two different ARIMA models are fitted on each marker: an ARIMA model, with no extra covariate (ii); and an ARIMA model adjusted on cumulative rainfalls of the previous weeks (iii), with a shift varying from 1 to 10 weeks. The optimal number of cumulative weeks is estimated by minimizing the prediction error (root mean square error, RMSE) assessed by cross-validation in the years 2016 and 2017. A likelihood-ratio test was used to compare the goodness of fit of statistical models. All parameters of ARIMA models are automatically selected using a stepwise procedure which minimizes the BIC, implemented in the *auto.arima* function of *forecast* package [39]. The Portmanteau test was used to conclude that no residual autocorrelation remained in the models [40]. This procedure allows investigation of the effect of rainfall and cumulative rainfalls on contamination markers; it also allows for the quantification of the number of cumulative weeks optimal to predict contamination.

Results

Contamination of the water over the 32 years

A total of 971 samples have been identified as positive for one or several microbial indicators among 25,467 samples collected over 32 years (365 months). This accounts for 3.8% of non-

compliant samples, unequally distributed over time. Indeed, during the period from 1989 to 2004 (175 months = 75% of the months), no contamination was reported.

Breakpoints in the yearly pattern of contamination

The time series of monthly water contamination frequencies showed significant shifts over the years for all indicators (IE, EC, TC, and SSRC). Change points and the associated 95% confidence intervals for total contamination (IE, EC, TC, and SSRC), as well as rainfalls, are summarized in [Table 1](#) (Breakpoint detection method).

Three breakpoints occurred over the “total contamination” series, defining four periods: i) before 1990, ii) between 1990 and 2005, iii) between 2005 and 2012, and iv) after 2012. Time series analysis also captured specific change-points for each specific contamination marker [i.e., 1990 and 2004 (TC); 2003 (EC); 2011 (SSRC) and 2012 (IE)]. For these periods, the monthly average of contaminated samples varied from 1.1% (the intermediate period from 1990 to 2005) to 9.5% (the last 5 years) ([Fig 2](#)). Periods 1 (from 1985 to 1990) and 3 (from 2005 to 2012) showed similar levels of contamination (4.7% and 4.2%). While the period from 1990 to 2005 was relatively free-from water contamination. The period from 2012 to 2017 showed a significant decrease in drinking water quality. Over the 30 years, no breakpoint or obvious trend was detected in the rainfall.

Over the whole series, and except for the 1990–2005 period, SSRC contamination events have continuously increased ([Fig 3d](#)), with the recent median of contamination events reaching 4.8% ([Fig 3k](#)). During the last period, IE contamination also increased, with median contamination events rising from 0 to 0.8% ([Fig 3k](#)). EC contaminated samples remained sporadic throughout the periods, with medians of the periods close to zero. However, the means of contamination increased very slightly from 0.1% ([Fig 3e](#)) to 0.7% ([Fig 3k](#)) (breakpoint in 2004). For TC, three out of four periods showed baseline contamination events with half of the months harboring 1% of contamination.

Change in monthly pattern of contamination

As the months harboring the highest contamination events also varied over time ([Fig 3](#)), the month effect had to be tested independently from the periods. The periodogram method and permutation test showed significant 12 months periodicity in data of several years for TC, IE, and rainfall (p-value < 0.05) ([S1 Table](#)). This means that TC and IE contamination events and rainfalls have preferentially occurred at specific months during the year. For SSRC, the test was barely significant (p-value ~ 0.05), suggesting that it suffers from a lack of power to detect

Table 1. Breakpoints in contamination markers and rainfall time series.

	TOTAL ^d	IE ^c	EC	TC	SSRC	Rainfall
Breakpoint n°1	1989(1) ^a [1989(9);1993(4)] ^b	-	-	1990(1) [1989(12);1991(7)]	-	-
Breakpoint n°2	2004(11) [2003(6);2005(3)]	-	2003(11) [1994(10);2004(9)]	2004(11) [2002(10);2004(12)]	-	-
Breakpoint n°3	2012(3) [2009(10);2012(6)]	2012(8) [2007(6);2014(2)]	-	-	2011(7) [2009(11);2011(9)]	-

^a Year and (month) when a breakpoint has occurred;

^b 95% Confidence intervals of time when a breakpoint has occurred;

^c Contamination markers, namely intestinal enterococci (IE), *Escherichia coli* (EC), total coliforms (TC) and spores of sulfite-reducing clostridia (SSRC);

^d Total contamination, regardless of markers.

<https://doi.org/10.1371/journal.pone.0218698.t001>

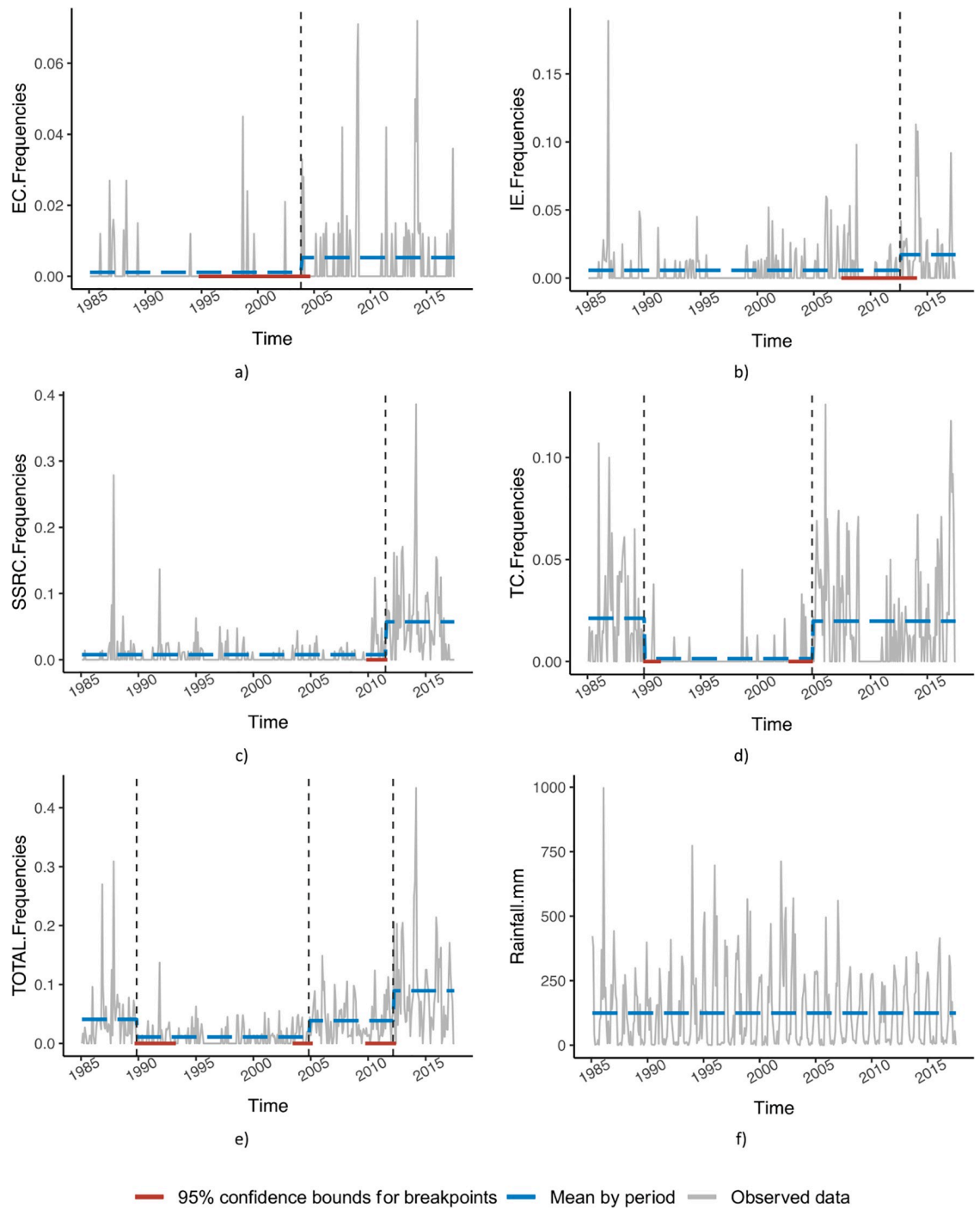


Fig 2. Time series of drinking water contamination frequencies in Antananarivo’s (Madagascar) water supply and rainfall from 1985 to 2017, using the period from breakpoints method. The time series are displayed in grey. The periods are represented by dashed vertical black lines; the mean of the time series within each period is indicated by a dashed blue line. Confidence intervals associated with change points are shown as red lines.

<https://doi.org/10.1371/journal.pone.0218698.g002>

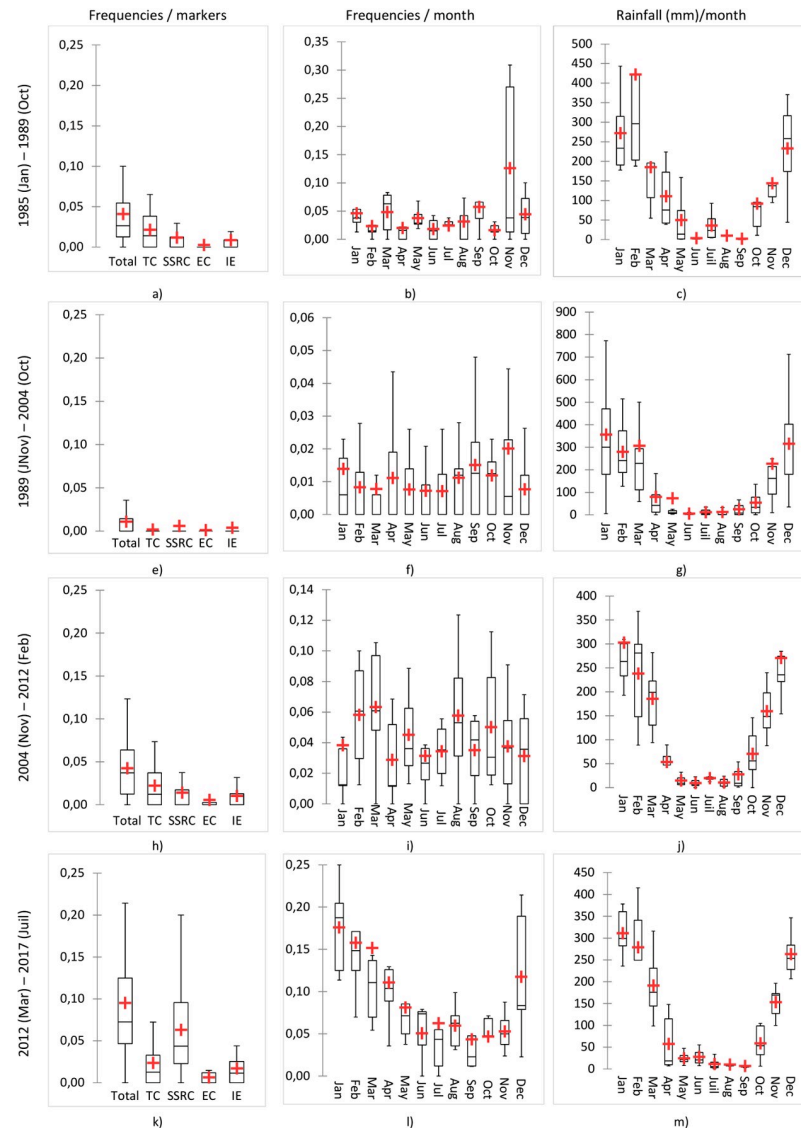


Fig 3. Distribution of drinking water contamination frequencies in Antananarivo's (Madagascar) water supply and rainfall from 1985 to 2017. Box plots are displayed with a mean (red cross).

<https://doi.org/10.1371/journal.pone.0218698.g003>

a specific pattern for this parameter. No month effect was detected for EC (p-value $\sim 0.3 > 0.05$).

From 1985 to 2004, November harbored the maximum of sample contamination accounting for the highest mean of the period, with 12.6% (Fig 3b) and 2% (Fig 3f), in the first and second period, respectively. In Antananarivo, November is also the month of the first heavy rainfall (Fig 3c, 3g, 3j and 3m). During the following periods, contamination events progressively increased preferentially at the beginning of the year, with means and medians of contaminated samples reaching 6% and 17% respectively in March (third period) and January (last period) (Fig 3i and 3l). This is in accordance with the rainiest months (Fig 3j and 3m). During the last 6 years, contamination events spread over the December to April period (Fig 3l). Thus, monthly contamination distribution can be superposed to rainfall distribution (Fig 3l and 3m).

Relationship between water contamination and rainfall

Profile contamination clustering. Correlation between the percentage of contaminated samples collected for one month and the rainfall measured during the same month was first queried using a clustering strategy conducted on the whole data set collected from March 2012 to the current date. For each month, rainfall, total contamination, IE, EC, TC, and SSRC were considered as variables for multiple component analysis (MCA) and automatic ascendant classification. The months grouped in a cluster and exhibited a similar profile of contamination. [Fig 4a](#) displays the clustering tree. Four clusters were determined according to the level of each contamination marker (IE, EC, TC, and SSRC). The scatter plot displays the distribution of all markers within each cluster. Rainfall and total contamination were also displayed ([Fig 4b](#)). Cluster 1, the largest, included 34 observations characterizing to months with low contamination in the context of low rainfall. Cluster 4, the smallest, included seven observations that demonstrated high contamination in TC and IE/EC, in the context of middle rainfall level. Clusters 4 and 3 exhibit similar total contamination. However, cluster 3 reported higher SSRC, lower TC, and IE/EC contamination and higher rainfall than cluster 4. This suggests that a similar total contamination rate might be associated with different contamination profiles. Cluster 2 demonstrated high contamination for all markers in the context of high rainfall.

In summary, during the dry seasons, the level of contamination was relatively low and mainly caused by SSRC (cluster 3). During the wet seasons, contamination was related to all other contamination markers (cluster 2) or by SSRC (cluster 3). Contamination by TC and IE/EC (cluster 4) was also more reported during the wet season.

The contamination profile also varied over the years. TC and EI/EC contaminations emerged three years ago and became predominant in 2017 (cluster no.4). Whereas in 2013, 2015, and 2016, contamination was mainly sustained by SSRC (cluster no. 3) and in 2012 and 2014 by all other markers (cluster no. 2). At the month level, contamination profiles varied cyclically according to the seasons. The wettest months of January and February showed high contamination, mainly caused by all types of microorganism (cluster no. 2) and SSRCs (cluster no. 3) respectively. This high contamination level occurred until May, regardless of the marker. Except during these first 5 months of the years, low or no contamination was observed, suggesting a rainfalls effect on emergence and persistence of contamination.

Rainfall and contamination modeling. According to previous data, the cumulative effect of the amount of rain fallen over previous weeks on contamination levels can be suspected. Three models (observed means, ARIMA model with no covariate, and ARIMA model adjusted to the optimal number of cumulative precipitations) were compared to select the one that best predicted the impact of cumulative rain on the occurrence of each contamination marker. The values fitted by the three models were reported ([Fig 5](#)), and determinants of best models were summarized in [Table 2](#).

The ARIMA model adjusted with cumulative weekly rainfall was found as the most accurate with the lowest BIC value and with a significant ratio test of likelihood (p -value < 0.05). The Portmanteau test concludes that no residual autocorrelation remained in the models ($p > 0.05$ for all models).

In summary, apart from EC, these models showed that weekly cumulative rainfalls had an impact on drinking water quality with different time lags according to the contamination markers. For total contamination, a lag of 5 weeks of cumulative rainfall led to the best model (BIC = -546.67) when comparing to the model with no covariate (BIC = -542.69, a p -value of the likelihood ratio test = $1.9e-03 < 0.05$). Prediction performance is also better than the other models ($7.95E-2 < 8.91E-2$ and $8.65E-2$).

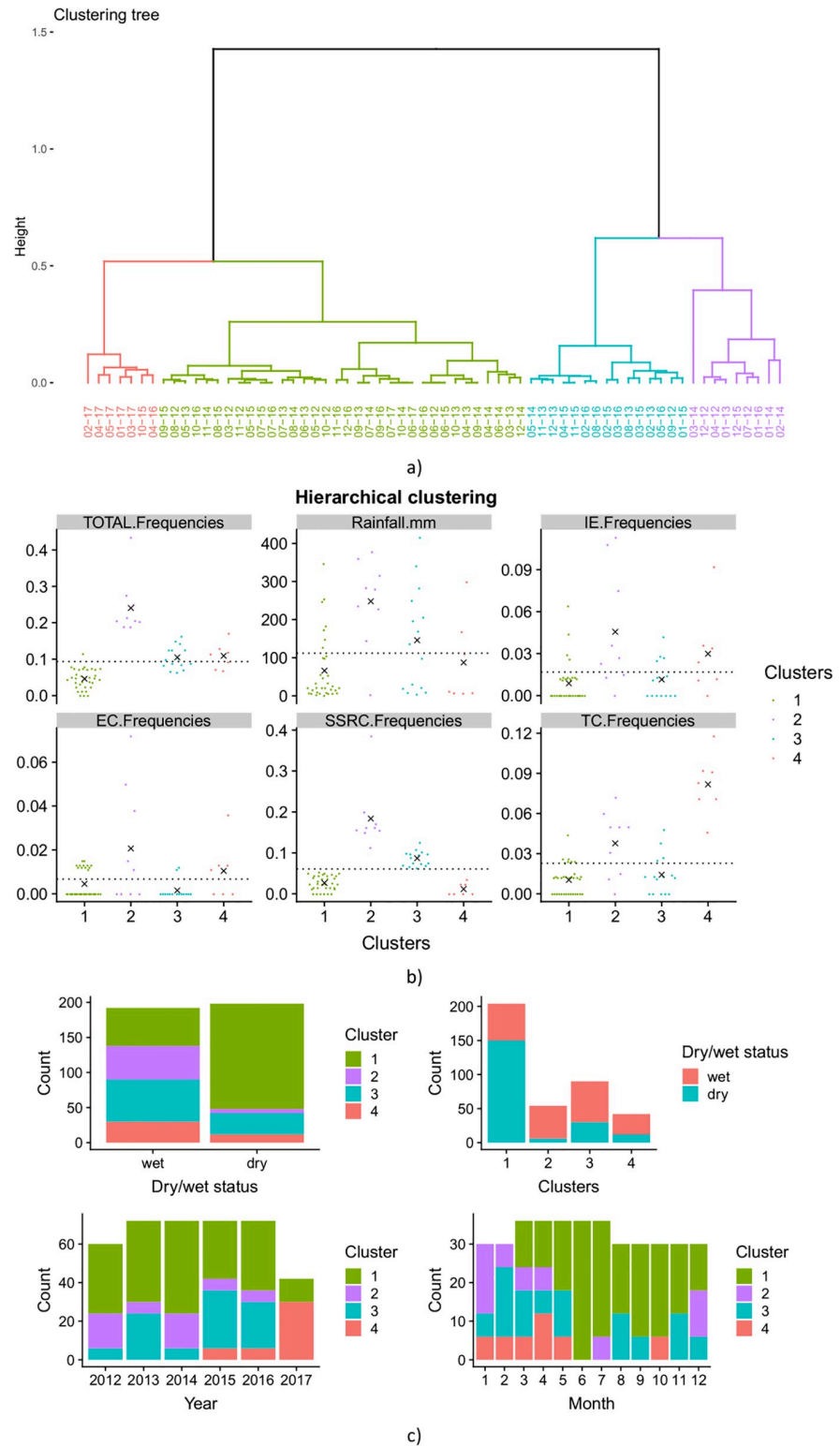


Fig 4. Hierarchical clustering of monthly observations from drinking water monitoring in Antananarivo's (Madagascar) water supply from 2012 to 2017. a) Clustering tree; b) Scatter plot displays the distribution of all markers within each cluster. The black crosses are the mean within the cluster of the corresponding variable. The dotted black line is the overall mean. c) Bar plots explore the repartition of each cluster by wet/dry seasons, by year and by months.

<https://doi.org/10.1371/journal.pone.0218698.g004>

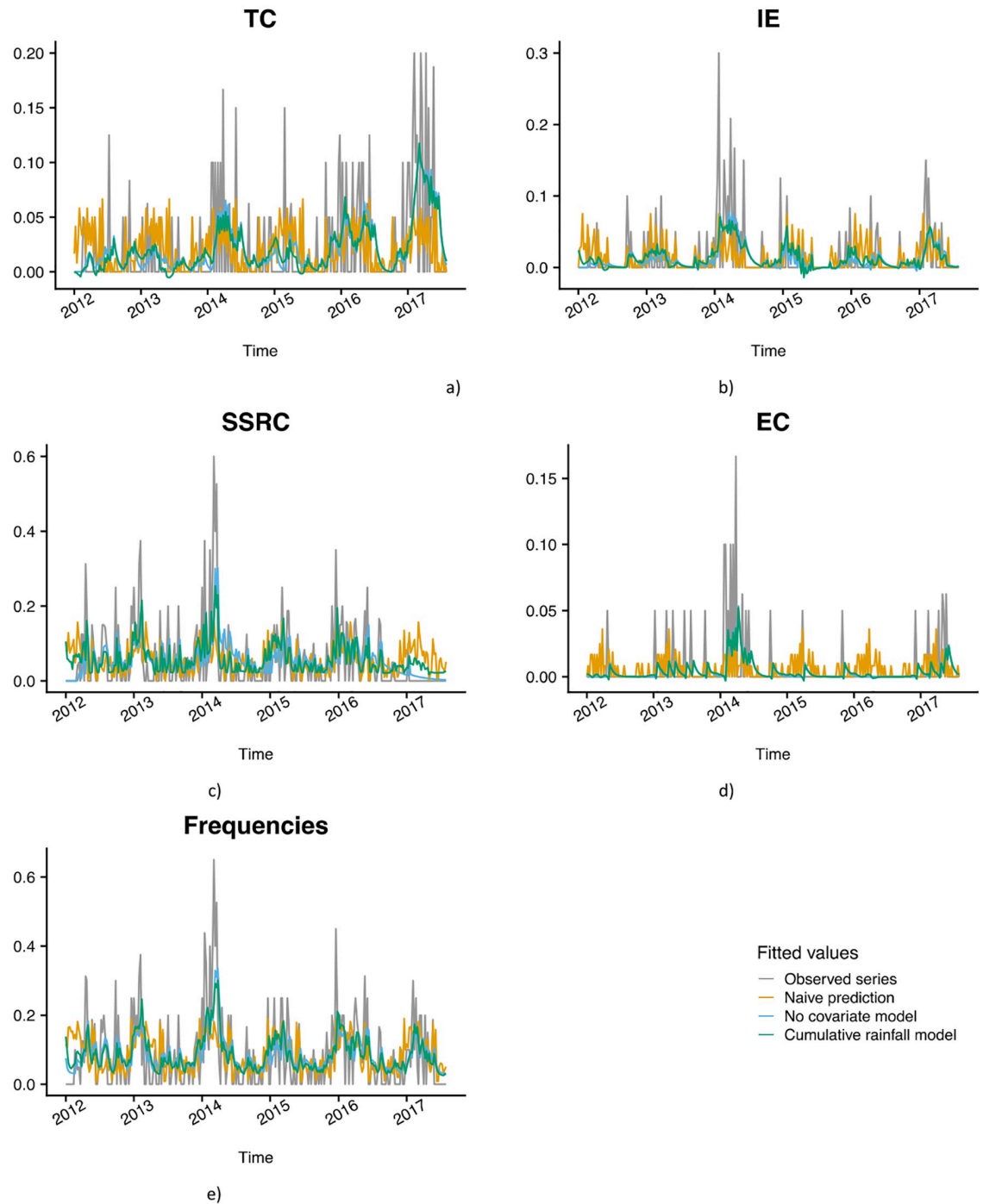


Fig 5. Modeling drinking water contamination in Antananarivo's (Madagascar) water supply from 2012 to 2017. The following figure shows the observed series in grey, the values fitted by the mean in orange, by the ARIMA model with no covariate in blue, and by the ARIMA model adjusted on the optimal number of cumulative rainfalls in green.

<https://doi.org/10.1371/journal.pone.0218698.g005>

For other specific markers and in agreement with MCA, the different lags suggest the chronological emergence of contamination markers after the weekly rainy periods: 1) SSRC contamination events generally occurred first after 4 weeks of cumulative rainfalls; 2) IE contamination events occurred after 5 weeks of cumulative rainfalls; 3) TC emerged last,

Table 2. Determinants of best ARIMA model adjusted to the optimal number of cumulative rainfalls.

Contamination markers ^a	Lag (weeks)	BIC ^b model	BIC no-covariate	Likelihood ratio ^c	Prediction model ^d	Prediction naïve	Prediction no-covariate
IE	5	-1119.84	-1118.34	7.4E-4	3.26E-2	3.62E-2	3.38E-2
EC	-	-1460.62	-1465.96	5.6E-1	1.44E-2	1.87E-2	1.46E-2
TC	8	-1010.19	-1011.11	2.95E-2	6.07E-2	6.07E-2	6.26E-2
SSRC	4	-620.49	-608.22	2.0E-5	6.26E-2	8.55E-2	6.61E-2
Total	5	-546.67	-542.62	1.9E-3	7.95E-2	8.91E-2	8.65E-2

^a Contamination markers, namely intestinal enterococci (IE), *Escherichia coli* (EC), total coliforms (TC) and spores of sulfite-reducing clostridia (SSRC);

^b Bayesian Information Criterion values for adjusted and no-covariate (reference) models (the lower, the better);

^c Likelihood ratio to test if the adjusted model is a better fit than the naïve model (values must be <0.05);

^d Prediction accuracy of the three models (the lower, the better): adjusted model over cumulative rainfall weeks (i), naïve model based on previously observed means (ii) and model with no-covariate.

<https://doi.org/10.1371/journal.pone.0218698.t002>

within 8 weeks of cumulative rainfalls. For EC, this procedure estimated that 3 weeks was the optimal cumulative rainfall (BIC = -1460.62). Nevertheless, the likelihood of the model does not significantly increase compared to the model with no covariate (BIC = -1465.96, a p-value of likelihood ratio test = $5.6e-01 > 0.05$). This suggests that the procedure is not able to detect how rainfall affects EC rate. Prediction error of the model adjusted on 3 weeks of cumulative rainfall (~ 1.44e-02) does not lead to an improvement of the prediction accuracy of the naïve model (~ 1.87e-02) nor of the ARIMA model with no covariate (~ 1.46e-02). This could be due to a lack of power of the model as EC contamination events were too sporadic (9% of the series).

In conclusion, the emergence of SSRC, IE, and TC are differentially linked to cumulative weekly precipitations, but no significant impact of cumulative rainfall could be detected for EC.

Discussion

Drinking water quality issues

Thirty-two-year monitoring of microbial indicators was performed in Antananarivo's full-scale drinking water distribution system, which operated under severe pressure from rapid and unplanned urbanization. The study showed that seasonal variations and significant long-term changes occurred in the microbiological quality of drinking water in the Antananarivo supply system. Large variations were observed in the occurrence of intestinal enterococci—EI (indicator of fecal pollution), total coliforms—TC (indicator of treatment efficiency or cleanliness and integrity of distribution systems) and clostridia spores—SSRC (indicator of filtration plant performance), following rainfall. Such seasonal variations in drinking water system performance were potentially due to rapid changes in raw water quality as a result of precipitation (e.g. increased stormwater flows and discharges, soil erosion, sporadic high turbidity) and an increased microbial load entering drinking water distribution [41] (e.g. overloading of the treatment process, adversely affecting disinfection efficiency) [17,42,43].

Long-term changes were also observed in the annual contamination level of TC, IE and SSRC. Such breakpoints (1993, 2004 and 2012) were potentially attributable to the treatment plant upgrades (Mandroseza II, in 1993, with an increase of 60,000 m³ of water per day), a gradual inability to meet quantity requirements since 2004, and environmental changes that gradually led to rapid and significant fluctuations in raw water quality (e.g. changes in land use, a deforested and urbanized watershed) [43–46]. On the other hand, the low proportion of

EC-contaminated samples has shown that, regardless of the ecological context or the technical performance of the treatment plan, the process has always been able to remove recent faecal contamination [47].

Water supply and demand issues: Signal of imbalance

Over the past 30 years, the capacity for drinking water treatment has not fully met the growing needs of residents. The population in 2017 was 2,904,000, a 5% increase per year from 1985. At the same time, daily water production increased by only 100,000 to 160,000 m³. In addition, the drinking water infrastructure was ageing and falling apart, with a production efficiency of around 60% [22,25,48].

Most pumps, basins, sand filters, storage reservoirs and underground water pipes were installed 60 years ago. Even with this system still in operation, it would need to be upgraded to meet exponential water demand (as an increase of 2% per year) [48]. The situation (e.g. age and no innovative design) required finding a balance that has reconciled duration and efficiency of treatment (nominal capacity of treatment plant) with daily water demand. However, the increase of technical problems, the decrease of yields, and the high seasonal changes in raw water did not allow a long-time balance to be maintained. Water demands in permanent excess of the nominal capacity resulted in a baseline remaining contamination by coliforms that characterized the water supply system.

The installation of the Mandroseza II treatment unit has led to a significant improvement in the microbiological quality of the water (statistical analysis of breakpoints). In practice, the implementation of the filtration step with the double-layer filter in complement of sand filtration has led to a sustainable reduction (more than 10 years) of contamination events in the supply system, especially samples contaminated by TC. Efficiency of clarification step was able to reduce TC contamination by a factor of three [49]. In 2004, the number of contamination events rose again to reach 4% of contaminated samples per month. The TC parameter governed this increase (+3%). The imbalance of the production system therefore shaped the CT contamination level of the water supply system [24,50].

In March 2017, a new subunit (Mandroseza II bis) was implemented to increase the capacity from 3,000 m³/h to 3,900 m³/h, but it was too soon to assess the impact of this on water quality. However, Antananarivo is expected to host nearly 3,400,000 inhabitants in 2020. Urbanization and demographics can again affect the balance between water supply and demand. The critical point will be the economic capacity to again upgrade infrastructures and to find a new economic model for water supply [51].

Ecological disruptions and damage to the water resource

Although there were no clear trends in the precipitation data, Antananarivo (since 2012) experienced successive extreme weather events, which led to episodes of high contamination during the first months of the year [52]. Cyclone Giovanna in February 2012 coincided with the start of the period with the highest contamination rates. The rains brought by cyclone Felleng in January 2013 raised river levels, with damage on water infrastructures. The rains of February 2015 triggered floods and the rising floodwaters have broken through several dams around the capital. Heavy rains that have hit the island since late 2014 were followed by Cyclone Chedza in January 2015. Since December 2015—and more precisely in January 2016—Antananarivo has also experienced torrential rains which caused significant damage. Enawo (a category-four tropical cyclone), hit Antananarivo in March 2017 and caused severe floods and landslides.

Significant associations between increased precipitation and greater occurrence of bacterial indicators in water samples were found, with specific lags in the effects of precipitation according to the different indicators. The emergence of SSRC and IE generally occurred within 4–5 weeks of rain, while TC appeared after 8 successive weeks of precipitation. The 4–8 weeks lag effect we observed can be explained by a cumulative phenomenon or a chain reaction that began with rainy season and that affected treatment efficiency, then the hygiene of supply network.

The emergence of the SSRC first was potentially attributed to soil leaching [53] during the first rains in November, which gradually overloaded the station with suspended matter, after 4 weeks. The Ikopa River watershed was severely impacted by erosion (e.g. deforestation, soils poorly protected by vegetation, agricultural practices) [54–57], that adversely affected clarification step and efficiency of disinfection [43]. Highlands cities that used surface water had contamination events, mainly sustained by the SSRC [58]. Failures in the treatment system appeared to have occurred, especially during wet periods.

The first IE emerged at week 5 after the beginning of heavy rainfalls. Their presence was potentially due to a loss of efficiency of filtration systems and chlorination steps (turbid water should be fully clarified to enable disinfection to be effective) and to a greater charge of suspended solids in raw water [59,60]. This increase in IE was only seen during the more recent period. Indeed, in 1995, the silting of the Ikopa River was estimated at 81 m³ per year per km² of the watershed, and sediments concentrated mainly upstream of dams (particularly Mandrozeza dam) [9,61–63]. Since then, the depth of Lake Mandrozeza had gradually decreased from 7.5 m to 3 m and has begun to be invaded by non-aquatic plants.

Demographic and ecological changes have also occurred, including deforestation of watersheds and disturbance of the protection perimeter related to urbanization. The Mandrozeza basin has increased from 30 to 50 hectares of the urbanized area [64]. Since then, although EC contamination events are not significant (median zero), the range of contaminated samples has increased. Nevertheless, the emergence of EC contamination is not significantly related to cumulative rainy weeks. The treatment system was able to limit the occurrence of EC, even though urban runoff could be heavily loaded with this bacterium [65].

After 8 weeks of cumulative rainfall (January–February), TC appeared. These contamination events were delayed and not directly related to precipitation. Unlike SSRC and IE, these contamination events seem related to another parameter. This event could be the accumulation of sediments or the deterioration of the cleanliness of the supply networks. The loss of filtration efficiency also creates conditions for the proliferation of TC in the supply network [21,66].

Bias induced by changes in monitoring

Over the last 30 years, some parameters have been ignored during water quality monitoring. Sample turbidity measurements, for example, have only been recorded since 2016. Similarly, the evaluation of organic matter in the water network (the simplest being the determination of permanganate oxidation) would also be necessary to assess hygiene. Monitoring of the chlorine level should allow the characterization of the response to this phenomenon. The chlorine demand resulting from the difference between the amount of chlorine added and the residual chlorine in the system tends to increase as the hygiene conditions of the system deteriorate. It is also likely that the disruption in 2012, which was characterized by a high level in SSRC, was related to the change in method and volume ($\times 5$) for the measurement of SSRC (NF T 90–415 vs. NF EN 26461–2). Apart from this case, no testing changes impacted on fecal contamination (EC and IE) and TC, which were highly stable during this period.

Conclusions

The bacteriological quality of the supplied water in Antananarivo has gradually deteriorated in recent years. Water supply infrastructure did not keep pace with population growth and the imbalance between production capacity and water demand has become critical (exponential urban growth and low production efficiency), with a serious impact on the quality of supplied water.

Unplanned urban expansion and land-cover change (deforested watershed) reinforced the impact of heavy rainfall on drinking water quality (high variation of suspended solids). Silting of lake resources and erosion were aggravating factors during rainy periods, introducing contamination markers attached to sediments into the supply system (i.e., spores of sulfite-reducing Clostridia and intestinal enterococci).

The overload of the filtration system mainly occurred after four weeks of cumulative rainfall favoring strong contamination in January and February. Regrowth conditions of bacteria were evident with the emergence of total coliforms after 8 weeks of cumulative rainfall. Consequently, the vulnerability to persistent contamination and biological instability generally persisted during rainy periods. On contrast, *Escherichia coli* were generally removed by the implemented treatment, even during periods of heavy rainfall.

The upgrading of the treatment plant in 1993 had a long and positive impact on drinking water quality, mainly in decreasing contamination events by total coliforms. Appropriate upgrading of the filtration process could be effective in improving the microbiological quality of the water in the supply system. Otherwise, a fair balance between the duration of filtration (flow rate) and the quantity of available treated water must be found.

Stability in testing methods and expansion of monitoring parameters were needed to better assess changes of the interplay between climate and environmental or technical context of water supply.

Supporting information

S1 Table. P-values from permutation test for testing yearly periodicity in contamination time-series data.

(DOCX)

Acknowledgments

We are grateful to Dr. Philippe Cecchi for methodological guidance and The Center of Bioinformatics, Biostatistics, and Integrative Biology (C3BI) of Institut Pasteur at Paris for research assistance.

Author Contributions

Conceptualization: Alexandra Bastaraud, Ronan Jambou.

Data curation: Jean-Marius Rakotondramanga, Jackson Mahazasoatra, Noro Ravaonindrina, Ronan Jambou.

Formal analysis: Emeline Perthame.

Investigation: Alexandra Bastaraud, Jean-Marius Rakotondramanga, Jackson Mahazasoatra, Noro Ravaonindrina.

Methodology: Alexandra Bastaraud, Ronan Jambou.

Project administration: Ronan Jambou.

Software: Emeline Perthame.

Supervision: Ronan Jambou.

Validation: Ronan Jambou.

Writing – original draft: Alexandra Bastaraud.

Writing – review & editing: Emeline Perthame, Ronan Jambou.

References

1. Cann K, Thomas D. Extreme water-related weather events and waterborne disease. *Epidemiol Infect* 2013; 141:671–686. <https://doi.org/10.1017/S0950268812001653> PMID: 22877498
2. Alexander KA, Heaney AK, Shaman J. Hydrometeorology and flood pulse dynamics drive diarrheal disease outbreaks and increase vulnerability to climate change in surface-water-dependent populations: A retrospective analysis. *PLoS Med* 2018; 15:e1002688. <https://doi.org/10.1371/journal.pmed.1002688> PMID: 30408029
3. Pendergrass AG, Knutti R, Lehner F, et al. Precipitation variability increases in a warmer climate. *Sci Rep* 2017; 7:17966. <https://doi.org/10.1038/s41598-017-17966-y> PMID: 29269737
4. Taxak AK, Murumkar AR, Arya DS. Long term spatial and temporal rainfall trends and homogeneity analysis in Wainganga basin, Central India. *Weather Clim Extrem* 2014; 4:50–61.
5. Kistemann T, Classen T, Koch C, et al. Microbial load of drinking water reservoir tributaries during extreme rainfall and runoff. *Appl Environ Microbiol* 2002; 68:2188–2197. <https://doi.org/10.1128/aem.68.5.2188-2197.2002> PMID: 11976088
6. Khan SJ, Deere D, Leusch FDL, et al. Extreme weather events: Should drinking water quality management systems adapt to changing risk profiles? *Water Res* 2015; 85:124–136. <https://doi.org/10.1016/j.watres.2015.08.018> PMID: 26311274
7. Göransson G, Larson M, Bendz D. Variation in turbidity with precipitation and flow in a regulated river system-river Göta Älv, SW Sweden. *Hydrol Earth Syst Sci* 2013; 17:2529–2542.
8. Hrdinka T, Novický O, Hanslík E, et al. Possible impacts of floods and droughts on water quality. *J Hydro-Environment Res* 2012; 6:145–150.
9. Rosario-Ortiz FL, Snyder SA, Suffet IH (Mel). Characterization of dissolved organic matter in drinking water sources impacted by multiple tributaries. *Water Res* 2007; 41:4115–4128. <https://doi.org/10.1016/j.watres.2007.05.045> PMID: 17659316
10. Delpla I, Jung A-V, Baures E, et al. Impacts of climate change on surface water quality in relation to drinking water production. *Environ Int* 2009; 35:1225–1233. <https://doi.org/10.1016/j.envint.2009.07.001> PMID: 19640587
11. Moors E, Singh T, Siderius C, et al. Climate change and waterborne diarrhoea in northern India: Impacts and adaptation strategies. *Sci Total Environ* 2013:468–469.
12. Olorunfoba EO, Folarin TB, Ayede AI. Hygiene and sanitation risk factors of diarrhoeal disease among under-five children in Ibadan, Nigeria. *Afr Health Sci* 2014; 14:1001–1011. <https://doi.org/10.4314/ahs.v14i4.32> PMID: 25834513
13. Howard G, Calow R, Macdonald A, et al. Climate change and water and sanitation: likely impacts and emerging trends for action. *Annu Rev Environ Resour* 2016; 41:253–276.
14. McDonald RI, Green P, Balk D, et al. Urban growth, climate change, and freshwater availability. *Proc Natl Acad Sci U S A* 2011; 108:6312–6317. <https://doi.org/10.1073/pnas.1011615108> PMID: 21444797
15. Ratan R, Venugopal V. Wet and dry spell characteristics of global tropical rainfall. *Water Resour Res* 2013; 49:3830–3841.
16. Razavi T, Switzman H, Arain A, et al. Regional climate change trends and uncertainty analysis using extreme indices: A case study of Hamilton, Canada. *Clim Risk Manag* 2016; 13:43–63.
17. Prest EI, Weissbrodt DG, Hammes F, et al. Long-term bacterial dynamics in a full-scale drinking water distribution system. *PLoS One* 2016; 11:e0164445. <https://doi.org/10.1371/journal.pone.0164445> PMID: 27792739
18. Hannah L, Dave R, Lowry PP, et al. Climate change adaptation for conservation in Madagascar. *Biol Lett* 2008; 4:590–594. <https://doi.org/10.1098/rsbl.2008.0270> PMID: 18664414

19. Van der Bruggen B, Borghgraef K, Vinckier C. Causes of water supply problems in urbanised regions in developing countries. *Water Resour Manag* 2010; 24:1885–1902.
20. Gleason JA, Fagliano JA. Effect of drinking water source on associations between gastrointestinal illness and heavy rainfall in New Jersey. *PLoS One* 2017; 12:e0173794. <https://doi.org/10.1371/journal.pone.0173794> PMID: 28282467
21. Hwang C, Ling F, Andersen GL, et al. Microbial community dynamics of an urban drinking water distribution system subjected to phases of chloramination and chlorination treatments. *Appl Environ Microbiol* 2012; 78:7856–7865. <https://doi.org/10.1128/AEM.01892-12> PMID: 22941076
22. United Nations, Departement of Economic and Social Affairs PD (2018). World Urbanization Prospects : The 2018 Revision, custom data acquired via website [Internet]. 2018 [cited 2019 May 13]. <https://population.un.org/wup/DataQuery/>
23. Peel MC, Finlayson BL, McMahon TA. Updated world map of the Köppen-Geiger climate classification. *Hydrol Earth Syst Sci* 2007; 11:1633–1644.
24. Brown R. IWRM Survey and Status Report: Namibia [Internet]. Global Water Partnership. In 2009 [cited 2019 May 12]. <https://www.gwp.org/globalassets/global/gwp-saf-files/madagascar-iwrm-report.pdf>
25. EAST. Etude de diagnostic AEP dans les 3 ème et 5 ème arrondissements de la Commune Urbaine d' Antananarivo [Internet]. 2016 [cited 2019 May 12]. https://www.pseau.org/outils/ouvrages/east_etude_diagnostic_aep_3eme_5eme_arrondissement_commune_urbaine_antananarivo.pdf
26. AFNOR. Essais des eaux—Recherche et dénombrement des spores de bactéries anaérobies sulfito-réductrices et de Clostridium sulfito-réducteurs—Méthode générale par incorporation en gélose en tubes profonds, NF T90-415, 1985.
27. AFNOR. Essais des eaux—Recherche et dénombrement des coliformes et des coliformes thermotolérants—Méthode générale par filtration sur membrane., NF T90-414, 1985.
28. AFNOR. Qualité de l'eau—Recherche et dénombrement des Escherichia coli et des bactéries coliformes—Partie 1 : méthode par filtration sur membrane, NF EN ISO 9308–1, 2000.
29. AFNOR. Essais des eaux—Recherche et dénombrement des enterocoques—Méthode générale par filtration sur membrane, XP T90-416, 1996.
30. AFNOR. Qualité de l'eau—Recherche et dénombrement des entérocoques intestinaux—Partie 2 : méthode par filtration sur membrane, NF EN ISO 7899–2, 2000.
31. AFNOR. Qualité de l'eau—Dénombrement des Escherichia coli et des bactéries coliformes—Partie 2 : méthode du nombre le plus probable, NF EN ISO 9308–2, 2014.
32. AFNOR Certification. Enterolert-DW / Quanti-Tray for the quantification of enterococci in drinking water: Certificate IDX 33/03-1, 2013.
33. AFNOR. Qualité de l'eau—Recherche et dénombrement des spores de micro-organismes anaérobies sulfito-réducteurs (Clostridia)—Partie 2 : méthode par filtration sur membrane, NF EN 26461–2, 1993.
34. Ministère de l'Energie et des Mines. DECRET N° 2004–635 du 15 juin 2004 Portant modification du décret n°2003–941 du 09 Septembre 2003 relatif à la surveillance de l'eau, au contrôle des eaux destinées à la consommation humaine et aux priorités d'accès à la ressource en eau [Internet]. 2004 p. 4. <http://www.observatoire-foncier.mg/file-library/DECRETN2004-635-du-15-juin-2004.pdf>
35. Zeileis A, Kleiber C, Walter K, et al. Testing and dating of structural changes in practice. *Comput Stat Data Anal* 2003; 44:109–123.
36. Bai J, Perron P. Computation and analysis of multiple structural change models. *J Appl Econom* 2003; 18:1–22.
37. Chan AK, Ripley B. Time Series Analysis: Package 'TSA' [Internet]. 2018 [cited 2019 May 12]. p. 1–79. <http://www.stat.uiowa.edu/~kchan/TSA.htm>
38. Blackford JU, Salomon RM, Waller NG. Detecting change in biological rhythms: A multivariate permutation test approach to Fourier-transformed data. *Chronobiol Int* 2009; 26:258–281. <https://doi.org/10.1080/07420520902772221> PMID: 19212840
39. Hyndman RJ, Khandakar Y. Automatic time series forecasting: The forecast package for R. *J Stat Softw* 2008; 27:1–22.
40. Mahdi E, Ian Mcleod A. Improved multivariate portmanteau test. *J Time Ser Anal* 2012; 33:211–222.
41. Jachimowski A. Factors affecting water quality in a water supply network. *J Ecol Eng* 2017; 18:110–117.
42. Liu G, Zhang Y, Knibbe W-J, et al. Potential impacts of changing supply-water quality on drinking water distribution: A review. *Water Res* 2017; 116:135–148. <https://doi.org/10.1016/j.watres.2017.03.031> PMID: 28329709
43. Edition F. WHO | Guidelines for drinking-water quality, 4th edition, incorporating the 1st addendum. Who 2018.

44. José Figueras M, Borrego JJ. New perspectives in monitoring drinking water microbial quality. *Int J Environ Res Public Health* 2010; 7:4179–4202. <https://doi.org/10.3390/ijerph7124179> PMID: 21318002
45. Haagsma J. Pathogenic anaerobic bacteria and the environment. *Rev Sci Tech l'OIE* 2016; 10:749–764.
46. Sathish S, Swaminathan K. Genetic diversity among toxigenic clostridia isolated from soil, water, meat and associated polluted sites in south india. *Indian J Med Microbiol* 2009; 27:311. <https://doi.org/10.4103/0255-0857.55443> PMID: 19736399
47. Edberg SC, Rice EW, Karlin RJ, et al. *Escherichia coli*: the best biological drinking water indicator for public health protection. *J Appl Microbiol* 2000; 88:106S–116S.
48. Exploitation Eau JIRAMA 2015 [Internet]. [cited 2019 May 13]. http://www.jirama.mg/index.php?w=scripts&f=Jirama-page.php&act=exp_eau
49. Stanfield G, Lechevallier M, Snozzi M. Treatment Efficiency. In 2003 [cited 2018 Sep 17]. p. 159–78. http://www.who.int/water_sanitation_health/dwq/9241546301_chap5.pdf
50. Jacobsen M, Webster M, Vairavamorthy K. The future of water in african cities [Internet]. The future of water in african cities. The World Bank; 2012 Oct [cited 2019 May 13]. <http://elibrary.worldbank.org/doi/book/10.1596/978-0-8213-9721-3>
51. Ricci PF, Ragaini RC, Goldstein R, Smith W. Global water quality, supply and demand: implications for megacities. In 2010 [cited 2019 May 13]. p. 443–67. http://federationofscientists.org/PMPanels/Pollution/Water_Quality.pdf
52. Hannah L, Dave R, Lowry PP, et al. Climate change adaptation for conservation in Madagascar. *Biol Lett* 2008; 4:590–594. <https://doi.org/10.1098/rsbl.2008.0270> PMID: 18664414
53. Stelma GN. Use of bacterial spores in monitoring water quality and treatment. *J Water Health* 2018; 16:491–500. <https://doi.org/10.2166/wh.2018.013> PMID: 30067232
54. Cox R, Bierman P, Jungers MC, et al. Erosion rates and sediment sources in Madagascar inferred from 10be analysis of lavaka, slope, and river sediment. *J Geol* 2009; 117:363–376.
55. Aldegheri M. Rivers and streams on Madagascar. In 1972 [cited 2019 May 13]. p. 261–310. http://horizon.documentation.ird.fr/exl-doc/pleins_textes/pleins_textes_5/b_fdi_30-30/32882.pdf
56. Chaperon P, Danloux J, Ferry L. Fleuves et rivières de Madagascar. Monographie hydrologique 10. In 1993 [cited 2019 May 13]. p. 883. <http://www.documentation.ird.fr/hor/fdi:37307>
57. Payet E, Dumas P, Pennober G. Modélisation de l'érosion hydrique des sols sur un bassin versant du sud-ouest de Madagascar, le Fiherenana. *Vertigo* [Internet]. 2012 Feb 7 [cited 2019 May 13]; (Volume 11 Numéro 3). <http://journals.openedition.org/vertigo/12591>
58. Bastaraud A, Rakotondramanga J, Mahazosaoatra J, et al. Environmental factors and the microbial quality of urban drinking water in a low-income country: The case of Madagascar. *Water* 2018; 10:1450.
59. Boehm AB, Sassoubre LM. Enterococci as indicators of environmental fecal contamination [Internet]; 2014 [cited 2019 Mar 13]. <http://www.ncbi.nlm.nih.gov/pubmed/24649503>
60. Byappanahalli MN, Nevers MB, Korajkic A, et al. *Enterococci* in the Environment. *Microbiol Mol Biol Rev* 2012; 76:685–706. <https://doi.org/10.1128/MMBR.00023-12> PMID: 23204362
61. Ramette M. Etude pour la protection contre les crues de la rive gauche de l'Ikopa et réglementation des zones inondables. Rapport de mission du 4 au 12/12/95] ARSIE [Internet]. 1995 [cited 2019 May 13]. <https://arsie.mg/fr/metadata/etude-pour-la-protection-contre-les-crues-de-la-rive—265706/edit>
62. Day T, Garratt R. *Lakes and Rivers*. *Lapl. A Nat. Hist.*, Chelsea House, 2014: 258.
63. Raharimahefa T, Kusky TM. Environmental monitoring of bombetoka bay and the Betsiboka estuary, Madagascar, using multi-temporal satellite data. *J Earth Sci* 2010; 21:210–226.
64. Razafindratsimba Dominique T. Quelques aspects de la gestion, de l'exploitation et du rapport à l'eau à Madagascar [Internet]. [cited 2018 Apr 9]. https://www.pseau.org/outils/ouvrages/universite_d_antananarivo_quelques_aspects_de_la_gestion_de_l_exploitation_et_du_rapport_a_l_eau_a_madagascar_2014.pdf
65. McCarthy DT. A traditional first flush assessment of *E. coli* in urban stormwater runoff. *Water Sci Technol* 2009; 60:2749–2757. <https://doi.org/10.2166/wst.2009.374> PMID: 19934495
66. Amanidaz N, Zafarzadeh A, Mahvi AH. The interaction between heterotrophic bacteria and coliform, fecal coliform, fecal *streptococci* bacteria in the water supply networks. *Iran J Public Health* 2015; 44:1685–1692. PMID: 26811820

Résumé en français

A Madagascar, parmi les menaces pour la santé publique, la population fait face aux maladies infectieuses pouvant toucher l'ensemble de la population, et constituer des risques sanitaires en permanence comme l'infection à *Plasmodium falciparum* (*P. falciparum*) et d'autres maladies infectieuses endémiques comme la peste ou encore des maladies émergentes tel que le COVID-19. Le système de surveillance épidémiologique et les programmes nationaux de contrôle des maladies infectieuses ont aussi été éprouvés dans le contexte de la pandémie de COVID-19. Selon l'Organisation Mondiale de la Santé (OMS), pendant la période pandémique de 2020–2021, environ 82% de cas et 95% de décès dus au paludisme dans le monde ont été survenus dans la région africaine de l'OMS, représentant une hausse allant de 211 millions à 234 millions de cas et de 542 000 à 593 000 décès de 2015–2020. De plus, entre 2020 et 2021, environ 13,4 millions de cas supplémentaires du paludisme, et une augmentation du nombre de décès de 386 400 à 597 400, auraient été attribuables à la mitigation des efforts de lutte due aux interventions non-pharmaceutiques pour faire face à la pandémie de COVID-19.

Dans le cadre de cette thèse, notre objectif consiste à mieux comprendre les dynamiques spatiales et temporelles de deux maladies infectieuses, le paludisme et le COVID-19, malgré la porosité (ensemble de manquements) du système de surveillance passive à Madagascar.

Pour ce faire, des approches de modélisation biostatistique et biomathématique ont été adoptées en utilisant des données de mesures indirectes de l'intensité de transmission : les mesures d'anticorps du *P. falciparum*, et l'excès de mortalité toutes causes pendant la pandémie de COVID-19. La première étude de cette thèse porte sur l'utilisation de données d'une étude randomisée transversale incluant 6 293 enfants pour identifier des facteurs associés d'exposition à l'infection plasmodiale dans les hautes terres, zone à très faible transmission. Des facteurs liés aux offres de soin (accès aux formations sanitaires, prises en charge communautaire, interventions de lutte antivectorielles), et liés à l'environnement et le climat (écologie des vecteurs) ont été étudiés. La seconde étude consiste à évaluer l'impact de la pandémie de COVID-19 dans la capitale, Antananarivo, par l'estimation de l'excès de décès durant les vagues de 2020–2021 à partir des registres de décès du Bureau Municipal d'Hygiène, représentant 45 959 enregistrements de décès hospitaliers et communautaires de toutes causes de 2016–2021.

Nos résultats issus de ces deux études ont pu accentuer l'importance des données spatiales ou temporelles désagrégées à l'échelle fine (réponses aux anticorps, facteurs environnementaux et climatiques) et des systèmes de surveillance optimaux (le registres de décès) pour évaluer, améliorer et adapter les programmes nationaux de lutte contre les maladies infectieuses dans les pays à revenu faible ou intermédiaire comme Madagascar.

Mots clés : épidémiologie, modélisation, système de surveillance, analyses spatiales et temporelles, paludisme, *Plasmodium falciparum*, COVID-19, SARS-CoV-2, excès de mortalité, Madagascar.

Résumé en anglais

In Madagascar, among the threats to public health, the population is faced with infectious diseases that can affect the entire population and constitute permanent health risks, such as *Plasmodium falciparum* (*P. falciparum*) infection and other endemic infectious diseases such as plague, as well as emerging diseases such as COVID-19. The epidemiological surveillance system and national infectious disease control programmes have also been tested in the context of the COVID-19 pandemic. According to the World Health Organization (WHO), during the 2020-2021 pandemic period, approximately 82% of cases and 95% of deaths due to malaria worldwide occurred in the WHO African Region, representing an increase in cases, from 211 million to 234 million, and deaths, from 542,000 to 593,000, from 2015-2020. Furthermore, between 2020 and 2021, approximately 13.4 million additional malaria cases, and an increase in deaths from 386,400 to 597,400, would have been attributable to the mitigation of control efforts due to non-pharmaceutical interventions to address the COVID-19 pandemic.

Our aim in this thesis is to gain a better understanding of the spatial and temporal dynamics of two infectious diseases, malaria and COVID-19, despite the porosity (set of shortcomings) of the passive surveillance system in Madagascar.

To this end, biostatistical and biomathematical modelling approaches were adopted using data from indirect measures of transmission intensity: *P. falciparum* antibody measurements, and all-cause excess mortality during the COVID-19 pandemic. The first study in this thesis uses data from a randomized cross-sectional survey involving 6,293 children to identify factors associated with residual malaria transmission in the highlands, an area of very low transmission. Factors related to the health care services (access to health facilities, community-based case management, vector control interventions) and to the environment and climate (vector ecology) were studied. The second study consists of assessing the impact of the COVID-19 pandemic in the capital, Antananarivo, by estimating the excess deaths during the 2020–2021 waves using the death registers referring to the Bureau Municipal d'Hygiène, representing 45,959 records of hospital and community deaths from 2016–2021.

Our results from these two studies have highlighted the importance of fine-scale disaggregated spatial or temporal data (antibody responses, environmental and climatic factors) and optimal surveillance systems (death registers) for evaluating, improving and adapting national infectious disease control programmes in low- and middle-income countries such as Madagascar.

Keywords: epidemiology, modelling, surveillance systems, spatial and temporal analyses, malaria, *Plasmodium falciparum*, COVID-19, SARS-CoV-2, excess mortality, Madagascar.